Proceedings to the 25th Workshop

What Comes Beyond the Standard Models

Bled, July 4–10, 2022

[Virtual Workshop]

July 11-12 2022

Edited by

Norma Susana Mankoč Borštnik
Holger Bech Nielsen
Astri Kleppe

_____

**The 25th Workshop *What Comes Beyond the Standard Models*,
4.– 10. July 2022, Bled
[Virtual Workshop, July 11-12, 2022]**

was organized by

Society of Mathematicians, Physicists and Astronomers of Slovenia

and sponsored by

Department of Physics, Faculty of Mathematics and Physics, University of Ljubljana

Society of Mathematicians, Physicists and Astronomers of Slovenia

Beyond Semiconductor (Matjaž Breskvar)

VIA (Virtual Institute of Astroparticle Physics), Paris

MDPI journal "Symmetry", Basel

MDPI journal "Physics", Basel

MDPI journal "Universe"", Basel

Scientific Committee

John Ellis, *King's College London / CERN*
Roman Jackiw, *MIT*
Masao Ninomiya, *Yukawa Institute for Theoretical Physics, Kyoto University*

Organizing Committee

Norma Susana Mankoč Borštnik
Holger Bech Nielsen
Maxim Yu. Khlopov

The Members of the Organizing Committee of the International Workshop "What Comes Beyond the Standard Models", Bled, Slovenia, state that the articles published in the Proceedings to the 25th Workshop "What Comes Beyond the Standard Models", Bled, Slovenia are refereed at the Workshop in intense in-depth discussions.

Workshops organized at Bled

▷ *What Comes Beyond the Standard Models*
  (June 29–July 9, 1998), Vol. **0** (1999) No. 1
  (July 22–31, 1999)
  (July 17–31, 2000)
  (July 16–28, 2001), Vol. **2** (2001) No. 2
  (July 14–25, 2002), Vol. **3** (2002) No. 4
  (July 18–28, 2003) Vol. **4** (2003) Nos. 2-3
  (July 19–31, 2004), Vol. **5** (2004) No. 2
  (July 19–29, 2005) , Vol. **6** (2005) No. 2
  (September 16–26, 2006), Vol. **7** (2006) No. 2
  (July 17–27, 2007), Vol. **8** (2007) No. 2
  (July 15–25, 2008), Vol. **9** (2008) No. 2
  (July 14–24, 2009), Vol. **10** (2009) No. 2
  (July 12–22, 2010), Vol. **11** (2010) No. 2
  (July 11–21, 2011), Vol. **12** (2011) No. 2
  (July 9–19, 2012), Vol. **13** (2012) No. 2
  (July 14–21, 2013), Vol. **14** (2013) No. 2
  (July 20–28, 2014), Vol. **15** (2014) No. 2
  (July 11–19, 2015), Vol. **16** (2015) No. 2
  (July 11–19, 2016), Vol. **17** (2016) No. 2
  (July 9–17, 2017), Vol. **18** (2017) No. 2
  (June 23–July 1, 2018), Vol. **19** (2018) No. 2
  (July 6–14, 2019), Vol. **20** (2019) No. 2
  (July 4–12, 2020), Vol. **21** (2020) No. 1
  (July 4–12, 2020), Vol. **21** (2020) No. 2
  (July 1–12, 2021), Vol. **22** (2021) No. 1
▷ *Hadrons as Solitons* (July 6–17, 1999)
▷ *Few-Quark Problems* (July 8–15, 2000), Vol. **1** (2000) No. 1
▷ *Selected Few-Body Problems in Hadronic and Atomic Physics* (July 7–14, 2001),
  Vol. **2** (2001) No. 1
▷ *Quarks and Hadrons* (July 6–13, 2002), Vol. **3** (2002) No. 3
▷ *Effective Quark-Quark Interaction* (July 7–14, 2003), Vol. **4** (2003) No. 1
▷ *Quark Dynamics* (July 12–19, 2004), Vol. **5** (2004) No. 1
▷ *Exciting Hadrons* (July 11–18, 2005), Vol. **6** (2005) No. 1
▷ *Progress in Quark Models* (July 10–17, 2006), Vol. **7** (2006) No. 1
▷ *Hadron Structure and Lattice QCD* (July 9–16, 2007), Vol. **8** (2007) No. 1
▷ *Few-Quark States and the Continuum* (September 15–22, 2008),
  Vol. **9** (2008) No. 1
▷ *Problems in Multi-Quark States* (June 29–July 6, 2009), Vol. **10** (2009) No. 1
▷ *Dressing Hadrons* (July 4–11, 2010), Vol. **11** (2010) No. 1
▷ *Understanding hadronic spectra* (July 3–10, 2011), Vol. **12** (2011) No. 1
▷ *Hadronic Resonances* (July 1–8, 2012), Vol. **13** (2012) No. 1
▷ *Looking into Hadrons* (July 7–14, 2013), Vol. **14** (2013) No. 1
▷ *Quark Masses and Hadron Spectra* (July 6–13, 2014), Vol. **15** (2014) No. 1
▷ *Exploring Hadron Resonances* (July 5–11, 2015), Vol. **16** (2015) No. 1

▷ *Quarks, Hadrons, Matter* (July 3–10, 2016), Vol. **17** (2016) No. 1
▷ *Advances in Hadronic Resonances* (July 2–9, 2017), Vol. **18** (2017) No. 1
▷ *Double-charm Baryons and Dimesons* (June 17–23, 2018), Vol. **19** (2018) No. 1
▷ *Electroweak Processes of Hadrons* (July 15–19, 2019), Vol. **20** (2019) No. 1
▷
　　○ *Statistical Mechanics of Complex Systems* (August 27–September 2, 2000)
　　○ *Studies of Elementary Steps of Radical Reactions in Atmospheric Chemistry* (August 25–28, 2001)

Contents

Preface in English and Slovenian Language

This year our series of workshops on "What Comes Beyond the Standard Models?" took place the twenty-fifth time. The series started in 1998 with the idea of organizing a workshop, in which participants would spend most of the time in discussions, confronting different approaches and ideas. The picturesque town of Bled by the lake of the same name, surrounded by beautiful mountains and offering pleasant walks, was chosen to stimulate the discussions.

The idea was successful and has developed into an annual workshop, which is taking place every year since 1998. Very open-minded and fruitful discussions have become the trade-mark of our workshop, producing several published works. It takes place in the house of Plemelj, which belongs to the Society of Mathematicians, Physicists and Astronomers of Slovenia.

Since the workshop is celebrating its anniversary, 25th, it is an opportunity to look at what has happened in the field of physics of elementary fermion and boson fields all this time. And what new the measurements together with the suggested theories have brought.

The technology and computer science has progressed in mean time astonishingly, enabling almost unbelievable measurements in all fields of physics, especially in the physics of fermion and boson fields and in cosmology.

The *standard model* assumptions have been confirmed without offering surprises. The last unobserved field assumed by the *standard model* as a field, the Higgs's scalar, detected in June 2012, was confirmed in March 2013. New and new measurements of masses of quarks and leptons and antiquarks and antileptons, of the mixing matrices of quarks and of leptons, of the Higgs's scalar, of bound states of quarks and leptons, offer new and new data. The waves of the gravitational field were detected in February 2016 and again 2017.

If we look at the collection of open questions that we set ourselves at the beginning and continuously supplemented in each workshop, it shows up that we are all the time mostly looking for an answer to the essential question: What is the next step beyond the *standard model*, which would offer not only the understanding of all the assumed properties for quarks and leptons and all the observed boson fields with the Higgs scalars included, but also for the observed phenomena in cosmology, like it is the understanding of the expansion rate of the universe, of the appearance of the dark matter, of black holes with their (second quantized) quantum nature included, of the necessity of the existence of the dark energy and many others.

When trying to understand the quantum nature of fermion and boson fields we are looking for the theory which is anomaly free and possibly renormalizable so that we would be able to predict properties of second quantized fields when proposing measurements.

If it turns out that these requirements lead to the dimension of space time which is higher than $(3 + 1)$ then the questions arise how does it happen that all the dimensions except the $(3 + 1)$-ones are hidden. How do consequently the internal spaces of fermion and boson fields manifest in d $= (3 + 1)$? And can such a theory be free of anomalies and renormalizable?

The observations of the galactic rotation curves are one of the strongest evidence that it is not only the ordinary matter which determines the properties of the galaxies. The direct measurements of the Dama/Libra experiment with more and more accuracy demonstrates the annual dependence of the number of events. One can hardly accept that these measurements are not connected with the dark matter needed to explain the rotational curves of galaxies and behaviour of clouds of galaxies, of whatever origin the dark matter is.
The measurements of the Hubble constant state that the universe is expanding and how fast does expend.
The cosmological measurements show up that there exist the black holes.

In all our annual workshops there have appeared innovative proposals for: **i.** Explaining the assumptions of the *standard model*, mostly with new unexplained assumptions. **ii.** Suggestions of what is the dark matter. **iii.** Suggestions for what causes inflation. **iv.** Suggestions what does determine the internal space of fermions and bosons. **v.** Suggestions how to avoid anomalies and make quantum theories of fields renormalizable. **vi.** How to suggest experiments which would show the next step beyond the *standard model*. **vii.** How does "Nature make the decision" about breaking of symmetries down to the noticeable ones, if coming from some higher dimension d? **viii.** Why is the metric of space-time Minkowskian and how is the choice of metric connected with the evolution of our universe(s)? **....** And many others.
In our proceedings there are papers (many of them later published in journals) discussing these problems and offering suggestions how to solve them.
In the last two Covid-19 years the ZOOM workshop replaced our ordinary workshops. It must be admitted that the ZOOM meetings can not replace the real meetings where all the questions are welcome even if answers need a long time to be presented.
Talks and discussions in our workshop are not at all talks in the usual way. Each talk as well as discussions lasted several hours, divided in two hours blocks, with a lot of questions, explanations, trials to agree or disagree from the audience or speakers side.
Although also on the ZOOM way of presentations several continuations of the same talk were planned and realized, yet the presence in real is much more effective.
This last, the jubilee workshop, was partly in "real" at Bled and partly by ZOOM. The topics presented and discussed in this workshop concern all the above mentioned open problems, illustrated by the question "How to understand Nature?"
We were trying to find the answers in several steps:

- How to make the next step beyond both standard models?
  - **o**   How to come beyond the *standard model* of the so far observed quarks and leptons and antiquarks and antileptons, appearing in families, and interacting with the electroweak, colour and scalar fields,
  - **o**   How to explain observed cosmological phenomena?
- How can we construct the anomalies-free renormalizable theory of all the so far observed fermions and all the so far observed boson fields?
  - **o**   Can this be done as well as for bound states and scattering states of fermion and boson fields?
  - **o**   How do symmetries contribute to bound states?
- Can we find the way to treat all the elementary fermion and boson fields in an unique way?
  - **o**   How to find the way to treat fermion and boson fields if space-time is indeed four dimensional?
  - **o**   How does "Nature make the decision" about breaking of symmetries down to the noticeable ones, if coming from some higher dimension d?
  - **o**   Why is the metric of space-time Minkowskian and how is the choice of metric connected with the evolution of our universe(s)?
  - **o**   What does cause the inflation of the universe?
  - **o**   When does the inflation appear? After the electroweak phase transition?
  - **o**   What does determine the colour scale?
- What is our universe made out of besides of the (mostly) first family baryonic matter?
  - **o**   How do black holes contribute to the dark matter?
- What is the role of symmetries in Nature?
- How to make experiments and how to propose the models so that the data would not be influenced too much by the proposed model?

Most of talks are "unusual" in the sense that they are trying to find out new ways of understanding and describing the observed phenomena.

The proceedings is divided into two parts. To the first part the invited talks, which appear in time and were refereed, contribute.
To the second part, called Discussion section, the contributions are presented, which started to be intensively discussed during the workshop but need more discussions so that the authors of different contributions would agree or disagree, or which seem to the authors of different contributions that they have many common points, expressed in a different way, which might lead to new ideas or new conclusions or new collaborations.
Some of discussions, started during the workshop, are not appearing in this proceedings and might continue next year and be ready for next proceedings.
The organizers are grateful to all the participants for the lively presentations and discussions and the good working atmosphere although most of participants appear virtually, what was lead by Maxim Khlopov.
The reader can find all the talks and soon also the whole Proceedings on the official website of the Workshop:
http://bsm.fmf.uni-lj.si/bled2022bsm/presentations.html,

and on the Cosmovia Forum https://bit.ly/bled2022bsm ..

Norma Mankoč Borštnik, Holger Bech Nielsen,
Maxim Khlopov, Astri Kleppe   *Ljubljana, December 2022*

1 Predgovor (Preface in Slovenian Language)

To leto je serija delavnic z naslovom „Kako preseči oba standardna modela, kozmološkega in elektrošibkega" ("What Comes Beyond the Standard Models?") stekla že petindvajsetič. Prva delavnica je stekla leta 1998 v želji, da bi udeleženci v izčrpnih diskusijah kritično soočali različne ideje in teorije. Slikovito mestece Bled, ob jezeru z enakim imenom, obkroženo s prijaznimi hribčki, nad katerimi kipijo slikovite gore, ki ponujajo prijetne sprehode in pohode, ponujajo priložnosti za diskusije.

Ideja je bila uspešna, razvila se je v vsakoletno delavnico, ki teče že ptindvajsetič. Zelo odprte, prijateljske in učinkovite diskusije so postale "blagovna znamka" naših delavnic, ideje, ki so se v diskusijah rodile, pa so pogosto botrovale objavljenim člankom. Delavnice domujejo v Plemljevi hiši na Bledu tik ob jezeru. Hišo je Društvu matematikov, fizikov in astronomov zapustil svetovno priznani slovenski matematik Jozef Plemelj.

Letošnje jubilejno leto ponuja priložnost, da pogledamo, kaj vse se je zgodilo v tem času v fiziki osnovnih fermionskih in bozonskih polj in v kozmologiji in kaj so novega v tem času ponudile meritve skupaj s predlaganimi teorijami.

Tehnologija in računalništvo sta medtem presenetljivo hitro napredovala in omogočila skoraj neverjetne meritve na vseh področjih fizike, tudi ali še posebej v fiziki fermionskih in bozonskih polj ter v kozmologiji.

Poskusi so potrdili predpostavke *standardnega modela* ne da bi prinesli kakršnekoli presenečenje. Zadnje polje, ki ga predpostavi *standardni model*, Higgsov skalar, ki je bil odkrit junija 2012, so potrdili v marcu 2013. Vedno bolj natančne meritve mas kvarkov in leptonov in antikvarkov in antileptonov, mešalnih matrik kvarkov in leptonov, mase Higgsovega skalarja, vezanih stanj kvarkov in leptonov, ponujajo nove in nove podatke. Valovanje gravitacijskega polja smo zaznali februarja 2016 in spet 2017.

Če pogledamo zbirko odprtih vprašanj, ki sva si jih s Holgerjem zastavila pred začetkom delavnic in ki smo jo ob vsaki delavnici sproti dopolnjevali, kaže, da ves čas iščemo odgovor na bistveno vprašanje: Kaj je naslednji korak, ki bo presegel *standardni model* in bo ponudil ne le razlago in razumevanje za vse predpostavljene lastnosti za kvarke in leptone in antikvarke in antileptone in za vsa doslej opažena bozonska polja, skupaj s Higgsovim skalarjem, ampak tudi za vse opažene pojave v vesolju, kot je na primer hitrost širjenja vesolja, pojav temne snovi, pomen singularnosti črnih luknenj kot kvantnega skupka fermionov in antifermionov in vseh bozonskih polj, vključno z gravitacijskim poljem v drugi kvantizaciji, kako je z nujnostjo obstoja temne energije in mnogih drugih opaženj. Ko poskušamo razumeti kvantno naravo fermionskih in bozonskih polj, iščemo teorijo, ki je brez anomalij in taka, da nam da končne prispevke za predlagane meritve.

Če se izkaže, da lahko uresničimo te zahteve le, če dovolimo, da ima prostor-čas več kot le opazljive $(3 + 1)$ razsežnosti, potem moramo odgovoriti na vprašanje, zakaj so vse razsežnosti razen $d = (3 + 1)$ skrite. Kako se tedaj v $d = (3 + 1)$

manifestirajo notranji prostori fermionskih in bozonskih polj? In ali je taka teorija lahko brez anomalij in ponudi končne prispevke za obravnane dogodke?

Merjenja hitrosti rotacije zvezd okoli centra galaksije in gibanja galaksij v jatah so ena najmočnejših dokazov, da ni le običajna snov, iz katere so zvezde, tista, ki določa lastnosti galaksij in jat galaksij. Tudi neposredne meritve eksperimenta Dama/Libra z vse večjo natančnostjo dokazujejo, da je izmerjeni letni odvisnosti števila dogodkov potrebno verjeti in da te dogodke povzroča temna snov, kakršenkoli že je njen izvor.
Meritve Hubblove konstante navajajo, kako hitro se vesolje širi.
Kozmološka merjenja kažejo, da črne luknje obstajajo.

Naše delavnice so ponudile inovativne predloge: **i.** Za razlago predpostavk *standardnega modela*, večinoma z novimi nepojasnjenimi predpostav-kami. **ii.** Za to, iz česa je temna snov. **iii.** Za pojav in vzrok inflacije vesolja. **iv.** Za to, kaj določa notranji prostor fermionov in bozonov. **v.** Kako se izogniti anomalijam in oblikovati kvantne teorije polj, ki jih je mogoče renormalizirati. **vi.** Kako predlagati poskuse, ki bi pokazali kaj je naslednji korak po *standardnem modelu*. **vii.** Kako se "Narava odloči" zlomiti simetrije od začetne v razsežnosti d do opaženih v d=(3+1)? **viii.** Zakaj je metrika prostora-časa metrika Minkovskega in kako je izbira metrike povezana z razvojem našega(ih) vesolja(ij)? **...** In mnogo drugih.
V objavljenih zbornikih in v pozneje objavljenih člankih v revijah so prispevki, ki razpravljajo o teh problemih in ponudijo predloge, kako probleme rešiti.
V zadnjih dveh letih Covida-19 je delavnica preko "ZOOM-a" nadomestila naše običajne delavnice. Treba je priznati, da srečanja preko interneta ne morejo nadomestiti pravih srečanj, kjer so vsa vprašanja dobrodošla, tudi če je za odgovore potrebno mnogo časa.
Pogovori in razprave na naših delavnicah sploh niso običajne diskusije. Razprave trajajo po več ur, razdeljene v dvourne bloke, z veliko vprašanji, razlagami, poskusi strinjanja ali nestrinjanja udeležencev in pojasnjevalca.
Čeprav so naše delavnice po internetu omogočile predstavitve del v več nadaljevanjih, je prisotnost v istem prostoru za prave razprave veliko bolj učinkovita.
Ta zadnja, jubilejna delavnica, je potekala delno na Bledu in delno po "ZOOM-u".
Teme, predstavljene in obravnavane na tej delavnici, se nanašajo na vse zgoraj omenjene teme, strnjene v vprašanje "kako razumeti Naravo".
Odgovore smo poskušali najti v več korakih:

- Kako najti naslednji korak, ki bo odgovoril na odprta vprašanja obeh modelov?
  o Kako poiskati teorijo, ki bo pojasnila vse privzetke *standardnega modela* kvarkov in leptonov ter antikvarkov in antileptonov, ki nastopajo v družinah in si izmenjujejo elektromagnetna, šibka, barvna in skalarna polja?
  o Kako razložiti doslej opažene kozmološke pojave?
- Kako poiskati renormalizabilno teorijo brez anomalij za vse poznane fermione in njihova umeritvena polja?

    o   Kako poiskati renormalizabilno teorijo brez anomalij tudi za vezana in sipana stanja fermionov in bozonov?

    o   Kako simetrije prispevajo k vezanim stanjem?

- Kako obravnavati vsa osnovna fermionska in bozonska polja na ekvivalenten način?

    o   Kako obravnavati fermionska in bozonska polja, če je prostor-čas res štirirazsežen?

    o   Kako se ″Narava odloči″ za zlom simetrij od začetne simetrije v d-razsežem prostotu-času do opaženih v d=(3+1)?

    o   Zakaj je metrika prostora-časa metrika Minkovskega in kako je izbira metrike povezana z razvojem našega vesolja?

    o   Kaj povzroča inflacijo vesolja?

    o   Kdaj se pojavi inflacija? Po elektrošibkem prehodu?

    o   Kaj določa barvno skalo?

- Iz česa je naše vesolje poleg iz barionov (večinoma iz prve družine kvarkov in leptonov)?

    o   Kako črne luknje prispevajo k temni snovi?

- Kakšna je vloga simetrij v naravi?
- Kako narediti poskuse in kako predlagati modele, da ne bi predlagani model preveč vplival na izmerjene podatke?

Večina prispevkov je ″nenavadnih″ v tem smislu, da poskušajo najti nove rešitve odprtih problemov.

Zbornik je razdeljen na dva dela. V prvi del so vključena vabljena predavanja, ki so prispela do organizatorjev pravočasno in so bila tudi recenzirana.
V drugem delu so zbrani prispevki, za katere avtorji menijo, da diskusije niso prinesle odločitve, do katere mere se avtorji strinjajo, ali nestrinjajo s predstavljenimi trditvami, ali pa avtorji menijo, da imajo različni pristopi mnogo skupnega ter lahko pripeljejo do novih idej ali novega razumevanja ali celo do sodelovanja.
Nekatere od diskusij, ki so se začele med delavnico, se v tem zborniku ne pojavijo. Morda se bodo nadaljevale na naslednji delavnici in bodo zapisane v naslednjem zborniku.
Organizatorji se iskreno zahvaljujejo vsem sodelujočim na delavnici za učinkovite predstavitve del, za živahne razprave in dobro delovno vzdušje, kljub temu, da je večina udeležencev sodelovala preko spleta, ki ga je vodil Maxim Yu. Khlopov.
Bralec najde vse pogovore in kmalu tudi celoten Zbornik na uradni spletni strani delavnice: http://bsm.fmf.uni-lj.si/bled2022bsm/presentations.html,
in na forumu Cosmovia https://bit.ly/bled2022bsm ..

Norma Mankoč Borštnik, Holger Bech Nielsen,
Maksim Khlopov, Astri Kleppe   *Ljubljana, december 2022*

1 New and recent results, and perspectives from DAMA/LIBRA–phase2

R. Bernabei, P. Belli, A. Bussolotti, V. Caracciolo, R. Cerulli, N. Ferrari, A. Leoncini, V. Merlo, F. Montecchia[***][1,2]
F. Cappella, A. d'Angelo, A. Incicchitti, A. Mattei[3,4]
C.J. Dai, X.H. Ma, X.D. Sheng, Z.P. Ye[†][5]

[1] Dip. di Fisica, Università di Roma Tor Vergata, Rome, Italy
[2] INFN, sez. Roma Tor Vergata, Rome, Italy
[3] Dip. di Fisica, Università di Roma La Sapienza, Rome, Italy
[4] INFN, sez. Roma, Rome, Italy
[5] Key Laboratory of Particle Astrophysics IHEP, Chinese Academy of Sciences, Beijing, PR China

Abstract. Here the results obtained by analysing other two annual cycles of DAMA/LIBRA–phase2 are presented and the long-standing model-independent annual modulation effect measured by DAMA deep underground at the Gran Sasso National Laboratory (LNGS) of the I.N.F.N. with different experimental configurations is summarized. In particular, profiting from a second generation high quantum efficiency photomultipliers and new electronics, the DAMA/LIBRA–phase2 apparatus ($\simeq 250$ kg highly radio-pure NaI(Tl)) has allowed the reaching of lower software energy threshold. Including the results of the two new annual cycles, the total exposure of DAMA/LIBRA–phase2 over 8 annual cycles is 1.53 ton $\times$ yr. The evidence of a signal that meets all the requirements of the model independent Dark Matter (DM) annual modulation signature is further confirmed: 11.8 σ C.L. in the energy region (1–6) keV. In the energy region between 2 and 6 keV, where data are also available from DAMA/NaI and DAMA/LIBRA–phase1, the achieved C.L. for the full exposure (2.86 ton $\times$ yr) is 13.7 σ; the modulation amplitude of the *single-hit* scintillation events is: (0.01014 ± 0.00074) cpd/kg/keV, the measured phase is (142.4 ± 4.2) days and the measured period is (0.99834 ± 0.00067) yr, values all well in agreement with those expected for DM particles. No systematics or side reaction able to mimic the exploited DM signature (i.e. to account for the whole measured modulation amplitude and to simultaneously satisfy all the requirements of the signature) has been found or suggested by anyone throughout some decades thus far.

Povzetek: Avtorji predstavijo rezultate zadnjih in vseh dosedanjih meritev na experimentu DAMA/LIBRA, ki meri letno modulacijo sipanja delcev, za katere zdaj že z veliko gotovostjo menijo, da so lahko samo delci *temne snovi*. Nacionalni laboratorij Gran Sasso (LNGS) I.N.F.N. se nahaja globoko pod zemljo. V teh letih so uporabili različne konfiguracije in vsebnosti merilcev ter poskrbeli za njihovo čistost in učinkovitost. V poskusu

---

[***] F. Montecchia also Dip. di Ing. Civile e Informatica, Universit'a di Roma Tor Vergata, Rome, Italy
[†] Z.P. Ye also University of Jinggangshan, Jiangxi, China

DAMA/LIBRA–phase2 ($\simeq$ 250 kg visoko radijsko čistega NaI(Tl)) uporabljajo drugo generacijov fotopomnoževalk z visoko kvantno učinkovitostjo in najsodobnejšo elektroniko, kar jim je omogočilo, da so znižali energijski prag, do katerega so meritve še zanesljive. Rezultati novih meritev letne modulacije trkov delcev *temne snovi* z delci v merilni aparaturi, ki so neodvisne od modela, potrjujejo stare meritve *temne snovi* (1.53 ton × leto) z 11,8 σ C.L.(stopnja zanesljivosti) v energijskem območju (1–6) KeV. V energijskem območju med (2 - 6) KeV, kjer so podatki zbrani že s poskusoma DAMA/NaI in DAMA/LIBRA–phase1, pa je C.L. (stopnja zanesljivost) za polno izpostavljenost (2,86 ton × leto) enaka 13,7 σ. Amplituda modulacije scintilacijskih dogodkov *single-hit* je: $(0, 01014 \pm 0, 00074)$ cpd/kg/keV, izmerjena faza je $(142, 4 \pm 4, 2)$ dni in izmerjeno obdobje je $(0, 99834 \pm 0, 00067)$ na leto. Vse te meritve so v skladu s predpostavko, da so izmerjene dogotke povzročili delci *temne snovi*. Noben drug dogodek, v zadnjih desetletjih so jih predlali kar nekaj, ni v skladu z izmerjenimi rezultati.

1.1   Introduction

The DAMA/LIBRA [1–23] experiment, as well as the pioneer DAMA/NaI [24–51], has the main aim to investigate the presence of DM particles in the galactic halo by exploiting the DM annual modulation signature (originally suggested in Ref. [52, 53]). In particular, the developed highly radio-pure NaI(Tl) target-detectors [1,6,9,54] ensure sensitivity to a wide range of DM candidates, interaction types and astrophysical scenarios (see e.g. Refs. [2, 14, 16–18, 25–32, 35–42], and in literature).

The investigated process is the DM annual modulation signature and related properties; as a consequence of the Earth's revolution around the Sun, which is moving in the Galaxy with respect to the Local Standard of Rest towards the star Vega near the constellation of Hercules, the Earth should be crossed by a larger flux of DM particles around $\simeq$ 2 June and by a smaller one around $\simeq$ 2 December (in the first case the Earth orbital velocity is summed to that of the solar system with respect to the Galaxy, while in the other one the two velocities are subtracted). Thus, this DM annual modulation signature is due to the Earth motion with respect to the DM particles constituting the Galactic Dark Halo.

The DM annual modulation signature is very distinctive since the effect induced by DM particles must simultaneously satisfy all the following requirements: the rate must contain a component modulated according to a cosine function (1) with one year period (2) and a phase that peaks roughly $\simeq$ 2 June (3); this modulation must only be found in a well-defined low energy range, where DM particle induced events can be present (4); it must apply only to those events in which just one detector of many actually "fires" (*single-hit* events), since the DM particle multi-interaction probability is negligible (5); the modulation amplitude in the region of maximal sensitivity must be $\lesssim$ 7% of the constant part of the signal for usually adopted halo distributions (6), but it can be larger in case of some proposed scenarios such as e.g. those in Ref. [55–59] (even up to $\simeq$ 30%). Thus this signature has many peculiarities and, in addition, it allows to test a wide range of parameters in many possible astrophysical, nuclear and particle physics scenarios. This DM signature might be mimicked only by systematic effects or side reactions able

to account for the whole observed modulation amplitude and to simultaneously satisfy all the requirements given above.

The description of the DAMA/LIBRA set-up and the adopted procedures during the phase1 and phase2 and other related arguments have been discussed in details e.g. in Refs. [1–6, 19–21, 23]. The radio-purity and details are discussed e.g. in Refs. [1–5, 54] and references therein. The adopted procedures provide sensitivity to large and low mass DM candidates inducing nuclear recoils and/or electromagnetic signals. The data of the former DAMA/NaI setup and, later, those of the DAMA/LIBRA–phase1 have already given (with high confidence level) positive evidence for the presence of a signal that satisfies all the requirements of the exploited DM annual modulation signature [2–5, 35, 36]. In particular, at the end of 2010 all the photomultipliers (PMTs) were replaced by a second generation PMTs Hamamatsu R6233MOD, with higher quantum efficiency (Q.E.) and with lower background with respect to those used in phase1, allowing the achievement of the software energy threshold at 1 keV as well as the improvement of some detector's features such as energy resolution and acceptance efficiency near software energy threshold [6]. The adopted procedure for noise rejection near software energy threshold and the acceptance windows are the same unchanged along all the DAMA/LIBRA–phase2 data taking, throughout the months and the annual cycles. The typical behaviour of the overall efficiency for *single-hit* events as a function of the energy is also shown in Ref. [6]; the percentage variations of the efficiency follow a gaussian distribution with $\sigma = 0.3\%$ and do not show any modulation with period and phase as expected for the DM signal (for a partial data release see Ref. [21]). At the end of 2012 new preamplifiers and special developed trigger modules were installed and the apparatus was equipped with more compact electronic modules [60]. In particular, the sensitive part of DAMA/LIBRA–phase2 set-up is made of 25 highly radio-pure NaI(Tl) crystal scintillators (5-rows by 5-columns matrix) having 9.70 kg mass each one; quantitative analyses of residual contaminants are given in Ref. [1]. In each detector two 10 cm long UV light guides (made of Suprasil B quartz) act also as optical windows on the two end faces of the crystal, and are coupled to two low background PMTs working in coincidence at single photoelectron level. The detectors are housed in a sealed low-radioactive copper box installed in the center of a low-radioactive Cu/Pb/Cd-foils/polyethylene/paraffin shield; moreover, about 1 m concrete (made from the Gran Sasso rock material) almost fully surrounds (mostly outside the barrack) this passive shield, acting as a further neutron moderator. The shield is decoupled from the ground by a metallic structure mounted above a concrete basement; a neoprene layer separates the concrete basement and the floor of the laboratory. The space between this basement and the metallic structure is filled by paraffin for several tens cm in height. A threefold-level sealing system prevents the detectors from contact with the environmental air of the underground laboratory and continuously maintains them in HP (high-purity) Nitrogen atmosphere. The whole installation is under air conditioning to ensure a suitable and stable working temperature. The huge heat capacity of the multi-tons passive shield ($\approx 10^6$ cal/°C) guarantees further relevant stability of the detectors' operating temperature. In particular, two independent systems of air conditioning are available for

redundancy: one cooled by water refrigerated by a dedicated chiller and the other operating with cooling gas. A hardware/software monitoring system provides data on the operating conditions. In particular, several probes are read out and the results are stored with the production data. Moreover, self-controlled computer based processes automatically monitor several parameters, including those from DAQ, and manage the alarms system. All these procedures, already experienced during DAMA/LIBRA–phase1 [1–5], allow us to control and to maintain the running conditions stable at a level better than 1% also in DAMA/LIBRA–phase2 (see e.g. Ref. [21, 23]).

During phase2 the light response of the detectors typically ranges from 6 to 10 photoelectrons/keV, depending on the detector. Energy calibration with X-rays/γ sources are regularly carried out in the same running condition down to few keV (for details see e.g. Ref. [1]); in particular, double coincidences due to internal X-rays from ^{40}K (which is at ppt levels in the crystals) provide (when summing the data over long periods) a calibration point at 3.2 keV close to the software energy threshold. The DAQ system records both *single-hit* events (where just one of the detectors fires) and *multiple-hit* events (where more than one detector fires) up to the MeV region despite the optimization is performed for the lowest energy.

1.2   Eight DAMA/LIBRA–phase2 annual cycles

Table 1.1 summarizes the details of the DAMA/LIBRA–phase2 annual cycles including the last two released ones. The first cycle was dedicated to commissioning and optimizations towards the achievement of the 1 keV software energy threshold [6]. On the other hand that cycle having: i) no data before/near Dec. 2, 2010 (the expected minimum of the DM signal); ii) data sets with some set-up modifications; iii) $(\alpha - \beta^2) = 0.355$ well different from 0.5 (i.e. the detectors were not being operational evenly throughout the year), cannot be used for the annual modulation studies; however, it has been used for other purposes [6, 13]. Thus (see Table 1.1) the considered annual cycles of DAMA/LIBRA–phase2 are eight for an exposure of 1.53 ton×yr. The cumulative exposure, when considering also the former DAMA/NaI and DAMA/LIBRA–phase1, is 2.86 ton×yr.

The total number of events collected for the energy calibrations during the eight annual cycles of DAMA/LIBRA–phase2 is about 1.6×10^8, while about 1.7×10^5 events/keV have been collected for the evaluation of the acceptance window efficiency for noise rejection near the software energy threshold [1, 6]. Finally, the duty cycle of the experiment is high, ranging between 76% and 86%: the routine calibrations and the data collection for the acceptance windows efficiency mainly affect it.

1.2.1   The annual modulation of the residual rate

In Fig. 1.1 the time behaviours of the experimental residual rates of the *single-hit* scintillation events in the (1–3), and (1–6) keV energy intervals are shown

Table 1.1: Details about the annual cycles of DAMA/LIBRA–phase2. The mean value of the squared cosine is $\alpha = \langle \cos^2 \omega(t - t_0) \rangle$ and the mean value of the cosine is $\beta = \langle \cos \omega(t - t_0) \rangle$ (the averages are taken over the live time of the data taking and $t_0 = 152.5$ day, i.e. June 2nd); thus, the variance of the cosine, $(\alpha - \beta^2)$, is $\simeq 0.5$ for a detector being operational evenly throughout the year.

DAMA/LIBRA–phase2 annual cycle	Period	Mass (kg)	Exposure (kg×day)	$(\alpha - \beta^2)$
1	Dec. 23, 2010 – Sept. 9, 2011	commissioning of phase2		
2	Nov. 2, 2011 – Sept. 11, 2012	242.5	62917	0.519
3	Oct. 8, 2012 – Sept. 2, 2013	242.5	60586	0.534
4	Sept. 8, 2013 – Sept. 1, 2014	242.5	73792	0.479
5	Sept. 1, 2014 – Sept. 9, 2015	242.5	71180	0.486
6	Sept. 10, 2015 – Aug. 24, 2016	242.5	67527	0.522
7	Sept. 7, 2016 – Sept. 25, 2017	242.5	75135	0.480
8	Sept. 25, 2017 – Aug. 20, 2018	242.5	68759	0.557
9	Aug. 24, 2018 – Oct. 3, 2019	242.5	77213	0.446
DAMA/LIBRA–phase2	Nov. 2, 2011 – Oct. 3, 2019	557109 kg×day $\simeq$ 1.53 ton×yr		0.501
DAMA/NaI + DAMA/LIBRA–phase1 + DAMA/LIBRA–phase2:			2.86 ton×yr	

for DAMA/LIBRA–phase2. The residual rates are calculated from the measured rate of the *single-hit* events after subtracting the constant part, as described in Refs. [2–5,35,36]. The null modulation hypothesis is rejected at very high C.L. by χ^2 test: $\chi^2 = 176$ and 202, respectively, over 69 d.o.f. ($P = 2.6 \times 10^{-11}$, and $P = 5.6 \times 10^{-15}$, respectively). The residuals of the DAMA/NaI data (0.29 ton × yr) are given in Ref. [2,5,35,36], while those of the DAMA/LIBRA–phase1 (1.04 ton × yr) in Ref. [2–5].

The former DAMA/LIBRA–phase1 and the new DAMA/LIBRA–phase2 residual rates of the *single-hit* scintillation events are reported in Fig. 1.2. The energy interval is from 2 keV, the software energy threshold of DAMA/LIBRA –phase1, up to 6 keV. The null modulation hypothesis is rejected at very high C.L. by χ^2 test: $\chi^2/d.o.f. = 240/119$, corresponding to P-value = 3.5×10^{-10}.

The *single-hit* residual rates of the DAMA/LIBRA–phase2 (Fig. 1.1) have been fitted with the function: $A \cos \omega(t - t_0)$, considering a period $T = \frac{2\pi}{\omega} = 1$ yr and a phase $t_0 = 152.5$ day (June 2nd) as expected by the DM annual modulation signature; this can be repeated for the only case of (2-6) keV energy interval when including also the former DAMA/NaI and DAMA/LIBRA–phase1 data. The goodness of the fits is well supported by the χ^2 test; for example, $\chi^2/d.o.f. = 81.6/68, 66.2/68, 130/155$ are obtained for the (1–3) keV and (1–6) keV cases of DAMA/LIBRA–phase2, and for the (2–6) keV case of DAMA/NaI, DAMA/LIBRA–phase1 and DAMA/LIBRA–phase2, respectively. The results of the best fits in the different cases are summarized in Table 1.2. In Table 1.2 also the cases when the period and the phase are kept free in the fitting procedure are shown. The period and the phase are well compatible with expectations for a DM annual modulation signal. In particular, the phase is consistent with about June 2nd and is fully consistent with the value independently determined by Maximum Likelihood analysis (see later). For com-
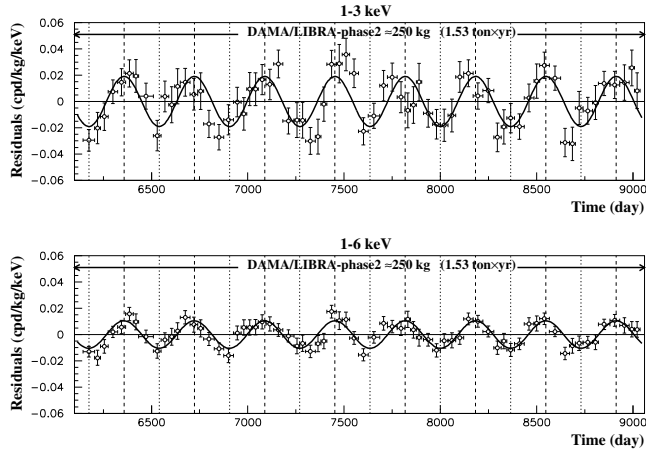
Fig. 1.1: Experimental residual rate of the *single-hit* scintillation events measured by DAMA/LIBRA–phase2 over eight annual cycles in the (1–3), and (1–6) keV energy intervals as a function of the time. The time scale is maintained the same of the previous DAMA papers for consistency. The data points present the experimental errors as vertical bars and the associated time bin width as horizontal bars. The superimposed curves are the cosinusoidal functional forms $A \cos \omega(t - t_0)$ with a period $T = \frac{2\pi}{\omega} = 1$ yr, a phase $t_0 = 152.5$ day (June 2nd) and modulation amplitudes, A, equal to the central values obtained by best fit on the data points of the entire DAMA/LIBRA–phase2. The dashed vertical lines correspond to the maximum expected for the DM signal (June 2nd), while the dotted vertical lines correspond to the minimum.
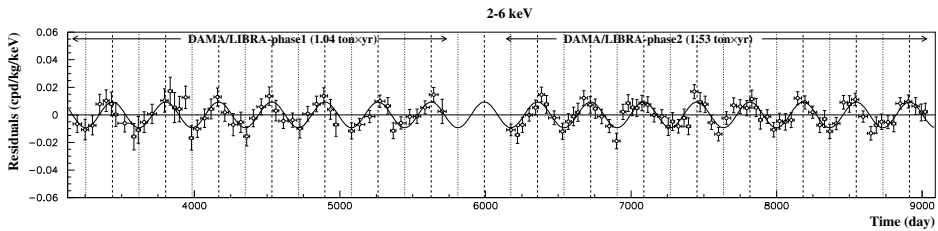
Fig. 1.2: Experimental residual rate of the *single-hit* scintillation events measured by DAMA/LIBRA–phase1 and DAMA/LIBRA–phase2 in the (2–6) keV energy intervals as a function of the time. The superimposed curve is the cosinusoidal functional forms $A \cos \omega(t - t_0)$ with a period $T = \frac{2\pi}{\omega} = 1$ yr, a phase $t_0 = 152.5$ day (June 2nd) and modulation amplitude, A, equal to the central value obtained by best fit on the data points of DAMA/LIBRA–phase1 and DAMA/LIBRA–phase2. For details see Fig. 1.1.

pleteness, we recall that a slight energy dependence of the phase could be expected (see e.g. Refs. [38,58,59,61–63]), providing intriguing information on the nature of Dark Matter candidate and related aspects.

Table 1.2: Modulation amplitude, A, obtained by fitting the *single-hit* residual rate of DAMA/LIBRA–phase2, as reported in Fig. 1.1, and also including the residual rates of the former DAMA/NaI and DAMA/LIBRA–phase1. It was obtained by fitting the data with the formula: $A \cos \omega(t - t_0)$. The period $T = \frac{2\pi}{\omega}$ and the phase t_0 are kept fixed at 1 yr and at 152.5 day (June 2nd), respectively, as expected by the DM annual modulation signature, and alternatively kept free. The results are well compatible with expectations for a signal in the DM annual modulation signature.

	A (cpd/kg/keV)	$T = \frac{2\pi}{\omega}$ (yr)	t_0 (days)	C.L.
DAMA/LIBRA–phase2:				
1-3 keV	(0.0191 ± 0.0020)	1.0	152.5	9.7 σ
1-6 keV	(0.01048 ± 0.00090)	1.0	152.5	11.6 σ
2-6 keV	(0.00933 ± 0.00094)	1.0	152.5	9.9 σ
1-3 keV	(0.0191 ± 0.0020)	(0.99952 ± 0.00080)	149.6 ± 5.9	9.6 σ
1-6 keV	(0.01058 ± 0.00090)	(0.99882 ± 0.00065)	144.5 ± 5.1	11.8 σ
2-6 keV	(0.00954 ± 0.00076)	(0.99836 ± 0.00075)	141.1 ± 5.9	12.6 σ
DAMA/LIBRA–phase1 + phase2:				
2-6 keV	(0.00941 ± 0.00076)	1.0	152.5	12.4 σ
2-6 keV	(0.00959 ± 0.00076)	(0.99835 ± 0.00069)	142.0 ± 4.5	12.6 σ
DAMA/NaI + DAMA/LIBRA–phase1 + phase2:				
2-6 keV	(0.00996 ± 0.00074)	1.0	152.5	13.4 σ
2-6 keV	(0.01014 ± 0.00074)	(0.99834 ± 0.00067)	142.4 ± 4.2	13.7 σ

1.2.2 Absence of background modulation

Since the background in the lowest energy region is essentially due to "Compton" electrons, X-rays and/or Auger electrons, muon induced events, etc., which are strictly correlated with the events in the higher energy region of the spectrum, if a modulation detected in the lowest energy region were due to a modulation of the background (rather than to a signal), an equal or larger modulation in the higher energy regions should be present. Thus, as done in previous data releases, absence of any significant background modulation in the energy spectrum for energy regions not of interest for DM. has also been verified in the present one. In particular, the measured rate integrated above 90 keV, R_{90}, as a function of the time has been analysed. Fig. 1.3 shows the distribution of the percentage variations of R_{90} with respect to the mean values for all the detectors in DAMA/LIBRA–phase2. It shows a cumulative gaussian behaviour with $\sigma \simeq 1\%$, well accounted for by the statistical spread provided by the used sampling time. Moreover, fitting the time behaviour of R_{90} including a term with phase and period as for DM particles, a modulation amplitude $A_{R_{90}}$ compatible with zero has been found for all the annual cycles (see Table 1.3). This also excludes the presence of any background modulation in the whole energy spectrum at a level much lower than the effect found in the lowest energy region for the *single-hit* scintillation events. In fact, otherwise – considering the R_{90} mean values – a modulation amplitude of order of tens cpd/kg would be present for each annual cycle, that is $\simeq 100$ σ far away from the measured values.
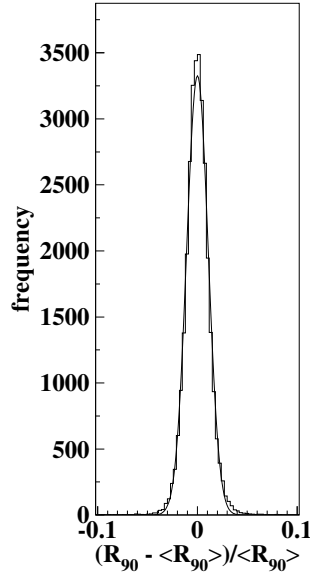
Fig. 1.3: Distribution of the percentage variations of R_{90} with respect to the mean values for all the detectors in the DAMA/LIBRA–phase2 (histogram); the superimposed curve is a gaussian fit.

Table 1.3: Modulation amplitudes, $A_{R_{90}}$, obtained by fitting the time behaviour of R_{90} in DAMA/LIBRA–phase2, including a term with a cosine function having phase and period as expected for a DM signal. The obtained amplitudes are compatible with zero, and incompatible ($\simeq 100\ \sigma$) with modulation amplitudes of tens cpd/kg. Modulation amplitudes, $A_{(6-14)}$, obtained by fitting the time behaviour of the residual rates of the *single-hit* scintillation events in the (6–14) keV energy interval. In the fit the phase and the period are at the values expected for a DM signal. The obtained amplitudes are compatible with zero.

DAMA/LIBRA–phase2 annual cycle	$A_{R_{90}}$ (cpd/kg)	$A_{(6-14)}$ (cpd/kg/keV)
2	(0.12±0.14)	(0.0032±0.0017)
3	-(0.08±0.14)	(0.0016±0.0017)
4	(0.07±0.15)	(0.0024±0.0015)
5	-(0.05±0.14)	-(0.0004±0.0015)
6	(0.03±0.13)	(0.0001±0.0015)
7	-(0.09±0.14)	(0.0015±0.0014)
8	-(0.18±0.13)	-(0.0005±0.0013)
9	(0.08±0.14)	-(0.0003±0.0014)

Similar results are obtained when comparing the *single-hit* residuals in the (1–6) keV with those in other energy intervals; for example Fig. 1.4 shows the *single-hit* residuals in the (1–6) keV and in the (10–20) keV energy regions, for the 8 annual cycles of DAMA/LIBRA–phase2 as if they were collected in a single annual cycle (i.e. binning in the variable time from the January 1st of each annual cycle).

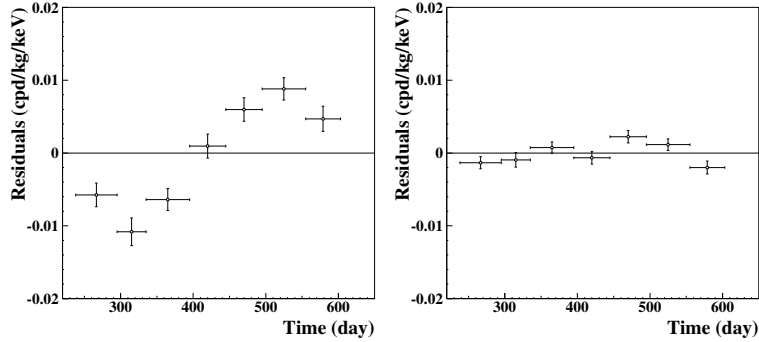Fig. 1.4: Experimental *single-hit* residuals in the (1–6) keV and in the (10–20) keV energy regions for DAMA/LIBRA–phase2 as if they were collected in a single annual cycle (i.e. binning in the variable time from the January 1st of each annual cycle). The data points present the experimental errors as vertical bars and the associated time bin width as horizontal bars. The initial time of the figures is taken at August 7th. A clear modulation satisfying all the peculiarities of the DM annual modulation signature is present in the lowest energy interval with A=(0.00956 ± 0.00090) cpd/kg/keV, while it is absent just above: A=(0.0007 ± 0.0005) cpd/kg/keV.

Moreover, Table 1.3 shows the modulation amplitudes obtained by fitting the time behaviour of the residual rates of the *single-hit* scintillation events in the (6–14) keV energy interval for the DAMA/LIBRA–phase2 annual cycles. In the fit the phase and the period are at the values expected for a DM signal. The obtained amplitudes are compatible with zero.

A further relevant investigation on DAMA/LIBRA–phase2 data has been performed by applying the same hardware and software procedures, used to acquire and to analyse the *single-hit* residual rate, to the *multiple-hit* one. Since the probability that a DM particle interacts in more than one detector is negligible, a DM signal can be present just in the *single-hit* residual rate. Thus, the comparison of the results of the *single-hit* events with those of the *multiple-hit* ones corresponds to compare the cases of DM particles beam-on and beam-off. This procedure also allows an additional test of the background behaviour in the same energy interval where the positive effect is observed.

In particular, in Fig. 1.5 the residual rates of the *single-hit* scintillation events collected during 8 annual cycles of DAMA/LIBRA–phase2 are reported, as collected in a single cycle, together with the residual rates of the *multiple-hit* events, in

the considered energy intervals. While, as already observed, a clear modulation, satisfying all the peculiarities of the DM annual modulation signature, is present in the *single-hit* events, the fitted modulation amplitude for the *multiple-hit* residual rate is well compatible with zero: (0.00030 ± 0.00032) cpd/kg/keV in the (1–6) keV energy region. Thus, again evidence of annual modulation with proper features as required by the DM annual modulation signature is present in the *single-hit* residuals (events class to which the DM particle induced events belong), while it is absent in the *multiple-hit* residual rate (event class to which only background events belong). Similar results were also obtained for the two last annual cycles of DAMA/NaI [36] and for DAMA/LIBRA–phase1 [2–5]. Since the same identical hardware and the same identical software procedures have been used to analyse the two classes of events, the obtained result offers an additional strong support for the presence of a DM particle component in the galactic halo.
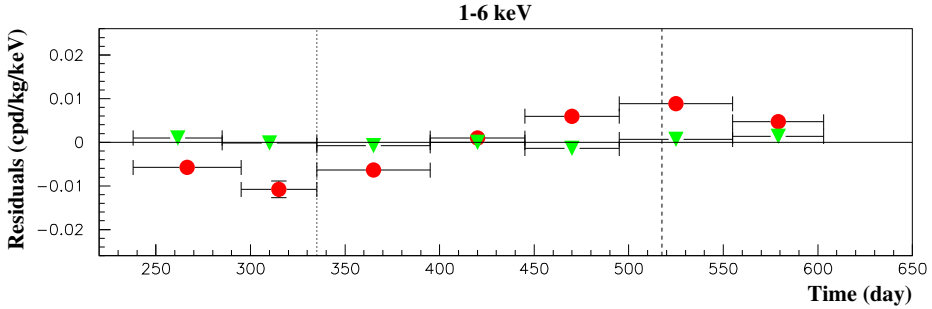
Fig. 1.5: Experimental residual rates of DAMA/LIBRA–phase2 *single-hit* events (filled red on-line circles), class of events to which DM events belong, and for *multiple-hit* events (filled green on-line triangles), class of events to which DM events do not belong. They have been obtained by considering for each class of events the data as collected in a single annual cycle and by using in both cases the same identical hardware and the same identical software procedures. The initial time of the figure is taken on August 7th. The experimental points present the errors as vertical bars and the associated time bin width as horizontal bars. Analogous results were obtained for DAMA/NaI (two last annual cycles) and DAMA/LIBRA–phase1 [2–5, 36].

In conclusion, no background process able to mimic the DM annual modulation signature (that is, able to simultaneously satisfy all the peculiarities of the signature and to account for the measured modulation amplitude) has been found or suggested by anyone throughout some decades thus far (see also discussions e.g. in Ref. [1–5, 7, 8, 19–21, 23, 34–36]).

1.3   The analysis in frequency

In order to perform the Fourier analysis of the data of DAMA/LIBRA–phase1 and of the present 8 annual cycles of phase2 in a wider region of considered frequency, the *single-hit* events have been grouped in 1 day bins. Due to the low statistics in
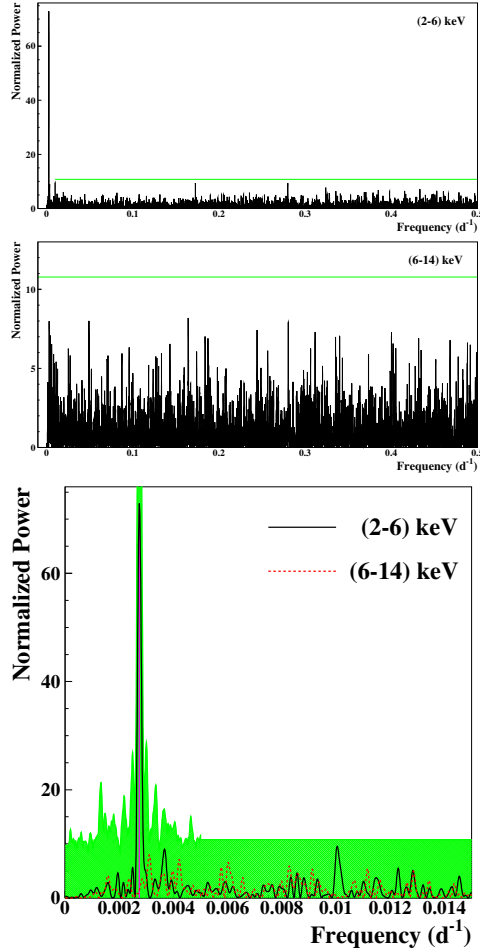
Fig. 1.6: Power spectra of the time sequence of the measured *single-hit* events for DAMA/LIBRA–phase1 and DAMA/LIBRA–phase2 grouped in 1 day bins. From top to bottom: spectra up to the Nyquist frequency for (2–6) keV and (6–14) keV energy intervals and their zoom around the $1 \, \mathrm{y}^{-1}$ peak, for (2–6) keV (solid line) and (6–14) keV (dotted line) energy intervals. The main mode present at the lowest energy interval corresponds to a frequency of $2.74 \times 10^{-3} \, \mathrm{d}^{-1}$ (vertical line, purple on-line). It corresponds to a period of $\simeq 1$ year. A similar peak is not present in the (6–14) keV energy interval. The shaded (green on-line) area in the bottom figure – calculated by Monte Carlo procedure – represents the 90% C.L. region where all the peaks are expected to fall for the (2–6) keV energy interval. In the frequency range far from the signal for the (2–6) keV energy region and for the whole (6–14) keV spectrum, the upper limit of the shaded region (90% C.L.) can be calculated to be 10.8 (continuous lines, green on-line).

each time bin, a procedure detailed in Ref. [64] has been applied. Fig. 1.6 shows the whole power spectra up to the Nyquist frequency and the zoomed ones: a clear peak corresponding to a period of 1 year is evident for the lowest energy interval, while the same analysis in the (6–14) keV energy region shows only aliasing peaks, instead. Neither other structure at different frequencies has been observed. To derive the significance of the peaks present in the periodogram, one can remind that the periodogram ordinate, z, at each frequency follows a simple exponential distribution e^{-z} in case of null hypothesis or white noise [65].
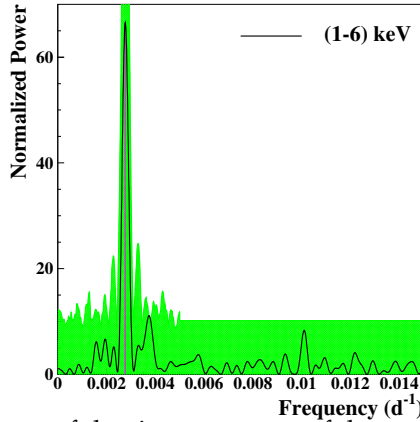
Fig. 1.7: Power spectrum of the time sequence of the measured *single-hit* events in the (1–6) keV energy interval for DAMA/LIBRA–phase2 grouped in 1 day bin. The main mode present at the lowest energy interval corresponds to a frequency of 2.77×10^{-3} d^{-1} (vertical line, purple on-line). It corresponds to a period of $\simeq$ 1 year. The shaded (green on-line) area – calculated by Monte Carlo procedure – represents the 90% C.L. region where all the peaks are expected to fall for the (1–6) keV energy interval.

Thus, if M independent frequencies are scanned, the probability to obtain values larger than z is: $P(> z) = 1 - (1 - e^{-z})^M$. In general M depends on the number of sampled frequencies, the number of data points N, and their detailed spacing. It turns out that $M \simeq N$ when the data points are approximately equally spaced and when the sampled frequencies cover the frequency range from 0 to the Nyquist one [66, 67]. In the present case, the number of data points used to obtain the spectra in Fig. 1.6 is $N = 5047$ (days measured over the 5479 days of the 15 DAMA/LIBRA–phase1 and phase2 annual cycles) and the full frequencies region up to Nyquist one has been scanned. Thus, assuming $M = N$, the significance levels $P = 0.10, 0.05$ and 0.01, correspond to peaks with heights larger than $z = 10.8, 11.5$ and 13.1, respectively, in the spectra of Fig 1.6. In the case below 6 keV, a signal is present; thus, to properly evaluate the C.L. the signal must be included. This has been done by a dedicated Monte Carlo procedure where a large number of similar experiments has been simulated. The 90% C.L. region (shaded, green on-line) where all the peaks are expected to fall for the (2–6) keV energy interval is

reported in Fig 1.6. Several peaks, satellite of the one year period frequency, are present.

Moreover, for each annual cycle of DAMA/LIBRA–phase1 and phase2, the annual baseline counting rates have been calculated for the (2–6) keV energy interval. Their power spectrum in the frequency range $0.00013 - 0.0019\,\mathrm{d}^{-1}$ (corresponding to a period range 1.4–21.1 year) has been calculated according to Ref. [5]. No statistically-significant peak is present at frequencies lower than $1\,\mathrm{y}^{-1}$. This implies that no evidence for a long term modulation in the counting rate is present.

Finally, the case of the (1–6) keV energy interval of the DAMA/LIBRA–phase2 data is reported in Fig. 1.7. As previously the only significant peak is the one corresponding to one year period. No other peak is statistically significant being below the shaded (green on-line) area obtained by Monte Carlo procedure.

In conclusion, apart from the peak corresponding to a 1 year period, no other peak is statistically significant either in the low and high energy regions.

1.4 The modulation amplitudes by the maximum likelihood approach

The annual modulation present at low energy can also be pointed out by depicting the energy dependence of the modulation amplitude, $S_m(E)$, obtained by maximum likelihood method considering fixed period and phase: $T = 1$ yr and $t_0 = 152.5$ day. For this purpose the likelihood function of the *single-hit* experimental data in the $k-$th energy bin is defined as: $L_k = \Pi_{ij} e^{-\mu_{ijk}} \frac{\mu_{ijk}^{N_{ijk}}}{N_{ijk}!}$, where N_{ijk} is the number of events collected in the i-th time interval (hereafter 1 day), by the j-th detector and in the k-th energy bin. N_{ijk} follows a Poisson's distribution with expectation value $\mu_{ijk} = [b_{jk} + S_i(E_k)]\,M_j\Delta t_i\Delta E\epsilon_{jk}$. The b_{jk} are the background contributions, M_j is the mass of the $j-$th detector, Δt_i is the detector running time during the i-th time interval, ΔE is the chosen energy bin, ϵ_{jk} is the overall efficiency. The signal can be written as:

$$S_i(E) = S_0(E) + S_m(E) \cdot \cos\omega(t_i - t_0),$$

where $S_0(E)$ is the constant part of the signal and $S_m(E)$ is the modulation amplitude. The usual procedure is to minimize the function $y_k = -2\ln(L_k) - \mathrm{const}$ for each energy bin; the free parameters of the fit are the $(b_{jk} + S_0)$ contributions and the S_m parameter.

The modulation amplitudes for the whole data sets: DAMA/NaI, DAMA /LIBRA–phase1 and DAMA/LIBRA–phase2 (total exposure 2.86 ton×yr) are plotted in Fig. 1.8; the data below 2 keV refer only to the DAMA/LIBRA–phase2 exposure (1.53 ton×yr). It can be inferred that positive signal is present in the (1–6) keV energy interval, while S_m values compatible with zero are present just above. All this confirms the previous analyses. The test of the hypothesis that the S_m values in the (6–14) keV energy interval have random fluctuations around zero yields $\chi^2/\mathrm{d.o.f.}$ equal to 20.3/16 (P-value = 21%).

For the case of (6–20) keV energy interval $\chi^2/\mathrm{d.o.f.} = 42.2/28$ (P-value = 4%). The obtained χ^2 value is rather large due mainly to two data points, whose centroids
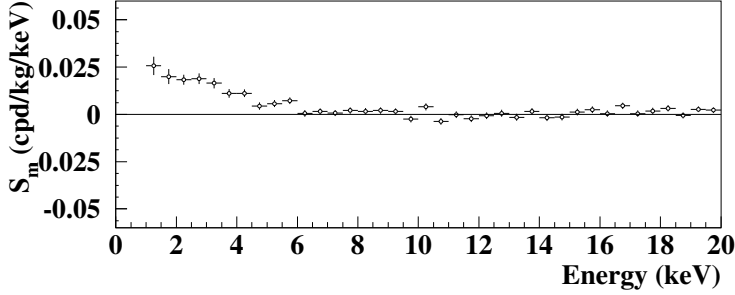
Fig. 1.8: Modulation amplitudes, S_m, for the whole data sets: DAMA/NaI, DAMA/LIBRA–phase1 and DAMA/LIBRA–phase2 (total exposure 2.86 ton×yr) above 2 keV; below 2 keV only the DAMA/LIBRA–phase2 exposure (1.53 ton × yr) is available and used. The energy bin ΔE is 0.5 keV. A clear modulation is present in the lowest energy region, while S_m values compatible with zero are present just above. In fact, the S_m values in the (6–20) keV energy interval have random fluctuations around zero with $\chi^2/\mathrm{d.o.f.}$ equal to 42.2/28 (P-value is 4%).

are at 16.75 and 18.25 keV, far away from the (1–6) keV energy interval. The P-values obtained by excluding only the first and either the points are 14% and 23%.

This method also allows the extraction of the S_m values for each detector. In particular, the modulation amplitudes S_m integrated in the range (2–6) keV for each of the 25 detectors for the DAMA/LIBRA–phase1 and DAMA/LIBRA–phase2 periods can be produced. They have random fluctuations around the weighted averaged value confirmed by the χ^2 analysis. Thus, the hypothesis that the signal is well distributed over all the 25 detectors is accepted.

As previously done for the other data releases [2–5, 19–21, 23], the S_m values for each detector for each annual cycle and for each energy bin have been obtained. The S_m are expected to follow a normal distribution in absence of any systematic effects. Therefore, the variable $x = \frac{S_m - \langle S_m \rangle}{\sigma}$ has been considered to verify that the S_m are statistically well distributed in the 16 energy bins ($\Delta E = 0.25$ keV) in the (2–6) keV energy interval of the seven DAMA/LIBRA–phase1 annual cycles and in the 20 energy bins in the (1–6) keV energy interval of the eight DAMA/LIBRA–phase2 annual cycles and in each detector. Here, σ are the errors associated to S_m and $\langle S_m \rangle$ are the mean values of the S_m averaged over the detectors and the annual cycles for each considered energy bin.

Defining $\chi^2 = \Sigma x^2$, where the sum is extended over all the 272 (192 for the 16th detector [4]) x values, $\chi^2/\mathrm{d.o.f.}$ values ranging from 0.8 to 2.0 are obtained, depending on the detector.

The mean value of the 25 $\chi^2/\mathrm{d.o.f.}$ is 1.092, slightly larger than 1. Although this can be still ascribed to statistical fluctuations, let us ascribe it to a possible systematics. In this case, one would derive an additional error to the modulation amplitude measured below 6 keV: $\leq 2.4 \times 10^{-4}$ cpd/kg/keV, if combining quadratically the

errors, or $\leq 3.6 \times 10^{-5}$ cpd/kg/keV, if linearly combining them. This possible additional error: $\leq 2.4\%$ or $\leq 0.4\%$, respectively, on the DAMA/LIBRA–phase1 and DAMA /LIBRA–phase2 modulation amplitudes is an upper limit of possible systematic effects coming from the detector to detector differences.

Among further additional tests, the analysis of the modulation amplitudes as a function of the energy separately for the nine inner detectors and the remaining external ones has been carried out for DAMA/LIBRA–phase1 and DAMA/LIBRA–phase2, as already done for the other data sets [2–5,19–21,23]. The obtained values are fully in agreement; in fact, the hypothesis that the two sets of modulation amplitudes belong to same distribution has been verified by χ^2 test, obtaining e.g.: χ^2/d.o.f. = 1.9/6 and 36.1/38 for the energy intervals (1–4) and (1–20) keV, respectively (ΔE = 0.5 keV). This shows that the effect is also well shared between inner and outer detectors.

Moreover, to test the hypothesis that the amplitudes, singularly calculated for each annual cycle of DAMA/LIBRA–phase1 and DAMA/LIBRA–phase2, are compatible and normally fluctuating around their mean values, the χ^2 test has been performed together with another independent statistical test: the *run test* (see e.g. Ref. [69]), which verifies the hypothesis that the positive (above the mean value) and negative (under the mean value) data points are randomly distributed. Both tests accept at 95% C.L. the hypothesis that the modulation amplitudes are normally fluctuating around the best fit values.

1.5 Investigation of the annual modulation phase

Finally, let us release the assumption of the phase value at $t_0 = 152.5$ day in the procedure to evaluate the modulation amplitudes, writing the signal as:

$$S_i(E) = S_0(E) + S_m(E) \cos \omega(t_i - t_0) + Z_m(E) \sin \omega(t_i - t_0) \qquad (1.1)$$
$$= S_0(E) + Y_m(E) \cos \omega(t_i - t^*).$$

For signals induced by DM particles one should expect: i) $Z_m \sim 0$ (because of the orthogonality between the cosine and the sine functions); ii) $S_m \simeq Y_m$; iii) $t^* \simeq t_0 = 152.5$ day. In fact, these conditions hold for most of the dark halo models; however, as mentioned above, slight differences can be expected in case of possible contributions from non-thermalized DM components (see e.g. Refs. [38,58,59,61–63]).

Considering cumulatively the data of DAMA/NaI, DAMA/LIBRA–phase1 and DAMA/LIBRA–phase2 the obtained 2σ contours in the plane (S_m, Z_m) for the (2–6) keV and (6–14) keV energy intervals are shown in Fig. 1.9–*left* while the obtained 2σ contours in the plane (Y_m, t^*) are depicted in Fig. 1.9–*right*. Moreover, Fig. 1.9 also shows only for DAMA/LIBRA–phase2 the 2σ contours in the (1–6) keV energy interval.

The best fit values in the considered cases (1σ errors) for S_m versus Z_m and Y_m versus t^* are reported in Table 1.4.
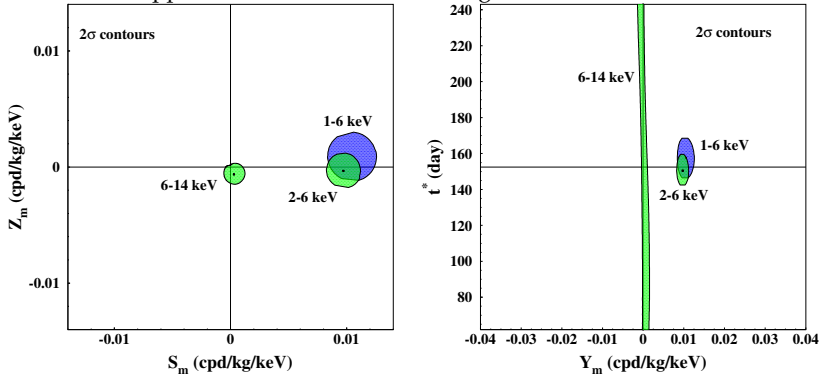
Fig. 1.9: 2σ contours in the plane (S_m, Z_m) (*left*) and in the plane (Y_m, t^*) (*right*) for: i) DAMA/NaI, DAMA/LIBRA–phase1 and DAMA/LIBRA–phase2 in the (2–6) keV and (6–14) keV energy intervals (light areas, green on-line); ii) only DAMA/LIBRA–phase2 in the (1–6) keV energy interval (dark areas, blue on-line). The contours have been obtained by the maximum likelihood method. A modulation amplitude is present in the lower energy intervals and the phase agrees with that expected for DM induced signals.

Table 1.4: Best fit values (1σ errors) for S_m versus Z_m and Y_m versus t^*, considering: i) DAMA/NaI, DAMA/LIBRA–phase1 and DAMA/LIBRA–phase2 in the (2–6) keV and (6–14) keV energy intervals; ii) only DAMA/LIBRA–phase2 in the (1–6) keV energy interval. See also Fig. 1.9.

E (keV)	S_m (cpd/kg/keV)	Z_m (cpd/kg/keV)	Y_m (cpd/kg/keV)	t^* (day)
DAMA/NaI+DAMA/LIBRA–phase1+DAMA/LIBRA–phase2:				
2–6	(0.0097 ± 0.0007)	$-(0.0003 \pm 0.0007)$	(0.0097 ± 0.0007)	(150.5 ± 4.0)
6–14	(0.0003 ± 0.0005)	$-(0.0006 \pm 0.0005)$	(0.0007 ± 0.0010)	undefined
DAMA/LIBRA–phase2:				
1–6	(0.0104 ± 0.0007)	(0.0002 ± 0.0007)	(0.0104 ± 0.0007)	(153.5 ± 4.0)

Finally, the Z_m values as function of the energy have also been determined by using the same procedure and setting S_m in eq. (1.1) to zero. The Z_m values as a function of the energy for DAMA/NaI, DAMA/LIBRA–phase1, and DAMA/LIBRA–phase2 data sets are expected to be zero. The χ^2 test applied to the data supports the hypothesis that the Z_m values are simply fluctuating around zero; in fact, in the (1–20) keV energy region the $\chi^2/\text{d.o.f.}$ is equal to 40.6/38 corresponding to a P-value = 36%.

The energy behaviors of Y_m and of phase t^* are also produced for the cumulative exposure of DAMA/NaI, DAMA/LIBRA–phase1, and DAMA/LIBRA–phase2; as in the previous analyses, an annual modulation effect is present in the lower energy intervals and the phase agrees with that expected for DM induced signals. No modulation is present above 6 keV and the phase is undetermined.

1.6 Perspectives

To further increase the experimental sensitivity of DAMA/LIBRA and to disentangle some of the many possible astrophysical, nuclear and particle physics scenarios in the investigation on the DM candidate particle(s), an increase of the exposure ($M \times t_{running}$, i.e. $t_{running}$ in our case at fixed M) in the lowest energy bin and a further decreasing of the software energy threshold are needed. This is pursued by running DAMA/LIBRA–phase2 and upgrading the experimental set-up to lower the software energy threshold below 1 keV with high acceptance efficiency.

Firstly, particular efforts for lowering the software energy threshold have been done in the already-acquired data of DAMA/LIBRA–phase2 by using the same technique as before with dedicated studies on the efficiency. As consequence, a new data point has been added in the modulation amplitude as function of energy down to 0.75 keV, see Fig. 1.10. A modulation is also present below 1 keV, from 0.75 keV. This preliminary result confirms the necessity to lower the software energy threshold by a hardware upgrade and an improved statistics in the first energy bin.
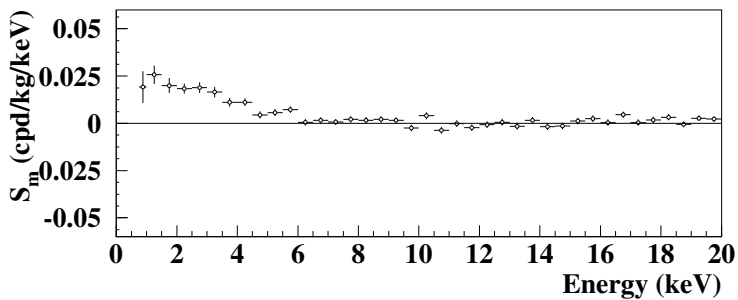
Fig. 1.10: As Fig. 1.8; the new data point below 1 keV, with software energy threshold at 0.75 keV, shows that an annual modulation is also present below 1 keV. This preliminary result confirms the necessity to lower the software energy threshold by a hardware upgrade and to improve the experimental error on the first energy bin.

This dedicated hardware upgrade of DAMA/LIBRA–phase2 is underway. It consists in equipping all the PMTs with miniaturized low background new concept preamplifiers and HV dividers mounted on the same socket, and related improvements of the electronic chain, mainly the use of higher vertical resolution 14-bit digitizers.

1.7 Conclusions

DAMA/LIBRA–phase2 confirms a peculiar annual modulation of the *single-hit* scintillation events in the (1–6) keV energy region satisfying all the many requirements of the DM annual modulation signature; the cumulative exposure by the

former DAMA/NaI, DAMA/LIBRA–phase1 and DAMA/LIBRA–phase2 is 2.86 ton × yr.

As required by the exploited DM annual modulation signature: 1) the *single-hit* events show a clear cosine-like modulation as expected for the DM signal; 2) the measured period is well compatible with the 1 yr period as expected for the DM signal; 3) the measured phase is compatible with the roughly $\simeq 152.5$ days expected for the DM signal; 4) the modulation is present only in the low energy (1–6) keV interval and not in other higher energy regions, consistently with expectation for the DM signal; 5) the modulation is present only in the *single-hit* events, while it is absent in the *multiple-hit* ones as expected for the DM signal; 6) the measured modulation amplitude in NaI(Tl) target of the *single-hit* scintillation events in the (2–6) keV energy interval, for which data are also available by DAMA/NaI and DAMA/LIBRA–phase1, is: (0.01014 ± 0.00074) cpd/kg/keV (13.7 σ C.L.).

No systematic or side processes able to mimic the signature, i.e. able to simultaneously satisfy all the many peculiarities of the signature and to account for the whole measured modulation amplitude, has been found or suggested by anyone throughout some decades thus far (for details see e.g. Ref. [1–5,7,8,19–23,35,36]). In particular, arguments related to any possible role of some natural periodical phenomena have been discussed and quantitatively demonstrated to be unable to mimic the signature (see references; e.g. Refs. [7,8]). Thus, on the basis of the exploited signature, the model independent DAMA results give evidence at 13.7σ C.L. (over 22 independent annual cycles and in various experimental configurations) for the presence of DM particles in the galactic halo.

The DAMA model independent evidence is compatible with a wide set of astrophysical, nuclear and particle physics scenarios for high and low mass candidates inducing nuclear recoil and/or electromagnetic radiation, as also shown in various literature. Moreover, both the negative results and all the possible positive hints, achieved so-far in the field, can be compatible with the DAMA model independent DM annual modulation results in many scenarios considering also the existing experimental and theoretical uncertainties; the same holds for indirect approaches. For a discussion see e.g. Ref. [5] and references therein.

The present new data released determine the modulation parameters with increasing precision and will allow us to disentangle with larger C.L. among different DM candidates, DM models and astrophysical, nuclear and particle physics scenarios. Finally, we stress that to efficiently disentangle among at least some of the many possible candidates and scenarios an increase of exposure in the new lowest energy bin and the decrease of the software energy threshold below the present 1 keV is important. The experiment is collecting data and the hardware efforts towards the lowering of the software energy threshold is in progress; a preliminary result below 1 keV is given.

References

1. R. Bernabei et al., Nucl. Instr. and Meth. A **592**, 297 (2008).
2. R. Bernabei et al., Eur. Phys. J. C **56**, 333 (2008).
3. R. Bernabei et al., Eur. Phys. J. C **67**, 39 (2010).

4. R. Bernabei et al., Eur. Phys. J. C **73**, 2648 (2013).
5. R. Bernabei et al., Int. J. of Mod. Phys. A **28**, 1330022 (2013).
6. R. Bernabei et al., J. of Instr. **7**, P03009 (2012).
7. R. Bernabei et al., Eur. Phys. J. C **72**, 2064 (2012).
8. R. Bernabei et al., Eur. Phys. J. C **74**, 3196 (2014).
9. DAMA coll., issue dedicated
    to DAMA, Int. J. of Mod. Phys. A **31** (2016) and refs therein.
10. R. Bernabei et al., Eur. Phys. J. C **74**, 2827 (2014).
11. R. Bernabei et al., Eur. Phys. J. C **62**, 327 (2009).
12. R. Bernabei et al., Eur. Phys. J. C **72**, 1920 (2012).
13. R. Bernabei et al., Eur. Phys. J. A **49**, 64 (2013).
14. R. Bernabei et al., Eur. Phys. J. C **75**, 239 (2015).
15. P. Belli et al., Phys. Rev. D **84**, 055014 (2011).
16. A. Addazi et al., Eur. Phys. J. C **75**, 400 (2015).
17. R. Bernabei et al., Int. J. of Mod. Phys. A **31**, 1642009 (2016).
18. R. Cerulli et al., Eur. Phys. J. C **77**, 83 (2017).
19. R. Bernabei et al., Universe **4**, 116 (2018).
20. R. Bernabei et al., Nucl. Phys. At. Energy **19**, 307 (2018).
21. R. Bernabei, Bled Workshops in Physics **19** n. 2, 27 (2018).
22. R. Bernabei et al., Nucl. Phys. At. Energy **20(4)**, 317 (2019).
23. R. Bernabei et al., Prog. Part. Nucl. Phys. **114**, 103810 (2020).
24. P. Belli, R. Bernabei, C. Bacci, A. Incicchitti, R. Marcovaldi, D. Prosperi,
    DAMA proposal to INFN Scientific Committee II, April 24th 1990.
25. R. Bernabei et al., Phys. Lett. B **389**, 757 (1996).
26. R. Bernabei et al., Phys. Lett. B **424**, 195 (1998).
27. R. Bernabei et al., Phys. Lett. B **450**, 448 (1999).
28. P. Belli et al., Phys. Rev. D **61**, 023512 (2000).
29. R. Bernabei et al., Phys. Lett. B **480**, 23 (2000).
30. R. Bernabei et al., Phys. Lett. B **509**, 197 (2001).
31. R. Bernabei et al., Eur. Phys. J. C **23**, 61 (2002).
32. P. Belli et al., Phys. Rev. D **66**, 043503 (2002)
33. R. Bernabei et al., Il Nuovo Cim. A **112**, 545 (1999).
34. R. Bernabei et al., Eur. Phys. J. C **18**, 283 (2000).
35. R. Bernabei el al., La Rivista del Nuovo Cimento **26** n.1, 1-73 (2003), and refs. therein.
36. R. Bernabei et al., Int. J. Mod. Phys. D **13**, 2127 (2004) and refs. therein.
37. R. Bernabei et al., Int. J. Mod. Phys. A **21**, 1445 (2006).
38. R. Bernabei et al., Eur. Phys. J. C **47**, 263 (2006).
39. R. Bernabei et al., Int. J. Mod. Phys. A **22**, 3155 (2007).
40. R. Bernabei et al., Eur. Phys. J. C **53**, 205 (2008).
41. R. Bernabei et al., Phys. Rev. D **77**, 023506 (2008).
42. R. Bernabei et al., Mod. Phys. Lett. A **23**, 2125 (2008).
43. R. Bernabei et al., Phys. Lett. B **408**, 439 (1997).
44. P. Belli et al., Phys. Lett. B **460**, 236 (1999).
45. R. Bernabei et al., Phys. Rev. Lett. **83**, 4918 (1999).
46. P. Belli et al., Phys. Rev. C **60**, 065501 (1999).
47. R. Bernabei et al., Il Nuovo Cimento A **112**, 1541 (1999).
48. R. Bernabei et al., Phys. Lett. B **515**, 6 (2001).
49. F. Cappella et al., Eur. Phys. J.-direct C **14**, 1 (2002).
50. R. Bernabei et al., Eur. Phys. J. A **23**, 7 (2005).
51. R. Bernabei et al., Eur. Phys. J. A **24**, 51 (2005).
52. K.A. Drukier et al., Phys. Rev. D **33**, 3495 (1986).

53. K. Freese et al., Phys. Rev. D **37**, 3388 (1988).
54. R. Bernabei and A. Incicchitti, Int. J. Mod. Phys. A **32**, 1743007 (2017).
55. D. Smith and N. Weiner, Phys. Rev. D **64**, 043502 (2001).
56. D. Tucker-Smith and N. Weiner, Phys. Rev. D **72**, 063509 (2005).
57. D. P. Finkbeiner et al, Phys. Rev. D **80**, 115008 (2009).
58. K. Freese et al., Phys. Rev. D **71**, 043516 (2005).
59. K. Freese et al., Phys. Rev. Lett. **92**, 111301 (2004).
60. P. Belli et al., Int. J. of Mod. Phys. A **31**, 1642005 (2016).
61. P. Gondolo et al., New Astron. Rev. **49**, 193 (2005).
62. G. Gelmini and P. Gondolo, Phys. Rev. D **64**, 023504 (2001).
63. F.S. Ling, P. Sikivie and S. Wick, Phys. Rev. D **70**, 123503 (2004).
64. G. Ranucci and M. Rovere, Phys. Rev. D **75**, 013010 (2007).
65. J.D. Scargle, Astrophys. J. **263**, 835 (1982).
66. W.H. Press et al., Numerical recipes in Fortran 77: the art of scientific computing, Cambridge University Press, Cambridge, England 1992, section 13.8.
67. J.H. Horne and S.L. Baliunas, Astrophys. J. **302**, 757 (1986).
68. R. Bernabei et al., Bled Workshop in Physics **15**, no. 2, 19 (2014).
69. W.T. Eadie et al., Statistical methods in experimental physics, ed. American Elsevier Pub. (1971).

2 Neutrino production by photons scattered on dark matter

V. Beylin

Institute of Physics, SFedU, Stachki av. 194, Rostov-on-Don, Russia, 344090
vitbeylin@gmail.com

Abstract. In the framework of hypercolor scenario of multicomponent Dark Matter, inelastic interaction of high energy photons with the Dark Matter candidates is considered. This reaction results in production of energetic leptons and neutrinos, and the Dark Matter particles also can be boosted. Total and differential cross sections have been calculated. The search of correlations between detected signals of high-energy photons and neutrinos can give an information on the Dark Matter scenario and dynamics.

Povzetek: Avtor obravnava neelastično sipanje visokoenergijskih fotonov na temni snovi, ki temno snov pospešijo, povzročijo pa tudi nastanek visokoenergijskih leptonov. Za temno snov uporabi hiperbarvni model, ki predvidi, da ima temna snov več komponent. Za to reakcijo izračuna totalni in parcialne sipalne preseke.

Keywords: hypercolor scenario, Dark Matter, high-enery photons, neutrino production. PACS: 12.60 - i, 96.50.S-,95.35.+d.

2.1 Introduction

Dark matter, which occupies such an important place in the observable Universe, both in its role in the formation of gravitating structures and in its contribution to the overall density of matter, still eludes the "hunters" - ground-based accelerators, measuring complexes and underground laboratories do not find obvious signals of birth, decay or interactions of these objects of unknown nature. Extending the region of the "hunting", physicists are studying in more detail the indirect possible manifestations of Dark Matter in various astrophysical phenomena [1–5, 7, 8, 8], actively analyzing the detected signals of cosmic rays and individual particles using space telescopes and interpreting observational data in the framework of various scenarios.
The so-called indirect methods of searching for traces of dark matter among numerous astrophysical phenomena simultaneously provide a testing ground for highlighting the most viable options for extending the Standard Model. Having no clues from Nature, we have to sort through the options for the DM construction from the main bricks of matter known to us; fermions, scalars, bosons, compound new hadrons or atoms, neutralinos from supersymmetry, axions, representatives

of the Dark World interacting with objects of our world by exchanging special mediators - dark bosons.

In all cases, we hope to find among the many studied reactions occurring in acts of interaction involving dark matter objects and parts of ordinary matter, unique events that carry information about the dynamics and origin of dark matter. As very important addition we consider events with high-energy neutrino and/or photons that are detected mostly by IceCube and LHAASO (and, certainly, by other ground observatories - because of unpredicted ways of cosmic strangers) [9–19]. Note, some interesting data can result from analysis of correlations between observed events with photons and neutrinos from close directions.

A special role has recently been played by the analysis of scattering by dark matter objects of particles generated by processes that take place at enormous densities and energies - in particular, in jets from powerful quasars (or blasars), in the vicinity of black holes. Depending on the DM scenario, possible, in principle, various observed signals: monochromatic photons from DM annihilation, high-energy particle fluxes during the decays of a hypothetical supermassive DM, continuous radiation in a certain energy range due to transitions between DM components, and so on.

In this paper, we consider the inelastic interaction of high-energy photons with DM particles. For definiteness, we work within the framework of the SM extension with additional heavy hyperquarks, this is the so-called hypercolor model in its minimal version with two doublets of new fermions and $SU(4)$ symmetry. In this case, it is possible to construct a vector interaction of hyperquark currents with the gauge bosons, providing the necessary smallness of the Pekin-Tackeuchi parameters. Further, in the framework of the llinear sigma model, by analogy with low-energy hadron physics, bound states of hyperfermions are introduced, i.e. new unstable hyperhadrons. On this path, a set of pseudo-Nambu-Goldstone states arises, of which several - the lightest neutral state of a hyperpion triplet and a hyper-diquark with a non-zero conserved hyperdron number - turn out to be stable. These states are interpreted as TM candidates. Some necessary technical details for the description of the process interested will be presented in Section 2. Section 3 contains results of calculations; discussion of results is placed in section Conclusions.

2.2   Dark Matter candidates in hypercolor scenario

Minimal model of the vector hypercolor SM extension contains one doublet of additional heavy H-fermions (H-quarks in confinement) with zero hypercharge. To provide the necessary smallness of Peskin-Takeuchi parameters, initial fields of H-fermions are redefined resulting in Dirac fields that interact vectorially with the gauge fields; extra $SU(2)_w$ symmetry ensures this electroweak interaction. An extra singlet scalar, $\tilde{\sigma}-$ meson, emerges to provide spontaneous symmetry breaking and, consequently, non-zero masses of new fields.

At the next stage, using the linear hyper-$\sigma-$ model (as it is done in the low-energy hadron physics), a new H-hadrons generated by H-quarks currents arize with some hierarchy in masses. Besides, the global $SO(4)$ breaking generates a set of

pseudo-Nambu-Goldstone (pNG) states, including a triplet of pseudoscalar H-pions and neutral H-baryon (H-diquark with the additive conserving quantum number) along with its antiparticle; H-pions possess a multiplicative conserved quantum number [20]. Thus, the neutral states, $\tilde{\pi}^0$ and B^0, $\bar{B}^0$, are stable in this scenario, so they can be interpreted as the DM candidates with equal masses at the tree level.

Note, the model which is used here to consider high energy photons scattering off the DM is described in detail in a series of papers [21–26]. That is why we do not repeat here all known elements of the scenario; remind only, the DM candidates masses were estimated from analysis of the DM burnout kinetics, and we get: $m_{DM} \sim 1\,\mathrm{TeV}$. The electroweak mass splitting in the H-pions triplet, i.e. between charged and neutral hyperpions, is nearly constant: $\Delta m_\pi \approx 0.16\,\mathrm{TeV}$. Mass splitting between H-pions and neutral H-baryon, another component of the DM, can be as large as $\approx (10 - 15)\,\mathrm{GeV}$ (see [27]). Mass of $\tilde{\sigma}-$ meson is connected with the H-pion mass and depends on the the mixing angle , θ, between $\tilde{\sigma}-$ and Higgs boson. This mixing should be small, $\sin\theta \lesssim 0.1$, so the standard Higgs boson has a small admixture of additional scalar state, $\tilde{\sigma}$. Note also that the density of H-baryons dominates over density of $\tilde{\pi}^0$ almost for all possible values of model parameters becaue of different origins of the DM components burning out at different rates [26]. The charged components of H-pion triplet decay, and the dominant channel is the following: $\tilde{\pi}^\pm \to \tilde{\pi}^0 l^\pm \nu_l$ with $\Gamma \approx 3 \cdot 10^{-15}\,\mathrm{GeV}$.

Certainly, the DM objects are neutral, so they do not interact with photons directly. However, in this scenario there is a class of tree-level diagrams which describe intermediate stage in the total process, $\gamma\tilde{\pi}^0 \to W^+\tilde{\pi}^- \to ll'\nu_l\nu_{l'}\tilde{\pi}^0$. Here, we know that charged H-pion decays into lepton and neutrino with $Br \approx 1$, and (in fact, intermediate) gauge $W-$ bosons also eventually decay into lepton-neutrino pairs. Correspondingly, we need only in hyperpion triplet properties. From this point of view, this DM component demonstrates possibilities of any WIMP scenario where the DM candidate interact with the standard gauge bosons in some way. Specific detail is: this scenario deal with heavy DM candidates, so to accelerate them the high energy transfer from the projectile is necessary.

In other words, H-pion as the DM component is the almost "pure" WIMP having tree level elctroweak links to the SM fields due to charged (unstable) components of H-pion triplet. Indeed, the model contains two types of stable neutral DM candidates, however, scatterings of photons off neutral H-pion are the most simple due to vertices which are shown in the following part of the model Lagrangian:

$$L_{EW} = igW_+^\mu(\tilde{\pi}^0\tilde{\pi}_{,\mu}^- - \tilde{\pi}_{,\mu}^0\tilde{\pi}^-) - ieA^\mu(\tilde{\pi}^-\tilde{\pi}_{,\mu}^+ - \tilde{\pi}_{,\mu}^-\tilde{\pi}^+) + eg\tilde{\pi}^0\tilde{\pi}^-A^\mu W_\mu^+ + \mathrm{h.c.} \quad (2.1)$$

The B^0 DM component participates in EW interactions only via fermion, vector and/or scalar (gauge boson, quark, H-quark or H-pion) loops and via (pseudo) scalar (Higgs boson, $\tilde{\sigma}$) exchanges, so, such stable H-diquark presents a hadronic type DM. Some comments on photons scattering off B^0, component will be done later.

2.3   Neutrino production by photons

Here, we consider inelastic interaction of photons with energies $\sim (1-10)\,\text{TeV}$ with the DM objects. Such process of leptons and neutrinos production by photons seems interesting because the yield of these secondary particles depends both on DM dynamics and distribution its density in space.

On origin of high-energy photons and neutrinos may be associated, in particular, with physics and structure of jets from active galaxies nucleus(AGN), events with these particles of $\text{TeV}-$ energies are repeatedly observed and analyzed [28–39]. So, there is a possibility for DM structures in the AGN vicinity to participate in the generation of leptons and neutrinos fluxes. Certainly, an analogous process is possible when high-energy photons are scattered by the DM clumps.

Then, in the framework of minimal hypercolor model we study the photons scattering off $\tilde{\pi}^0-$ component. Such reaction is the most simple, however, calculations of the total cross section with unstable final states were carried out in the continued mass approach(see [40] and references therein).

Three tree-level diagrams describing the photon scattering off $\tilde{\pi}^0$ are depicted in Fig.1 Note, there is an additional diagram (see Fig.2) which, however, gives a small contribution to the cross section, because we are interested in dominant configuration with small squared invariant mass of intermediate W-boson. Then, the sum of corresponding matrix elements is:

$$M_C + M_{\tilde{\pi}} + M_W = ige_\gamma^\alpha e_W^\mu \left(-g_{\mu\alpha} + \frac{(2k_1 - p_2)_\alpha (2p_1 - k_2)_\mu}{d_{\tilde{\pi}}} + \frac{(p_1 + k_1)_\beta}{d_W}\right.$$

$$\left. \cdot (g^{\nu\beta} - \frac{q_W^\nu q_W^\beta}{m_W^2}(g_{\mu\nu}(p_2 - 2k_2)_\alpha - g_{\nu\alpha}(2p_2 - k_2)_\mu + g_{\mu\alpha}(p_2 + k_2)_\nu)\right). \quad (2.2)$$

Here, propagators are denoted as $d_{\tilde{\pi}}$, d_W.

The squared matrix element is cumbersome, so the exact expression for the cross section of this sub-process is not shown here. Instead, we show dependencies of differential cross section on squared invariant mass of virtual W-boson, various masses of the DM target and energies of incident photon for fixed energies of final H-pion (see Fig.3). Analogous dependencies of differential cross section on squared invariant mass but fixed energies of virtual W-boson and for fixed energy of incident photon are shown in Fig.4. In fact, these two-dimensional curves are sections of three-dimensional graph for different values of the parameters; so, these curves contain information about the angle between products of W-boson decay (lepton and neutrino, in particular).

Of course, it is important to know not only differential cross section for the sub-process with virtual states (unstable charged H-pion and W-boson with known branching of decays into leptons and neutrinos) but total cross section of the process. This next step can be done using model of unstable particles with a smeared masses [40]. In this approximation the total cross section is presented in a factorized form:

$$\sigma_{tot}(s) = \int d\mu^2 \sigma_{tot}(s, \mu^2)\rho(\mu^2), \quad (2.3)$$

here μ^2 is the variable squared invariant mass of intermediate unstable state and

$$\rho(\mu^2) = \frac{1}{\pi} \frac{\sqrt{\mu^2}\Gamma(\mu^2)}{((\mu^2 - M^2(\mu^2))^2 + (\sqrt{\mu^2}\Gamma(\mu^2))^2)^2}$$

is the density of probability; integration goes over kinematically allowed region. Now, the total cross section for the whole process can be estimated with a good accuracy (note, the approach above was tested in a numerous reactions, and the accuracy was reliably evaluated as $\lesssim 5\,\%$).

Total cross section for the process of photons scattering off scalar DM candidates, $\gamma\tilde{\pi}^0 \to W^+\tilde{\pi}^- \to ll'\nu_l\nu_{l'}\tilde{\pi}^0$, in dependence of photons energy are presented in Fig.5. Here we consider not very high energies of photons, up to $10\,\mathrm{TeV}$ because for higher energies the photon flux is much lower. These results depend on the DM mass weakly, so we use here some referent value, $m_{DM} = 1\,\mathrm{TeV}$. Besides, we get the cross section almost stable in the energy region considered. This result indicates some possible correlations between detected high-energy photons and neutrinos fluxes - namely, neutrinos of high energy can be produced by photons scattered on the DM objects.

But this is not the whole story because there are loop contributions to neutrino+ leptons generation by the photons scattering off another DM component, stable H-baryon. However, this DM candidate presents other type of DM objects which do not interact with the gauge boson directly. So, one from possible contributions into such type reaction is shown in Fig.6. However, there should be also additional channels to transform a part of high-energy photons into fluxes of leptons and neutrinos. These are processes like $\gamma B^0 \to W^+W^-B^0$, $\gamma B^0 \to t\bar{t}B^0$, $\gamma B^0 \to ZB^0$ with subsequent decays of heavy standard quarks and gauge bosons. These interesting and promising channels of inelastic interactions of photons with the DM will be analyzed elsewhere.
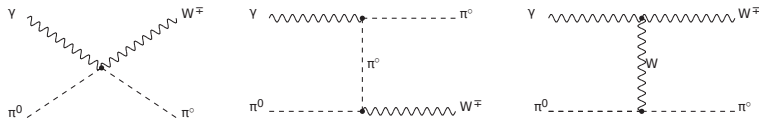
Fig. 2.1: Tree-level diagrams for the subprocess $\gamma\tilde{\pi}^0 \to W^\pm\tilde{\pi}^\pm$.
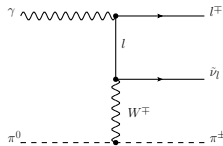
Fig. 2.2: Additional contribution to the scattering process.
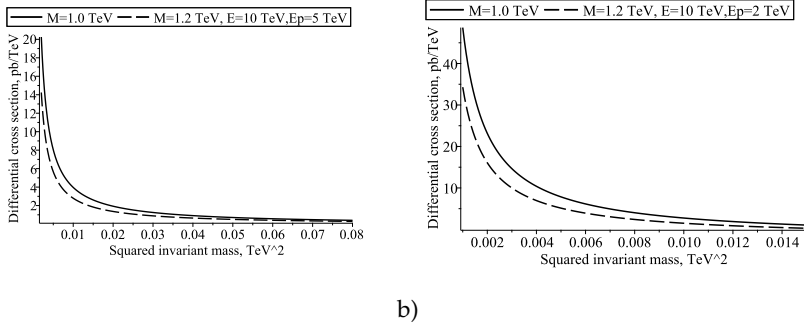
Fig. 2.3: Differential cross section in dependence on W-boson squared invariant mass for the incident photon energy $E_\gamma = 10$ TeV with the fixed energy of final H-pion: a) $E_{\tilde\pi} = 2$ TeV; b) $E_{\tilde\pi} = 5$ TeV.
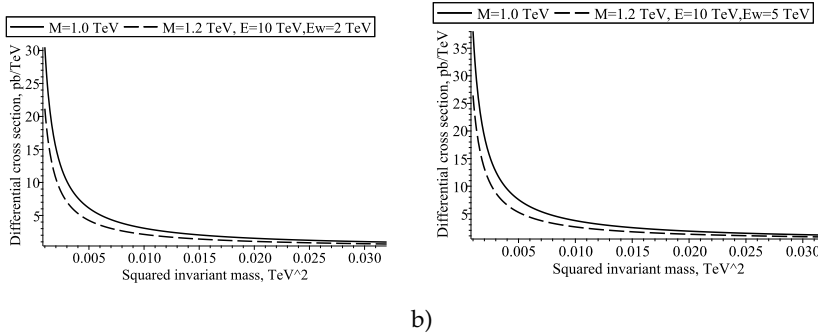
Fig. 2.4: Differential cross section in dependence on W-boson squared invariant mass for the incident photon energy $E_\gamma = 10$ TeV with the fixed energy of W-boson: a) $E_W = 2$ TeV; b) $E_W = 5$ TeV.
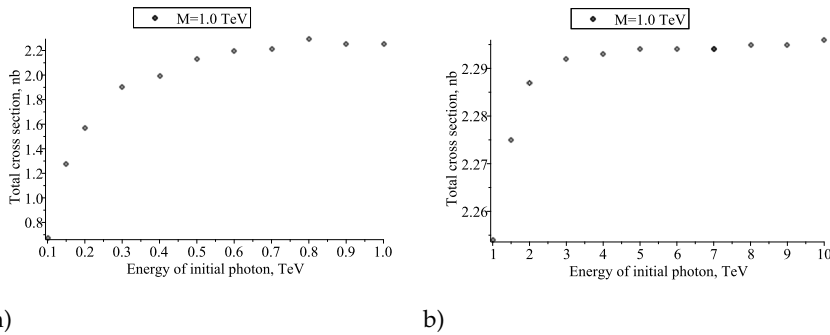
Fig. 2.5: Total cross section in dependence on photon energies energy; of incident photon: a) up to $E_\gamma = 1$ TeV; b) up to $E_\gamma = 10$ TeV.
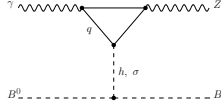
Fig. 2.6: One from possible loop-level diagrams for the subprocess $\gamma B^0 \to Z B^0$.

2.4 Conclusions and some open questions

So, for tree level production of leptons and neutrinos by inelastic scattering of high-energy photons off the DM we get $\sigma_{tot}(E_\gamma) \sim 10^0$ nb.

As it is seen from calculations, a significant part of E_γ is converted into energies of secondary leptons and neutrinos which are generated by decays of $W-$boson both in direct channel and from unstable light standard mesons due to hadronic decay channels of W.

At the time, a DM target is an active and necessary participant of the process, so, it also can get sufficiently large portion of photon energy, so the DM components can be accelerated up to energies $\sim (1-10)$ TeV or even larger depending on E_γ. Intensity of this reaction strongly depends on the DM density (the macroscopic cross section is $\sim \rho_{DM}$, the high-enery secondaries yield can be sufficiently enhanced when the scattering occurs in regions of high DM density.

It is an important notification because the main sources of high-energy photons are quasars(or blasars shining in the direction of the Earth) which emit dense and very fast fluxes of charged particles as jets (see references above); high-energy photons are radiated by these charged particles, so photons and neutrinos generated in quasars and blasars jets can be detected by ground observatories and cosmic telescopes. Inelastic scattering of photons off the DM most effectively occurs in the vicinity of quasars, i.e. close to active nuclei of galaxies. And it is in these regions of strongest gravity that the DM density is the largest.

Products of this collision of photon with the DM are approximately collimated with the initial photon direction for high E_γ. Flux of neutrinos produced with cross section $\sim (0.1-1)$ nb and energies $\sim (1-10)$ TeV should correlate with the initial photon flux, consequently, signals of TeV-photons detected by cosmic telescopes and ground observatories can be (approximately) synchronized with neutrinos of close energy which come from the nearly the same direction.

Possibly, interactions of such type affect on the DM density fluctuations at early stage of evolution when cosmological plasma is hot and contains a lot of the DM (neutral) objects and also the dense fluxes of photon radiaton. So, these processes can also affect on the density of photons and DM carriers throughot the radiation dominated era. In some sense, these processes can somewhat wash out dense DM clumps and fluctuations due to accelerating the DM particles of various masses.

It is, of course, a hard task to find out and separate from any other sources neutrinos and photons signals correlated in time and spatial direction, however, if it were discovered, it would mean obtaining an important information about the structure and dynamics of the DM and blasars jets, as well as about the DM spatial distribution and its ability to affect to dynamics and composition of cosmic rays in space.

In any case, it is worth considering such processes of photons transformation into leptons and neutrinos fluxes accompanying with the DM accelerated particles in all possible DM scenarios and for various characteristics of cosmological evolution stages. The DM plays an important role of an active and necessary catalyst of mutual transitions between various types of the SM particles. As it seems, such processes with the obligatory presence of the DM should be taken into acount when the early Universe dynamics and structure are studied.

Acknowledgements

References

1. J.L. Feng: Dark Matter Candidates from Particle Physics and Methods of Detection, Ann. Rev. Astron. Astrophys. **48**, 495 (2010).
2. L. Roszkowski, E.M. Sessolo, S. Trojanowski: WIMP dark matter candidates and searches, current status and future prospects, Rept.Progr.Phys. **81**, 066201 (2018), arXiv:1707.06277 [hep-ph].
3. M. Cirelli: Dark Matter Indirect searches: phenomenological and theoretical aspects, J. Phys.: Conf. Series. **447**, 447 (2013).
4. M.Yu. Khlopov: Introduction to the special issue on indirect dark matter searches, Int. J. Mod. Phys. A. **29**, 144302 (2014).
5. J.M. Gaskins: A review of indirect searches for particle dark matter. Contemp. Phys. **57**, 496525 (2016).
6. G. Arcadi, M. Dutra, P. Ghosh, M. Lindner, Y. Mambrini, M. Pierre, D. Profumo, F.S. Queiroz: The waning of the WIMP? A review of models, searches, and constraints. Eur. Phys. J. C **78**, 203 (2018).
7. K.M. Belotsky, E.A. Esipova, A.Kh. Kamaletdinov, E.S. Shlepkina, M.L. Solovyov: Indirect effects of dark matter. IJMPD. **28**, 1941011 (2019).
8. D. Gaggero, M. Valli: Impact of Cosmic-Ray Physics on Dark Matter Indirect Searches. Adv. in HEP, **2**018, 3010514 (2018).
9. Pierre Auger Collaboration: Searches for Ultra-High-Energy Photons at the Pierre Auger Observatory. Universe. **8(11)**, 579 (2022).
10. H. Abdallah et al (HESS collab.): Search for $\gamma-$Ray Line Signals from Dark Matter Annihilations in the Inner Galactic Halo from 10 Years of Observations with HESS, Phys. Rev. Lett. **120**, 201101 (2018).
11. E. Richard, et al. (Super-Kamiokande collab.): Measurements of the atmospheric neutrino flux by 430 Super-Kamiokande: energy spectra, geomagnetic effects, and solar modulation. Phys. Rev. D **94**, 052001 (2016).
12. H. Niederhausen, Y. Xu (IceCube Collab.): High Energy Astrophysical Neutrino Flux Measurement Using Neutrino-induced Cascades Observed in 4 Years of IceCube Data. PoS ICRC 2017 **2**017, 968 (2017).
13. A.A. Kochanov, A.D. Morozova, T.S. Sinegovskaya, S.I. Sinegovskiy: Behaviour of the high-energy neutrino flux in the Earth's atmosphere. Solar-Terrestrial Physics 2015, 1, 4.
14. A. Bhattacharya, R. Gandhi, A. Gupta: The Direct Detection of Boosted Dark Matter at High Energies and PeV events at IceCube, JCAP **1**503, 027 (2015).

15. J. Kopp, J, Liu, X-P. Wang: Boosted Dark Matter in IceCube and at the Galactic Center, JHEP **04**, 105 (2015).

16. B.L. Zhang, Z.-H. Lei, J. Tang: Constraints on cosmic-ray boosted DM in CDEX-10. arXiv:2008.07116 [hep-ph].

17. L.A. Fusco, F. Versari: Testing cosmic ray composition models with very large-volume neutrino telescopes. Eur. Phys. J. Plus **1**35, 624 (2020).

18. S. Bottai, S. Giurgola (EUSO Collab.): Downward neutrino induced EAS with EUSO detector. Proc. of 28th ICRC **2**003, 1113 (2020).

19. X. Baia, B. Bia, J. Bia, et al. (LHAASO Collab.): THE LARGE HIGH ALTITUDE AIR SHOWER OBSERVATORY. **2**019, arXiv: 1905.02773 [hep-ph].

20. Y. Bai, R.J. Hill: Weakly interacting stable hidden sector pions. Phys. Rev. D **82**, 111701 (2010).

21. R. Pasechnik, V. Beylin, V. Kuksa, G. Vereshkov: Chiral-symmetric technicolor with standard model Higgs boson. Phys. Rev. D **88**, 075009 (2013).

22. R. Pasechnik, V. Beylin, V. Kuksa, G. Vereshkov: Vector-like technineutron Dark Matter: is a QCD-type Technicolor ruled out by XENON100? Eur. Phys. J. C **2**728, 74 (2014).

23. R. Pasechnik, V. Beylin, V. Kuksa, G. Vereshkov: Composite scalar Dark Matter from vector-like $SU(2)$ confinement. Int. J. Mod. Phys. A **1**650036, 31 (2016).

24. V. Beylin, M. Bezuglov, V. Kuksa, N. Volchanskiy: An analysis of a minimal vector-like extension of the Standard Model. Adv. High Energy Phys. **2**017, 1765340 (2017).

25. V. Beylin, M. Khlopov, V. Kuksa, N. Volchanskiy: Hadronic and Hadron-Like Physics of Dark Matter. Symmetry, **1**1, 587 (2019).

26. V. Beylin, M. Bezuglov, V. Kuksa, E. Tretiakov, A. Yagozinskaya, A.: On the scattering of a high-energy cosmic ray electrons off the dark matter. Int.J.of Mod. Phys. A **6**(7), 34 (2019).

27. V. Beylin, V. Kuksa, M. Bezuglov: The multicomponent dark matter structure and its possible observed manifesttions. Proc. of 24th Workshop "What comes beyond the SM", **22**, 57 (2021), Bled, 2021.

28. A.V. Plavin et al.: Directional Association of TeV to PeV Astrophysical Neutrinos with Radio Blazars. Astrophys. Journ. **908**, 2 (2021).

29. M. Di Mauro: Characteristics of the Galactic Center excess measured with 11 years of Fermi-LAT data, Phys. Rev. D. **103**, 063029 (2021).

30. Z. Shah, N. Iqbal, A. Manzoor: Very-high-energy flat spectral radio quasar candidates. MNRAS. **515**, 3 (2022).

31. HESS Collab.:Resolving acceleration to very high energies along the Jet of Centaurus A. Nature.**582**, 356 (2020).

32. F.W. Stecker, M.H. Salomon: High energy neutrinos from quasars. Space Science Rev. **75**, 341 (1996).

33. M. Roncadelli et al: Very-high-energy quasars hint at ALPs. arXiv:1310.2829 [astro-ph.HE].

34. G. Bhatta: Blazar Jets as Possible Sources of Ultra-High Energy Photons: A Short Review. Universe **8(10)**, 513 (2022).

35. A. Shukla, K. Mannheim: Gamma-ray flares from relativistic magnetic reconnection in the jet of the quasar 3C 279. Nature Comm. **11**, 4176 (2020).

36. E.D. Bloom, J.D. Wells: Multi-GeV photons from electron–dark matter scattering near Active Galactic Nuclei. Phys. Rev. D **57**, 1299 (1998).

37. M. Gorchtein, S. Profumo, L. Ubaldi: Probing Dark Matter with AGN Jets. Phys.Rev. D **82**, 083514 (2010).

38. S. Profumo, L. Ubaldi: Cosmic Ray-Dark Matter Scattering: a New Signature of (Asymmetric) Dark Matter in the Gamma Ray Sky. JCAP **02**0, 1108 (2011).

39. V. Beylin, M. Bezuglov, V. Kuksa, E. Tretiakov: Quasielastic Lepton Scattering off Two-Component Dark Matter in Hypercolor Model. Symmetry, **12**, 5 (2020).
40. V.I. Kuksa, N.I. Volchanskiy: Factorization in the model of unstable particles with continuous masses. Cent. Eur. J. Phys. **11**, 182 (2013).

BLED WORKSHOPS
IN PHYSICS
VOL. 23, NO. 1

Proceedings to the 25*th* [*Virtual*]
Workshop
What Comes Beyond . . . *(p. 31)*
Bled, Slovenia, July 4–10, 2022

3   Elusive anomalies

L. Bonora

International School for Advanced Studies (SISSA),
Via Bonomea 265, 34136 Trieste, Italy

Abstract. Usually, in order to compute an anomaly (be it chiral or trace) with a perturbative method, the lowest significant order is sufficient. With the help of gauge or diffeomorphism invariance it uniquely identifies the anomaly. This note is a short review of the ambiguities that arise in the calculation of trace anomalies, and is meant, in particular, to signal cases in which the lowest perturbative order is not enough to unambiguously identify a trace anomaly. This may shed light on some recent contradictory results.

Povzetek: Ko želimo ugotoviti, če je teorija anomalna, največkrat zadošča, da izračunamo najnižji neničelni red v teoriji motenj in preverimo njeno umeritveno ali difeomorfno invarjanco. V tem prilspevku avtor na kratko predstavi težave, ki se pojavijo, če najnižji red v teoriji motenj ne zadostuje za nesporno odločitev ali je teorija anomalna. Prispevek bo morda pomagal osvetliti nekatere protislovne nedavno objavljene rezultate.

3.1   Introduction

The first manifestation of anomalies in QFT (the Adler-Bell-Jackiw anomaly) originated from an apparently technical problem: the constant shift of an integration variable in a fermion loop integral leads to a vanishing result (which, in turn, implies a conserved chiral current), except for the fact that this integral is UV divergent, so that the shift is illegal; on the contrary, a proper treatment of this problem leads to a non-vanishing result, which, in turn, implies an anomalous conservation law. The way it came up the first time might have seemed to be due to a technicality, but in fact it turned out to be the tip of an iceberg. On the one hand it was the first of a series of similar results that lead to the discovery of many anomalies: many currents which are classically conserved are not anymore so after quantization. On the other hand these anomalies were derived in a number of ways, both perturbative and nonperturbative, and it was discovered that they are far from wild, random violations of the conservation laws, but, on the contrary, they satisfy group theory motivated consistency conditions. Finally, the illuminating connection was found with the family's index theorem, illuminating, because it revealed that (consistent) anomalies represent obstructions to the existence of the inverse of the Dirac (or Dirac-Weyl) operator, i.e. to the very existence of the fermion propagator. The latter is a fundamental ingredient of a quantum theory, therefore consistent anomalies are a spy of its bad health.

In quite a similar way, after the ABJ anomalies, also anomalies in the trace of the energy-momentum tensor were found in theories where, classically, conformal invariance requires a traceless e.m. tensor, [1]. Strangely enough trace anomalies have lived a separate life from chiral anomalies, and any attempt to unify them has failed. Nevertheless it is true that both kind of anomalies are strictly linked to the existence of the inverse kinetic operator: to see it is enough, for instance, to consider that both the derivation of a current conservation law and the tracelessness condition within the path integral approach requires the existence of the inverse kinetic operator. Leaving aside, for the time being, this link between the two types of anomaly (chiral and trace) let us focus now on their differences.

It is not a mistery that the calculation of trace anomalies has led to some controversial results. The reason is, on the one hand, the ambiguity in the definition of trace anomaly and, on the other hand on the ambiguities intrinsic to their derivation. It was pointed out above that ABJ chiral anomaly arose from resolving an ambiguity in the definition of a loop integral. These types of ambiguities are the basic ones, and, of course, are present also in the case of trace anomalies. But they are not the only ones. The very definition of the trace anomaly in terms of perturbative amplitudes poses a problem. Let us denote by $\langle\langle T_{\mu\nu}(x)\rangle\rangle$ the full one-loop one-point e.m. tensor, i.e.

$$\langle\langle T_{\mu\nu}(x)\rangle\rangle = \sum_{n=0}^{\infty} \frac{i^n}{2^n n!} \int \prod_{i=1}^{n} d^4 x_i \sqrt{g(x_i)} h^{\mu_i \nu_i}(x_i) \langle 0|\mathcal{T}T_{\mu\nu}(x)T_{\mu_1\nu_1}(x_1)\dots T_{\mu_n\nu_n}(x_n)|0\rangle$$

(3.1)

where $\langle 0|\mathcal{T}T_{\mu\nu}(x)T_{\mu_1\nu_1}(x_1)\dots T_{\mu_n\nu_n}(x_n)|0\rangle$ are e.m. tensor correlators calculated with Feynman diagrams. Then we may proceed in two ways to compute the trace of this object. The first is to evaluate $g^{\mu\nu}(x)\langle\langle T_{\mu\nu}(x)\rangle\rangle$, i.e. to take the trace of the one-loop one-point e.m. tensor. The second is to evaluate $\langle\langle T_\mu^\mu(x)\rangle\rangle$, i.e. the one-loop one-point function of the e.m. trace (which is non-vanishing off-shell). In many examples these two quantities are different, therefore we face the problem of defining what we mean by trace anomaly. It turns out that the right definition is the difference between the two

$$T(x) = g^{\mu\nu}(x)\langle\langle T_{\mu\nu}(x)\rangle\rangle - \langle\langle T_\mu^\mu(x)\rangle\rangle$$

(3.2)

proposed by M. J. Duff, [2,3]. According to the physical interpretation in [4], it is entirely due to the violation of the equation of motion of the theory (remember that the trace of the e.m. tensor classically incorporates the equation of motion). But in the Feynman diagram approach there are other ambiguities. When regularizing the loop integral we are faced with more than one possibility, no matter what regularizing prescription we use, dimensional or Pauli-Villars, to name the most frequently used. These possibilities may lead to final results differing by local terms (this may happen also for chiral anomalies). Now, to proceed further, we have to introduce another ingredient that can be, and usually is, disregarded in the case of chiral anomalies: diffeomorphism invariance.The trace anomaly is the response of the functional integral under a rescaling of the metric. Therefore the properties of the metric are inevitably brought into the game, and one has to

check in particular that diffeomorphisms are conserved. This requires a recourse to cohomology. As we shall see in an example below, depending on the regularization prescription, the divergence of the e.m. tensor may be vanishing or non-vanishing, giving rise in the latter case to a cocycle of the diffeomorphisms. Such cocycle may be trivial, that is a counterterm can be added to the effective action which cancels this anomaly and, simultaneously, modify the trace anomaly. We shall refer to this as *the stabilizing or repairing* role of diffeomorphism conservation. In most situations this is what happens: a unique expression for the trace anomaly is identified, accompanied by conserved diffeomorphisms. In other words, as it should be, the final result does not depend on the regularization prescription. Said another way, a regularization prescription determines the anomaly up to trivial cocycles.

This is not the end of the story. There is another possible ambiguity which we would like to illustrate in this note. It is rather rare but plays a crucial role in specific cases and renders the lowest order calculation of the trace anomaly unusable. Such an ambiguity is triggered if the three-point function of the energy-momentum tensor (the lowest order as far as the calculation of the trace anomaly in 4d is concerned) vanishes identically. This may not happen for the full e.m. tensor, but it may happen for its odd-parity part. Since even-parity and odd-parity correlators split neatly we can treat them in the anomaly calculations as separate entities. When such vanishing occurs, the first term in (3.2) vanishes, but the second need not vanish. On the other hand the (odd-parity) divergence of the e.m. tensor at the (three-point level) vanishes identically and there is no possibility to adjust the effective action by adding counterterms in such a way as to unambiguously determine the trace anomaly. Now, in most cases the lowest order perturbative calculation is enough to determine trace or gauge anomalies completely, relying on gauge or diffeomorphism invariance, respectively. But in this case it is impossible, the problem is logically undecidable at the lowest perturbative order. The way out is to resort to higher order approximations or to a non-perturbative approach.

In this short note I would like to present an example of this pathological phenomenon. But, before, in order to appreciate it, it is necessary to understand the repairing mechanism of diffeomorphism conservation. For this reason I present in the next section a simple 2d example in which this mechanism works, and devote the third section to the non-working example. Throughout the paper the reference action will be that of a right-handed Weyl fermion

$$S = \int d^d x \sqrt{g}\, i\overline{\psi_R}\gamma^\mu \left(\partial_\mu + \frac{1}{2}\omega_\mu \right) \psi_R \tag{3.3}$$

where $g = \det(g_{\mu\nu})$, $\gamma^\mu = e^\mu_a \gamma^a$, ($\mu, \nu, \dots$ are world indices, $a, b, \dots$ are flat indices) and ω_μ is the spin connection:

$$\omega_\mu = \omega^{ab}_\mu \Sigma_{ab}$$

where $\Sigma_{ab} = \frac{1}{4}[\gamma_a, \gamma_b]$ are the Lorentz generators; $\psi_R = P_R\psi$, where $P_R = \frac{1+\gamma_*}{2}$, and γ^* is the appropriate chirality matrix. The reference classical e.m. tensor will be

$$T_{\mu\nu} = \frac{i}{4}\overline{\psi_R}\gamma_\mu \overset{\leftrightarrow}{\nabla}_\nu \psi_R + \{\mu \leftrightarrow \nu\} \tag{3.4}$$

The theory (3.3) is invariant under diffeomorphisms $\delta_\xi g_{\mu\nu} = \nabla_\mu \xi_\nu + \nabla_\nu \xi_\mu$ (∇ is the gravitational covariant derivative and $\xi_\mu = g_{\mu\nu} \xi^\nu$) and Weyl transformations $\delta_\omega g_{\mu\nu} = 2\omega g_{\mu\nu}$, where $\xi^\mu(x)$ and $\omega(x)$ are the relevant local parameters. As a consequence, classically,

$$\nabla^\mu T_{\mu\nu}(x) = 0, \qquad T_\mu^\mu(x) = 0 \qquad (3.5)$$

on shell.

3.2   A simple (working) example

In two dimensions, due to the anticommutativity of spinors, the spin connection drops out of the action (3.3). For ψ_R the action becomes

$$S = i \int d^2x \sqrt{g} \, \overline{\psi}_R \gamma^\mu \partial_\mu \psi_R \qquad (3.6)$$

Although this is not strictly necessary, we will further simplify it by absorbing the $\sqrt{g}$ into a redefinition of ψ: $\psi \to \widetilde{\psi} = g^{\frac{1}{4}} \psi$.

$$\widetilde{S} = i \int d^2x \, \overline{\widetilde{\psi}}_R \gamma^\mu \partial_\mu \widetilde{\psi}_R = i \int d^2x \, \overline{\widetilde{\psi}}_R \gamma^a e_a^\mu \partial_\mu \widetilde{\psi}_R \qquad (3.7)$$

Now let us write $e_a^\mu \approx \delta_a^\mu - \chi_a^\mu$ and make the identification $2\chi_a^\mu = h_a^\mu$, where $h_{\mu\nu}$ is the gravitational fluctuation field: $g_{\mu\nu} = \eta_{\mu\nu} + h_{\mu\nu}$. The fermion propagator is

$$\frac{i}{\not{p} + i\epsilon} \qquad (3.8)$$

and there is only one graviton-fermion-fermion (V_{ffg}) vertex given by

$$\frac{i}{8} \left[(p + p')_\mu \gamma_\nu + (p + p')_\nu \gamma_\mu \right] \frac{1 + \gamma_*}{2}. \qquad (3.9)$$

where p and p' are the two graviton momenta, one entering the other exiting. Other vertices will not be relevant.

Our purpose is to compute the two terms in eq.(3.2). In 2d the lowest order contribution is given by the two-point amplitudes

$$\eta^{\mu\nu} \langle 0|\mathcal{T} T_{\mu\nu}(x) T_{\lambda\rho}(y)|0\rangle \qquad \text{and} \qquad \langle 0|\mathcal{T} T_\mu^\mu(x) T_{\lambda\rho}(y)|0\rangle, \qquad (3.10)$$

respectively. Their Fourier transforms is provided by a Feynman (bubble) diagram with a fermion loop with momentum p and two external gravitons (one entering, one exiting) with momentum k. More in detail, considering the first term in (3.10) we have

$$\langle T_{\mu\nu}(x) T_{\lambda\rho}(y)\rangle = 4 \int \frac{d^2k}{(2\pi)^2} e^{-ik(x-y)} \widetilde{T}_{\mu\nu\lambda\rho}(k) \qquad (3.11)$$

with

$$\widetilde{T}_{\mu\nu\lambda\rho}(k) = -\frac{1}{64}\int\frac{d^2p}{(2\pi)^2}\,\text{tr}\left(\frac{1}{\slashed{p}}(2p-k)_\mu\gamma_\nu\frac{1+\gamma_*}{2}\frac{1}{\slashed{p}-\slashed{k}}(2p-k)_\lambda\gamma_\rho\frac{1+\gamma_*}{2}\right)+\left\{\begin{matrix}\mu\leftrightarrow\nu\\\lambda\leftrightarrow\rho\end{matrix}\right\}$$

(3.12)

The last bracket means that we have to add three more terms like the first so as to realize a symmetry under the exchanges $\mu\leftrightarrow\nu$, $\lambda\leftrightarrow\rho$. Moreover, we have to symmetrize with respect to the exchange $(\mu,\nu)\leftrightarrow(\lambda,\rho)$ (bosonic symmetry). The integral in (3.2) is UV divergent. We proceed to regularize it with dimensional regularization. To this end, as usual, we introduce extra space components of the momentum running around the loop, $p_\mu\to p_\mu+\ell_{\bar\mu}$ $(\ell_{\bar\mu}=\ell_2,\ldots,\ell_{\delta+1})$. So (3.2) becomes

$$\widetilde{T}^{(reg)}_{\mu\nu\lambda\rho}(k) = -\frac{1}{64}\int\frac{d^2p\,d^\delta\ell}{(2\pi)^{2+\delta}}\,\text{tr}\left(\frac{1}{\slashed{p}+\slashed{\ell}}(2p-k)_\mu\gamma_\nu\frac{1+\gamma_*}{2}\frac{1}{\slashed{p}+\slashed{\ell}-\slashed{k}}(2p-k)_\lambda\gamma_\rho\frac{1+\gamma_*}{2}\right).$$

(3.13)

Now let us recall that $\slashed{p}^2=p^2$, $\slashed{\ell}^2=-\ell^2$, $\slashed{p}\slashed{\ell}+\slashed{\ell}\slashed{p}=0$ and $[\gamma_*,\slashed{\ell}]=0$, while $\{\gamma_*,\slashed{p}\}=0$. Moreover $\text{tr}(\gamma_\mu\gamma_\nu\gamma_*)=-2^{1+\frac{\delta}{2}}\epsilon_{\mu\nu}$. Working out the γ-matrix algebra and performing a Wick rotation $k_0\to ik_0$ one can compute the loop integral. Here, for simplicity, we report only the even parity part of the trace and the divergence of the e.m. tensor:

$$\widetilde{T}^{E\,\mu}_{\mu\lambda\rho}(k) = \frac{i}{192\pi}\left[k_\lambda k_\rho + k^2\eta_{\lambda\rho}\right]$$

(3.14)

and

$$k^\mu\widetilde{T}^E_{\mu\nu\lambda\rho}(k) = -\frac{i}{384\pi}\left[k_\nu k_\lambda k_\rho + \frac{1}{2}k^2\left(\eta_{\nu\lambda}k_\rho+\eta_{\nu\rho}k_\lambda\right)\right]$$

(3.15)

where k_μ denotes the Euclidean momentum (in particular $k^2=-\mathbf{k}^2$). Next one anti-Fourier-transforms these amplitudes and, after returning to the Minkowski background, inserts them into (3.1). To obtain the corresponding integrated cocycles, one multiplies the first by ω and saturates the second with ξ^ν and integrate over space-time. The result are the two cocycles

$$\Delta_\omega = \frac{1}{2}\int d^2x\,\omega(x)\int d^2y\,h^{\lambda\rho}(y)\langle 0|\mathcal{T}T^\mu_\mu(x)T_{\lambda\rho}(y)|0\rangle_c =$$

(3.16)

$$=2\int d^2x\,\omega(x)\int d^2y\,h^{\lambda\rho}(y)\int\frac{d^2k}{(2\pi)^2}\,e^{-ik\cdot(x-y)}\widetilde{T}^\mu_{\mu\lambda\rho}(k) =$$

$$= \frac{1}{96\pi}\int d^2x\,\omega(x)\left[\partial_\lambda\partial_\rho h^{\lambda\rho}(x)-\Box h^\lambda_\lambda(x)\right]$$

and

$$\Delta_\xi = -\frac{1}{2}\int d^2x\,\xi^\nu(x)\int d^2y\,h^{\lambda\rho}(y)(-ik^\mu)e^{-ik\cdot(x-y)}\widetilde{T}_{\mu\nu\lambda\rho}(k)$$

$$= \frac{1}{192\pi}\int d^2x\,\xi^\nu(x)\left[\partial_\nu\partial_\lambda\partial_\rho h^{\lambda\rho}(x)-\partial_\lambda\Box h^\lambda_\nu(x)\right]$$

(3.17)

Let us recall that the parameters ξ^μ and ω, according to the rule of BRST quantization, are promoted to anti-commuting fields. The lowest order transformation rules for the metric is $\delta_\omega^{(0)} h_{\mu\nu} = 2\omega\eta_{\mu\nu}$ and $\delta_\xi h_{\mu\nu} = \partial_\mu\xi_\nu + \partial_\nu\xi_\mu$. Using this it is easy to prove that

$$\delta_\omega^{(0)}\Delta_\omega = 0, \qquad \delta_\xi^{(0)}\Delta_\xi = 0, \qquad \delta_\omega^{(0)}\Delta_\xi + \delta_\xi^{(0)}\Delta_\omega = 0. \tag{3.18}$$

Both trace and diffeomorphism cocycles are non-vanishing. However the diffeomorphism one is trivial. For let us consider the local counterterm

$$\mathcal{C}^{(even)} = \frac{1}{384\pi} \int d^2x \left(h_\rho^\gamma(x)\partial_\lambda\partial_\nu h^{\lambda\rho}(x) - h_{\lambda\rho}(x)\Box h^{\lambda\rho}(x) \right) \tag{3.19}$$

It is easy to prove that

$$\Delta_\xi^{\prime(even)} \equiv \Delta_\xi^{(even)} + \delta_\xi^{(0)}\mathcal{C}^{(even)} = 0 \tag{3.20}$$

Therefore diffeomorphisms are conserved. On the other hand the overall even trace cocycle becomes

$$\Delta_\omega^{\prime(even)} \equiv \Delta_\omega^{(even)} + \delta_\omega^{(0)}\mathcal{C}^{(even)} = \frac{1}{48\pi} \int d^2x\, \omega \left[\partial_\lambda\partial_\rho h^{\lambda\rho} - \Box h_\lambda^\lambda \right] \tag{3.21}$$

So far we have computed the first term of (3.2). We have to compute also the second, i.e. the second one in (3.10). The corresponding amplitude, once regulated, takes the form

$$\widetilde{\widetilde{T}}^\mu{}_{\mu\lambda\rho}(k) = -\frac{1}{64} \int \frac{d^2p\, d^\delta\ell}{(2\pi)^{2+\delta}} \mathrm{tr} \left(\frac{\not{p}+\not{\ell}}{p^2-\ell^2} (2\not{p}+2\not{\ell}-\not{k}) \frac{\not{p}-\not{k}}{(p-k)^2-\ell^2}(2p-k)_\lambda\gamma_\rho \frac{1+\gamma_*}{2} \right) \tag{3.22}$$

A direct calculation shows that it vanishes. Therefore the trace anomaly is determined by (3.21), which is the first order approximation of

$$A_\omega^{(even)} = \frac{1}{48\pi} \int d^2x\, \sqrt{g}\, \omega\, R \tag{3.23}$$

3.2.1   Another prescription

The regularizing prescription (3.2) is not the only possibility. We could have started from

$$\widetilde{T}'_{\mu\nu\lambda\rho}(k) = -\frac{1}{64} \int \frac{d^2p}{(2\pi)^2} \mathrm{tr} \left(\frac{1}{\not{p}}(2p-k)_\mu\gamma_\nu \frac{1}{\not{p}-\not{k}}(2p-k)_\lambda\gamma_\rho \frac{1+\gamma_*}{2} \right). \tag{3.24}$$

and regularize it as follows

$$\widetilde{T}^{(reg)\prime}_{\mu\nu\lambda\rho}(k) = -\frac{1}{32} \int \frac{d^2p\, d^\delta\ell}{(2\pi)^{2+\delta}} \mathrm{tr} \left(\frac{1}{\not{p}+\not{\ell}}(2p-k)_\mu\gamma_\nu \frac{1}{\not{p}+\not{\ell}-\not{k}}(2p-k)_\lambda\gamma_\rho \frac{1+\gamma_*}{2} \right).$$

We shall refer to it is the rightmost γ_* prescription. The result is now

$$\widetilde{T}^{\prime E \mu}_{\mu \lambda \rho}(k) = \frac{i}{96\pi} \Big[k_\lambda k_\rho + k^2 \eta_{\lambda \rho} \Big] \tag{3.25}$$

and

$$k^\mu \widetilde{T}^E_{\mu \nu \lambda \rho}(k) = 0 \tag{3.26}$$

Contrary to the previous prescription this one yields diffeomorphism invariance and the same trace cocycle (3.21). It remains for us to evaluate the second term of (3.2). The corresponding regulated amplitude is

$$\widetilde{\widetilde{T}}^{\prime \mu}_{\mu \lambda \rho}(k) \stackrel{reg}{=} -\frac{1}{32} \int \frac{d^2 p \, d^\delta \ell}{(2\pi)^{2+\delta}} \mathrm{tr} \left(\frac{\not{p} + \not{\ell}}{p^2 - \ell^2} \, (2\not{p} + 2\not{\ell} - \not{k}) \, \frac{\not{p} + \not{\ell} - \not{k}}{(p-k)^2 - \ell^2} (2p - k)_\lambda \gamma_\rho \frac{1 + \gamma_*}{2} \right)$$

$$\tag{3.27}$$

which, again, vanishes. Therefore the two prescriptions lead, as expected, to the same result, the trace anomaly (3.23), while diffeomorphisms are conserved (as far as the even parity part is concerned.).

In this section we have illustrated an example (probably the simplest one) of a perfectly working cohomological mechanism: the first prescription leads both to a trace and a diffeomorphism anomaly; however the latter is trivial and can be eliminated with a counterterm, which in turn modifies the trace anomaly giving it the final (minimal) form. The second prescription preserves diffeomorphism invariance and yields the previous final form of the trace anomaly. In the next section we shall see an example in which this mechanism cannot work.

3.3   The problematic example

The example we consider in the sequel is that of a right-handed Weyl fermion coupled to a non-trivial metric. The action is (3.3) with $d = 4$, but in this case the spin connection does not drop out. One can write the action as follows

$$S = \int d^4 x \, \sqrt{|g|} \left[\frac{i}{2} \overline{\psi_R} \gamma^\mu \overleftrightarrow{\partial}_\mu \psi_R - \frac{1}{4} \epsilon^{\mu abc} \omega_{\mu ab} \overline{\psi_R} \gamma_c \gamma_5 \psi_R \right] \tag{3.28}$$

where it is understood that the derivative applies to ψ_R and $\overline{\psi_R}$ only. We have used the relation $\{\gamma^a, \Sigma^{bc}\} = i \, \epsilon^{abcd} \gamma_d \gamma_5$. We expand $g_{\mu\nu}$ and e^a_μ as before, and, accordingly

$$\omega_{\mu ab} \, \epsilon^{\mu abc} = -\epsilon^{\mu abc} \, \partial_\mu \chi_{a\lambda} \chi^\lambda_b + \dots \tag{3.29}$$

Proceeding as in the previous 2d example, after some algebra the action takes the form

$$S \approx \int d^4 x \left[\frac{i}{2} (\delta^\mu_a - \chi^\mu_a) \overline{\psi_L} \gamma^a \overleftrightarrow{\partial}_\mu \psi_L + \frac{1}{4} \epsilon^{\mu abc} \partial_\mu \chi_{a\lambda} \chi^\lambda_b \, \overline{\psi}_L \gamma_c \gamma_5 \psi_L \right]$$

from which we can extract the Feynman rules. The fermion propagator and fermion-fermion-graviton vertex (V_{ffg}) are the same as before. In addition we have a two-fermion-two-graviton vertex (V_{ffgg})

$$\frac{1}{64} t_{\mu\nu\mu'\nu'\kappa\lambda} (k - k')^{\lambda} \gamma^{\kappa} \frac{1 + \gamma_5}{2} \tag{3.30}$$

where

$$t_{\mu\nu\mu'\nu'\kappa\lambda} = \eta_{\mu\mu'} \epsilon_{\nu\nu'\kappa\lambda} + \eta_{\nu\nu'} \epsilon_{\mu\mu'\kappa\lambda} + \eta_{\mu\nu'} \epsilon_{\nu\mu'\kappa\lambda} + \eta_{\nu\mu'} \epsilon_{\mu\nu'\kappa\lambda} \tag{3.31}$$

and the graviton momenta k, k' are incoming. Other vertices are irrelevant for the sequel.

This model has no even- nor odd-parity diffeomorphism anomalies, while it has both even and, as we shall see, odd-parity trace anomalies. The even part works much in the same way as in the previous 2d example. Our interest in this section is focused on the odd parity part. It is well-known that in 4d there cannot be odd-parity consistent diffeomorphism anomalies, but a priori we cannot exclude other (trivial) anomalies related to the trace anomalies (much like the (3.17) above). Therefore we have to verify that odd-parity divergence of the e.m. tensor vanishes. The relevant lowest order contribution (which we denote symbolically by $\langle \partial \cdot TTT \rangle$) may come from a triangle and a bubble diagram. The triangle diagram contains three fermion propagators and three V_{ffg} vertices. Taught by the 2d example we use the rightmost $\gamma_* \equiv \gamma_5$ prescription. The corresponding Fourier-transformed contribution after regularization is

$$q^{\mu} \widetilde{T}_{\mu\nu\lambda\rho\alpha\beta}^{(odd)}(k_1, k_2) = -\frac{1}{512} \int \frac{d^4 p \, d^{\delta} \ell}{(2\pi)^{4+\delta}} \, \mathrm{tr} \left[\left(\frac{\not{p} + \not{\ell}}{p^2 - \ell^2} (2p - k_1)_{\lambda} \gamma_{\rho} \, \frac{\not{p} - \not{k}_1 + \not{\ell}}{(p - k_1)^2 - \ell^2} \right. \right.$$

$$\left. \left. \times (2p - 2k_1 - k_2)_{\alpha} \gamma_{\beta} \, \frac{\not{p} - \not{q} + \not{\ell}}{(p - q)^2 - \ell^2} \left((2p - q) \cdot q \, \gamma_{\nu} - (2p - q)_{\nu} \not{q} \right) \right) \gamma_5 \right]$$

It is not difficult to show that it vanishes identically. Also the contribution from the bubble diagram, constructed with one V_{ffg}, one V_{ffgg} and two propagators, vanishes. Therefore we conclude that with this prescription diffeomorphisms are exactly preserved.

We next compute the odd parity contribution of the triangle and bubble diagram to the trace anomaly. At first sight this calculation does not seem to make sense, because a well known result of CFT claims that a conformal odd-parity three-point function $\langle 0| \mathcal{T} T_{\mu\nu}(x) T_{\mu'\nu'}(y) T_{\alpha\beta}(z) |0 \rangle^{(odd)}$ vanishes identically for algebraic reasons. This is confirmed by a direct calculation. In fact one can prove that, with both prescriptions above, $\langle 0| \mathcal{T} T_{\mu\nu}(x) T_{\mu'\nu'}(y) T_{\alpha\beta}(z) |0 \rangle^{(odd)}$ vanishes. So, at the lowest significant perturbative order, we can write:

$$\eta^{\mu\nu} \langle\!\langle T_{\mu\nu}(x) \rangle\!\rangle^{(odd)} = 0 \tag{3.32}$$

However according to the definition (3.2) we must compute also the second term with one insertion of a trace of the e.m. tensor (which we denote by $\langle tTT \rangle$). The

triangle diagram gives

$$\widetilde{T}_{\mu\nu\mu'\nu'}(k_1, k_2)= \tag{3.33}$$

$$= -\frac{1}{256} \int \frac{d^4p}{(2\pi)^4} \int \frac{d^\delta\ell}{(2\pi)^\delta} \text{Tr} \left\{ \frac{\not{p}+\not{\ell}}{p^2-\ell^2} \left[(2p-k_1)_\mu \gamma_\nu + (\mu \leftrightarrow \nu) \right] \frac{(\not{p}+\not{\ell}-\not{k}_1)}{(p-k_1)^2-\ell^2} \right.$$

$$\times [(2p-2k_1-k_2)_{\mu'}\gamma_{\nu'} + (\mu' \leftrightarrow \nu')] \frac{(\not{p}+\not{\ell}-\not{k}_1-\not{k}_2)}{(p-k_1-k_2)^2-\ell^2}(2\not{p}+2\not{\ell}-\not{k}_1-\not{k}_2)\left.\left(\frac{1+\gamma_5}{2}\right)\right\}.$$

$$\tag{3.34}$$

which, with the addition of the cross diagram, leads to the following result

$$\widetilde{T}_{\mu\nu\mu'\nu'}(k_1, k_2) = \frac{1}{6144\pi^2} k_1^\alpha k_2^\beta \left(\left(k_1^2 + k_2^2 + k_1 \cdot k_2\right) t_{\mu\nu\mu'\nu'\alpha\beta} - t^{(21)}_{\mu\nu\mu'\nu'\alpha\beta} \right),$$
$$\tag{3.35}$$

where

$$t^{(21)}_{\mu\nu\mu'\nu'\kappa\lambda} = k_{2\mu}k_{1\mu'}\epsilon_{\nu\nu'\kappa\lambda} + k_{2\nu}k_{1\nu'}\epsilon_{\mu\mu'\kappa\lambda} + k_{2\mu}k_{1\nu'}\epsilon_{\nu\mu'\kappa\lambda} + k_{2\nu}k_{1\mu'}\epsilon_{\mu\nu'\kappa\lambda}$$

$$\tag{3.36}$$

The contribution from the bubble diagram vanishes.

The conclusion of this computation is that the contribution to the odd-parity trace anomaly according to formula (3.2) comes solely from (3.35).

To simplify the derivation we set the external lines on-shell, $k_1^2 = k_2^2 = 0$. This requires a comment.

On shell conditions Putting the external lines on shell means that the corresponding fields have to satisfy the EOM of Einstein-Hilbert gravity $R_{\mu\nu} = 0$. In the linearized form this means

$$\Box\chi_{\mu\nu} = \partial_\mu\partial_\lambda\chi_\nu^\lambda + \partial_\nu\partial_\lambda\chi_\mu^\lambda - \partial_\mu\partial_\nu\chi_\lambda^\lambda = 0 \tag{3.37}$$

We also choose the De Donder gauge: $\Gamma^\lambda_{\mu\nu}g^{\mu\nu} = 0$, which at the linearized level becomes $2\partial_\mu\chi_\lambda^\mu - \partial_\lambda\chi_\mu^\mu = 0$. In this gauge (3.37) becomes

$$\Box\chi_{\mu\nu} = 0 \tag{3.38}$$

In momentum space this implies that $k_1^2 = k_2^2 = 0$. We remark that this does not trivially disrupt the cohomology, but define a restricted cohomology of the diffeomorphisms and the Weyl transformations: the latter is defined up to terms $\Box h_{\mu\nu}$ and $\Box\xi^\mu$. This is a well defined cohomology, under which we have, in particular,

$$\delta_\xi \left(2\partial_\mu\chi_\lambda^\mu - \partial_\lambda\chi_\mu^\mu \right) = 2\,\Box\xi_\lambda \approx 0 \tag{3.39}$$

i.e. in this restricted cohomology the De Donder gauge fixing is irrelevant. Similarly, the term corresponding in momentum space to $k_1^\alpha k_2^\beta \left(k_1^2 + k_2^2\right)t_{\mu\nu\mu'\nu'\alpha\beta}$

remains null after a restricted diffeomorphism transformation. The restricted co-homology has the same odd class (the Pontryagin one) as the unrestricted one, i.e. it completely determines it (this is not true for the even classes). Since we know that the final result must be covariant and that there is no covariant extension to all order of the term $k_1^\alpha k_2^\beta (k_1^2 + k_2^2) t_{\mu\nu\mu'\nu'\alpha\beta}$, the simplification of considering it null does not jeopardize it. This means that this term must be trivial in some way. We will comment on this below.

Overall contribution The overall one-loop contribution to the trace anomaly in momentum space, *as far as the parity violating part is concerned*, is given by (3.35). After returning to the Minkowski metric and Fourier-antitransforming it, we can extract the local expression of the trace anomaly, by replacing the results found so far in (3.1). The result, to lowest order, is

$$\langle\!\langle T_\mu^\mu(x) \rangle\!\rangle^{(odd)} \approx \frac{i}{768\pi^2} \epsilon^{\mu\nu\lambda\rho} \left(\partial_\mu \partial_\sigma h_\nu^\tau \partial_\lambda \partial_\tau h_\rho^\sigma - \partial_\mu \partial_\sigma h_\nu^\tau \partial_\lambda \partial^\sigma h_{\tau\rho} \right) \quad (3.40)$$

Since

$$\epsilon^{\mu\nu\lambda\rho} R_{\mu\nu}{}^{\sigma\tau} R_{\lambda\rho\sigma\tau} = \epsilon^{\mu\nu\lambda\rho} \left(\partial_\mu \partial_\sigma \chi_\nu^a \partial_\lambda \partial_a \chi_\rho^\sigma - \partial_\mu \partial_\sigma \chi_\nu^a \partial_\lambda \partial^\sigma \chi_{a\rho} \right) + ... \quad (3.41)$$

we obtain

$$\langle\!\langle T_\mu^\mu(x) \rangle\!\rangle^{(odd)} = \frac{i}{768\pi^2} \frac{1}{2} \epsilon^{\mu\nu\lambda\rho} R_{\mu\nu}{}^{\sigma\tau} R_{\lambda\rho\sigma\tau} \quad (3.42)$$

Now applying the definion (3.2) and recalling (3.32), we obtain the covariant expression of the parity violating part of the trace anomaly for a Weyl fermion

$$T[g](x) = \frac{i}{768\pi^2} \frac{1}{2} \epsilon^{\mu\nu\lambda\rho} R_{\mu\nu}{}^{\sigma\tau} R_{\lambda\rho\sigma\tau}. \quad (3.43)$$

3.3.1   The missing mechanism

The trace anomaly (3.43) coincides (up to a coefficient) with the KDS (Kimura-Delbourgo-Salam) anomaly of the chiral current in a theory of Dirac fermions immersed in a non-trivial metric background. In [6] this coincidence has been ex-plained. Therefore, is everything ok? No, because the term $k_1^\alpha k_2^\beta (k_1^2 + k_2^2) t_{\mu\nu\mu'\nu'\alpha\beta}$ we have disregarded has not been explained yet, and the attempt to explain it reveals an unexpected obstacle. It corresponds to an integrated anomalous term $\sim \int d^4x\, \omega\, \epsilon^{\mu\nu\lambda\rho} \partial_\mu \Box h_\nu^\alpha \partial^\lambda h_{\mu\alpha}$. There is no covariant expression that to the low-est order has this form. Therefore it must be a trivial term. Such a lowest order cocycle can be canceled by a counterterm $\sim \int d^4x\, h_\mu^\mu \epsilon^{\mu\nu\lambda\rho} \partial_\mu \Box h_\nu^\alpha \partial^\lambda h_{\mu\alpha}$. But this counterterm term destroys diffeomorphism invariance. There seems to be no way out.

Before surrendering, one may try to change the regularization prescription. For instance we might use the first prescription of the previous section. It is easy to see that with this new prescription diffeomorphisms are still conserved, as one can directly verify (and as it should be, because of the general theorem in [11]).

But the trace anomaly changes, both in its form and in its overall coefficient (even the bubble diagram gives a nontrivial contribution). This is a puzzle. We have seen above an example, but many others can be envisaged, where, after some calculations, nonzero trace anomalies and nonzero diffeomorphism anomalies appear in couples, and (unless the the diffeomorphism anomaly is non-trivial, which is not possible in 4d) by subtracting a counterterm we can recover diffeomorphism invariance and modify the trace anomaly to a minimal form. In other words diffeomorphism invariance plays a 'repairing' or 'stabilizing' role in cohomology. I.e. the diffeomorphism cohomology accompanies the regularization scheme in such a way that the latter preserves the cohomology class. However a necessary condition for this role to be effective is that the relevant amplitude be non-vanishing. Which is not what happens in our puzzling case. *In fact, the true origin of the puzzle is not the regularization scheme, but the accidental vanishing of the odd three-point function of the e.m. tensor.*

The next question is: does that mean that the perturbative calculation of the trace anomaly is impossible? The answer is: no, it is only more difficult. In our particular case the problem arises from the vanishing of the odd three-point function of the e.m. tensor. However the three-point function corresponds to the lowest possible order yielding a significant contribution to the calculation of the trace anomaly. But of course one should consider also the four-point function, the five-point function, and so on. In general there is no such accidental vanishing for the higher order functions. Therefore we should calculate, for instance, the odd four-point function of the energy-momentum tensor and compute both the trace and the divergence in the same way we have done for the three-point function. In this way the stabilizing effect of diffeomorphisms (together with the possible contribution of other graphs, such as the bubble one) would unfold undisturbed. The trouble here is the technical complexity. There is an easier way: a non-perturbative approach. Appropriate non-perturbative methods exist, they are the Seeley-Schwinger-DeWitt or heat kernel methods: the diffeomorphism invariance is inbuilt in them and, being non-perturbative, they encompass all the relevant higher order amplitudes. The relevant calculations have been carried out in [8] and more recently in [12] using a method à la Fujikawa. The two calculations lead to the same result, eq.(3.43), which is also in accord with the general formulas of [9].

Remark It is worth pointing out that a missing contribution from the perturbative calculation of an anomaly, such as the one we have come across above, is not rare. Let us consider, for instance, the (multiplet) non-Abelian covariant anomaly $\sim \epsilon^{\mu\nu\lambda\rho}\mathrm{tr}(T^a F_{\mu\nu}F_{\lambda\rho})$, which appears in the divergence of the chiral current in a theory of Dirac fermions coupled to a vector potential $V_\mu = V_\mu^a T^a$ (with curvature $F_{\mu\nu}$). This anomaly contains a quartic term in the potential $V_\mu = V_\mu^a T^a$, which can come only from a pentagon diagram. This diagram however is UV convergent. Therefore the quartic term cannot be produced through a perturbative calculation. It is nevertheless required by the conservation of the vector current in order to guarantee the invariance of the vector gauge symmetry (which plays a role analogous to the diffeomorphisms in solving the above puzzle).

3.4   Conclusions

The calculations for the odd-parity trace anomaly have led to controversial results, both with pertubative and non-perturbative methods. But while the non-perturbative approaches, if correctly employed, lead to unambiguous results, [8, 12], and some disagreements can be attributed to inappropriate methods of calculation (see [10] for a discussion), the perturbative ones are intrinsically ambiguous for the reason explained in the previous section. These encompass the perturbative derivations in [5–7, 12, 13]. As explained before the derivation of a trace anomaly is more complicated than the derivation of the more familiar chiral anomalies and involves the resolution of several ambiguities. The first ambiguity is related to the divergent integrals in the Feynman diagrams: it is resolved by a choice of regularization scheme. The second ambiguity lies in the very definition of the trace anomaly and is resolved by formula (3.2): as explained in [4] this formula selects the very violation of the equation of motion while excluding other irrelevant contributions. The third ambiguity is related to cohomology: there is no such thing as a trace anomaly unrelated to diffeomorphisms and other symmetries of the theory. A trace anomaly is a cocycle of the full symmetry of the theory. When we compute a trace anomaly we must make sure that no other symmetry is violated. Any mis-resolution of these ambiguities may lead to wrong results. For instance, if we compute only the first term in the definition (3.2) the odd parity trace anomaly disappears. Another example: it is always possible to find a counterterm that completely cancels the lowest order odd-parity trace anomaly, but it inevitably breaks diffeomorphism invariance.

The calculations in [5–7, 12] were made by resolving such ambiguities. But, as far as the odd-parity trace anomaly is concerned, there is a fourth ambiguity generated by the vanishing of the odd three-point amplitude of the e.m. tensor. As shown above this implies a dependence of the end result on the regularization scheme. As we have pointed out above, this ambiguity cannot be resolved within the lowest perturbative order, so that this problem is undecidable without going to higher orders of approximation or resorting to non-perturbative methods. Why the perturbative derivations of [5–7, 12] lead anyhow to the correct result is still to be explained.

At this point better avoid any misunderstanding. The true trace anomaly is given by (3.43). The aim of this note is to point out only the ambiguity of its lowest order perturbative derivation. Another example of the type considered before is related to the odd parity trace anomaly induced by a gauge field, a case recently re-examined in [14]. This is because the odd part of correlators $< TJJ >$ vanishes identically, just like the odd part of $< TTT >$. In this case there is no need to restrict the cohomology and, anyhow, an appropriate, and quite simple, non-perturbative approach unambiguously leads to a non-vanishing gauge induced trace anomaly, see [4]. But since in the literature on odd-parity trace anomalies is not univocal, it is worth pointing out that beside the explicit calculations there are also qualitative arguments. To emd this note we would like to briefly recall them. The first is based on the family's index theorem, [17]. This theorem can be thought of as expressing the obstructions to the existence of the inverse of the kinetic Dirac-

Weyl operator. Any variation of the path integral of the theory defined by the action (3.3), for instance in order to see its response under a Weyl transformation, inevitably involves such an inverse, i.e. the (full) fermion propagator. The relevant obstructions are expressed in terms of cohomological classes of the classifying space. Among them there are classes that give rise to the well-known chiral consistent anomalies, but in 4d there are also the Pontryagin and Chern classes. The latter are naturally associated to the trace anomaly, generated by the coupling to a background metric or a background gauge field, respectively. The second argument is more 'phenomenological': the Pontryagin class or the Chern class densities have the right properties and quantum numbers to couple to trace of the e.m. of a system such as (3.3), which violates parity. The experience teaches us that in such cases quantization usually excites such terms (with non vanishing coefficients). The only exceptions may come from (vector) gauge invariance and diffeomorphism invariance. But in this case the latter is satisfied with a non-vanishing Pontryagin term. So the pertinent question would rather be: why should it vanish?

References

1. D. M. Capper and M. J. Duff, *Trace Anomalies in Dimensional Regularization*, Nuovo Cim. **23 A** (1974) 173. *Conformal anomalies and the renormalizability problem in quantum gravity*, Phys. Lett. **53 A** (1975) 361.

2. M. J. Duff, *Twenty years of the Weyl anomaly*, Class. Quant. Grav. **11** (1994) 1387 [hep-th,9308075].

3. M. J. Duff, *Weyl, Pontryagin, Euler, Eguchi and Freund* , Jour. Phys. A: Mathematical and Theoretical, **53** (2020) 301001 [arXiv:2006.03574].

4. L.Bonora, *Perturbative and Non-Pertrubative Trace Anomalies*, Symmetry **13** (2021) 7, 1292. e-Print: 2107.07918 [hep-th]

5. L. Bonora, S. Giaccari and B. Lima de Souza, *Trace anomalies in chiral theories revisited*, JHEP **1407** (2014) 117 [arXiv:1403.2606 [hep-th]].

6. L. Bonora, A. D. Pereira and B. L. de Souza, *Regularization of energy-momentum tensor correlators and parity-odd terms*, JHEP **1506**, 024 (2015) [arXiv:1503.03326 [hep-th]].

7. L. Bonora, M. Cvitan, P. Dominis Prester, A. Duarte Pereira, S. Giaccari and T. Štemberga, *Axial gravity, massless fermions and trace anomalies*, Eur. Phys. J. C **77** (2017) 511 [arXiv:1703.10473 [hep-th]].

8. L. Bonora, M. Cvitan, P. Dominis Prester, S. Giaccari, M. Paulisic and T. Stemberga, *Axial gravity: a non-perturbative approach to split anomalies*, Eur. Phys. J. C **78** (2018) 652 [arXiv:1807.01249].

9. M. J. Duff and P. van Nieuwenhuizen, *Quantum inequivalence of different field representations*, Phys.Lett. 94B (1980) 179.

10. L. Bonora and R. Soldati, *On the trace anomaly for Weyl fermions*, [arXiv:arXiv:1909.11991[hep-th]], and references therein.

11. A. Zhiboedov, *A note on three-point functions of conserved currents*, arXiv:1206.6370 [hep-th].
    S. Jain, R. R. John, A. Mehta, A. A. Nizami and A. Suresh, *Momentum space parity-odd CFT 3-point functions*, JHEP **08** (2021) 089; e-Print: 2101.11635 [hep-th]

12. Chang-Yong Liu, *Investigation of Pontryagin trace anomaly using Pauli-Villars regularization*, arXiv:2202.13893 [hep-th]

13. S. Abdallah, S. A. Franchino-Viñas and M. B. Fröb, *Trace anomaly for Weyl fermions using the Breitenlohner-Maison scheme for γ^**, JHEP **03** (2021) 271 (2021) [arXiv:2101.11382 [hep-th]].

14. F. Bastianelli and L. Chiese, *Chiral fermions, dimensional regularization, and the trace anomaly* , arXiv:2203.11668 [hep-th].

15. R.Delbourgo and A.Salam *PCAC anomalies and Gravitation* preprint IC/72/86.

16. T. Kimura, *Divergence of Axial-Vector Current in the Gravitational Field*, Prog. Theor. Phys. **42** (1969) 1191.
    R.Delbourgo and A.Salam *The gravitational correctioin to PCAC*, Phys.Lett. **40B** (1972) 381.

17. M.F. Atiyah and I.M. Singer, *Dirac operators coupled to vector potentials*, Proc. Nat. Acad. Sci. **81** (1984), 2597.

BLED WORKSHOPS
IN PHYSICS
VOL. 23, NO. 1

Proceedings to the 25th [Virtual]
Workshop
What Comes Beyond . . . *(p. 45)*
Bled, Slovenia, July 4–10, 2022

4   Maximally Precise Tests of the Standard Model: Elimination of Perturbative QCD Renormalization Scale and Scheme Ambiguities

S. J. Brodsky
e-mail: sjbth@slac.stanford.edu

SLAC National Accelerator Laboratory, Stanford University

Abstract. The Principle of Maximum Conformality (PMC) systematically and rigorously eliminates order by order the renormalization scale and scheme ambiguities of perturbative QCD predictions, a topic central and crucial for testing the Standard Model to high precision. The QCD running coupling $\alpha_s(q^2)$ is defined to sum all β terms of a pQCD series as required by renormalization group invariance. The PMC thus generalizes the standard Gell-Mann Low scale-setting procedure for high precision tests of QED, where all vacuum polarization contributions are summed into the QED running coupling. The resulting series for pQCD matches the corresponding conformal theory, thus eliminating the non-convergent n-factorial renormalon growth of pQCD. The PMC predictions agree with QED scale-setting in the Abelian limit: PMC scale setting satisfies the property that calculations in QCD with N_C colors must analytically match those of Abelian QED theory in the $N_C \to 0$ limit. The PMC is also the theoretical principle underlying commensurate scale relations between observables which are independent of the choice of renormalization scheme. The number of active flavors n_f in the QCD β function is also correctly determined. It also satisfies the requirement that one must use the same scale-setting procedure in all sectors of a Grand-Unified Theory of QED, electroweak, and QCD interactions. I will also review a number of successful PMC predictions.

Keywords: renormalization scale setting, principle of maximum conformality, light-front holography, color confinement, QCD running coupling at all scales, Abelian limit.

4.1   Renormalization Scale Setting

It has become conventional to simply guess the renormalization scale and choose an arbitrary range of uncertainty when making perturbative QCD (pQCD) predictions. However, this *ad hoc* assignment of the renormalization scale and the estimate of the size of the resulting uncertainty leads to anomalous renormalization scheme-and-scale dependences. A valid perturbative prediction for any physical observable must be independent of the initial choices of the renormalization scale and the renormalization scheme; this is the central property of *renormalization group invariance* (RGI) [1–5]. In fact, relations between physical observables must be

independent of the theorist's choice of the renormalization scheme and the renormalization scale in any given scheme at any given order of pQCD. The *Principle of Maximum Conformality* (PMC) [6–8], which generalizes the conventional Gell-Mann-Low method [9] for scale-setting in perturbative QED to non-Abelian QCD, provides a rigorous method for achieving unambiguous scheme-independent, fixed-order predictions for observables consistent with the principles of the renormalization group. The resulting renormalization scale of the running coupling reflects the physics of the underlying quark and gluon subprocess.

A key problem in making precise perturbative QCD predictions has been the uncertainty in determining the renormalization scale μ of the running coupling $\alpha_s(\mu^2)$. The purpose of the running coupling in any gauge theory is to sum all terms involving the β function; in fact, when the renormalization scale is set properly, all non-conformal $\beta \neq 0$ terms in a perturbative expansion arising from renormalization are summed into the running coupling. The remaining terms in the perturbative series are then identical to that of a conformal theory; i.e., the corresponding theory with $\beta = 0$.

The above discussion was the motivation for the BLM (Brodsky-Lepage-Mackenzie) [10] procedure for QCD scale-setting at lowest order. The BLM procedure is generalized to all orders by using the PMC (the Principle of Maximum Conformality [6–8]. The PMC scale-setting procedure sets the renormalization scale $\alpha_s(Q_{\mathrm{PMC}}^2)$ at every order by absorbing the β terms appearing in the pQCD series. The resulting pQCD series thus the matches the corresponding conformal series with all β terms set to 0. The problematic $n!$"renormalon" divergence of a pQCD series associated with the nonconformal terms does not appear in the conformal series, and the conformal series is independent of the theorist's choice of renormalization scheme. This also means that relations between any two perturbatively calculable observables are scheme-independent. These relations are called "commensurate scale relations" [11]. There are no renormalization scale-setting ambiguities for precision tests of quantum electrodynamics. The scale of the QED running coupling at each order of the perturbative QED series is set to absorb all vacuum polarization diagrams; i.e. the β terms. The coefficients in the pQED series then matches the conformal theory; i.e. the corresponding perturbative series with $\beta = 0$. This defines the standard Gell-Mann-Low scale-setting procedure for high precision tests of QED, where all vacuum polarization contributions are summed into the QED running coupling. (For a review, see ref [12]). The same scale-setting procedure applies to the $SU(2) - U(1)$ theory of the electroweak interactions. [14]

An important analytic property of non-Abelian QCD with N_C colors is that it must agree analytically with Abelian QED in the $N_C \rightarrow 0$ limit, at fixed $\hat{\alpha}_s = C_F \alpha_s$ and fixed $\hat{n}_f = T \frac{n_f}{C_F}$ with $C_F = \frac{N_C^2 - 1}{2N_C}$ and $T - 1/2$. This is the "Abelian correspondence principle." [13] Thus the setting of the renormalization scale in QCD must agree with Gell-Mann-Low scale setting for QED in the $N_C \rightarrow 0$ limit. This analytic requirement is satisfied by the PMC. The PMC also satisfies the requirement that one must use the same scale-setting procedure in all sectors of a Grand-Unified Theory of QED, the electroweak interactions, and QCD [15].

As in QED, the renormalization scale in the PMC is fixed such that all β non-conformal terms are systematically eliminated from the perturbative series and

are resummed into the running coupling; this procedure results in a convergent, scheme-independent conformal series without factorial renormalon divergences. The resulting scale-fixed predictions relating physical observables using the PMC are thus *independent of the choice of renormalization scheme* – a key requirement of renormalization group invariance. The PMC predictions are also independent of the choice of the *initial* renormalization scale μ_0. Since the PMC sums all of the non-conformal terms associated with the QCD β function, it provides a rigorous method for eliminating renormalization scale ambiguities in quantum field theory. Predictions based on PMC scale setting also satisfy the self-consistency conditions of the renormalization group, including reflectivity, symmetry and transitivity [21]. The resulting PMC predictions thus satisfy all of the basic requirements of RGI.
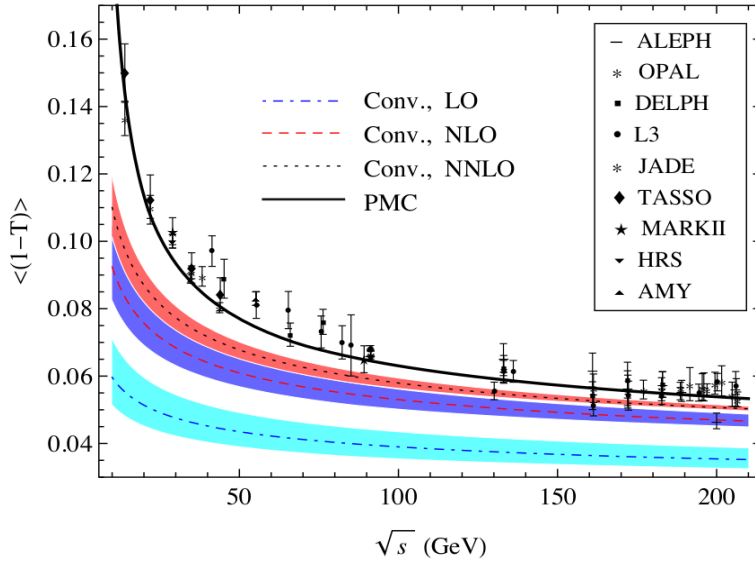
Fig. 4.1: The thrust mean value $\langle(1-T)\rangle$ for three-jet events versus the center-of-mass energy $\sqrt{s}$ using the conventional (Conv.) and PMC scale settings [42]. The dot-dashed, dashed and dotted lines are the conventional results at LO, NLO and NNLO, respectively. The solid line is the PMC result. The PMC prediction eliminates the renormalization scale μ uncertainty. The bands for theoretical predictions are obtained by varying $\mu \in [\sqrt{s}/2, 2\sqrt{s}]$. The experimental data points are taken from the ALEPH, DELPH, OPAL, L3, JADE, TASSO, MARKII, HRS and AMY experiments

.

The transition scale between the perturbative and nonperturbative domains of QCD can also be determined by using the PMC [17, 22–24], thus providing a procedure for setting the "factorization" scale for pQCD evolution. The running

coupling resums all of the $\{\beta_i\}$-terms by using the PMC, which naturally leads to a more convergent and renormalon-free pQCD series.

In more detail: the PMC scales are determined by applying the RGE of the QCD running coupling. By recursively applying the RGE one establishes a perturbative β-pattern at each order in a pQCD expansion. For example, the usual scale-displacement relation for the running couplings at two different scales Q_1 and Q_2 can be deduced from the RGE, which reads

$$
\begin{aligned}
a_{Q_2} = a_{Q_1} &- \beta_0 \ln\left(\frac{Q_2^2}{Q_1^2}\right) a_{Q_1}^2 + \left[\beta_0^2 \ln^2\left(\frac{Q_2^2}{Q_1^2}\right) - \beta_1 \ln\left(\frac{Q_2^2}{Q_1^2}\right)\right] a_{Q_1}^3 \\
&+ \left[-\beta_0^3 \ln^3\left(\frac{Q_2^2}{Q_1^2}\right) + \frac{5}{2}\beta_0\beta_1 \ln^2\left(\frac{Q_2^2}{Q_1^2}\right) - \beta_2 \ln\left(\frac{Q_2^2}{Q_1^2}\right)\right] a_{Q_1}^4 + \left[\beta_0^4 \ln^4\left(\frac{Q_2^2}{Q_1^2}\right)\right. \\
&\left. - \frac{13}{3}\beta_0^2\beta_1 \ln^3\left(\frac{Q_2^2}{Q_1^2}\right) + \frac{3}{2}\beta_1^2 \ln^2\left(\frac{Q_2^2}{Q_1^2}\right) + 3\beta_2\beta_0 \ln^2\left(\frac{Q_2^2}{Q_1^2}\right) - \beta_3 \ln\left(\frac{Q_2^2}{Q_1^2}\right)\right] a_{Q_1}^5 + \cdots,
\end{aligned}
$$

(4.1)

where $a_{Q_i} = \alpha_s(Q_i)/\pi$, the functions $\beta_0, \beta_1, \cdots$ are generally scheme dependent, which correspond to the one-loop, two-loop, $\cdots$, contributions to the RGE, respectively. The PMC utilizes this perturbative β-pattern to systematically set the scale of the running coupling at each order in a pQCD expansion.

The coefficients of the $\{\beta_i\}$-terms in the β-pattern can be identified by reconstructing the "degeneracy relations" [7, 8] among different orders. The degeneracy relations, which underly the conformal features of the resultant pQCD series by applying the PMC, are general properties of a non-Abelian gauge theory [25]. The PMC prediction achieved in this way resembles a skeleton-like expansion [34, 35]. The resulting PMC scales reflect the virtuality of the amplitudes relevant to each order, which are physical in the sense that they reflect the virtuality of the gluon propagators at a given order, as well as setting the effective number (n_f) of active quark flavors. The momentum flow for the process involving three-gluon vertex can be determined by properly dividing the total amplitude into gauge-invariant amplitudes [19]. Specific values for the PMC scales are computed as a perturbative expansion, so they have small uncertainties which can vary order-by-order. The PMC scales and the resulting fixed-order PMC predictions are to high accuracy independent of the initial choice of renormalization scale, e.g. the residual uncertainties due to unknown higher-order terms are negligibly small because of the combined suppression effect from both the exponential suppression and the α_s-suppression [7, 8].

When one applies the standard PMC procedures, different scales generally appear at each order; this is called the PMC multi-scale approach which often requires considerable theoretical analysis. To make the PMC scale-setting procedure simpler and more easily to be automatized, a single-scale approach (PMC-s), which achieves many of the same PMC goals, has been suggested in Ref. [16]. This method effectively replaces the individual PMC scale at each order by a single (effective) scale in the sense of a mean value theorem; e.g., it can be regarded as a weighted average of the PMC scales at each order derived under PMC multi-scale approach. The PMC-s inherits the main features of the multi-scale approach; for

example, its predictions are scheme independent, and the pQCD convergence is greatly improved due to the elimination of divergent renormalon terms.The single "PMC-s" scale shows stability and convergence with increasing order in pQCD, as observed by the e^+e^- annihilation cross-section ratio R_{e+e-} and the Higgs decay-width $\Gamma(H \to b\bar{b})$, up to four-loop level. Moreover, its predictions are again explicitly independent of the choice of the initial renormalization scale. Thus the PMC-s approach, which involves a simpler analysis, can be adopted as a reliable substitute for the PMC multi-scale approach, especially when one does not need detailed information at each order. We have given a detailed comparison of these two PMC approaches by comparing their predictions for three important quantities R_{e+e}, R_τ and $\Gamma_{H \to b\bar{b}}$ up to four-loop pQCD corrections [6]. The numerical results show that the single-scale PMCs method, which involves a somewhat simpler analysis, can serve as a reliable substitute for the full multi-scale PMCm method, and that it leads to more precise pQCD predictions with less residual scale dependence.

There are also cases in which additional momentum flows occur, whose scale uncertainties can also be eliminated by applying the PMC. For example, there are two types of log terms, $\ln(\mu/M_Z)$ and $\ln(\mu/M_t)$ [26–30], for the axial singlet r_S^A of the hadronic Z decays. By applying the PMC, one finds the optimal scale is $Q^{AS} \simeq 100$ GeV [32], indicating that the typical momentum flow for r_S^A is closer to M_Z than M_t. The PMC can also be systematically applied to multi-scale problems. The typical momentum flow can be distinct; thus, one should apply the PMC separately in each region. For example, two optimal scales arise at the N^2LO level for the production of massive quark-anti-quark pairs $(Q\bar{Q})$ close to threshold [33], with one being proportional to $\sqrt{\hat{s}}$ and the other to $v\sqrt{\hat{s}}$, where v is the Q and $\bar{Q}$ relative velocity. The PMC thus greatly improves the reliability and precision of QCD predictions at the LHC and other colliders [6] and greatly increases the sensitivity of experiments at the LHC to new physics beyond the Standard Model.

4.1.1   An overview of PMC renormalization-scale setting

The PMC procedure follows these steps

- First, we perform a pQCD calculation of an observable by using general regularization and renormalization procedures at an arbitrary initial renormalization scale μ and by taking any renormalization scheme. The initial renormalization scale can be arbitrarily chosen, which only needs to be large enough ($\mu >> \Lambda_{QCD}$) to ensure the reliability of the perturbative calculation. One may choose the renormalization scheme to be the usually adopted $\overline{MS}$-scheme; after applying the PMC, the final pQCD prediction will be shown to be independent to this choice, since the PMC is consistent with RGI.
- Second, we identify the non-conformal $\{\beta_i\}$-terms in the pQCD series. This can be achieved with the help of the degeneracy relations among different orders [7, 8], which identify which terms in the pQCD series are associated with the RGE and which terms are not.
  By using the displacement relation for the running coupling at any two scales, e.g. Eq.(4.1), one can obtain the general pattern of the $\{\beta_i\}$-terms at each order,

which naturally implies the wanted degeneracy relations among different terms; e.g., the coefficients for $\beta_0 a_\mu^2$, $\beta_1 a_\mu^3$, $\cdots$, $\beta_i a_\mu^{i+2}$ are the same. It has been demonstrated that the degeneracy relations hold using any renormalization scheme [25]. The dimensional-like $\mathcal{R}_\delta$-scheme provides a natural explanation of the degeneracy relations which are general properties of the non-Abelian gauge theory and underly the resulting conformal features of the pQCD series. Alternatively, one can use the δ dependence of the series to identify the $\{\beta_i\}$-terms [8]. One can also rearrange all the perturbative coefficients, which are usually expressed as an n_f-power series, into $\{\beta_i\}$-terms or non-$\{\beta_i\}$-terms. One needs to be careful using this method to ensure that the UV-free light-quark loops are not related to the $\{\beta_i\}$-terms; they should be identified as conformal terms and should be kept unchanged when doing the $n_f \to \{\beta_i\}$ transformation. The separation of UV-divergent and UV-free terms is very important. This fact has already been shown in QED case, in which electron-loop light-by-light contribution to the sixth-order muon anomalous moment is sizable but UV-free and should be treated as conformal terms [41]. There are many examples for the QCD case. For example, by carefully dealing with the UV-free light-by-light diagrams at the N^2LO level, the resulting PMC prediction agrees with the BaBar measurements within errors, thus provides a solution for the $\gamma\gamma^* \to \eta_c$ form factor puzzle [39].

In practice, one can also apply the PMC by directly dealing with the n_f-power series without transforming them into the $\{\beta_i\}$-terms [40]. This procedure is based on the observation that one can rearrange all the Feynman diagrams of a process in form of a cascade; i.e., the "new" terms emerging at each order can be equivalently regarded as a one-loop correction to all the "old" lower-order terms. All of the n_f-terms can then be absorbed into the running coupling following the basic β-pattern in the scale-displacement formula, i.e. Eq.(4.1). More explicitly, in this treatment, the PMC scales can be derived in the following way: The LO PMC scale Q_1 is obtained by eliminating all the n_f-terms with the highest power at each order, and at this step, the coefficients of the lower-power n_f-terms are changed simultaneously to ensure that the correct LO α_s-running is obtained; the NLO PMC scale Q_2 is obtained by eliminating the n_f-terms of one less power in the new series obtaining a third series with less n_f-terms; and so on until all n_f-terms are eliminated.

If the n_f-terms are treated correctly, the results for both treatments shall be equivalent since they lead to the same resummed "conformal" series up to all orders. Those two PMC approaches differ, however, at the non-conformal level, by predicting slightly different PMC scales of the running coupling. This difference arises due to different ways of resumming the non-conformal $\{\beta_i\}$-terms, but this difference decreases rapidly when additional loop corrections are included [25].

- Third, we absorb different types of $\{\beta_i\}$-terms into the running coupling via an order-by-order manner with the help of degeneracy relations. Different types of $\{\beta_i\}$-terms as determined from the RGE lead to different running behaviors of the running coupling at different orders, and hence, determine the distinct scales at each order. As a result, the PMC scales themselves are perturbative

expansion series in the running coupling. Since a different scale generally appears at each order, we call this approach as the PMC multi-scale approach.
- Finally, since all the non-conformal $\{\beta_i\}$-terms have been resummed into the running coupling, the remaining terms in the perturbative series will be identical to those of the corresponding conformal theory, thus leading to a generally scheme-independent prediction. Because of the uncalculated high-order terms, there is residual scale dependence for the PMC prediction. However such residual renormalization scale dependence is generally small either due to the perturbative nature of the PMC scales or due to the fast convergence of the conformal pQCD series [1]. This explains why one refers to the PMC method as "principle of maximum conformality". The scheme independence of the PMC prediction is a general result, satisfying the central property of RGI.

4.2   Some Recent Applications of PMC scale setting

In this section, some recent PMC applications, which show essential features of PMC and the importance of proper renormalization scale-setting are reviewed. Further details can be found in refs. [31,36–38]

The hadroproduction of the Higgs boson The total cross section for the production of Higgs boson at hadron colliders can be treated as the convolution of the hard-scattering partonic cross section $\hat{\sigma}_{ij}$ with the corresponding parton luminosity $\mathcal{L}_{ij}$, i.e.

$$\sigma_{H_1 H_2 \to HX} = \sum_{i,j} \int_{m_H^2}^{S} ds \, \mathcal{L}_{ij}(s, S, \mu_f) \hat{\sigma}_{ij}(s, L, R), \qquad (4.2)$$

where the parton luminosity

$$\mathcal{L}_{ij} = \frac{1}{S} \int_{s}^{S} \frac{d\hat{s}}{\hat{s}} f_{i/H_1}(x_1, \mu_f) f_{j/H_2}(x_2, \mu_f). \qquad (4.3)$$

Here the indices i, j run over all possible parton flavors in proton H_1 or H_2, $x_1 = \hat{s}/S$ and $x_2 = s/\hat{s}$. S denotes the hadronic center-of-mass energy squared, and $s = x_1 x_2 S$ is the subprocess center-of-mass energy squared. The subprocess cross section $\hat{\sigma}_{ij}$ depends on both the renormalization scale μ_r and the factorization scale μ_f, and the parton luminosity depends on μ_f. We define two ratios $L = \mu_f^2/m_H^2$ and $R = \mu_r^2/\mu_f^2$, where m_H is the Higgs boson mass. The parton distribution functions (PDF) underlying the parton luminosity $f_{i/H_\alpha}(x_\alpha, \mu_f)$ ($\alpha = 1$ or 2) describes the probability of finding a parton of type i with light-front momentum fraction between x_α and $x_\alpha + dx_\alpha$ in the proton H_α. The two-dimensional integration over

---

[1] By choosing a proper scale for the highest-order terms, whose value cannot be fixed, one can achieve a scheme-independent prediction due to commensurate scale relations among the predictions under different schemes [11].

s and $\hat{s}$ can be performed numerically by using the VEGAS program [44]. For this purpose, one can set $s = m_H^2(S/m_H^2)^{y_1}$ and $\hat{s} = s(S/s)^{y_2}$, and transform the two-dimensional integration into an integration over two variables $y_{1,2} \in [0,1]$. Analytic expressions using the $\overline{\text{MS}}$-scheme for the partonic cross section $\hat{\sigma}_{ij}$ up to N^2LO level can be found in Refs. [46, 47], which can be used for the PMC analysis. There are two types of large logarithmic terms $\ln(\mu_r/m_H)$ and $\ln(\mu_r/m_t)$ in $\hat{\sigma}_{ij}$. Thus a single guessed scale, using conventional scale-setting, such as $\mu_r = m_H$, cannot eliminate all of the large logarithmic terms. This explains why there are large K factors for the high-order terms, confirming the importance of achieving exact values for each order. The PMC uses the RGE to determine the optimal running behavior of α_s at each order, and the large scale uncertainty for each order using conventional scale setting can be eliminated. To be specific, the PMC introduces multiple scales for physical applications which depend on multiple kinematic variables, which is caused by the fact that different typical momentum flows could exist in different kinematic regions. Similar conditions have been observed in the hadronic Z decays [32] and the heavy-quark pair production via $q\bar{q}$ fusion [33]. For example, the process $q\bar{q} \rightarrow Q\bar{Q}$ near the heavy quark (Q) threshold involves not only the invariant variable $\hat{s} \sim 4M_Q^2$, but also the variable $v_{rel}^2\hat{s}$ with v_{rel} being the relative velocity, which enters the Sudakov final-state corrections.

	Tevatron	LHC			
$\sqrt{S}$	1.96 TeV	7 TeV	8 TeV	13 TeV	14 TeV
Conv.	$0.63^{+0.13}_{-0.11}$	$13.92^{+2.25}_{-2.06}$	$18.12^{+2.87}_{-2.66}$	$44.26^{+6.61}_{-6.43}$	$50.33^{+7.47}_{-7.31}$
PMC	$0.86^{+0.13}_{-0.12}$	$18.04^{+1.36}_{-1.32}$	$23.37^{+1.65}_{-1.59}$	$56.34^{+3.45}_{-3.00}$	$63.94^{+3.88}_{-3.30}$

Table 4.1: The total hadronic cross section σ_{sum} (in unit: pb) using the conventional (Conv.) and PMC scale-settings [48], where the uncertainties are for $\mu_r \in [m_H/2, 2m_H]$ and $\mu_f \in [m_H/2, 2m_H]$.

We use σ_{sum} to stand for the sum of the total hadronic production cross sections $\sigma_{(ij)}$ with $(ij) = (gg)$, $(q\bar{q})$, (gq), $(g\bar{q})$ and (qq'), respectively. Numerical results for σ_{sum} at the Tevatron and LHC are presented in Table 4.1 [48], where the uncertainties are for $\mu_r \in [m_H/2, 2m_H]$ and $\mu_f \in [m_H/2, 2m_H]$. As a comparison, the results using conventional scale-setting are also presented. After applying the PMC, σ_{sum} is increased by $\sim 37\%$ at the Tevatron, and by $\sim 30\%$ at the LHC for $\sqrt{S} = 7, 8, 13$ and 14 TeV, respectively.

To compare with the LHC measurements for Higgs boson production cross-section [49–51], one needs to include the contributions from other known production modes, such as the vector-boson fusion production process, the WH/ZH Higgs associated production process, the Higgs production associated with heavy quarks, etc. We use σ_{xH} to stand for the sum of those production cross sections from the channels via Z, W, $t\bar{t}$, $b\bar{b}$ and $\cdots$, and use σ_{EW} to stand for those production cross sections from the channels with electroweak corrections. The values of σ_{xH} and σ_{EW} are small in comparison to the dominant gluon-fusion σ_{ggH} contribution.

Decay channel	σ_{Incl}		
	7 TeV	8 TeV	13 TeV
$H \to \gamma\gamma$ [49–51]	35^{+13}_{-12}	$30.5^{+7.5}_{-7.4}$	$47.9^{+9.1}_{-8.6}$
$H \to ZZ^* \to 4l$ [49–51]	33^{+21}_{-16}	37^{+9}_{-8}	$68.0^{+11.4}_{-10.4}$
LHC-XS [56]	19.2 ± 0.9	24.5 ± 1.1	$55.6^{+2.4}_{-3.4}$
PMC	$21.21^{+1.36}_{-1.32}$	$27.37^{+1.65}_{-1.59}$	$65.72^{+3.46}_{-3.01}$

Table 4.2: Total inclusive cross sections (in unit: pb) for Higgs production at the LHC for the CM collision energies $\sqrt{S} = 7$, 8 and 13 TeV, respectively [48]. The inclusive cross section is $\sigma_{\text{Incl}} = \sigma_{\text{sum}} + \sigma_{xH} + \sigma_{\text{EW}}$.
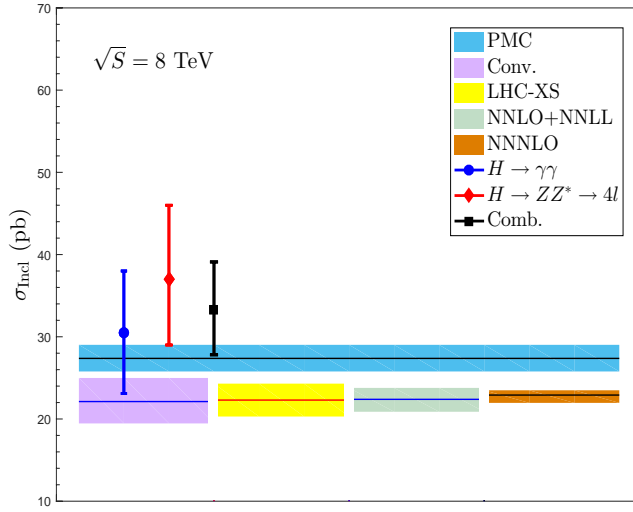
Fig. 4.2: Comparison of the N^{2}LO conventional versus PMC predictions for the total inclusive cross section σ_{Incl} [48] with the latest ATLAS measurements at 8 TeV [49]. The LHC-XS predictions [52], the N^{2}LO+NNLL prediction [57], and the N^{3}LO prediction [58] are presented as a comparison. The solid lines are central values.

Taking $\sqrt{S} = 8$ TeV and $m_H = 125$ GeV, one predicts $\sigma_{xH} = 3.08 + 0.10$ pb [49, 52]; the electro-weak correction up to two-loop level leads to a $+5.1\%$ shift with respect to the N^{2}LO-level QCD cross sections [54, 55]. Taking those contributions into consideration, the PMC predictions for the total inclusive cross section σ_{Incl} at the LHC for several center-of-mass (CM) collision energies are presented in Table 4.2; the LHC ATLAS predictions via $H \to \gamma\gamma$ and $H \to ZZ^* \to 4l$ decay channels [49, 50] are also given. The PMC results are larger than the central values of the LHC-XS prediction [56] by about 10%, 12% and 18% for $\sqrt{S} = 7$, 8 and 13 TeV, respectively, which shows a better agreement with the data. This is clearly

shown by Figure 4.2, in which a comparison of our present N^2LO conventional and PMC predictions for σ_{Incl} with the ATLAS measurements at 8 TeV is presented. Because of the large uncertainty for the ATLAS data, more data is needed to draw definite conclusions on the SM predictions. More accurate measurements with high integrated luminosity for $\sqrt{S}$=13 TeV will be helpful to test the PMC and conventional predictions.

$\sigma_{fid}(pp \to H \to \gamma\gamma)$	7 TeV	8 TeV	13 TeV
ATLAS data [59]	49 ± 18	$42.5^{+10.3}_{-10.2}$	52^{+40}_{-37}
CMS data [60]	-	-	84^{+13}_{-12}
ATLAS data [61]	-	-	60.4 ± 8.6
LHC-XS [56]	24.7 ± 2.6	31.0 ± 3.2	$66.1^{+6.8}_{-6.6}$
PMC prediction	$30.1^{+2.3}_{-2.2}$	$38.3^{+2.9}_{-2.8}$	$85.8^{+5.7}_{-5.3}$

Table 4.3: The fiducial cross section $\sigma_{fid}(pp \to H \to \gamma\gamma)$ (in unit: fb) at the LHC for CM collision energies $\sqrt{S}$ =7, 8 and 13 TeV, respectively [48].

It has been suggested that the fiducial cross section σ_{fid} can also be used to test the theoretical predictions, which is defined as

$$\sigma_{fid}(pp \to H \to \gamma\gamma) = \sigma_{Incl}\mathcal{B}_{H\to\gamma\gamma}\mathcal{A}. \tag{4.4}$$

The $\mathcal{A}$ is the acceptance factor, whose values for three typical proton-proton CM collision energies are [59], $\mathcal{A}|_{7TeV} = 0.620 \pm 0.007$, $\mathcal{A}|_{8TeV} = 0.611 \pm 0.012$ and $\mathcal{A}|_{13TeV} = 0.570 \pm 0.006$. The $\mathcal{B}_{H\to\gamma\gamma}$ is the branching ratio of $H \to \gamma\gamma$. By using the $\Gamma(H \to \gamma\gamma)$ with conventional scale-setting, the LHC-XS group predicts $\mathcal{B}_{H\to\gamma\gamma} = 0.00228 \pm 0.00011$ [52]. A PMC analysis for $\Gamma(H \to \gamma\gamma)$ up to three-loop or five-loop level has been given in Refs. [53, 133]. Using the formulae given there, we obtain $\Gamma(H \to \gamma\gamma)|_{PMC} = 9.34 \times 10^{-3}$ MeV for $m_H = 125$ GeV. Using this value, together with Higgs total decay width $\Gamma_{Total} = (4.07 \pm 0.16) \times 10^{-3}$ GeV [52], we obtain $\mathcal{B}_{H\to\gamma\gamma}|_{PMC} = 0.00229 \pm 0.00009$. The PMC predictions for $\sigma_{fid}(pp \to H \to \gamma\gamma)$ at the LHC are given in Table 4.3, where the ATLAS and CMS measurements [59–61] and the LHC-XS predictions [56] are also presented. The PMC fiducial cross sections are larger than the LHC-XS ones by $\sim 22\%$, $\sim 24\%$ and $\sim 30\%$ for $\sqrt{S}$ =7 TeV, 8 TeV and 13 TeV, respectively. Table 4.3 shows no significant differences between the measured fiducial cross sections and the SM predictions, and the PMC predictions show better agreement with the measurements at $\sqrt{S} = 7$ TeV and 8 TeV.

Top-quark pair production at hadron colliders and the top-quark pole mass As in the case of the hadronic production of the Higgs boson, the total cross section for the top-quark pair production at the hadronic colliders can also be written as the convolution of the factorized partonic cross section $\hat{\sigma}_{ij}$ with the parton

luminosities $\mathcal{L}_{ij}$:

$$\sigma_{H_1 H_2 \to t\bar{t}X} = \sum_{i,j} \int_{4m_t^2}^{S} ds \, \mathcal{L}_{ij}(s, S, \mu_f)\hat{\sigma}_{ij}(s, \alpha_s(\mu_r), \mu_r, \mu_f), \qquad (4.5)$$

where the parton luminosities $\mathcal{L}_{ij}$ has been defined in Eq.(4.3), and the partonic cross section $\hat{\sigma}_{ij}$ has been computed up to N^2LO level,

$$\hat{\sigma}_{ij} = \tfrac{1}{m_t^2}\left[f_{ij}^0(\rho, \mu_r, \mu_f)\alpha_s^2(\mu_r) + f_{ij}^1(\rho, \mu_r, \mu_f)\alpha_s^3(\mu_r) + f_{ij}^2(\rho, \mu_r, \mu_f)\alpha_s^4(\mu_r) + \mathcal{O}(\alpha_s^5)\right]$$
(4.6)

where $\rho = 4m_t^2/s$, $(ij) = \{(q\bar{q}), (gg), (gq), (g\bar{q})\}$ stands for the four production channels, respectively. In the literature, the perturbative coefficients up to N^2LO level have been calculated by various groups, e.g. Refs. [62–72]. More explicitly, the LO, NLO and N^2LO coefficients f_{ij}^0, f_{ij}^1 and f_{ij}^2 in an n_f-power series can be explicitly read from the HATHOR program [73] and the Top++ program [74]. By identifying the n_f-terms associated with the $\{\beta_i\}$-terms in the coefficients f_{ij}^0, f_{ij}^1 and f_{ij}^2, and by using the degeneracy relations of β-pattern at different orders, one can determine the correct arguments of the strong couplings at each order and hence the PMC scales at each order by using the RGE via a recursive way [97, 99]. The Coulomb-type corrections near the threshold region should be treated separately, since their contributions are enhanced by factors of π and are sizable (e.g. those terms are proportional to (π/v) or $(\pi/v)^2$ [33], where $v = \sqrt{1 - \rho}$, the heavy quark velocity). For this purpose, the Sommerfeld re-scattering formula is useful for a reliable prediction [75, 76].

	Conventional scale-setting				PMC scale-setting			
	LO	NLO	N^2LO	*Total*	LO	NLO	N^2LO	*Total*
$(q\bar{q})$ channel	4.87	0.96	0.48	6.32	4.73	1.73	−0.063	6.35
(gg) channel	0.48	0.41	0.15	1.04	0.48	0.48	0.15	1.14
(gq) channel	0.00	−0.036	0.0046	−0.032	0.00	−0.036	0.0046	−0.032
$(g\bar{q})$ channel	0.00	−0.036	0.0047	−0.032	0.00	−0.036	0.0047	−0.032
sum	5.35	1.30	0.64	7.29	5.21	2.14	0.096	7.43

Table 4.4: The top-quark pair production cross sections (in unit: pb) before and after PMC scale-setting at the Tevatron with $\sqrt{S} = 1.96$ TeV. $\mu_r = \mu_f = m_t$.

Numerical results for the total top-quark pair production cross sections at the hadronic colliders Tevatron and LHC for both conventional and PMC scale settings are presented in Tables 12.2, 4.5, 4.6, and 4.7, respectively. We have updated previous predictions by using $m_t = 173.3$ GeV [77] and the CTEQ version CT14 [78] as the PDF. The cross sections for the individual production channels, i.e. $(q\bar{q})$, (gq), $(g\bar{q})$ and (gg) channels are presented. In these tables, the initial choice of renormalization scale and factorization scale is fixed to be $\mu_r = \mu_f = m_t$.
We present the N^2LO top-quark pair production cross sections at the Tevatron and LHC for both conventional and PMC scale settings in Table 4.8, where four CM

	Conventional scale setting				PMC scale setting			
	LO	NLO	N²LO	Total	LO	NLO	N²LO	Total
$(q\bar{q})$ channel	23.37	3.42	1.86	28.69	22.32	7.23	−0.78	28.62
(gg) channel	80.40	46.87	10.87	138.15	80.10	54.70	8.77	145.54
(gq) channel	0.00	−0.43	1.41	1.03	0.00	−0.43	1.41	1.03
$(g\bar{q})$ channel	0.00	−0.44	0.24	−0.20	0.00	−0.44	0.24	−0.20
sum	103.77	49.42	14.38	167.67	102.42	61.06	9.64	174.98

Table 4.5: The top-quark pair production cross sections (in unit: pb) before and after PMC scale-setting at the LHC with $\sqrt{S} = 7$ TeV. $\mu_r = \mu_f = m_t$.

	Conventional scale setting				PMC scale setting			
	LO	NLO	N²LO	Total	LO	NLO	N²LO	Total
$(q\bar{q})$ channel	29.88	4.20	2.31	36.43	28.46	9.09	−1.06	36.29
(gg) channel	118.10	67.43	15.01	200.57	117.66	78.53	11.92	210.86
(gq) channel	0.00	0.18	2.02	2.18	0.00	0.18	2.02	2.18
$(g\bar{q})$ channel	0.00	−0.53	0.37	−0.15	0.00	−0.53	0.37	−0.15
sum	147.98	71.28	19.71	239.03	146.12	87.27	13.25	249.18

Table 4.6: The top-quark pair production cross sections (in unit: pb) before and after PMC scale-setting at the LHC with $\sqrt{S} = 8$ TeV. $\mu_r = \mu_f = m_t$.

	Conventional scale setting				PMC scale setting			
	LO	NLO	N²LO	Total	LO	NLO	N²LO	Total
$(q\bar{q})$ channel	66.47	8.30	4.73	79.58	62.86	19.38	−2.74	79.08
(gg) channel	415.06	224.43	43.36	682.98	413.52	259.35	32.56	713.60
(gq) channel	0.00	7.09	6.52	13.82	0.00	7.09	6.52	13.82
$(g\bar{q})$ channel	0.00	−0.25	1.59	1.33	0.00	−0.25	1.59	1.33
sum	481.53	239.57	56.20	777.72	476.38	285.57	37.93	807.83

Table 4.7: The top-quark pair production cross sections (in unit: pb) before and after PMC scale-setting at the LHC with $\sqrt{S} = 13$ TeV. $\mu_r = \mu_f = m_t$.

collision energies $\sqrt{S} = 1.96$ TeV, 7 TeV, 8 TeV, and 13 TeV, and three typical choices of initial renormalization scale $\mu_r = m_t/2$, m_t, and $2m_t$ have been assumed. Table 4.8 shows the PMC predictions for the top-pair total cross section: $\sigma_{\text{Tevatron}}^{1.96\text{TeV}} = 7.43_{-0.13}^{+0.14}$ pb at the Tevatron, $\sigma_{\text{LHC}}^{7\text{TeV}} = 175.0_{-3.5}^{+3.5}$ pb, $\sigma_{\text{LHC}}^{8\text{TeV}} = 249.2_{-4.9}^{+5.0}$ pb, and $\sigma_{\text{LHC}}^{13\text{TeV}} = 807.8_{-15.8}^{+16.0}$ pb at the LHC. These predictions agree with the Tevatron and LHC measurements within errors [79–95]. Table 4.8 shows that using conventional scale setting, the renormalization scale dependence of the N²LO-level cross section is about $6\% - 7\%$ for $\mu_r \in [m_t/2, 2m_t]$. Thus achieving the exact value for each order is important for a precise lower-order pQCD prediction, especially for those observables that are heavily dependent on the value at a particular order. By analyzing the N²LO pQCD series in detail, it is found that the renormalization scale dependence of each perturbative term is rather large using conventional scale setting [43]. On the other hand, by using the PMC, the cross sections at each order

	Conventional			PMC		
μ_r	$m_t/2$	m_t	$2m_t$	$m_t/2$	m_t	$2m_t$
$\sigma_{Tevatron}^{1.96\,TeV}$	7.54	7.29	7.01	7.43	7.43	7.43
$\sigma_{LHC}^{7\,TeV}$	172.07	167.67	160.46	174.97	174.98	174.99
$\sigma_{LHC}^{8\,TeV}$	244.87	239.03	228.94	249.16	249.18	249.19
$\sigma_{LHC}^{13\,TeV}$	792.36	777.72	746.92	807.80	807.83	807.86

Table 4.8: The N^2LO top-pair production cross sections for the Tevatron and LHC (in unit of pb), comparing conventional versus PMC scale settings. Here all production channels have been summed. Three typical choices for the initial renormalization scales $\mu_r = m_t/2$, m_t and $2m_t$ have been adopted.

are almost unchanged, indicating a nearly scale-independent prediction can be achieved even at lower orders. If one sets $\mu_r = m_t/2$ for conventional scale setting, the total cross section is close to the PMC prediction, whose pQCD convergence is also better than the cases of $\mu_r = m_t$ and $\mu_r = 2m_t$ as has been observed in Ref. [96]. Thus, the PMC provides support for "guessing" the optimal choice of $\mu_r \sim m_t/2$ using conventional scale setting [45].

After applying the PMC, we obtain the optimal scale of the top-quark pair production at each perturbative order in pQCD, and the resulting theoretical predictions are essentially free of the initial choice of renormalization scale. Thus a more accurate top-quark pole mass and a reasonable explanation of top-quark pair forward-backward asymmetry at the hadronic colliders can be achieved [43, 45, 98–100].

First, to fix the top-quark mass, one can compare the pQCD prediction on the top-quark pair production cross-section with the experimental data. For this purpose, one can define a likelihood function [101]

$$f(m_t) = \int_{-\infty}^{+\infty} f_{th}(\sigma|m_t) \cdot f_{exp}(\sigma|m_t) \, d\sigma. \tag{4.7}$$

Here $f_{th}(\sigma|m_t)$ is the normalized Gaussian distribution determined theoretically,

$$f_{th}(\sigma|m_t) = \frac{1}{\sqrt{2\pi}\Delta\sigma_{th}(m_t)} \exp\left[-\frac{(\sigma - \sigma_{th}(m_t))^2}{2\Delta\sigma_{th}^2(m_t)}\right]. \tag{4.8}$$

The top-quark pair production cross-section is a function of the top-quark pole mass m_t; its decrease with increasing m_t can be parameterized as [69]

$$\sigma_{th}(m_t) = \left(\frac{172.5}{m_t/GeV}\right)^4 \left(c_0 + c_1\left(\frac{m_t}{GeV} - 172.5\right) + c_2\left(\frac{m_t}{GeV} - 172.5\right)^2 + \right. \tag{4.9}$$
$$\left. + c_3\left(\frac{m_t}{GeV} - 172.5\right)^3,\right.$$

$$\tag{4.11}$$

where all masses are given in units of GeV. $\Delta\sigma_{th}(m_t)$ stands for the maximum error of the cross-section for a fixed m_t. One can estimate its value by using

the CT14 error PDF sets [78] with range of $\alpha_s(M_Z) \in [0.117, 0.119]$. The values for the coefficients $c_{0,1,2,3}$ can be determined by using a wide range of the top-quark pole mass, $m_t \in [160 \text{ GeV}, 190 \text{ GeV}]$. Here $\sigma_{th}(m_t)$ is defined as the cross-section at a fixed m_t, where all input parameters are set to be their central values, $[\sigma_{th}(m_t) + \Delta\sigma_{th}^+(m_t)]$ is the maximum cross-section within the allowable parameter range, and $[\sigma_{th}(m_t) - \Delta\sigma_{th}^-(m_t)]$ is the minimum value. The function $f_{exp}(\sigma|m_t)$ is the normalized Gaussian distribution determined experimentally,

$$f_{exp}(\sigma|m_t) = \frac{1}{\sqrt{2\pi}\Delta\sigma_{exp}(m_t)} \exp\left[-\frac{(\sigma - \sigma_{exp}(m_t))^2}{2\Delta\sigma_{exp}^2(m_t)}\right], \quad (4.12)$$

where $\sigma_{exp}(m_t)$ is the measured cross-section, and $\Delta\sigma_{exp}(m_t)$ is the uncertainty for $\sigma_{exp}(m_t)$. By evaluating the likelihood function, we obtain $m_t = 174.6^{+3.1}_{-3.2}$ GeV [98], where the central value is extracted from the maximum of the likelihood function, and the error ranges are obtained from the 68% area around the maximum. Because the PMC predictions have less uncertainty compared to the predictions by using conventional scale-setting, the precision of top-quark pole mass is dominated by the experimental errors. For example, the PMC determination for the pole mass via the combined dilepton and the lepton + jets channels data is about 1.8%, which is almost the same as that of the recent determination by the D0 collaboration, $172.8^{+3.4}_{-3.2}$ GeV [102], whose error is $\sim 1.9\%$.

A summary of the top-quark pole masses determined at both the Tevatron and LHC is presented in Figure 4.3, where the PMC predictions and previous predictions from other collaborations [87, 88, 101–107] are presented.

Second, it has been found that by applying the PMC, the SM predictions for the top-quark forward-backward asymmetry at the Tevatron are only 1σ deviation from the CDF and D0 measurements [43, 99, 100]. In fact, the PMC gives a scale-independent precise top-quark pair forward-backward asymmetry, $A_{FB}^{PMC} = 9.2\%$ and $A_{FB}(M_{t\bar{t}} > 450 \text{ GeV}) = 29.9\%$, in agreement with the corresponding CDF and D0 measurements [108–114]. The large discrepancies of the top-quark forward-backward asymmetry between the SM estimate and the Tevatron data are thus greatly reduced. Moreover, the PMC prediction for $A_{FB}(M_{t\bar{t}} > M_{cut})$ displays an "increasing-decreasing" behavior as M_{cut} is increased, consistent within errors with the measurements recently reported by D0 experiment [113].

The top-quark charge asymmetry at the LHC for the $pp \to t\bar{t}X$ process is defined as

$$A_C = \frac{N(\Delta|y| > 0) - N(\Delta|y| < 0)}{N(\Delta|y| > 0) + N(\Delta|y| < 0)}, \quad (4.13)$$

where $\Delta|y| = |y_t| - |y_{\bar{t}}|$ is the difference between the absolute rapidities of the top and anti-top quarks, and N is the number of events. Measurements of the top-quark charge asymmetry at the LHC have been reported in Refs. [115–120]. Figure 4.4 gives a summary of the LHC measurements, together with the theoretical predictions. In contrast to the Tevatron $p\bar{p} \to t\bar{t}X$ processes, the asymmetric channel $q\bar{q} \to t\bar{t}$ gives a small pQCD contribution to the top-pair production at the LHC, and the symmetric channel $gg \to t\bar{t}$ provides the dominant contribution. Thus, the predicted charge asymmetry at the LHC is smaller than the one at the
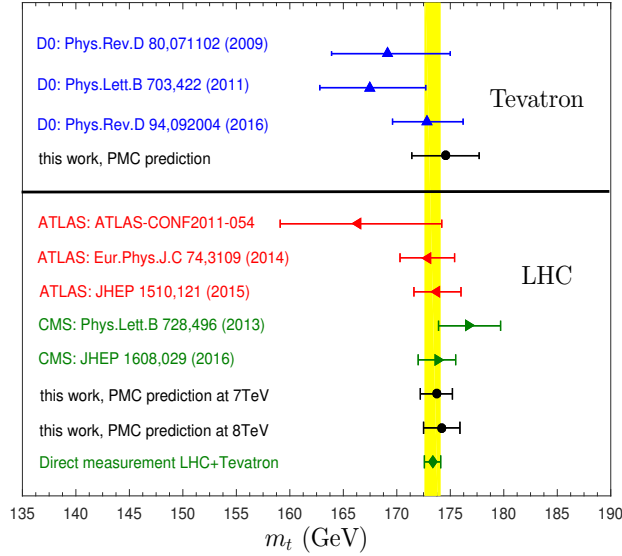
Fig. 4.3: A summary of the top-quark pole mass determined indirectly from the top-quark pair production channels at the Tevatron and LHC [98]. For reference, the combination of Tevatron and LHC direct measurements of the top-quark mass is presented as a shaded band, which gives $m_t = 173.34 \pm 0.76$ GeV [107].

Tevatron. Two typical SM predictions for the charge asymmetry at the LHC are: $A_C|_{7\text{TeV}} = (1.15 \pm 0.06)\%$ and $A_C|_{8\text{TeV}} = (1.02 \pm 0.05)\%$ [121]; $A_C|_{7\text{TeV}} = (1.23 \pm 0.05)\%$ and $A_C|_{8\text{TeV}} = (1.11 \pm 0.04)\%$ [122]. The uncertainties of the theoretical prediction are dominated by the choice of scale. The scale errors for conventional scale setting are obtained by varying $\mu_r \in [m_t/2, 2m_t]$, and fixing the factorization scale $\mu_f \equiv \mu_r$. As a representation, Figure 4.4 shows the prediction of Ref. [122]. On the other hand, the PMC prediction is almost scale independent and a more precise comparison with the data can be achieved.

The $\gamma\gamma^* \to \eta_c$ transition form factor The simplest exclusive charmonium production process, $\gamma^*\gamma \to \eta_c$, measured in two-photon collisions, provides another example of the importance of a proper scale-setting approach for fixed-order predictions. This is also helpful for testing Nonrelativistic QCD (NRQCD) theory [123]. One can define a transition form factor (TFF) $F(Q^2)$ via the following way [124]:

$$\langle \eta_c(p)|J^\mu_{EM}|\gamma(k, \varepsilon)\rangle = ie^2 \epsilon^{\mu\nu\rho\sigma}\varepsilon_\nu q_\rho k_\sigma F(Q^2), \qquad (4.14)$$

where J^μ_{EM} is the electromagnetic current evaluated at the time-like momentum transfer squared, $Q^2 = -q^2 = -(p - k)^2 > 0$. The BaBar collaboration has measured its value and parameterized it as $|F(Q^2)/F(0)| = 1/(1 + Q^2/\Lambda)$ [125], where $\Lambda = 8.5 \pm 0.6 \pm 0.7$ GeV^2. In the case of conventional scale setting, the renormalization scale is simply set as the typical momentum flow $\mu_Q = \sqrt{Q^2 + m_c^2}$; the
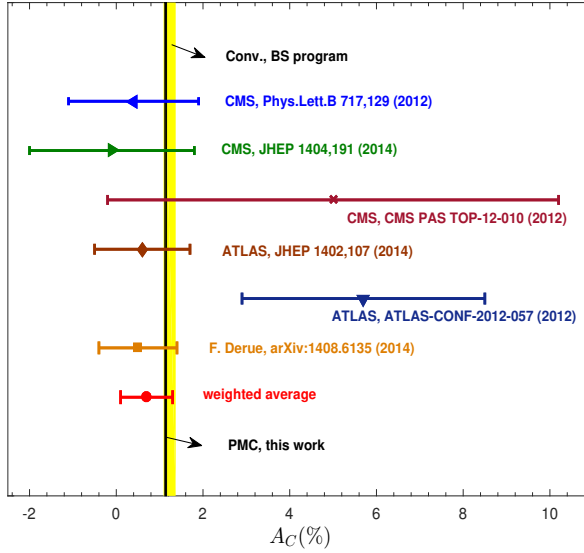
Fig. 4.4: The top-quark charge asymmetry A_C assuming conventional scale setting (Conv.) and PMC scale setting for $\sqrt{S} = 7$ TeV [45]; the error bars are for $\mu_r \in [m_t/2, 2m_t]$ and $\mu_f \in [m_t/2, 2m_t]$. As a comparison, the experimental results [115–120] and the prediction of Ref. [122] are also presented.

N^2LO NRQCD prediction cannot explain the BaBar measurements over a wide Q^2 range [126]. Here m_c is the c-quark mass and we set its value as 1.68 GeV. This disagreement cannot be solved by taking higher Fock states into consideration [127, 128].

Numerically, the choice of renormalization scale $\mu_r = \mu_Q$ leads to a substantially negative N^2LO contribution and hence a large $|F(Q^2)/F(0)|$, in disagreement with the data. Following the standard PMC scale-setting procedures, one can determine the PMC scale μ_r^{PMC} of the process by carefully dealing with the light-by-light diagrams at the N^2LO level. The determined PMC scale varies with momentum transfer squared Q^2 at which the TFF is measured, and it is independent of the initial choice of μ_r (thus the conventional scale uncertainty is eliminated). We present the PMC scale μ_r^{PMC} versus Q^2 in Figure 4.5, which is larger than the "guessed" value μ_Q in the small and large Q^2-regions. In the intermediate Q^2-region, e.g. $Q^2 \sim [20, 60]$ GeV^2, the discrepancy between μ_r^{PMC} and μ_Q is small; and the largest difference occurs at $Q^2 = 0$.

A comparison of the renormalization scale dependence for the ratio $|F(Q^2)/F(0)|$ is given in Figure 4.6, which is obtained by using the same input parameters as those of Refs. [39, 126]. It shows that the PMC prediction is independent of the initial choice of scale μ_r, whereas the conventional scale uncertainty is large, especially in low Q^2-region. The PMC prediction is close to the BaBar measurement. Thus
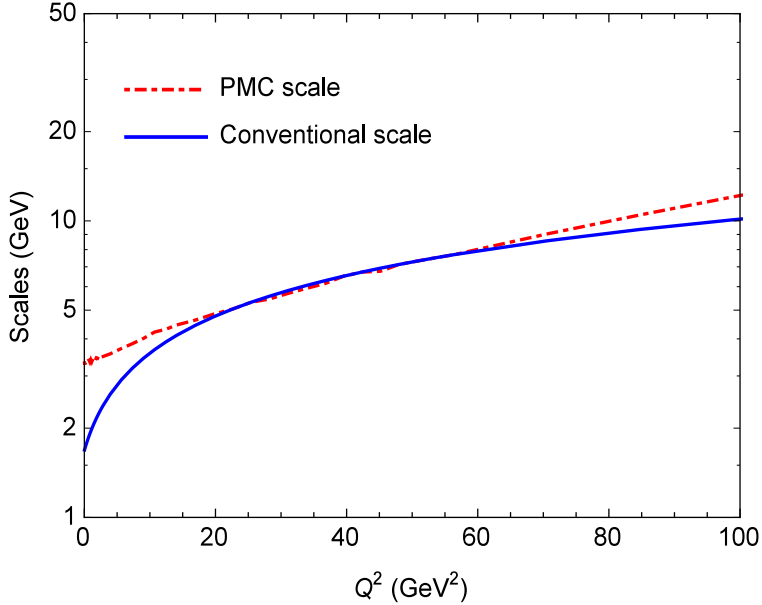
Fig. 4.5: The PMC scale of the transition form factor $F(Q^2)$ [39], defined in Eq.(4.14), versus Q^2. The conventional choice of scale $\mu_r = \mu_Q$ is presented as a comparison.

the application of PMC supports the applicability of NRQCD to hard exclusive processes involving heavy quarkonium.

The determination of the factorization scale is a separate issue from renormalization scale setting, since it is present even for a conformal theory. The factorization scale can be determined by matching nonperturbative bound-state dynamics with perturbative DGLAP evolution [157–159]. Recently, by using light-front holography [160, 161], it has been shown that the matching of high-and-low scale regimes of α_s can determine the scale which sets the interface between perturbative and nonperturbative hadron dynamics [17, 22–24]. Figure 4.6 also shows the factorization scale dependence for the ratio $|F(Q^2)/F(0)|$. In the case of conventional scale-setting, there is large factorization scale dependence. Choosing a smaller factorization scale could lower the N^2LO-level ratio $|F(Q^2)/F(0)|$ to a certain degree, but it cannot eliminate the large discrepancy with the data. In contrast, after applying the PMC, the prediction shows a small factorization scale dependence. This in some sense also shows the importance of a proper scale-setting approach. More explicitly, in the case $Q^2 = 0$, a large factorization scale uncertainty is observed using conventional scale-setting; i.e.,

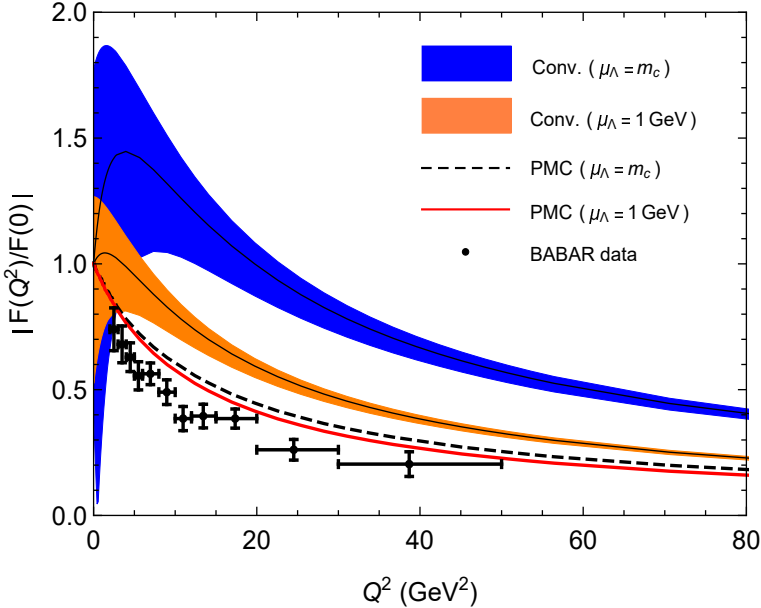$$F^{\text{Conv}}(0)|_{\mu_r = m_c} = 0.43c^{(0)}, \ 0.22c^{(0)}, \ -0.06c^{(0)} \tag{4.15}$$

Fig. 4.6: The ratio $|F(Q^2)/F(0)|$ up to N^2LO-level versus Q^2 using conventional (Conv.) and PMC scale-settings [39], where the BaBar data are presented as a comparison [125]. Two typical factorization scales, $\mu_\Lambda = 1$ GeV and m_c are adopted. The error bars are for $\mu_r^2 = [\mu_Q^2/2, 2\mu_Q^2]$ with $\mu_Q = \sqrt{Q^2 + m_c^2}$.

for factorization scale $\mu_\Lambda = 1$ GeV, m_c and $2m_c$, respectively. Here the LO coefficient $c^{(0)}$ is

$$c^{(0)} = \frac{4e_c^2 \langle \eta_c | \psi^\dagger \chi(\mu_\Lambda) | 0 \rangle}{(Q^2 + 4m_c^2)\sqrt{m_c}}, \tag{4.16}$$

where $e_c = +2/3$ is the c-quark electric charge, and $\langle \eta_c | \psi^\dagger \chi(\mu_\Lambda) | 0 \rangle$ represents the nonperturbative matrix-element which characterizes the probability of the $(c\bar{c})$-pair to form a η_c bound state. The magnitude of the negative N^2LO term increases with increasing μ_Λ, and the $F^{\text{Conv}}(0)$ is even negative for $\mu_\Lambda = 2m_c$. On the other hand, by applying the PMC, we obtain a reasonable small factorization scale dependence

$$F^{\text{PMC}}(0) = 0.61c^{(0)}, \quad 0.50c^{(0)}, \quad 0.34c^{(0)}. \tag{4.17}$$

again for $\mu_\Lambda = 1$ GeV, m_c and $2m_c$, respectively.

The conventional renormalization scheme-and-scale ambiguities for fixed-order pQCD predictions are caused by the mismatch of the perturbative coefficients and the QCD running coupling at any perturbative order. The elimination of such ambiguities relies heavily on how well we know the precise value and analytic properties of the strong coupling α_s. An extended RGE has been suggested to determine the α_s scheme-and-scale running behaviors simultaneously based on the conventional RGE,. However, those dependences are usually entangled with

each other and can only be solved perturbatively or numerically. More recently, a C-scheme coupling $\hat{\alpha}_s$ has been suggested, whose scheme-and-scale running behavior is exactly separated; it satisfies a RGE free of scheme-dependent $\{\beta_{i\geq 2}\}$-terms. The C-scheme coupling can be matched to a conventional coupling α_s via a proper choice of the parameter C. We have demonstrated that the C-dependence of the PMC predictions can be eliminated up to any fixed order; since the value of C is arbitrary, it means the PMC prediction is independent of any renormalization scheme. We have illustrated these features for three physical observables which are known up to the four-loop level.
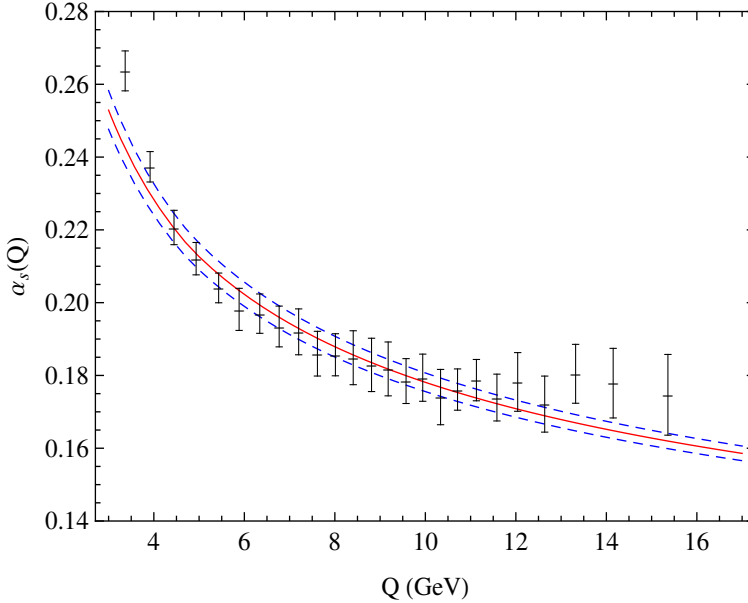
Fig. 4.7: The extracted $\alpha_s(Q)$ in the $\overline{\text{MS}}$-scheme from the comparison of PMC predictions with ALEPH data [129]. The error bars are from the experimental data. The three lines are the world average evaluated from $\alpha_s(M_Z) = 0.1181 \pm 0.0011$ [130].

The renormalization scale depends on kinematics such as thrust $(1 - T)$ for three jet production via e^+e^- annihilation. A definitive advantage of using the PMC is that since the PMC scale varies with $(1 - T)$, we can extract directly the strong coupling α_s at a wide range of scales using the experimental data at single center-of-mass-energy, $\sqrt{s} = M_Z$. In the case of conventional scale setting, the predictions are scheme-and-scale dependent and do not agree with the precise experimental results; the extracted coupling constants in general deviate from the world average. In contrast, after applying the PMC, we obtain a comprehensive and self-consistent analysis for the thrust variable results including both the differential distributions and the mean values [42]. Using the ALEPH data [129], the extracted α_s are

presented in Figure 4.7. It shows that in the scale range of 3.5 GeV $< Q <$ 16 GeV (corresponding $(1 - T)$ range is $0.05 < (1 - T) < 0.29$), the extracted α_s are in excellent agreement with the world average evaluated from $\alpha_s(M_Z)$.

The PMC provides first-principle predictions for QCD; it satisfies renormalization group invariance and eliminates the conventional renormalization scheme-and-scale ambiguities, greatly improving the precision of tests of the Standard Model and the sensitivity of collider experiments to new physics. Since the perturbative coefficients obtained using the PMC are identical to those of a conformal theory, one can derive all-orders commensurate scale relations between physical observables evaluated at specific relative scales.

Because the divergent renormalon series does not appear in the conformal perturbative series generated by the PMC, there is an opportunity to use resummation procedures such as the PA approach to predict the values of the uncalculated higher-order terms and thus to increase the precision and reliability of pQCD predictions. We have shown that if the PMC prediction for the conformal series for an observable has been determined at order α_s^n, then the $[N/M] = [0/n-1]$-type PA series provides an important estimate for the higher-order terms.

An essential property of renormalizable SU(N)]/U(1) gauge theories, is "Intrinsic Conformality," [131]. It underlies the scale invariance of physical observables and can be used to resolve the conventional renormalization scale ambiguity *at every order* in pQCD. This reflects the underlying conformal properties displayed by pQCD at NNLO, eliminates the scheme dependence of pQCD predictions and is consistent with the general properties of the PMC. We have also introduced a new method [131] to identify the conformal and β terms which can be applied either to numerical or to theoretical calculations and in some cases allows infinite resummation of the pQCD series, The implementation of the PMC$_\infty$ can significantly improve the precision of pQCD predictions; its implementation in multi-loop analysis also simplifies the calculation of higher orders corrections in a general renormalizable gauge theory. This method has also been used to improve the NLO pQCD prediction for $t\bar{t}$ pair production and other processes at the LHC, where subtle aspects of the renormalization scale of the three-gluon vertex and multi gluon amplitudes, as well as large radiative corrections to heavy quarks at threshold play a crucial role. The large discrepancy of pQCD predictions with the forward-backward asymmetry measured at the Tevatron is significantly reduced from 3 σ to approximately 1 σ. The PMC has also been used to precisely determine the QCD running coupling constant $\alpha_s(Q^2)$ over a wide range of Q^2 from event shapes for electron-positron annihilation measured at a single energy $\sqrt{s}$ [132]. The PMC method has also been applied to a spectrum of LHC processes including Higgs production, jet shape variables, and final states containing a high p_T photon plus heavy quark jets, all of which, sharpen the precision of the Standard Model predictions.

4.3 Extending the Predictive Power of Perturbative QCD Using the Principle of Maximum Conformality and Bayesian Analysis

In addition to the evaluation of high-order loop contributions, the precision and predictive power of perturbative QCD (pQCD) predictions depends on two important issues: (1) how to achieve a reliable, convergent fixed-order series, and (2) how to reliably estimate the contributions of unknown higher-order terms. The recursive use of renormalization group equation, together with the Principle of Maximum Conformality (PMC), eliminates the renormalization scheme-and-scale ambiguities of the conventional pQCD series. The result is a conformal, scale-invariant series of finite order which also satisfies all of the principles of the renormalization group. In a recent paper [18] a novel Bayesian-based approach is proposed to estimate the size of the unknown higher order contributions based on an optimized analysis of probability distributions. One finds that by using the PMC conformal series, in combination with the Bayesian analysis, one can consistently achieve high degree of reliability estimates for the unknown high order terms. Thus the predictive power of pQCD can be greatly improved. This procedure has been applied to three pQCD observables: R_{e+e-} R_τ and $\Gamma(H \to b\bar{b})$, which are each known up to four loops in pQCD. Numerical analyses confirm that by using the convergent and scale-independent PMC conformal series, one can achieve reliable Bayesian probability estimates for the unknown higher-order contributions. For further details, see Ref. [18]

4.4 Color Confinement, Light-Front Holography, and the QCD Coupling at all Scales

A key problem in hadron physics is to obtain a first approximation to QCD which can accurately predict not only the spectroscopy of hadrons, but also the light-front wave functions which underly their properties and dynamics. Guy de Téramond, Guenter Dosch, and I [15] have shown that a mass gap and a fundamental color confinement scale can be derived from light-front holography – the duality between five-dimensional anti-de Sitter (AdS) space physical 3+1 spacetime using light-front time. The combination of superconformal quantum mechanics [13, 134], light-front quantization [2] and the holographic embedding on a higher dimensional gravity theory [5] (gauge/gravity correspondence) has led to new analytic insights into the structure of hadrons and their dynamics [7, 9, 15–17, 148]. This new approach to nonperturbative QCD dynamics, *holographic light-front QCD*, has led to effective semi-classical relativistic bound-state equations for arbitrary spin [8], and it incorporates fundamental properties which are not apparent from the QCD Lagrangian, such as the emergence of a universal hadron mass scale, the prediction of a massless pion in the chiral limit, and remarkable connections between the spectroscopy of mesons, baryons and tetraquarks across the full hadron spectrum [39–41, 151].

Light-Front Hamiltonian theory provides a causal, frame-independent, ghost-free nonperturbative formalism for analyzing gauge theories such as QCD. Remarkably,

LF theory in 3+1 physical space-time is holographically dual to five-dimensional AdS space, if one identifies the LF radial variable ζ with the fifth coordinate z of AdS_5. If the metric of the conformal AdS_5 theory is modified by a dilaton of the form $e^{+\kappa^2 z^2}$, one obtains an analytically-solvable Lorentz-invariant color-confining LF Schrödinger equations for hadron physics. The parameter κ of the dilaton becomes the fundamental mass scale of QCD, underlying the color-confining potential of the LF Hamiltonian and the running coupling $\alpha_s(Q^2)$ in the nonperturbative domain. When one introduces super-conformal algebra, the result is "Holographic LF QCD", which not only predicts a unified Regge-spectroscopy of mesons, baryons, and tetraquarks, arranged as supersymmetric 4-plets, but also the hadronic LF wavefunctions which underly form factors, structure functions, and other dynamical phenomena. In each case, the quarks and antiquarks cluster in hadrons as 3_C diquarks, so that mesons, baryons and tetraquarks all obey a two-body $3_C - \bar{3}_C$ LF bound-state equation. Thus tetraquarks are compact hadrons, as fundamental as mesons and baryons. Holographic LF QCD also leads to novel phenomena such as the color transparency of hadrons produced in hard-exclusive reactions traversing a nuclear medium and asymmetric intrinsic heavy-quark distributions $Q(x) \neq \bar{Q}(x)$, appearing at high x in the non-valence higher Fock states of hadrons.

Phenomenological extensions of the holographic QCD approach have also led to nontrivial connections between the dynamics of form factors and polarized and unpolarized quark distributions with pre-QCD nonperturbative approaches such as Regge theory and the Veneziano model [18, 19, 136]. As discussed in the next section, it also predicts the analytic behavior of the QCD coupling $\alpha_s(Q^2)$ in the nonperturbative domain [17, 139].

4.4.1   The QCD Coupling at All Scales

The QCD running coupling can be defined [154] at all momentum scales from any perturbatively calculable observable, such as the coupling $\alpha_{g_1}^s(Q^2)$ which is defined from measurements of the Bjorken sum rule. At high momentum transfer, such "effective charges" satisfy asymptotic freedom, obey the usual pQCD renormalization group equations, and can be related to each other without scale ambiguity by commensurate scale relations [11]. The dilaton $e^{+\kappa^2 z^2}$ soft-wall modification [156] of the AdS_5 metric, together with LF holography, predicts the functional behavior in the small Q^2 domain [139]: $\alpha_{g_1}^s(Q^2) = \pi e^{-Q^2/4\kappa^2}$. Measurements of $\alpha_{g_1}^s(Q^2)$ are remarkably consistent with this predicted Gaussian form. The predicted coupling is thus finite at $Q^2 = 0$.

We have also shown how the parameter κ, which determines the mass scale of hadrons in the chiral limit, can be connected to the mass scale Λ_s controlling the evolution of the perturbative QCD coupling [17, 139, 140]. This connection can be done for any choice of renormalization scheme, including the $\overline{MS}$ scheme, as seen in Fig. 4.8. The relation between scales is obtained by matching at a scale Q_0^2 the nonperturbative behavior of the effective QCD coupling, as determined from light-front holography, to the perturbative QCD coupling with asymptotic

freedom. The result of this perturbative/nonperturbative matching at the analytic inflection point is an effective QCD coupling which is defined at all momenta.
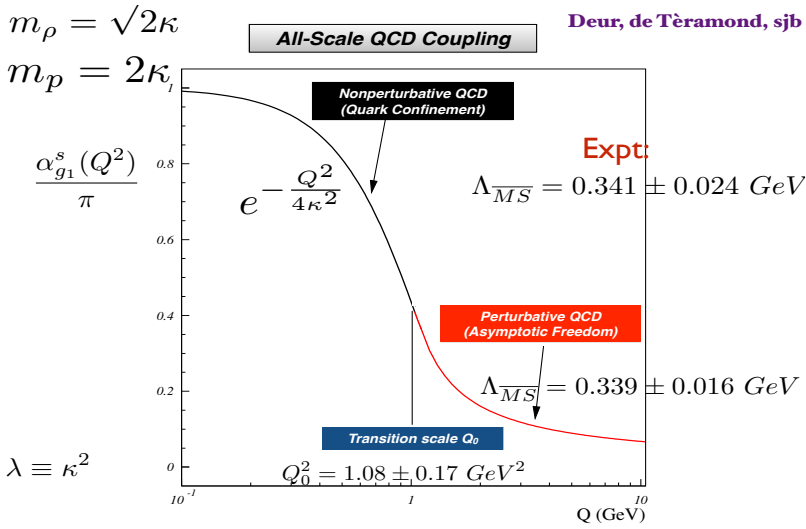
Let us assume that the QED, electroweak, and QCD gauge theories satisfy grand unification. One can then argue that each of their gauge couplings at $Q^2 = 0$ in the unified theory. is independent of the choice of renormalization scheme. The nonperturbative behavior of $\alpha_s(Q^2)$ is driven by the color confining potential $U(\zeta^2) = \kappa^4 \zeta^2$, where κ^2, like the hadron masses, is scheme independent. The coupling has no UV divergences in the nonperturbative domain. Thus $\alpha_{QCD}(Q^2)$ is analytically universal and scheme independent for Q^2 below the transition scale, the infection point, and It becomes scheme dependent only above that scale.

Knowing the QCD coupling in the nonperturbative and timelike domains also can have important implications for QCD predictions, For example, PMC scale-setting can require knowledge of the coupling outside of its usual spacelike and perturbative domains. The analytic determination of $\alpha_s(Q^2)$ over all domains will clearly greatly increase the precision and reliability of QCD predictions.
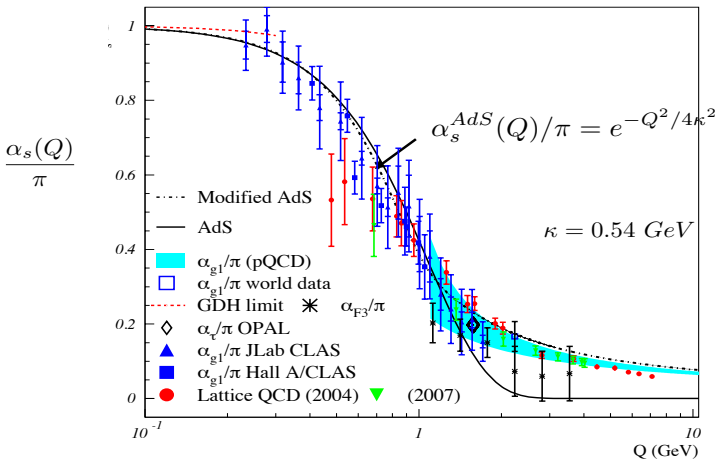
4.5   Summary

It has become conventional to simply guess the renormalization scale and choose an arbitrary range of uncertainty when making perturbative QCD (pQCD) predictions. However, this *ad hoc* assignment of the renormalization scale and the estimate of the size of the resulting uncertainty leads to anomalous renormalization scheme-and-scale dependences. In fact, relations between physical observables must be independent of the theorist's choice of the renormalization scheme, and the renormalization scale in any given scheme at any given order of pQCD is not ambiguous. The *Principle of Maximum Conformality* (PMC), which generalizes the conventional Gell-Mann-Low method for scale-setting in perturbative QED to non-Abelian QCD, provides a rigorous method for achieving unambiguous scheme-independent, fixed-order predictions for observables consistent with the principles of the renormalization group. The renormalization scale of the running coupling depends dynamically on the virtuality of the underlying quark and gluon subprocess and thus the specific kinematics of each event.

The renormalization scale in the PMC is fixed such that all β nonconformal terms are eliminated from the perturbative series and are resummed into the running coupling; this procedure results in a convergent, scheme-independent conformal series without factorial renormalon divergences. The resulting scale-fixed predictions for physical observables using the PMC are also *independent of the choice of renormalization scheme* – a key requirement of renormalization group invariance. The PMC predictions are also independent of the choice of the *initial* renormalization scale μ_0. Other important properties of the PMC are that the resulting series are free of renormalon resummation problems, and the predictions agree with QED scale-setting in the Abelian limit. The PMC is also the theoretical principle underlying the BLM procedure, commensurate scale relations between observables, and the scale-setting method used in lattice gauge theory. The number of active flavors n_f in the QCD β function is also correctly determined. We have also showed that a single global PMC scale, valid at leading order, can be derived

$$m_\rho = \sqrt{2}\kappa$$

$$m_p = 2\kappa$$

All-Scale QCD Coupling

Deur, de Tèramond, sjb

$$\frac{\alpha_{g_1}^s(Q^2)}{\pi}$$

Nonperturbative QCD
(Quark Confinement)

Expt:

$$\Lambda_{\overline{MS}} = 0.341 \pm 0.024 \; GeV$$

$$e^{-\frac{Q^2}{4\kappa^2}}$$

Perturbative QCD
(Asymptotic Freedom)

$$\Lambda_{\overline{MS}} = 0.339 \pm 0.016 \; GeV$$

Transition scale Q_0

$$\lambda \equiv \kappa^2$$

$$Q_0^2 = 1.08 \pm 0.17 \; GeV^2$$

Q (GeV)

Running Coupling from Light-Front Holography and AdS/QCD

Analytic, defined at all scales, IR Fixed Point

$$\frac{\alpha_s(Q)}{\pi}$$

$$\alpha_s^{AdS}(Q)/\pi = e^{-Q^2/4\kappa^2}$$

$$\kappa = 0.54 \; GeV$$

- ∙∙∙∙∙ Modified AdS
- —— AdS
- α_{g_1}/π (pQCD)
- □ α_{g_1}/π world data
- ∙∙∙∙∙ GDH limit ✳ α_{F3}/π
- ◇ α_τ/π OPAL
- ▲ α_{g_1}/π JLab CLAS
- ■ α_{g_1}/π Hall A/CLAS
- ● Lattice QCD (2004) ▼ (2007)

Q (GeV)

AdS/QCD dilaton captures the higher twist corrections to effective charges for Q < 1 GeV

$$e^\varphi = e^{+\kappa^2 z^2}$$

Deur, de Teramond, sjb

Fig. 4.8: (A). Prediction from LF Holography for the QCD running coupling $\alpha_{g_1}^s(Q^2)$. The magnitude and derivative of the perturbative and nonperturbative coupling are matched at the scale Q_0. This matching connects the perturbative scale $\Lambda_{\overline{MS}}$ to the nonperturbative scale κ which underlies the hadron mass scale. (B). Comparison of the predicted nonperturbative coupling with measurements of the effective charge $\alpha_{g_1}^s(Q^2)$ defined from the Bjorken sum rule. See Ref. [140].

from basic properties of the perturbative QCD cross section. We have given a detailed comparison of these PMC approaches by comparing their predictions for three important quantities R_{e+e}, R_τ and $\Gamma_{H\to b\bar{b}}$ up to four-loop pQCD corrections. The numerical results show that the single-scale PMCs method, which involves a somewhat simpler analysis, can serve as a reliable substitute for the full multi-scale PMCm method, and that it leads to more precise pQCD predictions with less residual scale dependence. The PMC thus greatly improves the reliability and precision of QCD predictions at the LHC and other colliders. As we have demonstrated, the PMC also has the potential to greatly increase the sensitivity of experiments at the LHC to new physics beyond the Standard Model.

Acknowledgements

References

1. E. C. G. Stueckelberg and A. Petermann, 26 499 1953.
2. C. G. Callan, Jr., 2 1541 1970.
3. K. Symanzik, 18 227 1970.
4. N. N. Bogoliubov and D. V. Shirkov, 103 391 1955.
5. A. Peterman, 53 157 1979.
6. S. J. Brodsky and L. Di Giustino, "Setting the Renormalization Scale in QCD: The Principle of Maximum Conformality," Phys. Rev. D **86**, 085026 (2012) doi:10.1103/PhysRevD.86.085026 [arXiv:1107.0338 [hep-ph]].
7. M. Mojaza, S. J. Brodsky and X. G. Wu, 110 192001 2013.
8. S. J. Brodsky, M. Mojaza and X. G. Wu, Phys. Rev. D **89**, 014027 (2014) doi:10.1103/PhysRevD.89.014027 [arXiv:1304.4631 [hep-ph]].
9. M. Gell-Mann and F. E. Low, Phys. Rev. **95**, 1300-1312 (1954) doi:10.1103/PhysRev.95.1300
10. S. J. Brodsky, G. P. Lepage and P. B. Mackenzie, Phys. Rev. D **28**, 228 (1983) doi:10.1103/PhysRevD.28.228
11. S. J. Brodsky and H. J. Lu, "Commensurate scale relations in quantum chromodynamics," Phys. Rev. D **51**, 3652-3668 (1995) doi:10.1103/PhysRevD.51.3652 [arXiv:hep-ph/9405218 [hep-ph]].
12. L. Di Giustino, [arXiv:2205.03689 [hep-ph]].
13. S. J. Brodsky and P. Huet, Phys. Lett. B **417**, 145-153 (1998) doi:10.1016/S0370-2693(97)01209-4 [arXiv:hep-ph/9707543 [hep-ph]].

14. M. Bohm, H. Spiesberger and W. Hollik, Fortsch. Phys. **34**, 687-751 (1986) doi:10.1002/prop.19860341102

15. M. Binger and S. J. Brodsky, Phys. Rev. D **69**, 095007 (2004) doi:10.1103/PhysRevD.69.095007 [arXiv:hep-ph/0310322 [hep-ph]].

16. J. M. Shen, X. G. Wu, B. L. Du and S. J. Brodsky, Phys. Rev. D **95**, no.9, 094006 (2017) doi:10.1103/PhysRevD.95.094006 [arXiv:1701.08245 [hep-ph]].

17. A. Deur, S. J. Brodsky and G. F. de Téramond, "Connecting the hadron mass scale to the fundamental mass scale of quantum chromodynamics," https://www.sciencedirect.com/science/article/pii/S0370269315007388?via[https://arxiv.org/abs/1409.5488 arXiv:1409.5488 [hep-ph]];

18. J. M. Shen, Z. J. Zhou, S. Q. Wang, J. Yan, Z. F. Wu, X. G. Wu and S. J. Brodsky, [arXiv:2209.03546 [hep-ph]].

19. M. Binger and S. J. Brodsky, 74 2006 054016.

20. S. J. Brodsky, G. F. de Téramond and H. G. Dosch, "Threefold complementary approach to holographic QCD," http://www.sciencedirect.com/science/article/pii/S0370269313010198 Phys. Lett. B **729**, 3 (2014) [http://arxiv.org/abs/arXiv:1302.4105 arXiv:1302.4105 [hep-th]].

21. S. J. Brodsky and X. G. Wu, 86 054018 2012.

22. A. Deur, S. J. Brodsky and G. F. de Teramond, 757 275 2016.

23. A. Deur, S. J. Brodsky and G. F. de Teramond, 90 1 2016.

24. A. Deur, J. M. Shen, X. G. Wu, S. J. Brodsky and G. F. de Teramond, 773 98 2017.

25. H. Y. Bi, X. G. Wu, Y. Ma, H. H. Ma, S. J. Brodsky and M. Mojaza, 748 13 2015.

26. P. A. Baikov, K. G. Chetyrkin and J. H. Kühn, 101 012002 2008.

27. P. A. Baikov, K. G. Chetyrkin and J. H. Kühn, 104 132004 2010.

28. I. O. Goriachuk, A. L. Kataev and V. S. Molokoedov, JHEP **05**, 028 (2022) doi:10.1007/JHEP05(2022)028 [arXiv:2111.12060 [hep-ph]].

29. P. A. Baikov, K. G. Chetyrkin, J. H. Kühn and J. Rittinger, 714 62 2012.

30. P. A. Baikov, K. G. Chetyrkin, J. H. Kühn and J. Rittinger, 108 222003 2012.

31. X. G. Wu, J. M. Shen, B. L. Du, X. D. Huang, S. Q. Wang and S. J. Brodsky, Prog. Part. Nucl. Phys. **108**, 103706 (2019) doi:10.1016/j.ppnp.2019.05.003 [arXiv:1903.12177 [hep-ph]].

32. S. Q. Wang, X. G. Wu and S. J. Brodsky, 90 037503 2014.

33. S. J. Brodsky, A. H. Hoang, J. H. Kühn and T. Teubner, 359 355 1995.

34. H. J. Lu and C. A. R. Sa de Melo, 273 260 1991.

35. H. J. Lu, 45 1217 1992.

36. X. D. Huang, J. Yan, H. H. Ma, L. Di Giustino, J. M. Shen, X. G. Wu and S. J. Brodsky, [arXiv:2109.12356 [hep-ph]].

37. S. Q. Wang, X. G. Wu, J. M. Shen and S. J. Brodsky, Chin. Phys. C **45**, no.11, 113102 (2021) doi:10.1088/1674-1137/ac1bfd [arXiv:2011.00535 [hep-ph]].

38. H. M. Yu, W. L. Sang, X. D. Huang, J. Zeng, X. G. Wu and S. J. Brodsky, JHEP **01**, 131 (2021) doi:10.1007/JHEP01(2021)131 [arXiv:2007.14553 [hep-ph]].

39. S. Q. Wang, X. G. Wu, W. L. Sang and S. J. Brodsky, 97 094034 2018.

40. S. J. Brodsky and X. G. Wu, 85 034038 2012.

41. J. Aldins, T. Kinoshita, S. J. Brodsky and A. J. Dufner, 23 441 1969.

42. S. Q. Wang, S. J. Brodsky, X. G. Wu and L. Di Giustino, arXiv:1902.01984 [hep-ph].

43. S. Q. Wang, X. G. Wu, Z. G. Si and S. J. Brodsky, 93 014004 2016.

44. G. P. Lepage, 27 192 1978.

45. S. Q. Wang, X. G. Wu, Z. G. Si and S. J. Brodsky, 90 114034 2014.

46. C. Anastasiou and K. Melnikov, 646 220 2002.

47. V. Ravindran, J. Smith and W. L. van Neerven, 665 325 2003.

48. S. Q. Wang, X. G. Wu, S. J. Brodsky and M. Mojaza, 94 053003 2016.

49. G. Aad *et al.* [ATLAS Collaboration], 115 091801 2015.
50. The ATLAS collaboration [ATLAS Collaboration], ATLAS-CONF-2015-069.
51. The ATLAS collaboration [ATLAS Collaboration], ATLAS-CONF-2017-047.
52. S. Heinemeyer *et al.* [LHC Higgs Cross Section Working Group], CERN-2013-004.
53. Q. Yu, X. G. Wu, S. Q. Wang, X. D. Huang, J. M. Shen and J. Zeng, arXiv:1811.09179 [hep-ph].
54. S. Actis, G. Passarino, C. Sturm and S. Uccirati, 811 182 2009.
55. S. Actis, G. Passarino, C. Sturm and S. Uccirati, 670 12 2008.
56. D. de Florian *et al.* [LHC Higgs Cross Section Working Group], CERN-2017-002-M.
57. D. de Florian and M. Grazzini, 718 117 2012.
58. C. Anastasiou, C. Duhr, F. Dulat, F. Herzog and B. Mistlberger, 114 212001 2015.
59. The ATLAS collaboration [ATLAS Collaboration], ATLAS-CONF-2015-060.
60. The CMS Collaboration [CMS Collaboration], CMS-PAS-HIG-17-015.
61. The ATLAS collaboration [ATLAS Collaboration], ATLAS-CONF-2018-028.
62. P. Nason, S. Dawson and R. K. Ellis, 303 607 1988.
63. P. Nason, S. Dawson and R. K. Ellis, 327 49 1989.
64. W. Beenakker, H. Kuijf, W. L. van Neerven and J. Smith, 40 54 1989.
65. W. Beenakker, W. L. van Neerven, R. Meng, G. A. Schuler and J. Smith, 351 507 1991.
66. M. Czakon, P. Fiedler and A. Mitov, 110 252004 2013.
67. S. Moch and P. Uwer, 78 034003 2008.
68. M. Czakon and A. Mitov, 824 111 2010.
69. M. Beneke, P. Falgari, S. Klein and C. Schwinn, 855 695 2012.
70. N. Kidonakis, 82 114030 2010.
71. P. Baernreuther, M. Czakon and A. Mitov, 109 132001 2012.
72. M. Czakon and A. Mitov, 1301 080 2013.
73. M. Aliev, H. Lacker, U. Langenfeld, S. Moch, P. Uwer and M. Wiedermann, 182 1034 2011.
74. M. Czakon and A. Mitov, 185 2930 2014.
75. K. Hagiwara, Y. Sumino and H. Yokoya, 666 71 2008.
76. Y. Kiyo, J. H. Kühn, S. Moch, M. Steinhauser and P. Uwer, 60 375 2009.
77. The ATLAS and CMS Collaborations [ATLAS Collaboration], ATLAS-CONF-2012-095.
78. S. Dulat, *et al.*, 93 033006 2016.
79. T. A. Aaltonen *et al.* [CDF and D0 Collaborations], 89 072001 2014.
80. S. Chatrchyan *et al.* [CMS Collaboration], 1305 065 2013.
81. G. Aad *et al.* [ATLAS Collaboration], 73 2328 2013.
82. S. Chatrchyan *et al.* [CMS Collaboration], 73 2386 2013.
83. G. Aad *et al.* [ATLAS Collaboration], 92 072005 2015.
84. S. Chatrchyan *et al.* [CMS Collaboration], 85 112007 2012.
85. G. Aad *et al.* [ATLAS Collaboration], 711 244 2012.
86. S. Chatrchyan *et al.* [CMS Collaboration], 77 15 2017.
87. G. Aad *et al.* [ATLAS Collaboration], 74 3109 2014.
88. V. Khachatryan *et al.* [CMS Collaboration], 1608 029 2016.
89. V. Khachatryan *et al.* [CMS Collaboration], 76 128 2016.
90. V. Khachatryan *et al.* [CMS Collaboration], 739 23 2014.
91. G. Aad *et al.* [ATLAS Collaboration], 91 112013 2015.
92. V. Khachatryan *et al.* [CMS Collaboration], 77 172 2017.
93. V. Khachatryan *et al.* [CMS Collaboration], 116 052002 2016.
94. The ATLAS Collaboration [ATLAS Collaboration], ATLAS-CONF-2015-049.
95. M. Aaboud *et al.* [ATLAS Collaboration], 761 136 2016.
96. M. Czakon, D. Heymes and A. Mitov, 1704 071 2017.
97. S. J. Brodsky and X. G. Wu, 86 014021 2012.

98. S. Q. Wang, X. G. Wu, Z. G. Si and S. J. Brodsky, 78 237 2018.
99. S. J. Brodsky and X. G. Wu, 109 042002 2012.
100. S. J. Brodsky and X. G. Wu, 85 114040 2012.
101. M. Aaboud *et al.* [ATLAS Collaboration], ATLAS-CONF-2011-054.
102. V. M. Abazov *et al.* [D0 Collaboration], 94 092004 2016.
103. S. Chatrchyan *et al.* [CMS Collaboration], 728 496 2014.
104. V. M. Abazov *et al.* [D0 Collaboration], 703 422 2011.
105. G. Aad *et al.* [ATLAS Collaboration], 1510 121 2015.
106. V. M. Abazov *et al.* [D0 Collaboration], 80 071102 2009.
107. The ATLAS, CDF, CMS and D0 Collaborations [ATLAS and CDF and CMS and D0 Collaborations], arXiv:1403.4427 [hep-ex].
108. T. Aaltonen *et al.* [CDF Collaboration], 101 202001 2008.
109. T. Aaltonen *et al.* [CDF Collaboration], 83 092002 2013.
110. T. Aaltonen *et al.* [CDF Collaboration], 87 092002 2013.
111. V. M. Abazov *et al.* [D0 Collaboration], 100 142002 2008.
112. V. M. Abazov *et al.* [D0 Collaboration], 84 112005 2011.
113. V. M. Abazov *et al.* [D0 Collaboration], 90 072011 2014.
114. V. M. Abazov *et al.* [D0 Collaboration], 92 052007 2015.
115. S. Chatrchyan *et al.* [CMS Collaboration], 717 129 2012.
116. S. Chatrchyan *et al.* [CMS Collaboration], 1404 191 2014.
117. The CMS Collaboration [CMS Collaboration], CMS-PAS-TOP-12-010.
118. G. Aad *et al.* [ATLAS Collaboration], 1402 107 2014.
119. The ATLAS Collaboration [ATLAS Collaboration], ATLAS-CONF-2012-057.
120. F. Derue [ATLAS Collaboration], arXiv:1408.6135 [hep-ex].
121. J. H. Kühn and G. Rodrigo, 1201 063 2012.
122. W. Bernreuther and Z. G. Si, 86 034026 2012.
123. G. T. Bodwin, E. Braaten and G. P. Lepage, 51 1125 1995.
124. G. P. Lepage and S. J. Brodsky, 22 2157 1980.
125. J. P. Lees *et al.* [BaBar Collaboration], 81 052010 2010.
126. F. Feng, Y. Jia and W. L. Sang, 115 222001 2015.
127. H. K. Guo, Y. Q. Ma and K. T. Chao, 83 114038 2011.
128. Y. Jia, X. T. Yang, W. L. Sang and J. Xu, 1106 097 2011.
129. A. Heister *et al.* [ALEPH Collaboration], 35 457 2014.
130. C. Patrignani *et al.* [Particle Data Group], 40 100001 2016.
131. L. Di Giustino, S. J. Brodsky, S. Q. Wang and X. G. Wu, "Infinite-order scale-setting using the principle of maximum conformality: A remarkably efficient method for eliminating renormalization scale ambiguities for perturbative QCD," Phys. Rev. D **102**, no.1, 014015 (2020) doi:10.1103/PhysRevD.102.014015 [arXiv:2002.01789 [hep-ph]].
132. S. Q. Wang, S. J. Brodsky, X. G. Wu, J. M. Shen and L. Di Giustino, "Novel method for the precise determination of the QCD running coupling from event shape distributions in electron-positron annihilation," Phys. Rev. D **100**, no.9, 094010 (2019) doi:10.1103/PhysRevD.100.094010 [arXiv:1908.00060 [hep-ph]].
133. S. Q. Wang, X. G. Wu, X. C. Zheng, G. Chen and J. M. Shen, 41 075010 2014.
134. V. de Alfaro, S. Fubini and G. Furlan, "Conformal invariance in quantum mechanics," http://link.springer.com/article/10.1007
135. S. Fubini and E. Rabinovici, "Superconformal quantum mechanics," https://www.sciencedirect.com/science/article/abs/pii/055032138490422X?via
136. R. S. Sufian, G. F. de Téramond, S. J. Brodsky, A. Deur and H. G. Dosch, Analysis of nucleon electromagnetic form factors from light-front holographic QCD: The space-like region, https://journals.aps.org/prd/abstract/10.1103/PhysRevD.95.014011Phys. Rev. D **95**, 014011 (2017) [https://arxiv.org/abs/1609.06688`arXiv:1609.06688 [hep-ph]`].

137. G. F. de Téramond, T. Liu, R. S. Sufian, H. G. Dosch, S. J. Brodsky and A. Deur, "Universality of generalized parton distributions in light-front holographic QCD," https://journals.aps.org/prl/abstract/10.1103/PhysRevLett.120.182001Phys. Rev. Lett. **120**, 182001 (2018) [https://arxiv.org/abs/1801.09154`arXiv:1801.09154 [hep-ph]`].

138. T. Liu, R. S. Sufian, G. F. de Téramond, H. G. Dosch, S. J. Brodsky and A. Deur, Unified description of polarized and unpolarized quark distributions in the proton, https://journals.aps.org/prl/abstract/10.1103/PhysRevLett.124.082003Phys. Rev. Lett. **124**, 082003 (2020) [https://arxiv.org/abs/1909.13818`arXiv:1909.13818 [hep-ph]`].

139. S. J. Brodsky, G. F. de Téramond and A. Deur, "Nonperturbative QCD coupling and its β function from light-front holography," https://journals.aps.org/prd/abstract/10.1103/PhysRevD.81.096010Phys. Rev. D **81**, 096010 (2010) [https://arxiv.org/abs/1002.3948`arXiv:1002.3948 [hep-ph]`].

140. S. J. Brodsky, G. F. de Téramond, A. Deur and H. G. Dosch, "The Light-Front Schrödinger Equation and the Determination of the Perturbative QCD Scale from Color Confinement: A First Approximation to QCD," Few Body Syst. **56**, no.6-9, 621-632 (2015) doi:10.1007/s00601-015-0964-1 [arXiv:1410.0425 [hep-ph]].
A. Deur, S. J. Brodsky and G. F. de Téramond, " On the interface between perturbative and nonperturbative QCD," Phys. Lett. B **757**, 275 (2016) [https://arxiv.org/abs/1601.06568`arXiv:1601.06568 [hep-ph]`].

141. L. Zou and H. G. Dosch, "A very practical guide to light front holographic QCD" [https://arxiv.org/abs/1801.00607`arXiv:1801.00607 [hep-ph]`].

142. P. A. M. Dirac, " Forms of relativistic dynamics," http://rmp.aps.org/abstract/RMP/v21/i3/p392₁$Rev. Mod. Phys.$ 21, 392(1949).

143. J. M. Maldacena, "The large-N limit of superconformal field theories and supergravity," https://link.springer.com/article/10.1023[http://arXiv.org/abs/hep-th/9711200`arXiv:hep-th/9711200`].

144. G. F. de Téramond and S. J. Brodsky, " Light-front holography: A first approximation to QCD," http://prl.aps.org/abstract/PRL/v102/i8/e081601 Phys. Rev. Lett. **102**, 081601 (2009) [http://arXiv.org/abs/0809.4899`arXiv:0809.4899 [hep-ph]`].

145. G. F. de Téramond, H. G. Dosch and S. J. Brodsky, " Baryon spectrum from superconformal quantum mechanics and its light-front holographic embedding," https://journals.aps.org/prd/abstract/10.1103/PhysRevD.91.045040Phys. Rev. D **91**, 045040 (2015) [http://arxiv.org/abs/1411.5243`arXiv:1411.5243 [hep-ph]`].

146. H. G. Dosch, G. F. de Téramond and S. J. Brodsky, "Superconformal baryon-meson symmetry and light-front holographic QCD," https://journals.aps.org/prd/abstract/10.1103/PhysRevD.91.085016Phys. Rev. D **91**, 085016 (2015) [http://arxiv.org/abs/1501.00959`arXiv:1501.00959 [hep-th]`].

147. S. J. Brodsky, G. F. de Téramond, H. G. Dosch and J. Erlich, "Light-front holographic QCD and emerging confinement," https://www.sciencedirect.com/science/article/abs/pii/S0370157315002306?via[https://arxiv.org/abs/1407.8131`arXiv:1407.8131 [hep-ph]`].

148. S. J. Brodsky, G. F. de Téramond and H. G. Dosch, "Light-front holography and supersymmetric conformal algebra: A novel approach to hadron spectroscopy, structure, and dynamics," [https://arxiv.org/abs/2004.07756`arXiv:2004.07756 [hep-ph]`].

149. G. F. de Téramond, H. G. Dosch and S. J. Brodsky, "Kinematical and dynamical aspects of higher-spin bound-state equations in holographic QCD," https://journals.aps.org/prd/abstract/10.1103/PhysRevD.87.075005Phys. Rev. D **87**, 075005 (2013) [https://arxiv.org/abs/1301.1651`arXiv:1301.1651 [hep-ph]`].

150. H. G. Dosch, G. F. de Téramond and S. J. Brodsky, "Super-symmetry across the light and heavy-light hadronic spectrum," https://journals.aps.org/prd/abstract/10.1103/PhysRevD.92.074010Phys. Rev. D **92**, 074010 (2015) [https://arxiv.org/abs/1504.05112`arXiv:1504.05112 [hep-ph]`].

151. H. G. Dosch, G. F. de Téramond and S. J. Brodsky, "Super-symmetry across the light and heavy-light hadronic spectrum II," https://journals.aps.org/prd/abstract/10.1103/PhysRevD.95.034016Phys. Rev. D **95**, 034016 (2017) [https://arxiv.org/abs/1612.02370`arXiv:1612.02370 [hep-ph]`].

152. M. Nielsen and S. J. Brodsky, "Hadronic superpart-ners from a superconformal and supersymmetric algebra," https://journals.aps.org/prd/abstract/10.1103/PhysRevD.97.114001Phys. Rev. D **97**, 114001 (2018) [https://arxiv.org/abs/1802.09652`arXiv:1802.09652 [hep-ph]`].

153. M. Nielsen, S. J. Brodsky, G. F. de Téramond, H. G. Dosch, F. S. Navarra and L. Zou, "Supersymmetry in the double-heavy hadronic spectrum," https://journals.aps.org/prd/abstract/10.1103/PhysRevD.98.034002Phys. Rev. D **98**, 034002 (2018) [https://arxiv.org/abs/1805.11567`arXiv:1805.11567 [hep-ph]`].

154. G. Grunberg, 95 70 1980.

155. A. P. Trawiński, S. D. Głazek, S. J. Brodsky, G. F. de Téramond and H. G. Dosch, "Effective confining potentials for QCD," https://journals.aps.org/prd/abstract/10.1103/PhysRevD.90.074017Phys. Rev. D **90**, 074017 (2014) [https://arxiv.org/abs/1403.5651`arXiv:1403.5651 [hep-ph]`].

156. A. Karch, E. Katz, D. T. Son and M. A. Stephanov, Linear confinement and AdS/QCD, https://journals.aps.org/prd/abstract/10.1103/PhysRevD.74.015005Phys. Rev. D **74**, 015005 (2006) [https://arxiv.org/abs/hep-ph/0602229`arXiv:hep-ph/0602229`].

157. V. N. Gribov and L. N. Lipatov, 15 438 1972.

158. G. Altarelli and G. Parisi, 126 298 1977.

159. Y. L. Dokshitzer, 46 641 1977.

160. S. J. Brodsky and G. F. de Teramond, PoS QCD **-TNT-II**, 008 (2011) [arXiv:1112.4212 [hep-th]].

161. G. F. de Teramond and S. J. Brodsky, arXiv:1203.4025 [hep-ph].

BLED WORKSHOPS
IN PHYSICS
VOL. 23, NO. 1

*Proceedings to the 25th [Virtual]
Workshop*
What Comes Beyond . . . *(p. 75)*
Bled, Slovenia, July 4–10, 2022

5   Predictions of Additional Baryons and Mesons

Paul H. Frampton
paul.h.frampton@gmail.com

Dipartimento di Matematica e Fisica "Ennio De Giorgi",
Università del Salento, Via Arnesano, 73100 Lecce, Italy

Abstract. We discuss the predictions of the bilepton model which is an extension of the standard model in which the group $SU(2) \times U(1)$ is changed to $SU(3) \times U(1)$ and the fermion families are treated non-sequentially with the third assigned differently from the first two. Cancellation of triangle anomalies and asymptotic freedom require three families. The predicted new physics includes bileptons and three heavy quarks $\mathcal{D}$. $\mathcal{S}$ and $\mathcal{T}$. QCD will bind the heavy quarks to light quarks and to each other to form baryons and mesons which, unlike bileptons, are beyond the reach of the LHC but accessible in a hypothetical 100 TeV proton-proton collider.

Povzetek: Snov, ki jo gradijo kvarki in leptoni ter ter njihova umeritvena polja, prispeva komaj dvajsetino entropije. Avtor išče odgovor s predlogom, da prispeva k entropiji vesolja poleg temne snovi, ki v pretežni meri določa gibanje snovi v galaksijah in v intergalaktičnem prostoru, ipredvsem zjemno masivna temna snov iz prvobitnih črnih lukenj.

5.1   Introduction

In this talk we shall discuss what now seems likely to be the first new particle beyond the standard model and which is now being actively searched for at the LHC. The bilepton model, a better name than the 331-Model, was invented as an example of what then was expected to be a new class of models which require the existence three families. That invention was in 1992 [1] but it required a couple more years to realise that the expected new class of models has only one member.

We remain optimistic that LHC can find a discovery signal for the bilepton gauge boson in the remainder of 2022. What we can say generally is that to invent a model which is beyond the standard model, one generally aims to both (i)address and solve a question unanswered within the standard model, and to (ii) provide explicit predictions which are testable. The bilepton model beautifully fulfils both of these criteria.

Although not a sub-theory, the model originated from studying an interesting $SU(15)$ model [2] in which the 224 gauge bosons couple to all possible pairs of the 15 states

$$(u, d)_\alpha; (\bar{u})_\alpha; (\bar{d})_\alpha; (\nu_e.e); (\bar{e}). \tag{5.1}$$

Every gauge boson therefore has a well-defined B and L so there can be no proton decay by tree-level gauge boson exchange.

In the $SU(15)$ model there is one unaesthetic feature that anomalies are cancelled by adding mirror fermions as in $15 + \bar{15}$. But persisting further, we considered the subgroups in $SU(15) \to SU(12)_q \times SU(3)_l$, especially the $SU(3)_l$ which contains an antitriplet (e^+, ν_e, e^-) where the $|L| = |Q| = 2$ bilepton can first be seen, coupling electron to positron.

The question then was: can a chiral model contain bileptons? After hundreds of trials and errors we found only one solution of the anomaly cancellation equations. This required non-sequential families where the third is assigned differently from the first two and explains why there must be three families. This is the bilepton model. It provides an answer to Rabi's famous question when the muon was discovered in 1936: "Who ordered that?"

The non-sequentiality of families offers one explanation for the failure of the $SU(5)$ model studied first in 1974 [3,4] then in hundreds of other papers. $SU(5)$ assumed sequentiality of families of the form $3(10 + \bar{5})$.

In 1977 Weinberg [5] and in 1984 Glashow [6] both considered upgrading the electroweak $SU(2)$ of the standard model to $SU(3)$ but overlooked the assignments which explain three families.

5.2   Bilepton model

The gauge group is:

$$SU(3)_C \times SU(2)_L \times U(1)_X \tag{5.2}$$

The simplest choice for the electric charge is

$$Q = \frac{1}{2}\lambda_L^3 + \left(\frac{\sqrt{3}}{2}\right)\lambda_L^8 + X\left(\frac{\sqrt{3}}{\sqrt{2}}\right)\lambda^9 \tag{5.3}$$

where

$$\text{Tr}(\lambda_L^a \lambda_L^b) = 2\delta^{ab} \tag{5.4}$$

and

$$\lambda^9 \equiv \left(\frac{\sqrt{2}}{\sqrt{3}}\right)\text{diag}(1, 1, 1) \tag{5.5}$$

Thus a triplet has charges $(X + 1, X, X - 1)$.

Leptons are treated democratically in each
of the three families. They are colour singlets in antitriplets of $SU(3)_L$:

$(e^+, \nu_e, e^-)_L$

$(\mu^+, \nu_\mu, \mu^-)_L$

$(\tau^+, \nu_\tau, \tau^-)_L$

All have $X = 0$.

Quarks in the first family are assigned to a left-handed triplet plus three singlets
of $SU(3)_L$.

$(u^\alpha, d^\alpha, D^\alpha)_L \ (\bar{u}_\alpha)_L, (\bar{d}_\alpha)_L, (\bar{D}_\alpha)_L$

Similarly for the second family

$(c^\alpha, s^\alpha, S^\alpha)_L \ (\bar{c}_\alpha)_L, (\bar{s}_\alpha)_L, (\bar{S}_\alpha)_L$

The X values are for the triplets are $X = -1/3$ and for the singlets $X = -2/3, +1/3, +4/3$
respectively. The electric charge of the new quarks D, S is $-4/3$.

The quarks of the third family are treated differently. They are assigned to a
left-handed antitriplet and three singlets under $SU(3)_L$

$(b^\alpha, t^\alpha, T^\alpha)_L \ (\bar{b}_\alpha)_L, (\bar{t}_\alpha)_L, (\bar{T}_\alpha)_L$

The antitriplet has $X = +2/3$ and the singlets carry $X = +1/3, -2/3, -5/3$ respec-
tively. The new quark T has $Q = 5/3$.

Some of the relevant LHC phenomenology is discussed in [7]. A refined mass
estimate [8] for the bilepton is is $M(Y^{\pm\pm}) = (1.29 \pm 0.06)$ TeV where *faute de mieux*
it was assumed that the symmetry breaking of $SU(3)_L$ is closely similar to that of
$SU(2)_L$. It will be pleasing if the physical mass is consistent with this.

5.3   New Quarks

Because the quarks are in triplets and anti-triplets of $SU(3)_L$, rather than only in
doublets of $SU(2)_L$ as in the standard model, there is necessarily an additional
quark in each family. In the first and second families they are the $\mathcal{D}$ and $\mathcal{S}$ respec-
tively, both with charge $Q = -4/3$ and lepton number $L = +2$. In the third family
is the $\mathcal{T}$ with charge $Q = +5/3$ and lepton number $L = -2$. All the three TeV scale
quarks are colour triplets with spin-$\frac{1}{2}$ and baryon number $B = \frac{1}{3}$. Their masses are
yet to be measured but may be expected to be below the ceiling of 4.1TeV which

is the upper limit for symmetry breaking of $SU(3)_L$ and probably above 1TeV. By analogy with the known quarks, one might expect $M(\mathcal{T}) > M(\mathcal{S}) > M(\mathcal{D})$, although without experimental data this is conjecture.

The heavy quarks and antiquarks will be bound to light quarks and antiquarks, and to each other, to form an interesting spectroscopy of mesons and baryons. Let us first display, in Tables 1, 2 the TeV mesons, then in Tables 3,4,5 the TeV baryons. The charge conjugate states are equally expected, and will reverse the signs of Q and L.

5.4   Additional Baryons and Mesons

.

Table 5.1: TeV mesons $\mathcal{Q}\bar{q}$

$\mathcal{Q}$	$\bar{q}$	Q	L
$\mathcal{D}/\mathcal{S}$	$\bar{u}$ etc.	-2	+2
$\mathcal{D}/\mathcal{S}$	$\bar{d}$ etc.	-1	+2
$\mathcal{T}$	$\bar{u}$ etc.	+1	-2
$\mathcal{T}$	$\bar{d}$ etc.	+2	-2

Although the $\mathcal{Q}$ masses are unknown, it may be reasonable first to make a preliminary discussion of these states by assuming that

$$M(\mathcal{T}) > M(\mathcal{S}) + 2M_t > M(\mathcal{D}) + 4M_t \qquad (5.6)$$

where M_t is the top quark mass so that the lightest of the TeV baryons and mesons are those containing just one $\mathcal{D}$ quark or one $\bar{\mathcal{D}}$ antiquark. The next lightest are the TeV baryons and mesons containing just one $\mathcal{S}$ quark or one $\bar{\mathcal{S}}$ antiquark.

We begin by discussing the decay modes of the $\mathcal{D}\bar{q}$ mesons in Table 1, focusing on final states from the first family. The decays of $\mathcal{D}$ include, taking care of L conservation,

Table 5.2: TeV mesons $\mathcal{Q}\bar{\mathcal{Q}}$

$\mathcal{Q}$	$\bar{\mathcal{Q}}$	Q	L
$\mathcal{D}/\mathcal{S}$	$\bar{\mathcal{D}}/\bar{\mathcal{S}}$	0	0
$\mathcal{D}/\mathcal{S}$	$\bar{\mathcal{T}}$	-3	+4
$\mathcal{T}$	$\bar{\mathcal{T}}$	0	0

Table 5.3: TeV baryons $\mathcal{Q}qq$

$\mathcal{Q}$	qq	Q	L
$\mathcal{D}/\mathcal{S}$	dd etc.	-2	+2
$\mathcal{D}/\mathcal{S}$	ud etc.	-1	+2
$\mathcal{D}/\mathcal{S}$	uu etc.	0	+2
$\mathcal{T}$	dd etc.	+1	-2
$\mathcal{T}$	ud etc.	+2	-2
$\mathcal{T}$	uu etc,	+3	-2

Table 5.4: TeV baryons $\mathcal{Q}\mathcal{Q}q$

$\mathcal{Q}\mathcal{Q}$	q	Q	L
$(\mathcal{D}/\mathcal{S})(\mathcal{D}/\mathcal{S})$	d etc.	-3	+4
$(\mathcal{D}/\mathcal{S})(\mathcal{D}/\mathcal{S})$	u etc.	-2	+4
$(\mathcal{D}/\mathcal{S})\mathcal{T}$	d etc.	0	0
$(\mathcal{D}/\mathcal{S})\mathcal{T}$	u etc.	+1	0
$\mathcal{T}\mathcal{T}$	d etc.	+3	-4
$\mathcal{T}\mathcal{T}$	u etc.	+4	-4

$$\mathcal{D} \rightarrow d + Y^-$$
$$\rightarrow d + (e^- + \nu_e)$$
$$\rightarrow d + (\mu^- + \nu_\mu)$$
$$\rightarrow d + (\tau^- + \nu_\tau)$$

$$(5.7)$$

Table 5.5: TeV baryons $\mathcal{QQQ}$

$\mathcal{QQQ}$	Q	L
$(\mathcal{D}/\mathcal{S})(\mathcal{D}/\mathcal{S})(\mathcal{D}/\mathcal{S})$	-4	+6
$(\mathcal{D}/\mathcal{S})(\mathcal{D}/\mathcal{S})\mathcal{T}$	-1	+2
$(\mathcal{D}/\mathcal{S})\mathcal{T}\mathcal{T}$	+2	-2
$\mathcal{T}\mathcal{T}\mathcal{T}$	+5	-6

which implies that decays of the $(\mathcal{D}\bar{u})$ meson include

$$
\begin{aligned}
(\mathcal{D}\bar{u}) &\to \pi^- + (e^- + \nu_e) \\
&\to \pi^- + (\mu^- + \nu_\mu) \\
&\to \pi^- + (\tau^- + \nu_\tau)
\end{aligned}
$$

(5.8)

and variants thereof where π^- is replaced by any other non-strange negatively charged meson. The d in Eq.(5.7) can be replaced by s or b which subsequently decay.

An alternative to Eq.(5.7) is

$$
\begin{aligned}
\mathcal{D} &\to u + Y^{--} \\
&\to u + (e^- + e^-) \\
&\to u + (\mu^- + \mu^-) \\
&\to u + (\tau^- + \tau^-)
\end{aligned}
$$

(5.9)

which implies additional decay modes of the $(\mathcal{D}\bar{u})$ meson which include

$$
\begin{aligned}
(\mathcal{D}\bar{u}) &\to \pi^0 + (e^- + e^-) \\
&\to \pi^0 + (\mu^- + \mu^-) \\
&\to \pi^0 + (\tau^- + \tau^-)
\end{aligned}
$$

(5.10)

and variants obtained by flavour replacements. Eqs.(5.8) and (5.10), and their generalisations to other flavours, suffice to illustrate the richness of $(\mathcal{D}\bar{u})$ decays.

Turning to the meson $\mathcal{D}\bar{d}$, we can use Eq.(5.7) to identify amongst its possible decays

$$(\mathcal{D}\bar{d}) \rightarrow \pi^0 + (e^- + \nu_e)$$
$$\rightarrow \pi^0 + (\mu^- + \nu_\mu)$$
$$\rightarrow \pi^0 + (\tau^- + \nu_\tau)$$

$$(5.11)$$

and variants thereof where π^0 is replaced by any other non-strange neutral meson. When u in Eq.(5.7) is replaced by c or t which subsequently decay, we arrive at many other decay channels additional to Eq.(5.11).

Employing instead the $\mathcal{D}$ decays in Eq.(5.9) implies additional decay modes of $(\mathcal{D}\bar{d})$ meson that include

$$(\mathcal{D}\bar{d}) \rightarrow \pi^+ + (e^- + e^-)$$
$$\rightarrow \pi^+ + (\mu^- + \mu^-)$$
$$\rightarrow \pi^+ + (\tau^- + \tau^-)$$

$$(5.12)$$

and variants obtained by flavour replacement. Eqs.(5.11) and (5.12), merely illustrate a few of the simplest $(\mathcal{D}\bar{d})$ decays. There are many more.

Next we consider the lightest TeV baryons in Table 3 with $\mathcal{Q} = \mathcal{D}$. Using the $\mathcal{D}$ decays from Eq.(5.7) we find for $(\mathcal{D}uu)$ decay

$$(\mathcal{D}uu) \rightarrow p + (l_i^- + \nu_i).$$

$$(5.13)$$

together with flavour rearrangements. Here, as in subsequent equations, $i = e, \mu, \tau$.

Alternatively, the $\mathcal{D}$ decays from Eq.(5.9) lead to

$$(\mathcal{D}uu) \rightarrow N^{*++} + Y^{--}.$$
$$\rightarrow p + \pi^+ + (l_i^- + l_i^-)..$$

$$(5.14)$$

Looking at the TeV baryon $(\mathcal{D}ud)$ the respective sets of decays corresponding to Eq.(5.7) are

$$(\mathcal{D}ud) \rightarrow n + (l_i^- + \nu_i)$$

$$(5.15)$$

where only the simplest light baryon is exhibited.

Corresponding to $\mathcal{D}$ decays in Eq.(5.9) there are also

$$(\mathcal{D}ud) \rightarrow p + (l_i^- + l_i^-)$$

$$(5.16)$$

in the simplest cases.

Finally, of the $(\mathcal{D}qq)$ TeV baryons, we write out the decays for $(\mathcal{D}dd)$, first for the $\mathcal{D}$ decays in Eq.(5.7)

$$
\begin{aligned}
(\mathcal{D}dd) &\to N^{*-} + Y^- \\
&\to n + \pi^- + (l_i^- + \nu_i).
\end{aligned}
$$

$$(5.17)$$

within flavour variations.

With the Eq.(5.9) decays of $\mathcal{D}$ there are also decays

$$
(\mathcal{D}dd) \to n + (l_i^- + l_i^-)
$$

$$(5.18)$$

again with more possibilities by choosing alternative flavours.

We now replace the TeV quark $\mathcal{D}$ by the next heavier TeV quark $\mathcal{S}$ and repeat our study of decays whereupon we shall encounter the first example of decay not only to the known quarks but also to a TeV quark.

The TeV quark $\mathcal{S}$ has possible decay channels

$$
\begin{aligned}
\mathcal{S} &\to d + Y^- \\
&\to d + (e^- + \nu_e) \\
&\to d + (\mu^- + \nu_\mu) \\
&\to d + (\tau^- + \nu_\tau) \\
&\to \mathcal{D} + Z' \\
&\to d + (e^- + \nu_e) + (e^+ + e^-) \\
&\to d + (e^- + \nu_e) + (\mu^+ + \mu^-) \\
&\to d + (e^- + \nu_e) + (\tau^+ + \tau^-) \\
&\to d + (\mu^- + \nu_\mu) + (e^+ + e^-) \\
&\to d + (\mu^- + \nu_\mu) + (\mu^+ + \mu^-) \\
&\to d + (\mu^- + \nu_\mu) + (\tau^+ + \tau^-) \\
&\to d + (\tau^- + \nu_\tau) + (e^+ + e^-) \\
&\to d + (\tau^- + \nu_\tau) + (\mu^+ + \mu^-) \\
&\to d + (\tau^- + \nu_\tau) + (\tau^+ + \tau^-)
\end{aligned}
$$

$$(5.19)$$

where we note the opening up of channels due to $\mathcal{S} \to \mathcal{D}$ decay.

With Eq.(5.19) in mind, the decays of the TeV meson $(\mathcal{S}\bar{u})$ include

$$(\mathcal{S}\bar{u}) \rightarrow \pi^- + (l_i^- + \nu_i)$$
$$\rightarrow \pi^- + (l_i^- + \nu_i) + (l_j^+ + l_j^-)$$

$$(5.20)$$

where the second line involves a $\mathcal{D}$ intermediary.

An alternative to Eq.(5.19) is

$$\mathcal{S} \rightarrow u + Y^{--}$$
$$\rightarrow u + (e^- + e^-)$$
$$\rightarrow u + (\mu^- + \mu^-)$$
$$\rightarrow u + (\tau^- + \tau^-)$$

$$(5.21)$$

which implies additional decay modes of $(\mathcal{S}\bar{u})$

$$(\mathcal{S}\bar{u}) \rightarrow \pi^0 + (l_i^- + l_i^-)$$

$$(5.22)$$

and variants which replace π^0 by another neutral non-strange meson. Eqs.(5.20) and (5.22), illustrate sufficiently $(\mathcal{S}\bar{u})$ decays.

Turning to the meson $(\mathcal{S}\bar{d})$, we can use Eq.(5.19) to identify its possible decays

$$(\mathcal{S}\bar{d}) \rightarrow \pi^0 + (l_i^- + \nu_i)$$

$$(5.23)$$

When u in Eq.(5.19) is replaced by c or t which subsequently decay, we arrive at many other decay channels additional to Eq.(5.23).

Employing instead the $\mathcal{S}$ decays in Eq.(5.21) implies additional decay modes of $(\mathcal{S}\bar{d})$ that include

$$(\mathcal{S}\bar{d}) \rightarrow \pi^+ + (l_i^- + l_i^-)$$

$$(5.24)$$

and variants obtained by flavour replacement. Eqs.(5.23) and (5.24), illustrate only a few of the simplest $(\mathcal{S}\bar{d})$ decays. There are many more.

Next we consider the lightest TeV baryons in Table 3 with one $\mathcal{Q} = \mathcal{S}$. Using the $\mathcal{S}$ decays from Eq.(5.19) we find for $(\mathcal{S}uu)$ decay

$$(\mathcal{S}uu) \rightarrow p + (l_i^- + \nu_i).$$

$$(5.25)$$

together with flavour rearrangements.

Alternatively, the $\mathcal{S}$ decays from Eq.(5.21) lead to

$$(\mathcal{S}uu) \to N^{*++} + (l_i^- + l_i^-)..$$
$$\to p + \pi^+ + (l_i^- + l_i^-).$$

(5.26)

Looking at the TeV baryon $(\mathcal{S}ud)$ the respective sets of decays corresponding to Eq.(5.19) are

$$(\mathcal{S}ud) \to n + (l_i^- + \nu_i)$$

(5.27)

where only the simplest version is exhibited.

Corresponding to the $\mathcal{S}$ decays in Eq.(5.21) there are the decays

$$(\mathcal{S}ud) \to p + (l_i^- + l_i^-)$$

(5.28)

For baryon $(\mathcal{S}dd)$, firstly from the $\mathcal{S}$ decays in Eq.(5.19) we have

$$(\mathcal{S}dd) \to N^{*-} + Y^-$$
$$\to n + \pi^- + (l_i^- + \nu_i).$$

(5.29)

within flavour variations.

Secondly, from the Eq.(5.21) decays of $\mathcal{S}$ there are baryon decays of the type

$$(\mathcal{S}dd) \to n + (l_i^- + l_i^-)$$

(5.30)

with more possibilities by choosing alternative flavours.

5.5   Discussion

We could continue further to study decays of all the baryons and mesons in our Tables. However, it seems premature to do so, until we know from experimental data the masses and mixings of $\mathcal{D}, \mathcal{S}, \mathcal{T}$. We remark only that the type of lepton cascade which we have exhibited in Eq.(5.19) becomes ever more prevalent as the lepton number of the decaying hadron increases.

We may expect, by analogy with the top quark mass being close to the weak scale that the mass of the $\mathcal{T}$ quark, although probably below 4.1 TeV for the symmetry-breaking reason discussed *ut supra*, might be not much below. For example it might exceed 3 TeV whereupon the mass of a $(\mathcal{T}\mathcal{T}\mathcal{T})$ baryon could exceed 9 TeV. Since this baryon has high lepton number, it must be pair produced and such production is far beyond the reach of the 14 TeV LHC. Its study would require a 100 TeV collider of the type presently under preliminary discussion. As a foretaste of the physics accessible to such a hypothetical collider, the simplest decay of the $(\mathcal{T}\mathcal{T}\mathcal{T})$ baryon we can find is

$$p + 4(e^+) + 2(\bar{\nu}_e).$$

which would be very exciting to confirm.

At the time of writing, the particles exhibited in our Tables are conjectural. After the bilepton is discovered the existence of all the additional baryons and mesons in our five Tables would become sharp predictions.

The bilepton resonance in $\mu^\pm\mu^\pm$ has been the subject of searches by the ATLAS and CMS Collaborations at the LHC, starting in March 2021. In March 2022, ATLAS published an inconclusive result [9] about the existence of the resonance, putting only a lower mass limit $M_Y > 1.08$ TeV. CMS has better momentum resolution and, what is the same thing, charge identification than ATLAS and should be able to investigate the bilepton resonance proper. The high sensitivity of CMS is a result of serendipity because it was designed in 1993 not for the bilepton but to search for heavy Z-primes [11]. A second serendipity was an accidental 2015 meeting in London between us and Sir Tejinder Virdee who helped design the CMS detector.

Our strong belief in the existence of the bilepton lies partly in the close relationship between the 1961 paper [10] which solved the parity puzzle and our 1992 paper [1] which solved the family puzzle. We regard these two papers which span three decades as well-matched bookends,

According to our calculations [7], the Run 2 data with 139/fb collected by 2018 are sufficient for a CMS discovery of the bilepton. If not, future LHC runs up to their target integrated luminosity of 4/ab can provide 28 times as many events and bilepton discovery would be merely postponed. We do hope, however, that a great discovery will be made by the LHC within six months from today (July 25, 2022).

Note added:
We answer here one interesting question received after our talk: Why are these heavy states not as unstable as the top quark which lives for less than a trillion trillionth of a second? The answer is that they decay via bilepton exchange. This fact renders their lifetimes a trillion times longer than the top quark lifetime.

Acknowlegement

We thank the organisers Norma Borstnik, Maxim Khlopov and Holger Nielsen for their invitation to present this talk.

References

1. P.H. Frampton,
   Phys. Rev. Lett. **69,** 2889 (1992).
2. P.H. Frampton and B.-H. Lee,
   Phys. Rev Lett. **64,** 619 (1990).
3. H. Georgi and S.L. Glashow,
   Phys. Rev. Lett. **32,** 438 (1974).
4. H. Georgi, H.R. Quinn and S. Weinberg,
   Phys. Rev. Lett. **33,** 451 (1974).
5. B.W.Lee and S.Weinberg,
   Phys.Rev. Lett. **38,** 1237 (1977).
6. S.L. Glashow,
   Fifth Workshop on Grand Unification.
   World Scientific Publishing Company (1984).
7. G. Corcella, C, Coriano, A, Costantini and P.H. Frampton,
   Phys. Lett. **B773,** 544 (2017); *ibid*. **B785,** 73 (2018);
   ibid. **B826,** 136904 (2022).
8. C. Coriano and P.H. Frampton,
   Mod. Phys. Lett. **A36,** 2150118 (2021).
9. ATLAS Collaboration,
   ATLAS-CONF-2022-010 (March 2022).
10. S.L. Glashow,
    Nucl. Phys. **22,** 579 (1961).
11. T. Virdee,
    Several private communications beginning in 2015.

6 Possibility of Additional Intergalactic and Cosmological Dark Matter

Paul H. Frampton
paul.h.frampton@gmail.com

Dipartimento di Matematica e Fisica "Ennio De Giorgi",
Università del Salento, Via Arnesano, 73100 Lecce, Italy

Abstract. The entropies of the known entities in the universe add to a total which is some twenty orders of magnitude below the holographic limit. Based on an assumption that the entropies should saturate the limit, we suggest that there exists dark matter, in the form of extremely massive primordial black holes, in addition to the dark matter known to exist inside galaxies and clusters of galaxies.

Povzetek: Avtor ponudi napovedi bileptonskega modela, ki je razširitev standardnega modela, v katerem zamenja grupo $SU(2) \times U(1)$ z grupo $SU(3) \times U(1)$. S podobno spremembo grupe poseže tudi v število družin kvarkov in leptonov, pričemer meni, da zahteva odprava trikotniške anomalije in asimptotska svoboda teorije tri družine kvarkov in leptonov. Napoveduje tri nove težke kvarke, $\mathcal{D}$. $\mathcal{S}$ in $\mathcal{T}$, in nova vezana stanja dileptonov. Dileptone bodo izmerili na LHC, novi barioni in mezoni pa potrebujejo protonski trkalnik, ki bi dosegel 100Tev.

Keywords: Dark matter; Entropy of the universe; Black holes.

6.1 Introduction

In particle theory, the concept of entropy is usually not regarded as fundamental. Particle theorists rarely even use the word entropy. For one elementary particle, entropy is neither defined nor useful.

In general relativity and cosmology, the situation is different. For black holes, entropy is a central and useful concept. We shall in this talk argue that the origin and nature of cosmological dark matter can be best understood by consideration of the entropy of the universe.

We have made such an argument some years ago but that discussion was perhaps too diluted by considering simultaneously dark matter being made from elementary particles such as WIMPs and axions. In this talk, we dispose of microscopic candidates in one paragraph. The standard model of particle theory (SM) has two examples of lack of naturalness, the Higgs boson and the strong CP problem. Our position is that to understand these we still need to understand better the SM itself. Regarding the strong CP problem, it is too *ad hoc* to posit a spontaneously broken global symmetry and consequences which include an axion. Concerning the WIMP, the idea that dark matter experiences weak interactions arose from assuming TeV-scale supersymmetry which is now disfavoured by LHC data. To identify the dark matter, we therefore instead look up at the night sky.

Assuming dark matter is astrophysical, and that the reason for its existence lies in the Second Law of Thermodynamics, we shall be led uniquely to the dark matter constituent as the Primordial Black Hole (PBH). We must admit that there is no observational evidence for any PBH, but according to our discussion PBHs must exist. In the ensuing discussion, we shall speculate that they exist in abundance in three tiers of mass up to and including extremely high masses which are far greater than the masses of galaxy clusters and approach closely to the mass of the visible universe.

Because PBH entropy goes like mass squared, we are mainly interested in masses satisfying $M_{PBH} > 100 M_\odot$. Within the Milky Way, we use the acronym PIMBH for intermediate mass PBHs in the mass range $10^2 M_\odot < M_{PIMBH} < 10^5 M_\odot$. Outside the Milky Way we entertain all masses $10^2 M_\odot < M_{PBH} < 10^{22} M_\odot$. Of these, we use PSMBH for supermassive PBHs in the mass range $10^6 M_\odot < M_{PSMBH} < 10^{11} M_\odot$ and PEMBH for extra massive PBHs with $10^{12} M_\odot < M_{PEMBH} < 10^{22} M_\odot$.

Although the visible universe (VU) is not a black hole, its Schwartzschild radius is about 68% of its physical radius, 30 Gly versus 44 Gly, so it is remarkably close. This curious fact seems to have no bearing on the nature of dark matter. Acronyms will be useful: CMB is the familiar cosmic microwave background while CIB refers to its counterpart, cosmic infra-red background.

6.2   Entropy

We begin with the premise that the early universe be regarded in an approximate sense as a thermodynamically-isolated system for the purposes of our discussion. It certainly contains a number of particles, $\sim 10^{80}$, vastly larger than the numbers normally appearing in statistical mechanics, such as Avogadro's number, $\sim 6 \times 10^{23}$ molecules per mole.

No heat ever enters or leaves and it can be considered as though its surface were covered by a perfect thermal insulator. It is impracticable to solve all the Boltzmann transport equations so it is mandatory to use thermodynamic arguments, provided that we may argue that the system is proximate to thermal equilibrium.

Making the then-unsupported assumption in 1872 of atoms and molecules, Boltz-mann discovered the quantity $S(t)$ in terms of the molecular momentum distribu-tion function $f(\mathbf{p}, t)$

$$S(t) = -\int d\mathbf{p} f(\mathbf{p}, t) \log f(\mathbf{p}.t) \tag{6.1}$$

which satisfies

$$\left(\frac{dS(t)}{dt}\right) \geq 0 \tag{6.2}$$

and can be identified with the thermodynamic entropy. The crucial inequality, Eq(6.2), the Second Law, was derived for non-equilibrium systems assuming only the Boltzmann transport equations and the ergodic hypothesis.

Ascertaining the nature of the dark matter can be regarded as a detective's mission and there are useful clues in the visible universe. We can made an inventory of the entropies of the known objects in the visible universe, using a venerable source, Weinberg's 1972 book.

Let us model the visible universe as containing 10^{11} galaxies each of mass $10^{12} M_\odot$ and each containing one central SMBH with mass $10^7 M_\odot$. We recall the dimen-sionless entropy of a black hole $S/k(M_{BH} = \eta M_\odot) \sim 10^{78} \eta^2$. Then the inventory is

- SMBHs $\sim 10^{103}$
- Photons $\sim 10^{88}$
- Neutrinos $\sim 10^{88}$
- Baryons $\sim 10^{80}$

We regard this entropy inventory as a **<u>first clue</u>**. From the point of view of en-tropy the universe would be only infinitesimally changed if everything except the SMBHs were removed. This suggests that more generally black holes totally dominate the entropy, as we shall find in the sequel.

A second remarkable fact about the visible universe is the near-perfect black-body spectrum of the CMB which originated some 300,000 years after the beginning of the present expansion era, or after the Big Bang in a more familiar language. We are not tied to a Big Bang which we believe will eventually be replaced by a bounce from contraction to expansion in cyclic cosmology.

The precise CMB spectrum is a **<u>second clue</u>** about dark matter. It suggests that the plasma of electrons and protons prior to recombination is in excellent thermal equilibrium, and hence the matter sector was in thermal equilibrium for the first 300,000 years. This, combined with the thermal isolation mentioned already, underwrites the use of entropy, and the second law, during this period.

A **third clue** and final one about dark matter lies with the holographic principle [5] which provides an upper limit on the entropy of the visible universe, the area of its

surface in units of the Planck length. Given it present co-moving radius 44 Gly this requires $S_{Universe}/k \leq 10^{123}$. The entropy of the contents which is so bounded might nevertheless equal this limit which is many orders of magnitude higher than the total entropy in the limited inventory listed above. That this may be the case is based only on our cosmological intuition that the universe is beautiful.

In a this talk we investigate the possibility that PBHs aaturate the holographic entropy bound [1] and entertain the possibility of extremely high masses up to $10^{22}M_{\odot}$. Just a few of these could saturate the maximum entropy bound but here we discuss such a situation more generally.

One might reasonably be concerned that such objects might be inconsistent with existing knowledge in astronomy and cosmology? To our knowledge, there is no serious contradiction. There are at least three places where such a theory might be challenged. Firstly, there are limits on the cosmological principle which asserts the large-scale homogeneity and isotropy of the universe. Secondly, if PBHs are formed during the era of Large-Scale Structure formation, they might conceivably play a deleterious röle. Thirdly and finally, one might also worry about whether the theory leaves inviolate the precise thermal spectrum and isotropy of the CMB? On the third point, consistency requires only that additional non-thermalised photons are absent or sufficiently suppressed.

It is appropriate to refer to the high mass objects as additional dark matter because they are not associated with specific galaxies or clusters of galaxies but are located elsewhere in the universe. The total mass of additional dark is expected to be comparable in order of magnitude to that of dark matter inside galaxies and clusters but its total entropy is extremely much greater. Indeed, we would say that the possibility of equalling the holographic bound can be uniquely achieved only with the presence of additional dark matter in the form of extremely massive black holes.

Another relevant consideration is PBH production. The mass governed by the horizon size at cosmic time t is

$$M_{PBH} = 10^5 M_{\odot} \left(\frac{t}{1 \text{ second}} \right) \tag{6.3}$$

so that taking $t < 300,000y$ to precede recombination when the CMB originates would require that

$$M_{PBH} < M_{cmb} \sim 10^{18} M_{\odot} \tag{6.4}$$

However, it is possible that more massive PBHs may be formed later provided they do not produce photons which disturb the CMB spectrum.

As examples of higher masses we take $10^7 M_{\odot}$ and $10^{14} M_{\odot}$ respectively. According to Eq.(6.3) theses are produced at $t = 100s$ and $t = 30y$. For the largest mass mentioned above, $10^{22} M_{\odot}$, the formation time in Eq.(6.3) is $t = 3Gy$ which is quite recent cosmologically.

In reality, we might expect a smoother PBH mass spectrum than suggested by these monochromatic examples. However, at least one PBH formation model [6] does suggest quasi-monochromatic formation so we must consider all possibilities.

6.3   The Great Attractor

It was pointed out by Dressler [3] that the peculiar velocities of certain galaxies point to the existence of a specific mass overdensity which corresponds to what he called the Great Attractor with mass $M_{GA} \sim 10^{18} M_\odot$. This the only such overdensity in a volume $\sim (1Gpc)^3$ so assuming a uniform density within the visible universe there could be a few thousand of them. The approximate equality of M_{GA} with M_{cmb} in Eq.(6.4) is presumably accidental.

For our present purposes, we shall assume that the Great Attractor is a PBH, and use it as a jumping off point to posit the existence in the visible universe of truly cosmological size PBHs. The size of the GA is comparable to that of the Milky Way ~ 100kpc. For a PBH with mass $10^{22} M_\odot$ the Schwarzschild radius is comparable to that of the visible universe and too large to be detectable on a plot like Fig 2 in Reference [3].

In Table 1, we summarise the entropy properties for two examples of intergalactic dark matter.

We see from Table 1 that they suggest an opportunity to approach the holographic upper bound because if we take the maximum allowed number of GAs their entropy adds to $S/k \sim 10^{117}$ just a million times less than the limit.

To put this in perspective, we recall the dark matter suggested in [4] and which could be the correct explanation for the dark matter inside of galaxies such as the Milky Way. If we take those intermediate-mass black holes to all have mass $100 M_\odot$ their entropy adds to only $S/k \sim 10^{103}$ which is approximately the same as the entropy of the supermassive black holes (SMBHs) known to reside at galactic centres. Of the known objects in the universe, SMBHs overwhelmingly dominate the entropy. Nevertheless, their entropy falls mysteriously short of the holographic limit by a huge factor of some twenty orders of magnitude.

Table 6.1: Values of Schwarzschild radius and Dimensionless entropy.

Mass	Schwarzschild radius	Entropy S/k
$10^{18} M_\odot$	100 kpc	10^{114}
$10^{22} M_\odot$	1 Gpc	10^{122}

We are here exploring the assumption[1] that the content of the universe possesses entropy adding to the holographic limit. Initially our expectation was to find this possibility excluded but all we would say now is that it must involve a significant quantity of additional dark matter.

Looking at the universe from the viewpoint of entropy is very different from the viewpoint of mass. For example, it is well known that normal matter is only 5% in a mass pie-chart. In an entropy pie-chart, however, with only the known objects, baryonic matter provides only 10^{-25} of total entropy which diminishes its importance much further.

In the context of the additional dark matter model being discussed in the present article, normal matter would provide only an infinitesimal fraction ($\sim 10^{-45}$) of the total entropy, the rest being dark matter.

6.4   Maximal Additional Dark Matter

From the entropy viewpoint, it is interesting that the visible universe is so close to being itself a black hole in the sense that its Schwarzschild radius $9\,\mathrm{Gpc}$ is some two thirds of the co-moving radius $13.5\,\mathrm{Gly}$,

In terms of mass-energy, this is merely a restatement of the fact that the present density is close to the critical density. But for entropy it is extremely puzzling, because the known content has only an infinitesimally tiny fraction of its maximum possible value. This suggests that there is something dominating the cosmological entropy which is being overlooked.

The only candidate to fill this rôle is, to our knowledge, extremely massive black holes, such as those in Table 1, which may be regarded as a straightforward extension of the dark matter in galaxies and supermassive black holes in galactic cores, all here assumed to be PBHs.

We have no prejudice about the mass function of extremely massive PBHs. It may be a smooth function or a series of almost monochromatic steps as suggested by some numerical work [6]. Here we discuss the latter possibility.

First, we reconsider the Great Attractor mass, M_{GA}, and the viable possibility of one thousand PBHs of this size. As we have seen, these can contribute $S/k \sim 10^{117}$ to the entropy of the universe, much more than the supermassive black holes, $\sim 10^{103}$.

The other, higher, mass scale mentioned *ut supra* was M_{cp} which was taken to be the largest mass which is consistent with present evidence supporting the

---

[1] This assumption is not part of, but is additional to, the holographic principle [5] as proposed first by 't Hooft in 1993. Our additional assumption may be necessary in order to describe Nature.

cosmological principle. Each such black hole provides a contribution to dimensionless entropy which is only one order of magnitude below the holographic limit. Therefore, no more than a few are allowed. If these exist, then saturating the maximum allowed entropy can easily be fulfilled.

6.5   James Webb Space Telescope

At large red-shifts $Z > 15$, a population of PBHs would be expected to accrete matter and emit in X-ray and UV radiation which will be redshifted into the CIB to be probed for the first time by the James Webb Space Telescope which could therefore provide support for PBH formation.

Analysis of a specific PBH formation model supports this idea that the JWST observations in the infrared could provide relevant information about whether PBHs really are formed in the early universe. This is important because although we have plenty of evidence for the existence of black holes, whether any of them is primordial is not known. The gravitational wave detectors LIGO, VIRGO and KAGRA have discovered mergers in black hole binaries with initial black holes in the mass range $3-85M_\odot$. We suspect that all or most of these are not primordial but that is only conjecture. The supermassive black holes at galactic centres, including Sgr A* at the centre of the Milky Way, are well established and are primordial in our toy model. Whether that is the case in Nature is unknown.

Because of the no-hair theorem that black holes are completely characterised by their mass, spin and electric charge (usually taken to be zero), there is no way to tell directly whether a given black hole is primordial or the result of gravitational collapse of a star. The distinction between a primordial and a non-primordial black hole can be made only from knowledge of its history. For example, if it existed before star formation, it must be primordial. The infra-red data from JWST will able to provide insight into the central question of PBH formation.

A second deep insight likely to be provided by the JWST is whether or not Population III stars existed at high red shifts. Their existence looks inevitable from metallicity arguments. Our Sun and other typical stars have a surprisingly high metallicity close to 2%. Such stars cannot be formed directly from the primordial gases which have vanishing metallicity so there must be, and is, an earlier generation of Poplulation II stars with metallicities orders of magnitude below that of the Sun. Even this is insufficient to account for the existence of the Sun and therefore Population III stars are expected to have existed at $Z > 15$. These extremely low metallicity stars would have lifetimes of only about ten million years and have long ago disappeared. Evidence from the infra-red observations by the JWST could find evidence of Population III stars, if they really existed.

It is familiar to study a mass-energy pie-chart of the universe with approximately 5% baryonic normal matter, 25% dark matter and 70% dark energy. The entropy

pie-chart is very different if the toy model considered in this papers resembles Nature. The slices corresponding to normal matter and dark energy are extremely thin and the pie is essentially all dark matter.

In this talk we have attempted to justify better that entropy and the second law applied to the early universe provide a *raison d'être* for the dark matter. We propose that the dark matter constituents are PBHs with a very wide range of masses from $10^2 M_\odot$ to $10^{22} M_\odot$.

Since it has never been observed except by its gravity, it does seem most likely that dark matter has no direct or even indirect connection to the standard model of strong and electroweak interactions in particle theory. The three clues we have mentioned: the dominance of black holes in the entropy inventory, the CMB spectrum and the holographic entropy maximum all hint toward PBHs as the dark matter constituent.

Assuming that the maximum entropy limit suggested by holography is saturated the mass function for the PBHs must extend to maximally high mass values.

6.6   Testability

So far, our discussion has been highly speculative and has populated the visible universe with objects which may well be the most massive ever contemplated. The nearest may be [7] which considered almost as massive black holes. From the point of view of entropy, all these very massive black holes are a natural extension of the dark matter expected inside galaxies and clusters.

Thus, dark matter in this generalised sense permeates all of space not as condensed clumps of mass but spread out on all scales up to cosmological ones. This occurrence of such extremely massive black holes seems *inevitable*, if we adopt the hypothesis that the bulk contents of the universe possess an entropy which saturates the holographic limit.

An obvious question is how to test this novel view of the universe. Additional great attractors, along the lines of [3], if they exist, require better technology to observe galaxy distributions at larger distances. As for the most extreme black holes comparable to the size of the universe itself, we are unaware of any good and practicable observational test.

There is the important question of whether and how PBHs were formed. According to Eq.(6.3), masses $10^{18} M_\odot$ and $10^{22} M_\odot$ would be formed at, respectively, t = 300ky and 3Gy so there can be natural concern about distorting too much the CMB and of adversely affecting the formation of large-scale structure.

One possibility would be to test the PBH theory by numerical dark matter simulations, similar to those pioneered in [7], but this seems very challenging because

they give a qualitatively acceptable result for the Large Scale Structure independent of the mass of the dark matter constituents. It is conceivable that more powerful computers than presently available will be able to discriminate between the predicted LSS estimated both with and without such large PBHs. In a similar vein, more advanced technology in telescope construction, both terrestrial and in space, is necessary to make astronomical observations sensitive enough to detect the existence of more examples similar to the Great Attractor.

Discussion of the central assumption of this article, that the holographic entropy maximum is reached by summing the entropies of all the objects within the universe might prove fruitless but hopefully not. What prompted us to publish this discussion was partly the response "pure cowardice" by Dirac when asked why he did not predict the positron in his 1928 paper which announced the discovery of his eponymous equation.

Acknowlegement

References

1. P.H. Frampton,
   `arXiv:2202.04432[astro-ph.GA]`.
2. N. Secrest, *et al.*,
   Astrophys. J. Lett. **908,** L51 (2021).
   `arXiv:2009.14826[astro-ph.CO]`.
3. A. Dressler,
   Nature **350,** 391 (1991).
4. P.H. Frampton,
   Mod.Phys. Lett. **A31,** 1650093 (2016).
   `arXiv:1510.00400[hep-ph]`.
5. G. 't Hooft,
   in SalamFestschrift.
   Editors: A. Ali, D. Amati and J. Ellis. (1993).
   `arXiv:gr-qc/9310026`.
6. P.H. Frampton, M. Kawasaki, F. Takahashi and T. Yanagida.
   JCAP **04**:023 (2010).
   `arXiv:1001.2308 [hep-ph]`.
7. B. Carr, F. Kuhnel and L. Visinelli,
   MNRAS **501,** 2029 (2021).
   `arXiv:2008.08077[astro-ph.CO]`.
8. J.F. Navarro, C.S. Frenk and S.D.M. White,
   Astrophys. J. **462,** 563 (1996).
   `arXiv:astro-ph/9508025`.
   ibid. **490,** 493 (1997).
   `arXiv:astro-ph/9611107`.

7 Near-inflection point inflation and production of dark matter during reheating

Anish Ghoshal[1], Gaetano Lambiase[2], Supratik Pal[3], Arnab Paul[4], Shiladitya Porey[5]

[1]Institute of Theoretical Physics, Faculty of Physics, University of Warsaw,ul. Pasteura 5, 02-093 Warsaw, Poland, email: anish.ghoshal@fuw.edu.pl
[2]Dipartimento di Fisica "E.R. Caianiello", Universita' di Salerno, I-84084 Fisciano (Sa), Italy Gruppo Collegato di Salerno, I-84084 Fisciano (Sa), Italy,email:lambiase@sa.infn.it
[3]Physics and Applied Mathematics Unit, Indian Statistical Institute, Kolkata-700108, India Technology Innovation Hub on Data Science, Big Data Analytics and Data Curation, Indian Statistical Institute, Kolkata-700108, India, email:supratik@isical.ac.in,
[4]Physics and Applied Mathematics Unit, Indian Statistical Institute, Kolkata-700108, India, Indian School of Physical Sciences, Indian Association for the Cultivation of Science, Kolkata-700032, India, email:arnabpaul9292@gmail.com,
[5]Department of Physics and Astronomy, Novosibirsk State University, email: shiladityamailbox@gmail.com

Abstract. We study slow roll single field inflationary scenario and the production of non-thermal fermionic dark matter, together with standard model Higgs, during reheating. For the inflationary scenario, we have considered two models of polynomial potential – one is symmetric about the origin and another one is not. We fix the coefficients of the potential from the current Cosmic Microwave Background (CMB) data from *Planck*/BICEP. Next, we explore the allowed parameter space on the coupling (y_χ) with inflaton and mass (m_χ) of dark matter (DM) particles (χ) produced during reheating and satisfying CMB and several other cosmological constraints.

http://arxiv.org/abs/2211.15061

7.1 Introduction

Cosmic inflation which is postulated as a fleeting cosmological epoch, occurred at the very early time of the universe. During this primordial epoch, spacetime expanded exponentially resulting in statistical homogeneity and isotropy on large angular scales, the exceedingly flat universe, and providing a proper explanation for the horizon problem. In addition to that, inflation can generate quantum fluctuations, which transform into scalar and tensor perturbations. Scalar perturbation acts as the mechanism for the formation of the large-scale structure, while tensor perturbation is responsible for generating gravitational wave. The simplest way to fabricate such an epoch is to assume that the universe was dominated by the energy density of a single scalar field, called inflaton, minimally coupled to gravity

and having canonical kinetic energy, slowly rolling along the slope of the potential. However, current data from CMB measurements, e.g. *Planck* [1] and BICEP [2], favour plateau-like potential over the inflaton-potential of the form $V(\phi) \propto \phi^p$ with p $\geq$ 1. One of the other alternatives to get such a potential is to consider inflection-point inflation.

On the other hand, CMB measurements suggest that approximately one-quarter of the total mass-energy density of the present universe is in the form of Dark Matter (DM) whose true nature is still not known with certainty. All proposed possible particles of DM can be categorized into two groups - Weakly Interacting Massive Particles (WIMP) and Feebly Interacting Massive Particles (FIMP). Till now, the signature of the presence of WIMP particles has not been detected in particle detector experiments [3]. In that case, FIMP which were never in thermal equilibrium with the relativistic plasma of the universe, seems more favorable as the viable DM candidate [4].

In the paper [5] we studied a single unified model of inflation and the production of non-thermal dark matter particles. For the inflationary part, we have considered two small-field inflection point inflationary scenarios. We have also assumed direct coupling between the inflaton and the DM, a vector-like fermionic field χ which transforms as gauge singlet under the SM gauge groups. The inflaton either decays to DM or may undergo scattering with the dark sector to produce the observed relic. As we will see, additional irreducible gravitational interaction may also mediate the DM production, either by 2-to-2 annihilation of the Standard Model (SM) Higgs bosons or of the inflatons during the reheating era.

This paper is organized as follows: in Section 7.2, we discuss the condition of getting an inflection point for a single field potential. In Section 7.3, we study the slow roll inflationary scenario for two potentials and find the location of inflection point and fix the coefficients of the potentials from CMB data. Reheating and production of dark matter have been discussed in Section 7.5. Section 7.6 contains conclusion.

7.2   Inflection-point inflation models

Near the location of the inflection point, the potential takes a plateau-like shape. Because of that, inflection point of the inflationary potential is important for the slow roll inflationary scenario. If inflaton starts rolling along the potential from the vicinity of the inflection point, the number of e-foldings (described in Section 7.3) increases without significant change in the inflaton value.

To determine the stationary inflection point of an inflationary potential $\mathcal{V}(\psi)$ of a single scalar field ψ, we need the solution of

$$\frac{d\mathcal{V}}{d\psi} = \frac{d^2\mathcal{V}}{d\psi^2} = 0 \,. \tag{7.1}$$

In the following sections (Section 7.3) we discuss two different slow roll small-field inflationary scenarios, where each of the inflationary potentials possesses an inflection point.

7.3   Slow roll inflationary scenario

The Lagrangian density we are interested in, is given by in $\hbar = c = k_B = 1$ unit,

$$\mathcal{L}_I = \frac{M_P^2}{2}\mathcal{R} + \mathcal{L}_{KE,INF} + U_{INF} + \mathcal{L}_{KE,\chi} - U_\chi(\chi) + \mathcal{L}_{KE,H} - U_H(H) + \mathcal{L}_{reh}, \tag{7.2}$$

where $M_P \simeq 2.4 \times 10^{18}$ GeV is the reduced Planck mass and $\mathcal{R}$ is the Ricci scalar with metric-signature $(+,-,-,-)$. $\mathcal{L}_{KE,INF}$ and U_{INF} are respectively the kinetic energy and potential energy term of the single scalar inflaton. Since, those two terms are function of inflaton, they alter when we change the model of inflation. In this work, we use Φ to symbolize inflaton for Model I inflation and φ for Model II. Accordingly,

$$U_{INF} \equiv U_\Phi = V_0 + a\,\Phi - b\,\Phi^2 + d\,\Phi^4 \qquad \text{(for Model I)}, \tag{7.3}$$

$$U_\varphi = p\,\varphi^2 - q\,\varphi^4 + w\,\varphi^6 \qquad \text{(for Model II)}. \tag{7.4}$$

Here V_0, a, b, d, p, q, and w are all assumed to be positive, real; and we choose $d, w > 0$. The potential of Eq. (7.3) contains a term of linear order of inflaton. Due to this term U_Φ is not symmetric about the origin. On the contrary, the U_φ is symmetric about the origin. In Eq. (7.2), $\mathcal{L}_{KE,\chi}$, and $\mathcal{L}_{KE,H}$ represent the kinetic energy of the vector-like fermionic DM, χ, and Standard Model (SM) Higgs field, H, respectively. And the potential term for χ and H are given by -

$$U_\chi(\chi) = m_\chi \bar{\chi}\chi, \tag{7.5}$$

$$U_H(H) = -m_H^2 H^\dagger H + \lambda_H \left(H^\dagger H\right)^2. \tag{7.6}$$

Furthermore, the last term on the right side of Eq. (7.2), $\mathcal{L}_{reh}$, takes care of the interactions of χ and H with $\Phi(\varphi)$ during reheating and it is defined as

$$\mathcal{L}_{reh} \equiv \begin{cases} \mathcal{L}_{reh,I} = -y_\chi \Phi\bar{\chi}\chi - \lambda_{12}\Phi H^\dagger H - \lambda_{22}\Phi^2 H^\dagger H & \text{(for Model I)}, \\ \mathcal{L}_{reh,II} = -y_\chi \varphi\bar{\chi}\chi - \lambda_{12}\varphi H^\dagger H - \lambda_{22}\varphi^2 H^\dagger H & \text{(for Model II)}, \end{cases} \tag{7.7}$$

where λ_{12}, λ_{22}, and Yukawa-like y_χ are the couplings of SM Higgs and fermionic DM with inflaton.

During the slow roll inflationary epoch, contribution from the terms except the first three terms in Eq. (7.2) is negligible. The slow-roll condition is measured in terms of four potential-slow-roll parameters – $\epsilon_V, \eta_V, \xi_V$, and σ_V. During slow roll inflationary epoch, $|\epsilon_V|, |\eta_V|, |\xi_V|, |\sigma_V| \ll 1$. These four potential-slow-roll

parameters for Model I are defined as

$$\epsilon_V \approx \frac{M_P^2}{2}\left(\frac{U'_\Phi}{U_\Phi}\right)^2 = M_P^2 \frac{\left(a - 2b\,\Phi + 4d\,\Phi^3\right)^2}{2\left(\Phi\left(a - b\,\Phi + d\,\Phi^3\right) + V_0\right)^2}\,, \tag{7.8}$$

$$\eta_V \approx M_P^2 \frac{U''_\Phi}{U_\Phi} = -M_P^2 \frac{2\left(b - 6d\,\Phi^2\right)}{\Phi\left(a - b\,\Phi + d\,\Phi^3\right) + V_0}\,, \tag{7.9}$$

$$\xi_V \approx M_P^4 \frac{U'_\Phi U'''_\Phi}{U_\Phi^2} = M_P^4 \frac{24d\,\Phi\left(a - 2b\,\Phi + 4d\,\Phi^3\right)}{\left(\Phi\left(a - b\,\Phi + d\,\Phi^3\right) + V_0\right)^2}\,, \tag{7.10}$$

$$\sigma_V \approx M_P^6 \frac{{U'_\Phi}^2 U''''_\Phi}{U_\Phi^3} = M_P^6 \frac{24d\left(a - 2b\,\Phi + 4d\,\Phi^3\right)^2}{\left(\Phi\left(a - b\,\Phi + d\,\Phi^3\right) + V_0\right)^3}\,. \tag{7.11}$$

Here, prime denotes derivative with respect to inflaton. For Model II inflation, the potential-slow-roll parameters are

$$\epsilon_V = M_P^2 \frac{2\left(p\varphi - 2q\varphi^3 + 3w\varphi^5\right)^2}{\left(p\varphi^2 - q\varphi^4 + w\varphi^6\right)^2}\,, \tag{7.12}$$

$$\eta_V = M_P^2 \frac{2\left(p - 6q\varphi^2 + 15w\varphi^4\right)}{p\varphi^2 - q\varphi^4 + w\varphi^6}\,, \tag{7.13}$$

$$\xi_V = M_P^4 \frac{48\varphi^2\left(-q + 5w\varphi^2\right)\left(p - 2q\varphi^2 + 3w\varphi^4\right)}{\left(p\varphi^2 - q\varphi^4 + w\varphi^6\right)^2}\,, \tag{7.14}$$

$$\sigma_V = M_P^6 \frac{96\left(-q + 15w\varphi^2\right)\left(p\varphi - 2q\varphi^3 + 3w\varphi^5\right)^2}{\left(p\varphi^2 - q\varphi^4 + w\varphi^6\right)^3}\,. \tag{7.15}$$

By the time any one of these slow-roll parameters becomes ~ 1 at $\Phi \sim \Phi_{\text{end}}$ (for Model I) or at $\varphi \sim \varphi_{\text{end}}$ (for Model II), slow roll inflation terminates. The duration of slow roll inflation is measured in terms of the total number of e-foldings, $\mathcal{N}_{\text{CMB, tot}}$ as

$$\mathcal{N}_{\text{CMB, tot}} = M_P^{-2} \int_{\Phi_{\text{end}}(\varphi_{\text{end}})}^{\Phi_{\text{CMB}}(\varphi_{\text{CMB}})} \frac{U_{\text{INF}}}{U'_{\text{INF}}}\, d\Phi(\varphi) = \int_{\Phi_{\text{end}}(\varphi_{\text{end}})}^{\Phi_{\text{CMB}}(\varphi_{\text{CMB}})} \frac{1}{\sqrt{2\epsilon_V}}\, d\Phi(\varphi)\,, \tag{7.16}$$

where $\Phi_{\text{CMB}}(\varphi_{\text{CMB}})$ is the inflaton value at which the length scale, which had previously left the causal horizon during inflation, has reentered during the period of recombination.

Moreover, inflation generates primordial scalar and tensor perturbations. The primordial scalar and tensor power spectrum for 'k'-th Fourier mode are defined as

$$\mathcal{P}_s(k) = A_s\left(\frac{k}{k_*}\right)^{n_s - 1 + (1/2)\alpha_s \ln(k/k_*) + (1/6)\beta_s\,(\ln(k/k_*))^2}\,, \tag{7.17}$$

$$\mathcal{P}_h(k) = A_t\left(\frac{k}{k_*}\right)^{n_t + (1/2)dn_t/d\ln k\,\ln(k/k_*) + \cdots}\,, \tag{7.18}$$

where $k_* = 0.05\text{Mpc}^{-1}$; n_s and n_t are the scalar and tensor spectral index, α_s is the running of scalar spectral index, and β_s is called the 'running of running'.

Moreover, in Eq. (7.17)-(7.18), A_s and A_t are the normalizations. The relation between A_s and inflationary potential is

$$A_s \approx \frac{U_{INF}}{24\pi^2 M_P^4 \, \epsilon_V} \approx \frac{2U_{INF}}{3\pi^2 M_P^4 \, r} \, .$$

(7.19)

Here, r is the tensor-to-scalar ratio. r, n_s, α_s and β_s depend on potential-slow-roll parameters as

$$r = \frac{A_t}{A_s} \approx 16\epsilon_V \, . \qquad n_s = \frac{d \ln \mathcal{P}_s}{d \ln k} = 1 + 2\eta_V - 6\epsilon_V \, ,$$

(7.20)

$$\alpha_s \equiv \frac{dn_s}{d \ln k} = 16\epsilon_V \eta_V - 24\epsilon_V^2 - 2\xi_V \, .$$

(7.21)

$$\beta_s \equiv \frac{d^2 n_s}{d \ln k^2} = -192\epsilon_V^3 + 192\epsilon_V^2 \eta_V - 32\epsilon_V \eta_V^2 - 24\epsilon_V \xi_V + 2\eta_V \xi_V + 2\sigma_V \, .$$

(7.22)

The observed values of all these inflation parameters measured at $\Phi = \Phi_{CMB}$ (at $k_* \simeq 0.05 \text{Mpc}^{-1}$) from *Planck*, *WMAP*, and other CMB observations are presented in Table 7.1. [1]

Table 7.1: *CMB constraints on inflationary parameters.*

$\ln(10^{10} A_s)$	3.047 ± 0.014	68%, TT,TE,EE+lowE+lensing+BAO	[1]
n_s	0.9647 ± 0.0043	68%, TT,TE,EE+lowE+lensing+BAO	[1]
$dn_s/d \ln k$	0.0011 ± 0.0099	68%, TT,TE,EE+lowE+lensing+BAO	[1]
$d^2 n_s/d \ln k^2$	0.009 ± 0.012	68%, TT,TE,EE+lowE+lensing+BAO	[1]
r	$0.014^{+0.010}_{-0.011}$ and < 0.036	95%, BK18, BICEP3, *Keck Array* 2020, and *WMAP* and *Planck* CMB polarization	[1,2,7,8]

7.3.1 Estimating coefficients from CMB data

In this subsection, we find the location of inflection points and also, fix the coefficient of the potentials of both inflationary models, mentioned in Eq. (7.3) and Eq. (7.4), from the CMB data. At first, we start the calculation with Model I. Solution of Eq. (7.1) provides the location of inflection point for Model I potential

$$\Phi_0 = \frac{3a}{4b} \qquad \text{when } d = \frac{8b^3}{27a^2} \, .$$

(7.23)

To fix the coefficients of the potential of Eq. (7.3), following [9,10], we can write

$$\begin{pmatrix} \Phi_{CMB} & \Phi_{CMB}^2 & \Phi_{CMB}^4 \\ 1 & 2\Phi_{CMB} & 4\Phi_{CMB}^3 \\ 0 & 2 & 12\Phi_{CMB}^2 \end{pmatrix} \begin{pmatrix} a \\ b \\ d \end{pmatrix} = \begin{pmatrix} U_\Phi(\Phi_{CMB}) - V_0 \\ U_\Phi'(\Phi_{CMB}) \\ U_\Phi''(\Phi_{CMB}) \end{pmatrix} ,$$

(7.24)

---

[1] T and E corresponds to temperature and E-mode polarisation of CMB.

where d is known from Eq. (7.23) and $U_\Phi(\Phi_{CMB})$, $U'_\Phi(\Phi_{CMB})$ and $U''_\Phi(\Phi_{CMB})$ can be derived using Eq. (7.8), (7.9), (7.10), (7.19), (7.20) as

$$U_\Phi(\Phi_{CMB}) = \frac{3}{2} A_s r \pi^2 M_P^4, \tag{7.25}$$

$$U'_\Phi(\Phi_{CMB}) = \frac{3}{2} \sqrt{\frac{r}{8}} \left(A_s r \pi^2 \right) M_P^3, \tag{7.26}$$

$$U''_\Phi(\Phi_{CMB}) = \frac{3}{4} \left(\frac{3r}{8} + n_s - 1 \right) \left(A_s r \pi^2 \right) M_P^2. \tag{7.27}$$

Using these together with Table 7.1, we can find the coefficients of the potential. However, for cosmological purpose, it is adequate to design the potential in a way such that Φ_{CMB} is adjacent to Φ_0 [11]. In order to implement this, let us modify the potential (Eq. (7.3)) as

$$U_\Phi(\Phi) = V_0 + A\,\Phi - B\,\Phi^2 + d\,\Phi^4, \tag{7.28}$$

with $A = a(1-\beta_1^I)$, $B = b(1-\beta_2^I)$ (where β_1^I, β_2^I are dimensionless) and in the limit $\beta_1^I, \beta_2^I \to 0$, the slope of the potential vanishes at Φ_0. Using this modification, we have found the benchmark value for this potential which is exhibited in Table 7.2, and using this value, the evolution of the potential and slow roll parameters with Φ are illustrated in Fig. 7.1. From this Fig. 7.1 it is clear that $\sigma_V, \xi_V, \epsilon_V < |\eta_V|$. Besides, at $\Phi = \Phi_{CMB}$, $\epsilon_V, |\eta_V|, \xi_V, \sigma_V << 1$, and at $\Phi = \Phi_{end}$, $|\eta_V| \simeq 1$. This last condition leads to the ending of slow roll phase.

Table 7.2: *Benchmark value for linear term potential (Model I) (Φ_{min} is the minimum of potential in Eq. (7.28))*

V_0/M_P^4	a/M_P^3	b/M_P^2	d	β_1^I	β_2^I
2.788×10^{-19}	9.29×10^{-19}	6.966×10^{-18}	1.16×10^{-16}	6×10^{-7}	6×10^{-7}

Φ_{CMB}/M_P	Φ_{end}/M_P	Φ_{min}/M_P	Φ_0/M_P
0.1	0.098889	-0.200045	0.100022

r	n_s	A_s	e-folding	α_s	β_s
9.87606×10^{-12}	0.960249	2.10521×10^{-9}	53.75	-1.97×10^{-3}	-3.92×10^{-5}

Next, we follow similar steps for the inflationary potential of Model II. The potential of Eq. (7.4) has an inflection point at

$$\varphi_0 = \frac{\sqrt{q}}{\sqrt{3\,w}} \qquad \text{for } p = \frac{q^2}{3\,w}. \tag{7.29}$$

Likewise, we can also redefine the potential Model II as

$$U_\varphi(\varphi) = p\,\varphi^2 - Q\,\varphi^4 + W\,\varphi^6, \tag{7.30}$$
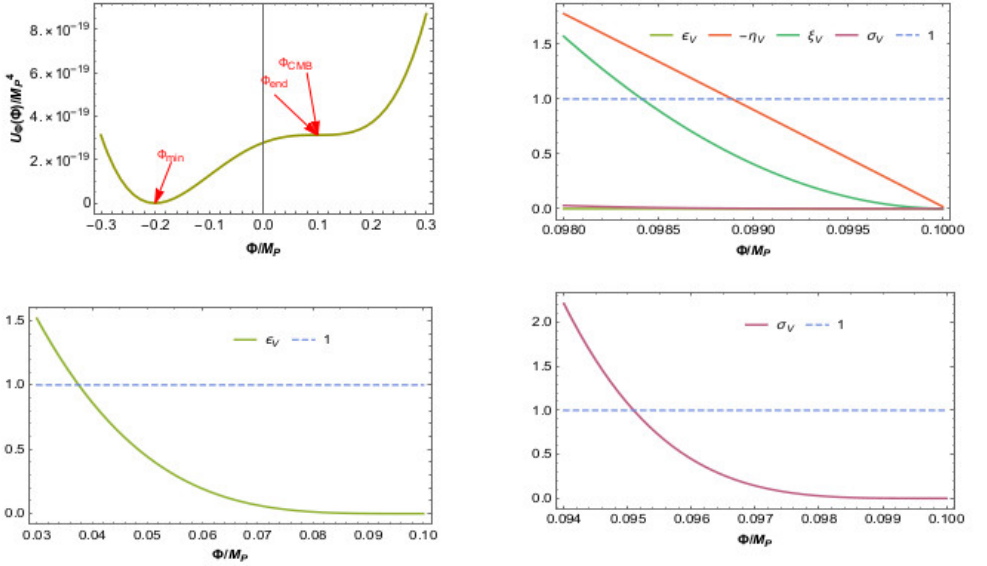
Fig. 7.1: *In the top-left panel: normalised inflaton-potential of Model I inflation as a function of 'φ/M_P' for benchmark value shown in Table 7.2. The evolution of inflationary slow-roll parameters ($\epsilon_V, -\eta_V, \xi_V, \sigma_V$) as a function of Φ/M_P is presented in the top-right panel; second row - left panel: ϵ_V, and second row – right panel: σ_V of Model I slow roll inflation against Φ/M_P are shown individually for benchmark values listed in Table 7.2. The dashed line is for 1. Whenever $|\eta_V|$ becomes ~ 1, the slow roll inflation ends. From these figures, it is clearly visible that $|\epsilon_V| < |\sigma_V| < |\xi_V| < |\eta_V|$ during the slow-roll regime.*

such that $Q = q(1 - \beta_1^{II})$ and $W = w(1 - \beta_2^{II})$ and $\beta_1^{II}, \beta_2^{II}$ have zero mass dimension. Then, we can estimate p, q and w, and the values are mentioned in Table 7.3. For this value, the variation of $U_\varphi(\varphi)$ of Eq. (7.30) and $\epsilon_V, |\eta_V|, \xi_V, \sigma_V$ as a function of φ is shown in Fig. 7.2. The slow roll inflationary phase ends at φ_{end} when $|\eta_V| \simeq 1$ (because for Model II $\epsilon_V < |\eta_V|$).
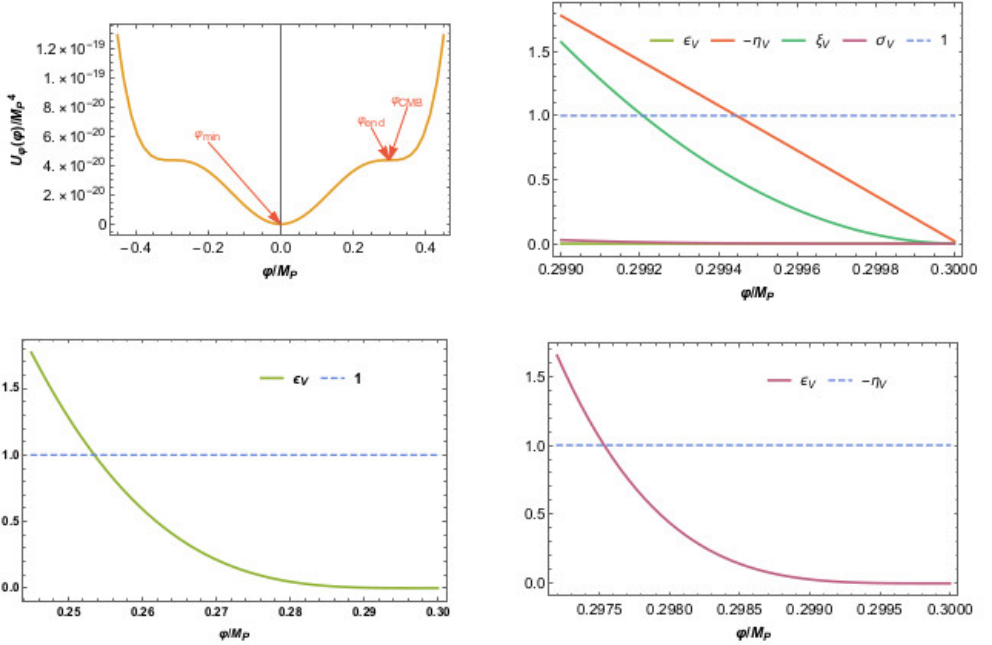
Fig. 7.2: *Top-left panel: evolution of normalised inflaton-potential of Model II for bench-mark value from Table 7.3. Top-right panel: absolute values of four slow roll parameters ($\epsilon_V, -\eta_V, \xi_V, \sigma_V$) are plotted against φ/M_P. Left and right panel of the second row displays ϵ_V and σ_V, respectively, against φ/M_P for benchmark values mentioned in Table 7.3. The dashed line indicates 1. These graphs demonstrate that $|\epsilon_V| < |\sigma_V| < |\xi_V| < |\eta_V| < 1$ during the slow-roll inflation, similar to what we have found in Model I.*

Table 7.3: *Benchmark values for sextic potential ($\varphi_{\min}$ is the minimum of potential Eq. (7.30))*

p/M_P^2	q	wM_P^2	β_1^{II}	β_2^{II}
1.45×10^{-18}	1.62×10^{-17}	5.98×10^{-17}	1.53×10^{-8}	1.53×10^{-8}

φ_{CMB}/M_P	φ_{end}/M_P	$\varphi_{\min}/M_P$	φ_0/M_P
0.3	0.299444	0	0.300011

r	n_s	A_s	e-folding	α_s	β_s
1.4×10^{-12}	0.96001	2.10521×10^{-9}	60.247	-1.487×10^{-3}	-2.972×10^{-5}

7.4   Stability analysis

In this section, we attempt to determine the upper bound of y_χ and λ_{12} so that $\mathcal{L}_{\mathrm{reh,I}}$ and $\mathcal{L}_{\mathrm{reh,II}}$ do not affect the inflationary scenario set forth in Section 7.3.

The Coleman–Weinberg (CW) radiative correction at 1-loop order to the inflaton-potential is given by [6] -

$$V_{CW} = \sum_j \frac{n_j}{64\pi^2} (-1)^{2s_j} \widetilde{m}_j^4 \left[\ln \left(\frac{\widetilde{m}_j^2}{\mu^2} \right) - c_j \right].$$ (7.31)

Here, $j \equiv H, \chi$ and inflaton; $n_{H,\chi} = 4$, n_j for inflaton is 1. Furthermore, $s_H = 0$, $s_\chi = 1/2$, and $s_{\Phi(\varphi)} = 0$. $\widetilde{m}_j$ is inflaton dependent mass of the component j and μ is the renormalization scale, which is taken $\sim \Phi_0$ (for Model I) or φ_0 (for Model II). Besides, $c_j = \frac{3}{2}$. Now, the second derivative of the CW term w.r.t. inflaton is

$$V_{CW}'' = \sum_j \frac{n_j}{32\pi^2} (-1)^{2s_j} \left\{ \left[\left((\widetilde{m}_j^2)' \right)^2 + \widetilde{m}_j^2 (\widetilde{m}_j^2)'' \right] \ln \left(\frac{\widetilde{m}_j^2}{\mu^2} \right) - \widetilde{m}_j^2 (\widetilde{m}_j^2)'' \right\}.$$ (7.32)

In the next two subsections, we investigate the stability relative to the couplings y_χ and λ_{12} for the two inflation-potentials (Eq. (7.28)) and Eq. (7.30)) we have considered.

7.4.1   Stability analysis for linear term inflation

From Eq. (7.7), the field-depended mass of the χ and H are respectively

$$\widetilde{m}_\chi^2(\Phi) = (m_\chi + y_\chi \Phi)^2,$$ (7.33)
$$\widetilde{m}_H^2(\Phi) = m_H^2 + \lambda_{12}\Phi.$$ (7.34)

For the stability of the inflation-potential, the terms of the order of λ_{12}^2 and y_χ^2 on the right-hand side in Eq. (7.32) should be less than corresponding tree level terms from Eq. (7.28) -

$$V_{tree}''(\Phi_0) \equiv U_\Phi''(\Phi_0) = \frac{32b^3\Phi_0^2}{9a^2} - 2b(1 - \beta),$$ (7.35)

where $\beta_1^I = \beta_2^I = \beta^I$ (as we have chosen the benchmark value $\beta_1^I = \beta_2^I$). The second derivative (Eq. (7.32)) of CW term for Higgs field is

$$|V_{CW,H}''| = \frac{\lambda_{12}^2}{8\pi^2} \ln \left(\frac{\lambda_{12}\Phi}{\Phi_0^2} \right).$$ (7.36)

The upper bound of the value of λ_{12} at $\Phi \sim \Phi_0$ can be deduced from $|V_{CW,H}''| < V_{tree}''(\Phi_0)$, and it is depicted on the right panel of Fig. 7.3. Thus, allowed value of λ_{12}/M_P is $< 5.283 \times 10^{-12}$.
Similarly, for y_χ,

$$\left| V_{CW,\chi}'' \right| = \frac{1}{8\pi^2} \left(6\Phi^2 y_\chi^4 \ln \left(\frac{\Phi^2 y_\chi^2}{\Phi_0^2} \right) - 2\Phi^2 y_\chi^4 \right).$$ (7.37)

The upper bound on y_χ around $\Phi \sim \Phi_0$ can be obtained from $\left| V_{CW,\chi}'' \right| < V_{tree}''(\Phi_0)$ which is exhibited on the left panel of Fig. 7.3, and it gives $y_\chi < 4.578 \times 10^{-6}$.
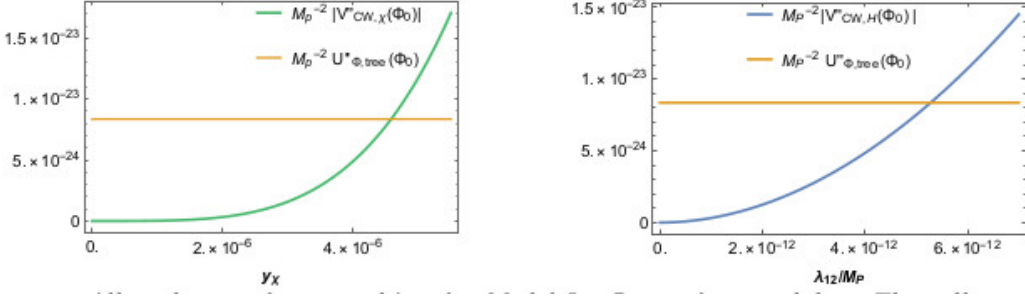
Fig. 7.3: *Allowed range for y_χ and λ_{12} for Model I inflation from stability. The yellow colored line represents the value of tree level potential of Model I at Φ_0. The green and blue colored lines indicate the CW correction due to χ and H, respectively.*

7.4.2 Stability analysis for sextic inflation

In this model, inflaton is φ. Accordingly, the field-depended mass of the fermionic field and Higgs field are respectively

$$\widetilde{m}_\chi^2(\varphi) = (m_\chi + y_\chi \varphi)^2 \,, \tag{7.38}$$

$$\widetilde{m}_H^2(\varphi) = m_H^2 + \lambda_{12}\varphi \,. \tag{7.39}$$

From Eq. (7.30)

$$V''_{\text{tree}}(\varphi_0) \equiv U''_\varphi(\varphi_0) = \frac{2q^2}{3w} - 12(1-\beta^{II})q\varphi_0^2 + 30(1-\beta^{II})w\varphi_0^4 \,, \tag{7.40}$$

where $\beta_1^{II} = \beta_2^{II} = \beta^{II}$ (because we have chosen $\beta_1^{II} = \beta_2^{II}$ in our benchmark value). Following the steps similar to the ones mentioned in Section 7.4.1, for λ_{12} Eq. (7.32) results in

$$|V''_{\text{CW,H}}| = \frac{\lambda_{12}^2}{8\pi^2} \ln\left(\frac{\lambda_{12}\varphi}{\varphi_0^2}\right) \,, \tag{7.41}$$

and for y_χ

$$|V''_{\text{CW},\chi}| = \frac{1}{8\pi^2}\left(6\varphi^2 y_\chi^4 \ln\left(\frac{\varphi^2 y_\chi^2}{\varphi_0^2}\right) - 2\varphi^2 y_\chi^4\right). \tag{7.42}$$

In this inflationary case, upper bound on λ_{12} and y_χ around $\varphi \sim \varphi_0$ comes from $|V''_{\text{CW,H}}| < V''_{\text{tree}}(\varphi_0)$, and $\left|V''_{\text{CW},\chi}\right| < V''_{\text{tree}}(\varphi_0)$, respectively. These have been shown in Fig. 7.4. The upper bounds are $y_\chi < 6.9 \times 10^{-7}$, and $\lambda_{12}/M_P < 3.58 \times 10^{-13}$.

7.5 Reheating and Dark Matter

As soon as the slow roll epoch ends, inflaton quickly drops to the minimum of the potential and starts coherent oscillation about that minimum. If $\Phi_{\min}$ (in Model
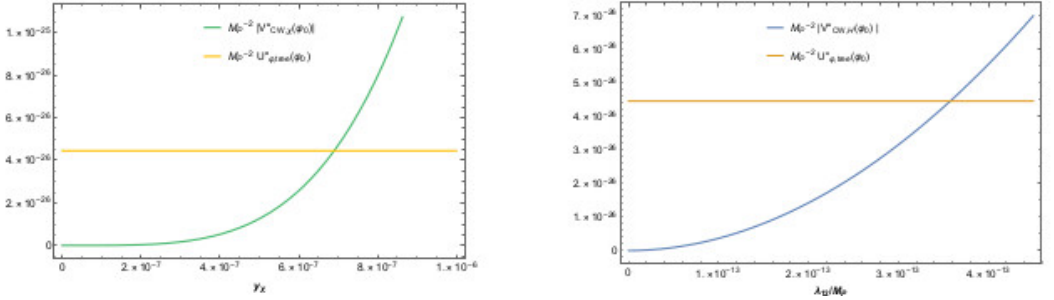
Fig. 7.4: *From the stability analysis of Model II inflation, allowed range for y_χ and λ_{12}. The green and blue colored lines result from CW correction for χ and H, and they are compared with the value of tree-level potential of at φ_0 (yellow colored horizontal line).*

I) and $\varphi_{\min}$ (in Model II) are the locations of minimum of the inflaton potential respectively, then effective mass of the inflaton in two inflationary models are

$$\frac{m_{\Phi(\varphi)}}{M_P} = \begin{cases} \left(M_P^{-2} U''_\Phi(\Phi)|_{\Phi=\Phi_{\min}}\right)^{1/2} = 6.465 \times 10^{-9} & \text{(for Model I)}, \\ \left(M_P^{-2} U''_\varphi(\varphi)|_{\varphi=\varphi_{\min}}\right)^{1/2} = 1.705 \times 10^{-9} & \text{(for Model II)}. \end{cases} \tag{7.43}$$

This oscillating field acts as a non-relativistic fluid without any pressure when averaged over a number of coherent oscillations. The energy density of this inflaton decreases due to two reasons - Hubble expansion and decay to relativistic SM Higgs particle h and DM particle χ following the Lagrangian density of Eq. (7.7) and Eq. (**??**). The decay width of inflaton to h and χ are

$$\Gamma_{\Phi(\varphi)\to hh} \simeq \frac{\lambda_{12}^2}{8\pi\, m_{\Phi(\varphi)}}, \qquad \Gamma_{\Phi(\varphi)\to\chi\chi} \simeq \frac{y_\chi^2\, m_{\Phi(\varphi)}}{8\pi}. \tag{7.44}$$

To satisfy present-day relic density of photons and baryons, we are considering $\Gamma_{\Phi(\varphi)\to hh} > \Gamma_{\Phi(\varphi)\to\chi\chi}$ such that total decay width of inflaton $\Gamma = \Gamma_{\Phi(\varphi)\to\chi\chi} + \Gamma_{\Phi(\varphi)\to hh} \simeq \Gamma_{\Phi(\varphi)\to hh}$. Hence,

$$\Gamma = \begin{cases} 6.15 \times 10^6 \frac{\lambda_{12}^2}{M_P} & \text{(for Model I)}, \\ 2.33 \times 10^7 \frac{\lambda_{12}^2}{M_P} & \text{(for Model II)}. \end{cases} \tag{7.45}$$

Now, the branching ratio for the production of χ is

$$Br = \frac{\Gamma_{\Phi(\varphi)\to\chi\chi}}{\Gamma_{\Phi(\varphi)\to\chi\chi} + \Gamma_{\Phi(\varphi)\to hh}} \simeq \frac{\Gamma_{\Phi(\varphi)\to\chi\chi}}{\Gamma_{\Phi(\varphi)\to hh}} = m_{\Phi(\varphi)}^2 \left(\frac{y_\chi}{\lambda_{12}}\right)^2 \tag{7.46}$$

$$= \begin{cases} 4.18 \times 10^{-17} \left(\frac{y_\chi}{\lambda_{12}}\right)^2 M_P^2 & \text{(for Model I)}, \\ 2.91 \times 10^{-18} \left(\frac{y_\chi}{\lambda_{12}}\right)^2 M_P^2 & \text{(for Model II)}. \end{cases} \tag{7.47}$$

These produced particles cause the development of the local-thermal relativistic fluid of the universe and consequently, raise the temperature of the universe.

At the beginning of reheating, due to the small value of couplings to inflaton, $\Gamma < \mathcal{H}(\text{ß})$, where $\mathcal{H} \equiv \mathcal{H}(\text{ß})$ is the Hubble parameter and ß is the cosmological scale factor. Meanwhile, $\mathcal{H}$ continues to decrease. At the moment when $\mathcal{H}$ becomes $\sim \Gamma$, the temperature of the universe is called as reheating temperature, T_{rh}, and it is can be computed as [12]

$$T_{rh} = \sqrt{\frac{2}{\pi}} \left(\frac{10}{g_\star}\right)^{1/4} \sqrt{M_P} \sqrt{\Gamma} = \begin{cases} 1095.07\,\lambda_{12} & \text{(for Model I)}, \\ 2132.09\lambda_{12} & \text{(for Model II)}. \end{cases} \tag{7.48}$$

We have assumed $g_\star = 106.75$. At temperature below T_{rh}, the universe behaves as if it is dominated by relativistic particles [13]. Additionally, we have assumed here that the process of particle production from inflaton is instantaneous [14]. In general, reheating is not an instantaneous process. The maximum temperature of the universe during the whole process of reheating may be many orders greater than T_{rh} and it can be estimated as [14]

$$T_{max} = \Gamma^{1/4} \left(\frac{60}{g_\star \pi^2}\right)^{1/4} \left(\frac{3}{8}\right)^{2/5} \mathcal{H}_I^{1/4} M_P^{1/2}, \tag{7.49}$$

where $\mathcal{H}_I$ is the value of the Hubble parameter at the beginning of reheating when no particle, including the DM, is produced. This can be taken as

$$\mathcal{H}_I \simeq \begin{cases} \sqrt{\frac{U_\Phi(\Phi_0)}{3M_P^2}} = 3.23 \times 10^{-10} M_P & \text{(for Model I)}, \\ \sqrt{\frac{U_\varphi(\varphi_0)}{3M_P^2}} = 1.206 \times 10^{-10} M_P & \text{(for Model II)}. \end{cases} \tag{7.50}$$

The Eq. (7.48)with $T_{rh} \gtrsim 4\text{MeV}$ puts down the lower limit on λ_{12}

$$\frac{\lambda_{12}}{M_P} \gtrsim \begin{cases} 1.52 \times 10^{-24} & \text{(for Model I)}, \\ 7.82 \times 10^{-25} & \text{(for Model II)}. \end{cases} \tag{7.51}$$

From Eq. (7.49), we can write

$$\frac{T_{max}}{T_{rh}} = \left(\frac{3}{8}\right)^{2/5} \left(\frac{\mathcal{H}_I}{\mathcal{H}(T_{rh})}\right)^{1/4}, \tag{7.52}$$

where

$$\mathcal{H}(T_{rh}) = \frac{\pi}{3M_P} \sqrt{\frac{g_\star}{10}} T_{rh}^2. \tag{7.53}$$

The allowed ranges for T_{max}/T_{rh} for two inflationary models are shown in Fig. 7.5. The upper limit for the allowed region comes from Eq. (7.52) and the lower limit from the fact that $T_{rh} \gtrsim 4\text{MeV}$ which is needed for successful Big Bang nucleosynthesis (BBN) [15].

7.5.1 Dark Matter Production and Relic Density

In this subsection, we estimate, following Ref. [12], the amount of DM produced during reheating and compared it with DM relic density of the present-day universe. The Boltzmann equation for the evolution of DM number density, n_χ, of
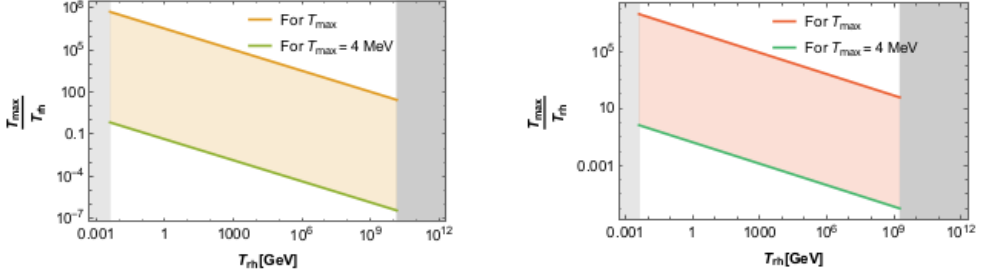
Fig. 7.5: *Allowed range (colored region) for* T_{max}/T_{rh}*: left panel is for Model I inflation, where right panel is for the Model II. The green color line points to* T_{max}/T_{rh} *when* $T_{max} = 4MeV$*. The gray colored area indicates the lower (*$T_{rh} \not< 4MeV$*) and upper bound on* T_{rh} *obtained from the stability analysis (see Eq. (7.36) and Eq. (7.41)).*

DM particles is -

$$\frac{dn_\chi}{dt} + 3\mathcal{H} n_\chi = \gamma, \qquad (7.54)$$

where t is the physical time, γ is the rate of production of DM per unit volume. Then the evolution equation of comoving number density, $N_\chi = n_\chi ß^3$ (ß(t) is the cosmological scale factor, as mentioned earlier), of DM particles

$$\frac{dN_\chi}{dt} = ß^3 \gamma. \qquad (7.55)$$

While the temperature, T of the universe is $T_{max} > T > T_{rh}$, the energy density of the universe is dominated by inflaton and the first Friedman equation leads to [12]

$$\mathcal{H} = \frac{\pi}{3} \sqrt{\frac{g_\star}{10}} \frac{T^4}{M_P T_{rh}^2}. \qquad (7.56)$$

Therefore, energy density of inflaton

$$\rho_{\Phi(\varphi)} = \frac{\pi^2 g_\star}{30} \frac{T^8}{T_{rh}^4}. \qquad (7.57)$$

Since, during reheating, ρ_Φ behaves as a non-relativistic fluids, $\rho_{\Phi(\varphi)} \propto ß^{-3}$, the scale factor behaves as

$$ß \propto T^{-8/3}. \qquad (7.58)$$

Using Eq. (7.56) and (7.58) in Eq. (7.55) we obtain

$$\frac{dN_\chi}{dT} = -\frac{8M_P}{\pi} \left(\frac{10}{g_\star}\right)^{1/2} \frac{T_{rh}^{10}}{T^{13}} ß^3(T_{rh}) \gamma. \qquad (7.59)$$

DM Yield, Y_χ is defined as the ratio of the number density of DM to the entropy density of photons, i.e., $Y_\chi = \frac{n_\chi(T)}{s(T)}$, where entropy density $s(T) = \frac{2\pi^2}{45} g_{\star,s} T^3$ and

$g_{\star,s}$ is the effective number of degrees of freedom of the constituents of the relativistic fluid. If we assume that there is no entropy generation in any cosmological process, after reheating epoch, then the evolution of Y_χ can be expressed as

$$\frac{dY_\chi}{dT} = -\frac{135}{2\pi^3 \, g_{\star,s}} \sqrt{\frac{10}{g_\star}} \frac{M_P}{T^6} \, \gamma \, . \tag{7.60}$$

We are assuming that the DM particles, produced during reheating, were never in thermal equilibrium with the relativistic fluid of the universe. Those DM particles contribute to the cold dark matter (CDM) density of the present universe. Thus, following Table 7.4, present-day CDM yield [12] is

$$Y_{CDM,0} = \frac{4.3. \times 10^{-10}}{m_\chi} \, , \tag{7.61}$$

where m_χ is expressed in GeV. Now, the amount of DM produced during reheating through decay or via scattering in both Model I and Model II, has been estimated and compared with $Y_{CDM,0}$ in the following part of this subsection.

Table 7.4: *Data about CDM ($h_{CMB} \approx 0.674$)*

Ω_{CDM}	$0.120 \, h_{CMB}^{-2}$	
ρ_c	$1.878 \times 10^{-29} \, h_{CMB}^2 \, \mathrm{gcm}^{-3}$	[16]
s_0	$2891.2 \, (T/2.7255K)^3 \, \mathrm{cm}^{-3}$	

Inflaton decay If DM particles are generated from the inflaton decay

$$\gamma = 2Br \, \Gamma \, \frac{\rho_{\Phi(\varphi)}}{m_{\Phi(\varphi)}} \, . \tag{7.62}$$

Substituting this in Eq. (7.60), the DM yield from the decay of inflaton,

$$Y_{\chi,0} \simeq \frac{3}{\pi} \frac{g_\star}{g_{\star,s}} \sqrt{\frac{10}{g_\star}} \frac{M_P \, \Gamma}{m_{\Phi(\varphi)} \, T_{rh}} Br = \frac{3}{\pi} \frac{g_\star}{g_{\star,s}} \sqrt{\frac{10}{g_\star}} \frac{M_P}{T_{rh}} \frac{(y_\chi)^2}{8\pi} \tag{7.63}$$

$$= 1.163 \times 10^{-2} M_P \frac{y_\chi^2}{T_{rh}} \, . \tag{7.64}$$

Here, we assume $g_{\star,s} = g_\star$. Equating Eq. (7.64) with Eq. (7.61), we get the condition to generate the complete CDM energy density -

$$T_{rh} \simeq 6.49 \times 10^{25} y_\chi^2 m_\chi \, . \tag{7.65}$$

Fig. 7.6 depicts the allowed range of the coupling y_χ from Eq. (7.65), to generate the complete CDM density of the contemporary universe only via the decay channel of inflaton. From this figure, we can deduce that the allowed range for y_χ and m_χ to construct the CDM density of the universe is $10^{-10} \gtrsim y_\chi \gtrsim 10^{-15}$ (for $2.5 \times 10^3 \, \mathrm{GeV} \lesssim m_\chi \lesssim 8.1 \times 10^9 \, \mathrm{GeV}$ in Model I) and $10^{-11} \gtrsim y_\chi \gtrsim 10^{-15}$ (for $8.4 \times 10^3 \, \mathrm{GeV} \lesssim m_\chi \lesssim 2 \times 10^9 \, \mathrm{GeV}$ in Model II).
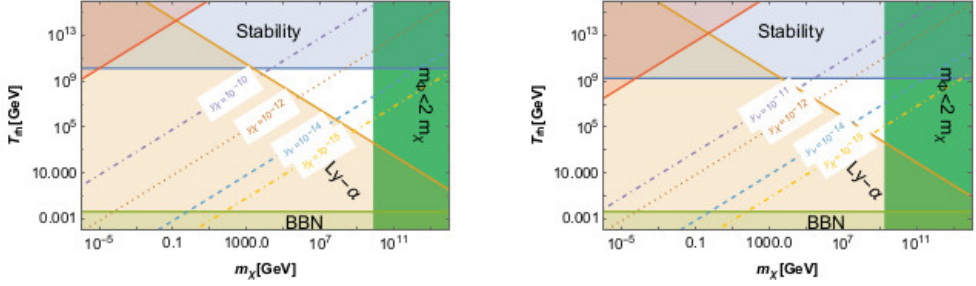
Fig. 7.6: *The allowed region (unshaded) for the Yukawa-like coupling y_χ to produce the complete CDM of the present universe: left panel is for Model I inflation and right for Model II inflation. The constraints (colored regions) are from (a) BBN (light green colored region): $T_{rh} > 4 MeV$, (b) from stability analysis (blue colored region): $T_{rh} \simeq 1.388 \times 10^{10} GeV$ (for Model I) or $T_{rh} \simeq 1.83 \times 10^9 GeV$ (for Model II) from the upper bound of λ_{12} from Eq. (7.36) or Eq. (7.41), (c) stability (red-colored region): from the upper bound of y_χ from Eq. (7.37) or Eq. (7.42), (d) (deep green region): m_χ must be $< m_\Phi/2$ (Model I) or $< m_\varphi/2$ (Model II), (e) (light peach-colored region): Ly-α : $T_{rh} \gtrsim (2m_\Phi)/m_\chi$ or $T_{rh} \gtrsim (2m_\varphi)/m_\chi$ [12].*

DM production from scattering channel In this work, we consider the 2-to-2 scattering processes which contribute significantly in DM production, as mentioned in [12]. When graviton acts as the mediator for the production of DM particles from non-relativistic inflaton via 2-to-2 scattering, then the DM yield [12]

$$Y_{IS,0} \simeq \frac{g_\star^2}{81920 g_{\star,s}} \sqrt{\frac{10}{g_\star}} \left(\frac{T_{rh}}{M_P}\right)^3 \left[\left(\frac{T_{max}}{T_{rh}}\right)^4 - 1\right] \frac{m_\chi^2}{m_{\Phi(\varphi)}^2} \left(1 - \frac{m_\chi^2}{m_{\Phi(\varphi)}^2}\right)^{3/2}. \tag{7.66}$$

In Fig. 7.7, $Y_{IS,0}$ (actually $m_\chi Y_{IS,0}$ with $m_\chi Y_{CDM,0}$) is compared with $Y_{CDM,0}$ for different m_χ as a function of T_{rh}. Hence, it is shown there that the yield of DM produced via scattering (Eq. (7.66)) is not significant compared to the present CDM density.

DM particles can also be produced from the scattering of SM particles via graviton mediation. In that case,

$$\gamma = \alpha \frac{T^8}{M_P^4}, \tag{7.67}$$

where $\alpha \simeq 1.1 \times 10^{-3}$. Due to the presence of M_P^4 in the denominator, it is expected that the production of DM through this process is less compared to previous ones and thus, we neglect.

When inflaton acts as mediator for the production of DM from 2-to-2 scattering of SM particles, production of DM (yield) only through that channel results in

$$Y_{SMi,0} \simeq \frac{135 \, y_\chi^2 \lambda_{12}^2}{4\pi^8 \, g_{\star,s}} \sqrt{\frac{10}{g_\star}} \frac{M_P \, T_{rh}}{m_{\Phi(\varphi)}^4}, \qquad \text{for } T_{rh} \ll m_{\Phi(\varphi)}, T_{rh} > T. \tag{7.68}$$
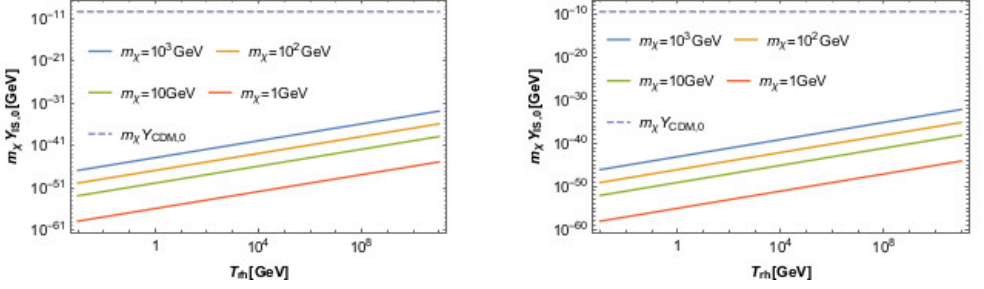
Fig. 7.7: $m_\chi \times$ *yield of DM generated from the 2-to-2 scattering with graviton as mediator for different values of* m_χ. *The left panel shows the result for Model I and the right panel for Model II inflation.*

$Y_{SMi,0} \sim 10^{-60}$ ($\sim 10^{-62}$) for $T_{rh} \sim 10^5 \text{GeV} \simeq 10^{-5} m_\Phi$ (m_φ) for $g_\star = g_{\star,s} = 106.75$, $\lambda_{12} \sim 10^{-12}$ (10^{-13}) and $y_\chi \sim 10^{-6}$ (10^{-7}). Therefore, the DM produced from 2-to-2 scattering during reheating is insignificant in comparison to total CDM density of the universe.

7.6   Conclusions and Discussion

We investigated a simple possibility of a scalar inflaton and a non-thermal fermionic particle that originated during the reheating epoch and acted as the CDM. Satisfying the correct relic density of DM and other CMB bounds, we discovered the following features of our analysis:

- We investigated two polynomial potential models for slow roll single field cosmic inflation. Each of these models features an inflection point. Moreover, due to the presence of a term corresponding to the linear power of inflaton (see Eq. (7.3)), the potential of Model I is not symmetric about the origin. In contrast, the potential of Model II (Eq. (7.4)) is symmetric under the transformation of $\varphi \to -\varphi$.

- We computed the coefficients of the potentials of both models satisfying the current CMB bounds and under the assumption of near-inflection point inflationary scenario. We also found $n_s \sim 0.96$, $r \sim 10^{-12}$, $\alpha_s \sim 10^{-3}$, and $\beta_s \sim 10^{-8}$ (see Table 7.2 and Table 7.3).

- We assumed that inflaton decays to SM Higgs (H) together with DM (χ). From stability analysis of the inflation-potential in Fig. 7.3 and Fig. 7.4, we deduced that the upper bounds of the couplings for two decay channels are $\lambda_{12}/M_P \lesssim \mathcal{O}(10^{-12})$ and $y_\chi \lesssim \mathcal{O}(10^{-6})$. The former upper bound defines the highest permissible value of T_{rh}.

- We studied the formation of non-thermal vector-like fermionic DM particles, during reheating from the inflaton decay. The rate of DM creation through this decay is temperature dependent; when the temperature of the universe's relativistic fluid increases during reheating, the rate of DM generation reduces

(Eq. (7.60)). Fig. 7.5 depicts the permissible range for the ratio of the highest temperature T_{max} to the reheating temperature T_{rh} during that period, T_{max}/T_{rh}. For $T_{rh} = 4\text{MeV}$, the ratio might reach $\mathcal{O}(10^7)$. The permitted range of T_{max}/T_{rh} is determined by the inflection point (see Eq. (7.49) and Eq. (7.50)). Because we chose the CMB scale around the inflection point, the inflection point determines the CMB observables, such as n_s and r on one hand, and controls the production regimes (via T_{max}) of DM and consequently DM relic on the other hand.

- Fig. 7.6 depicts the allowed region in $T_{rh}-m_\chi$ space for two models of potential we have considered and the constraints on that space are coming from bound on T_{rh} from BBN, radiative stability analysis of the potential for slow roll inflation, Ly-α bound, and the maximum possible value of m_χ for the effective mass of the inflaton. From this figure we can conclude that χ produced only through the decay of inflaton may explain the total density of CDM of the current universe if $10^{-10} \gtrsim y_\chi \gtrsim 10^{-15}$ (for $2.5 \times 10^3\,\text{GeV} \lesssim m_\chi \lesssim 8.1 \times 10^9\,\text{GeV}$ in Model I) and $10^{-11} \gtrsim y_\chi \gtrsim 10^{-15}$ (for $8.4 \times 10^3\,\text{GeV} \lesssim m_\chi \lesssim 2 \times 10^9\,\text{GeV}$ in Model II).

- χ can also be produced from 2-to-2 scattering of either SM particles or inflatons. Among all those scattering processes, the promising one is – from the scattering of inflaton with graviton as the mediator. In Fig. 7.7 we showed that Y_χ produced through 2-to-2 scattering of inflaton with graviton as mediator, is more than the DM production via other scattering channels, and it is $Y_{IS,0} \sim \mathcal{O}(10^{-36})$ for $T_{rh} = 10^8$ GeV, $m_\chi = 10^3$ GeV. But, $Y_{IS,0}$ produced through this channel is much less than $Y_{CDM,0}$ and thus χ produced through 2-to-2 scattering channels can contribute only a negligible fraction of $Y_{CDM,0}$.

In conclusion, we consider two members of the beyond the standard model physics - inflaton and the non-thermal DM, to connect the CMB data and the DM mystery. This work can be further extended to study the formation of Primordial Black Holes for inflection point inflationary scenario, non-Gaussianities in the CMB spectrum, and generation of Gravitational Waves which can be tested from future CMB experiments.

Acknowledgement

References

1. N. Aghanim *et al.* [Planck], Astron. Astrophys. **641**, A6 (2020) [erratum: Astron. Astrophys. **652**, C4 (2021)] doi:10.1051/0004-6361/201833910 [arXiv:1807.06209 [astro-ph.CO]].

2. P. A. R. Ade *et al.* [BICEP/Keck], [arXiv:2203.16556 [astro-ph.CO]].

3. J. Aalbers *et al.* [LZ], [arXiv:2207.03764 [hep-ex]].

4. J. Billard, M. Boulay, S. Cebrián, L. Covi, G. Fiorillo, A. Green, J. Kopp, B. Majorovits, K. Palladino and F. Petricca, *et al.* Rept. Prog. Phys. **85**, no.5, 056201 (2022) doi:10.1088/1361-6633/ac5754 [arXiv:2104.07634 [hep-ex]].

5. A. Ghoshal, G. Lambiase, S. Pal, A. Paul and S. Porey, JHEP **09**, 231 (2022) doi:10.1007/JHEP09(2022)231 [arXiv:2206.10648 [hep-ph]].

6. M. Drees and Y. Xu, JCAP **09**, 012 (2021) doi:10.1088/1475-7516/2021/09/012 [arXiv:2104.03977 [hep-ph]].

7. P. A. R. Ade *et al.* [BICEP and Keck], Phys. Rev. Lett. **127**, no.15, 151301 (2021) doi:10.1103/PhysRevLett.127.151301 [arXiv:2110.00483 [astro-ph.CO]].

8. P. Campeti and E. Komatsu, [arXiv:2205.05617 [astro-ph.CO]].

9. S. Hotchkiss, A. Mazumdar and S. Nadathur, JCAP **02**, 008 (2012) doi:10.1088/1475-7516/2012/02/008 [arXiv:1110.5389 [astro-ph.CO]].

10. A. Chatterjee and A. Mazumdar, JCAP **01**, 031 (2015) doi:10.1088/1475-7516/2015/01/031 [arXiv:1409.4442 [astro-ph.CO]].

11. J. Garcia-Bellido and E. Ruiz Morales, Phys. Dark Univ. **18**, 47-54 (2017) doi:10.1016/j.dark.2017.09.007 [arXiv:1702.03901 [astro-ph.CO]].

12. N. Bernal and Y. Xu, Eur. Phys. J. C **81**, no.10, 877 (2021) doi:10.1140/epjc/s10052-021-09694-5 [arXiv:2106.03950 [hep-ph]].

13. E. W. Kolb, A. Notari and A. Riotto, Phys. Rev. D **68**, 123505 (2003) doi:10.1103/PhysRevD.68.123505 [arXiv:hep-ph/0307241 [hep-ph]].

14. D. J. H. Chung, E. W. Kolb and A. Riotto, Phys. Rev. D **60**, 063504 (1999) doi:10.1103/PhysRevD.60.063504 [arXiv:hep-ph/9809453 [hep-ph]].

15. G. F. Giudice, E. W. Kolb and A. Riotto, Phys. Rev. D **64**, 023508 (2001) doi:10.1103/PhysRevD.64.023508 [arXiv:hep-ph/0005123 [hep-ph]].

16. P. A. Zyla *et al.* [Particle Data Group], PTEP **2020**, no.8, 083C01 (2020) doi:10.1093/ptep/ptaa104

BLED WORKSHOPS
IN PHYSICS
VOL. 23, NO. 1

Proceedings to the 25th [Virtual]
Workshop
What Comes Beyond . . . *(p. 114)*
Bled, Slovenia, July 4–10, 2022

8 Quark masses and mixing from a SU(3) gauge family symmetry

A. Hernandez-Galeana

Departamento de Física, ESFM - Instituto Politécnico Nacional.
U. P. "Adolfo López Mateos". C. P. 07738, Ciudad de México, México.
e-mail: ahernandez@ipn.mx

Abstract. Within a broken local vector-like $SU(3)$ family symmetry, we address the problem of the hierarchical spectrum of quark masses and mixing. In this scenario heavy fermions, top and bottom quarks and tau lepton become massive at tree level from **Dirac See-saw** mechanisms implemented by the introduction of a new set of $SU(2)_L$ weak singlets vector-like fermions U, D, E, N, with N a sterile neutrino. Light fermions, quarks and leptons obtain masses from loop radiative corrections mediated by the massive $SU(3)$ gauge bosons.
We provide a parameter space region where this framework can account for the known hierarchical spectrum of quark masses and mixing, and simultaneously suppress properly the current experimental constraints on $K^o - \bar{K}^o$ and $D^o - \bar{D}^o$ meson mixing. In addition, we find out that the mass of the $SU(2)_L$ weak singlet vector-like D quark introduced in this scenario may lie within a few TeV's region, and hence within current LHC possibilities.

Povzetek: Avtor predstavi svoj predlog modela z umeritveno družinsko simetrijo $SU(3)$, ki poskrbi za mase kvarkov in leptonov in za mešalni matriki. Uvede šibke singlete fermionov $SU(2)_L$ (U, D, E, N, N je nevtralni nevtrino), ki prinesejo kvarkoma t in b ter leptonu tau maso že na drevesnem nivoju preko **Dirac**ovega mehanizma **See-saw**. Za maso ostalih kvarkov in leptonov poskrbijo massivna umeritvena polja družinske simetrije $SU(3)$ s popravki v naslednjem redu.
Avtor predstavi območje parametrov, znotraj katerega so dobljeni rezulati skladni z eksperimenti $K^o - \bar{K}^o$ in $D^o - \bar{D}^o$. Masa kvarka D je nekaj TeV, torej v dosegu trenutnih zmogljivosti LHC.

Keywords: Quark masses and mixing, Flavor symmetry, Dirac See-saw mechanism.

8.1 Introduction

In this report we study the quark masses and mixing within the framework of a broken $SU(3)$ gauged family symmetry model [1, 2]. This framework introduce a hierarchical mass generation mechanism in which light fermions become massive from radiative corrections, mediated by the massive gauge bosons associated to the $SU(3)$ family symmetry that is spontaneously broken, while the masses of the

top and bottom quarks as well as for the tau lepton, are generated at tree level from "Dirac See-saw"mechanisms implemented by the introduction of a new set of $SU(2)_L$ weak singlets U, D, E and N vector-like fermions.

Flavor physics and rare processes play an important role to test any Beyond Standard Model(BSM) physics proposal, and hence, it is crucial to compute the the $\Delta F = 2$ processes [3]- [6] in neutral mesons at tree level exchange diagrams mediated by the horizontal gauge bosons.

Previous theories addressing the problem of quark and lepton masses and mixing with spontaneously broken $SU(3)$ gauge symmetry of generations include the ones with chiral $SU(3)$ family symmetry [8]- [12], as well as other $SU(3)$ family symmetry proposals [7], [13]- [16].

8.2 $SU(3)$ **family symmetry model**

The model is based on the gauge symmetry

$$G \equiv SU(3) \otimes SU(3)_C \otimes SU(2)_L \otimes U(1)_Y \tag{8.1}$$

where $SU(3)$ is a completely vector-like and universal gauged family symmetry. That is, the corresponding gauge bosons couple equally to Left and Right Handed ordinary Quarks and Leptons, with g_H, g_s, g and g' the corresponding coupling constants. The content of fermions assumes the standard model quarks and leptons:

$$\Psi_q^o = (3, 3, 2, \frac{1}{3})_L \quad , \quad \Psi_l^o = (3, 1, 2, -1)_L \tag{8.2}$$

$$\Psi_u^o = (3, 3, 1, \frac{4}{3})_R \quad , \quad \Psi_d^o(3, 3, 1, -\frac{2}{3})_R \quad , \quad \Psi_e^o = (3, 1, 1, -2)_R \tag{8.3}$$

where the last entry is the hypercharge Y, with the electric charge defined by $Q = T_{3L} + \frac{1}{2}Y$.

The model includes two types of extra fermions: Right Handed Neutrinos: $\Psi_{\nu_R}^o = (3, 1, 1, 0)_R$, introduced to cancel anomalies [7], and a new family of $SU(2)_L$ weak singlet vector-like fermions: Vector like quarks $U_L^o, U_R^o = (1, 3, 1, \frac{4}{3})$ and $D_L^o, D_R^o = (1, 3, 1, -\frac{2}{3})$, Vector Like electrons: $E_L^o, E_R^o = (1, 1, 1, -2)$, and New Sterile Neutrinos: $N_L^o, N_R^o = (1, 1, 1, 0)$.

The particle content and gauge symmetry assignments are summarized in Table 8.1. Notice that all $SU(3)$ non-singlet fields transform as the fundamental representation under the $SU(3)$ symmetry.

	$SU(3)$	$SU(3)_C$	$SU(2)_L$	$U(1)_Y$
ψ_q^o	3	3	2	$\frac{1}{3}$
ψ_{uR}^o	3	3	1	$\frac{4}{3}$
ψ_{dR}^o	3	3	1	$-\frac{2}{3}$
ψ_l^o	3	1	2	-1
ψ_{eR}^o	3	1	1	-2
$\psi_{\nu R}^o$	3	1	1	0
$U_{L,R}^o$	1	3	1	$\frac{4}{3}$
$D_{L,R}^o$	1	3	1	$-\frac{2}{3}$
$E_{L,R}^o$	1	1	1	-2
$N_{L,R}^o$	1	1	1	0
Φ^u	3	1	2	-1
Φ^d	3	1	2	+1
η_1 , η_2	3	1	1	0

Table 8.1: Particle content and charges under the gauge symmetry

8.3 $SU(3)$ **family symmetry breaking**

$SU(3)$ family symmetry is broken spontaneously by heavy SM singlet scalars $\eta_1 = (3, 1, 1, 0)$ and $\eta_2 = (3, 1, 1, 0)$ in the fundamental representation of $SU(3)$, with the "Vacuum ExpectationValues" (VEV's):

$$\langle\eta_1\rangle^T = (\Lambda_1, 0, 0) \quad , \quad \langle\eta_2\rangle^T = (0, \Lambda_2, 0) \, . \tag{8.4}$$

It is worth to mention that these two scalars in the fundamental representation is the minimal set of scalars to break down completely the $SU(3)$ family symmetry.
The interaction of the $SU(3)$ gauge bosons to the SM massless fermions is

$$i\mathcal{L}_{int,SU(3)} = g_H \, (f_1^o \, , \, f_2^o \, , \, f_3^o) \, \gamma_\mu \begin{pmatrix} \frac{Z_1^\mu}{2} + \frac{Z_2^\mu}{2\sqrt{3}} & \frac{Y_1^{+\mu}}{\sqrt{2}} & \frac{Y_2^{+\mu}}{\sqrt{2}} \\ \frac{Y_1^{-\mu}}{\sqrt{2}} & -\frac{Z_2^\mu}{\sqrt{3}} & \frac{Y_3^{+\mu}}{\sqrt{2}} \\ \frac{Y_2^{-\mu}}{\sqrt{2}} & \frac{Y_3^{-\mu}}{\sqrt{2}} & -\frac{Z_1^\mu}{2} + \frac{Z_2^\mu}{2\sqrt{3}} \end{pmatrix} \begin{pmatrix} f_1^o \\ f_2^o \\ f_3^o \end{pmatrix} \tag{8.5}$$

where g_H is the $SU(3)$ coupling constant, Z_1, Z_2 and $Y_j^\pm = \frac{Y_j^1 \mp i Y_j^2}{\sqrt{2}}$, $j = 1, 2, 3$ are the eight gauge bosons.
Thus, the contribution to the horizontal gauge boson masses from the VEV's of Eq.(8.4) read

- $\langle\eta_1\rangle$: $\frac{g_H^2 \Lambda_1^2}{2}(Y_1^+ Y_1^- + Y_2^+ Y_2^-) + \frac{g_H^2 \Lambda_1^2}{4}(Z_1^2 + \frac{Z_2^2}{3} + 2Z_1 \frac{Z_2}{\sqrt{3}})$
- $\langle\eta_2\rangle$: $\frac{g_H^2 \Lambda_2^2}{2}(Y_1^+ Y_1^- + Y_3^+ Y_3^-) + g_H^2 \Lambda_2^2 \frac{Z_2^2}{3}$

The "Spontaneous Symmetry Breaking" (SSB) of $SU(3)$ occurs in two stages

$$SU(3)_F \times G_{SM} \xrightarrow{\langle \eta_2 \rangle} SU(2)_F \times G_{SM} \xrightarrow{\langle \eta_1 \rangle} G_{SM}$$
$$Z_1, Y_2^{\pm}$$

Notice that the hierarchy of scales $\Lambda_2 > \Lambda_1$ yield an "approximate SU(2) global symmetry" in the spectrum of SU(2) gauge boson masses of order $g_H \Lambda_1$.

Therefore, neglecting tiny contributions from electroweak symmetry breaking, the gauge boson masses read

$$(M_1^2 + M_2^2) Y_1^+ Y_1^- + M_1^2 Y_2^+ Y_2^- + M_2^2 Y_3^+ Y_3^-$$
$$+ \frac{1}{2} M_1^2 Z_1^2 + \frac{1}{2} \frac{M_1^2 + 4M_2^2}{3} Z_2^2 + \frac{1}{2}(M_1^2)\frac{2}{\sqrt{3}} Z_1 Z_2 \quad (8.6)$$

$$M_1^2 = \frac{g_H^2 \Lambda_1^2}{2} \quad , \quad M_2^2 = \frac{g_H^2 \Lambda_2^2}{2} \quad (8.7)$$

	Z_1	Z_2
Z_1	M_1^2	$\frac{M_1^2}{\sqrt{3}}$
Z_2	$\frac{M_1^2}{\sqrt{3}}$	$\frac{M_1^2 + 4M_2^2}{3}$

Table 8.2: $Z_1 - Z_2$ mixing mass matrix

8.4 Electroweak symmetry breaking

The "Electroweak Symmetry Breaking" (EWSB) is achieved by the Higgs fields Φ_i^u and Φ_i^d, which transform simultaneously as triplets under SU(3) and as Higgs doublets with hypercharges -1 and $+1$ under the SM, respectively, explicitly:

$$\Phi^u = \begin{pmatrix} \begin{pmatrix} \phi^o \\ \phi^- \end{pmatrix}_1^u \\ \begin{pmatrix} \phi^o \\ \phi^- \end{pmatrix}_2^u \\ \begin{pmatrix} \phi^o \\ \phi^- \end{pmatrix}_3^u \end{pmatrix} \quad , \quad \Phi^d = \begin{pmatrix} \begin{pmatrix} \phi^+ \\ \phi^o \end{pmatrix}_1^d \\ \begin{pmatrix} \phi^+ \\ \phi^o \end{pmatrix}_2^d \\ \begin{pmatrix} \phi^+ \\ \phi^o \end{pmatrix}_3^d \end{pmatrix}$$

with the VEV's

$$\langle \Phi^u \rangle = \begin{pmatrix} \frac{1}{\sqrt{2}} \begin{pmatrix} v_{u1} \\ 0 \end{pmatrix} \\[8pt] \frac{1}{\sqrt{2}} \begin{pmatrix} v_{u2} \\ 0 \end{pmatrix} \\[8pt] \frac{1}{\sqrt{2}} \begin{pmatrix} v_{u3} \\ 0 \end{pmatrix} \end{pmatrix} \quad , \quad \langle \Phi^d \rangle = \begin{pmatrix} \frac{1}{\sqrt{2}} \begin{pmatrix} 0 \\ v_{d1} \end{pmatrix} \\[8pt] \frac{1}{\sqrt{2}} \begin{pmatrix} 0 \\ v_{d2} \end{pmatrix} \\[8pt] \frac{1}{\sqrt{2}} \begin{pmatrix} 0 \\ v_{d3} \end{pmatrix} \end{pmatrix}$$

The contributions from $\langle \Phi^u \rangle$ and $\langle \Phi^d \rangle$ generate the W and Z_o SM gauge boson masses

$$\frac{g^2}{4} (v_u^2 + v_d^2) W^+ W^- + \frac{(g^2 + g'^2)}{8} (v_u^2 + v_d^2) Z_o^2 \tag{8.8}$$
$$+ \text{ tiny contribution to the SU(3) gauge boson masses and mixing}$$
$$\text{with } Z_o,$$

$v_u^2 = v_{1u}^2 + v_{2u}^2 + v_{3u}^2$, $v_d^2 = v_{1d}^2 + v_{2d}^2 + v_{3d}^2$. So, if $M_W \equiv \frac{1}{2} g\, v$, we may write $v = \sqrt{v_u^2 + v_d^2} \approx 246 \text{ GeV}$.

8.5   Fermion masses

8.5.1   Dirac See-saw mechanisms

SM quarks and leptons get tree level mass contribution after EWSB from the generic diagram in Fig. 1

The gauge symmetry $G \equiv SU(3) \times G_{SM}$, the fermion content, and the transformation of the scalar fields, all together, avoid Yukawa couplings between SM fermions. The allowed Yukawa couplings involve terms between the SM fermions and the corresponding vector-like fermions U, D, E and N. The scalars and fermion content allow the gauge invariant Yukawa couplings

$$h_u \, \overline{\psi_q^o} \, \Phi^u \, U_R^o \; + \; h_{1u} \, \overline{\psi_{uR}^o} \, \eta_1 \, U_L^o \; + \; h_{2u} \, \overline{\psi_{uR}^o} \, \eta_2 \, U_L^o \; + \; M_U \, \overline{U_L^o} \, U_R^o$$

$$h_d \, \overline{\psi_q^o} \, \Phi^d \, D_R^o \; + \; h_{1d} \, \overline{\psi_{dR}^o} \, \eta_1 \, D_L^o \; + \; h_{2d} \, \overline{\psi_{dR}^o} \, \eta_2 \, D_L^o \; + \; M_D \, \overline{D_L^o} \, D_R^o$$

$$h_\nu \, \overline{\psi_l^o} \, \Phi^u \, N_R^o \; + \; h_{1\nu} \, \overline{\psi_{\nu R}^o} \, \eta_1 \, N_L^o \; + \; h_{2\nu} \, \overline{\psi_{\nu R}^o} \, \eta_2 \, N_L^o \; + \; m_D \, \overline{N_L^o} \, N_R^o$$

$$h_e \, \overline{\psi_l^o} \, \Phi^d \, E_R^o \; + \; h_{1e} \, \overline{\psi_{eR}^o} \, \eta_1 \, E_L^o \; + \; h_{2e} \, \overline{\psi_{eR}^o} \, \eta_2 \, E_L^o \; + \; M_E \, \overline{E_L^o} \, E_R^o$$
$$+ h.c$$

Neutrinos may also obtain left-handed and right-handed Majorana masses both from tree level and radiative corrections.

$$h_L \; \overline{\psi_l^o} \; \Phi^u \; (N_L^o)^c \; + \; m_L \; \overline{N_L^o} \; (N_L^o)^c$$

$$h_{1R} \; \overline{\psi_{\nu R}^o} \; \eta_1 \; (N_R^o)^c \; + \; h_{2R} \; \overline{\psi_{\nu R}^o} \; \eta_2 \; (N_R^o)^c \; + \; m_R \; \overline{N_R^o} \; (N_R^o)^c \; + h.c$$

When the involved scalar fields acquire VEV's, we get in the gauge basis $\psi_{L,R}^o{}^T = (e^o, \mu^o, \tau^o, E^o)_{L,R}$, the mass terms $\bar{\psi}_L^o \mathcal{M}^o \psi_R^o + h.c$, where

$$\mathcal{M}^o = \begin{pmatrix} 0 & 0 & 0 & h\,v_1 \\ 0 & 0 & 0 & h\,v_2 \\ 0 & 0 & 0 & h\,v_3 \\ h_1\Lambda_1 & h_2\Lambda_2 & 0 & M \end{pmatrix} \equiv \begin{pmatrix} 0 & 0 & 0 & a_1 \\ 0 & 0 & 0 & a_2 \\ 0 & 0 & 0 & a_3 \\ b1 & b2 & 0 & M \end{pmatrix}. \tag{8.9}$$

$\mathcal{M}^o$ is diagonalized by applying a biunitary transformation $\psi_{L,R}^o = V_{L,R}^o \, \chi_{L,R}$.

$$V_L^{o\,T} \mathcal{M}^o \, V_R^o = \mathrm{Diag}(0, 0, -\lambda_3, \lambda_4) \tag{8.10}$$

$$V_L^{o\,T} \mathcal{M}^o \mathcal{M}^{o\,T} \, V_L^o = V_R^{o\,T} \mathcal{M}^{o\,T} \mathcal{M}^o \, V_R^o = \mathrm{Diag}(0, 0, \lambda_3^2, \lambda_4^2), \tag{8.11}$$

where λ_3 and λ_4 are the nonzero eigenvalues, λ_4 being the fourth heavy fermion mass, and λ_3 of the order of the top, bottom and tau mass for u, d and e fermions, respectively. We see from Eqs.(8.10,8.11) that from tree level there exist two massless eigenvalues associated to the light fermions:

8.6   One loop contribution to fermion masses

The one loop diagram of Fig.8.1 gives the generic contribution to the mass term $m_{ij} \, \bar{e}_{iL}^o e_{jR}^o$,
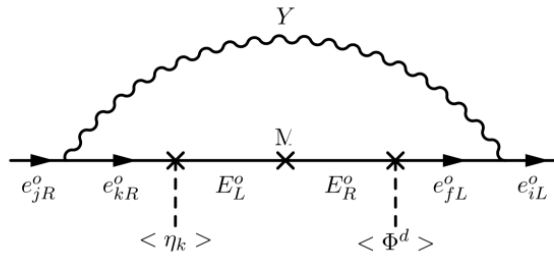

Fig. 8.1: Generic one loop diagram mass contribution

$$m_{ij} = c_Y \frac{\alpha_H}{\pi} \sum_{k=3,4} m_k^o \, (V_L^o)_{ik} (V_R^o)_{jk} f(M_Y, m_k^o) \qquad , \qquad \alpha_H \equiv \frac{g_H^2}{4\pi}, \qquad (8.12)$$

M_Y being the mass of the gauge boson, c_Y is a factor coupling constant, $m_3^o = -\lambda_3$ and $m_4^o = \lambda_4$, and $f(x, y) = \frac{x^2}{x^2 - y^2} \ln \frac{x^2}{y^2}$,

$$\sum_{k=3,4} m_k^o \, (V_L^o)_{ik} (V_R^o)_{jk} f(M_Y, m_k^o) = \frac{a_i \, b_j \, M}{\lambda_4^2 - \lambda_3^2} F(M_Y), \qquad (8.13)$$

$i = 1, 2, 3$, $j = 1, 2$, and $F(M_Y) \equiv \frac{M_Y^2}{M_Y^2 - \lambda_4^2} \ln \frac{M_Y^2}{\lambda_4^2} - \frac{M_Y^2}{M_Y^2 - \lambda_3^2} \ln \frac{M_Y^2}{\lambda_3^2}$. Adding up all possible one loop diagramss, we get the contribution $\bar{\psi}_L^o \mathcal{M}_1^o \psi_R^o + h.c.$,

$$\mathcal{M}_1^o = \begin{pmatrix} D_{11} & D_{12} & 0 & 0 \\ D_{21} & D_{22} & 0 & 0 \\ D_{31} & D_{32} & D_{33} & 0 \\ 0 & 0 & 0 & 0 \end{pmatrix} \frac{\alpha_H}{\pi}, \qquad (8.14)$$

$$D_{11} = \mu_{11}\left(\frac{F_{Z_1}}{4} + \frac{F_{Z_2}}{12} + F_m\right) + \frac{1}{2}\mu_{22}F_1 \; ; \; D_{12} = \mu_{12}\left(-\frac{F_{Z_2}}{6} - F_m\right)$$

$$D_{21} = \mu_{21}\left(-\frac{F_{Z_2}}{6} - F_m\right) \; ; \qquad\qquad D_{22} = \frac{1}{2}\mu_{11}F_1 + \frac{1}{3}\mu_{22}F_{Z_2}$$

$$D_{31} = \mu_{31}\left(-\frac{F_{Z_1}}{4} + \frac{F_{Z_2}}{12}\right) \; ; \qquad\qquad D_{32} = \mu_{32}\left(-\frac{F_{Z_2}}{6} + F_m\right)$$

$$D_{33} = \frac{1}{2}(\mu_{11}F_2 + \mu_{22}F_3)$$

$$F_1 \equiv F(M_{Y_1}) \quad , \quad F_2 \equiv F(M_{Y_2}) \quad , \quad F_3 \equiv F(M_{Y_3}) \qquad (8.15)$$

$$F_{Z_1} = \cos^2 \phi \, F(M_-) + \sin^2 \phi \, F(M_+) \qquad (8.16)$$

$$F_{Z_2} = \sin^2 \phi \, F(M_-) + \cos^2 \phi \, F(M_+) \qquad (8.17)$$

$$F_m = \frac{\cos\phi \sin\phi}{2\sqrt{3}} \left[F(M_+) - F(M_-)\right]. \qquad (8.18)$$

F_{Z_1}, F_{Z_2} are the contributions from the diagrams mediated by the Z_1, Z_2 gauge bosons, F_m comes from the $Z_1 - Z_2$ mixing diagrams, with M_1, M_2, M_-, M_+ the horizontal boson mass eigenvalues, Eqs.(7-11),

$$\mu_{ij} = \frac{a_i \, b_j \, M}{\lambda_4^2 - \lambda_3^2} = \frac{a_i \, b_j}{a \, b} \lambda_3 \, c_\alpha \, c_\beta, \qquad (8.19)$$

$c_\alpha = \cos\alpha, c_\beta = \cos\beta, s_\alpha = \sin\alpha, s_\beta = \sin\beta$ are mixing angles from the diagonalization of $\mathcal{M}^o$. Therefore, up to one loop corrections the fermion masses are

$$\bar{\psi}^o_L \mathcal{M}^o\, \psi^o_R + \bar{\psi}^o_L \mathcal{M}^o_1\, \psi^o_R = \bar{\chi}_L\, \mathcal{M}\, \chi_R\,, \tag{8.20}$$

where $\psi^o_{L,R} = V^o_{L,R}\, \chi_{L,R}$, and $\mathcal{M} \equiv \left[\mathrm{Diag}(0,0,-\lambda_3,\lambda_4) + V^{o\,T}_L \mathcal{M}^o_1\, V^o_R \right]$, namely:

$$\mathcal{M} = \begin{pmatrix} m_{11} & m_{12} & c_\beta\, m_{13} & s_\beta\, m_{13} \\[2mm] m_{21} & m_{22} & c_\beta\, m_{23} & s_\beta\, m_{23} \\[2mm] c_\alpha\, m_{31} & c_\alpha\, m_{32} & (-\lambda_3 + c_\alpha c_\beta\, m_{33}) & c_\alpha s_\beta\, m_{33} \\[2mm] s_\alpha\, m_{31} & s_\alpha\, m_{32} & s_\alpha c_\beta\, m_{33} & (\lambda_4 + s_\alpha s_\beta\, m_{33}) \end{pmatrix}, \tag{8.21}$$

The diagonalization of $\mathcal{M}$, Eq.(8.21) gives the physical masses for u and d quarks, e charged leptons and ν Dirac neutrino masses. Using a new biunitary transformation $\chi_{L,R} = V^{(1)}_{L,R}\, \Psi_{L,R}$; $\bar{\chi}_L\, \mathcal{M}\, \chi_R = \bar{\Psi}_L\, V^{(1)\,T}_L \mathcal{M}\, V^{(1)}_R\, \Psi_R$, with $\Psi_{L,R}{}^T = (f_1, f_2, f_3, F)_{L,R}$ the mass eigenfields, that is

$$V^{(1)\,T}_L \mathcal{M}\, \mathcal{M}^T\, V^{(1)}_L = V^{(1)\,T}_R \mathcal{M}^T\, \mathcal{M}\, V^{(1)}_R = \mathrm{Diag}(m_1^2, m_2^2, m_3^2, M_F^2)\,, \tag{8.22}$$

$m_1^2 = m_e^2$, $m_2^2 = m_\mu^2$, $m_3^2 = m_\tau^2$ and $M_F^2 = M_E^2$ for charged leptons. So, the rotations from massless to mass fermion eigenfields in this scenario reads

$$\psi^o_L = V^o_L\, V^{(1)}_L\, \Psi_L \qquad \text{and} \qquad \psi^o_R = V^o_R\, V^{(1)}_R\, \Psi_R \tag{8.23}$$

8.6.1   Quark Mixing Matrix V_{CKM}

We recall that vector like quarks are $SU(2)_L$ weak singlets, and hence the interaction of L-handed up and down quarks; $f^o_{uL}{}^T = (u^o, c^o, t^o)_L$ and $f^o_{dL}{}^T = (d^o, s^o, b^o)_L$, to the W charged gauge boson is

$$\frac{g}{\sqrt{2}}\, \bar{f}^o_{uL} \gamma_\mu f^o_{dL} W^{+\mu} = \frac{g}{\sqrt{2}}\, \bar{\Psi}_{uL}\, (V_{CKM})_{4\times4}\, \gamma_\mu \Psi_{dL}\, W^{+\mu}\,, \tag{8.24}$$

where the non-unitary quark mixing matrix V_{CKM} of dimension 4×4 is

$$(V_{CKM})_{4\times4} = [(V^o_{uL}\, V^{(1)}_{uL})_{3\times4}]^T\, (V^o_{dL}\, V^{(1)}_{dL})_{3\times4} \tag{8.25}$$

8.7   Numerical results for quark masses and mixing

As an example of the possible spectrum of quark masses and mixing from this scenario, we show up the following fit of parameters at the M_Z scale [17]

Using the input values for the horizontal boson masses, Eq.(8), and the coupling constant of the $SU(3)$ family symmetry:

$$M_1 = 2800 \text{ TeV} \quad , \quad M_2 = 10^3 \, M_1 \quad , \quad \frac{\alpha_H}{\pi} = 0.05 \, , \tag{8.26}$$

we write the tree level $\mathcal{M}_q^o$, and up to one loop corrections $\mathcal{M}_q$ quark mass matrices, as well as the corresponding mass eigenvalues and mixing:

d-quarks:

Tree level see-saw mass matrix:

$$\mathcal{M}_d^o = \begin{pmatrix} 0 & 0 & 0 & 817.977 \\ 0 & 0 & 0 & 9224.67 \\ 0 & 0 & 0 & 4139.08 \\ 3.072 \times 10^6 & -132120.0 & 9.1 \times 10^6 \end{pmatrix} \text{MeV} \, , \tag{8.27}$$

the mass matrix up to one loop corrections:

$$\mathcal{M}_d = \begin{pmatrix} 0. & -2.31807 & -48.2688 & -16.3033 \\ 46.5611 & 20.7889 & -0.89430 & -0.30206 \\ -20.8102 & 46.5138 & -2859.86 & 130.424 \\ -0.02081 & 0.04651 & 0.38614 & 9.61 \times 10^6 \end{pmatrix} \text{MeV} \, , \tag{8.28}$$

the d-quark mass eigenvalues

$$(\, m_d, m_s, m_b, M_D \,) = (\, 2.97 \,, \, 51 \,, \, 2860.72 \,, \, 9.61 \times 10^6 \,) \, \text{MeV} \, , \tag{8.29}$$

and the product of mixing matrices:

$$V_{d\,L} = V_{d\,L}^o \, V_{d\,L}^{(1)} = \begin{pmatrix} -0.99508 & -0.01754 & -0.09742 & 8.0 \times 10^{-5} \\ 0.09608 & -0.40801 & -0.90790 & 9.218 \times 10^{-4} \\ 0.02382 & 0.91280 & -0.40769 & 4.136 \times 10^{-4} \\ -1.87 \times 10^{-5} & 7.19 \times 10^{-10} & 1.34 \times 10^{-5} & 0.99999 \end{pmatrix} \tag{8.30}$$

$$V_{d\,R} = V_{d\,R}^o \, V_{d\,R}^{(1)} = \begin{pmatrix} 0.02236 & -0.01754 & -0.94709 & 0.31970 \\ 0.91254 & -0.40802 & 0.02446 & -0.01374 \\ 0.40833 & 0.91280 & -0.00726 & -2.19 \times 10^{-9} \\ 0.00569 & -6.24 \times 10^{-8} & 0.31994 & 0.94741 \end{pmatrix} \tag{8.31}$$

u-quarks:

$$\mathcal{M}_u^o = \begin{pmatrix} 0 & 0 & 0 & 23924.3 \\ 0 & 0 & 0 & 216134. \\ 0 & 0 & 0 & 104083. \\ 8.65 \times 10^{10} & -6.91 \times 10^9 & 0 & 6.96 \times 10^{10} \end{pmatrix} \text{MeV} \, , \tag{8.32}$$

$$\mathcal{M}_u = \begin{pmatrix} 0 & -150.079 & -678.614 & -845.855 \\ 4.02292 & 586.756 & 2635.9 & 3285.51 \\ -1.92554 & 2086.27 & -172961. & 18797.7 \\ -2.61 \times 10^{-6} & 0.00282 & 0.02045 & 1.11 \times 10^{11} \end{pmatrix} \text{MeV}, \tag{8.33}$$

the u-quark mass eigenvalues

$$(m_u, m_c, m_t, M_U) = (1.38, 638.36, 172995, 1.11 \times 10^{11}) \text{MeV} \tag{8.34}$$

and the product of mixing matrices:

$$V_{uL} = V_{uL}^o V_{uL}^{(1)} = \begin{pmatrix} 0.97438 & 0.20022 & -0.10239 & 1.45 \times 10^{-7} \\ 0.00044 & -0.45700 & -0.88946 & 1.38 \times 10^{-6} \\ -0.224887 & 0.866634 & -0.445389 & 6.31 \times 10^{-7} \\ 0 & 5.44 \times 10^{-8} & 1.52 \times 10^{-6} & 1. \end{pmatrix} \tag{8.35}$$

$$V_{uR} = V_{uR}^o V_{uR}^{(1)} = \begin{pmatrix} -0.00007 & 0.07222 & -0.6247 & 0.77751 \\ -0.00087 & 0.99734 & 0.03791 & -0.06217 \\ 1. & 0.00087 & -0.00001 & 0 \\ 7.09 \times 10^{-7} & 0.00936 & 0.77994 & 0.62578 \end{pmatrix} \tag{8.36}$$

and the quark mixing matrix:

$$V_{CKM} = \begin{pmatrix} -0.97491 & -0.22255 & -0.00364 & -0.000014 \\ -0.22250 & 0.97402 & 0.04208 & -0.000046 \\ 0.00581 & -0.04184 & 0.99910 & -0.001012 \\ 3.24 \times 10^{-9} & 1.07 \times 10^{-8} & -1.52 \times 10^{-6} & 1.54 \times 10^{-9} \end{pmatrix} \tag{8.37}$$

8.8   ΔF = 2 Processes in Neutral Mesons

The $SU(3)$ family gauge bosons contribute to new FCNC's, in particular they mediate $K^o - \bar{K}^o$, $D^o - \bar{D}^o$ mixing via single exchange from the depicted diagram in Fig.8.2

The Z_1, $Y_2^{\pm}$ ($Y_2^{\pm} = \frac{Y_2^1 \mp i Y_2^2}{\sqrt{2}}$) gauge bosons become massive at the second stage of the $SU(3)$ symmetry breaking, and have flavor changing couplings in both left- and right-handed fermions, and then contribute the $\Delta F = 2$ effective operators

$$\mathcal{O}_{LL} = (\bar{d}_L \gamma_\mu s_L)(\bar{d}_L \gamma^\mu s_L) \quad , \quad \mathcal{O}_{RR} = (\bar{d}_R \gamma_\mu s_R)(\bar{d}_R \gamma^\mu s_R) \tag{8.38}$$

$$\mathcal{O}_{LR} = (\bar{d}_L \gamma_\mu s_L)(\bar{d}_R \gamma^\mu s_R) \tag{8.39}$$

The $SU(3)$ couplings to fermions when written in the mass basis yield the effective couplings
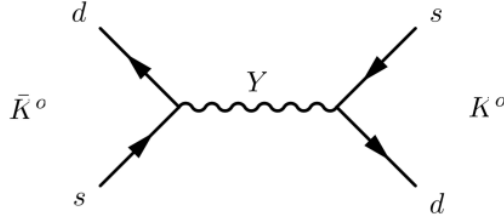
Fig. 8.2: Generic tree level exchange contribution to $K^o - \bar{K}^o$ from the SU(3) family gauge bosons.

$$\mathcal{H}_{SU(2)} = \frac{g_H^2}{4M_1^2} \left[\delta_L^2\, \mathcal{O}_{LL} + \delta_R^2\, \mathcal{O}_{RR} + \delta_{LR}^2\, \mathcal{O}_{LR}\right] \tag{8.40}$$

The suppression of the generic meson mixing couplings $\frac{z_{ij}}{\Lambda^2}(\bar{q}_{iL}\gamma^\mu P_L\, q_j)^2$ come out as follows

8.8.1 $K^o - \bar{K}^o$ meson mixing

$$\delta_L = 0.0392053 \qquad , \qquad \frac{M_1}{\frac{g_H}{2}|\delta_L|} = 101667.\ \text{TeV's}$$

$$\delta_R = 0.372337 \qquad , \qquad \frac{M_1}{\frac{g_H}{2}|\delta_R|} = 10705.\ \text{TeV's} \tag{8.41}$$

$$\sqrt{|\delta_{LR}|} = 0.170869\ , \qquad \frac{M_1}{\frac{g_H}{2}\sqrt{|\delta_{LR}|}} = 23327.\ \text{TeV's}$$

8.8.2 $D^o - \bar{D}^o$ meson mixing

$$\delta_L = 0.000201739\ , \qquad \frac{M_1}{\frac{g_H}{2}|\delta_L|} = 1.97 \times 10^7\ \text{TeV's}$$

$$\delta_R = 0.000872865\ , \qquad \frac{M_1}{\frac{g_H}{2}|\delta_R|} = 4.56 \times 10^6\ \text{TeV's} \tag{8.42}$$

$$\sqrt{|\delta_{LR}|} = 0.49322\ , \qquad \frac{M_1}{\frac{g_H}{2}\sqrt{|\delta_{LR}|}} = 8081.33\ \text{TeV's}$$

These values are within the suppression required for BSM contributions reported for instance in the review "CKM Quark - Mixing Matrix" in PDG2022 [18].

8.9   Conclusions

We have updated the analysis of quark masses and mixing within the context of a broken local vector-like $SU(3)$ family symmetry, which combines tree level "Dirac See-saw" mechanisms and radiative corrections to implement a successful hierarchical spectrum for fermion masses and mixing.

We provided a parameter space region where this scenario can accommodate the known hierarchy spectrum of quark masses and mixing, and simultaneously suppress properly the $\Delta S = 2$ and $\Delta C = 2$ processes. Furthermore, the $SU(2)_L$ weak singlet vector-like D quark mass turns out to lie within a few TeV region.

8.10   Acknowledgements

References

1. A. Hernandez-Galeana, Rev. Mex. Fis. **Vol. 50(5)**, (2004) 522. hep-ph/0406315.
2. A. Hernandez-Galeana, Bled Workshops in Physics, (ISSN:1580-4992), **Vol. 19, No. 2**, (2018) Pag. 299; **Vol. 18, No. 2**, (2017) Pag. 56; **Vol. 17, No. 2**, (2016) Pag. 36; arXiv:1612.07388[hep-ph]; **Vol. 16, No. 2**, (2015) Pag. 47; arXiv:1602.08212[hep-ph]; **Vol. 15, No. 2**, (2014) Pag. 93; arXiv:1412.6708[hep-ph]; **Vol. 14, No. 2**, (2013) Pag. 82; arXiv:1312.3403[hep-ph]; **Vol. 13, No. 2**, (2012) Pag. 28; arXiv:1212.4571[hep-ph]; **Vol. 12, No. 2**, (2011) Pag. 41; arXiv:1111.7286[hep-ph]; **Vol. 11, No. 2**, (2010) Pag. 60; arXiv:1012.0224[hep-ph]; Bled Workshops in Physics,**Vol. 10, No. 2**, (2009) Pag. 67; arXiv:0912.4532[hep-ph];
3. E. Golowich, J. Hewett, S. Pakvasa, and A. Petrov, Phys. Rev. D **76**, 095009 (2007).
4. E. Golowich, J. Hewett, S. Pakvasa, and A. Petrov, Phys. Rev. D **79**, 114030 (2009).
5. M. Kirk, A. Lenz, and T. Rauh, arXiv:1711.02100[hep-ph]; T. Jubb, M. Kirk, A. Lenz, and G. Tetlalmatzi-Xolocotzi, arXiv:1603.07770[hep-ph];
6. C. Bobeth, A. J. Buras, A. Celis, and M. Junk, arXiv:1703.04753[hep-ph]; A. J. Buras, arXiv:1611.06206[hep-ph]; arXiv:1609.05711[hep-ph];
7. T. Yanagida, Phys. Rev. D **20**, 2986 (1979).
8. Z.G. Berezhiani: The weak mixing angles in gauge models with horizontal symmetry: A new approach to quark and lepton masses, Phys. Lett. B **129**, 99 (1983).
9. Z. Berezhiani and M. Yu.Khlopov: Theory of broken gauge symmetry of families, Sov.J.Nucl.Phys. **51**, 739 (1990).
10. Z. Berezhiani and M. Yu.Khlopov: Physical and astrophysical consequences of family symmetry breaking, Sov.J.Nucl.Phys. **51**, 935 (1990).
11. A. S. Sakharov and M. Yu. Khlopov: Horizontal unification as the phenomenology of the theory of "everything", Phys.Atom.Nucl. **57**, 651 (1994).
12. Z. Berezhiani, M. Yu.Khlopov and R. R. Khomeriki: On the possible test of quantum flavor dynamics in the searches for rare decays of heavy particles, Sov.J.Nucl.Phys. **52**, 344 (1990).
13. J.L. Chkareuli, C.D. Froggatt, and H.B. Nielsen, Nucl. Phys. B **626**, 307 (2002).

14. T. Appelquist, Y. Bai and M. Piai: SU(3) Family Gauge Symmetry and the Axion, Phys. Rev. D **75**, 073005 (2007).
15. T. Appelquist, Y. Bai and M. Piai: Neutrinos and SU(3) family gauge symmetry, Phys. Rev. D **74**, 076001 (2006).
16. T. Appelquist, Y. Bai and M. Piai: Quark mass ratios and mixing angles from SU(3) family gauge symmetry, Phys. Lett. B **637**, 245 (2006).
17. Zhi-zhong Xing, He Zhang and Shun Zhou, Phys. Rev. D **86**, 013013 (2012).
18. R.L. Workman et al. (Particle Data Group), Prog. Theor. Exp. Phys. **2022**, 083C01 (2022)

8.11   Appendix

8.11.1   Diagonalization of the generic Dirac See-saw mass matrix

$$\mathcal{M}^o = \begin{pmatrix} 0 & 0 & 0 & a_1 \\ 0 & 0 & 0 & a_2 \\ 0 & 0 & 0 & a_3 \\ b_1 & b_2 & 0 & c \end{pmatrix} \tag{8.43}$$

The tree level $\mathcal{M}^o$ 4×4 See-saw mass matrix is diagonalized by a biunitary transformation $\psi_L^o = V_L^o \chi_L$ and $\psi_R^o = V_R^o \chi_R$. The diagonalization of $\mathcal{M}^o \mathcal{M}^{o\,T}$ ($\mathcal{M}^{o\,T} \mathcal{M}^o$) yield the nonzero eigenvalues

$$\lambda_3^2 = \frac{1}{2}\left(B - \sqrt{B^2 - 4D}\right) \quad , \quad \lambda_4^2 = \frac{1}{2}\left(B + \sqrt{B^2 - 4D}\right) \tag{8.44}$$

and rotation mixing angles

$$\cos\alpha = \sqrt{\frac{\lambda_4^2 - a^2}{\lambda_4^2 - \lambda_3^2}} \quad , \quad \sin\alpha = \sqrt{\frac{a^2 - \lambda_3^2}{\lambda_4^2 - \lambda_3^2}} ,$$

$$\tag{8.45}$$

$$\cos\beta = \sqrt{\frac{\lambda_4^2 - b^2}{\lambda_4^2 - \lambda_3^2}} \quad , \quad \sin\beta = \sqrt{\frac{b^2 - \lambda_3^2}{\lambda_4^2 - \lambda_3^2}} .$$

$$B = a^2 + b^2 + c^2 = \lambda_3^2 + \lambda_4^2 \quad , \quad D = a^2 b^2 = \lambda_3^2 \lambda_4^2 , \tag{8.46}$$

$$a^2 = a_1^2 + a_2^2 + a_3^2 \quad , \quad b^2 = b_1^2 + b_2^2 \tag{8.47}$$

The rotation matrices V_L^o, V_R^o admit several parametrizations related to the two zero mass eigenstates, for instance

$$V_L^o = \begin{pmatrix} c_1 & s_1 c_2 & s_1 s_2 c_\alpha & s_1 s_2 s_\alpha \\ -s_1 & c_1 c_2 & c_1 s_2 c_\alpha & c_1 s_2 s_\alpha \\ 0 & -s_2 & c_2 c_\alpha & c_2 s_\alpha \\ 0 & 0 & -s_\alpha & c_\alpha \end{pmatrix} \quad , \quad V_R^o = \begin{pmatrix} 0 & c_r & s_r c_\beta & s_r s_\beta \\ 0 & -s_r & c_r c_\beta & c_r s_\beta \\ 1 & 0 & 0 & 0 \\ 0 & 0 & -s_\beta & c_\beta \end{pmatrix}$$

$$a_p = \sqrt{a_1^2 + a_2^2} \quad , \quad a = \sqrt{a_p^2 + a_3^2} \quad , \quad b = \sqrt{b_1^2 + b_2^2}$$

$$s_1 = \frac{a_1}{a_p} \quad , \quad c_1 = \frac{a_2}{a_p} \quad , \quad s_2 = \frac{a_p}{a} \quad , \quad c_2 = \frac{a_3}{a} \quad , \quad s_r = \frac{b_1}{b} \quad , \quad c_r = \frac{b_2}{b}$$

$$a_1 = s_1 s_2 a \quad , \quad a_2 = c_1 s_2 a \quad , \quad a_3 = c_2 a \quad , \quad b_1 = s_r b \quad , \quad b_2 = c_r b$$

BLED WORKSHOPS
IN PHYSICS
VOL. 23, NO. 1

Proceedings to the 25th [Virtual]
Workshop
What Comes Beyond . . . *(p. 128)*
Bled, Slovenia, July 4–10, 2022

9 Evolution and Possible Forms of Primordial Antimatter and Dark Matter celestial objects

Maxim Yu. Khlopov, O.M. Lecian
email: khlopov@apc.in2p3.f
email:orchideamaria.lecian@uniroma1.it

Institute of Physics, Southern Federal University,Rostov on Don, Russia
Virtual Institute of Astropartcie physics, Paris, France and
National Research Nuclear University "MEPHI", Moscow, Russia;
Sapienza University of Rome,
Faculty of Medicine and Pharmacy,
Viale Regina Elena, 324 - 00185 Rome, Italy;
Sapienza University of Rome,
Faculty of Medicine and Dentistry,
Piazzale Aldo Moro, 5 - 00185 Rome, Italy;
Kursk State University,
Faculty of Physics, Mathematics and Information Sciences,
Chair of Algebra, Geometry and Didactics of Mathematics Theory,
ul. Radis'c'eva, 33, aud. 201, Kursk, Russia

Abstract. The structure and evolution of Primordial Antimatter domains and Dark matter objects are analysed. Relativistic low- density antimatter domains are described. The Relativistic FRW perfect-fluid solution is found for the characterization of i) ultra- high density antimatter domains, ii) high-density antimatter domains, and iii) dense anti- matter domains. The possible sub-domains structures is analyzed. The structures evolved to the time of galaxy formation are outlined. Comparison is given with other primordial celestial objects. The features of antistars are outlined. In the case of WIMP dark matter clumps, the mechanisms of their survival to the present time are discussed. The cosmological features of neutrino clumping due to fifth force are examined.

Povzetek: Članek obravnava strukturo in dinamiko domen anti-snovi majhne gostote in temne snovi v zgodnjem vesolju. Avtorja opišeta domene antisnovi z relativistično idealno tekočino in poiščeta rešitve za majhne, srednje velike in velike gostote tekočine. Dinamiko domen antisnovi spremljata do nastanka galaksij in obravnavata njihovo preživetje do danes. Študirata tudi kozmološke posledice združevanja nevtrinov zaradi pete sile.

Keywords: perfect-fluid plasma solution; nonhomogeneus baryosynthesis, antimatter; cosmology, celestial bodies.

9.1 Introduction

The formation of antimatter regions and antimatter domains in a matter/antimatter asymmetric Universe has long been studied according to the properties of the

pertinent celestial objects, as well as to the observational signatures expected, i.e. the energetic gamma rays descending from the matter-antimatter interaction at the boundaries of the antimatter domains. Several scenarios can be envisaged, i.e. also ones in which strong antimatter inhomogeneities interact with the surrounding medium (see [1,3,4,4,5] for review and references).

The mechanisms of survival for the antimatter domains can be analyzed.

Comparison with other celestial bodies enables one to extrapolate the properties of both the formation and evolution of such celestial bodies, as well as the interactions under which the celestial bodies are formed.

In the present paper, low-density antimatter domains will be revised in the non-relativistic description, under the suitable hypotheses. The Relativistic diffusion equation of low-density antimatter domains will be solved; the Relativistic radius and the Relativistic spherical shell interaction width will be calculated.

Dense antimatter domains will be introduced and classified according to the density, i.e. ultra-high density antimatter domains, very-high density ones and high-density ones. The Relativistic FRW diffusion equation of dense antimatter domains will be solved in the perfect-fluid FRW plasma solution. The Relativistic radius of the dense antimatter domains in the FRW symmetry and the Relativistic spherical shell interaction width in the FRW symmetry will be calculated; the calculated expressions will be shown to depend on the Relativistic quantities in a non-trivial manner.

Baryon subdomains inside the antimatter domains will be investigated; in particular, the analysis will be conduced in the cases pertinent to the epoch before the second phase transition and that after the second phase transition. This way, the formation of non-trivial structures will be assessed; more in detail, 'Swiss-cheese' structures and 'Chinese-boxes' structures will be reconducted to the analytical quantification.

Antimatter-excess regions will be explored wrt the diffusion process taking place at the boundary regions.

The density of antimatter domains at the time of galaxy formation will be written down.

Experimental-verification methods will be recapitulated for antimatter domains in a matter/antimatter asymmetric Universe within the framework of inhomogeneous baryosynthesis. The investigation methods for these purposes will be specialized to the study of the γ-ray background and of the expected anti-Helium. Further experimental purposes will be recalled.

Comparison with other celestial bodies will be brought. The features of antimatter celestial bodies in the Galaxy, WIMP dark-matter clumps and Fifth-Force neutrino lumps will be revised for the sake of the study of the formation mechanisms, the Universe-evolution survival models, and of the interaction ruling the structure of the celestial bodies.

9.2   Low-density antimatter domain: diffusion equation

The Relativistic diffusion equation of

$n_{\bar{b}}$ the antibaryon number density as a function of n_b the baryon number density, and n_γ the photon number density reads [6]

$$\frac{dn_{\bar{b}}}{dt} = -\frac{3d}{R} < \sigma v > n_{\bar{b}} n_b - \beta n_{\bar{b}} \qquad (9.1)$$

being R the antimatter domain non-Relativistic radius, and d the antimatter domain spherical shell boundary interaction width; furthermore, $< \sigma v >$ antibaryon-baryon annihilation cross-section within the interaction region is defined, and β the FRW Relativistic factor is introduced.

Being $\bar{r}$ the antibaryon-to-photon ratio and r baryon-to-photon ratio
the Relativistic FRW diffusion equation of low-density domains rewrites

$$\bar{r} = -\frac{3d}{R} < \sigma v > r n_\gamma \bar{r} - \beta \bar{r} \qquad (9.2)$$

9.2.1   Low-density antimatter domains: non-Relativistic approximation

The non-Relativistic diffusion equation of low-density antimatter domains can be approximated after neglecting $\beta \bar{r}$, and posing $< \sigma v > r n_\gamma \Delta t \sim 1$, and solved as

$$\frac{\bar{r}_\tau}{\bar{r}_0} = exp[-\frac{3d}{R} \int_{t_0}^{t_\tau} < \sigma v > r n_\gamma dt] \qquad (9.3)$$

9.2.2   Low-density antimatter domains: Relativistic solution

The Relativistic diffusion equation of low-density antimatter domains under the assumption $\beta \bar{r} << 1$ can be solved as

$$\frac{d}{dt_\tau}(ln[\frac{r_\tau}{r_0} - \tilde{\beta}(t_\tau - t_0)]) = -\frac{1}{3}\left(\frac{4\pi}{3}\right)^{1/3} \frac{\delta(t_\tau)}{a(t_\tau)^{1/3}} \qquad (9.4)$$

with $\tilde{\beta} = -beta$.
The Relativistic quantities $d \to \delta(t)$ Relativistic spherical-shell width interaction region, and $a(t) = \frac{4\pi R(t)^3}{3}$ FRW volume have been upgraded.

9.3   General implemetation- Relativistic

After hypothesizing $-\beta n_{\bar{b}} \equiv \tilde{\beta}$ small but not negligible, and $\tilde{\beta} \simeq const$, the following solution is found

$$ln[\frac{\bar{r}_f}{\bar{r}_0} - \tilde{\beta}\Delta t] \simeq -\frac{\delta}{3a}\Delta t \qquad (9.5)$$

in the case of perturbed Minkowski space-time.
In the case of an FRW symmetry, the following solution is written

$$\frac{d}{dt_\tau}ln[\frac{\bar{r}_f}{\bar{r}_0} - \tilde{\beta}\Delta t] \simeq -\frac{\delta(t_\tau)}{3a(t_\tau)} \qquad (9.6)$$

9.4 Perfect-fluid Relativistic FRW equation of dense antimatter domains

The prefect-fluid FRW diffusion equation of the antibaryon number density writes

$$\frac{dn_{\bar{b}}}{dt} = -\frac{3d}{R} < \sigma v >_{ext} n_{\bar{b}} n_b - \beta n_{\bar{b}} + Q(\vec{r}, p, t) - \frac{n_{\bar{b}}}{t_d} +$$
$$+ \sum_i F_i(p, \dot{p}; ...) - f(\rho_E, \vec{p}; R_d, l_d; \vec{v}_T, v_f; \tilde{i}) - \mu \nabla^2 n_{\bar{b}} \qquad (9.7)$$

Here, $< \sigma v >_{ext}$ is cross-section of the antibaryon-baryon annihilation process at the boundary of the antimatter domain, $Q(\vec{r}, p, t)$ is a source term (can be neglected), $F_i(p, \dot{p}; ...)$ are further terms depending on the momentum (can be neglected), $f(\rho_E, \vec{p}; R_d, l_d; \vec{v}_T, v_f; \tilde{i})$ is plasma characterization in terms of the viscosity properties and of the turbulent velocity (can be neglected), $\frac{n_{\bar{b}}}{t_d} \simeq < \tilde{\sigma}\tilde{v} >_{int} n_{\bar{b}} n_b$ is the decay rate inside the interior of the domain, $t_d = const?$ is the time scale of annihilation, $< \sigma v >_{int}$ is cross-section of the antibaryon-baryon annihilation process in the interior of the antimatter domain, $\beta n_{\bar{b}}$ accounts for the FRW homogeneous Relativistic expansion of the universe, and μ is the chemical potential, i.e. $\tilde{\mu}n_{\bar{b}} = -\mu \nabla^2 n_{\bar{b}}$ for the self-similarity properties of the equation.

9.5 Dense antimatter domains

By construction, both the antibaryon density and the baryon one are much higher than average baryon density in all the Universe;
several cases can be distinguished:
i) **ultra-high densities**

the antibaryon excess and baryon ones start to exceed the contribution of thermal quark-antiquark pairs before QCD phase transition

ii) **very-high densities** the antibaryon density and the baryon ones exceed the contribution of plasma and radiation after the QCD phase transition

iii) **high densities** the antibaryon densities and the baryon ones exceed the DM density

9.5.1 i) ultra-high density antimatter domains

Let $n_{\bar{b}}$ be the number density of antibaryons. The following diffusion equation is outlined

$$\frac{dn_{\bar{b}}}{dt} = -\frac{3d}{R} < \sigma v >_{ext} n_{\bar{b}} n_b - \beta n_{\bar{b}} - \mu \nabla^2 n_{\bar{b}} \equiv -\frac{n_{\bar{b}}}{t_s} - \beta n_{\bar{b}} + \tilde{\beta} + \tilde{\mu} \qquad (9.8)$$

and solved as

$$\ln[\frac{\bar{r}_\tau}{\bar{r}_0} - (\tilde{\beta} + \tilde{\mu})(t_\tau - t_0)] = -\frac{1}{3}\left(\frac{4\pi}{3}\right)^{1/3} < \sigma v >_{ext} m_\gamma \int_{t_i}^{t_\tau} \frac{\delta(t)}{(a(t))^{1/3}} dt \qquad (9.9)$$

with $a(t) = 4\pi R(t)^3/3$ the Relativistic FRW volume, and $d \to \delta(t)$ the Relativistic interaction spherical-shell width, which simplifies as

$$\frac{d}{dt_\tau}\left(\ln\left[\frac{\bar{r}_\tau}{\bar{r}_0} - (\tilde{\beta} + \tilde{\mu})(t_\tau - t_0)\right]\right) = -\frac{1}{3}\left(\frac{4\pi}{3}\right)^{1/3} < \sigma v >_{ext} rn_\gamma \frac{\delta(t_\tau)}{(a(t_\tau))^{1/3}} \quad (9.10)$$

Relativistic expression for the radius of the antimatter domain Relativistic expression for the radius of the antimatter domain reads

$$(a(t_\tau))^{1/3} = -\left(\frac{3}{4\pi}\right)^{1/3} \frac{< \sigma v >_{ext} rn_\gamma \delta(t_\tau)}{3} \frac{\left[\frac{\bar{r}_\tau}{\bar{r}_0} - (\tilde{\beta} + \tilde{\mu})(t_\tau - t_0)\right]}{\frac{d}{dt_\tau}\left[\frac{\bar{r}_\tau}{\bar{r}_0} - (\tilde{\beta} + \tilde{\mu})(t_\tau - t_0)\right]} \quad (9.11)$$

Relativistic expression for the interaction width Relativistic expression for the interaction width is obtained as

$$\delta(t_\tau) \sim -\left(\frac{3}{4\pi}\right)^{1/3} \frac{3(a(t_\tau))^1/3}{< \sigma v >_{ext} rn_\gamma} \frac{\frac{d}{dt_\tau}\left[\frac{\bar{r}_\tau}{\bar{r}_0} - (\tilde{\beta} + \tilde{\mu})(t_\tau - t_0)\right]}{\left[\frac{r_\tau}{r_0} - (\tilde{\beta} + \tilde{\mu})(t_\tau - t_0)\right]} \quad (9.12)$$

The relativistic expression of the interaction width of the antimatter domain depends therefore also on the Relativistic radius in a non-trivial manner, i.e. as a prefactor.

9.5.2   ii) **very-high-density antimatter domains**

In the case of very-high-density antimatter domains, the diffusion equation of the baryon number density becomes

$$\frac{dn_{\bar{b}}}{dt} = -\frac{3d}{R} < \sigma v >_{ext} n_{\bar{b}}n_b - \beta n_{\bar{b}} - \frac{n_{\bar{b}}}{t_d} - \mu\nabla^2 n_{\bar{b}} \equiv -\frac{n_{\bar{b}}}{t_s} - \beta n_{\bar{b}} - \frac{n_{\bar{b}}}{t_d} - \mu\nabla^2 n_{\bar{b}} \quad (9.13)$$

solved as

$$\ln\left[\frac{\bar{r}_\tau}{\bar{r}_0} + < \tilde{\sigma}\tilde{\mu} >_{int j} rn_\gamma\bar{r} - (\tilde{\beta} + \tilde{\mu})(t_\tau - t_0)\right] = -\frac{1}{3}\left(\frac{4\pi}{3}\right)^{1/3}\int_{t_i}^{t_\tau} \frac{\delta(t)}{(a(t))^{1/3}}dt \quad (9.14)$$

with $a(t) = 4\pi R(t)^3/3$ Relativistic FRW volume, and $d \to \delta(t)$ Relativistic interaction spherical-shell width

$$\frac{d}{dt_\tau}\left(\ln\left[\frac{\bar{r}_\tau}{\bar{r}_0} + < \tilde{\sigma}\tilde{\mu} >_{int j} rn_\gamma\bar{r}(t_\tau - t_0) - (\tilde{\beta} + \tilde{\mu})(t_\tau - t_0)\right]\right) = -\frac{1}{3}\left(\frac{4\pi}{3}\right)^{1/3}\frac{\delta(t_\tau)}{(a(t_\tau))^{1/3}} \quad (9.15)$$

Relativistic expression of the radius of the antimatter domain The Relativistic expression of the radius of very-high-density antimatter domains is obtained as

$$(a(t_\tau))^{1/3} = -\left(\frac{3}{4\pi}\right)^{1/3}\frac{< \sigma v >_{ext} rn_\gamma \delta(t_\tau)}{3}.$$

$$\cdot\frac{\left[\frac{\bar{r}_\tau}{\bar{r}_0} + < \tilde{\sigma}\tilde{\mu} >_{int j} rn_\gamma\bar{r}(t_\tau - t_0) - (\tilde{\beta} + \tilde{\mu})(t_\tau - t_0)\right]}{\frac{d}{dt_\tau}\left[\frac{\bar{r}_\tau}{\bar{r}_0} - + < \tilde{\sigma}\tilde{\mu} >_{int j} rn_\gamma\bar{r}(t_\tau - t_0) - (\tilde{\beta} + \tilde{\mu})(t_\tau - t_0)\right]} \quad (9.16)$$

Relativistic expression of the spherical shell interaction width The Relativistic expression of the spherical shell interaction width of very-high density antimatter domains is

$$\delta(t_\tau) \sim -\left(\frac{3}{4\pi}\right)^{1/3} \frac{3(a(t_\tau))^{1/3}}{<\sigma v>_{ext} rn_\gamma} \frac{\frac{d}{dt_\tau}[\frac{\bar{r}_\tau}{\bar{r}_0} + <\bar{\sigma}\bar{\mu}>_{int j} rn_\gamma \bar{r}(t_\tau - t_0) - (\bar{\beta} + \bar{\mu})(t_\tau - t_0)]}{[\frac{\bar{r}_\tau}{\bar{r}_0} + <\bar{\sigma}\bar{\mu}>_{int j} rn_\gamma \bar{r}(t_\tau - t_0) - (\bar{\beta} + \bar{\mu})(t_\tau - t_0)]} \tag{9.17}$$

The Relativistic expression of the interaction width of the antimatter domain depends therefore also on the Relativistic radius in a non-trivial manner, i.e. as a prefactor.

9.5.3 iii) high-density antimatter domains

The diffusion equation of the antibaryon number density of high-density antimatter domains is characterized as

$$\frac{dn_{\bar{b}}}{dt} = -\frac{3d}{R} <\sigma v>_{ext} n_{\bar{b}} n_b - \frac{n_{\bar{b}}}{t_d} - \mu \nabla^2 n_{\bar{b}} \equiv$$

$$\equiv -\frac{3d}{R} <\sigma v>_{ext} n_{\bar{b}} n_b - \frac{n_{\bar{b}}}{t_s} - \frac{n_{\bar{b}}}{t_d} - \mu \nabla^2 n_{\bar{b}} \tag{9.18}$$

and solved as

$$\ln[\frac{\bar{r}_\tau}{\bar{r}_0} - (\tilde{\mu})(t_\tau - t_0)] = -\frac{1}{3}\left(\frac{4\pi}{3}\right)^{1/3} <\sigma v>_{ext} rn_\gamma \int_{t_i}^{t_\tau} \frac{\delta(t)}{(a(t))^{1/3}} dt \tag{9.19}$$

Here, $a(t) = 4\pi R(t)^3/3$ is the Relativistic FRW volume, and $d \to \delta(t)$ is the Relativistic interaction spherical-shell width.
Eq. (9.19) rewrites

$$\frac{d}{dt_\tau}(\ln[\frac{\bar{r}_\tau}{\bar{r}_0} - (\tilde{\mu})(t_\tau - t_0)]) = -\frac{1}{3}\left(\frac{4\pi}{3}\right)^{1/3} <\sigma v>_{ext} rn_\gamma \frac{\delta(t_\tau)}{(a(t_\tau))^{1/3}} \tag{9.20}$$

Relativistic expression for the radius of the antimatter domain In the case of high-density antimatter domains, the Relativistic expression for the radius of the antimatter domain is expressed as

$$(a(t_\tau))^{1/3} = -\left(\frac{3}{4\pi}\right)^{1/3} \frac{<\sigma v>_{ext} rn_\gamma \delta(t_\tau)}{3} \frac{[\frac{\bar{r}_\tau}{\bar{r}_0} - \tilde{\mu}(t_\tau - t_0)]}{\frac{d}{dt_\tau}[\frac{\bar{r}_\tau}{\bar{r}_0} - \tilde{\mu}(t_\tau - t_0)]} \tag{9.21}$$

Relativistic expression for the spherical shell interaction width The Relativistic expression for the spherical shell interaction width of high-density antimatter domains is solved as

$$\delta(t_\tau) \sim -\left(\frac{3}{4\pi}\right)^{1/3} \frac{3(a(t_\tau))^{1/3}}{<\sigma v>_{ext} rn_\gamma} \frac{\frac{d}{dt_\tau}[\frac{\bar{r}_\tau}{\bar{r}_0} - \tilde{\mu}(t_\tau - t_0)]}{[\frac{\bar{r}_\tau}{\bar{r}_0} - \tilde{\mu}(t_\tau - t_0)]} \tag{9.22}$$

The Relativistic expression of the spherical-shell interaction width of the antimatter domain depends therefore also on the Relativistic radius in a non-trivial manner, i.e. as a prefactor.

9.6   Conditions and evolution of different types of of strong primordial inhomogeneities in non-homogeneous baryosynthesis

In the case of non-homogeneous primordial baryosynthesis, various types of scenarios can accomplish: antimatter consisting of axion-like particles; closed walls for baryogenesis with excess of antibaryons, and phase fluctuations such that a baryon excess is created everywhere and with non-homogeneous distribution. To avoid large-scale fluctuations, the fluctuations have to be imposed to be small. In the latter cases of small fluctuations, the following inequality holds

$$\frac{3B}{4\pi R(t)^3} >> \rho_B \tag{9.23}$$

The diffusion process of the model is described as follows.

Three Regions can be outlined:
1) the **dense antimatter domain** of radius $R \leq R_1$ of antibaryon number density $n_{b\ 1}$, and of chemical potential μ_1,
2) the **outer spherical shell** region of radius $R_1 \leq R \leq R_2$ of antibaryon number density $n_{b\ 2}$, and of chemical potential μ_2,
where the diffusion process happens, and 3) the outmost region of radius $R_3 \geq R_2$ of antibaryon number density $n_{b\ 3}$ of low antimatter density.

The chemical potentials of related to the three regions are assumed to be small but not negligible, i.e.
$|\tilde{\mu_1}| << 1$, $|\tilde{\mu_2}| << 1$, and $|\tilde{\mu_3}| << 1$. The differential equation of the antibaryon number density in Region 1) is

$$\frac{n_{b\ 1}}{dt} = -\mu_1 \nabla^2 n_{b\ 1} \sim \tilde{\mu_1} n_{b\ 1}; \tag{9.24}$$

The differential equation of the antibaryon number density in Region 2) is

$$\frac{n_{b\ 2}}{dt} = -\mu_2 \nabla^2 n_{b\ 2} \sim \tilde{\mu_2} n_{b\ 2} \tag{9.25}$$

The differential equation of the antibaryon number density in Region 3)

$$\frac{n_{b\ 3}}{dt} = -\mu_3 \nabla^2 n_{b\ 3} \sim \tilde{\mu_3} n_{b\ 3} \tag{9.26}$$

The solutions of Eq. (9.24), Eq. (9.6) and (9.25)
must satisfy the continuity conditions

$$n_{b\ 1}(t, R_1) = n_{b\ 2}(t, R_1) \tag{9.27}$$

on the boundary of Region 1), and

$$n_{b\ 2}(t, R_2) = n_{b\ 3}(t, R_2) \tag{9.28}$$

on the boundary of Region 2).

9.7   Dense Baryon subdomains

It is possible to hypothesize the presence of antibaryons inside the baryon subdomains, which exceed the survival size of volume $V_j = 4\pi R_j^3/3$; such a possibilty is dependent on the second phase transition.

For axion-like particles, it is dependent on the QCD phase transition.

Two possibilities are outlined, i.e. according to whether the description is taken before the Λ_{QCD} phase transition, or after it.

I) In the case $\Lambda < \Lambda_{QCD}$, the baryon number density n_b in a baryon subdomain filled with (grazing) antibaryons obey the following plasma characterization

$$\frac{dn_b}{dt} = - <\sigma v>_{j\ ext} n_b n_{\bar{b}} - <\sigma v>_{j\ int} n_b n_{\bar{b}} - \mu \nabla^2 n_b \qquad (9.29)$$

The following perfect-fluid Relativistic FRW solution is found

$$-\sqrt{4\pi}3 \frac{\tilde{\delta}(t_\tau)}{3\tilde{a}(t_\tau)} r_{int} \bar{r}_{int} n_\gamma <\sigma v>_{j\ ext} =$$

$$= \frac{d}{dt_\tau} \ln[r_{int} \bar{r}_{int} n_{\gamma\ int} <\sigma v>_{j\ ext} + -\tilde{\mu}(t_\tau - t_0)+] \qquad (9.30)$$

In the case II) $\Lambda > \Lambda_{QCD}$ the baryon number density n_b in a baryon subdomain without free antibaryons inside

is described by the following plasma characterization

$$\frac{dn_b}{dt} = - <\sigma v>_{j\ ext} n_b n_{\bar{b}} - \mu \nabla^2 n_b \qquad (9.31)$$

The following perfect-fluid Relativistic FRW solution is found

$$-\sqrt{4\pi}3 \frac{\delta(\tilde{t}_\tau)}{3\tilde{a}(t_\tau)} r_{int} \bar{r}_{int} n_\gamma <\sigma v>_{j\ ext} = \frac{d}{dt_\tau} \ln[+\tilde{\mu}(t_\tau - t_0)] \qquad (9.32)$$

9.8   Further structures

Further structures can be analysed, according to the presence of baryon subdomain(s) inside the antibaryon domain.

9.8.1   'Swiss-cheese' structures

A description of 'Swiss-cheese' structures can be hypothesized as an antimatter domain containing one matter domain, in the simplest instance, and more complicated 'Swiss-cheese' structures, such as an antimatter domain containing several matter subdomains.

Antibaryon domain containing one baryon subdomain In the case of an antibaryon domain containing one baryon subdomain, the antibaryon number density obeys the differential equation

$$\frac{dn_{\bar{b}}}{dt} = -\frac{3d}{R} < \tilde{\sigma}\tilde{v} >_{ext} n_{\bar{b}}n_b - \beta n_{\bar{b}} + Q(\vec{r}, p, t) - \frac{n_{\bar{b}}}{t_d} + + F_i(p, \dot{p}; ...)+$$

$$-\mu\nabla^2 n_{\bar{b}} - \frac{3d_i}{R_i} < \hat{\sigma}_i\hat{v}_i > n_{\bar{b}}n_{bi} - \mu_i\nabla^2 n_{\bar{b}} \qquad (9.33)$$

Swiss-cheese structure: baryon domain containing several baryon subdomains

$$\frac{dn_{\bar{b}}}{dt} = -\frac{3d}{R} < \tilde{\sigma}\tilde{v} >_{ext} n_{\bar{b}}n_b - \beta n_{\bar{b}} + Q(\vec{r}, p, t) - \frac{n_{\bar{b}}}{t_d} +$$

$$+ \sum_{i=1}^{i=I} \left(F_i(p, \dot{p}; ...) - \mu\nabla^2 n_{\bar{b}} - \frac{3d_i}{R_i} < \hat{\sigma}_i\hat{v}_i > n_{\bar{b}}n_{bi} - \mu_i\nabla^2 n_{\bar{b}} \right) \qquad (9.34)$$

Chinese-boxes structures 'Chinese-boxes' structures are described as

$$\frac{dn_{\bar{b}}}{dt} = -\frac{3d}{R} < \sigma v >_{ext} n_{\bar{b}}n_b - \beta n_{\bar{b}} + Q(\vec{r}, p, t) - \frac{n_{\bar{b}}}{t_d} - \mu\nabla^2 n_{\bar{b}}$$

$$- \sum_{i=1}^{i=I} \left[F_i(p, \dot{p}; ...) - \mu\nabla^2 n_{\bar{b}_i} - \frac{3d_i}{R_i} < \sigma_v >_{i\ ext} n_{\bar{b}}n_{b_i} \right] + \sum_{j=1}^{j=J} [F_j(p, \dot{p}; ...)$$

$$-\mu\nabla^2 n_{\bar{b}_j} - \frac{3d_j}{R_j} < \sigma_v >_{j\ ext} n_{\bar{b}}n_{b_j}] \qquad (9.35)$$

9.9   Galaxy formation: Relativistic density of the surviving domains

The present section is aimed at studying the density of the antimatter domains at the time of galaxy formation.

9.9.1   Plasma characterization

The plasma characterization of the antimatter domains at the time of galaxy formation is given after the condition

$$< \sigma v >_{int} r = 0, \qquad (9.36)$$

i.e. after the antibaryon/baryon interactions in the interior of the antimatter domains have exhausted.
The following conditions are taken into account:

$$\tilde{\mu}(t_\tau - t_0)n_\gamma << 1, \qquad (9.37)$$

and

$$\tilde{\beta}(t_\tau - t_0)n_\gamma << 1, \tag{9.38}$$

with

$$(\tilde{\mu} + \tilde{\beta})(t_\tau - t_0)n_\gamma << 1, \tag{9.39}$$

i.e. that the chemical-potential etrms and the Relativistic FWR terms be small but not negligible.

i) **ultra-high-density antimatter domains** In the case of ultra-high-density anti-matter domains, the antimatter-domain density at the time of galaxy formation reads

$$\frac{\bar{r}_\tau n_\gamma}{a(t_\tau)} = \frac{1}{a(t_\tau)} \frac{n_\gamma}{\frac{1}{\bar{r}_0} + (\tilde{\beta} + \tilde{\mu})(t_\tau - t_0)n_\gamma} \cdot$$

$$\cdot \exp\left[\frac{1}{3} \left(\frac{4\pi}{3} \right)^{1/3} < \sigma v >_{ext} r_0 n_\gamma \int_{t_0}^{t_\tau} \frac{\delta t}{a(t)} dt \right] \tag{9.40}$$

ii) **very-high-density antimatter domains** In the case of very-high density anti-matter domains, the antimatter-domain density at the time of galaxy formation is

$$\frac{\bar{r}_\tau n_\gamma}{a(\tau)} = \frac{1}{a(t_\tau)} \frac{n_\gamma}{\frac{1}{\bar{r}_0 n_\gamma} + (\tilde{\beta} + \tilde{\mu})(t_\tau - t_0)n_\gamma} \cdot$$

$$\exp^{\frac{1}{3}} \left(\frac{4\pi}{3} \right)^{1/3} < \sigma v >_{ext} r_0 n_\gamma \int_{t_0}^{t_\tau} \frac{\delta t}{a(t)} dt \tag{9.41}$$

iii) **high-density antimatter domains** In the case of high-density antimatter domains, the antimatter-domain density at the time of galaxy formation becomes

$$\frac{\bar{r}_\tau n_\gamma}{a(\tau)} = \frac{1}{a(t_\tau)} \frac{n_\gamma}{\frac{n_\gamma}{\bar{r}_0} + \tilde{\mu}(t_\tau - t_0)n_\gamma} e^{\frac{1}{3}} \left(\frac{4\pi}{3} \right)^{1/3} < \sigma v >_{ext} r_0 n_\gamma \int_{t_0}^{t_\tau} \frac{\delta t}{a(t)} dt \tag{9.42}$$

9.10   Experimental verification

The signatures of the experimental verification of the existence of antimatter do-mains have to be analysed. In particular, the γ-ray background is expected to be modified after the baryon/antibaryon interaction within the boundary interaction region of the antimatter domains. Furthermore, the detection of anti-Helium flux after the AMS2 experiment is awaited.

The properties of pp atoms have been studied in [7] In [8], the γ-ray spectrum originated after the p$\bar{p}$ annihilation in liquid Hydrogen is analysed by means of two spectrometers. As a result, no exotic narrow peacks are evidentiated, and the upper limit is calculated.

The γ-ray signal due to matter-antimatter annihilation on the boundary of an anti-matter domain can therefore be analyzed [9]; the hypotheses of a matter/antimatter

symmetric Universe and of a matter/antimatter asymmetric Universe can be scrutinized and compared.

In the case of a matter/antimatter-symmetric Universe: more γ-rays than the observed quantities are predicted; therefore, a matter/antimatter-symmetric Universe is possible iff the present Universe is one consisting of the matter quantity.

The $p\bar{p}$ interaction process is studied as resolving in photons after the π^0 decay. Be $\bar{g}$ the mean photon multiplicity;

each $p\bar{p}$ annihilation process is estimated to produce $\bar{g} \simeq 3.8$ electrons and positrons, and an approximate similar number of photons.

The annihilation electrons are described at a redshift y s.t. $20 < y < 1100$.

The mechanisms that control the electrons motion must therefore be studied. Such mechanisms are evaluated to be the cosmological redshift, the collision with CBR photons, and the collision with ambient plasma electrons.

At the considered values of the redshift, the collisions with CBR photons are considered the most important control mechanism of the electron trajectory.

For initially-Relativistic electrons of energy $E_0 = \gamma_0 m_e$, the dependece of the width of the reheated zone where the electrons produced after the annihilations directly deposit energy into the fluid, i.e. the electron range, on γ_0 is negligible.

The inclusive photon spectrum in the $p\bar{p}$ process is normalized to $\bar{g}$; the average number of photons made per unit volume is calculated: the transport equation of the photons scatter and redshift, (which lead to a spectral flux of annihilation photons), is therefore assessed. A conservative lower limit for the γ-ray signal can this way estimated.

The γ-rays energy is expected to be of order $100MeV - 10Mev$ at modern times; a different value can be expected for the opaque universe at the early stages).

The results are awaited after the experiment $AMS2$ as far as the presence of the anti-Helium flux is concerned.

9.11   Further experimental verifications

Further experimental verifications of a matter/antimatter Universe can be expected .

As an example [10], annihilation and transformation of annihilating matter's rest mass into energy particles and radiation with 100% efficiency can be looked for at different length scales.

A substantial lack of antimatter on the Earth is evidentiated within the due limits.

A lack of antimatter in the vicinity of the Earth is found.

Matter asymmetry in the Solar System can be revealed within the study of the:

Solar wind, i.e. the continuous outflow of particles from the Sun. For antiplanets of radius r and distance d from the Earth intercepting the Solar wind, the expected annihilation flux is

$F(\gamma = 100MeV) \sim 10^8 (r/d)^2$ photons cm^{-2} s^{-1}.

At scales larger than the Solar System, i.e. at the Galaxy scales, the γ-ray analysis must be investigated (γ-ray detectors have better detection capabilities and localization ones at $E \sim 100$ MeV than neutrino detectors). Antimatter mixed in with matter inside our Galaxy's gas at $E \sim 100$ MeV is expected to be present in a matter/antimatter-symmetric Universe.

Models can be postulated [11], such that SUSY-condensate baryogenesis models motivate the possibilities of antimatter domains in the Universe.

In this case, vast antimatter structures in Early-Universe evolution possible after initial space distribution at the inflationary stage of the quantum fluctuation field $\phi(r, t_0)$, unharmonic potential of the field carrying the baryon charge, and inflationary expansion of the initially microscopic baryon distribution. The vast antimatter regions are calculated to be separated at distances larger than 10 Mpc from the Earth, and separated from the matter ones by baryonically-empty voids. Such models are not ruled out after

cosmic rays data, γ-rays ones, and CMB anisotropy ones.

Antimatter in a matter/antimatter-symmetric Universe can be further verified [12] after the presence of antimatter at the Galactic scale and above.

As far as hydrogen in "clouds" is concerned, the experimental verification is based on the observation of γ-rays from their directions, compatible with π^0 decay, and non-observation of a γ excess. In this case, form the observational data, the antibaryon presence in the media is calculated not to exceed one part in 10^{15}.

The instance of galaxy-antigalaxy collisions can be studied. Such events have not been verified after devices s.t. Antennae pair NGC4038(9). Clusters of certain galaxies, dense enough and active in order to allow for intergalactic hot plasma in the central parts (at temperatures of order ~ 10 keV: it is therefore possible to verify the presence of antimatter as a few parts per million from the observation of absence of enough γ-ray excess on the thermal spectral tail.

Large antimatter regions with sizes larger than the critical surviving size can be verified in different observational proofs [13]. The absence of anti-Helium in the cosmic rays and annihilation signals can be consistent as an indicator: their fraction in the Galaxy is smaller than 10^{-4}. The antimatter islands must be separated from a space filled with matter at least by the distance of about 1Mpc.

For this, the possibility for antimatter islands (antistars) in the Galaxy still allowed [14].

Large antimatter regions with high antimatter density evolve to single galaxies [15]. They are detected after particular content of anti-Helium and anti-deuterium.

Further Cosmic antimatter searches can be pursued [16]. The presence of antistars in our Galaxy can be verified after the possibility to detect antinuclei with $Z \geq 2$. Domain sizes of the scale of galaxies or scales of galaxy clusters can be testified after antimatter cosmic rays (CR) originating from the nearest domain for uniform domains, non-uniform domains, and condensed antimatter bodies (i.e. antistars, antiplanetoids). The upper limit of antistars in the Milky Way has been estimated as 10^7 (i.e. 10^{-4} of the total number of stars). Antistars can be described as con-

fined into compact structures separated from the matter environment and able to survive for a longer period rather than in gas clouds. Antistars are not expected to be strong γ-ray emitters, unless they at least cross a galactic cloud or impact on other condensed bodies.

The lower limit on the distance of the nearest antistar [17] has been set as ~ 30 pc. The upper limit on the fraction of antistars in the Andromeda Galaxy has been estimated as $\sim 10^{-3}$.

Experimental verification of presence of matter regions and antimatter ones in a matter/antimatter-symmetric universe should be studied after the pre-recombinational signals and the post-recombinational ones.
The prerecombination signal [18] allows one for the verification of the presence of domains of larger size. The assumption that matter domains and antimatter ones were in contact before the last scattering exhibits such effects after which contact and annihilation significantly distort the radiation from the last-scattering surface: a single domain boundary, or a fraction , can be detectable; differently, the absence of such signatures rules out a matter/antimatter-symmetric universe.

The postrecombination signal [18] would consists of the observable unobserved γ-ray flux, due to nuclear annihilation rate of matter/antimatter near domain boundaries; the a resulting relic diffuse γ-ray flux exceeds the observed cosmic diffuse γ spectrum, so that a matter/antimatter-symmetric Universe is ruled out unless the matter region consists of almost the entire Universe

9.12   Antistars

The analysis of the mean free path of the cross section of the matter/antimatter annihilation products in the interaction spherical shell boundary of the antistars is conisistent for the comparison with the γ-ray-background constraints [19].
After the compilation of the 10-years Fermi Large Area Telescope (LAT) γ-ray-sources catalog, constraints on the abundance of antistars around the Sun are obtained: 14 antistar candidates are present around the Sun. In particular, they have been chosen as they are not associated with any objects belonging to established γ-ray source classes, and exhibit a spectrum compatible with baryon-antibaryon annihilation [20].

9.13   Antimatter celestial objects in the Galaxy

The exist observational evidences of the existence of antimatter celestial objects in the Milky Way; more in detail [21], they are point-like sources of gamma radiation, and diffuse galactic γ-ray background, where the latter possible antimatter sources are to be verified after an anomalous abundance of chemical (anti-)elements around it possibly measured by spectroscopy, anti-nuclei in cosmic

rays, and more exotic events, where large amounts of matter and antimatter interact. In the latter case, star-antistar annihilation can be considered: huge energy produced, even though their total destruction is prevented by the radiation pressure produced in the collision; and collision of a star and an anti-star with similar masses is calculated to provoke a peculiar result.

9.13.1 Antistars

The creation of stellar-like objects in the very early universe [22], from the QCD phase transition until the BBN and later, can be witnessed as the presence of some of the celestial objects created which can consist of antimatter. The α cosmological baryon asymmetry $\alpha = \frac{N_B}{N_\gamma}$ can be close to unity, i.e. much larger than the observed value $\alpha \simeq 6 \cdot 10^{-10}$. The ratio α can also be negative: this way, the amount of antimatter constituting compact objects in the Galaxy is expected.

9.14   WIMP's clumps

9.14.1   Neutralino clumps

Within the standard cosmological scenario (FRW with its thermal history, inflationary-produced primordial fluctuation spectrum and with a hierarchical clustering), the neutralino clumps [23] undergo tidal destruction in the hierarchical clustering (i.e. the smaller clumps are captured by the larger clumps) at early stages of the structure-formation process, starting from a time of clump detachment from the Universe expansion.
In the case of small-scale dark-matter clumps, a mass function can be calculated for the survived clumps: the tidal destruction of clumps by the Galactic disk, the life-time of clumps in the central stellar bulge, and the life-time of clumps in the stellar halo spheroid can be calculated; as a result, the minimal mass is the evaluated as the Moon-scale mass.

9.14.2   Neutralino annihilation in the Galaxy

Within the standard cosmological scenario, neutralino annihilation of small-scale neutralino clumps [24] would produce a signal from the galactic halo: the clump destruction is due to larger-scale clumps, gravitational field of the galactic disk, stars in the galactic bulge, and stars in the galactic halo.
The mutual tidal clumps interactions would become important at early stages of hierarchical clustering, and for the galactic halo formation.
The hierarchical clustering implies clumps surviving the hierarchical clustering to be continuously destroyed by interactions with the galactic disk and stars. This way,

20% of neutralino clumps surviving the hierarchical clustering between the Earth and the Moon can 'survive the Sun position' because of tidal destruction due to Galactic disk. Furthermore, the diminishing of the expected DM annihilation signal from the galactic halo would be awaited.

9.14.3   Small-scale DM clumps

The clumps scenarios comprehend spherical models, non-spherical models, and clumps around topological defects [25].
The possible observational verifications are established DM-particles direct detection, record of clumps in gravitational-wave detectors, neutralino stars, baryons in clumps, and clump motion in the Sky sphere.

9.15   Fifth-Force neutrino lumps

9.15.1   Fifth-Force codifications

The Fifth Force potential can be codified as [26], [27]

$$V(r) = \frac{\tilde{G}m_1}{r}\left(1 + \alpha e^{-r/\lambda}\right) = G\frac{m_1 m_2}{r}\left(1 + e^{-\beta\frac{\phi}{r}}\right) = \frac{m_1 m_2}{r}\left(G + \frac{G}{\Delta G}\right). \quad (9.43)$$

Such a codification allows for the description of dark-matter gravitational clustering.

9.15.2   Modellizations for neutrino cosmology

The parameter β is intended as the Fifth-Force parameter, and $\phi - \nu$ coupling is postulated.
The fifth force is requested to be subdominant with respect to the gravitational force [28], [29]. As an example, the request can be expressed as

$$\beta = -\frac{d\ln m_\nu}{d\phi}. \quad (9.44)$$

Is is also possibe to set a λ comoving length scale larger than the typical lump sizes, but smaller than their typical distances, such that the mean distance between neighboring lumps be of order $100h^{-1}\,\text{Mpc}$.
l lumps of masses M_l are expressed via smoothed fields $\hat{\phi}$. The effective coupling

$$\beta_l = -\frac{d\ln M_l}{d\hat{\phi}} \quad (9.45)$$

is worked out.

9.15.3   Applications for fluids of composite objects

Neutrino lumps are described within a hydrodynamic framework, i.e. endowed with a balance equation [29], and a stability equation [30] based on the Tolman-Oppenheimer-Volkoff equation.

Within the framework of the $\phi - \nu$ coupled fluid, neutrino fluctuations are hypothesized to grow under the effect of the Fifth-Force [31].
Non-Relativistic neutrino clusters under the effect of the fifth-force are hypothesized at scales estimated to be around a few 10–100Mpc. A statistical distribution of neutrino lumps is expressed as a function of the mass at different redshifts $z \geq 1$.
The oscillating structure formation is described as at the time a large number of neutrinos were staying in gravitationally-bounded lumps at $z = 1.3$.

9.15.4   Formation of large-scale neutrino lumps in a recent cosmological epoch

Within the framework of a $\phi - \nu$ interaction, the non-linear features of the Fifth-Force can be outlined [32].
The averaged interaction strength $< \beta >$ of the neutrinos in a neutrino lump reads

$$< \beta >= -M \frac{d \ln < m_\nu >}{d\phi}. \tag{9.46}$$

The effective suppression of the ϕ- mediated attractive force between neutrino lumps is proportional to 2β. In particular, the attraction between two equal lumps is reduced by a factor $\left(\frac{<\beta>}{\beta} \right)^2$. Furthermore, the characteristic time scale for the infall increased by a factor $\frac{\beta}{<\beta>}$ compared to the consideration excluding non-linear effects and thus results in a slow down of the infall: the time scale for the clumping of lumps to larger lumps enhanced by a factor $\left(\frac{\beta}{<\beta>} \right)^2$.
In the interior of the lump, the possibility of a time variation of fundamental constants results much smaller than the cosmological evolution; therefore, it is possible to reconcile the cosmological variations of the fine structure constant with geophysical bounds.

9.15.5   CMB verification for neutrino lumps

Within the framework of a $\phi - \nu$ interaction, the integrated Sachs-Wolfe effect of CMB [33] can be considered. The size of the gravitational potential induced by the neutrino lumps, and the time evolution of the gravitational potential induced by the neutrino lumps have to be analyzed.
as a result, a proportionality between the scalar potential and the neutrino-induced gravitational potential is found as

$$\beta \delta \phi = 2\beta^2 \Phi_\nu \tag{9.47}$$

for the local potential and the cosmological-averaged potential.

The population of lumps of size ≥ 100Mpc can lead to observable effects from the CMB anisotropies for low angular momenta.

9.16   Outlook and perspectives

Evolution of antimatter domains have been studied: an analysis of low-density antimatter domains and dense antimatter domains has been performed. More in detail, ultra-high density antimatter domains, very-high density antimatter domains, and high-density antimatter domains.
Experimental verification of their signatures consists of the search for confirmation

in the observed γ-ray background, and for the expected anti-Helium flux in AMS02 experiment.

Comparison with other celestial objects has been accomplished: study of formation mechanisms, Universe-evolution survival models, and comparison of interactions characterizing the structure of the celestial bodies has been performed.

Acknowledgements

References

1. M.Yu.Khlopov: What comes after the Standard model? Prog.Part. Nucl. Phys. **116**, 103824 (2021).
2. Khlopov, M. Cosmological Reflection of Particle Symmetry. Symmetry **8**, 81 (2016).
3. V.M. Chechetkin, M.Y. Khlopov, M.G. Sapozhnikov, Y.B. Zeldovich: Astrophysical aspects of antiproton interaction with He (Antimatter in the Universe). Phys. Lett. B **118**, 329 (1982).
4. A.D. Dolgov: Matter and antimatter in the universe. Nucl. Phys. Proc. Suppl. **113**, 40 (2002)
5. M.Y. Khlopov, S.G. Rubin, A.S. Sakharov: Possible origin of antimatter regions in the baryon dominated universe. Phys. Rev. D **62**, 083505 (2000). Phys.Rev. Lett **99**, 123 (1999). Place, Year. Proceedings ..., Publisher, Place, Year.
6. M.Y. Khlopov, R.V. Konoplich, R. Mignani, S.G. Rubin, A.S. Sakharov: Physical origin, evolution and observational signature of diffused antiworld, Astropart. Phys. **12**, 367 (2000).
7. S. Ahmad et al.: First observation of K X-rays from $\bar{p}p$ atoms, Phys. Lett. B **157**, 333 (1985).
8. L. Adiels et al.: Search for narrow signals in the γ-spectrum from proton-antiproton annihilation at rest, Phys. Lett. B **182**, 40 (1986).

9. A.G. Cohen, A. De Rujula, S.L. Glashow: A Matter-Antimatter Universe? Astrophys. J. **495**, 539 (1998).
10. P.S. Coppi: How Do We Know Antimatter Is Absent?, in: Jennifer Chan and Lilian DePorcel Editors: Proceedings SLAC Summer Institute on Particle Physics (SSI04), USA, SLAC-Report-484, 1996.
11. D.Kirilova: Baryogenesis model predicting antimatter in the Universe, Nucl. Phys. B-Proceedings Supplements **122**, 404 (2003).
12. A. De Rújula: Avatars of a Matter-Antimatter Universe, in: J. Tran Thanh Van Editor: Proceedings 32nd Rencontres de Moriond: High-Energy Phenomena in Astrophysics, Ed. Frontieres, France, 1997.
13. L. Canetti, M. Drewes, M. Shaposhnikov: Matter and Antimatter in the Universe New J. Phys. **14**, 095012 (2012).
14. A.D. Dolgov, V.A. Novikov, M.I. Vysotsky: How to see an antistar, J. Exp. Th. Phys. Lett. **98**, 519 (2014).
15. A. V. Grobov, S. G. Rubin: Formation and Search of Large Scale Antimatter Regions, Int. J. Mod. Phys. D **24**, 1550093 (2015).
16. D. Casadei: Searches for Cosmic Antimatter, *Frontiers in Cosmic Ray Research*, Nova Science Publishers, Hauppauge, New York, USA, 2007.
17. A. Dudarewicz, A.W. Wolfendale: Anti-matter in the Universe on very large scales, Mon. N. R. Astr. Soc.**268**, 609 (1994).
18. A.G. Cohen, A. De Rújula, S.L. Glashow: A Matter-Antimatter Universe?, Astrophys. J. **495**, 539 (1998).
19. A.D. Dolgov: Antimatter in the Milky Way, Preprint arXiv:2112.15255 [astro-ph.GA].
20. S. Dupourqué, L. Tibaldo, P. von Ballmoos: Constraints on the antistar fraction in the Solar System neighborhood from the 10-year Fermi Large Area Telescope γ-ray source catalog, Phys. Rev. D **103** 083016 (2021).
21. C. Bambi, A. D. Dolgov: Antimatter in the Milky Way, Nucl. Phys. B **784**, 132 (2007).
22. A. D. Dolgov, S. I. Blinnikov: Stars and Black Holes from the very Early Universe, Phys. Rev. D **89**, 021301 (2014).
23. V. Berezinsky, V. Dokuchaev, Y. Eroshenko: Destruction of small-scale dark matter clumps in the hierarchical structures and galaxies, Phys. Rev. D **77**, 083519 (2008).
24. V. Berezinsky, V. Dokuchaev, Y. Eroshenko: Dark Matter Annihilation in the Galaxy, Phys. Atom. Nucl. **69**, 2068 (2006).
25. V. Berezinsky, V. Dokuchaev, Y. Eroshenko: Small-scale clumps of dark matter, Usp. Fiz. Nauk **184**, 3 (2014).
26. A. Nusser, S. S. Gubser, and P. J. Peebles: Structure formation with a long-range scalar dark matter interaction, Phys. Rev. D **71**, 083505 (2005).
27. W. A. Hellwing and R. Juszkiewicz: Dark matter gravitational clustering with a long-range scalar interaction, Phys. Rev. D **80**, 083522 (2009).
28. S. Casas, V. Pettorino, C. Wetterich: Dynamics of neutrino lumps in growing neutrino quintessence, Phys. Rev. D **94**, 103518 (2016).
29. Y. Ayaita, M. Weber, C. Wetterich: Neutrino Lump Fluid in Growing Neutrino Quintessence, Phys. Rev. D **87**, 043519 (2013).
30. A. E. Bernardini and O. Bertolami: Stability of mass varying particle lumps Phys.Rev. D **80**, 123011 (2009), arXiv:0909.1541 [gr-qc]
31. M. Baldi, V. Pettorino, L. Amendola and C. Wetterich: Oscillating non-linear large-scale structures in growing neutrino quintessence, Mon. Not. R. Astron. Soc. **418**, 214 (2011).
32. N.J. Nunes, L. Schrempp, C. Wetterich: Mass freezing in growing neutrino quintessence, Phys. Rev. D83 **083523** 2011.
33. V. Pettorino, N. Wintergerst, L. Amendola, C. Wetterich: Neutrino lumps and the Cosmic Microwave Background, Phys. Rev. D **82**, 123001 (2010).

10 The Problem of Particle-Antiparticle in Particle Theory

Felix M Lev

Artwork Conversion Software Inc.
509 N. Sepulveda Blvd Manhattan Beach CA 90266 USA
Email: felixlev314@gmail.com

Abstract. The title of this workshop is: "What comes beyond standard models?". Standard models are based on standard Poincare invariant quantum theory (SQT). Here irreducible representations (IRs) of the Poincare algebra are such that in each IR, the energies are either ≥ 0 or ≤ 0. In the first case, IRs are associated with particles and in the second case — with antiparticles, while particles for which all additive quantum numbers (electric charge, baryon and lepton quantum numbers) equal zero are called neutral. However, SQT is a special degenerate case of finite quantum theory (FQT) in the formal limit $p \to \infty$ where p is a characteristic of a ring in FQT. In FQT, one IR of the symmetry algebra describes a particle and its antiparticle simultaneously, and there are no conservation laws of additive quantum numbers. One IR in FQT splits into two standard IRs with positive and negative energies as a result of symmetry breaking in the formal limit $p \to \infty$. The construction of FQT is one of the most fundamental (if not the most fundamental) problems of particle theory.

Povzetek: Standardni modeli temeljijo na standardni Poincarejevi invariantni kvantni teoriji (SQT). Nerazcepne upodobitve (IR) Poincarejeve algebre privzamejo, da imajo delci (fermioni) pozitivno energijo, antifermioni (antidelci) pa negativno energijo. Nevtralne imenujemo fermione, ki ne nosijo nabojev in je njihovo barionsko ali leptonsko število enako nič. SQT je poseben primer končne kvantne teorije (FQT)v limiti $p \to \infty$, kjer je p radij ustrezne sfere. FQT opiše hkrati delce in antidelce in ne ohranja aditivnih kvantnih števil. Avtor meni, da je konstruiranje FQT eno najbolj nujnih, če ne kar osnovni problem fizike osnovnih delcev.

Keywords: irreducible representations, particle-antiparticle, de Sitter symmetry
PACS numbers: 02.20.Sv, 03.65.Ta, 11.30-j, 11.30.Cp, 11.30.Ly

10.1 Introduction: problems with the physical interpretation of the Dirac equation

Modern fundamental particle theories (QED, QCD and electroweak theory) are based on the concept of particle-antiparticle. Historically, this concept has arisen as a consequence of the fact that the Dirac equation has solutions with positive and negative energies. The solutions with positive energies are associated with particles, and the solutions with negative energies - with corresponding antiparticles. And when the positron was found, it was treated as a great success of the

Dirac equation. Another great success is that in the approximation $(v/c)^2$ the Dirac equation reproduces the fine structure of the hydrogen atom with a very high accuracy.

However, now we know that there are problems with the physical interpretation of the Dirac equation. For example, in higher order approximations, the probabilistic interpretation of non-quantized Dirac spinors is lost because the coordinate description implies that they are described by representations induced from non-unitary representations of the Lorenz algebra. Moreover, this problem exists not only for the Dirac spinors but for any functions described by relativistic covariant equations (Klein-Gordon, Dirac, Rarita-Schwinger and others). As shown by Pauli [1] in the case of fields with an integer spin there is no invariant subspace where the spectrum of the charge operator has a definite sign while in the case of fields with a half-integer spin there is no invariant subspace where the spectrum of the energy operator has a definite sign. It is also known that the description of the electron in the external field by the Dirac spinor is not accurate (e.g., it does not take into account the Lamb shift).

Another fundamental problem in the interpretation of the Dirac equation is as follows. One of the key principles of quantum theory is the principle of superposition. This principle states that if ψ_1 and ψ_2 are possible states of a physical system then $c_1\psi_1 + c_2\psi_2$, when c_1 and c_2 are complex coefficients, also is a possible state. The Dirac equation is the linear equation, and, if $\psi_1(x)$ and $\psi_2(x)$ are solutions of the equation, then $c_1\psi_1(x) + c_2\psi_2(x)$ also is a solution, in agreement with the principle of superposition. In the spirit of the Dirac equation, there should be no separate particles the electron and the positron. It should be only one particle which can be called electron-positron such that electron states are the states of this particle with positive energies, positron states are the states of this particle with negative energies and the superposition of electron and positron states should not be prohibited. However, in view of charge conservation, baryon number conservation, and lepton numbers conservations, the superposition of a particle and its antiparticle is prohibited.

Modern particle theories are based on Poincare (relativistic) symmetry. In these theories, elementary particles are described by irreducible representations (IRs) of the Poincare algebra. Such IRs have a property that energies in them can be either strictly positive or strictly negative but there are no IRs where energies have different signs. The objects described by positive-energy IRs are called particles, and objects described by negative-energy IRs are called antiparticles, and energies of both, particles and antiparticles become positive after second quantization. In this situation, there are no elementary particles which are superpositions of a particle and its antiparticle, and as explained above, this is not in the spirit of the Dirac equation.

In particle theories, only quantized Dirac spinors $\psi(x)$ are used. Here, by analogy with non-quantized spinors, x is treated as a point in Minkowski space. However, $\psi(x)$ is an operator in the Fock space for an infinite number of particles. Each particle in the Fock space can be described by its own coordinates (in the approximation when the position operator exists — see e.g., [3]). **In view of this fact, the following natural question arises: why do we need an extra coordinate x which**

does not have any physical meaning because it does not belong to any particle and so is not measurable? Moreover, I can ask the following seditious question: in quantum theory, do we need Minkowski space at all?

When there are many bodies, the impression may arise that they are in some space but this is only an impression. In fact a background space-time (e.g., Minkowski space) is only a mathematical concept needed in classical theory. For illustration, consider quantum electromagnetic theory. Here we deal with electrons, positrons and photons. In the approximation when the position operator exists, each particle can be described by its own coordinates. The coordinates of the background Minkowski space do not have a physical meaning because they do not refer to any particle and therefore are not measurable. However, in classical electrodynamics we do not consider electrons, positrons and photons. Here the concepts of the electric and magnetic fields $(E(x), B(x))$ have the meaning of the average contribution of all particles in the point x of Minkowski space.

This situation is analogous to that in statistical physics. Here we do not consider each particle separately but describe the average contribution of all particles by temperature, pressure etc. Those quantities have a physical meaning not for each separate particle but for ensembles of many particles.

A justification of the presence of x in quantized Dirac spinors $\psi(x)$ is that in quantum field theories (QFT) the Lagrangian density depends on the four-vector x, but this is only the integration parameter which is used in the intermediate stage. The goal of the theory is to construct the S-matrix, and when the theory is already constructed one can forget about Minkowski space because no physical quantity depends on x. This is in the spirit of the Heisenberg S-matrix program according to which in relativistic quantum theory it is possible to describe only transitions of states from the infinite past when $t \to -\infty$ to the distant future when $t \to \infty$.

The fact that the theory gives the S-matrix in the momentum representation does not mean that the coordinate description is excluded. In typical situations, the position operator in momentum representation exists not only in the nonrelativistic case but in the relativistic case as well. In the latter case, it is known, for example, as the Newton-Wigner position operator [3] or its modifications. However, as pointed out even in textbooks on quantum theory, the coordinate description of elementary particles can work only in some approximations. In particular, even in most favorable scenarios, for a massive particle with the mass m its coordinate cannot be measured with the accuracy better than the particle Compton wave length $\hbar/mc$.

10.2 Is Poincare symmetry the most general symmetry in particle theory?

The above discussion of the problems with Dirac spinors was based on the assumption that Poincare (relativistic) symmetry is the most general symmetry in particle theory, and Standard Model is based on this assumption. But suppose that I ask a question: why not to consider particle theory based on Galilei (nonrelativistic) symmetry? Probably, most physicists will immediately say that this question is silly because everybody knows that Poincare symmetry is more general

(fundamental) than Galilei one and many facts in particle physics show that Galilei symmetry does not work here. But suppose that I am not a physicist, I do not know experimental data and I ask whether the fact that Poincare symmetry is more general than Galilei one follows only from mathematics? Is this question legitimate?

In his famous paper "Missed Opportunities" [5] Dyson explains that the fact that Poincare symmetry is more general than Galilei one follows from pure mathematical considerations. The Poincare group is more symmetric that the Galilei one: the former contains a formal parameter c (I even do not discuss its physical meaning), and the latter can be obtained from the former by a procedure called contraction when formally $c \to \infty$.

In view of this observation, I can ask whether Poincare symmetry is most general, maybe there are groups more symmetric that Poincare one such that the Poincare group can be obtained from these more symmetric groups by contraction? In his paper Dyson explains that indeed the de Sitter (dS) and anti-de Sitter (AdS) groups are more symmetric than Poincare one and the transition from the former to the latter is described by contraction when a parameter R (see below) goes to infinity. At the same time, since dS and AdS groups are semisimple, they have a maximum possible symmetry and cannot be obtained from more symmetric groups by contraction.

The paper [5] appeared in 1972, i.e., 50 years ago, and, in view of Dyson's results, a question arises why the fundamental particle theories are still based on Poincare symmetry and not dS or AdS ones. The parameter R arises from particle theory but in the literature it is often interpreted as the radius of the universe. Probably, physicists believe that, since R is even much greater than sizes of stars, the dS and AdS symmetries can play an important role only in cosmology and there is no need to use them for describing elementary particles. I believe that this argument is not consistent because usually more general theories shed a new light on standard concepts, and my talk is a good illustration of this point.

In Sec. 10.3 I describe the concept of symmetry on quantum level. In Secs. 10.7 and 10.8 I consider the concept of particle-antiparticle for dS and AdS symmetries in standard quantum theory and in a quantum theory based on finite mathematics (FQT). Here I give a popular explanation why standard concepts of particle-antiparticle, electric charge and baryon number have only a limited meaning when the symmetry in FQT is broken to Poincare or standard AdS symmetries. Finally, Sec. 19.3 is discussion. I describe all physical quantities in units $c = \hbar = 1$.

10.3   Symmetry on quantum level

In the usual treatment of relativistic quantum theory, the approach to symmetry on quantum level follows. Since the Poincare group is the group of motions of Minkowski space, quantum states should be described by representations of this group. This implies that the representation generators commute according to the

commutation relations of the Poincare group Lie algebra:

$$[P^\mu, P^\nu] = 0, \quad [P^\mu, M^{\nu\rho}] = -i(\eta^{\mu\rho}P^\nu - \eta^{\mu\nu}P^\rho),$$
$$[M^{\mu\nu}, M^{\rho\sigma}] = -i(\eta^{\mu\rho}M^{\nu\sigma} + \eta^{\nu\sigma}M^{\mu\rho} - \eta^{\mu\sigma}M^{\nu\rho} - \eta^{\nu\rho}M^{\mu\sigma}) \quad (10.1)$$

where $\mu, \nu = 0, 1, 2, 3$, P^μ are the operators of the four-momentum, $M^{\mu\nu}$ are the operators of Lorentz angular momenta, and $\eta^{\mu\nu}$ is such that $\eta^{00} = -\eta^{11} = -\eta^{22} = -\eta^{33} = 1$ and $\eta^{\mu\nu} = 0$ if $\mu \neq \nu$. This approach is in the spirit of Klein's Erlangen program in mathematics.

However, as noted in Sec. 18.2 and discussed in detail in [3], in quantum theory, the concept of space-time background does not have a physical meaning. As argued in [3,5], the approach should be the opposite. Each system is described by a set of linearly independent operators. By definition, the rules how they commute with each other define the symmetry algebra. In particular, *by definition*, Poincare symmetry on quantum level means that the operators commute according to Eq. (18.1). This definition does not involve Minkowski space at all. In particular, the fact that $\eta^{\mu\nu}$ coincides with the metric tensor in Minkowski space, does not imply that this space is involved. I am very grateful to Leonid Avksent'evich Kondratyuk for explaining me this definition during our collaboration.

By analogy with the definition of Poincare symmetry on quantum level, the definition of dS symmetry on quantum level should not involve the fact that the dS group is the group of motions of dS space. Instead, *the definition* is that the operators M^{ab} ($a, b = 0, 1, 2, 3, 4$, $M^{ab} = -M^{ba}$) describing the system under consideration satisfy the commutation relations *of the dS Lie algebra*, i.e.,

$$[M^{ab}, M^{cd}] = -i(\eta^{ac}M^{bd} + \eta^{bd}M^{ac} - \eta^{ad}M^{bc} - \eta^{bc}M^{ad}) \quad (10.2)$$

where η^{ab} is such that $\eta^{00} = -\eta^{11} = -\eta^{22} = -\eta^{33} = -\eta^{44} = 1$ and $\eta^{ab} = 0$ if $a \neq b$. The *definition* of AdS symmetry on quantum level is given by the same equations but $\eta^{44} = 1$.

The procedure of contraction from dS and AdS symmetries to Poincare one is defined as follows. If we *define* the operators P^ν as $P^\nu = M^{\nu 4}/R$ where R is a parameter with the dimension $\texttt{length}$ then in the formal limit when $R \to \infty$, $M^{\nu 4} \to \infty$ but the quantities P^ν are finite, Eqs. (18.2) become Eqs. (18.1). This procedure is the same for the dS and AdS symmetries.

The above contraction is analogous to the contraction from Poincare symmetry to Galilei one, where the parameter of contraction is c. On quantum level, R and c are only the parameters describing the relations between Lie algebras of higher and lower symmetries. On classical level, the physical meaning of c is well-known, while R is the radius of the dS or AdS space. A detailed discussion of the both contractions is described in a vast literature, in particular, in [3] where it has been proposed the following

Definition: *Let theory A contain a finite nonzero parameter and theory B be obtained from theory A in the formal limit when the parameter goes to zero or infinity. Suppose that, with any desired accuracy, theory A can reproduce any result of theory B by choosing a value of the parameter. On the contrary, when the limit is already taken, one cannot return back to theory A, and theory B cannot reproduce all results of theory A. Then theory A*

is more general (fundamental) than theory B and theory B is a special degenerate case of theory A.

As proved in [3], dS and AdS symmetries are more general (fundamental) than Poincare symmetry. The latter is a special degenerate case of the former in the formal limit $R \rightarrow \infty$. As noted above, in contrast to Dyson's approach based on Lie groups, our approach is based on Lie algebras. Then, as proved in [3], classical theory is a special degenerate case of quantum one in the formal limit $\hbar \rightarrow 0$, and nonrelativistic theory (NT) is a special degenerate case of relativistic one (RT) in the formal limit $c \rightarrow \infty$. In the literature the above facts are explained from physical considerations but, as shown in [3] they can be proved mathematically by using properties of Lie algebras. In particular, since, from mathematical point of view, de Sitter symmetry is more general (fundamental) than Poincare one, there should exist physical phenomena which can be explained by de Sitter symmetries but cannot be explained by Poincare symmetry. Below I will discuss such phenomena.

10.4   Problems with describing nature by classical mathematics

Standard quantum theory (SQT) is based on classical mathematics involving limits, infinitesimals, continuity etc. Mathematical education at physics departments develops a belief that classical mathematics is the most fundamental mathematics, while, for example, discrete and finite mathematics is something inferior what is used only in special applications. And many mathematicians have a similar belief. Historically it happened so because more than 300 years ago Newton and Leibniz proposed the calculus of infinitesimals, and, since that time, a titanic work has been done on foundation of classical mathematics. This problem has not been solved till the present time, but for most physicists and many mathematicians the most important thing is not whether a rigorous foundation exists but that in many cases standard mathematics works with a very high accuracy.

The idea of infinitesimals was in the spirit of existed experience that any macroscopic object can be divided into arbitrarily large number of arbitrarily small parts, and, even in the 19th century, people did not know about atoms and elementary particles. But now we know that when we reach the level of atoms and elementary particles, standard division loses its usual meaning and in nature there are no arbitrarily small parts and no continuity.

For example, typical energies of electrons in modern accelerators are millions of times greater than the electron rest energy, and such electrons experience many collisions with different particles. If it were possible to break the electron into parts, then it would have been noticed long ago.

Another example is that if we draw a line on a sheet of paper and look at this line by a microscope then we will see that the line is strongly discontinuous because it consists of atoms. That is why standard geometry (the concepts of continuous lines and surfaces) can work well only in the approximation when sizes of atoms are neglected, standard macroscopic theory can work well only in this approximation etc.

Of course, when we consider water in the ocean and describe it by differential equations of hydrodynamics, this works well but this is only an approximation

since water consists of atoms. However, it seems unnatural that even quantum theory is based on continuous mathematics. Even the name "quantum theory" reflects a belief that nature is quantized, i.e., discrete, and this name has arisen because in quantum theory some quantities have discrete spectrum (i.e., the spectrum of the angular momentum operator, the energy spectrum of the hydrogen atom etc.). But this discrete spectrum has appeared in the framework of classical mathematics.

I asked physicists and mathematicians whether, in their opinion, the indivisibility of the electron shows that in nature there are no infinitesimals, and standard division does not work always. Some mathematicians say that sooner or later the electron will be divided. On the other hand, as a rule, physicists agree that the electron is indivisible and in nature there are no infinitesimals. They say that, for example, dx/dt should be understood as $\Delta x/\Delta t$ where Δx and Δt are small but not infinitesimal. I ask them: but you work with dx/dt, not $\Delta x/\Delta t$. They reply that since mathematics with derivatives works well then there is no need to philosophize and develop something else (and they are not familiar with finite mathematics).

One of the key problems of modern quantum theory is the problem of infinities: the theory gives divergent expressions for the S-matrix in perturbation theory. In renormalized theories, the divergencies are eliminated by the renormalization procedure where finite observable quantities are formally expressed as products of singularities. Although this procedure is not well substantiated mathematically, in some cases it results in excellent agreement with experiment. Probably the most famous case is that the results for the electron and muon magnetic moments obtained at the end of the 40th agree with experiment at least with the accuracy of eight decimal digits (see, however, a discussion in [6]). In view of this and other successes of quantum theory, most physicists believe that agreement with the data is much more important than the rigorous mathematical substantiation.

At the same time, in nonrenormalized theories, infinities cannot be eliminated by the renormalization procedure, and this a great obstacle for constructing quantum gravity based on quantum field theory (QFT). As the famous physicist and the Nobel Prize laureate Steven Weinberg writes in his book [7]: *"Disappointingly this problem appeared with even greater severity in the early days of quantum theory, and although greatly ameliorated by subsequent improvements in the theory, it remains with us to the present day"*. The title of Weinberg's paper [8] is "Living with infinities".

In view of efforts to describe discrete nature by continuous mathematics, my friend told me the following joke: "A group of monkeys is ordered to reach the Moon. For solving this problem each monkey climbs a tree. The monkey who has reached the highest point believes that he has made the greatest progress and is closer to the goal than the other monkeys". Is it reasonable to treat this joke as a hint on some aspects of the modern science? Indeed, people invented continuity and infinitesimals which do not exist in nature, created problems for themselves and now apply titanic efforts for solving those problems.

The founders of quantum theory and scientists who essentially contributed to it were highly educated. But they used only classical mathematics, and even now finite mathematics is not a part of standard education for physicists. The

development of quantum theory has shown that the theory contains anomalies and divergences. Most physicists considering those problems, worked in the framework of classical mathematics and did not acknowledge that they arise just because this mathematics was used.

10.5   Quantum theory based on finite mathematics

Several well-known physicists, including the Nobel Prize laureates Gross, Nambu and Schwinger, discussed approaches when quantum theory involves finite mathematics. While classical mathematics starts from the ring of integers $Z = (-\infty, ... -1, 0, 1, ...\infty)$, finite mathematics rejects infinities from the beginning. It starts from the ring $R_p = (0, 1, 2, ...p - 1)$ where addition, subtraction and multiplication are performed as usual but modulo p, and p is called the characteristic of the ring. In number theory, p is the usual notation for the characteristic and this has nothing to do with the fact that in particle theory the notation p is used for denoting a particle four-momentum.

Since the operations in R_p are modulo p, then, if p is odd, one can say that R_p contains the numbers $(-(p-1)/2, ... -1, 0, 1, ...(p-1)/2)$. Then, if elements of Z are depicted as integer points on the x axis of the xy plane, the elements of R_p can be depicted as points of the circle in Figure 1 and analogously if p is even.
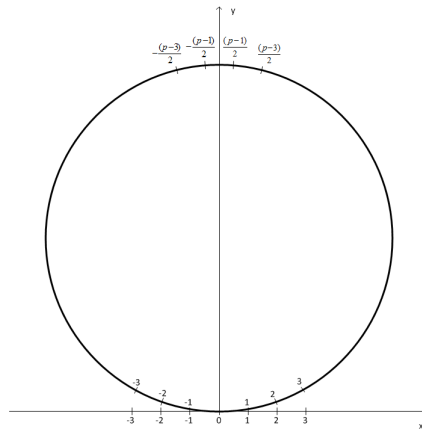

Fig. 10.1: Relation between R_p and Z

The analogy between R_p and the circle follows from the following observations. If we take an element of R_p and successively add 1 to it, then after p steps we will return to the original element because addition in R_p is modulo p. This is analogous to the fact that if we are moving along the circle in the same direction then, sooner or later, we will arrive to the initial point.

Figure 1 is natural from the following historical analogy. For many years people believed that the Earth was flat and infinite, and only after a long period of time they realized that it was finite and curved. It is difficult to notice the curvature

when we deal only with distances much less than the radius of the curvature. Analogously, when we deal with numbers the modulus of which is much less than p, the results are the same in Z and R_p, i.e., we do not notice the "curvature" of R_p. This "curvature" is manifested only when we deal with numbers the modulus of which is comparable to p.

As proved in my book [3], as follows from **Definition**, classical mathematics (involving the concepts of limits, infinitesimals, continuity etc.) is a special degenerate case of finite mathematics in the formal limit when the characteristic p of the ring or field in the latter goes to infinity. Therefore standard dS and AdS symmetries over the field of complex numbers can be generalized to dS and AdS symmetries over a finite ring or field of characteristic p.

We use the abbreviation FQT (finite quantum theory) to denote quantum theory over the ring or field of characteristic p. Since mathematically FQT is more general (fundamental) than SQT, there are physical phenomena which can be explain only by FQT but cannot be explained by SQT. An example of such a phenomenon is discussed in Sec. 10.8, for other examples —see [3].

10.6   Particles and antiparticles in Poincare invariant theories

As noted in Sec. 18.2, solutions of the Dirac equation with positive energies are associated with particles and solution with negative energies — with antiparticles. It has been noted that there are problems with the interpretation of the non-quantized Dirac spinor $\psi(x)$ and for the quantized Dirac spinor the problem is that the quantity x does not have the physical meaning. Elementary particles in Poincare invariant theory are described by IRs of the Poincare algebra by selfadjoint operators. Therefore a problem arises whether the concept of particle-antiparticle can be defined proceeding only from such IRs without mentioning the nonphysical parameter x.

Let p^ν be the four-momentum of a particle in Poincare invariant theory. Define $p^2 = p^\nu p_\nu$, where a sum over repeated indices is assumed. Then for usual particles $p^2 \geq 0$ while for tachyons $p^2 < 0$. The existence of tachyons is a problem, and we will consider only usual particles. Then the mass of the particle can be defined as a nonnegative number m such that $m^2 = p^2$.

The energy E of a particle with the momentum p and mass m equals $\pm(m^2+p^2)^{1/2}$. The choice of the sign of the square root is only the matter of convention but not the matter of principle. Depending on this sign, there are IRs where energies can be only either positive or negative while the probability to have zero energy is zero.

When we consider a system consisting of particles and antiparticles then the energy sign of both, particles and antiparticles should be the same. Indeed, consider, for example a system of two particles with the same mass m and let the momenta p_1 and p_2 be such that the total momentum $p_1 + p_2$ equals zero. Then, if the energy of particle 1 is positive, and the energy of particle 2 is negative then the total four-momentum of the system would be zero what contradicts experimental data. By convention, the energy sign of all particles and antiparticles in question is chosen to be positive. For this purpose, the procedure of second quantization

is defined such that after the second quantization the energies of antiparticles become positive. Then the mass of any particle is the minimum value of its energy in the case when the momentum equals zero.

Suppose now that we have two particles such that particle 1 has the mass m_1, spin s_1 and is characterized by some additional quantum numbers (e.g., electric charge, baryon quantum number etc.), and particle 2 has the mass m_2, spin $s_2 = s_1$ and all additional quantum numbers characterizing particle 2 equal the corresponding additional quantum numbers for particle 1 with the opposite sign. A question arises when particle 2 can be treated as an antiparticle for particle 1. Is it necessary that m_1 should be exactly equal m_2 or they can slightly differ each other? In particular, can we guarantee that the mass of the positron exactly equals the mass of the electron, the mass of the proton exactly equals the mass of the antiproton etc.?

If particle 2 (for some reasons) is treated as an antiparticle for particle 1, and the particles are considered only on the level of IRs, then the relation between m_1 and m_2 is fully arbitrary. However, in QFT, $m_1 = m_2$ because IRs for a particle and its antiparticle are combined together in the framework of a local field. For example, the Dirac spinor combines together two IRs for the electron and positron. However, as noted in Sec. 18.2, this procedure encounters the following problems:

- The quantity x in quantized fields $\psi(x)$ does not have a physical meaning.
- There is no probabilistic interpretation of $\psi(x)$ because it is described by a non-unitary representation of the Poincare algebra.
- Although $\psi(x)$ satisfies a linear equation, a superposition of solutions with positive and negative energies is prohibited.

A usual statement in the literature is that in QFT the fact that $m_1 = m_2$ follows from the CPT theorem which is a consequence of locality since *we construct* local covariant fields from a particle and its antiparticle with equal masses. However, as noted in Sec. 18.2, since on quantum level there are problems with the physical interpretation of covariant fields and the quantity x, the very meaning of locality on quantum level is problematic.

Also, a question arises what happens if locality is only an approximation: in that case the equality of masses is exact or approximate? Consider a simple model when electromagnetic and weak interactions are absent. Then the fact that the proton and the neutron have equal masses has nothing to do with locality; it is only a consequence of the fact that the proton and the neutron belong to the same isotopic multiplet. In other words, they are simply different states of the same object—the nucleon.

Since the concept of locality is not formulated in terms of selfadjoint operators, this concept does not have a clear physical meaning, and this fact has been pointed out even in known textbooks (see e.g. [9]). Therefore, QFT does not give a physical proof that $m_1 = m_2$. Note also that in Poincare invariant quantum theories there can exist elementary particles for which all additional quantum numbers are zero. Such particles are called neutral because they coincide with their antiparticles. In Secs. 10.7 and 10.8 I consider how the concept of particle-antiparticle in treated for dS and AdS invariant theories, respectively.

10.7   Particles and antiparticles in dS invariant theories

The descriptions of elementary particles in the dS and AdS cases are considerably different. In the former case all the operators $M^{\nu 4}$ ($\nu = 0, 1, 2, 3$) are on equal footing. Therefore, M^{04} can be treated as the Poincare analog of the energy only in the approximation when R is rather large. In the general case, the sign of M^{04} cannot be used for the classification of IRs.

In his book [7] Mensky describes the implementation of dS IRs when the representation space is the three-dimensional unit sphere in the four-dimensional space. In this implementation, there exist one-to-one relations between the northern hemisphere and the upper Lorentz hyperboloid with positive Poincare energies and between the southern hemisphere and the lower Lorentz hyperboloid with negative Poincare energies, while points on the equator correspond to infinite Poincare energies. However, the operators of IRs are not singular in the vicinity of the equator and, since the equator has measure zero, the properties of wave functions on the equator are not important.

Since the number of states in dS IRs is twice as big as the number of states in IRs of the Poincare algebras, one might think that each IR of the dS algebra describes a particle and its antiparticle simultaneously. However, a detailed analysis in [3] shows that states described by dS IRs cannot be characterized as particles or antiparticles in the usual meaning.

For example, let us call states with the support of their wave functions on the northern hemisphere as particles and states with the support on the southern hemisphere as their antiparticles. Then states which are superpositions of a particle and its antiparticle obviously belong to the representation space under consideration, i.e., they are not prohibited.

As noted in Sec. 18.2, in the spirit of the Dirac equation, there should be no separate particles the electron and the positron. It should be only one particle which can be called electron-positron such that electron states are the states of this particle with positive energies, positron states are the states of this particle with negative energies and, as follows from the principle of superposition in quantum theory, the superposition of electron and positron states should not be prohibited. *However, since in standard particle theory, charge conservation is treated as more fundamental than the principle of superposition, the superposition of a particle and its antiparticle is prohibited.*

However, we see that in the dS case the situation is in the spirit of the Dirac equation: there are no independent particles and antiparticles, there are only objects described by IRs of the dS algebra, and, if states of each object with positive energies are called particle states and states with negative energies — antiparticle states, superpositions of such states are not prohibited. *Therefore, in the dS case, the principle of superposition is stronger than the electric charge conservation.* Note that the law of electric charge conservation comes from classical physics. The existing experimental data confirms that this law takes place. However, a problem arises whether those data describe all possible situations. We discuss this problem below. As noted in Sec. 10.3, dS symmetry is more general than Poincare one, and the latter can be treated as a special degenerate case of the former in the formal limit

$R \to \infty$. This means that, with any desired accuracy, any phenomenon described in the framework of Poincare symmetry can be also described in the framework of dS symmetry if R is chosen to be sufficiently large, but there also exist phenomena for explanation of which it is important that R is finite and not infinitely large (see [3]).

As shown in [3,9], dS symmetry is broken in the formal limit $R \to \infty$ because one IR of the dS algebra splits into two IRs of the Poincare algebra with positive and negative energies and with equal masses. Therefore, the fact that the masses of particles and their corresponding antiparticles are equal to each other, can be explained as a consequence of the fact that observable properties of elementary particles can be described not by exact Poincare symmetry but by dS symmetry with a very large (but finite) value of R. In contrast to QFT, for combining a particle and its antiparticle into one object, there in no need to assume locality and involve local field functions because a particle and its antiparticle already belong to the same IR of the dS algebra (compare with the above remark about the isotopic symmetry in the proton-neutron system).

The fact that dS symmetry is higher than Poincare one is clear even from the fact that, in the framework of the latter symmetry, it is not possible to describe states which are superpositions of states on the upper and lower hemispheres. Therefore, breaking the IR into two independent IRs defined on the northern and southern hemispheres obviously breaks the initial symmetry of the problem. This fact is in agreement with the Dyson observation (mentioned above) that dS group is more symmetric than Poincare one.

When $R \to \infty$, standard concepts of particle-antiparticle, electric charge and baryon and lepton quantum numbers are restored, i.e., in this limit, superpositions of particle and antiparticle become prohibited because now a particle and its antiparticle belong to different IRs. Therefore, those concepts arise as a result of symmetry breaking, i.e., they are not universal.

10.8   Particles and antiparticles in AdS invariant theories

In theories where the symmetry algebra is the AdS algebra, the structure of IRs is known (see e.g., [3,12]). The operator M^{04} is the AdS analog of the energy operator. Let W be the Casimir operator $W = \frac{1}{2} \sum M^{ab} M_{ab}$ where a sum over repeated indices is assumed. As follows from the Schur lemma, the operator W has only one eigenvalue in every IR. By analogy with Poincare invariant theory, we will not consider AdS tachyons and then one can define the AdS mass μ such that $\mu \geq 0$ and μ^2 is the eigenvalue of the operator W.

As noted in Sec. 10.3, the procedure of contraction from the AdS algebra to the Poincare one involves the definition of P^{ν} such that $M^{\nu 4} = RP^{\nu}$. This relation has a physical meaning only if R is rather large. In that case the AdS mass μ and the Poincare mass m are related as $\mu = Rm$, and the relation between the AdS and Poincare energies is analogous. Since AdS symmetry is more general (fundamental) then Poincare one then μ is more general (fundamental) than m. In contrast to the Poincare masses and energies, the AdS masses and energies are dimensionless. From cosmological considerations (see e.g., [3]), the value of R is

usually accepted to be of the order of 10^{26} m. Then the AdS masses of the electron, the Earth and the Sun are of the order of 10^{39}, 10^{93} and 10^{99}, respectively. The fact that even the AdS mass of the electron is so large might be an indication that the electron is not a true elementary particle. In addition, the present accepted upper level for the photon mass is $10^{-17}ev$. This value seems to be an extremely tiny quantity. However, the corresponding AdS mass is of the order of 10^{16}, and so, even the mass which is treated as extremely small in Poincare invariant theory might be very large in AdS invariant theory.

In the AdS case there are IRs with positive and negative energies, and they belong to the discrete series [3, 12]. Therefore, by analogy with standard particle theory, one can define particles and antiparticles. Consider first the construction of positive energy IRs. We start from "the rest state" where the AdS energy equals the AdS mass μ_1. Then we obtain the states with the AdS energies $\mu_1, \mu_1 + 1, \mu_1 + 2, ...\infty$ (see Figure 2). Analogously, if μ_2 is the AdS mass of the antiparticle, we start from the state where the energy equals $-\mu_2$ and obtain the states with the AdS energies $-\mu_2, -\mu_2 - 1, -\mu_2 - 2, ... - \infty$. (see Figure 2) Therefore, the situation is pretty much analogous to that in Poincare invariant theories, and there is no way to conclude whether the mass of a particle equals the mass of the corresponding antiparticle. In view of the results in this and preceding sections, we conclude that the descriptions of elementary particles in the cases of dS and AdS symmetries are considerably different. In the dS case, one IR describes particle and antiparticle states simultaneously and their superpositions are not prohibited, i.e. the principle of superposition is more fundamental than the conservation of electric charge and other additive quantum numbers. On the other hand, in the AdS case, the situation is analogous to that in Poincare invariant theories; in particular the electric charge conservation is more fundamental than the principle of superposition.

So, a question arises which of those possibilities in SQT is more physical. However, as discussed in [3], FQT is more general (fundamental) than SQT, in FQT it is also possible to define the concepts of dS and AdS symmetries and here the dS and AdS cases are physically equivalent. Below we will consider a direct generalization of the AdS symmetry from SQT to FQT.

The description of the energy spectrum in standard IRs of the AdS algebra has been given above. We will now explain why in FQT the spectrum is different, and in FQT the situation is similar to that in standard dS case but not standard AdS one because IRs in FQT contain both, positive and negative energies. Let us note first that, while in SQT the quantity μ can be an arbitrary real number, in FQT μ is an element of R_p. As noted above, if p is odd then R_p contains the elements $-(p - 1)/2, ... - 1, 0, 1, ...(p - 1)/2$ (see Figure 1) and the case when p is even is analogous. For definiteness, we consider the case when p is odd.

By analogy with the construction of positive energy IRs in SQT, in FQT we start the construction from "the rest state", where the AdS energy is positive and equals μ. Then we act on this state by raising operators and gradually get states with higher and higher energies, i.e., $\mu + 1, \mu + 2, ...$ However, now we are moving not along the straight line but along the circle in Figure 1 and, in contrast to the situation in SQT, we cannot obtain infinitely large numbers. When we reach the state with the energy $(p - 1)/2$, the next state has the energy $(p - 1)/2 + 1 = (p + 1)/2$ and, since
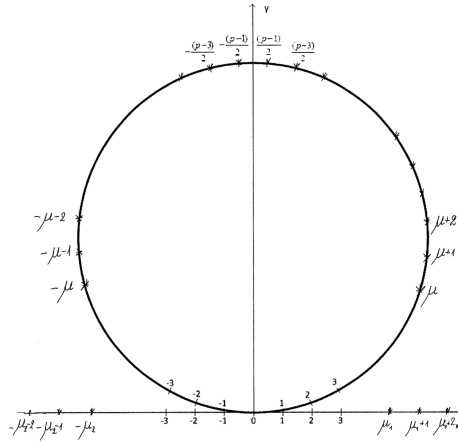
Fig. 10.2: Spectrum of Energies of Elementary Particle

the operations are modulo p, this value also can be denoted as $-(p-1)/2$ i.e., it may be called negative. When this procedure is continued, one gets the energies $-(p-1)/2+1 = -(p-3)/2, -(p-3)/2+1 = -(p-5)/2, \dots$ and, as shown in [3], the procedure finishes when the energy $-\mu$ is reached (see Figure 2).

Therefore, in contrast to the situation in SQT, in FQT IRs are finite-dimensional (and even finite since the ring R_p and its complex extension $R_p + iR_p$ are finite). By analogy with the dS case in SQT, one can say that the states with the energies $\mu, \mu+1, \mu+2, \dots$ refer to a particle and states with the energies $\dots -\mu-2, -\mu-1, -\mu$ — to an antiparticle. Therefore, in FQT the mass of a particle automatically equals the mass of the corresponding antiparticle. This is an example when FQT can solve a problem which standard quantum AdS theory cannot. By analogy with the situation in the dS case, for combining a particle and its antiparticle together, there is no need to involve additional coordinate fields because a particle and its antiparticle are already combined in the same IR.

Then, since states which are superpositions of particles and antiparticles belong to the representation space, we conclude by analogy with the situation in Sec. 10.7, that in FQT there are no superselection rules which prohibit superpositions of states with opposite electric charges, baryon quantum numbers etc. Moreover, the representation operators of the enveloping algebra can perform transformations $particle \leftrightarrow antiparticle$.

As shown in Ref. [3], in the formal limit $p \to \infty$, one IR in FQT splits into two standard IRs of the AdS algebra with positive and negative energies. This result seems natural from Figure 2 since the spectrum of positive energies becomes $\mu, \mu+1, \mu+2, \dots \infty$ and the spectrum of negative energies becomes $-\infty, \dots -\mu -$

$2, -\mu - 1, -\mu$ by analogy with the spectrum in SQT (see Figure 2). Therefore, in this limit the concept of particle-antiparticle and the superselection rules have the usual meaning. In turn, in situations when one can define the quantity R such that the contraction to the Poincare algebra works with a high accuracy, one can describe particles and antiparticles in the framework of Poincare symmetry.

Even from the fact that in standard quantum theory, there are no superpositions of states belonging to a particle and its antiparticle, it is clear that symmetry described by one IR in FQT is higher than symmetry described by two IRs obtained from one IR in FQT in the formal limit $p \to \infty$. Therefore standard concepts of particle-antiparticle and superselection rules arise as a result of symmetry breaking, i.e., they are not universal.

10.9   Discussion

As explained in Sec. 10.6, in quantum theory based on Poincare symmetry, the concept of particle-antiparticle arises because IRs have the property that energies in them can be either positive or negative, and there are no IRs where energies have different signs. Then IRs with positive energies are associated with particles and IRs with negative energies — with antiparticles, and superpositions of particles and antiparticles are prohibited because they belong to different IRs. As shown in Sec. 10.8, in SQT based on AdS symmetry, the situation is analogous.

On the other hand, as shown in Secs. 10.7 and 10.8, in SQT based on dS symmetry and in FQT, IRs contain states with both, positive and negative energies. If states with positive energies are called particle states and states with negative energies — antiparticle states then their superpositions are not prohibited because they belong to the same IR. The principle of superposition is a fundamental principle of quantum theory but in SQT based on Poincare and AdS symmetries, superpositions of particles and antiparticles are prohibited because they contradict the electric charge conservation, baryon number conservation etc. Therefore, in those cases, e.g., the electric charge conservation is treated as more fundamental than the principle of superposition but in SQT based on dS symmetry and in FQT the situation is the opposite.

One might think that for this reason the latter theories are not physical but in fact they are more physical than the former theories. The matter is that, as explained in Secs. 10.7 and 10.8:

- Standard Poincare invariant theory arises as a result of symmetry breaking at $R \to \infty$ in dS invariant quantum theory because in this limit one IR in the latter splits into two IRs in the former.
- Standard Poincare and AdS invariant theories arise as a result of symmetry breaking at $p \to \infty$ in FQT because in this limit one IR in the latter splits into two IRs in the former.

Then experimentally the electric charge conservation, baryon number conservation etc. are observed with a very high accuracy as a consequence of the fact that at the present stage of the universe the quantities R and p are extremely high and then standard quantum theory based on Poincare symmetry works with a very

high accuracy. However, there are reasons to think [3] that at early stages of the universe those quantities were much less than now . That is why at those stages the conservation of the electric charge and baryon quantum number did not take place. As argued in [13], this is the reason of the baryon asymmetry of the universe. The present fundamental particle theories are based on Poincare invariant QFT, and, as noted in Sec. 10.6, for solving the problem why a particle and its antiparticle have equal masses, those theories involve local quantized field $\psi(x)$ where x does not belong to any particle and is simply a parameter arising from the second quantization of a non-quantized field. So, the physical meaning of x is not clear. Although QFT has many successes, it also has problems because, as noted, for example, in the textbook [9], $\psi(x)$ is an operatorial distribution, and the product of distributions at the same point is not a well defined mathematical operation.

As explained in Secs. 10.7 and 10.8, in quantum theories based on dS symmetry and FQT, the masses of a particle and the corresponding antiparticle are automatically equal, and this is achieved without introducing local quantized fields. However, as noted above, in those theories the concepts of particle-antiparticle and additive quantum numbers differ from standard ones because one IR combines together a particle and its antiparticle. The construction of such theories is one of the most fundamental (if not the most fundamental) problems of particle theory.

References

1. W. Pauli: The connection between spin and statistics, Phys. Rev. **58**, 716–722 (1940).
2. F. Lev: Finite mathematics as the foundation of classical mathematics and quantum theory. With application to gravity and particle theory. ISBN 978-3-030-61101-9. Springer, https://www.springer.com/us/book/9783030611002 (2020).
3. T.D. Newton and E.P. Wigner: Localized States for Elementary Systems, Rev. Mod. Phys. **21**, 400–405 (1949).
4. F.G. Dyson: Missed Opportunities. Bull. Amer. Math. Soc., **78**, 635–652 (1972).
5. F.M. Lev: de Sitter Symmetry and Quantum Theory, Phys. Rev. D**85**, 065003 (2012).
6. O. Consa: Something is wrong in the state of QED, arXiv preprint (2021), https://arxiv.org/abs/2110.02078.
7. S. Weinberg: The Quantum Theory of Fields, Vol. I, Cambridge University Press, Cambridge, UK, 1999.
8. S. Weinberg: Living with Infinities, arXiv preprint (2009), https://arxiv.org/abs/0903.0568.
9. N.N. Bogolubov, A.A. Logunov, A.I. Oksak and I.T. Todorov: General Principles of Quantum Field Theory, Nauka: Moscow (1987).
10. F.M. Lev: Could Only Fermions Be Elementary? J. Phys. A: Mathematical and Theoretical, **A37**, 3285-3304 (2004).
11. M.B. Mensky: Method of Induced Representations. Space-time and Concept of Particles. Moscow: Nauka (1976)
12. N.T. Evans: Discrete Series for the Universal Covering Group of the 3+2 de Sitter Group, J. Math. Phys. **8**, 170-184 (1967).
13. F.M. Lev: The Concept of Particle-Antiparticle and the Baryon Asymmetry of the Universe, Physics of Particles and Nuclei Letters, **18**, 729-737 (2021).

11   Clifford odd and even objects, offering description of internal space of fermion and boson fields, respectively, open new insight into next step beyond standard model

N. S. Mankoč Borštnik

Department of Physics, University of Ljubljana
SI-1000 Ljubljana, Slovenia
norma.mankoc@fmf.uni-lj.si

Abstract. In a long series of works the author demonstrated, together with collaborators, that the model named the *spin-charge-family* theory offers the explanation for all in the *standard model* assumed properties of fermion and boson fields, with the families of fermions and the Higgs's scalars included. The theory starts with a simple action in $\geq (13+1)$-dimensional space-time with massless fermions which interact with massless gravitational fields only (vielbeins and the two kinds of spin connection fields). The internal spaces of fermion and boson fields are described by the Clifford odd and even objects, respectively. The corresponding odd and even "basis vectors" in a tensor product with the basis in ordinary momentum or coordinate space define the creation and annihilation operators, which explain the second quantization postulates for fermion and boson fields. The break of the starting symmetry leads at low energies to the action for families of quarks and leptons and the corresponding gauge fields, with Higgs's fields included, offering several predictions and several explanations of the observed cosmological phenomena. The properties of the odd dimensional spaces are also discussed.

Povzetek: V dolgem nizu člankov je avtorica, skupaj s sodelavci, pokazala, da ponuja model, ki ga avtorica poimenuje teorija *spinov-nabojev-družin*, razlago za vse v *standardnem modelu* privzete lastnosti fermionskih in bozonskih polj, vključno z družinami fermionov in Higgsovimi skalarji. Teorija predpostavi preprosto akcijo v $\geq (13+1)$-razsežnem prostoru-času, v kateri fermioni nimajo mase, interagirajo pa samo z brezmasnim gravitacijskim poljem (tetradani, ki določajo gravitacijsko polje v običajnem prostoru in dvema vrstama spinskih povezav, ki so umeritvena polja Lorentzovih transformacij v notranjem prostoru fermionov). Notranji prostor fermionov opiše avtorica z "bazičnimi vektorji", ki so lihi objekti Clifordove algebre, notranji prostor bozonov pa s Clifordovo sodimi objekti. Ustrezni lihi in sodi "bazični vektorji" v tenzorskem produktu z bazo v prostoru gibalnih količin definirajo kreacijske in anihilacijske operatorje antikomutirajočih fermionskih polj in komutirajočih bozonskih polj, kar pojasni postulate za drugo kvantizacijo za fermionska in bozonska polja. Zlomitev začetne simetrije akcije vodi pri nizkih energijah do akcije kot jo predpostavi *standardni model*— za družine kvarkov in leptonov in za ustrezna umeritvena polja ter za Higgsove skalarje. Teorija ponuja števine napovedi in pojasni vzroke za kozmološka opažanja. Predstavi tudi lastnosti Clifordovih objektov v prostorih z lihim številom dimenzij.

Keywords: Second quantization of fermion and boson fields in Clifford space; beyond the standard model; Kaluza-Klein-like theories in higher dimensional space, explanation of appearance of families of fermions, scalar fields, fourth family, dark matter.

11.1   Introduction

The *standard model* (with massive neutrinos added) has been experimentally confirmed without raising any serious doubts so far on its assumptions, which remain unexplained [1].

The assumptions of the *standard model* has in the literature several explanations, mostly with many new not explained assumptions. The most popular seem to be the grand unifying theories ([1–6].

Among the questions for which the answers are needed are:

i. Where do fermions, quarks and leptons, originate?

ii. Why do family members, quarks and leptons, manifest so different masses if they all start as massless?

iii. Why are charges of quarks and leptons so different and why have the left handed family members so different charges from the right handed ones?

iv. Where do antiquarks and antileptons originate?

v. Where do families of quarks and leptons originate and how many families do exist?

vi. What is the origin of boson fields, of vector fields which are the gauge fields of fermions?

vii. What is the origin of the Higgs's scalars and the Yukawa couplings?

viii. How are scalar fields connected with the origin of families and how many scalar fields determine properties of the so far (and others possibly be) observed fermions and of weak bosons?

ix. Why have the scalar fields half integer weak and hyper charge? Do possibly exist also scalar fields with the colour charges in the fundamental representation ?

ix. Could all boson fields, with the scalar fields included, have a common origin?

x. Where does the *dark matter* originate? Does the *dark matter* consist of fermions?

xi. Where does the "ordinary" matter-antimatter asymmetry originate?

xii. Where does the dark energy originate?

xiii. How can we understand the postulates of the second quantized fermion and boson fields?

xiv. What is the dimension of space? $(3 + 1)$?, $((d − 1) + 1)$?, ∞?

xv. Are all the fields indeed second quantized with the gravity included? And consequently are all the systems second quantized (although we can treat them in simplified versions, like it is the first quantization and even the classical treatment), with the black holes included?

xvi. And many others.

---

[1] This introduction is similar to the one appearing in the arxiv:2210.07004. Also most of sections and subsections are similar. There are, however, some new parts added.

In a long series of works ([1–3, 5, 23, 25, 27–29, 31, 32] and the references therein), the author has succeeded, together with collaborators, to find the answer to many of the above, and also to other open questions of the *standard model*, as well as to several open cosmological questions, with the model named the *spin-charge-family* theory. The more work is put into the theory the more answers the theory offers. The theory assumes that the space has more than $(3 + 1)$ dimensions, it must have $d \geq (13 + 1)$, so that the subgroups of the $SO(13, 1)$ group, describing the internal space of fermions by the superposition of odd products of the Clifford objects γ^a's, manifest from the point of view of $d = (3 + 1)$-dimensional space the spins, handedness and charges assumed for massless fermions in the *standard model*. Correspondingly each irreducible representation of the $SO(13, 1)$ group carrying the quantum numbers of quarks and leptons and antiquarks and antileptons, represents one of families of fermions, the quantum numbers of which are determined by the second kind of the Clifford objects, by $\tilde{\gamma}^a$ (by $\tilde{S}^{ab}$ $(= \frac{i}{4} \{\tilde{\gamma}^a, \tilde{\gamma}^b\}_-)$).

Fermions interact in $d = (13 + 1)$ with gravity only, with vielbeins (the gauge fields of momenta) and the two kinds of the spin connection fields, the gauge fields of the two kinds of the Lorentz transformations in the internal space of fermions, of $S^{ab} (= \frac{i}{4} \{\gamma^a, \gamma^b\}_-)$ and of $\tilde{S}^{ab}$ $(= \frac{i}{4} \{\tilde{\gamma}^a, \tilde{\gamma}^b\}_-)$.

The theory assumes a simple starting action ([5] and the references therein) for the second quantized massless fermion and antifermion fields, and the corresponding massless boson fields in $d = 2(2n + 1)$-dimensional space

$$\mathcal{A} = \int d^d x \, E \, \frac{1}{2} \, (\bar{\psi} \gamma^a p_{0a} \psi) + h.c. +$$

$$\int d^d x \, E \, (\alpha R + \tilde{\alpha} \tilde{R}),$$

$$p_{0a} = f^\alpha{}_a p_{0\alpha} + \frac{1}{2E} \{p_\alpha, E f^\alpha{}_a\}_-,$$

$$p_{0\alpha} = p_\alpha - \frac{1}{2} S^{ab} \omega_{ab\alpha} - \frac{1}{2} \tilde{S}^{ab} \tilde{\omega}_{ab\alpha},$$

$$R = \frac{1}{2} \{f^{\alpha[a} f^{\beta b]} \, (\omega_{ab\alpha,\beta} - \omega_{ca\alpha} \omega^c{}_{b\beta})\} + h.c.,$$

$$\tilde{R} = \frac{1}{2} \{f^{\alpha[a} f^{\beta b]} \, (\tilde{\omega}_{ab\alpha,\beta} - \tilde{\omega}_{ca\alpha} \tilde{\omega}^c{}_{b\beta})\} + h.c.. \qquad (11.1)$$

Here [2] $f^{\alpha[a} f^{\beta b]} = f^{\alpha a} f^{\beta b} - f^{\alpha b} f^{\beta a}$. f^a_α, and the two kinds of the spin connection fields, $\omega_{ab\alpha}$ (the gauge fields of S^{ab}) and $\tilde{\omega}_{ab\alpha}$ (the gauge fields of $\tilde{S}^{ab}$), manifest in $d = (3 + 1)$ as the known vector gauge fields and the scalar gauge fields taking

---

[2] $f^\alpha{}_a$ are inverted vielbeins to $e^a{}_\alpha$ with the properties $e^a{}_\alpha f^\alpha{}_b = \delta^a{}_b$, $e^a{}_\alpha f^\beta{}_a = \delta^\beta_\alpha$, $E = \det(e^a{}_\alpha)$. Latin indices $a, b, .., m, n, .., s, t, ..$ denote a tangent space (a flat index), while Greek indices $\alpha, \beta, .., \mu, \nu, ..\sigma, \tau, ..$ denote an Einstein index (a curved index). Letters from the beginning of both the alphabets indicate a general index ($a, b, c, ..$ and $\alpha, \beta, \gamma, ..$), from the middle of both the alphabets the observed dimensions $0, 1, 2, 3$ ($m, n, ..$ and $\mu, \nu, ..$), indexes from the bottom of the alphabets indicate the compactified dimensions ($s, t, ..$ and $\sigma, \tau, ..$). We assume the signature $\eta^{ab} = diag\{1, -1, -1, \cdots, -1\}$.

care of masses of quarks and leptons and antiquarks and antileptons and the weak boson fields [27] [3]

While in any even dimensional space the superposition of odd products of γ^a's, forming the Clifford odd "basis vectors", offer the description of the internal space of fermions with the half integer spins, (manifesting in $d = (3+1)$ properties of quarks and leptons and antiquarks and antileptons, with the families included if $d = (13+1)$, the superposition of even products of γ^a's, forming the Clifford even "basis vectors", offer the description of the internal space of boson fields with integer spins, manifesting as gauge fields of the corresponding Clifford odd "basis vectors".

From the point of view of $d = (3+1)$ one family of the Clifford odd "basis vectors" with $2^{\frac{d=14}{2}-1}$ members manifest spins, handedness and charges of quarks and leptons and antiquarks and antileptons appearing in $2^{\frac{d=14}{2}-1}$ families, while their Hermitian conjugated partners appear in another group of $2^{\frac{d}{2}-1}$ members in $2^{\frac{d}{2}-1}$ families [4].

The Clifford even "basis vectors" appear in two groups, each with $2^{\frac{d}{2}-1} \times 2^{\frac{d}{2}-1}$ members, with the Hermitian conjugated partners within the same group and have correspondingly no families. The Clifford even "basis vectors" manifest from the point of view of $d = (3+1)$ all the properties of the vector gauge fields before the electroweak break and for the scalar fields causing the electroweak break (as assumed by the *standard model*).

Tensor products of the Clifford odd and Clifford even "basis vectors" (describing the internal space of fermions and bosons, respectively) with the basis in ordinary space form the creation operators to which the "basis vectors" transfer either anticommutativity or commutativity. The Clifford odd "basis vectors" transfer their anticommutativity to creation operators and to their Hermitian conjugated partners annihilation operators for fermions. The Clifford even "basis vectors" transfer their commutativity to creation operators and annihilation operators for bosons. Correspondingly the anticommutation properties of creation and annihilation operators of fermions explain the second quantization postulates of Dirac for fermion fields, while the commutation properties of creation and annihilation operators for bosons explain the corresponding second quantization postulates for boson fields [5].

In Sect. 11.2 the Grassmann and the Clifford algebra are explained and creation and annihilation operators described as a tensor products of the "basis vectors"

---

[3] Since the multiplication with either γ^a's or $\tilde{\gamma}^a$'s changes the Clifford odd "basis vectors" into the Clifford even objects, and even "basis vectors" commute, the action for fermions can not include an odd numbers of γ^a's or $\tilde{\gamma}^a$'s, what the simple starting action of Eq. (19.1) does not. In the starting action γ^a's and $\tilde{\gamma}^a$'s appear as $\gamma^0\gamma^a\hat{p}_a$ or as $\gamma^0\gamma^c S^{ab}\omega_{abc}$ and as $\gamma^0\gamma^c \tilde{S}^{ab}\tilde{\omega}_{abc}$.

[4] The appearance of the condensate of two right handed neutrinos causes that the number of the observed families reduces to two at low energies decoupled groups of four groups.

[5] The creation and annihilation operators for either fermion or boson fields with the momenta zero, have no dynamics, and consequently no influence on clusters of fermion and boson fields.

offering explanation of the internal spaces of fermion (by the Clifford odd algebra) and boson (by the Clifford even algebra) fields and the basis in ordinary space.
In Subsect. 11.2.1 the "basis vectors" are introduced and their properties presented.
In Subsect. 11.2.2 the properties of the Clifford odd and even "basis vectors" are demonstrated in the toy model in $d = (5 + 1)$. The simplest cases with $d = (1 + 1)$ and $d = (3 + 1)$ are also added.
In Subsect. 11.2.3 the properties of the creation and annihilation operators for the second quantized fields are described.
In Sect. 11.3 a short overview of the achievements and predictions so far of the *spin-charge-family* theory is presented,
Sect. 11.4 presents what the reader could learn from the main contribution of this talk.
In Sect. 11.5 the properties of Clifford odd and Clifford even "basis vectors" in odd dimensional spaces are presented, demonstrating how much properties of "basis vectors" in odd dimensional spaces differ from the properties in even dimensional spaces.

11.2   Creation and annihilation operators for fermions and bosons

The second quantization postulates for fermions [16–18] require that the creation operators and their Hermitian conjugated partners annihilation operators, depending on a finite dimensional basis in internal space, that is on the space of half integer spins and on charges described by the fundamental representations of the appropriate groups, and on continuously infinite number of momenta (or coordinates) ([5], Subsect. 3.3.1), fulfil anticommutation relations.
The second quantization postulates for bosons [16–18] require that the creation and annihilation operators, depending on finite dimensional basis in internal space, that is on the space of integer spins and on charges described by the adjoint representations of the same groups, and on continuously infinite number of momenta (or coordinates) ([5], Subsect. 3.3.1), fulfil commutation relation.
I demonstrate in this talk that using the Clifford algebra to describe the internal space of fermions and bosons, the creation and annihilation operators which are tensor products of the internal basis and the momentum/coordinate basis, not only fulfil the appropriate anticommutation relations (for fermions) or commutation relations (for bosons) but also have the required properties for either fermion fields (if the internal space is described with the Clifford odd products of γ^a's) or for boson fields (if the internal space is described with the Clifford even products of γ^a's). The Clifford odd and Clifford even "basic vectors" correspondingly offer the explanation for the second quantization postulates for fermions and bosons, respectively.
There are two Clifford subalgebras which can be used to describe the internal space of fermions and of bosons, each with 2^d members. In each of the two subalgebras there are $2 \times 2^{\frac{d}{2}-1} \times 2^{\frac{d}{2}-1}$ Clifford odd and $2 \times 2^{\frac{d}{2}-1} \times 2^{\frac{d}{2}-1}$ Clifford even "basic vectors" which can be used to describe the internal space of fermion fields, the

Clifford odd "basic vectors", and of boson fields, the Clifford even "basic vectors" in any even d. d $= (13 + 1)$ offers the explanation for all the properties of fermion fields, with families included, and of boson fields which are the gauge fields of fermion fields.

In any even d, d $= 2(2n + 1)$ or d $= 4n$, any of the two Clifford subalgebras offers twice $2^{\frac{d}{2}-1}$ irreducible representations, each with $2^{\frac{d}{2}-1}$ members, which can represent "basis vectors" and their Hermitian conjugated partners. Each irreducible representation offers in d $= (13 + 1)$ the description of the quarks and the antiquarks and the leptons and the antileptons (with the right handed neutrinos and left handed antineutrinos included in addition to what is) assumed by the *standard model*.

There are obviously only one kind of fermion fields and correspondingly also of their gauge fields observed. There is correspondingly no need for two Clifford subalgebras.

The reduction of the two subalgebras to only one with the postulate in Eq. (19.6), (Ref. [5], Eq. (38)) solves this problem. At the same time the reduction offers the quantum numbers for each of the irreducible representations of the Clifford subalgbebra left, γ^a's, when fermions are concerned ([5] Subsect. 3.2).

Boson fields have no families as it will be demonstrated.

Grassmann and Clifford algebras

The internal space of anticommuting or commuting second quantized fields can be described by using either the Grassmann or the Clifford algebras [1–3,31]. What follows is a short overview of Subsect.3.2 of Ref. [5] and of references cited in [5]. In Grassmann d-dimensional space there are d anticommuting (operators) θ^a, and d anticommuting operators which are derivatives with respect to θ^a, $\frac{\partial}{\partial\theta_a}$,

$$\{\theta^a, \theta^b\}_+ = 0, \qquad \{\frac{\partial}{\partial\theta_a}, \frac{\partial}{\partial\theta_b}\}_+ = 0,$$

$$\{\theta_a, \frac{\partial}{\partial\theta_b}\}_+ = \delta_{ab}, (a, b) = (0, 1, 2, 3, 5, \cdots, d). \qquad (11.2)$$

Defining [32]

$$(\theta^a)^\dagger = \eta^{aa}\frac{\partial}{\partial\theta_a}, \quad \text{leads to} \quad (\frac{\partial}{\partial\theta_a})^\dagger = \eta^{aa}\theta^a, \qquad (11.3)$$

with $\eta^{ab} = diag\{1, -1, -1, \cdots, -1\}$.

θ^a and $\frac{\partial}{\partial\theta_a}$ are, up to the sign, Hermitian conjugated to each other. The identity is the self adjoint member of the algebra. The choice for the following complex properties of θ^a and correspondingly of $\frac{\partial}{\partial\theta_a}$ are made

$$\{\theta^a\}^* = (\theta^0, \theta^1, -\theta^2, \theta^3, -\theta^5, \theta^6, ..., -\theta^{d-1}, \theta^d),$$

$$\{\frac{\partial}{\partial\theta_a}\}^* = (\frac{\partial}{\partial\theta_0}, \frac{\partial}{\partial\theta_1}, -\frac{\partial}{\partial\theta_2}, \frac{\partial}{\partial\theta_3}, -\frac{\partial}{\partial\theta_5}, \frac{\partial}{\partial\theta_6}, ..., -\frac{\partial}{\partial\theta_{d-1}}, \frac{\partial}{\partial\theta_d}). \quad (11.4)$$

The are 2^d superposition of products of θ^a, the Hermitian conjugated partners of which are the corresponding superposition of products of $\frac{\partial}{\partial\theta_a}$.

There exist two kinds of the Clifford algebra elements (operators), γ^a and $\tilde{\gamma}^a$, expressible with θ^a's and their conjugate momenta $p^{\theta a} = i \frac{\partial}{\partial \theta_a}$ [2], Eqs. (11.2, 11.3),

$$\gamma^a = (\theta^a + \frac{\partial}{\partial \theta_a}), \quad \tilde{\gamma}^a = i(\theta^a - \frac{\partial}{\partial \theta_a}),$$
$$\theta^a = \frac{1}{2}(\gamma^a - i\tilde{\gamma}^a), \quad \frac{\partial}{\partial \theta_a} = \frac{1}{2}(\gamma^a + i\tilde{\gamma}^a),$$

$$(11.5)$$

offering together $2 \cdot 2^d$ operators: 2^d are superposition of products of γ^a and 2^d of $\tilde{\gamma}^a$. It is easy to prove, if taking into account Eqs. (11.3, 11.5), that they form two anticommuting Clifford subalgebras, $\{\gamma^a, \tilde{\gamma}^b\}_+ = 0$, Refs. ([5] and references therein)

$$\{\gamma^a, \gamma^b\}_+ = 2\eta^{ab} = \{\tilde{\gamma}^a, \tilde{\gamma}^b\}_+ ,$$
$$\{\gamma^a, \tilde{\gamma}^b\}_+ = 0, \quad (a, b) = (0, 1, 2, 3, 5, \cdots, d),$$
$$(\gamma^a)^\dagger = \eta^{aa} \gamma^a, \quad (\tilde{\gamma}^a)^\dagger = \eta^{aa} \tilde{\gamma}^a .$$

$$(11.6)$$

While the Grassmann algebra offers the description of the "anticommuting integer spin second quantized fields" and of the "commuting integer spin second quantized fields" [5,35], the Clifford algebras which are superposition of odd products of either γ^a's or $\tilde{\gamma}^a$'s offer the description of the second quantized half integer spin fermion fields, which from the point of the subgroups of the $SO(d-1, 1)$ group manifest spins and charges of fermions and antifermions in the fundamental representations of the group and subgroups.

The superposition of even products of either γ^a's or $\tilde{\gamma}^a$'s offer the description of the commuting second quantized boson fields with integer spins (as we can see in [9] and shall see in this contribution) which from the point of the subgroups of the $SO(d-1, 1)$ group manifest spins and charges in the adjoint representations of the group and subgroups.

The following *postulate*, which determines how does $\tilde{\gamma}^a$'s operate on γ^a's, reduces the two Clifford subalgebras, γ^a's and $\tilde{\gamma}^a$'s, to one, to the one described by γ^a's [2, 14, 29, 31, 32]

$$\{\tilde{\gamma}^a B = (-)^B i B \gamma^a\} |\psi_{oc} >,$$

$$(11.7)$$

with $(-)^B = -1$, if B is (a function of) an odd products of γ^a's, otherwise $(-)^B = 1$ [14], $|\psi_{oc} >$ is defined in Eq. (19.8) of Subsect. 11.2.1.

After the postulate of Eq. (19.6) it follows:

a. The Clifford subalgebra described by $\tilde{\gamma}^a$'s looses its meaning for the description of the internal space of quantum fields.

b. The "basis vectors" which are superposition of an odd or an even products of γ^a's obey the postulates for the second quantization fields for fermions or bosons, respectively, Sect.11.2.1.

c. It can be proven that the relations presented in Eq. (19.3) remain valid also after

the postulate of Eq. (19.6). The proof is presented in Ref. ([5], App. I, Statement 3a.

d. Each irreducible representation of the Clifford odd "basis vectors" described by γ^a's are equipped by the quantum numbers of the Cartan subalgebra members of $\tilde{S}^{ab}$, chosen in Eq. (19.4), as follows

$$
\begin{aligned}
& \mathcal{S}^{03}, \mathcal{S}^{12}, \mathcal{S}^{56}, \cdots, \mathcal{S}^{d-1\,d}, \\
& S^{03}, S^{12}, S^{56}, \cdots, S^{d-1\,d}, \\
& \tilde{S}^{03}, \tilde{S}^{12}, \tilde{S}^{56}, \cdots, \tilde{S}^{d-1\,d}, \\
& \mathcal{S}^{ab} = S^{ab} + \tilde{S}^{ab} = i\,(\theta^a \frac{\partial}{\partial \theta_b} - \theta^b \frac{\partial}{\partial \theta_a}).
\end{aligned}
\tag{11.8}
$$

After the postulate of Eq. (19.6) no vector space of $\tilde{\gamma}^a$'s needs to be taken into account for the description of the internal space of either fermions or bosons, in agreement with the observed properties of fermions and bosons. Also the Grassmann algebra is reduced to only one of the Clifford subalgebras. The operators $\tilde{\gamma}^a$'s describe from now on properties of fermion and boson "basis vectors" determined by superposition of products of odd or even numbers of γ^a's, respectively.

$\tilde{\gamma}^a$'s equip each irreducible representation of the Lorentz group (with the infinitesimal generators $S^{ab} = \frac{i}{4}\{\gamma^a, \gamma^b\}_-$) when applying on the Clifford odd "basis vectors" (which are superposition of odd products of $\gamma^{a's}$) with the family quantum numbers (determined by $\tilde{S}^{ab} = \frac{i}{4}\{\tilde{\gamma}^a, \tilde{\gamma}^b\}_-$).

Correspondingly the Clifford odd "basis vectors" (they are superposition of an odd products of γ^a's) form $2^{\frac{d}{2}-1}$ families, with the quantum number f, each family have $2^{\frac{d}{2}-1}$ members, m. They offer the description of the second quantized fermion fields.

The Clifford even "basis vectors" (they are superposition of an even products of γ^a's) have no families as we shall see in what follows, but they do carry both quantum numbers, f and m. They offer the description of the second quantized boson fields as the gauge fields of the second quantized fermion fields. The generators of the Lorentz transformations in the internal space of the Clifford even "basis vectors" are $\mathcal{S}^{ab} = S^{ab} + \tilde{S}^{ab}$.

Properties of the Clifford odd and the Clifford even "basis vectors" are discussed in the next subsection.

11.2.1 "Basis vectors" of fermions and bosons

After the reduction of the two Clifford subalgebras to only one, Eq. (19.6), we only need to define "basis vectors" for the case that the internal space of second quantized fields is described by superposition of odd or even products γ^a's [6].

Let us use the technique which makes "basis vectors" products of nilpotents and projectors [2, 3, 13, 14] which are eigenvectors of the (chosen) Cartan subalgebra

---

[6] In Ref. [5] the reader can find in Subsects. (3.2.1 and 3.2.2) definitions for the "basis vectors" for the Grassmann and the two Clifford subalgebras, which are products of nilpotents and projectors chosen to be eigenvactors of the corresponding Cartan subalgebra members of the Lorentz algebras presented in Eq. (19.4).

members, Eq. (19.4), of the Lorentz algebra in the space of γ^a's, either in the case of the Clifford odd or in the case of the Clifford even products of γ^a's .

There are $\frac{d}{2}$ members of the Cartan subalgebra, Eq. (19.4), in even dimensional spaces.

One finds for any of the $\frac{d}{2}$ Cartan subalgebra member, S^{ab} or $\tilde{S}^{ab}$, both applying on a nilpotent $\overset{ab}{(k)}$ or on projector $\overset{ab}{[k]}$

$$\overset{ab}{(k)} := \frac{1}{2}(\gamma^a + \frac{\eta^{aa}}{ik}\gamma^b)\,, \quad (\overset{ab}{(k)})^2 = 0\,,$$

$$\overset{ab}{[k]} := \frac{1}{2}(1 + \frac{i}{k}\gamma^a\gamma^b)\,, \quad (\overset{ab}{[k]})^2 = \overset{ab}{[k]}$$

the relations

$$S^{ab}\,\overset{ab}{(k)} = \frac{k}{2}\,\overset{ab}{(k)}\,, \qquad \tilde{S}^{ab}\,\overset{ab}{(k)} = \frac{k}{2}\,\overset{ab}{(k)}\,,$$

$$S^{ab}\,\overset{ab}{[k]} = \frac{k}{2}\,\overset{ab}{[k]}\,, \qquad \tilde{S}^{ab}\,\overset{ab}{[k]} = -\frac{k}{2}\,\overset{ab}{[k]}\,, \qquad (11.9)$$

with $k^2 = \eta^{aa}\eta^{bb}$, demonstrating that the eigenvalues of S^{ab} on nilpotents and projectors expressed with γ^a's differ from the eigenvalues of $\tilde{S}^{ab}$ on nilpotents and projectors expressed with γ^a's, so that $\tilde{S}^{ab}$ can be used to equip each irreducible representation of S^{ab} with the "family" quantum number. [7]

We define in even d the "basis vectors" as algebraic, $*_A$, products of nilpotents and projectors so that each product is eigenvector of all $\frac{d}{2}$ Cartan subalgebra members. We recognize in advance that the superposition of an odd products of γ^a's, that is the Clifford odd "basis vectors", must include an odd number of nilpotents, at least one, while the superposition of an even products of γ^a"s, that is Clifford even "basis vectors", must include an even number of nilpotents or only projectors.

To define the Clifford odd "basis vectors", we shall see that they have properties appropriate to describe the internal space of the second quantized fermion fields, and the Clifford even "basis vectors", we shall see that they have properties appropriate to describe the internal space of the second quantized boson fields, we need to know the relations for nilpotents and projectors

$$\overset{ab}{(k)} := \frac{1}{2}(\gamma^a + \frac{\eta^{aa}}{ik}\gamma^b)\,, \quad \overset{ab}{[k]} := \frac{1}{2}(1 + \frac{i}{k}\gamma^a\gamma^b)\,,$$

$$\overset{ab}{(\tilde{k})} := \frac{1}{2}(\tilde{\gamma}^a + \frac{\eta^{aa}}{ik}\tilde{\gamma}^b)\,, \quad \overset{ab}{[\tilde{k}]} := \frac{1}{2}(1 + \frac{i}{k}\tilde{\gamma}^a\tilde{\gamma}^b)\,, \qquad (11.10)$$

---

[7] The reader can find the proof of Eq. (19.7) in Ref. [5], App. (I).

which can be derived after taking into account Eq. (19.3)

$$\gamma^a \stackrel{ab}{(k)} = \eta^{aa} \stackrel{ab}{[-k]}, \quad \gamma^b \stackrel{ab}{(k)} = -ik \stackrel{ab}{[-k]}, \quad \gamma^a \stackrel{ab}{[k]} = \stackrel{ab}{(-k)}, \quad \gamma^b \stackrel{ab}{[k]} = -ik\eta^{aa} \stackrel{ab}{(-k)},$$

$$\tilde{\gamma}^a \stackrel{ab}{(k)} = -i\eta^{aa} \stackrel{ab}{[k]}, \quad \tilde{\gamma}^b \stackrel{ab}{(k)} = -k \stackrel{ab}{[k]}, \quad \tilde{\gamma}^a \stackrel{ab}{[k]} = i \stackrel{ab}{(k)}, \quad \tilde{\gamma}^b \stackrel{ab}{[k]} = -k\eta^{aa} \stackrel{ab}{(k)},$$

$$\stackrel{ab}{(k)}^\dagger = \eta^{aa} \stackrel{ab}{(-k)}, \quad (\stackrel{ab}{(k)})^2 = 0, \quad \stackrel{ab}{(k)}\stackrel{ab}{(-k)} = \eta^{aa} \stackrel{ab}{[k]},$$

$$\stackrel{ab}{[k]}^\dagger = \stackrel{ab}{[k]}, \quad (\stackrel{ab}{[k]})^2 = \stackrel{ab}{[k]}, \quad \stackrel{ab}{[k]}\stackrel{ab}{[-k]} = 0,$$

$$\stackrel{ab}{(k)}\stackrel{ab}{[k]} = 0, \quad \stackrel{ab}{[k]}\stackrel{ab}{(k)} = \stackrel{ab}{(k)}, \quad \stackrel{ab}{(k)}\stackrel{ab}{[-k]} = \stackrel{ab}{(k)}, \quad \stackrel{ab}{[k]}\stackrel{ab}{(-k)} = 0,$$

$$\stackrel{ab}{(\tilde{k})}^\dagger = \eta^{aa} \stackrel{ab}{(-\tilde{k})}, \quad (\stackrel{ab}{(\tilde{k})})^2 = 0, \quad \stackrel{ab}{(\tilde{k})}\stackrel{ab}{(-\tilde{k})} = \eta^{aa} \stackrel{ab}{[\tilde{k}]},$$

$$\stackrel{ab}{[\tilde{k}]}^\dagger = \stackrel{ab}{[\tilde{k}]}, \quad (\stackrel{ab}{[\tilde{k}]})^2 = \stackrel{ab}{[\tilde{k}]}, \quad \stackrel{ab}{[\tilde{k}]}\stackrel{ab}{[-\tilde{k}]} = 0,$$

$$\stackrel{ab}{(\tilde{k})}\stackrel{ab}{[\tilde{k}]} = 0, \quad \stackrel{ab}{[\tilde{k}]}\stackrel{ab}{(\tilde{k})} = \stackrel{ab}{(\tilde{k})}, \quad \stackrel{ab}{(\tilde{k})}\stackrel{ab}{[-\tilde{k}]} = \stackrel{ab}{(\tilde{k})}, \quad \stackrel{ab}{[\tilde{k}]}\stackrel{ab}{(-\tilde{k})} = 0. \tag{11.11}$$

Looking at relations in Eq. (19.9) it is obvious that the properties of the "basis vectors" which include odd number of nilpotents differ essentially from the "basis vectors" which include even number of nilpotents.
One namely recognizes:

i. Since the Hermitian conjugated partner of a nilpotent $\stackrel{ab}{(k)}^\dagger$ is $\eta^{aa} \stackrel{ab}{(-k)}$ and since neither S^{ab} nor $\tilde{S}^{ab}$ nor both can transform odd products of nilpotents to belong to one of the $2^{\frac{d}{2}-1}$ members of one of $2^{\frac{d}{2}-1}$ irreducible representations (families), the Hermitian conjugated partners of the Clifford odd "basis vectors" must belong to a different group of $2^{\frac{d}{2}-1}$ members of $2^{\frac{d}{2}-1}$ families.

Since S^{ac} transforms $\stackrel{ab}{(k)} *_A \stackrel{cd}{(k')}$ into $\stackrel{ab}{[-k]} *_A \stackrel{cd}{[-k']}$, while $\tilde{S}^{ab}$ transforms $\stackrel{ab}{[-k]} *_A \stackrel{cd}{[-k']}$ into $\stackrel{ab}{(-k)} *_A \stackrel{cd}{(-k')}$ it is obvious that the Hermitian conjugated partners of the Clifford odd "basis vectors" must belong to the same group of $2^{\frac{d}{2}-1} \times 2^{\frac{d}{2}-1}$ members. Projectors are self adjoint.

ii. Since an odd products of γ^a's anticommute with another group of an odd product of γ^a, the Clifford odd "basis vectors" anticommute, manifesting in a tensor product with the basis in ordinary space together with the corresponding Hermitian conjugated partners properties of the anticommutation relations postulated by Dirac for the second quantized fermion fields.
The Clifford even "basis vectors" correspondingly fulfil the commutation relations for the second quantized boson fields.

iii. The Clifford odd "basis vectors" have all the eigenvalues of the Cartan subalgebra members equal to either $\pm\frac{1}{2}$ or to $\pm\frac{i}{2}$.
The Clifford even "basis vectors" have all the eigenvalues of the Cartan subalgebra members $\mathcal{S}^{ab}$ equal to either ± 1 and zero or to $\pm i$ and zero.

Let us define odd an even "basis vectors" as products of nilpotents and projectors in even dimensional spaces.

a. *Clifford odd "basis vectors"*

The Clifford odd "basis vectors" must be products of an odd number of nilpotents and the rest, up to $\frac{d}{2}$, of projectors, each nilpotent and projector must be the "eigenstate" of one of the members of the Cartan subalgebra, Eq. (19.4), correspondingly are the "basis vectors" eigenstates of all the members of the Lorentz algebras: S^{ab}'s determine $2^{\frac{d}{2}-1}$ members of one family, $\tilde{S}^{ab}$'s transform each member of one family to the same member of the rest of $2^{\frac{d}{2}-1}$ families.

Let us name the Clifford odd "basis vectors" $\hat{b}_f^{m\dagger}$, where m determines membership of 'basis vectors' in any family and f determines a particular family. The Hermitian conjugated partner of $\hat{b}_f^{m\dagger}$ is named by $\hat{b}_f^{m} = (\hat{b}_f^{m\dagger})^{\dagger}$.

Let us start in $d = 2(2n + 1)$ with the "basis vector" $\hat{b}_1^{1\dagger}$ which is the product of only nilpotents, all the rest members belonging to the $f = 1$ family follow by the application of $S^{01}, S^{03}, \ldots, S^{0d}, S^{15}, \ldots, \tilde{S}^{1d}, S^{5d} \ldots, S^{d-2\,d}$. The algebraic product mark $*_A$ is skipped.

$$d = 2(2n + 1),$$

$$\hat{b}_1^{1\dagger} = \overset{03}{(+i)}\overset{12}{(+)}\overset{56}{(+)} \cdots \overset{d-1\,d}{(+)},$$

$$\hat{b}_1^{2\dagger} = \overset{03}{[-i]}\overset{12}{[-]}\overset{56}{(+)} \cdots \overset{d-1\,d}{(+)},$$

$$\cdots$$

$$\hat{b}_1^{2^{\frac{d}{2}-1}\dagger} = \overset{03}{[-i]}\overset{12}{[-]}\overset{56}{(+)} \ldots \overset{d-3\,d-2}{[-]}\overset{d-1\,d}{[-]},$$

$$\cdots. \tag{11.12}$$

The Hermitian conjugated partners of the Clifford odd "basis vector" $\hat{b}_1^{m\dagger}$, presented in Eq. (11.12), are

$$d = 2(2n + 1),$$

$$\hat{b}_1^{1} = \overset{03}{(-i)}\overset{12}{(-)} \cdots \overset{d-1\,d}{(-)},$$

$$\hat{b}_1^{2} = \overset{03}{[-i]}\overset{12}{[-]}\overset{56}{(-)} \cdots \overset{d-1\,d}{(-)},$$

$$\cdots$$

$$\hat{b}_1^{2^{\frac{d}{2}-1}\dagger} = \overset{03}{[-i]}\overset{12}{[-]}\overset{56}{(-)}\overset{78}{[-]} \ldots \overset{d-3\,d-2}{[-]}\overset{d-1\,d}{[-]},$$

$$\cdots. \tag{11.13}$$

In $d = 4n$ the choice of the starting "basis vector" with maximal number of nilpotents must have one projector

$$d = 4n,$$

$$\hat{b}_1^{1\dagger} = \overset{03}{(+i)}\overset{12}{(+)} \cdots \overset{d-1\,d}{[+]},$$

$$\hat{b}_1^{2\dagger} = \overset{03}{[-i]}\overset{12}{[-]}\overset{56}{(+)} \cdots \overset{d-1\,d}{[+]},$$

$$\cdots$$

$$\hat{b}_1^{2^{\frac{d}{2}-1}\dagger} = \overset{03}{[-i]}\overset{12}{[-]}\overset{56}{(+)} \ldots \overset{d-3\,d-2}{[-]}\overset{d-1\,d}{[+]},$$

$$\cdots. \tag{11.14}$$

The Hermitian conjugated partners of the Clifford odd "basis vector" $\hat{b}_1^{m\dagger}$, presented in Eq. (11.14), follow if all nilpotents $\overset{ab}{(k)}$ are transformed into $\eta^{aa} \overset{ab}{(-k)}$. For either $d = 2(2n + 1)$ or for $d = 4n$ all the $2^{\frac{d}{2}-1}$ families follow by applying $\tilde{S}^{ab}$'s on all the members of the starting family. (Or one can find the starting $\hat{b}_f^1$ for all families f and then generate all the members $\hat{b}_f^m$ from $\hat{b}_f^1$ by the application of $\tilde{S}^{ab}$ on the starting member.)

It is not difficult to see that all the "basis vectors" within any family as well as the "basis vectors" among families are orthogonal, that is their algebraic product is zero, and the same is true for the Hermitian conjugated partners, what can be proved by the algebraic multiplication using Eq.(19.9).

$$\hat{b}_f^{m\dagger} *_A \hat{b}_{f'}^{m'\dagger} = 0, \quad \hat{b}_f^m *_A \hat{b}_{f'}^{m'} = 0, \quad \forall m, m', f, f'. \tag{11.15}$$

If we require that each family of "basis vectors", determined by nilpotents and projectors described by γ^a's, carries the family quantum number determined by $\tilde{S}^{ab}$ and define the vacuum state on which "basis vectors" apply as

$$|\psi_{oc}> = \sum_{f=1}^{2^{\frac{d}{2}-1}} \hat{b}_f^m *_A \hat{b}_f^{m\dagger} |1>, \tag{11.16}$$

it follows that the Clifford odd "basis vectors" obey the relations

$$\hat{b}_f^m *_A |\psi_{oc}> = 0.|\psi_{oc}>,$$
$$\hat{b}_f^{m\dagger} *_A |\psi_{oc}> = |\psi_f^m>,$$
$$\{\hat{b}_f^m, \hat{b}_{f'}^{m'}\}_{*A+}|\psi_{oc}> = 0.|\psi_{oc}>,$$
$$\{\hat{b}_f^{m\dagger}, \hat{b}_{f'}^{m'\dagger}\}_{*A+}|\psi_{oc}> = 0.|\psi_{oc}>,$$
$$\{\hat{b}_f^m, \hat{b}_f^{m'\dagger}\}_{*A+}|\psi_{oc}> = \delta^{mm'}\delta_{ff'}|\psi_{oc}>, \tag{11.17}$$

while the normalization $<\psi_{oc}|\hat{b}_{f'}^{m'\dagger} *_A \hat{b}_f^{m\dagger} *_A |\psi_{oc}> = \delta^{mm'}\delta_{ff'}$ is used and the anticommutation relation mean $\{\hat{b}_f^{m\dagger}, \hat{b}_{f'}^{m'\dagger}\}_{*A+} = \hat{b}_f^{m\dagger} *_A \hat{b}_{f'}^{m'\dagger} + \hat{b}_{f'}^{m'\dagger} *_A \hat{b}_f^{m\dagger}$. If we write the creation and annihilation operators as the tensor, $*_T$, products of "basis vectors" and the basis in ordinary space, the creation and annihilation operators fulfil the Dirac's anticommutation postulates since the "basis vectors" transfer their anticommutativity to creation and annihilation operators. It turns out that not only the Clifford odd "basis vectors" offer the description of the internal space of fermions, they offer the explanation for the second quantization postulates for fermions as well.

Table 11.1, presented in Subsect. 11.2.2, illustrates the properties of the Clifford odd "basis vectors" on the case of $d = (5 + 1)$.

b. *Clifford even "basis vectors"*

The Clifford even "basis vectors" must be products of an even number of nilpotents and the rest, up to $\frac{d}{2}$, of projectors, each nilpotent and projector in a product must be the "eigenstate" of one of the members of the Cartan subalgebra, Eq. (19.4),

correspondingly are the "basis vectors" eigenstates of all the members of the Lorentz algebra: S^{ab}'s and $\tilde{S}^{ab}$'s generate from the starting "basis vector" all the $2^{\frac{d}{2}-1} \times 2^{\frac{d}{2}-1}$ members of one group which includes as well the Hermitian conjugated partners of any member. $2^{\frac{d}{2}-1}$ members of the group are products of projectors only. They are self adjoint.

There are two groups of Clifford even "basis vectors" with $2^{\frac{d}{2}-1} \times 2^{\frac{d}{2}-1}$ members each. The members of one group are not connected with the members of another group by either by S^{ab}'s or $\tilde{S}^{ab}$'s or both.

Let us name the Clifford even "basis vectors" $^{i}\hat{\mathcal{A}}_{f}^{m\dagger}$, where $i = (I, II)$ denotes that there are two groups of Clifford even "basis vectors", while m and f determine membership of 'basis vectors' in any of the two groups, I or II. Let me repeat that the Hermitian conjugated partner of any "basis vector" appears either in the case of $^{I}\hat{\mathcal{A}}_{f}^{m\dagger}$ or in the case of $^{II}\hat{\mathcal{A}}_{f}^{m\dagger}$ within the same group.

Let us write down the Clifford even "basis vectors" as a product of an even number of nilpotents and the rest of projectors, so that the Clifford even "basis vectors" are eigenvectors of all the Cartan subalgebra members, and let us name them as follows

$$d = 2(2n+1)$$

$$^{I}\hat{\mathcal{A}}_{1}^{1\dagger} = \overset{03}{(+i)}\overset{12}{(+)} \cdots \overset{d-1\,d}{[+]} \,, \qquad ^{II}\hat{\mathcal{A}}_{1}^{1\dagger} = \overset{03}{(-i)}\overset{12}{(+)} \cdots \overset{d-1\,d}{[+]} \,,$$

$$^{I}\hat{\mathcal{A}}_{1}^{2\dagger} = \overset{03}{[-i]}\overset{12}{[-]}\overset{56}{(+)} \cdots \overset{d-1\,d}{[+]} \,, \qquad ^{II}\hat{\mathcal{A}}_{1}^{2\dagger} = \overset{03}{[+i]}\overset{12}{[-]}\overset{56}{(+)} \cdots \overset{d-1\,d}{[+]} \,,$$

$$^{I}\hat{\mathcal{A}}_{1}^{3\dagger} = \overset{03}{(+i)}\overset{12}{(+)}\overset{56}{(+)} \cdots \overset{d-3\,d-2}{[-]}\overset{d-1\,d}{(-)} \,, \quad ^{II}\hat{\mathcal{A}}_{1}^{3\dagger} = \overset{03}{(-i)}\overset{12}{(+)}\overset{56}{(+)} \cdots \overset{d-3\,d-2}{[-]}\overset{d-1\,d}{(-)} \,,$$

$$\cdots \qquad\qquad \cdots$$

$$d = 4n$$

$$^{I}\hat{\mathcal{A}}_{1}^{1\dagger} = \overset{03}{(+i)}\overset{12}{(+)} \cdots \overset{d-1\,d}{(+)} \,, \qquad ^{II}\hat{\mathcal{A}}_{1}^{1\dagger} = \overset{03}{(-i)}\overset{12}{(+)} \cdots \overset{d-1\,d}{(+)} \,,$$

$$^{I}\hat{\mathcal{A}}_{1}^{2\dagger} = \overset{03}{[-i]}\overset{12}{[-i]}\overset{56}{(+)} \cdots \overset{d-1\,d}{(+)} \,, \qquad ^{II}\hat{\mathcal{A}}_{1}^{2\dagger} = \overset{03}{[+i]}\overset{12}{[-i]}\overset{56}{(+)} \cdots \overset{d-1\,d}{(+)} \,,$$

$$^{I}\hat{\mathcal{A}}_{1}^{3\dagger} = \overset{03}{(+i)}\overset{12}{(+)}\overset{56}{(+)} \cdots \overset{d-3\,d-2}{[-]}\overset{d-1\,d}{[-]} \,, \quad ^{II}\hat{\mathcal{A}}_{1}^{3\dagger} = \overset{03}{(-i)}\overset{12}{(+)}\overset{56}{(+)} \cdots \overset{d-3\,d-2}{[-]}\overset{d-1\,d}{[-]}$$

$$\cdots \qquad\qquad \cdots \tag{11.18}$$

There are $2^{\frac{d}{2}-1} \times 2^{\frac{d}{2}-1}$ Clifford even "basis vectors" of the kind $^{I}\hat{\mathcal{A}}_{f}^{m\dagger}$ and there are $2^{\frac{d}{2}-1} \times 2^{\frac{d}{2}-1}$ Clifford even "basis vectors" of the kind $^{II}\hat{\mathcal{A}}_{f}^{m\dagger}$.

Table 11.1, presented in Subsect. 11.2.2, illustrates properties of the Clifford odd and Clifford even "basis vectors" on the case of $d = (5 + 1)$. Looking at this particular case it is easy to evaluate properties of either even or odd "basis vectors". I shall present here the general results which follow after careful inspection of properties of both kinds of "basis vectors".

The Clifford even "basis vectors" belonging to two different groups are orthogonal due to the fact that they differ in the sign of one nilpotent or one projectors, or the algebraic products of members of one group give zero according to Eq. (19.9).

$$^{I}\hat{\mathcal{A}}_{f}^{m\dagger} *_{A} {}^{II}\hat{\mathcal{A}}_{f}^{m\dagger} = 0 = {}^{II}\hat{\mathcal{A}}_{f}^{m\dagger} *_{A} {}^{I}\hat{\mathcal{A}}_{f}^{m\dagger} \,. \tag{11.19}$$

The members of each of this two groups have the property

$$^{I,II}\hat{\mathcal{A}}_f^{m\dagger} \ *_A \ ^{I,II}\hat{\mathcal{A}}_{f'}^{m'\dagger} \to \begin{cases} ^{I,II}\hat{\mathcal{A}}_{f'}^{m\dagger}, \text{only one for } \forall f', \\ \qquad\qquad\qquad\text{or zero}. \end{cases} \tag{11.20}$$

Two "basis vectors" $^{I}\hat{\mathcal{A}}_f^{m\dagger}$ and $^{I}\hat{\mathcal{A}}_{f'}^{m'\dagger}$, the algebraic product, $*_A$, of which gives nonzero contribution, "scatter" into the third one $^{I}\hat{\mathcal{A}}_{f'}^{m\dagger}$. The same is true also for the "basis vectors" $^{II}\hat{\mathcal{A}}_f^{m\dagger}$.

Let us write the commutation relations for Clifford even "basis vectors" taking into account Eq. (11.20).

   i.   In the case that $^{I}\hat{\mathcal{A}}_f^{m\dagger} *_A {}^{I}\hat{\mathcal{A}}_{f'}^{m'\dagger} \to {}^{I}\hat{\mathcal{A}}_{f'}^{m\dagger}$ and $^{I}\hat{\mathcal{A}}_{f'}^{m'\dagger} *_A {}^{I}\hat{\mathcal{A}}_f^{m\dagger} = 0$ it follows

$$\{^{I}\hat{\mathcal{A}}_f^{m\dagger}, \ ^{I}\hat{\mathcal{A}}_{f'}^{m'\dagger}\}_{*_A -} \to \begin{cases} ^{I}\hat{\mathcal{A}}_{f'}^{m\dagger}, & (\text{if } \quad ^{I}\hat{\mathcal{A}}_f^{m\dagger} *_A {}^{I}\hat{\mathcal{A}}_{f'}^{m'\dagger} \to {}^{I}\hat{\mathcal{A}}_{f'}^{m\dagger} \\ & \text{and } \ ^{I}\hat{\mathcal{A}}_{f'}^{m'\dagger} *_A {}^{I}\hat{\mathcal{A}}_f^{m\dagger} = 0), \end{cases} \tag{11.21}$$

   ii.   In the case that $^{I}\hat{\mathcal{A}}_f^{m\dagger} *_A {}^{I}\hat{\mathcal{A}}_{f'}^{m'\dagger} \to {}^{I}\hat{\mathcal{A}}_{f'}^{m\dagger}$ and $^{I}\hat{\mathcal{A}}_{f'}^{m'\dagger} *_A {}^{I}\hat{\mathcal{A}}_f^{m\dagger} \to {}^{I}\hat{\mathcal{A}}_f^{m'\dagger}$ it follows

$$\{^{I}\hat{\mathcal{A}}_f^{m\dagger}, \ ^{I}\hat{\mathcal{A}}_{f'}^{m'\dagger}\}_{*_A -} \to \begin{cases} ^{I}\hat{\mathcal{A}}_{f'}^{m\dagger} - {}^{I}\hat{\mathcal{A}}_f^{m'\dagger}, & (\text{if } \quad ^{I}\hat{\mathcal{A}}_f^{m\dagger} *_A {}^{I}\hat{\mathcal{A}}_{f'}^{m'\dagger} \to {}^{I}\hat{\mathcal{A}}_{f'}^{m\dagger} \\ & \text{and } \ ^{I}\hat{\mathcal{A}}_{f'}^{m'\dagger} *_A {}^{I}\hat{\mathcal{A}}_f^{m\dagger} \to {}^{I}\hat{\mathcal{A}}_f^{m'\dagger}), \end{cases} \tag{11.22}$$

   iii.   In all other cases we have

$$\{^{I}\hat{\mathcal{A}}_f^{m\dagger}, \ ^{I}\hat{\mathcal{A}}_{f'}^{m'\dagger}\}_{*_A -} = 0 . \tag{11.23}$$

$\{^{I}\hat{\mathcal{A}}_f^{m\dagger}, \ ^{I}\hat{\mathcal{A}}_{f'}^{m'\dagger}\}_{*_A -}$ means $^{I}\hat{\mathcal{A}}_f^{m\dagger} *_A {}^{I}\hat{\mathcal{A}}_{f'}^{m'\dagger} - {}^{I}\hat{\mathcal{A}}_{f'}^{m'\dagger} *_A {}^{I}\hat{\mathcal{A}}_f^{m\dagger}$.

It remains to evaluate the algebraic application, $*_A$, of the Clifford even "basis vectors" $^{I}\hat{\mathcal{A}}_f^{m\dagger}$ on the Clifford odd "basis vectors" $\hat{b}_{f'}^{m'\dagger}$. One finds

$$^{I}\hat{\mathcal{A}}_{f'}^{m\dagger} *_A \hat{b}_f^{m'\dagger} \to \begin{cases} \hat{b}_f^{m\dagger}, \\ \text{or zero}. \end{cases} \tag{11.24}$$

For each $^{I}\hat{\mathcal{A}}_f^{m\dagger}$ there are among $2^{\frac{d}{2}-1} \times 2^{\frac{d}{2}-1}$ members of the Clifford odd "basis vectors" (describing the internal space of fermion fields) $2^{\frac{d}{2}-1}$ members, $\hat{b}_{f'}^{m'\dagger}$, fulfilling the relation of Eq. (11.24). All the rest $(2^{\frac{d}{2}-1} \times (2^{\frac{d}{2}-1} - 1)$, give zero contributions.

Eq. (11.24) clearly demonstrates that $^{I}\hat{\mathcal{A}}_f^{m\dagger}$ transforms the Clifford odd "basis vector" in general into another Clifford odd "basis vector", transfering to the Clifford odd "basis vector" an integer spin.

We can obviously conclude that the Clifford even "basis vectors" offer the description of the gauge fields to the corresponding fermion fields.

While the Clifford odd "basis vectors" offer the description of the internal space of the second quantized anticommuting fermion fields, appearing in families, the Clifford even "basis vectors" offer the description of the internal space of the second quantized commuting boson fields, having no families and manifesting as the gauge fields of the corresponding fermion fields.

11.2.2 Example demonstrating properties of Clifford odd and even "basis vectors" for $d = (1 + 1)$, $d = (3 + 1)$, $d = (5 + 1)$

'

Subsect. 11.2.2 demonstrates properties of the Clifford odd and even "basis vectors" in special cases when $d = (1 + 1)$, $d = (3 + 1)$, and $d = (5 + 1)$.

Let us start with the simplest case:

d=(1+1)

There are 4 ($2^{d=2}$) "eigenvectors" of the Cartan subalgebra members S^{01} and $\mathcal{S}^{01}$ of the Lorentz algebra S^{ab} and $\mathcal{S}^{ab}$, Eq. (19.4), representing one Clifford odd "basis vector" $\hat{b}_1^{1\dagger} = \overset{01}{(+i)}$ (m=1), appearing in one family (f=1) and correspondingly one Hermitian conjugated partner $\hat{b}_1^{1} = \overset{01}{(-i)}$ [8] and two Clifford even "basis vector" $^{I}\mathcal{A}_1^{1\dagger} = \overset{01}{[+i]}$ and $^{II}\mathcal{A}_1^{1\dagger} = \overset{01}{[-i]}$, each of them is self adjoint.
Correspondingly we have two Clifford odd

$$\hat{b}_1^{1\dagger} = \overset{01}{(+i)}, \quad \hat{b}_1^{1} = \overset{01}{(-i)}$$

and two Clifford even

$$^{I}\mathcal{A}_1^{1\dagger} = \overset{01}{[+i]}, \quad ^{II}\mathcal{A}_1^{1\dagger} = \overset{01}{[-i]}$$

"basis vectors".
The first two Clifford odd "basis vectors" are Hermitian conjugated to each other. I make a choice that $\hat{b}_1^{1\dagger}$ is the "basis vector", the second Clifford odd object is its Hermitian conjugated partner. Defining the handedness as $\Gamma^{(1+1)} = \gamma^0 \gamma^1$ it follows, using Eq. (19.5), that $\Gamma^{(1+1)} \hat{b}_1^{1\dagger} = \hat{b}_1^{1\dagger}$, which means that $\hat{b}_1^{1\dagger}$ is the right handed "basis vector".
We could make a choice of left handed "basis vector" if choosing $\hat{b}_1^{1\dagger} = \overset{01}{(-i)}$, but the choice of handedness would remain only one.
Each of the two Clifford even "basis vectors" is self adjoint $((^{I,II}\mathcal{A}_1^{1\dagger})^\dagger = {}^{I,II}\mathcal{A}_1^{1\dagger})$.

---

[8] It is our choice which one, $\overset{01}{(+i)}$ or $\overset{01}{(-i)}$, we chose as the "basis vector" $\hat{b}_1^{1\dagger}$ and which one is its Hermitian conjugated partner. The choice of the "basis vector" determines the vacuum state $|\psi_{oc} >$, Eq. (19.8). For $\hat{b}_1^{1\dagger} = \overset{01}{(+i)}$, the vacuum state is $|\psi_{oc} >= \overset{01}{[-i]}$ (due to the requirement that $\hat{b}_1^{1\dagger}|\psi_{oc} >$ is nonzero) which is the Clifford even object.

Let us notice, taking into account Eqs. (19.5, 19.9), that

$$\{\hat{b}^1_1(\equiv(\overset{01}{-i})) *_A \hat{b}^{1\dagger}_1(\equiv(\overset{01}{+i}))\}|\psi_{oc}> = {}^{II}\mathcal{A}^{1\dagger}_1(\equiv[\overset{01}{-i}])|\psi_{oc}> = |\psi_{oc}>,$$

$$\{\hat{b}^{1\dagger}_1(\equiv(\overset{01}{+i})) *_A \hat{b}^1_1(\equiv(\overset{01}{-i}))\}|\psi_{oc}> = 0,$$

$${}^{I}\mathcal{A}^{1\dagger}_1(\equiv[\overset{01}{+i}]) *_A \hat{b}^1_1(\equiv(\overset{01}{+i}))|\psi_{oc}> = \hat{b}^1_1(\equiv(\overset{01}{+i}))|\psi_{oc}>,$$

$${}^{I}\mathcal{A}^{1\dagger}_1(\equiv[\overset{01}{+i}]) \hat{b}^1_1(\equiv(\overset{01}{-i}))|\psi_{oc}> = 0.$$

We find that

$${}^{I}\mathcal{A}^{1\dagger}_1 *_A {}^{II}\mathcal{A}^{1\dagger}_1 = 0 = {}^{II}\mathcal{A}^{1\dagger}_1 *_A {}^{I}\mathcal{A}^{1\dagger}_1.$$

From the case $d = (3+1)$ we can learn a little more:

d=(3+1)

There are 16 ($2^{d=4}$) "eigenvectors" of the Cartan subalgebra members (S^{03}, S^{12}) and ($\mathcal{S}^{03}, \mathcal{S}^{12}$) of the Lorentz algebras S^{ab} and $\mathcal{S}^{ab}$, Eq. (19.4), in $d = (3+1)$.
There are two families ($2^{\frac{4}{2}-1}$, f=(1,2)) with two ($2^{\frac{4}{2}-1}$, m=(1,2)) members each of the Clifford odd "basis vectors" $\hat{b}^{m\dagger}_f$, with $2^{\frac{4}{2}-1} \times 2^{\frac{4}{2}-1}$ Hermitian conjugated partners $\hat{b}^m_f$ in a separate group (not reachable by S^{ab}).
There are $2^{\frac{4}{2}-1} \times 2^{\frac{4}{2}-1}$ members of the group of ${}^{I}\mathcal{A}^{m\dagger}_f$, which are Hermitian conjugated to each other or are self adjoint, all reachable by $\mathcal{S}^{ab}$ from any starting "basis vector ${}^{I}\mathcal{A}^{1\dagger}_1$.
And there is another group of $2^{\frac{4}{2}-1} \times 2^{\frac{4}{2}-1}$ members of ${}^{II}\mathcal{A}^{m\dagger}_f$, again either Hermitian conjugated to each other or are self adjoint. All are reachable from the starting vector ${}^{II}\mathcal{A}^{1\dagger}_1$ by the application of $\mathcal{S}^{ab}$.
Again we can make a choice of either right or left handed Clifford odd "basis vectors", but not of both handedness. Making a choice of the right handed "basis vectors"

$$
\begin{array}{cccc}
 & f=1 & f=2 & \\
\tilde{S}^{03} = \frac{i}{2}, \tilde{S}^{12} = -\frac{1}{2}, & \tilde{S}^{03} = -\frac{i}{2}, \tilde{S}^{12} = \frac{1}{2}, & S^{03}, & S^{12} \\
\hat{b}^{1\dagger}_1 = (\overset{03}{+i})[\overset{12}{+}] & \hat{b}^{1\dagger}_2 = [\overset{03}{+i}](\overset{12}{+}) & \frac{i}{2} & \frac{1}{2} \\
\hat{b}^{2\dagger}_1 = [\overset{03}{-i}](\overset{12}{-}) & \hat{b}^{2\dagger}_2 = (\overset{03}{-i})[\overset{12}{-}] & -\frac{i}{2} & -\frac{1}{2},
\end{array}
$$

we find for the Hermitian conjugated partners of the above "basis vectors"

$$
\begin{array}{cccc}
S^{03} = -\frac{i}{2}, S^{12} = \frac{1}{2}, & S^{03} = \frac{i}{2}, S^{12} = -\frac{1}{2}, & \tilde{S}^{03}, & \tilde{S}^{12} \\
\hat{b}^1_1 = (\overset{03}{-i})[\overset{12}{+}] & \hat{b}^1_2 = [\overset{03}{+i}](\overset{12}{-}) & -\frac{i}{2} & -\frac{1}{2} \\
\hat{b}^2_1 = [\overset{03}{-i}](\overset{12}{+}) & \hat{b}^2_2 = (\overset{03}{+i})[\overset{12}{-}] & \frac{i}{2} & \frac{1}{2}.
\end{array}
$$

Let us notice that if we look at the subspace $SO(1,1)$ with the Clifford odd "basis vectors" with the Cartan subalgebra member S^{03} of the space $SO(3,1)$, and neglect

the values of S^{12}, we do have $\hat{b}_1^{1\dagger} \overset{03}{=}(+i)$ and $\hat{b}_2^{2\dagger} \overset{03}{=}(-i)$, which have opposite handedness $\Gamma^{(1,1)}$ in $d = (1+1)$, but they have different "charges" S^{12} in $d = (3+1)$. In the whole internal space all the Clifford odd "basis vectors" have only one handedness.

We further find that $|\psi_{oc}> = \frac{1}{\sqrt{2}}(\overset{03}{[-i]}\overset{12}{[+]} + \overset{03}{[+i]}\overset{12}{[+]})$. All the Clifford odd "basis vectors" are orthogonal: $\hat{b}_f^{m\dagger} *_A \hat{b}_{f'}^{m'\dagger} = 0$.

For the Clifford even "basis vectors" we find two groups of either self adjoint members or with the Hermitian conjugated partners within the same group. The two groups are not reachable by $\mathcal{S}^{03}$. We have for ${}^I\mathcal{A}_f^{m\dagger}$, $m = (1,2), f = (1,2)$

$$
\begin{array}{cc}
\mathcal{S}^{03}\ \mathcal{S}^{12} & \mathcal{S}^{03}\ \mathcal{S}^{12} \\
{}^I\mathcal{A}_1^{1\dagger} =\overset{03}{[+i]}\overset{12}{[+]}\quad 0 \quad 0 \;,\; {}^I\mathcal{A}_2^{1\dagger} =\overset{03}{(+i)}\overset{12}{(+)}\quad i \quad 1 \\
{}^I\mathcal{A}_1^{2\dagger} =\overset{03}{(-i)}\overset{12}{(-)}\; -i \; -1 \;,\; {}^I\mathcal{A}_2^{2\dagger} =\overset{03}{[-i]}\overset{12}{[-]}\quad 0 \quad 0\,,
\end{array}
$$

and for ${}^{II}\mathcal{A}_f^{m\dagger}$, $m = (1,2), f = (1,2)$

$$
\begin{array}{cc}
\mathcal{S}^{03}\ \mathcal{S}^{12} & \mathcal{S}^{03}\ \mathcal{S}^{12} \\
{}^{II}\mathcal{A}_1^{1\dagger} =\overset{03}{[+i]}\overset{12}{[-]}\quad 0 \quad 0 \;,\; {}^{II}\mathcal{A}_2^{1\dagger} =\overset{03}{(+i)}\overset{12}{(-)}\quad i \quad 1 \\
{}^{II}\mathcal{A}_1^{2\dagger} =\overset{03}{(-i)}\overset{12}{(+)}\; -i \; 1 \;,\; {}^{II}\mathcal{A}_2^{2\dagger} =\overset{03}{[-i]}\overset{12}{[+]}\quad 0 \quad 0\,.
\end{array}
$$

The Clifford even "basis vectors" have no families. ${}^I\mathcal{A}_f^{m\dagger} *_A {}^I\mathcal{A}_{f'}^{m'\dagger} = 0$, for any (m, m', f, f').

$d = (5 + 1)$

In Table 11.1 the $64\,(= 2^{d=6})$ "eigenvectors" of the Cartan subalgebra members of the Lorentz algebra S^{ab} and $\mathcal{S}^{ab}$, Eq. (19.4), are presented. The Clifford odd "basis vectors", they appear in $4\,(= 2^{\frac{d=6}{2}-1})$ families, each family has 4 members, are products of an odd number of nilpotents, that is either of three nilpotents or of one nilpotent. They appear in Table 11.1 in the group named odd $I\,\hat{b}_f^{m\dagger}$. Their Hermitian conjugated partners appear in the second group named odd $II\,\hat{b}_f^m$. Within each of these two groups, the members are orthogonal, Eq. (11.15), which means that the algebraic product of $\hat{b}_f^{m\dagger} *_A \hat{b}_{f'}^{m'\dagger} = 0$ for all (m, m', f, f'). This can be checked by using relations in Eq. (19.9). Equivalently, the algebraic products of their Hermitian conjugated partners are also orthogonal among themselves. The "basis vectors" and their Hermitian conjugated partners are normalized as follows

$$< \psi_{oc}|\hat{b}_f^m *_A \hat{b}_{f'}^{m'\dagger}|\psi_{oc}> = \delta^{mm'}\delta_{ff'}, \tag{11.25}$$

since the vacuum state $|\psi_{oc}> = \frac{1}{\sqrt{2^{\frac{d=6}{2}-1}}} (\overset{03}{[-i]}\overset{12}{[-]}\overset{56}{[-]} + \overset{03}{[-i]}\overset{12}{[+]}\overset{56}{[+]} + \overset{03}{[+i]}\overset{12}{[-]}\overset{56}{[+]}$

$+ \overset{03}{[+i]}\overset{12}{[+]}\overset{56}{[-]})$ is normalized to one: $< \psi_{oc}|\psi_{oc}> = 1$.

The longer overview of the properties of the Clifford odd "basis vectors" and their Hermitian conjugated partners for the case $d = (5 + 1)$ can be found in Ref. [5].

The Clifford even "basis vectors" are products of an even number of nilpotents, of either two or none in this case. They are presented in Table 11.1 in two groups, each with $16 (= 2^{\frac{d=6}{2}-1} \times 2^{\frac{d=6}{2}-1})$ members, as $even\, I\, \mathcal{A}_f^{m\dagger}$ and $even\, II\, \mathcal{A}_f^{m\dagger}$. One can easily check, using Eq. (19.9), that the algebraic product $^I\mathcal{A}_f^{m\dagger} *_A {}^{II}\mathcal{A}_{f'}^{m'\dagger} = 0, \forall (m, m', f.f')$, Eq. (11.19). The longer overview of the Clifford even "basis vectors" and their Hermitian conjugated partners for the case $d = (5 + 1)$- can be found in Ref. [9].

While the Clifford odd "basis vectors" are (chosen to be) right handed, $\Gamma^{(5+1)} = 1$, have their Hermitian conjugated partners opposite handedness [9]

While the Clifford odd "basis vectors" have half integer eigenvalues of the Cartan subalgebra members, Eq.(19.4), that is of S^{03}, S^{12}, S^{56} in this particular case of $d = (5 + 1)$, the Clifford even "basis vectors" have integer spins, obtained by $\mathcal{S}^{03} = S^{03} + \tilde{S}^{03}, \mathcal{S}^{12} = S^{12} + \tilde{S}^{12}, \mathcal{S}^{56} = S^{56} + \tilde{S}^{56}$.

Let us check what does the algebraic application, $*_A$, of $^I\hat{\mathcal{A}}_{f=3}^{m\dagger}, m = (1, 2, 3, 4)$, presented in Table 11.1 in the third column of $even\, I$, do on the Clifford odd "basis vectors" $\hat{b}_{f=1}^{m=1\dagger}$, presented as the first $odd\, I$ "basis vector" in Table 11.1. This can easily be evaluated by taking into account Eq. (19.5) for any m.

$$^I\hat{\mathcal{A}}_3^{m\dagger} *_A \hat{b}_1^{1\dagger}(\equiv \overset{03}{(+i)}\overset{12}{[+]}\overset{56}{[+]}):$$

$$^I\hat{\mathcal{A}}_3^{1\dagger}(\equiv \overset{03}{[+i]}\overset{12}{[+]}\overset{56}{[+]}) *_A \hat{b}_1^{1\dagger}(\equiv \overset{03}{(+i)}\overset{12}{[+]}\overset{56}{[+]}) \rightarrow \hat{b}_1^{1\dagger}, \text{selfadjoint}$$

$$^I\hat{\mathcal{A}}_3^{2\dagger}(\equiv \overset{03}{(-i)}\overset{12}{(-)}\overset{56}{[+]}) *_A \hat{b}_1^{1\dagger} \rightarrow \hat{b}_1^{2\dagger}(\equiv \overset{03}{[-i]}\overset{12}{(-)}\overset{56}{[+]}),$$

$$^I\hat{\mathcal{A}}_3^{3\dagger}(\equiv \overset{03}{(-i)}\overset{12}{[+]}\overset{56}{(-)}) *_A \hat{b}_1^{1\dagger} \rightarrow \hat{b}_1^{3\dagger}(\equiv \overset{03}{[-i]}\overset{12}{[+]}\overset{56}{(-)}),$$

$$^I\hat{\mathcal{A}}_3^{4\dagger}(\equiv \overset{03}{[+i]}\overset{12}{(-)}\overset{56}{(-)}) *_A \hat{b}_1^{1\dagger} \rightarrow \hat{b}_1^{4\dagger}(\equiv \overset{03}{(+i)}\overset{12}{(-)}\overset{56}{(-)}). \tag{11.26}$$

The sign $\rightarrow$ means that the relation is valid up to the constant. $^I\hat{\mathcal{A}}_3^{1\dagger}$ is self adjoint, the Hermitian conjugated partner of $^I\hat{\mathcal{A}}_3^{2\dagger}$ is $^I\hat{\mathcal{A}}_4^{1\dagger}$, of $^I\hat{\mathcal{A}}_3^{3\dagger}$ is $^I\hat{\mathcal{A}}_2^{1\dagger}$ and of $^I\hat{\mathcal{A}}_3^{4\dagger}$ is $^I\hat{\mathcal{A}}_1^{1\dagger}$.

We can conclude that the algebraic, $*_A$, application of $^I\hat{\mathcal{A}}_3^{m\dagger}(\equiv \overset{03}{(-i)}\overset{12}{[+]}\overset{56}{(-)})$ on $\hat{b}_1^{1\dagger}$ leads to the same or another family member of the same family $f = 1$, namely to $\hat{b}_1^{m\dagger}, m = (1, 2, 3, 4)$.

Calculating the eigenvalues of the Cartan subalgebra members, Eq. (19.4), before and after the algebraic multiplication, $*_A$, one sees that $^I\hat{\mathcal{A}}_3^{m\dagger}$ carry the integer eigenvalues of the Cartan subalgebra members, namely of $\mathcal{S}^{ab} = S^{ab} + \tilde{S}^{ab}$, since they transfer when applying on the Clifford odd "basis vector" to it the integer eigenvalues of the Cartan subalgebra members, changing the Clifford odd "basis vector" into another Clifford odd "basis vector".

We therefore find out that the algebraic application of $^I\hat{\mathcal{A}}_3^{m\dagger}, m = 1, 2, 3, 4$, on $\hat{b}_1^{1\dagger}$ transforms $\hat{b}_1^{1\dagger}$ into $\hat{b}_1^{m\dagger}, m = (1, 2, 3, 4)$. Similarly we find that the algebraic application of $^I\hat{\mathcal{A}}_4^m, m = (1, 2, 3, 4)$ on $\hat{b}_1^{2\dagger}$ transforms $\hat{b}_1^{2\dagger}$ into $\hat{b}_1^{m\dagger}, m = (1, 2, 3, 4)$.

---

[9] The handedness $\Gamma^{(d)}$, one of the invariants of the group $SO(d)$, with the infinitesimal generators of the Lorentz group S^{ab}, is defined as $\Gamma^{(d)} = \alpha \varepsilon_{a_1 a_2 \ldots a_{d-1} a_d} S^{a_1 a_2} \cdot S^{a_3 a_4} \cdots S^{a_{d-1} a_d}$, with α chosen so that $\Gamma^{(d)} = \pm 1$.

Table 11.1: $2^d = 64$ "eigenvectors" of the Cartan subalgebra of the Clifford odd and even algebras — the superposition of odd and even products of γ^a's — in $d = (5+1)$-dimensional space are presented, divided into four groups. The first group, odd I, is chosen to represent "basis vectors", named $\hat{b}_f^{m\dagger}$, appearing in $2^{\frac{d}{2}-1} = 4$ "families" (f = 1, 2, 3, 4), each "family" with $2^{\frac{d}{2}-1} = 4$ "family" members (m = 1, 2, 3, 4). The second group, odd II, contains Hermitian conjugated partners of the first group for each family separately, $\hat{b}_f^m = (\hat{b}_f^{m\dagger})^\dagger$. Either odd I or odd II are products of an odd number of nilpotents, the rest are projectors. The "family" quantum numbers of $\hat{b}_f^{m\dagger}$, that is the eigenvalues of $(\tilde{S}^{03}, \tilde{S}^{12}, \tilde{S}^{56})$, are for the first *odd I* group written above each "family", the quantum numbers of the members (S^{03}, S^{12}, S^{56}) are written in the last three columns. For the Hermitian conjugated partners of *odd I*, presented in the group *odd II*, the quantum numbers (S^{03}, S^{12}, S^{56}) are presented above each group of the Hermitian conjugated partners, the last three columns tell eigenvalues of $(\tilde{S}^{03}, \tilde{S}^{12}, \tilde{S}^{56})$. The two groups with the even number of γ^a's, *even I* and *even II*, each has their Hermitian conjugated partners within its own group, have the quantum numbers f, that is the eigenvalues of $(\tilde{S}^{03}, \tilde{S}^{12}, \tilde{S}^{56})$, written above column of four members, the quantum numbers of the members, (S^{03}, S^{12}, S^{56}), are written in the last three columns.

"basis vectors" $(\tilde{S}^{03}, \tilde{S}^{12}, \tilde{S}^{56})$	m →	f = 1 $(\frac{i}{2}, -\frac{1}{2}, -\frac{1}{2})$	f = 2 $(-\frac{i}{2}, -\frac{1}{2}, \frac{1}{2})$	f = 3 $(-\frac{i}{2}, \frac{1}{2}, -\frac{1}{2})$	f = 4 $(\frac{i}{2}, \frac{1}{2}, \frac{1}{2})$	S^{03}	S^{12}	S^{56}
		03 12 56	03 12 56	03 12 56	03 12 56			
odd I $\hat{b}_f^{m\dagger}$	1	(+i)[+][+]	[+i][+](+)	[+i](+)[+]	(+i)(+)(+)	$\frac{i}{2}$	$\frac{1}{2}$	$\frac{1}{2}$
	2	[−i](−)[+]	(−i)(−)(+)	(−i)[−][+]	[−i][−](+)	$-\frac{i}{2}$	$-\frac{1}{2}$	$\frac{1}{2}$
	3	[−i][+](−)	(−i)[+][−]	(−i)(+)(−)	[−i](+)[−]	$-\frac{i}{2}$	$\frac{1}{2}$	$-\frac{1}{2}$
	4	(+i)(−)(−)	[+i](−)[−]	[+i][−](−)	(+i)[−][−]	$\frac{i}{2}$	$-\frac{1}{2}$	$-\frac{1}{2}$
(S^{03}, S^{12}, S^{56}) →		$(-\frac{i}{2}, \frac{1}{2}, \frac{1}{2})$ 03 12 56	$(\frac{i}{2}, \frac{1}{2}, -\frac{1}{2})$ 03 12 56	$(\frac{i}{2}, -\frac{1}{2}, \frac{1}{2})$ 03 12 56	$(-\frac{i}{2}, -\frac{1}{2}, -\frac{1}{2})$ 03 12 56	$\tilde{S}^{03}$	$\tilde{S}^{12}$	$\tilde{S}^{56}$
odd II $\hat{b}_f^m$	1	(−i)[+][+]	[+i][+](−)	[+i](−)[+]	(−i)(−)(−)	$-\frac{i}{2}$	$-\frac{1}{2}$	$-\frac{1}{2}$
	2	[−i](+)[+]	(+i)(+)(−)	(+i)[−][+]	[−i][−](−)	$\frac{i}{2}$	$\frac{1}{2}$	$-\frac{1}{2}$
	3	[−i][+](+)	(+i)[+][−]	(+i)(−)(+)	[−i](−)[−]	$\frac{i}{2}$	$-\frac{1}{2}$	$\frac{1}{2}$
5	−1	−1						
	4	(−i)(+)(+)	[+i](+)[−]	[+i][−](+)	(−i)[−][−]	$-\frac{i}{2}$	$\frac{1}{2}$	$\frac{1}{2}$
$(\tilde{S}^{03}, \tilde{S}^{12}, \tilde{S}^{56})$ →		$(-\frac{1}{2}, \frac{1}{2}, \frac{1}{2})$ 03 12 56	$(\frac{1}{2}, -\frac{1}{2}, \frac{1}{2})$ 03 12 56	$(-\frac{1}{2}, -\frac{1}{2}, -\frac{1}{2})$ 03 12 56	$(\frac{1}{2}, \frac{1}{2}, -\frac{1}{2})$ 03 12 56	S^{03}	S^{12}	S^{56}
even I $^I A_f^m$	1	[+i](+)(+)	(+i)[+](+)	[+i][+][+]	(+i)(+)[+]	$\frac{i}{2}$	$\frac{1}{2}$	$\frac{1}{2}$
	2	(−i)[−](+)	[−i](−)(+)	(−i)(−)[+]	[−i][−](+)	$-\frac{i}{2}$	$-\frac{1}{2}$	$\frac{1}{2}$
	3	(−i)(+)[−]	[−i][+][−]	[−i](+)[−]	[−i](+)(−)	$-\frac{i}{2}$	$\frac{1}{2}$	$-\frac{1}{2}$
	4	[+i][−][−]	(+i)(−)[−]	[+i](−)(−)	(+i)[−](−)	$\frac{i}{2}$	$-\frac{1}{2}$	$-\frac{1}{2}$
$(\tilde{S}^{03}, \tilde{S}^{12}, \tilde{S}^{56})$ →		$(\frac{i}{2}, \frac{1}{2}, \frac{1}{2})$ 03 12 56	$(-\frac{i}{2}, -\frac{1}{2}, \frac{1}{2})$ 03 12 56	$(\frac{i}{2}, -\frac{1}{2}, \frac{1}{2})$ 03 12 56	$(-\frac{i}{2}, \frac{1}{2}, -\frac{1}{2})$ 03 12 56	S^{03}	S^{12}	S^{56}
even II $^{II} A_f^m$	1	[−i](+)(+)	(−i)[+](+)	[−i][+][+]	(−i)(+)[+]	$-\frac{i}{2}$	$\frac{1}{2}$	$\frac{1}{2}$
	2	(+i)[−](+)	[+i](−)(+)	(+i)(−)[+]	[+i][−](+)	$\frac{i}{2}$	$-\frac{1}{2}$	$\frac{1}{2}$
	3	(+i)(+)[−]	[+i][+][−]	(+i)[+](−)	[+i](+)(−)	$\frac{i}{2}$	$\frac{1}{2}$	$-\frac{1}{2}$
	4	[−i][−][−]	(−i)(−)[−]	[−i](−)(−)	(−i)[−](−)	$-\frac{i}{2}$	$-\frac{1}{2}$	$-\frac{1}{2}$

The algebraic application of $^I\hat{\mathcal{A}}_2^m$, $m = (1,2,3,4)$ on $\hat{b}_1^{3\dagger}$ transforms $\hat{b}_1^{3\dagger}$ into $\hat{b}_1^{m\dagger}$, $m = (1,2,3,4)$. And the algebraic application of $^I\hat{\mathcal{A}}_1^m$, $m = (1,2,3,4)$ on $\hat{b}_1^{4\dagger}$ transforms $\hat{b}_1^{4\dagger}$ into $\hat{b}_1^{m\dagger}$, $m = (1,2,3,4)$.

The statement of Eq. (11.24) is therefore demonstrated on the case of $d = (5+1)$. It remains to stress and illustrate in the case of $d = (5+1)$ some general properties of the Clifford even "basis vector" $^I\hat{\mathcal{A}}_f^{m\dagger}$ when they apply on each other. Let us denote the self adjoint member in each group of "basis vectors" of particular f as $^I\hat{\mathcal{A}}_f^{m_0\dagger}$. We easily see that

$$\{^I\hat{\mathcal{A}}_f^{m\dagger}, {}^I\hat{\mathcal{A}}_f^{m'\dagger}\}_- = 0, \quad \text{if } (m,m') \neq m_0 \text{ or } m = m_0 = m', \forall f,$$
$$^I\hat{\mathcal{A}}_f^{m\dagger} *_A {}^I\hat{\mathcal{A}}_f^{m_0\dagger} \to {}^I\hat{\mathcal{A}}_f^{m\dagger}, \quad \forall m, \forall f. \tag{11.27}$$

In Table 11.1 we see that in each column of either $even \, ^I\hat{\mathcal{A}}_f^{m\dagger}$ or of $even \, ^{II}\hat{\mathcal{A}}_f^{m\dagger}$ there is one self adjoint $^{I,II}\hat{\mathcal{A}}_f^{m_0\dagger}$. We also see that two "basis vectors" $^I\hat{\mathcal{A}}_f^{m\dagger}$ and $^I\hat{\mathcal{A}}_f^{m'\dagger}$ of the same f and of $(m,m') \neq m_0$ are orthogonal. We only have to take into account Eq. (19.9), which tells that

$$\overset{ab}{(k)}\overset{ab}{[k]}= 0, \quad \overset{ab}{[k]}\overset{ab}{(k)}=\overset{ab}{(k)}, \quad \overset{ab}{(k)}\overset{ab}{[-k]}=\overset{ab}{(k)}, \quad \overset{ab}{[k]}\overset{ab}{(-k)}= 0.$$

These relations tell us that $^I\hat{\mathcal{A}}_4^{1\dagger} *_A {}^I\hat{\mathcal{A}}_3^{2\dagger} = {}^I\hat{\mathcal{A}}_3^{1\dagger}$, what illustrates Eq. (11.23), while $^I\hat{\mathcal{A}}_3^{2\dagger} *_A {}^I\hat{\mathcal{A}}_4^{1\dagger} = {}^I\hat{\mathcal{A}}_4^{2\dagger}$ illustrating Eq. (11.22), while $^I\hat{\mathcal{A}}_3^{1\dagger} *_A {}^I\hat{\mathcal{A}}_4^{2\dagger} = 0$ illustrates Eq. (11.21).

Table 11.2 presents the Clifford even "basis vectors" $^I\hat{\mathcal{A}}_f^{m\dagger}$ for $d = (5+1)$ with the properties: **i.** They are products of an even number of nilpotents, $\overset{ab}{(k)}$, with the rest up to $\frac{d}{2}$ of projectors, $\overset{ab}{[k]}$. **ii.** Nilpotents and projectors are eigenvectors of the Cartan subalgebra members $\mathcal{S}^{ab} = S^{ab} + \tilde{S}^{ab}$, Eq. (19.4), carrying the integer eigenvalues of the Cartan subalgebra members.
iii. They have their Hetmitian conjugated partners within the same group of $^I\hat{\mathcal{A}}_f^{m\dagger}$ with $2^{\frac{d}{2}-1} \times 2^{\frac{d}{2}-1}$ members.
iv. They have properties of the boson gauge fields. When applying on the Clifford odd "basis vectors" (offering the description of the fermion fields) they transform the Clifford odd "basis vectors" into another Clifford odd "basis vectors", transferring to the Clifford odd "basis vectors" the integer spins with respect to the $SO(d-1,1)$ group, while with respect to subgroups of the $SO(d-1,1)$ group they transfer appropriate superposition of the eigenvalues (manifesting the properties of the adjoint representations of the corresponding groups).

To demonstrate that the Clifford even "basis vectors" have properties of the gauge fields of the corresponding Clifford odd "basis vectors" we study properties of the $SU(3) \times U(1)$ subgroups of the Clifford odd and Clifford even "basis vectors".
We present in Eqs. (11.28, 11.29) the superposition of members of Cartan subalgebra, Eq. (19.4), for S^{ab} for the Clifford odd "basis vectors", for the subgroups $SO(3,1) \times U(1)$ $(N_\pm^3, \tau)$ and for the subgroups $SU(3) \times U(1)$: (τ', τ^3, τ^8). The same relations can be used

also for the corresponding operators determining the "family" quantum numbers ($\tilde{N}^3_\pm$, $\tilde{\tau}$) of the Clifford odd "basis vectors', if S^{ab}'s are replaced by $\tilde{S}^{ab}$'s. For the Clifford even objects $\mathcal{S}^{ab}(= S^{ab} + \tilde{S}^{ab})$ must replace S^{ab}.

$$N^3_\pm(= N^3_{(L,R)}) := \frac{1}{2}(S^{12} \pm iS^{03}), \quad \tau = S^{56}, \tag{11.28}$$

$$\tau^3 := \frac{1}{2}(-S^{12} - iS^{03}), \qquad \tau^8 = \frac{1}{2\sqrt{3}}(-iS^{03} + S^{12} - 2S^{56}),$$

$$\tau' = -\frac{1}{3}(-iS^{03} + S^{12} + S^{56}). \tag{11.29}$$

Let us, for example, algebraically apply $^I\hat{\mathcal{A}}^2_3 (\equiv \overset{03}{(-i)} \overset{12}{(-)} \overset{56}{[+]})$, denoted by $\odot\odot$ on Table 11.2, carrying ($\tau^3 = 0, \tau^8 = -\frac{1}{\sqrt{3}}, \tau' = \frac{2}{3}$), represented also on Fig. 11.2 by $\odot\odot$, on the Clifford odd "basis vector" $\hat{b}^{1\dagger}_1 (\equiv \overset{03}{(+i)} \overset{12}{(+)} \overset{56}{(+)})$, presented on Table 11.1, with ($\tau^3 = 0, \tau^8 = 0, \tau' = -\frac{1}{2}$), as we can calculate using Eq. (11.29) and which is represented on Fig. 11.1 by a square as a singlet. $^I\hat{\mathcal{A}}^2_3$ transforms $\hat{b}^{1\dagger}_1$ (by transferring to $\hat{b}^{1\dagger}_1$ ($\tau^3 = 0, \tau^8 = -\frac{1}{\sqrt{3}}, \tau' = \frac{2}{3}$)) to $\hat{b}^{1\dagger}_2$ with ($\tau^3 = 0, \tau^8 = -\frac{1}{\sqrt{3}}, \tau' = \frac{1}{6}$), belonging on Fig. 11.1 to the triplet, denoted by $\bigcirc$. The corresponding gauge fields, presented on Fig. 11.2, if belonging to the sextet, would transform the triplet of quarks among themselves.
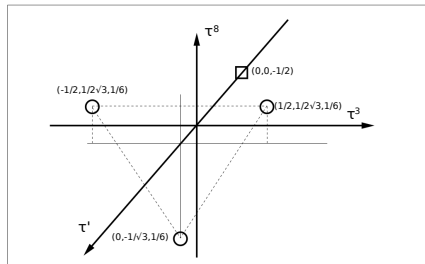
Fig. 11.1: Representations of the subgroups $SU(3)$ and $U(1)$ of the group $SO(5, 1)$, the properties of which appear in Table 11.1, are presented. (τ^3, τ^8 and τ') can be calculated if using Eqs.(11.28, 11.29). On the abscissa axis, on the ordinate axis and on the third axis the eigenvalues of the superposition of the three Cartan subalgebra members, τ^3, τ^8, τ' are presented. One notices one triplet, denoted by $\bigcirc$ with the values $\tau' = \frac{1}{6}$, ($\tau^3 = -\frac{1}{2}, \tau^8 = \frac{1}{2\sqrt{3}}, \tau' = \frac{1}{6}$), ($\tau^3 = \frac{1}{2}, \tau^8 = \frac{1}{2\sqrt{3}}, \tau' = \frac{1}{6}$), ($\tau^3 = 0, \tau^8 = -\frac{1}{\sqrt{3}}, \tau' = \frac{1}{6}$), respectively, and one singlet denoted by the square. ($\tau^3 = 0, \tau^8 = 0, \tau' = -\frac{1}{2}$). The triplet and the singlet appear in four families.

In the case of the group $SO(6)$ ($SO(5, 1)$indeed), manifesting as $SU(3) \times U(1)$ and representing the $SU(3)$ colour group and $U(1)$ the "fermion" quantum number, embedded into $SO(13, 1)$ the triplet would represent quarks and the singlet leptons. The corresponding gauge of the fields, presented on Fig. 11.2, if belonging to the sextet, would transform the triplet of quarks among themselves, changing the

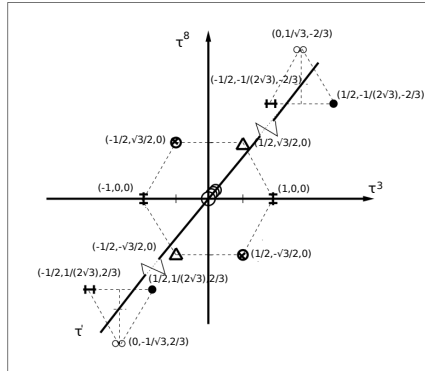colour and leaving the "fermion" quantum number equal to $\frac{1}{6}$.

Fig. 11.2: The Clifford even "basis vectors" $^I\hat{\mathcal{A}}_f^m$, in the case that d $=$ $(5+1)$, are presented with respect to the eigenvalues of the commuting operators of the subgroups SU(3) and U(1) of the group SO(5,1): $\tau^3 = \frac{1}{2}(-\mathcal{S}^{12} - i\mathcal{S}^{03})$, $\tau^8 = \frac{1}{2\sqrt{3}}(\mathcal{S}^{12} - i\mathcal{S}^{03} - 2\mathcal{S}^{56})$, $\tau' = -\frac{1}{3}(\mathcal{S}^{12} - i\mathcal{S}^{03} + \mathcal{S}^{56})$. Their properties appear in Table 11.2. The abscissa axis carries the eigenvalues of τ^3, the ordinate axis of τ^8 and the third axis the eigenvalues of τ', One notices four singlets with $(\tau^3 = 0, \tau^8 = 0, \tau' = 0)$, denoted by $\bigcirc$, representing four self adjoint Clifford even "basis vectors" $^I\hat{\mathcal{A}}_f^m$, one sextet of three pairs with $\tau' = 0$, Hermitian conjugated to each other, denoted by $\triangle$ (with $(\tau' = 0, \tau^3 = -\frac{1}{2}, \tau^8 = -\frac{3}{2\sqrt{3}})$ and $(\tau' = 0, \tau^3 = \frac{1}{2}, \tau^8 = \frac{3}{2\sqrt{3}})$), respectively, by $\ddagger$ (with $(\tau' = 0, \tau^3 = -1, \tau^8 = 0)$ and $(\tau' = 0, \tau^3 = 1, \tau^8 = 0)$, respectively, and by $\otimes$ (with $(\tau' = 0, \tau^3 = \frac{1}{2}, \tau^8 = -\frac{3}{2\sqrt{3}})$ and $(\tau' = 0, \tau^3 = -\frac{1}{2}, \tau^8 = \frac{3}{2\sqrt{3}})$), respectively, and one triplet, denoted by $\star\star$ with $(\tau' = \frac{2}{3}, \tau^3 = \frac{1}{2}, \tau^8 = \frac{1}{2\sqrt{3}})$, by $\bullet$ with $(\tau' = \frac{2}{3}, \tau^3 = -\frac{1}{2}, \tau^8 = \frac{1}{2\sqrt{3}})$, and by $\odot\odot$ with $(\tau' = \frac{2}{3}, \tau^3 = 0, \tau^8 = -\frac{1}{\sqrt{3}})$, as well as one antitriplet, Hermitian conjugated to the triplet, denoted by $\star\star$ with $(\tau' = -\frac{2}{3}, \tau^3 = -\frac{1}{2}, \tau^8 = -\frac{1}{2\sqrt{3}})$, by $\bullet$ with $(\tau' = -\frac{2}{3}, \tau^3 = \frac{1}{2}, \tau^8 = -\frac{1}{2\sqrt{3}})$, and by $\odot\odot$ with $(\tau' = -\frac{2}{3}, \tau^3 = 0, \tau^8 = \frac{1}{\sqrt{3}})$.

We can see that $^I\hat{\mathcal{A}}_3^{m\dagger}$ with $(m = 2, 3, 4)$, if applied on the SU(3) singlet $\hat{b}_1^{1\dagger}$ with $(\tau' = -\frac{1}{2}, \tau^3 = 0, \tau^8 = 0)$, transforms it to $\hat{b}_1^{m=2,3,4)\dagger}$, respectively, which are members of the SU(3) triplet. All these Clifford even "basis vectors" have τ' equal to $\frac{2}{3}$, changing correspondingly $\tau' = -\frac{1}{2}$ into $\tau' = \frac{1}{6}$ and bringing the needed values of τ^3 and τ^8.

In Table 11.2 we find $(6+4)$ Clifford even "basis vectors" $^I\hat{\mathcal{A}}_f^{m\dagger}$ with $\tau` = 0$. Six of them are Hermitian conjugated to each other — the Hermitian conjugated partners are denoted by the same geometric figure on the third column. Four of them are self adjoint and correspondingly with $(\tau' = 0, \tau^3 = 0, \tau^8 = 0)$, denoted in the third column of Table 11.2 by $\bigcirc$. The rest 6 Clifford even "basis vectors" belong to one

triplet with $\tau' = \frac{2}{3}$ and (τ^3, τ^8) equal to $[(0, -\frac{1}{\sqrt{3}}), (-\frac{1}{2}, \frac{1}{2\sqrt{3}}), (\frac{1}{2}, \frac{1}{2\sqrt{3}})]$ and one antitriplet with $\tau' = -\frac{2}{3}$ and $((\tau^3, \tau^8)$ equal to $[(-\frac{1}{2}, -\frac{1}{2\sqrt{3}}), (\frac{1}{2}, -\frac{1}{2\sqrt{3}}), (0, \frac{1}{\sqrt{3}})]$. Each triplet has Hermitian conjugated partner in antitriplet and opposite. In Table 11.2 the Hermitian conjugated partners of the triplet and antitriplet are denoted by the same signum: $({}^{I}\hat{\mathcal{A}}_1^{1\dagger}, {}^{I}\hat{\mathcal{A}}_3^{4\dagger})$ by $\star\star$, $({}^{I}\hat{\mathcal{A}}_2^{1\dagger}, {}^{I}\hat{\mathcal{A}}_3^{3\dagger})$ by $\bullet$, and $({}^{I}\hat{\mathcal{A}}_3^{2\dagger}, {}^{I}\hat{\mathcal{A}}_4^{1\dagger})$ by $\odot\odot$.

The octet and the two triplets are presented in Fig. 11.2.

Table 11.2: The Clifford even "basis vectors" ${}^{I}\hat{\mathcal{A}}_f^{m\dagger}$, each of them is the product of projectors and an even number of nilpotents, and each is the eigenvector of all the Cartan subalgebra members, $\mathcal{S}^{03}$, $\mathcal{S}^{12}$, $\mathcal{S}^{56}$, Eq. (19.4), are presented for $d = (5 + 1)$-dimensional case. Indexes m and f determine $2^{\frac{d}{2}-1} \times 2^{\frac{d}{2}-1}$ different members ${}^{I}\hat{\mathcal{A}}_f^{m\dagger}$. In the third column the "basis vectors" ${}^{I}\hat{\mathcal{A}}_f^{m\dagger}$ which are Hermitian conjugated partners to each other (and can therefore annihilate each other) are pointed out with the same symbol. For example, with $\star\star$ are equipped the first member with $m = 1$ and $f = 1$ and the last member of $f = 3$ with $m = 4$. The sign $\bigcirc$ denotes the Clifford even "basis vectors" which are self adjoint $({}^{I}\hat{\mathcal{A}}_f^{m\dagger})^{\dagger} = {}^{I}\hat{\mathcal{A}}_{f'}^{m'\dagger}$. It is obvious that † has no meaning, since ${}^{I}\hat{\mathcal{A}}_f^{m\dagger}$ are self adjoint or are Hermitian conjugated partner to another ${}^{I}\hat{\mathcal{A}}_{f'}^{m'\dagger}$. This table represents also the eigenvalues of the three commuting operators $\mathcal{N}_{L,R}^3$ and $\mathcal{S}^{56}$ of the subgroups $SU(2) \times SU(2) \times U(1)$ of the group $SO(5, 1)$ and the eigenvalues of the three commuting operators τ^3, τ^8 and τ' of the subgroups $SU(3) \times U(1)$.

f	m	*	${}^{I}\hat{\mathcal{A}}_f^{m\dagger}$	$\mathcal{S}^{03}$	$\mathcal{S}^{12}$	$\mathcal{S}^{56}$	$\mathcal{N}_L^3$	$\mathcal{N}_R^3$	τ^3	τ^8	τ'
I	1	$\star\star$	$\overset{03}{[+i]}\overset{12}{(+)}\overset{56}{(+)}$	0	1	1.	$\frac{1}{2}$	$\frac{1}{2}$	$-\frac{1}{2}$	$-\frac{1}{2\sqrt{3}}$	$-\frac{2}{3}$
	2	$\triangle$	$\overset{03}{(-i)}\overset{12}{[-]}\overset{56}{(+)}$	$-i$	0	1	$\frac{1}{2}$	$-\frac{1}{2}$	$-\frac{1}{2}$	$-\frac{3}{2\sqrt{3}}$	0
	3	$\ddagger$	$\overset{03}{(-i)}\overset{12}{(+)}\overset{56}{[-]}$	$-i$	1	0	1	0	-1	0	0
	4	$\bigcirc$	$\overset{03}{[+i]}\overset{12}{[-]}\overset{56}{[-]}$	0	0	0	0	0	0	0	0
II	1	$\bullet$	$\overset{03}{(+i)}\overset{12}{[+]}\overset{56}{(+)}$	i	0	1	$-\frac{1}{2}$	$\frac{1}{2}$	$\frac{1}{2}$	$-\frac{1}{2\sqrt{3}}$	$-\frac{2}{3}$
	2	$\otimes$	$\overset{03}{[-i]}\overset{12}{(-)}\overset{56}{(+)}$	0	-1	1	$-\frac{1}{2}$	$-\frac{1}{2}$	$\frac{1}{2}$	$-\frac{3}{2\sqrt{3}}$	0
	3	$\bigcirc$	$\overset{03}{[-i]}\overset{12}{[+]}\overset{56}{[-]}$	0	0	0	0	0	0	0	0
	4	$\ddagger$	$\overset{03}{(+i)}\overset{12}{(-)}\overset{56}{[-]}$	i	-1	0	-1	0	1	0	0
III	1	$\bigcirc$	$\overset{03}{[+i]}\overset{12}{[+]}\overset{56}{[+]}$	0	0	0	0	0	0	0	0
	2	$\odot\odot$	$\overset{03}{(-i)}\overset{12}{(-)}\overset{56}{[+]}$	$-i$	-1	0	0	-1	0	$-\frac{1}{\sqrt{3}}$	$\frac{2}{3}$
	3	$\bullet$	$\overset{03}{(-i)}\overset{12}{[+]}\overset{56}{(-)}$	$-i$	0	-1	$\frac{1}{2}$	$-\frac{1}{2}$	$-\frac{1}{2}$	$\frac{1}{2\sqrt{3}}$	$\frac{2}{3}$
	4	$\star\star$	$\overset{03}{[+i]}\overset{12}{(-)}\overset{56}{(-)}$	0	-1	-1	$-\frac{1}{2}$	$-\frac{1}{2}$	$\frac{1}{2}$	$\frac{1}{2\sqrt{3}}$	$\frac{2}{3}$
IV	1	$\odot\odot$	$\overset{03}{(+i)}\overset{12}{(+)}\overset{56}{[+]}$	i	1	0	0	1	0	$\frac{1}{\sqrt{3}}$	$-\frac{2}{3}$
	2	$\bigcirc$	$\overset{03}{[-i]}\overset{12}{[-]}\overset{56}{[+]}$	0	0	0	0	0	0	0	0
	3	$\otimes$	$\overset{03}{[-i]}\overset{12}{(+)}\overset{56}{(-)}$	0	1	-1	$\frac{1}{2}$	$\frac{1}{2}$	$-\frac{1}{2}$	$\frac{3}{2\sqrt{3}}$	0
	4	$\triangle$	$\overset{03}{(+i)}\overset{12}{[-]}\overset{56}{(-)}$	i	0	-1	$-\frac{1}{2}$	$\frac{1}{2}$	$\frac{1}{2}$	$\frac{3}{2\sqrt{3}}$	0

Fig. 11.2 represents the $2^{\frac{d}{2}-1} \times 2^{\frac{d}{2}-1}$ members ${}^{I}\hat{\mathcal{A}}_{f}^{m}$ of the Clifford even "basis vectors" for the case that d = (5 + 1). The properties of ${}^{I}\hat{\mathcal{A}}_{f}^{m}$ are presented also in Table 11.2. There are in this case again 16 members. Manifesting the structure of subgroups $SU(3) \times U(1)$ of the group $SO(5,1)$ they are represented as eigenvectors of the superposition of the Cartan subalgebra members $(\mathcal{S}^{03}, \mathcal{S}^{12}, \mathcal{S}^{56})$, that is with $\tau^3 = \frac{1}{2}(-\mathcal{S}^{12} - i\mathcal{S}^{03})$, $\tau^8 = \frac{1}{2\sqrt{3}}(\mathcal{S}^{12} - i\mathcal{S}^{03} - 2\mathcal{S}^{56})$, and $\tau' = -\frac{1}{3}(\mathcal{S}^{12} - i\mathcal{S}^{03} + \mathcal{S}^{56})$. There are four self adjoint Clifford even "basis vectors" with $(\tau^3 = 0, \tau^8 = 0, \tau' = 0)$, one sextet of three pairs Hermitian conjugated to each other, one triplet and one antitriplet with the members of the triplet Hermitian conjugated to the corresponding members of the antitriplet and opposite. These 16 members of the Clifford even "basis vectors" ${}^{I}\hat{\mathcal{A}}_{f}^{m}$ are the boson "partners" of the Clifford odd "basis vectors" $\hat{b}_{f}^{m\dagger}$, presented in Fig. 11.1 for one of four families, anyone. The reader can check that the algebraic application of ${}^{I}\hat{\mathcal{A}}_{f}^{m}$, belonging to the triplet, transforms the Clifford odd singlet, denoted on Fig. 11.1 by a square, to one of the members of the triplet, denoted on Fig. 11.1 by the circle $\bigcirc$.

Looking at the boson fields ${}^{I}\hat{\mathcal{A}}_{f}^{m\dagger}$ from the point of view of subgroups $SU(3) \times U(1)$ of the group $SO(5+1)$ we will recognize in the part of fields forming the octet the colour gauge fields of quarks and leptons and antiquarks and antileptons.

11.2.3 Second quantized fermion and boson fields the internal spaces of which are described by the Clifford basis vectors.

We learned in the previous subsection that in even dimensional spaces (d = 2(2n + 1) or d = 4n) the Clifford odd and the Clifford even "basis vectors", which are the superposition of the Clifford odd and the Clifford even products of γ^a's, respectively, offer the description of the internal spaces of fermion and boson fields.

The Clifford odd algebra offers $2^{\frac{d}{2}-1}$ "basis vectors" $\hat{b}_{f}^{m\dagger}$, appearing in $2^{\frac{d}{2}-1}$ families (with the family quantum numbers determined by $\tilde{S}^{ab} = \frac{i}{2}\{\tilde{\gamma}^a, \tilde{\gamma}^b\}_{-}$), which together with their $2^{\frac{d}{2}-1} \times 2^{\frac{d}{2}-1}$ Hermitian conjugated partners $\hat{b}_{f}^{m}$ fulfil the postulates for the second quantized fermion fields, Eq. (11.17) in this paper, Eq.(26) in Ref. [5], explaining the second quantization postulates of Dirac.

The Clifford even algebra offers $2^{\frac{d}{2}-1} \times 2^{\frac{d}{2}-1}$ "basis vectors" of ${}^{I}\hat{\mathcal{A}}_{f}^{m\dagger}$ (and the same number of ${}^{II}\hat{\mathcal{A}}_{f}^{m\dagger}$) with the properties of the second quantized boson fields manifesting as the gauge fields of fermion fields described by the Clifford odd "basis vectors" $\hat{b}_{f}^{m\dagger}$.

The Clifford odd and the Clifford even "basis vectors" are chosen to be products of nilpotents, $\overset{ab}{(k)}$ (with the odd number of nilpotents if describing fermions and the even number of nilpotents if describing bosons), and projectors, $\overset{ab}{[k]}$. Nilpotents and projectors are (chosen to be) eigenvectors of the Cartan subalgebra members of the Lorentz algebra in the internal space of S^{ab} for the Clifford odd "basis vectors" and of $\mathcal{S}^{ab}(= S^{ab} + \tilde{S}^{ab})$ for the Clifford even "basis vectors".

To define the creation operators, either for fermions or for bosons besides the "basis vectors" defining the internal space of fermions and bosons also the basis in

ordinary space in momentum or coordinate representation is needed. Here Ref. [5], Subsect. 3.3 and App. J is overviewed.

Let us introduce the momentum part of the single particle states. The longer version is presented in Ref. [5] in Subsect. 3.3 and in App. J.

$$|\vec{p}> = \hat{b}_{\vec{p}}^{\dagger}|0_p>, \quad <\vec{p}| =< 0_p|\hat{b}_{\vec{p}},$$
$$<\vec{p}|\vec{p}'> = \delta(\vec{p}-\vec{p}') =< 0_p|\hat{b}_{\vec{p}}\,\hat{b}_{\vec{p}'}^{\dagger}|0_p>,$$
$$\text{leading to}$$
$$\hat{b}_{\vec{p}'},\hat{b}_{\vec{p}}^{\dagger} = \delta(\vec{p}'-\vec{p}), \qquad (11.30)$$

with the normalization $< 0_p|0_p> = 1$. While the quantized operators $\hat{\vec{p}}$ and $\hat{\vec{x}}$ commute $\{\hat{p}^i,\hat{p}^j\}_- = 0$ and $\{\hat{x}^k,\hat{x}^l\}_- = 0$, it follows for $\{\hat{p}^i,\hat{x}^j\}_- = i\eta^{ij}$. One correspondingly finds

$$<\vec{p}|\vec{x}> = < 0_{\vec{p}}|\hat{b}_{\vec{p}}\,\hat{b}_{\vec{x}}^{\dagger}|0_{\vec{x}}> = (< 0_{\vec{x}}|\hat{b}_{\vec{x}}\,\hat{b}_{\vec{p}}^{\dagger}|0_{\vec{p}}>)^{\dagger}$$
$$\{\hat{b}_{\vec{p}}^{\dagger},\hat{b}_{\vec{p}'}^{\dagger}\}_- = 0, \qquad \{\hat{b}_{\vec{p}},\hat{b}_{\vec{p}'}\}_- = 0, \qquad \{\hat{b}_{\vec{p}},\hat{b}_{\vec{p}'}^{\dagger}\}_- = 0,$$
$$\{\hat{b}_{\vec{x}}^{\dagger},\hat{b}_{\vec{x}'}^{\dagger}\}_- = 0, \qquad \{\hat{b}_{\vec{x}},\hat{b}_{\vec{x}'}\}_- = 0, \qquad \{\hat{b}_{\vec{x}},\hat{b}_{\vec{x}'}^{\dagger}\}_- = 0,$$
$$\{\hat{b}_{\vec{p}},\hat{b}_{\vec{x}}^{\dagger}\}_- = e^{i\vec{p}\cdot\vec{x}}\frac{1}{\sqrt{(2\pi)^{d-1}}}, \qquad \{\hat{b}_{\vec{x}},\hat{b}_{\vec{p}}^{\dagger}\}_- = e^{-i\vec{p}\cdot\vec{x}}\frac{1}{\sqrt{(2\pi)^{d-1}}}, \qquad (11.31)$$

.
The internal space of either fermion or boson fields has the finite number of "basis vectors", $2^{\frac{d}{2}-1}\times 2^{\frac{d}{2}-1}$, the momentum basis is continuously infinite.

The creation operators for either fermions or bosons must be a tensor product, $*_T$, of both contributions, the "basis vectors" describing the internal space of fermions or bosons and the basis in ordinary, momentum or coordinate, space.
The creation operators for a free massless fermion of the energy $p^0 = |\vec{p}|$, belonging to a family f and to a superposition of family members m applying on the vacuum state $|\psi_{oc}> *_T |0_{\vec{p}}>$ can be written as ([5], Subsect.3.3.2, and the references therein)

$$\hat{b}_f^{s\dagger}(\vec{p}) = \sum_m c^{sm}{}_f(\vec{p})\,\hat{b}_{\vec{p}}^{\dagger}\,*_T\,\hat{b}_f^{m\dagger}, \qquad (11.32)$$

where the vacuum state for fermions $|\psi_{oc}> *_T |0_{\vec{p}}>$ includes both spaces, the internal part, Eq.(19.8), and the momentum part, Eq. (11.30) (in a tensor product for a starting single particle state with zero momentum, from which one obtains the other single fermion states of the same "basis vector" by the operator $\hat{b}_{\vec{p}}^{\dagger}$ which pushes the momentum by an amount $\vec{p}$ [10]).

---

[10] The creation operators and their Hermitian conjugated partners annihilation operators in the coordinate representation can be read in [5] and the references therein: $\hat{b}_f^{s\dagger}(\vec{x},x^0) = \sum_m \hat{b}_f^{m\dagger}\int_{-\infty}^{+\infty}\frac{d^{d-1}p}{(\sqrt{2\pi})^{d-1}}c^{ms}{}_f(\vec{p})\,\hat{b}_{\vec{p}}^{\dagger}\,e^{-i(p^0x^0-\epsilon\vec{p}\cdot\vec{x})}$ ([5], subsect. 3.3.2., Eqs. (55,57,64) and the references therein).

The creation operators fulfil the anticommutation relations for the second quantized fermion fields

$$\{\hat{b}_{f'}^{s'}(\vec{p}'),\, \hat{b}_f^{s\dagger}(\vec{p})\}_+ \,|\psi_{oc} > |0_{\vec{p}} > \,=\, \delta^{ss'}\delta_{ff'}\,\delta(\vec{p}' - \vec{p})\,|\psi_{oc} > |0_{\vec{p}} >,$$

$$\{\hat{b}_{f'}^{s'}(\vec{p}'),\, \hat{b}_f^{s}(\vec{p})\}_+ \,|\psi_{oc} > |0_{\vec{p}} > \,=\, 0 \cdot |\psi_{oc} > |0_{\vec{p}} >,$$

$$\{\hat{b}_{f'}^{s'\dagger}(\vec{p}'),\, \hat{b}_f^{s\dagger}(\vec{p})\}_+ \,|\psi_{oc} > |0_{\vec{p}} > \,=\, 0 \cdot |\psi_{oc} > |0_{\vec{p}} >,$$

$$\hat{b}_f^{s\dagger}(\vec{p})\,|\psi_{oc} > |0_{\vec{p}} > \,=\, |\psi_f^s(\vec{p}) >$$

$$\hat{b}_f^{s}(\vec{p})\,|\psi_{oc} > |0_{\vec{p}} > \,=\, 0 \cdot |\psi_{oc} > |0_{\vec{p}} >$$

$$|p^0| = |\vec{p}|. \tag{11.33}$$

The creation operators $\hat{b}_f^{s\dagger}(\vec{p}))$ and their Hermitian conjugated partners annihilation operators $\hat{b}_f^{s}(\vec{p})$, creating and annihilating the single fermion states, respectively, fulfil when applying on the vacuum state, $|\psi_{oc} > *_T |0_{\vec{p}} >$, the anticommutation relations for the second quantized fermions, postulated by Dirac (Ref. [5], Subsect. 3.3.1, Sect. 5). [11]

To write the creation operators for boson fields we must take into account that boson gauge fields have the space index α, describing the α component of the boson field in the ordinary space [12]. We therefore add the space index α as follows

$$^I\hat{\mathcal{A}}_{f\alpha}^{m\dagger}(\vec{p}) \,=\, \hat{b}_{\vec{p}}^\dagger \,*_T\, \mathcal{C}^m_{f\alpha}\, ^I\hat{\mathcal{A}}_f^{m\dagger}. \tag{11.34}$$

We treat free massless bosons of momentum $\vec{p}$ and energy $p^0 = |\vec{p}|$ and of particular "basis vectors" $^I\hat{\mathcal{A}}_f^{m\dagger}$'s which are eigenvectors of all the Cartan subalgebra members [13], $\mathcal{C}^m_{f\alpha}$ carry the space index α of the boson field. Creation operators operate on the vacuum state $|\psi_{oc_{ev}} > *_T |0_{\vec{p}} >$ with the internal space part just a constant, $|\psi_{oc_{ev}} >= |1 >$, and for a starting single boson state with a zero momentum from which one obtains the other single boson states with the same "basis vector" by the operators $\hat{b}_{\vec{p}}^\dagger$ which push the momentum by an amount $\vec{p}$, making also $\mathcal{C}^m_{f\alpha}$ depending on $\vec{p}$.

For the creation operators for boson fields in a coordinate representation we find using Eqs. (11.30, 11.31)

$$^I\hat{\mathcal{A}}_{f\alpha}^{m\dagger}(\vec{x}, x^0) \,=\, \int_{-\infty}^{+\infty} \frac{d^{d-1}p}{(\sqrt{2\pi})^{d-1}}\, ^I\hat{\mathcal{A}}_{f\alpha}^{m\dagger}(\vec{p})\, e^{-i(p^0 x^0 - \varepsilon \vec{p}\cdot\vec{x})}\big|_{p^0=|\vec{p}|}. \tag{11.35}$$

---

[11] The anticommutation relations of Eq. (11.33) are valid also if we replace the vacuum state, $|\psi_{oc} > |0_{\vec{p}} >$, by the Hilbert space of Clifford fermions generated by the tensor product multiplication, $*_{T_H}$, of any number of the Clifford odd fermion states of all possible internal quantum numbers and all possible momenta (that is of any number of $\hat{b}_f^{s\dagger}(\vec{p})$ of any $(s, f, \vec{p})$), Ref. ([5], Sect. 5.).

[12] In the *spin-charge-family* theory the Higgs's scalars origin in the boson gauge fields with the vector index $(7, 8)$, Ref. ([5], Sect. 7.4.1, and the references therein).

[13] In general the energy eigenstates of bosons are in superposition of $^I\hat{\mathcal{A}}_f^{m\dagger}$. One example, which uses the superposition of the Cartan subalgebra eigenstates manifesting the $SU(3) \times U(1)$ subgroups of the group $SO(6)$, is presented in Fig. 11.2.

To understand what new does the Clifford algebra description of the internal space of fermion and boson fields, Eqs. (11.34, 11.35, 11.32), bring to our understanding of the second quantized fermion and boson fields and what new can we learn from this offer, we need to relate $\sum_{ab} c^{ab} \omega_{ab\alpha}$ and $\sum_{mf} {}^{I}\hat{\mathcal{A}}_f^{m\dagger} \mathcal{C}_\alpha^{mf}$, recognizing that ${}^{I}\hat{\mathcal{A}}_f^{m\dagger} \mathcal{C}_\alpha^{mf}$ are eigenstates of the Cartan subalgebra members, while $\omega_{ab\alpha}$ are not.

The gravity fields, the vielbeins and the two kinds of the spin connection fields, $f^a{}_\alpha$, $\omega_{ab\alpha}$, $\tilde{\omega}_{ab\alpha}$, respectively, are in the *spin-charge-family* theory (unifying spins, charges and families of fermions and offering not only the explanation for all the assumptions of the *standard model* but also for the increasing number of phenomena observed so far) the only boson fields in $d = (13+1)$, observed in $d = (3+1)$ besides as gravity also as all the other boson fields with the Higgs's scalars included [27]. We therefore need to relate

$$\{\frac{1}{2} \sum_{ab} S^{ab} \, \omega_{ab\alpha}\} \sum_m \beta^{mf} \, \hat{b}_f^{m\dagger}(\vec{p}) \text{ relate to } \{ \sum_{m'f'} {}^{I}\hat{\mathcal{A}}_{f'}^{m'\dagger} \, \mathcal{C}_\alpha^{m'f'} \} \sum_m \beta^{mf} \, \hat{b}_f^{m\dagger}(\vec{p}) \, ,$$

$$\forall f \text{ and } \forall \beta^{mf} \, ,$$

$$\mathcal{S}^{cd} \sum_{ab} (c^{ab}{}_{mf} \, \omega_{ab\alpha}) \text{ relate to } \mathcal{S}^{cd} \, ({}^{I}\hat{\mathcal{A}}_f^{m\dagger} \, \mathcal{C}_\alpha^{mf}) \, ,$$

$$\forall \, (m, f) \, ,$$

$$\forall \text{ Cartan subalgebra member} \tag{11.36}$$

Let be repeated that ${}^{I}\hat{\mathcal{A}}_f^{m\dagger}$ are chosen to be the eigenvectors of the Cartan subalgebra members, Eq. (19.4). Correspondingly we can relate a particular ${}^{I}\hat{\mathcal{A}}_f^{m\dagger} \mathcal{C}_\alpha^{mf}$ with such a superposition of $\omega_{ab\alpha}$'s which is the eigenvector with the same values of the Cartan subalgebra members as there is a particular ${}^{I}\hat{\mathcal{A}}_f^{m\dagger} \mathcal{C}_\alpha^{mf}$. We can do this in two ways:

i.   Using the first relation in Eq. (11.36). On the left hand side of this relation S^{ab}'s apply on $\hat{b}_f^{m\dagger}$ part of $\hat{b}_f^{m\dagger}(\vec{p})$. On the right hand side ${}^{I}\hat{\mathcal{A}}_f^{m\dagger}$ apply as well on the same "basis vector" $\hat{b}_f^{m\dagger}$.

ii.   Using the second relation, in which $\mathcal{S}^{cd}$ apply on the left hand side on $\omega_{ab\alpha}$'s

$$\mathcal{S}^{cd} \sum_{ab} c^{ab}{}_{mf} \, \omega_{ab\alpha} = \sum_{ab} c^{ab}{}_{mf} \, i \, (\omega_{cb\alpha} \eta^{ad} - \omega_{db\alpha} \eta^{ac} + \omega_{ac\alpha} \eta^{bd} - \omega_{ad\alpha}) \tag{11.37}$$

on each $\omega_{ab\alpha}$ separately; $c^{ab}{}_{mf}$ are constants to be determined from the second relation, where on the right hand side of this relation $\mathcal{S}^{cd}(= S^{cd} + \tilde{S}^{cd})$ apply on the "basis vector" ${}^{I}\hat{\mathcal{A}}_f^{m\dagger}$ of the corresponding gauge field.

Let us conclude this section by pointing out that either the Clifford odd "basis vectors" $\hat{b}_f^{m\dagger}$ or the Clifford even "basis vectors" ${}^{i}\hat{\mathcal{A}}_f^{m\dagger}$, $i = (I, II)$ have in any even d $2^{\frac{d}{2}-1} \times 2^{\frac{d}{2}-1}$ members, while $\omega_{ab\alpha}$ as well as $\tilde{\omega}_{ab\alpha}$ have each for each α $\frac{d}{2}(d-1)$ members. It is needed to find out what new does this difference bring into the - unifying theories of the Kaluza-Klein theories are.

11.3   Short overview and achievements of *spin-charge-family* theory

The *spin-chare-family* theory [1,2,23,25,27–32] is a kind of the Kaluza-Klein theories [27,38–45] since it is built on the assumption that the dimension of space-time is $\geq (13+1)$ [14], and that the only interaction among fermions is the gravitational one (vielbeins, the gauge fields of momenta, and two kinds of the spin connection fields, the gauge fields of S^{ab} and of $\tilde{S}^{ab}$ [15]).

This theory assumes as well that the internal space of fermion and boson fields are described by the Clifford odd and Clifford even algebra, respectively [6,7] [16].

The theory is offering the explanation for all the assumptions of the *standard model*, unifying not only charges, but also spins, charges and families, [36,37,46,48,51] and consequently offering the explanation for the appearance of families of quarks and leptons and antiquarks and antileptons, of vector gauge fields [27], of Higgs's scalar field and the Yukawa couplings [28,30,32,36], for the differences in masses among quarks and leptons [46,51], for the matter-antimatter asymmetry in the universe [51], for the *dark matter* [49], making several predictions.

The *spin-charge-family* theory shares with the Kaluza-Klein like theories their weak points, like: **a.** Not yet solved the quantization problem of the gravitational field [17]. **b.** The spontaneous symmetry breaking which would at low energies manifest the observed almost massless fermions [30,32,34,39]. The spontaneously break of the starting symmetry of $SO(13+1)$ with the condensate of the two right handed neutrinos (with the family quantum numbers of the group of four families, which does not include the observed three families ([19], Table III), ([5], Table 6) bringing masses of the scale $\propto 10^{16}$ GeV or higher to all the vector and scalar gauge fields, which interact with the condensate [25] is promising to show the right way [32–34].

The scalar fields (scalar fields are the spin connection fields with the space index α higher than $(0,1,2,3)$) with the space index $(7,8)$ offer, after gaining constant non zero vacuum values, the explanation for the Higgs's scalar and the Yukawa couplings. They namely determine the mass matrices of quarks and leptons and antiquarks and antileptons. In Refs. [24,27] it is pointed out that the spin connection

---

[14] d $= (13+1)$ is the smallest dimension for which the subgroups of the group $SO(13,1)$ offer the description of spins and charges of fermions assumed by the *standard model* and correspondingly also of boson gauge fields.

[15] If there are no fermions present both spin connection fields are expressible with vielbeins ([5], Eq. (103)).

[16] Fermions and bosons internal spaces are assumed to be superposition of odd products of γ^a's (fermion fields) or of even products of γ^a's (boson fields) what offers the explanation for the second quantized postulates of Dirac [16]. The "basis vectors" of the internal spaces namely determine anticommutativity or commutativity of the corresponding creation and annihilation operators.

[17] The description of the internal space of fermions and bosons as superposition of odd (for fermion fields) or even (for boson fields) products of the Clifford objects γ^a's seems very promising in looking for a new way to second quantization of all fields, with gravity included, as discussed in this talk.

gauge fields do manifest in $d = (3+1)$ as the ordinary gravity and all the observed vector and scalar gauge fields.

The *spin-charge-family* theory assumes a simple starting action for second quantized massless fermion and the corresponding gauge boson fields in $d = (13+1)$-dimensional space, presented in Eq. (19.1).

The fermion part of the action, Eq. (19.1), can be rewritten in the way that it manifests in $d = (3+1)$ in the low energy regime before the electroweak break by the *standard model* postulated properties of: **i.** Quarks and leptons and antiquarks and antileptons with the spins, handedness, charges and family quantum numbers. Their internal space is described by the Clifford odd "basis vectors" which are eigenvectors of the Cartan subalgebra of S^{ab} and $\tilde{S}^{ab}$, Eqs. (19.4, 11.29, 11.28).

ii. Couplings of fermions to the vector gauge fields, which are the superposition of gauge fields $\omega^{st}{}_\alpha$, Sect. 6.2 in Ref. [5], with the space index $\alpha = (0, 1, 2, 3)$ and with the charges determined by the Cartan subalgebra of S^{ab} and $\tilde{S}^{ab}$ manifesting the symmetry of space $(d-4)$, and to the scalar gauge fields [1, 2, 23, 24, 26, 29, 31, 36, 37, 48–50] with the space index $\alpha \geq 5$ and the charges determined by the Cartan subalgebra of S^{ab} and $\tilde{S}^{ab}$ (as explained in the case of the vector gauge fields), and which are superposition of either $\omega^{st}{}_\alpha$ or $\tilde{\omega}^{ab}{}_\alpha$,

$$\mathcal{L}_f = \bar{\psi}\gamma^m(p_m - \sum_{A,i} g^{Ai}\tau^{Ai}A_m^{Ai})\psi +$$
$$\{\sum_{s=7,8} \bar{\psi}\gamma^s p_{0s}\,\psi\} +$$
$$\{\sum_{t=5,6,9,\ldots,14} \bar{\psi}\gamma^t p_{0t}\,\psi\}, \tag{11.38}$$

where $p_{0s} = p_s - \frac{1}{2}S^{s's"}\omega_{s's"s} - \frac{1}{2}\tilde{S}^{ab}\tilde{\omega}_{abs}$, $p_{0t} = p_t - \frac{1}{2}S^{t't"}\omega_{t't"t} - \frac{1}{2}\tilde{S}^{ab}\tilde{\omega}_{abt}$, with $p_{0s} = e_s^\alpha p_{0\alpha}$, $m \in (0, 1, 2, 3)$, $s \in (7, 8)$, $(s', s") \in (5, 6, 7, 8)$, (a, b) (appearing in $\tilde{S}^{ab}$) run within either $(0, 1, 2, 3)$ or $(5, 6, 7, 8)$, t runs $\in (5, \ldots, 14)$, $(t', t")$ run either $\in (5, 6, 7, 8)$ or $\in (9, 10, \ldots, 14)$. The spinor function ψ represents all family members of all the $2^{\frac{7+1}{2}-1} = 8$ families.

The first line of Eq. (11.38) determines in $d = (3+1)$ the kinematics and dynamics of fermion fields coupled to the vector gauge fields [23, 27, 31]. The vector gauge fields are the superposition of the spin connection fields ω_{stm}, $m = (0, 1, 2, 3)$, $(s, t) = (5, 6, \cdots, 13, 14)$, and are the gauge fields of S^{st}, Subsect. (6.2.1) of Ref. [5]. The reader can find in Sect. 6 of Ref. [5] a quite detailed overview of the properties which the massless fermion and boson fields appearing in the simple starting action, Eq. (19.1), (the later only as gravitational fields) manifest in $d = (3+1)$ as all the observed fermions — quarks and leptons and antiquarks and antileptons in each family — appearing in twice four families, with the lower four families including the observed three families of quarks and leptons and antiquarks and antileptons. The higher four families offer the explanation for the dark matter [49]. Table 5 and Eq. (110) of Ref. [5] explain that the scalar fields with the space index $\alpha = (7, 8)$ carry the weak charge $\tau^{13} = \pm\frac{1}{2}$ and the hyper charge $Y = \mp\frac{1}{2}$, just as assumed by the *standard model*.

Masses of families of quarks and leptons are determined by the superposition of the scalar fields, Eq. (108-120) of Ref. [5], appearing in two groups, each of them manifesting the symmetry $SU(2) \times SU(2) \times U(1)$ [18].

The scalar gauge fields with the space index $(7, 8)$ determine correspondingly the symmetry of mass matrices of quarks and leptons ([5], Eq. (111)) which appear in two groups as the scalar fields do [49, 51]. In Table 5 in Ref. [5]) the symmetry $SU(2) \times SU(2) \times U(1)$ for each of the two groups is presented and explained.

Although spontaneous symmetry braking of the starting symmetry has not (yet consistently enough) been studied and the coupling constants of the scalar fields among themselves and with quarks and leptons are not yet known, the known symmetry of mass matrices, presented in Eq. (111) of Ref. [5], enables to determine parameters of mass matrices from the measured data of the 3×3 sub mixing matrices and the masses of the measured three families of quarks and leptons.

Although the known 3×3 submatrix of the unitary 4×4 matrix enables to determine 4×4 matrix, the measured 3×3 mixing sub matrix is even for quarks far accurately enough measured, so that we only can predict the matrix elements of the 4×4 mixing matrix for quarks if assuming that masses (times c^2) of the fourth family quarks are heavy enough, that is above one TeV [46, 49]. The new measurements of the matrix elements among the observed 3 families agree better with the predictions obtained by the *sspin-charge-family* theory than the old measurements. The reader can find predictions in Refs. ([50, 51]) and the overview in Ref. ([5], Subsect. 7.3.1).

The upper group of four families offers the explanation for the *dark matter*, to which the quarks and leptons from the (almost) stable of the upper four families mostly contribute. The reader can find the report on this proposal for the *dark matter* origin in Ref. [49] and a short overview in Subsect. 7.3.1 of [5], where the appearance, development and properties of the *dark matter* are discussed. The upper four families predict nucleons of very heavy quarks with the nuclear force among nucleons which is correspondingly very different from the known one [49, 52].

Besides the scalar fields with the space index $\alpha = (7, 8)$, which manifest in $d = (3 + 1)$ as scalar gauge fields with the weak and hyper charge $\pm\frac{1}{2}$ and $\mp\frac{1}{2}$, respectively, and which gaining at low energies constant values make families of quarks and leptons and the weak gauge field massive, there are in the starting action, Eqs. (19.1), additional scalar gauge fields with the space index $\alpha = (9, 10, 11, 12, 13, 14)$. They are with respect to the space index α either triplets or antitriplets causing transitions from antileptons into quarks and from antiquarks into quarks and back.

---

[18] The assumption that the symmetry $SO(13, 1)$ first breaks into $SU(3) \times U(1) \times SO(7, 1)$ makes that quarks and leptons distinguish only in the part $SU(3) \times U(1)$, while the $SO(7, 1)$ part is identical separately for quarks and leptons and separately for antiquarks and antileptons. Table 7 of Ref. [5], presenting one family, which includes quarks and leptons and antiquarks and antileptons, manifests these properties. The $\omega_{ab\alpha}$, with the space index $(7, 8)$ carry with respect to the flat index ab only quantum numbers $Q, Y, \tau^4, (Q (= \tau^{13} + Y), \tau^{13} (= \frac{1}{2}(S^{56} - S^{78}), Y (= \tau^4 + \tau^{23})$ and $\tau^4 = -\frac{1}{3}(S^{9\,10} + S^{11\,12} + S^{13\,14})$, the flat index (ab) of $\tilde{\omega}_{ab\alpha}$, with the space index $(7, 8)$, includes all $(0, 1, \ldots, 8)$ correspondingly forming the symmetry $SU(2) \times SU(2) \times U(1)$.

Their properties are presented in Ref. [25] and briefly in Table 9 and Fig. 1 of Ref. [5].

Concerning this second point we proved on the toy model of $d = (5+1)$ that the break of symmetry can lead to (almost) massless fermions [34].

In $d = (3+1)$-dimensional space — at low energies — the gauge gravitational fields manifest as the observed vector gauge fields [27], which can be quantized in the usual way.

The author is in mean time trying to find out (together with the collaborators) how far can the *spin-charge-family* theory — starting in $d = (13+1)$-dimensional space with a simple and "elegant" action, Eq. (19.1) — reproduce in $d = (3+1)$ the observed properties of quarks and leptons [23, 25, 27–32], the observed vector gauge fields, the scalar field and the Yukawa couplings, the appearance of the *dark matter* and of the matter-antimatter asymmetry, as well as the other open questions, connecting elementary fermion and boson fields and cosmology.

The work done so far on the *spin-charge-family* theory seems promising.

11.4   Conclusions

In the *spin-charge-family* theory [1, 2, 5, 23, 25, 27–32] the Clifford odd algebra is used to describe the internal space of fermion fields. The Clifford odd "basis vectors" — the superposition of odd products of γ^a's — in a tensor product with the basis in ordinary space form the creation and annihilation operators, in which the anticommutativity of the "basis vectors" is transferred to the creation and annihilation operators for fermions, offering the explanation for the second quantization postulates for fermion fields.

The Clifford odd "basis vectors" have all the properties of fermions: Half integer spins with respect to the Cartan subalgebra members of the Lorentz algebra in the internal space of fermions in even dimensional spaces ($d = 2(2n+1)$ or $d = 4n$), as discussed in Subsects. (11.2.1, 11.2.3).

With respect to the subgroups of the $SO(d-1, 1)$ group the Clifford odd "basis vectors" appear in the fundamental representations, as illustrated in Subsects. 11.2.2. In this article it is demonstrated that the Clifford even algebra is offering the description of the internal space of boson fields. The Clifford even "basis vectors" — the superposition of even products of γ^a's — in a tensor product with the basis in ordinary space form the creation and annihilation operators which manifest the commuting properties of the second quantized boson fields, offering explanation for the second quantization postulates for boson fields [9]. The Clifford even "basis vectors" have all the properties of bosons: Integer spins with respect to the Cartan subalgebra members of the Lorentz algebra in the internal space of bosons, as discussed in Subsects. (11.2.1, 11.2.3).

With respect to the subgroups of the $SO(d-1, 1)$ group the Clifford even "basis vectors" manifest the adjoint representations, as illustrated in Subsect. 11.2.2.

There are two kinds of anticommuting algebras [2]: The Grassmann algebra, offering in d-dimensional space $2 \cdot 2^d$ operators (2^d θ^a's and 2^d $\frac{\partial}{\partial \theta_a}$'s, Hermitian

conjugated to each other, Eq. (11.3)), and the two Clifford subalgebras, each with 2^d operators named γ^a's and $\tilde{\gamma}^a$'s, respectively, [2, 13, 14], Eqs. (11.2-19.3).

The operators in each of the two Clifford subalgebras appear in two groups of $2^{\frac{d}{2}-1} \times 2^{\frac{d}{2}-1}$ of the Clifford odd operators (the odd products of either γ^a's in one subalgebra or of $\tilde{\gamma}^a$'s in the other subalgebra), which are Hermitian conjugated to each other: In each Clifford odd group of any of the two subalgebras there appear $2^{\frac{d}{2}-1}$ irreducible representation each with the $2^{\frac{d}{2}-1}$ members and the group of their Hermitian conjugated partners.

There are as well the Clifford even operators (the even products of either γ^a's in one subalgebra or of $\tilde{\gamma}^a$'s in another subalgebra) which again appear in two groups of $2^{\frac{d}{2}-1} \times 2^{\frac{d}{2}-1}$ members each. In the case of the Clifford even objects the members of each group of $2^{\frac{d}{2}-1} \times 2^{\frac{d}{2}-1}$ members have the Hermitian conjugated partners within the same group, Subsect. 11.2.1, Table 11.1.

The Grassmann algebra operators are expressible with the operators of the two Clifford subalgebras and opposite, Eq. (11.5). The two Clifford subalgebras are independent of each other, Eq. (19.3), forming two independent spaces.

Either the Grassmann algebra [15, 20] or the two Clifford subalgebras can be used to describe the internal space of anticommuting objects, if the superposition of odd products of operators (θ^a's or γ^a's, or $\tilde{\gamma}^a$'s) are used to describe the internal space of these objects. The commuting objects must be superposition of even products of operators (θ^a's or γ^a's or $\tilde{\gamma}^a$'s).

No integer spin anticommuting objects have been observed so far, and to describe the internal space of the so far observed fermions only one of the two Clifford odd subalgebras are needed.

The problem can be solved by reducing the two Clifford sub algebras to only one, the one (chosen to be) determined by γ^{ab}'s. The decision that $\tilde{\gamma}^a$'s apply on γ^a as follows: $\{\tilde{\gamma}^a B = (-)^B i B\gamma^a\}|\psi_{oc} >$, Eq. (19.6), (with $(-)^B = -1$, if B is a function of an odd products of γ^a's, otherwise $(-)^B = 1$) enables that $2^{\frac{d}{2}-1}$ irreducible representations of $S^{ab} = \frac{i}{2}\{\gamma^a, \gamma^b\}_-$ (each with the $2^{\frac{d}{2}-1}$ members) obtain the family quantum numbers determined by $\tilde{S}^{ab} = \frac{i}{2}\{\tilde{\gamma}^a, \tilde{\gamma}^b\}_-$.

The decision to use in the *spin-charge-family* theory in d $= 2(2n + 1)$, $n \geq 3$ (d $\geq (13+1)$ indeed), the superposition of the odd products of the Clifford algebra elements γ^a's to describe the internal space of fermions which interact with the gravity only (with the vielbeins, the gauge fields of momenta, and the two kinds of the spin connection fields, the gauge fields of S^{ab} and $\tilde{S}^{ab}$, respectively), Eq. (19.1), offers not only the explanation for all the assumed properties of fermions and bosons in the *standard model*, with the appearance of the families of quarks and leptons and antiquarks and antileptons ([5] and the references therein) and of the corresponding vector gauge fields and the Higgs's scalars included [27], but also for the appearance of the *dark matter* [49] in the universe, for the explanation of the matter/antimatter asymmetry in the universe [25], and for several other observed phenomena, making several predictions [37, 47, 48, 50].

Recognition that the use of the superposition of the even products of the Clifford algebra elements γ^a's to describe the internal space of boson fields, what appear

to manifest all the properties of the observed boson fields, as demonstrated in this articles, makes clear that the Clifford algebra offers not only the explanation for the postulates of the second quantized anticommuting fermion fields but also for the postulates of the second quantized boson fields.

The relations in Eq. (11.36)

$$\{\frac{1}{2}\sum_{ab}S^{ab}\,\omega_{ab\alpha}\}\sum_{m}\beta^{mf}\,\hat{b}_{f}^{m\dagger}(\vec{p})\text{ relate to }\{\sum_{m'f'}{}^{I}\hat{\mathcal{A}}_{f'}^{m'\dagger}\,\mathcal{C}_{\alpha}^{m'f'}\}\sum_{m}\beta^{mf}\,\hat{b}_{f}^{m\dagger}(\vec{p}),$$

$$\forall f\text{ and }\forall\beta^{mf},$$

$$\mathcal{S}^{cd}\sum_{ab}(c^{ab}{}_{mf}\,\omega_{ab\alpha})\text{ relate to }\mathcal{S}^{cd}\,({}^{I}\hat{\mathcal{A}}_{f}^{m\dagger}\,\mathcal{C}_{\alpha}^{mf}),$$

$$\forall\,(m,f),$$

$$\forall\text{ Cartan subalgebra member }\mathcal{S}^{cd},$$

offers the possibility to replace the covariant derivative $p_{0\alpha}$

$$p_{0\alpha}=p_{\alpha}-\frac{1}{2}S^{ab}\omega_{ab\alpha}-\frac{1}{2}\tilde{S}^{ab}\tilde{\omega}_{ab\alpha}$$

in Eq. (19.1) with

$$p_{0\alpha}=p_{\alpha}-\sum_{mf}{}^{I}\hat{\mathcal{A}}_{f}^{m\dagger I}\mathcal{C}_{f\alpha}^{m}-\sum_{mf}{}^{I}\widehat{\tilde{\mathcal{A}}}_{f}^{m\dagger}\,{}^{I}\widetilde{\mathcal{C}}_{f\alpha}^{m},$$

where the relation among ${}^{I}\widehat{\tilde{\mathcal{A}}}_{f}^{m\dagger}\,{}^{I}\widetilde{\mathcal{C}}_{f\alpha}^{m}$ and ${}^{II}\widehat{\tilde{\mathcal{A}}}_{f}^{m\dagger}\,{}^{II}\widetilde{\mathcal{C}}_{f\alpha}^{m}$ with respect to $\omega_{ab\alpha}$ and $\tilde{\omega}_{ab\alpha}$, not discussed directly in this article, needs additional study and explanation.

Although the properties of the Clifford odd and even "basis vectors" and correspondingly of the creation and annihilation operators for fermion and boson fields are, hopefully, clearly demonstrated in this article, yet the proposed way of the second quantization of fields, the fermion and the boson ones, needs further study to find out what new can the description of the internal space of fermions and bosons bring in understanding of the second quantized fields.

Let be added that in even dimensional spaces the Clifford odd "basis vectors" carry only one handedness, either right or left, depending on the definition of handedness and the choice of the "basis vectors". Their Hermitian conjugated partners carry opposite handedness. The "basis vectors" in the subspace of the whole space do have both handedness. In odd dimensional spaces ($d=(2n+1)$) the operator of handedness is a superposition of an odd products of γ^{a}'s. The eigenstates of the operator of handedness must be therefore the superposition of the Clifford odd and the Clifford even "basis vectors". These eigenstates can have either right or left handed. The properties of "basis vectors" in odd dimensional spaces are demonstrated in the App. 11.5 of this contribution for $d=1$ and $d=(2+1)$ spaces.

It looks like that this study, showing up that the Clifford algebra can be used to describe the internal spaces of fermion and boson fields in an equivalent way, offering correspondingly the explanation for the second quantization postulates

for fermion and boson fields, is opening the new insight into the quantum field theory, since studies of the interaction of fermion fields with boson fields and of boson fields with boson fields so far looks very promising.

The study of properties of the second quantized boson fields, the internal space of which is described by the Clifford even algebra, has just started and needs further consideration. Studying properties of "basis vectors" in odd dimensional spaces might help to understand anomalies of quantum fields.

11.5 Examples demonstrating properties of Clifford odd and even "basis vectors" in odd dimensional spaces for $d = (1)$, $d = (2 + 1)$

The *spin-charge-family* theory, using even dimensional spaces, $d = (13 + 1)$ indeed, offers the explanation for all the assumptions of the *standard model*, explaining as well the postulates for the second quantization of fermion and boson fields. The internal space of fermions is in this theory described by "basis vectors" which are superposition of odd products of γ^a's while the internal space of bosons is described by "basis vectors" which are superposition of even products of γ^a's. Subsect. 11.2.2 demonstrates properties of the Clifford odd and even "basis vectors" in special cases when $d = (1 + 1)$, $d = (3 + 1)$, and $d = (5 + 1)$.

Let us discuss here odd dimensional spaces, which have very different properties:

i. While in even dimensional spaces the Clifford odd "basis vectors" have $2^{\frac{d}{2}-1}$ members m in $2^{\frac{d}{2}-1}$ families f, $\hat{b}_f^{m\dagger}$, and their Hermitian conjugated partners appear in a separate group of $2^{\frac{d}{2}-1}$ members in $2^{\frac{d}{2}-1}$ families, there are in odd dimensional spaces some of the $2^{\frac{d}{2}-1} \times 2^{\frac{d}{2}-1} = 2^{d-2}$ Clifford odd "basis vectors" self adjoint and have correspondingly some of the Hermitian conjugated partners in another group with 2^{d-2} members.

ii. In even dimensional spaces the Clifford even "basis vectors" $^i\hat{\mathcal{A}}_f^{m\dagger}$, $i = (1, 2)$, appear in two orthogonal groups, each with $2^{\frac{d}{2}-1} \times 2^{\frac{d}{2}-1}$ members and each with the Hermitian conjugated partners within the same group, $2^{\frac{d}{2}-1}$ of them are self adjoint. In odd dimensional spaces the Clifford even "basis vectors" appear in two groups, each with $2^{\frac{d}{2}-1} \times 2^{\frac{d}{2}-1} = 2^{d-2}$ members, which are either self adjoint or have their Hermitian conjugated partners in another group. Not all the members of one group are orthogonal to the members of another group, only the self adjoint ones are orthogonal.

iii. While $\hat{b}_f^{m\dagger}$ have in even dimensional spaces one handedness only (either right or left, depending on the definition of handedness), in odd dimensional spaces the operator of handedness is a Clifford odd object, still commuting with S^{ab}, which is the product of odd number of γ^a's and correspondingly transforms the Clifford odd "basis vectors" into Clifford even "basis vectors" and opposite. Correspondingly are the eigenvectors of handedness the superposition of the Clifford odd and the Clifford even "basis vectors". Correspondingly there are in odd dimensional

spaces right handed and left handed eigenvectors of the operator of handedness.

Let us illustrate the above mentioned properties of the "basis vectors" in odd dimensional spaces, starting with the simplest case:

d=(1)

There is one Clifford odd "basis vector"

$$\hat{b}_1^{1\dagger} = \gamma^0$$

and one Clifford even "basis vectors"

$$^i\hat{\mathcal{A}}_1^{1\dagger} = 1\,.$$

The operator of handedness $\Gamma^{(0+1)} = \gamma^0$ transforms $\hat{b}_1^{1\dagger}$ into identity $^i\hat{\mathcal{A}}_1^{1\dagger}$ and $^i\hat{\mathcal{A}}_1^{1\dagger}$ into $\hat{b}_1^{1\dagger}$.

The two eigenvectors of the operator of handedness are

$$\frac{1}{\sqrt{2}}(\gamma^0 + 1)\,, \quad \frac{1}{\sqrt{2}}(\gamma^0 - 1)\,,$$

with the handedness $(+1, -1)$, that is of right and left handedness. respectively.

d=(2+1)

There are twice $2^{d=3-2} = 2$ Clifford odd "basis vectors". We chose as the Cartan subalgebra member S^{01} of S^{ab}: $\hat{b}_1^{1\dagger} =\overset{01}{[-i]}\gamma^2$, $\hat{b}_1^{2\dagger} =\overset{01}{(+i)}$, $\hat{b}_2^{1\dagger} =\overset{01}{(-i)}$, $\hat{b}_2^{2\dagger} =\overset{01}{[+i]}\gamma^2$, with the properties

$$
\begin{array}{ccc}
f = 1 & f = 2 & \\
\tilde{S}^{01} = \frac{i}{2} & \tilde{S}^{01} = -\frac{i}{2}, & S^{01} \\
\hat{b}_1^{1\dagger} =\overset{01}{[-i]}\gamma^2 & \hat{b}_2^{1\dagger} =\overset{01}{(-i)} & -\frac{i}{2} \\
\hat{b}_1^{2\dagger} =\overset{01}{(+i)} & \hat{b}_2^{2\dagger} =\overset{03}{[+i]}\gamma^2 & \frac{i}{2},
\end{array}
$$

$\hat{b}_1^{1\dagger}$ and $\hat{b}_2^{2\dagger}$ are self adjoint (up to a sign), $\hat{b}_1^{2\dagger} =\overset{01}{(+i)}$ and $\hat{b}_2^{1\dagger} =\overset{01}{(-i)}$ are Hermitian conjugated to each other.

In odd dimensional spaces the "basis vectors" are not separated from their Hermitian conjugated partners and are correspondingly not well defined.

The operator of handedness is (chosen up to a sign to be) $\Gamma^{(2+1)} = i\gamma^1\gamma^2\gamma^2$.

There are twice $2^{(d=3)-2} = 2$ Clifford even "basis vectors". We choose as the Cartan subalgebra member $\mathcal{S}^{01}$: $^I\hat{\mathcal{A}}_1^{1\dagger} =\overset{01}{[+i]}$, $^I\hat{\mathcal{A}}_1^{2\dagger} =\overset{01}{(-i)}\gamma^2$, $^{II}\hat{\mathcal{A}}_2^{1\dagger} =\overset{01}{[-i]}$, $^{II}\hat{\mathcal{A}}_2^{2\dagger} =\overset{01}{(+i)}\gamma^2$, with the properties

$$
\begin{array}{cccc}
& \mathcal{S}^{01} & & \mathcal{S}^{01} \\
{}^{I}\hat{\mathcal{A}}_1^{1\dagger} = [\overset{01}{+i}] & 0 & {}^{II}\hat{\mathcal{A}}_2^{1\dagger} = [\overset{01}{-i}] & 0 \\
{}^{I}\hat{\mathcal{A}}_1^{2\dagger} = (\overset{01}{-i})\,\gamma^2 & -i & {}^{II}\hat{\mathcal{A}}_2^{2\dagger} = (\overset{03}{+i})\,\gamma^2 & i,
\end{array}
$$

${}^{I}\hat{\mathcal{A}}_1^{1\dagger} = [\overset{01}{+i}]$ and ${}^{II}\hat{\mathcal{A}}_2^{1\dagger} = [\overset{01}{-i}]$ are self adjoint, ${}^{I}\hat{\mathcal{A}}_1^{2\dagger} = (\overset{01}{-i})\,\gamma^2$ and ${}^{II}\hat{\mathcal{A}}_2^{2\dagger} = (\overset{03}{+i})\,\gamma^2$ are Hermitian conjugated to each other.

In odd dimensional spaces the two groups of the Clifford even "basis vectors" are not orthogonal.

Let us find the eigenvectors of the operator of handedness $\Gamma^{(2+1)} = i\gamma^0\gamma^1\gamma^2$. Since it is the Clifford odd object its eigenvectors are superposition of Clifford odd and Clifford even "basis vectors".
It follows

$$
\begin{aligned}
\Gamma^{(2+1)}\{[\overset{01}{-i}] \pm i\,[\overset{01}{-i}]\,\gamma^2\} &= \mp\{[\overset{01}{-i}] \pm i\,[\overset{01}{-i}]\,\gamma^2\}, \\
\Gamma^{(2+1)}\{(\overset{01}{+i}) \pm i\,(\overset{01}{+i})\,\gamma^2\} &= \mp\{(\overset{01}{+i}) \pm i\,(\overset{01}{+i})\,\gamma^2\}, \\
\Gamma^{(2+1)}\{[\overset{01}{+i}] \pm i\,[\overset{01}{+i}]\,\gamma^2\} &= \pm\{[\overset{01}{+i}] \pm i\,[\overset{01}{+i}]\,\gamma^2\}, \\
\Gamma^{(2+1)}\{(\overset{01}{-i})\,\gamma^2 \pm i\,(\overset{01}{-i})\} &= \pm\{(\overset{01}{-i})\,\gamma^2 \pm i\,(\overset{01}{-i})\},
\end{aligned}
$$

We can conclude that neither Clifford odd nor Clifford even "basis vectors" have in odd dimensional spaces the properties which they demonstrate in even dimensional spaces.
i. In odd dimensional spaces the "basis vectors" are not separated from their Hermitian conjugated partners and are correspondingly not well defined, that is we can not define creation and annihilation operators as a tensor products of "basis vectors" and basis in momentum space.
In odd dimensional spaces the two groups of the Clifford even "basis vectors" are not orthogonal, only self adjoint "basis vectors" are orthogonal, the rest of "basis vectors" have their Hermitian conjugated partners in another group.
ii. The Clifford odd operator of handedness allows left and right handed superposition of Clifford odd and Clifford even "basis vectors".

11.5.1 Acknowledgment

References

1. H. Georgi, in *Particles and Fields* (edited by C. E. Carlson), A.I.P., 1975; Google Scholar.

2. H. Fritzsch and P. Minkowski, *Ann. Phys.* **93** (1975) 193.

3. J. Pati and A. Salam, *Phys.Rev.* **D 8** (1973) 1240.

4. H. Georgy and S.L. Glashow, *Phys. Rev. Lett.* **32** (1974) 438.
5. Y. M. Cho, *J. Math. Phys.* **16** (1975) 2029.
6. Y. M. Cho, P. G. O. Freund, *Phys. Rev.* **D 12** (1975) 1711.
7. N. Mankoč Borštnik, "Spin connection as a superpartner of a vielbein", *Phys. Lett.* **B 292** (1992) 25-29.
8. N. Mankoč Borštnik, "Spinor and vector representations in four dimensional Grassmann space", *J. of Math. Phys.* **34** (1993) 3731-3745.
9. N. Mankoč Borštnik, "Unification of spin and charges in Grassmann space?", hep-th 9408002, IJS.TP.94/22, Mod. Phys. Lett.**A (10)** No.7 (1995) 587-595.
10. N. S. Mankoč Borštnik, H. B. Nielsen, "How does Clifford algebra show the way to the second quantized fermions with unified spins, charges and families, and with vector and scalar gauge fields beyond the *standard model*", Progress in Particle and Nuclear Physics, http://doi.org/10.1016.j.ppnp.2021.103890 .
11. N. S. Mankoč Borštnik, "How Clifford algebra can help understand second quantization of fermion and boson fields", [arXiv: 2210.06256. physics.gen-ph].
12. N. S. Mankoč Borštnik, "Clifford odd and even objects offer description of internal space of fermions and bosons, respectively, opening new insight into the second quantization of fields", The 13$^{\text{th}}$ Bienal Conference on Classical and Quantum Relativistic Dynamics of Particles and Fields IARD 2022, Prague, $6 - 9$ June [http://arxiv.org/abs/2210.07004].

13. N.S. Mankoč Borštnik, H.B.F. Nielsen, "Understanding the second quantization of fermions in Clifford and in Grassmann space", *New way of second quantization of fermions — Part I and Part II*, in this proceedings [arXiv:2007.03517, arXiv:2007.03516].
14. N. S. Mankoč Borštnik, "How do Clifford algebras show the way to the second quantized fermions with unified spins, charges and families, and to the corresponding second quantized vector and scalar gauge field ", Proceedings to the 24$^{\text{rd}}$ Workshop "What comes beyond the standard models", 5 - 11 of July, 2021, Ed. N.S. Mankoč Borštnik, H.B. Nielsen, D. Lukman, A. Kleppe, DMFA Založništvo, Ljubljana, December 2021, [arXiv:2112.04378] .
15. N.S. Mankoč Borštnik, H.B.F. Nielsen, "Understanding the second quantization of fermions in Clifford and in Grassmann space" *New way of second quantization of fermions — Part I and Part II*, Proceedings to the 22$^{\text{nd}}$ Workshop "What comes beyond the standard models", 6 - 14 of July, 2019, Ed. N.S. Mankoč Borštnik, H.B. Nielsen, D. Lukman, DMFA Založništvo, Ljubljana, December 2019, [arXiv:1802.05554v4, arXiv:1902.10628].
16. P.A.M. Dirac *Proc. Roy. Soc. (London)*, **A 117** (1928) 610.
17. H.A. Bethe, R.W. Jackiw, "Intermediate quantum mechanics", New York : W.A. Benjamin, 1968.
18. S. Weinberg, "The quantum theory of fields", Cambridge, Cambridge University Press, 2015.
19. N.S. Mankoč Borštnik, H.B.F. Nielsen, "New way of second quantized theory of fermions with either Clifford or Grassmann coordinates and *spin-charge-family* theory " [arXiv:1802.05554v4,arXiv:1902.10628].
20. D. Lukman, N. S. Mankoč Borštnik, "Properties of fermions with integer spin described with Grassmann algebra", Proceedings to the 21$^{\text{st}}$ Workshop "What comes beyond the standard models", 23 of June - 1 of July, 2018, Ed. N.S. Mankoč Borštnik, H.B. Nielsen, D. Lukman, DMFA Založništvo, Ljubljana, December 2018 [arxiv:1805.06318,

arXiv:1902.10628].

21. N.S. Mankoč Borštnik, H.B.F. Nielsen, *J. of Math. Phys.* **43**, 5782 (2002) [arXiv:hep-th/0111257].

22. N.S. Mankoč Borštnik, H.B.F. Nielsen, "How to generate families of spinors", *J. of Math. Phys.* **44** 4817 (2003) [arXiv:hep-th/0303224].

23. N.S. Mankoč Borštnik, "Spin-charge-family theory is offering next step in understanding elementary particles and fields and correspondingly universe", Proceedings to the Conference on Cosmology, Gravitational Waves and Particles, IARD conferences, Ljubljana, 6-9 June 2016, The 10th Biennial Conference on Classical and Quantum Relativistic Dynamics of Particles and Fields, J. Phys.: Conf. Ser. 845 012017 [arXiv:1409.4981, arXiv:1607.01618v2].

24. N.S. Mankoč Borštnik, "The attributes of the Spin-Charge-Family theory giving hope that the theory offers the next step beyond the Standard Model", Proceedings to the 12th Bienal Conference on Classical and Quantum Relativistic Dynamics of Particles and Fields IARD 2020, Prague, $1 - 4$ June 2020 by ZOOM.

25. N.S. Mankoč Borštnik, "Matter-antimatter asymmetry in the *spin-charge-family* theory", *Phys. Rev.* **D 91** (2015) 065004 [arXiv:1409.7791].

26. N. S. Mankoč Borštnik, "How far has so far the Spin-Charge-Family theory succeeded to explain the Standard Model assumptions, the matter-antimatter asymmetry, the appearance of the Dark Matter, the second quantized fermion fields...., making several predictions", Proceedings to the 23rd Workshop "What comes beyond the standard models", 4 - 12 of July, 2020 Ed. N.S. Mankoč Borštnik, H.B. Nielsen, D. Lukman, DMFA Založništvo, Ljubljana, December 2020, [arXiv:2012.09640]

27. N.S. Mankoč Borštnik, D. Lukman, "Vector and scalar gauge fields with respect to d $= (3 + 1)$ in Kaluza-Klein theories and in the *spin-charge-family theory*", *Eur. Phys. J. C* **77** (2017) 231.

28. N.S. Mankoč Borštnik, "The *spin-charge-family* theory explains why the scalar Higgs carries the weak charge $\pm\frac{1}{2}$ and the hyper charge $\mp\frac{1}{2}$", Proceedings to the 17th Workshop "What comes beyond the standard models", Bled, 20-28 of July, 2014, Ed. N.S. Mankoč Borštnik, H.B. Nielsen, D. Lukman, DMFA Založništvo, Ljubljana December 2014, p.163-82 [arXiv:1502.06786v1] [arXiv:1409.4981].

29. N.S. Mankoč Borštnik N S, "The spin-charge-family theory is explaining the origin of families, of the Higgs and the Yukawa couplings", *J. of Modern Phys.* **4** (2013) 823 [arXiv:1312.1542].

30. N.S. Mankoč Borštnik, H.B.F. Nielsen, "The spin-charge-family theory offers understanding of the triangle anomalies cancellation in the standard model", *Fortschritte der Physik, Progress of Physics* (2017) 1700046.

31. N.S. Mankoč Borštnik, "The explanation for the origin of the Higgs scalar and for the Yukawa couplings by the *spin-charge-family* theory", *J.of Mod. Physics* **6** (2015) 2244-2274, http://dx.org./10.4236/jmp.2015.615230 [arXiv:1409.4981].

32. N.S. Mankoč Borštnik and H.B. Nielsen, "Why nature made a choice of Clifford and not Grassmann coordinates", Proceedings to the 20th Workshop "What comes beyond the standard models", Bled, 9-17 of July, 2017, Ed. N.S. Mankoč Borštnik, H.B. Nielsen, D. Lukman, DMFA Založništvo, Ljubljana, December 2017, p. 89-120 [arXiv:1802.05554v1v2].

33. N.S. Mankoč Borštnik and H.B.F. Nielsen, "Discrete symmetries in the Kaluza-Klein theories", *JHEP* 04:165, 2014 [arXiv:1212.2362].

34. D. Lukman, N.S. Mankoč Borštnik and H.B. Nielsen, "An effective two dimensionality cases bring a new hope to the Kaluza-Klein-like theories", *New J. Phys.* 13:103027, 2011.

35. N. S. Mankoč Borštnik, Second quantized "anticommuting integer spin fields", sent to arXiv.

36. A. Borštnik, N.S. Mankoč Borštnik, "Left and right handedness of fermions and bosons", J. of Phys. G: Nucl. Part. Phys.**24**(1998)963-977, hep-th/9707218.

37. A. Borštnik Bračič, N. S. Mankoč Borštnik, "On the origin of families of fermions and their mass matrices", hep-ph/0512062, Phys Rev. **D 74** 073013-28 (2006).

38. T. Kaluza, "On the unification problem in Physics", *Sitzungsber. d. Berl. Acad.* (1918) 204, O. Klein, "Quantum theory and five-dimensional relativity", *Zeit. Phys.* **37**(1926) 895.

39. E. Witten, "Search for realistic Kaluza-Klein theory",*Nucl. Phys.* **B 186** (1981) 412.

40. M. Duff, B. Nilsson, C. Pope, *Phys. Rep.* **C 130** (1984)1, M. Duff, B. Nilsson, C. Pope, N. Warner, *Phys. Lett.* **B 149** (1984) 60.

41. T. Appelquist, H. C. Cheng, B. A. Dobrescu, *Phys. Rev.* **D 64** (2001) 035002.

42. M. Saposhnikov, P. TinyakovP 2001 *Phys. Lett.* **B 515** (2001) 442 [arXiv:hep-th/0102161v2].

43. C. Wetterich,*Nucl. Phys.* **B 253** (1985) 366.

44. The authors of the works presented in *An introduction to Kaluza-Klein theories*, Ed. by H. C. Lee, World Scientific, Singapore 1983.

45. M. Blagojević, *Gravitation and gauge symmetries*, IoP Publishing, Bristol 2002.

46. M. Breskvar, D. Lukman, N. S. Mankoč Borštnik, "On the Origin of Families of Fermions and Their Mass Matrices — Approximate Analyses of Properties of Four Families Within Approach Unifying Spins and Charges", Proceedings to the 9th Workshop "What Comes Beyond the Standard Models", Bled, Sept. 16 - 26, 2006, Ed. by Norma Mankoč Borštnik, Holger Bech Nielsen, Colin Froggatt, Dragan Lukman, DMFA Založništvo, Ljubljana December 2006, p.25-50, hep-ph/0612250.

47. G. Bregar, M. Breskvar, D. Lukman, N.S. Mankoč Borštnik, "Families of Quarks and Leptons and Their Mass Matrices", Proceedings to the 10th international workshop "What Comes Beyond the Standard Model", 17 -27 of July, 2007, Ed. Norma Mankoč Borštnik, Holger Bech Nielsen, Colin Froggatt, Dragan Lukman, DMFA Založništvo, Ljubljana December 2007, p.53-70, hep-ph/0711.4681.

48. G. Bregar, M. Breskvar, D. Lukman, N.S. Mankoč Borštnik, "Predictions for four families by the Approach unifying spins and charges" *New J. of Phys.* **10** (2008) 093002, hep-ph/0606159, hep/ph-07082846.

49. G. Bregar, N.S. Mankoč Borštnik, "Does dark matter consist of baryons of new stable family quarks?", *Phys. Rev. D* **80**, 083534 (2009), 1-16.

50. G. Bregar, N.S. Mankoč Borštnik, "Can we predict the fourth family masses for quarks and leptons?", Proceedings (arxiv:1403.4441) to the 16 th Workshop "What comes beyond the standard models", Bled, 14-21 of July, 2013, Ed. N.S. Mankoč Borštnik, H.B. Nielsen, D. Lukman, DMFA Založništvo, Ljubljana December 2013, p. 31-51, http://arxiv.org/abs/1212.4055.

51. G. Bregar, N.S. Mankoč Borštnik, "The new experimental data for the quarks mixing matrix are in better agreement with the *spin-charge-family* theory predictions", Proceedings to the 17th Workshop "What comes beyond the standard models", Bled, 20-28 of July, 2014, Ed. N.S. Mankoč Borštnik, H.B. Nielsen, D. Lukman, DMFA Založništvo, Ljubljana December 2014, p.20-45 [arXiv:1502.06786v1] [arxiv:1412.5866].

52. N.S. Mankoč Borštnik, M. Rosina, "Are superheavy stable quark clusters viable candidates for the dark matter?", International Journal of Modern Physics D (IJMPD) **24** (No. 13) (2015) 1545003.

12 A Unified Solution to the Big Problems of the Standard model

R. N. Mohapatra[a], N. Okada[b]

[a] Maryland Center for Fundamental Physics and Department of Physics, University of Maryland, College Park, Maryland 20742, USA
[b] Department of Physics, University of Alabama, Tuscaloosa, Alabama 35487, USA

Abstract. We present a unified model that solves four major problems of the standard model i.e. neutrino masses, origin of matter, strong CP problem and dark matter. We use the Affleck-Dine (AD) mechanism for this purpose, with the AD-field playing the role of inflaton and where its cosmological evolution leads to the origin of matter. The model relates the neutrino masses to the baryon to photon ratio of the universe. The dark matter in the model is the axion field used to solve the strong CP problem. The model has two testable predictions: (i) a near massless Majorana fermion which contributes to $\Delta N_{eff} \sim 0.1$ in the early universe, which can be tested in the upcoming CMB-S4 experiment, and (ii) the required value of the reheat temperature implies that the lightest neutrino mass is so small that it predicts the neutrinoless double beta decay parameter $< m_{eff} >$ is between 2 to 5 meV.

12.1 Introduction

The standard model (SM) despite its experimental successes is an incomplete model. Its major deficiencies are its inability to explain three experimental observations : (i) small neutrino masses; (ii) matter-anti-matter asymmetry in the universe; (iii) the dark matter of the universe. A fourth theoretical problem with the SM is why strong CP violating parameter θ is so small (i.e. $\theta \leq 10^{-10}$). In an attempt to address the first three of these problems, we recently proposed an extension of the SM [1] using the framework of the Affleck-Dine (AD) mechanism [2] for leptogenesis. In this model, a complex scalar field, called AD field here, generates the lepton asymmetry as it evolves from the early stage of the universe. Our model [1] provides an example of how to implement leptogenesis in a minimal model with radiative neutrino masses. The AD field also played the role of inflaton whose non-minimal coupling to gravity leads to a viable model of inflation in the early universe. Thus the AD field played a key role in not only implementing leptogenesis but also in generating neutrino masses as well as the inflationary expansion. In this paper, we show how a similar but a more economical version of the model in Ref. [1] can provide an axion solution to the strong CP problem.
We work within the invisible axion model framework [6–9], of KSVZ type, where the Peccei-Quinn (PQ) symmetry breaking scale is in the range of $10^9 - 10^{12}$ GeV as required by astrophysical considerations. The PQ symmetry breaking also

provides a lepton number breaking term involving the AD field which is crucial to AD leptogenesis.

Our starting point is how to implement leptogenesis in minimal models for small neutrino masses. As is well known, connecting the origin of neutrino masses to the matter-antimatter asymmetry via the mechanism of leptogenesis [10] is an attractive possibility and has been the subject of great deal of activity over the past decades [11, 12]. However, this connection is most compelling only for the case of type I seesaw mechanism [13–17] with two or three right handed neutrinos. On the other hand, there are other very interesting mechanisms for generating small neutrino masses, such as type II, type III and inverse seesaw as well as loop models (see for some example of loop models [18–21] and an exhaustive review in Ref. [22]). In the latter class of models, it becomes necessary to add extra particles to implement leptogenesis. These extra particles do not have anything to do with neutrino mass generation but are put in solely to implement leptogenesis. For a discussion of traditional leptogenesis and the need for extra particles, see Ref. [24] for type II seesaw, Refs. [25, 26] for inverse seesaw, and Ref. [23] for loop models. For one class of loop models for neutrino masses, we showed in Ref. [1] that use of AD mechanism provides a way to avoid adding extra particles to generate the lepton asymmetry., which in combination with the sphalerons, leads to baryon asymmetry of the universe [27]. (For a recent discussion of AD leptogenesis in the context of minimal type II seesaw models, see Ref. [39].)

Our goal in this paper is to provide a new one loop model for neutrino masses, where AD leptogenesis works, without adding extra particles and to show how this model also provides a solution to the strong CP problem.

Typically, in the AD mechanism, one relies on the cosmological evolution of a lepton number carrying complex scalar field (called here AD field and denoted here by Φ), with the Lagrangian of the model explicitly breaking lepton number (L), which plays an essential role in the generation of lepton asymmetry. While the L-breaking term could have any form, we choose it to have a quadratic form in the Φ field i.e. a Φ^2 term, since with that particular choice, an analytic form for the baryon to entropy ratio can be derived. The neutrino masses in this case arise from the same lepton number breaking Φ^2 term in the Lagrangian. Thus, neutrino masses are a consequence of AD leptogenesis. Of course, neutrinos in this kind of scenario are naturally Majorana type fermions. There are then restrictions on the parameters of the model following from phenomenological and cosmological consistency. For example, in the AD leptogenesis models, the L asymmetry created by the AD field typically gets transferred to the SM sector at the inflation reheat temperature T_R. So any lepton number washout interactions must decouple at temperature T_* with $T_* \gg T_R$. Furthermore, one must have $T_R > T_{sph}$ (where T_{sph} is the sphaleron decoupling temperature) for the lepton asymmetry to be converted to baryon asymmetry. While these constraints put a strong restriction on the model parameters, there is still a wide range of them where the model works, as we show below.

The model in this paper is similar to that of Ref. [1], though somewhat more economical with the neutrino mass arising from a different diagram. As in Ref. [1], we adopt a scheme where the inflaton and the AD fields are one and the same,

unlike many original AD scenarios [2,28–30], thus providing unification of inflation and leptogenesis [31–40]. We find it convenient to adopt the particular scenario proposed in Ref. [36,37], although we believe it can be extended to other types of AD models as well. We include a complex singlet field to implement the PQ solution to the strong CP problem. Adding the axion solution to strong CP in inflation models can lead to complications due to large iso-curvature perturbations if PQ symmetry is broken during the inflationary period or domain wall problem if the scale is below the inflation scale. We show how to avoid these problems. A distinguishing feature of our model is that cosmological consistency requires the existence of a near massless Majorana fermion which contributes $\Delta N_{eff} \sim 0.1$ at the Big Bang Nucleosynthesis (BBN) epoch, This prediction can be tested in the upcoming CMB-S4 experiment [41]. We also show that the constraints on the reheat temperature after inflation predict a rate for the neutrinoless double beta decay, which can provide another test of the model. These two predictions are generic, not dependent on the choice of model parameters and can therefore test the basic framework.

This paper is organized as follows: in sec. 2, we present an outline of the model and isolate its symmetries; in sec. 3, we discuss the evolution of the universe in this picture, and discuss leptogenesis and one loop generation of neutrino mass in sec. 4; in sec. 5, we discuss the constraints on the model parameters and provide a benchmark set and in sec. 6, dark matter candidate in the model is discussed; in sec. 7, we comment on other possible implications of this model. Sec. 8 is devoted to a summary of the results.

12.2   The model

The model is based on the SM gauge group $SU(3)_c \times SU(2)_L \times U(1)_Y$. The particle content is listed in Table I. In addition to the SM particle content, we introduce the following new fields i.e. an AD field Φ, which is an SM singlet scalar and carries a lepton number -1, a scalar $SU(2)_L$ doublet σ with hypercharge $Y = +1$ and lepton number -1, three Majorana fermionic SM singlets χ_i. To them, we add the field complex scalar field Δ, which carries $L = -1$ and the PQ charge -1 as in Table I. The most general gauge invariant and $U(1)_{PQ} \times U(1)_L$ invariant Lagrangian of the model (in addition to the straightforward kinetic terms) is given symbolically by

$$\mathcal{L} = \mathcal{L}_{kin} + \mathcal{L}_{inf}(\Phi, R) - V(\Phi, \Delta, \sigma, H) + \mathcal{L}_Y. \tag{12.1}$$

Here, $\mathcal{L}_Y$ is the PQ invariant Yukawa Lagrangian given by

$$\mathcal{L}_Y = Y_u q H u^c + Y_d q \tilde{H} d^c + Y_\ell \ell \tilde{H} e^c + Y_Q \Delta Q Q^c + (Y_\sigma)_{ai} \ell_a \sigma \chi_i + \frac{1}{2} \sum_i \mu_{ii} \chi_i \chi_i + h.c., \tag{12.2}$$

and

$$V(\Phi, \Delta, H, \sigma) = m_\Phi^2 |\Phi|^2 + \lambda |\Phi|^4 + \left(\lambda' (\Delta)^2 (\Phi^2) + \beta m_\sigma \Phi H^\dagger \sigma + h.c. \right) \tag{12.3}$$
$$- M_\Delta^2 |\Delta|^2 + \lambda_\Delta |\Delta|^4 + \lambda_{mix} |\Delta|^2 |\Phi|^2.$$

Field	$U(1)_{PQ}$	SM quantum number	L
Fermion			
ℓ_a	$+1$	$(1, 2, -1)$	$+1$
e_a^c	-1	$(1, 1, +2)$	-1
q	$+1$	$(3, 2, +1/3)$	0
u^c	-1	$(3^*, 1, -4/3)$	0
d^c	-1	$(3^*, 1, +2/3)$	0
Q	-1	$(3, 1, -2/3)$	$+1/2$
Q^c	$+2$	$(1, 3^*, 1, +2/3)$	$+1/2$
χ_i	0	$(1, 1, 0)$	0
Scalars			
σ	-1	$(1, 2, +1)$	-1
H	0	$(1, 2, +1)$	0
Φ	$+1$	$(1, 1, 0)$	$+1$
Δ	-1	$(1, 1, 0)$	-1

Table 12.1: Particle content of the model responsible for one loop neutrino mass and dark matter and PQ symmetry. χ_i are new fermionic fields, Q and Q^c are new heavy quarks that help implementing the PQ mechanism. The subscript a goes over lepton flavors and i goes over χ flavors with $a, i = 1, 2, 3$. The PQ charge of the different fields are shown in the second column. The SM $SU(3)_c \times SU(2)_L \times U(1)_Y$ quantum numbers are in the third column.

Here, Δ is the field whose imaginary part is the axion field. $\mathcal{L}_{inf}$ denotes the non-minimal Φ coupling to gravity of the form $\mathcal{L}_{inf} = -\frac{1}{2}(M_P^2 + \xi|\Phi|^2)R$ (see, for example, Refs. [42,43]) and it plays a crucial role in implementing successful inflation, R is the Ricci scalar, and $M_P = 2.4 \times 10^{18}$ GeV is the reduced Planck mass. Note that the field σ has a lepton number (as does Φ) and χ being a Majorana fermion has zero lepton number. Without loss of generality, we can work in a basis where the χ fields are mass eigenstates

We note using Table I that the Lagrangian has an exact global symmetry, $U(1)_{PQ}$ as well as a lepton number symmetry $U(1)_L$. The model also has an automatic Z_2 symmetry even after $U(1)_{PQ}$ breaking under which the fields Φ, χ, σ are odd and the rest of the fields are even. This Z_2 symmetry remains exact and allows for χ_1 (the lightest among the Z_2-odd particles) to be absolutely stable. For subsequent discussion, we assume the following mass hierarchy among the various particles: $\mu_{11}, m_H, m_\ell \ll m_\Phi \leq \mu_{22}, \mu_{33}, m_\sigma$. As we will see below, this allows Φ to decay only via a three body decay mode that involves the field χ_1 in the final state i.e. $\Phi \to \ell_a + \chi_1 + H$. As we show below, this will allow us to relate the reheat temperature T_R directly only to the unknown lightest active neutrino mass, which in turn allows us to choose T_R appropriately.

Once the Field Δ acquires a vacuum expectation value (vev), it will generate the $\epsilon m_\Phi^2 \Phi^2$ term, with $\epsilon m_\Phi^2 = \lambda' f_{PQ}^2/2$. This term breaks lepton number required for neutrino mass generation as well as for AD leptogenesis. The Δ vev will also give rise to the axion field which prior to the QCD scale will remain as a massless

particle and solve the strong CP problem. Since Φ field does not have a vev, its imaginary part does not contribute to the axion field.

As we show in a subsequent section, one loop Majorana masses for all neutrinos are proportional to ϵ whereas the baryon to entropy ratio generated by the AD mechanism is inversely proportional to ϵ [1,36], thereby relating the neutrino mass with the lepton asymmetry in a way different from traditional leptogenesis.

12.3   Inflation and evolution of the AD field

To discuss inflation in this model, note that there are two scalar singlets Φ and Δ unlike the model in Ref. [1] which only had the field Φ at the epoch of inflation. The field Δ is the mother-field of the axion and implements the PQ symmetry, as already stated above. We couple only one of them non-minimally to gravity i.e. $\mathcal{L}_{\text{inf}} = -\frac{1}{2}(M_P^2 + \xi_\Phi|\Phi|^2)R$. This kind of a non-minimal gravity coupling emerges naturally within a supergravity embedding of the model. We do not discuss this here.

To discuss the evolution of the two scalars in the early universe, we expand the fields into the radial and polar parts as $\Phi = \frac{1}{\sqrt{2}}\varphi e^{i\theta}$ and $\Delta = \frac{1}{\sqrt{2}}\rho e^{i\delta}$. The Φ part of the potential in the Einstein frame then looks like:

$$V_E(\varphi,\rho) \simeq \frac{V(\varphi,\rho)}{\left(1 + \xi\frac{\varphi^2}{M_P^2}\right)^2} \tag{12.4}$$

with

$$V(\varphi,\rho) = \frac{1}{2}m_\Phi^2\varphi^2 + \frac{1}{4}\lambda\varphi^4 - \frac{1}{2}M_\Delta^2\rho^2 + \frac{1}{4}\lambda_\Delta\rho^4 + \frac{1}{2}\lambda'\rho^2\varphi^2\cos(2\theta+2\delta) + \frac{1}{4}\lambda_{\text{mix}}\rho^2\varphi^2 \tag{12.5}$$

Note the negative sign in front of the ρ mass, which leads to PQ symmetry breaking. During inflation, $\varphi \sim M_P$ and as a result, the effective potential for ρ turns out to be

$$V(\rho) \sim \frac{1}{2}(-M_\Delta^2 + \lambda_{\text{mix}}M_P^2)\rho^2 + \frac{1}{4}\lambda_\Delta\rho^4 + \frac{\lambda'}{2}M_P^2\rho^2\cos(2\theta+2\delta). \tag{12.6}$$

We see that by setting $\lambda' \ll \lambda_{\text{mix}}$ and $\lambda_{\text{mix}}M_P^2 > M_\Delta^2$, the mass square of the ρ field is now positive. We therefore expect the ρ field to quickly settle to its minimum at $\langle\rho\rangle = 0$ and therefore to play no role in inflation or generating curvature fluctuation.

To discuss inflation, we proceed as follows: For $\varphi \geq M_P$, the potential in the Einstein frame is a constant, which leads to inflation. As the field φ rolls down the potential, its value goes down and inflation ends as the slow roll parameters become of order one. After that the effect of the coupling of φ to the Ricci scalar becomes unimportant. The angle θ can take an arbitrary value when the inflation begins ($\theta = \mathcal{O}(1)$ is naturally assumed), making the real and imaginary parts of

the Φ field different. It is this difference which plays a key role in the development of the baryon asymmetry as the φ becomes smaller.

After inflation ends, the φ field behaves like radiation while the φ^4 term is dominating the inflaton potential and its value goes down like $\varphi \sim a(t)^{-1}$, where $a(t)$ is the scale factor. The rest of the story is same as in the paper [36] and concisely explained in Ref. [40]: When the φ field gets smaller and reaches its value $\varphi_{oscil} \sim m_\Phi/\sqrt{\lambda}$, the φ^4 term becomes unimportant and the quadratic terms in the Lagrangian dominate Φ evolution. This leads to a damped harmonic oscillatory behavior of the real and imaginary parts of Φ with different frequencies due to the presence of the lepton number breaking term $\epsilon m_\Phi^2 \Phi^2$. Using the lepton asymmetry formula $n_L \simeq -\mathrm{Im}(\dot{\Phi}\Phi^*)$, we can then calculate the lepton asymmetry that survives below the reheat temperature. This gives the formula discussed in the next section. The only difference between our case and Ref. [1] is the appearance of the Δ field as an independent field at this temperature. This is because as φ becomes smaller, the mass square of the Δ field becomes negative and PQ symmetry breaks down as φ becomes negligible and we get $\langle\rho\rangle = f_{PQ} = M_\Delta/\sqrt{\lambda_\Delta}$. The ρ field then remains stuck there and effectively generates the lepton number breaking term $\epsilon m_\Phi^2 \Phi^2$.

To realize the scalar field evolution discussed above, the parameters in the scalar potential must be suitably arranged. During inflation, the PQ symmetry is unbroken and hence $M_\Delta^2 < \lambda_{mix} M_P^2$. Well before the damped harmonic oscillation of the Φ field begins, ρ must be settled down at $\langle\rho\rangle = f_{PQ}$ to generate the $\epsilon m_\Phi^2 \Phi^2$ term. This leads to a condition, $M_\Delta^2 = \lambda_\Delta f_{PQ}^2 > \lambda_{mix} \varphi_{oscil}^2 \sim (\lambda_{mix}/\lambda) m_\Phi^2$. In addition, we impose $\lambda_{mix} f_{PQ}^2 < m_\Phi^2$ in order not to change the formula for the lepton asymmetry presented in the next section. We find that all conditions are easily satisfied.

12.4   Lepton asymmetry

Coming to generation of lepton asymmetry, we note that the different initial values of the real and imaginary parts of the AD field Φ i.e. $\phi_1 \neq \phi_2$ introduces the CP violation required by the Sakharov's criterion for leptogenesis and leads to lepton asymmetry $n_L = \mathrm{Im}(\dot{\Phi}^*\Phi)$ while the Φ field is oscillating. This asymmetry gets transmitted to the standard model leptons when Φ decays to $\ell + \chi_1 + H$ and reheats the universe to the temperature $T = T_R$. There are restrictions on the value of the reheat temperature T_R which imposes constraints on the parameters of the model. We must have $T_R \geq T_{sph} \sim 140$ GeV, where T_{sph} is the sphaleron decoupling temperature. This is required so that the lepton asymmetry can be converted to the baryon asymmetry. Furthermore $T_R < T_*$, where T_* denotes the temperature at which lepton number washout processes such as $H\sigma^\dagger \leftrightarrow H^\dagger\sigma$ mediated by ϵ interaction decouples from the cosmic soup.

We estimate the reheat temperature by $T_R \simeq \sqrt{\Gamma_\Phi M_P}$ and find by using the formula for neutrino mass (see the next section) that it is proportional only to the lightest neutrino mass in the normal neutrino mass hierarchy scheme and the latter being unknown at the moment, the T_R value can be adjusted as desired. Here, Γ_Φ is the total decay width of the inflaton/AD field Φ to $\ell + \chi_1 + H$ (since $m_\sigma > m_\Phi$). This

part of the discussion is similar to that in Ref. [1]. We choose χ_1 and H fields to be lighter than the Φ field.

We choose parameters such that $T_R = Km_\Phi$ with $K < 1$. This helps to prevent the inverse decay $\ell + \chi_1 + H \rightarrow \Phi$ so that the lepton asymmetry generated by Φ evolution is transmitted to the SM fields. In the next section, we will see the constraints imposed by this requirement on our model.

We first note that in such a leptogenesis scenario, the lepton number to entropy ratio is given by [36]

$$\frac{n_L}{s} \simeq \frac{T_R^3}{\epsilon\, m_\Phi^2\, M_P}\sin2\theta \simeq 10^{-10}. \tag{12.7}$$

This formula is valid in our scenario despite the presence of the field Δ since it gets a vev around 10^{12} GeV and effectively decouples from the Φ evolution.

An important input into this estimate of n_L/s is the reheat temperature $T_R = Km_\Phi$, which must be less than the AD field mass m_Φ, i.e. $K < 1$ as already noted. This implies the following relation between m_Φ, ϵ and K i.e.

$$m_\Phi \simeq 10^{-10}\frac{\epsilon}{K^3}M_P. \tag{12.8}$$

12.5   Neutrino mass, reheat temperature and washout decoupling

In this section, we first look at the one loop neutrino mass generation in our model and then its relation to the reheat temperature and the decoupling temperature T_* of the dangerous L-violating washout process that could potentially erase the lepton asymmetry. Our main goal will be to establish that in our model, we can satisfy the essential requirement that $T_{sph} \leq T_R \leq T_*$. For this purpose, we will assume the following mass hierarchy among the fields, as already stated above,

$$m_\sigma, \mu_{22}, \mu_{33} > m_\Phi \gg \mu_{11}. \tag{12.9}$$

We will see later on that the χ_1 mass μ_{11} actually has to be in the eV range or below if it is not to over-close the universe.

Neutrino mass

The diagram for one loop neutrino mass is given in Fig. 1. We then estimate the light neutrino mass as

$$m_\nu = \frac{v_{wk}^2\beta^2\epsilon m_\Phi^2}{16\pi^2 m_\sigma^4}Y_\sigma\mu Y_\sigma^T \equiv X^{-2}Y_\sigma\mu Y_\sigma^T, \tag{12.10}$$

where $X^{-2} = \frac{v_{wk}^2\beta^2\epsilon m_\Phi^2}{16\pi^2 m_\sigma^4}$, and $\mu = \mathrm{diag}(\mu_{11},\mu_{22},\mu_{33})$. For the second and third generation neutrinos, this one loop result must give a value of $\mathcal{O}(10^{-10})$ GeV for m_ν. It turns out that for $(Y_\sigma)_{2a,3a} \sim 1$, $\epsilon \sim 10^{-5}$, $\beta \sim 1$, $m_\Phi \sim 10^6$ GeV, and $m_\sigma = \mu_{22} = \mu_{33} \sim 10^{6.5}$ GeV, we get the correct value for the neutrino masses of second and third generations. The resulting neutrino masses will then fit the oscillation data. The situation for the lightest neutrino mass m_{ν_1} is however much
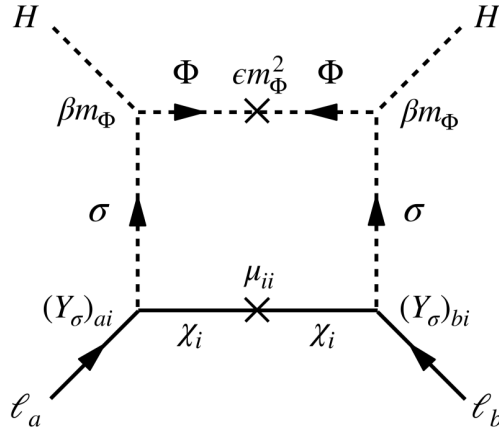
Fig. 12.1: Feynman diagram responsible for one loop neutrino mass. Arrows indicate the flow of the lepton number. The lower cross denotes the Majorana mass insertion of $(\mu)_{ii}$ while the upper cross is for the insertion of ϵm_Φ^2.

smaller as we discuss below. Anyway, the neutrino oscillation fits do not determine the value of m_{ν_1}.

Reheat temperature and m_{ν_1}

Let us now evaluate the reheat temperature in terms of the parameters of the model. For that, we need the decay width of the AD field Φ whose only decay mode is $\Phi \to \ell_a + \chi_1 + H$ and it is given by

$$\Gamma_\Phi \simeq \frac{\beta^2}{32\pi^3} \frac{m_\Phi^5}{m_\sigma^4} \sum_a (Y_\sigma)_{a1}^* (Y_\sigma)_{a1}. \tag{12.11}$$

Now using the formula above for neutrino mass, we note that

$$\sum_a (Y_\sigma)_{a1}^* (Y_\sigma)_{a1} Y_{\sigma,a1}^* Y_{\sigma,a1} \simeq \frac{16\pi^2 m_\sigma^2}{v_{wk}^2 \epsilon \beta^2} \frac{m_{\nu_1}}{\mu_1} \equiv X^2 \frac{m_{\nu_1}}{\mu_{11}}$$

where we have used $m_\nu = U_{MNS}^* D_\nu U_{MNS}^\dagger$ with $D_\nu = \mathrm{diag}(m_{\nu_1}, m_{\nu_2}, m_{\nu_3})$ and the neutrino mixing matrix U_{MNS}.

This leads to the important connection between T_R and m_{ν_1} i.e.

$$T_R \simeq \frac{\beta x^2}{4\pi\sqrt{2\pi}} X \sqrt{\frac{m_{\nu_1}}{\mu_{11}} m_\Phi M_P} = \frac{m_\Phi^2}{v_{wk}\sqrt{2\pi\epsilon}} \left(\frac{m_{\nu_1} M_P}{\mu_{11} m_\Phi}\right)^{1/2}, \tag{12.12}$$

where $x = \frac{m_\Phi}{m_\sigma}$. Thus as claimed earlier, this T_R is related to the experimentally undetermined neutrino observable m_{ν_1} and can be adjusted to satisfy our constraint $T_{sph} \leq T_R < T_*$. Turning this around, we predict m_{ν_1} for each benchmark choice of parameters to be close to zero. For example, when $\epsilon \simeq 10^{-5}$ and $m_\Phi \simeq 10^6$

GeV and $m_\sigma \simeq 10^{6.5}$ GeV, we get $T_R \simeq 10^5$ GeV for $m_{\nu_1}/\mu_{11} \sim 10^{-26}$ while satisfying $n_L/s \sim 10^{-10}$. With μ_{11} in the eV range (as we argue below), m_{ν_1} is almost massless.

Note that reheat requires that the mass of one of the three χ fields must be much lighter than σ, Φ and the Higgs field, as given in Eq. (12.11). In this case, as we will discuss below, χ_1 decouples from the SM thermal plasma when it is relativistic and can over-close the universe if it is heavier than a few eV (like the neutrino). Therefore, we conclude that χ_1 must have a mass lighter than an eV to be cosmologically acceptable.

There is however no symmetry which guarantees its small mass but nonetheless, we have checked that all loop corrections to its mass are proportional to the neutrino mass and are suppressed, making its small mass technically natural. The leading one loop contribution to μ_{11} is

$$\delta\mu_{11} \sim \frac{1}{16\pi^2}(m_\nu)_{ab}(Y_\sigma)_{a1}(Y_\sigma)_{b1}\frac{\beta^2 \epsilon v_{wk}^2 m_\Phi^2}{m_\sigma^4}, \tag{12.13}$$

parameter	value(set 1)	value(set 2)
ϵ	10^{-5}	10^{-3}
K	0.1	0.1
m_Φ	10^6 GeV	10^8 GeV
m_σ	$10^{6.5}$ GeV	$10^{8.5}$ GeV
β	~ 1	~ 1
m_{χ_1}	≤ 1 eV	≤ 1 eV
m_{ν_1}	~ 0 eV	~ 0 eV

Table 12.2: Two sets of benchmark parameters that satisfy all the constraints considered in the model. They cover all points in between and thus represent a broad parameter space of the model.

12.6   Prediction of ΔN_{eff} in the model

We note from the benchmark parameters given in Table II that the mass of χ_1 fermion is near zero. This is required because of the following reason: Below T_R, the χ_1 is in equilibrium with the SM plasma through $\chi_1 - \ell$ coupling, and it decouples from the plasma at $T_D \sim 1$ TeV (100 TeV) for the choice of benchmark parameters $m_\sigma \sim 10^{6.5}$ GeV ($10^{8.5}$ GeV). Thus, the χ_1 field decouples from the thermal plasma when relativistic and as a result the ratio n_{χ_1}/n_γ remains fixed apart from small dilution due to entropy release when other particles annihilate. This means that unless the mass of χ_1 is below an eV, it will dominate the energy density (and hence the expansion rate) of the universe, making the theory unacceptable. The χ_1 field therefore behaves like a hot dark matter with very small contribution to the universe's energy density Ω. Clearly such a new sub-eV mass particle will leave its imprint on the cosmic microwave background (CMB).

Using the entropy conservation for the SM plasma and the χ_1 system after the decoupling T_D, we evaluate the temperature T_{χ_1} of the χ_1 system at the BBN epoch:

$$(T_{\chi_1})^3 = \frac{g_*^{SM}(T_{BBN})}{g_*^{SM}(T_D)} T_{BBN}^3, \tag{12.14}$$

where T_{BBN} is the temperature of the SM plasma at the BBN ($T_{BBN} \sim 1$ MeV), and $g_*^{SM}(T)$ is the effective relativistic degrees of freedom of the SM plasma at temperature T. Since $g_*^{SM}(T \geq 100 \text{GeV}) = 106.75$ and $g_*^{SM}(T_{BBN}) = 10.75$, we evaluate the extra neutrino species from the χ_1 energy density at the BBN era to be $\Delta N_{eff} = 10.75/106.75 \sim 0.1$. This is within the reach of the next generation CMB experiment CMB-S4 [41] being planned. This is a generic feature of the model, not dependent on the choice of parameters.

12.7   Comments

We now make several comments on the model:

- In this model, dark matter is provided by the axion by setting $f_{PQ} \sim 10^{12}$ GeV.
- The heavy color triplet field Q, Q^c has mass of order of the PQ breaking scale. Although they are super-heavy and stable, they are much heavier than the reheat temperature and therefore are not present in the early universe after the reheat when the Hubble phase starts.
- Due to the presence of only one color triplet fermion coupled to the axion field, the domain wall number $N_{DW} = 1$. So after the instanton effects kick in there is no domain wall problem.
- A prediction of our model is the absence of the right handed neutrinos; so discovery of a right handed neutrino will rule out our model. Similarly, due to the absence of three right-handed neutrinos, our model does not allow for a gauged $B - L$ symmetry [44,45]. So any experimental evidence (see for instance [46–49]) for a $B - L$ Z' boson would rule out this model.
- For all our plausible and acceptable scenarios, we find the lightest active neutrino mass to be close to zero. As a result for this normal mass hierarchy scenario, the neutrinoless double beta decay parameter has a lower limit of $\langle m_{\beta\beta} \rangle \geq 0.08$ meV.
- The model has a near massless Majorana field (χ_1) coupling to leptons. It contributes to $\Delta N_{eff} \simeq 0.1$, which can be probed by future precision CMB experiments such as CMB-S4. While there is no symmetry which guarantees its tiny mass, we have checked that it is protected from loop corrections being tiny.
- The parameter λ' that mixes the Δ and Φ fields turns out to be very small to give the right order of magnitude for ϵm_Φ^2. It becomes bigger as Φ mass is increased. While we do not address the naturalness issue of parameters in the model here, we do note that this mixed term is only multiplicatively renormalized due to quantum corrections and therefore its small value is technically natural. Alternatively, one could envisage a supersymmetric embedding of the model, where small values of λ' will be more natural.

- We have shown only two benchmark points in Table II but the model works at all points in the range between these two sets with ϵ appropriately adjusted e.g. for $m_\Phi \sim 10^7$ GeV, $\epsilon \simeq 10^{-4}$.

12.8   Summary

We have presented an optimal extension of the standard model that provides a unified explanation of several of its puzzles i.e. neutrino masses, dark matter compatible with current direct detection constraints, inflation and baryogegenesis via the Affleck-Dine mechanism and a solution to the strong CP problem via the axion. The model adds only three heavy singlet Majorana fermions (χ_i) to the standard model, supplemented by a single lepton number carrying a complex SM doublet scalar boson σ, the singlet lepton number carrying AD field Φ, and a PQ charge carrying field Δ that implements the strong CP problem solution. All the four features of the model are interconnected: for instance, baryon asymmetry and the neutrino mass are inversely related to each other. The reheat temperature is proportional to the lightest active neutrino mass. We give two benchmark points where all the constraints of the model are satisfied.

Acknowledgement

References

1. R. N. Mohapatra and N. Okada, JHEP **03**, 092 (2022) [arXiv:2201.06151 [hep-ph]].
2. I. Affleck and M. Dine, Nucl. Phys. B **249**, 361-380 (1985).
3. R. D. Peccei and H. R. Quinn, Phys. Rev. Lett. **38**, 1440-1443 (1977).
4. S. Weinberg, Phys. Rev. Lett. **40**, 223-226 (1978).
5. F. Wilczek, Phys. Rev. Lett. **40**, 279-282 (1978).
6. J. E. Kim, Phys. Rev. Lett. **43**, 103 (1979).
7. M. A. Shifman, A. I. Vainshtein and V. I. Zakharov, Nucl. Phys. B **166**, 493-506 (1980).
8. M. Dine, W. Fischler and M. Srednicki, Phys. Lett. B **104**, 199-202 (1981).
9. A. R. Zhitnitsky, Sov. J. Nucl. Phys. **31**, 260 (1980).
10. M. Fukugita and T. Yanagida, Phys. Lett. B **174**, 45-47 (1986).
11. W. Buchmuller, P. Di Bari and M. Plumacher, Annals Phys. **315**, 305-351 (2005) [arXiv:hep-ph/0401240 [hep-ph]].
12. D. Bodeker and W. Buchmuller, Rev. Mod. Phys. **93**, no.3, 3 (2021) [arXiv:2009.07294 [hep-ph]].
13. P. Minkowski, "$\mu \to e + \gamma$ at a Rate of One Out of 10^9 Muon Decays?" Phys. Lett. B **67**, 421 (1977).
14. R. N. Mohapatra and G. Senjanović, "Neutrino Mass and Spontaneous Parity Nonconservation", Phys. Rev. Lett. **44**, 912 (1980).

15. T. Yanagida, "Horizontal gauge symmetry and masses of neutrinos", *Workshop on unified theories and baryon number in the universe*, edited by A. Sawada and A. Sugamoto (KEK, Tsukuba, 1979);

16. M. Gell-Mann, P. Ramond and R. Slansky, "Complex Spinors and Unified Theories", *Supergravity*, edited by P. Van Niewenhuizen and D. Freedman (North Holland, Amsterdam, 1980).

17. S. L. Glashow, *The Future of Elementary Particle Physics,* NATO Sci. Ser. B 61 (1980) 687.

18. A. Zee, Phys. Lett. B **93**, 389 (1980) [erratum: Phys. Lett. B **95**, 461 (1980)].

19. D. Chang and R. N. Mohapatra, Phys. Rev. Lett. **58**, 1600 (1987).

20. K. S. Babu, Phys. Lett. B **203**, 132-136 (1988).

21. L. M. Krauss, S. Nasri and M. Trodden, Phys. Rev. D **67**, 085002 (2003) [arXiv:hep-ph/0210389 [hep-ph]].

22. For a recent review of radiative neutrino mass models, see Y. Cai, J. Herrero-García, M. A. Schmidt, A. Vicente and R. R. Volkas, "From the trees to the forest: a review of radiative neutrino mass models," Front. in Phys. **5**, 63 (2017) [arXiv:1706.08524 [hep-ph]].

23. H. Zhou and P. H. Gu, Nucl. Phys. B **927**, 184-195 (2018) [arXiv:1708.04207 [hep-ph]].

24. T. Hambye, New J. Phys. **14**, 125014 (2012) [arXiv:1212.2888 [hep-ph]].

25. M. Aoki, N. Haba and R. Takahashi, PTEP **2015**, no.11, 113B03 (2015) [arXiv:1506.06946 [hep-ph]].

26. K. Agashe, P. Du, M. Ekhterachian, C. S. Fong, S. Hong and L. Vecchi, JHEP **04**, 029 (2019) [arXiv:1812.08204 [hep-ph]].

27. V. A. Kuzmin, V. A. Rubakov and M. E. Shaposhnikov, Phys. Lett. B **155**, 36 (1985).

28. M. Dine, L. Randall and S. D. Thomas, Phys. Rev. Lett. **75**, 398-401 (1995) [arXiv:hep-ph/9503303 [hep-ph]].

29. K. Enqvist and A. Mazumdar, Phys. Rept. **380**, 99-234 (2003) [arXiv:hep-ph/0209244 [hep-ph]].

30. R. Allahverdi and A. Mazumdar, New J. Phys. **14**, 125013 (2012).

31. J. M. Cline, M. Puel and T. Toma, Phys. Rev. D **101**, no.4, 043014 (2020) [arXiv:1909.12300 [hep-ph]];

32. Y. Y. Charng, D. S. Lee, C. N. Leung and K. W. Ng, Phys. Rev. D **80**, 063519 (2009) [arXiv:0802.1328 [hep-ph]].

33. M. P. Hertzberg and J. Karouby, Phys. Lett. B **737**, 34-38 (2014) [arXiv:1309.0007 [hep-ph]]; Phys. Rev. D **89**, no.6, 063523 (2014) [arXiv:1309.0010 [hep-ph]].

34. N. Takeda, Phys. Lett. B **746**, 368-371 (2015) [arXiv:1405.1959 [astro-ph.CO]].

35. C. M. Lin and K. Kohri, Phys. Rev. D **102**, no.4, 043511 (2020) [arXiv:2003.13963 [hep-ph]].

36. A. Lloyd-Stubbs and J. McDonald, Phys. Rev. D **103**, 123514 (2021). [arXiv:2008.04339 [hep-ph]].

37. E. Babichev, D. Gorbunov and S. Ramazanov, Phys. Lett. B **792**, 228-232 (2019). [arXiv:1809.08108 [astro-ph.CO]].

38. M. Kawasaki and S. Ueda, JCAP **04**, 049 (2021) [arXiv:2011.10397 [hep-ph]].

39. N. D. Barrie, C. Han and H. Murayama, Phys. Rev. Lett. **128**, no.14, 141801 (2022) [arXiv:2106.03381 [hep-ph]]; JHEP **05**, 160 (2022) [arXiv:2204.08202 [hep-ph]].

40. R. N. Mohapatra and N. Okada, Phys. Rev. D **104**, no.5, 055030 (2021) [arXiv:2107.01514 [hep-ph]].

41. K. N. Abazajian *et al.* [CMB-S4], [arXiv:1610.02743 [astro-ph.CO]].

42. F. L. Bezrukov and M. Shaposhnikov, Phys. Lett. B **659**, 703-706 (2008) [arXiv:0710.3755 [hep-th]].

43. N. Okada, M. U. Rehman and Q. Shafi, Phys. Rev. D **82**, 043502 (2010) [arXiv:1005.5161 [hep-ph]].

44. R. E. Marshak and R. N. Mohapatra, Phys. Lett. B **91**, 222-224 (1980).
45. A. Davidson, Phys. Rev. D **20**, 776 (1979).
46. A. Das, N. Okada and D. Raut, Phys. Rev. D **97**, no.11, 115023 (2018) [arXiv:1710.03377 [hep-ph]]; Eur. Phys. J. C **78**, no.9, 696 (2018) [arXiv:1711.09896 [hep-ph]].
47. K. Asai, A. Das, J. Li, T. Nomura and O. Seto, [arXiv:2206.12676 [hep-ph]].
48. P. S. B. Dev, B. Dutta, K. J. Kelly, R. N. Mohapatra and Y. Zhang, JHEP **07**, 166 (2021) [arXiv:2104.07681 [hep-ph]].
49. For a recentt experimental search for the $B - L$ Z' boson, see Yu. M. Andreev et al. NA64 collaboration, arXiv:2207.09979 .

13   Dusty Dark Matter Pearls Developed

H.B. Nielsen[1], C. D. Froggatt[2]

[1]Niels Bohr Institute, hbech@nbi.dk
[2]Glasgow University, Colin.Froggatt@glasgow.ac.uk

Abstract. We briefly review and update our earlier published model for dark matter consisting of nanometer size bubbles of a new speculated vacuum phase in which some ordinary material, e.g. carbon, is present under high pressure caused by the surface tension of the domain wall surrounding the bubble. These bubbles or pearls are surrounded by dust grains, and it is one of the new points of the present article that this dust grain rather than being a three-dimensional blob of ordinary matter is a lower dimensional object of some lower Hausdorff dimension. We make several order of magnitude fits and find rather good agreement for our model. However we must imagine that the very high - 3.5 kev - homolumo gap assumed present in the highly compressed medium inside the bubble has influenced the neighbouring dust, so as to make it significantly harder than usual dust. This is to ensure that we obtain the correct order of magnitude for the velocity in the collisions between dark matter particles at which the cross section falls strongly with increasing velocity.

The dark matter pearls lose their surrounding dust in passing through the earth's atmosphere and impacting the earth. They must reach down with their terminal velocity through the shielding to the DAMA observatory in less than a year, so that there is no problem in obtaining the seasonal variation effect the DAMA experiment has observed. This is easier to achieve with a sufficiently high pearl mass and this mass is not so strongly restricted once the dust grain is lower dimensional.

13.1   Introduction

What dark matter really consists of is one of greatest mysteries in physics today, and we have long worked on the proposal that it consists of bubbles of a new phase of the vacuum into which is filled some ordinary material, such as probably carbon in the form of highly compressed diamond [1–11]. Our main assumption not based simply on the Standard Model is that there are several possible phases of the vacuum with *the same energy density* [12–17]. So it is only the surface tension S of the surface between the "new" vacuum inside the bubble and the usual vacuum outside the bubbles which keeps the diamond under high pressure. Apart from our new speculation of there existing several phases of the vacuum, a speculation

with the help of which we *pre*dicted the mass of the Higgs boson [16] before it was found, our model is based only on the Standard Model, an achievement not usually managed by models for the dark matter.

At the present, in spite of the gravitational force from the dark matter fitting the motions of the stars and galaxies and cosmology well, the remarkable facts are that

- The majority of the underground experiments - in particular the Xenon ones [18–20] - do *not* see any dark matter hitting the Earth, and
- Accelerators - LHC is the most hopeful - have *not* been able to see any dark matter either.

13.2 Pearl

The dark matter particles or pearls are composed of:

- A nm-size bubble of a new speculated vacuum filled with highly compressed atomic stuff, say carbon.
- A surrounding dust particle of "metallicity" material [21, 22] such as C, O, Si, Fe, ..., presumably of some non-integer Hausdorff dimension about 2 or 1. This atomic matter is influenced by the electrons being partly in a superposition of being inside the bubble of the new vacuum, where there is very high homolumo gap between filled and unfilled electron states [11]. This influences the dust grain material so as to make it denser and harder.

Pearls interact with:

- other dark matter particles and thereby provide an example of self-interacting dark matter (SIDM) [23].
- atomic matter.

The most important evidence for our model may be that we find the energy value of 3.5 keV in *three* different places as a possible favourite energy level difference for dark matter:

- From places in outer space with a lot of dark matter, galaxy clusters, Andromeda and the Milky Way Center, as the energy of an unexpected X-ray line [24–29], and strangely also from Tycho supernova remnant [30].
- As the average energy of the DAMA dark matter events [31, 32].
- As an average energy for the electron recoil excess[1] in the XENON1T experiment [33].

Dust easily gets of lower than 3 dimensions because the growing of a dust grain takes place by molecules (monomers) almost one by one being attached to the grain as it is at the time and by grains colliding and sticking together. Such growing could easily make the dimension non-integer. This idea of a dust grain with a
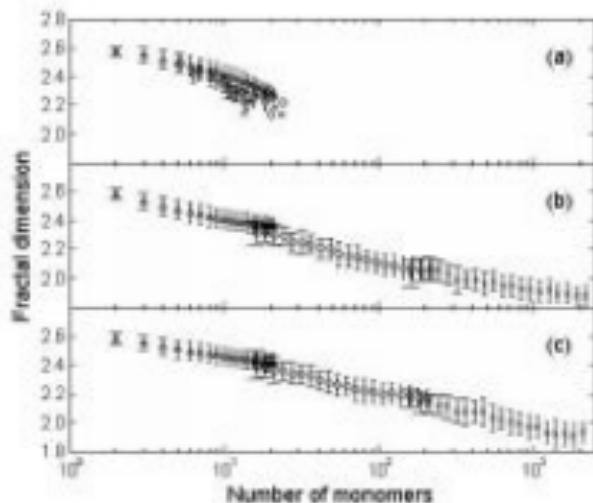
Fig. 13.1: Fractal dimensions of dust grain given by the Hausdorff dimension from [35].

fractal dimension has been studied in [35] and results from this paper are given in Figure 13.1.

An example of such a fractal cosmic dust grain built up from 1024 monomers [36] is given in Figure 13.2.

It is indeed very likely that such a dust grain would collect on top of one of our pearls, which in itself is very much like a seed atom. We may illustrate that in Figure 13.3 by drawing our little pearl as a bubble of new vacuum inside the dust grain.

If typically the grain size is $0.1\,\mu m$ and the bubble size is $1\,nm = 0.001\,\mu m$, then the bubble is about 100 times smaller than the dust grain.

13.3   Achievements

Important achievements of our model:

- Explain that only DAMA "sees" the dark matter by the particles interacting so strongly as to be quite slow and unable to knock nuclei so as to make observable signals. Instead the DAMA signal is explained as due to emission

---

[1] The results from the more sensitive XENONnT detector were published [34] shortly after this School. XENONnT reduces the low energy electron recoil background to a factor of 5 lower than in XENON1T and observe no electron excess above background.
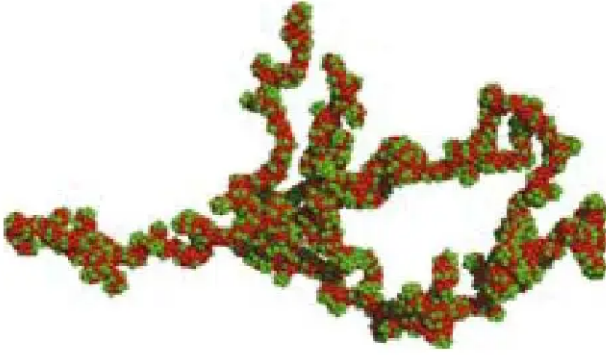
Рис. 3. Фрактальная модель космической пылинки [5]

Fig. 13.2: Picture of Fractal Cosmic Dust Grain constructed from 1024 monomers [36].
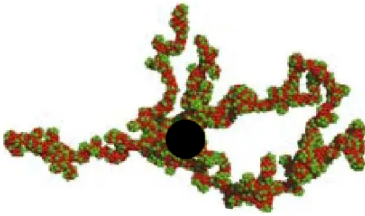
Рис. 3. Фрактальная модель космической пылинки [5]

Fig. 13.3: The little dot inserted in the foregoing figure 13.2 here symbolizes the bubble of new vacuum. It is supposedly much heavier than the rest of the dust grain.

of electrons from pearls in an excited state with the "remarkable 3.5 keV energy".

Actually Xenon1T may have seen these electrons from the dark matter particle *decays* as the mysterious electron recoil excess.

- The favourite frequency of electron or photon emission of the dark matter particles is due to a homolumo gap in the material inside the bubble of the new vacuum. This gap should be equal to the 3.5 keV.

- We have made a rather complicated calculation of what happens when the bubbles - making up the main part of the dark matter particle - hit each other and the surface/skin/domain wall contract and how one gets out a part of the energy as 3.5 keV X-rays [7]. We fit with one parameter both the very frequency 3.5 keV, and the over all intensity of the corresponding X-ray line observed from galaxy clusters etc. This production mechanism gives an

intensity proportional to the dark matter density squared and we use the results of the analysis of Cline and Frey [37] whose model shares this property.

- We explain why - otherwise mysteriously - the 3.5 keV line was seen by Jeltema and Profumo [30] from the Tycho supernova remnant and probably also problems with the Perseus galaxy cluster 3.5 keV X-ray observations. This is by claiming the excitation of the bubbles come from cosmic radiation in the supernova remnant.

- According to expectations from ideal dark matter that only interacts essentially by gravity there should be e.g in a dwarf galaxy a concentrated peak or cusp of dark matter, but that seems not to be true. The inner density profile rather seems to be flat as expected for self-interacting dark matter [23]. Correa [38] can fit the dwarf galaxy star velocities by the hypothesis that dark matter particles interact with each other with a cross section over mass ratio increasing for lower velocity, as shown in Figure 13.4. We fit the cross section over mass velocity dependence of hers. But we need a "hardening" of the dust around the bubbles.
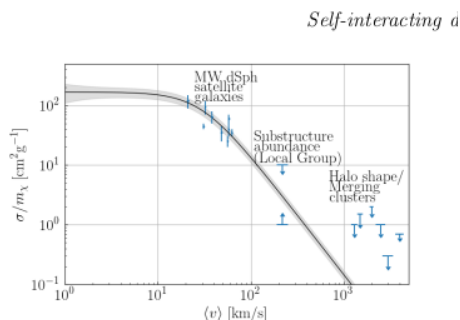
Figure 7. Same as Fig. 6, but extended to cover the range of MW-(~200 km/s) and cluster-size (~1000 – 5000 km/s) haloes' velocities. The figure shows upper and lower limits for σ/m_χ taken for substructure abundance studies (e.g. Volgelsberger et al. 2012 and Zavala et al. 2013), as well as based on halo shape/ellipticity studies and cluster lensing surveys (see text).

Fig. 13.4: Extract from Correa's paper illustrating the fits of the cross section to mass ratio obtained for different dwarf galaxies, as a function of the estimated velocity for the relevant galaxy.

13.4   Impact

We imagine that the dark matter pearls lose their dust grain in the atmosphere or at least, if not before, by the penetration into the earth shielding, and that they at the
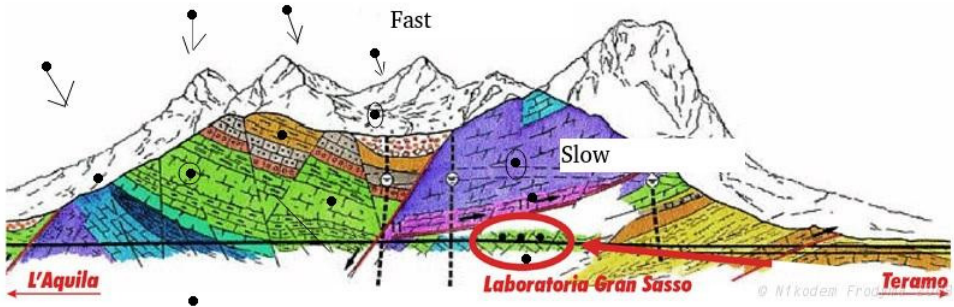
Fig. 13.5: The mountains above the Gran Sasso laboratories.

same time get excited by means of the energy from the braking of the pearls. For a very small number of the pearls this excitation energy gets radiated first much later when the pearl has passed through the earth shielding to the underground detectors, so as to deliver X-ray radiation with just the characteristic 3.5 keV energy per photon. The energy is delivered we guess by electrons or photons. Thus experiments like the xenon experiments do not "see" it when looking for nucleus-caused events. Only DAMA, which does not notice if it is from nuclei or from electrons, does not throw electron-caused events away as something else. The dark matter pearls come in with high speed (galactic velocity), but get stopped down to much lower speed by interaction with the shielding mountains, whereby they also get excited to emit 3.5 keV X-rays or *electrons*.

13.5 Calculations

The percentages of the matter in the Universe are as follows:

- 27% dark matter (while 68% of a form of energy known as dark energy, and 5 % ordinary matter).

The elements heavier than hydrogen and helium make up of order 1% of ordinary matter and are known as "metals". The comoving density of these "metals" together is [21]

$$\text{"metal density"} = 5.48 * 10^6 M_\odot \text{Mpc}^{-3} \tag{13.1}$$
$$= 3.71 * 10^{-31} \text{kg/m}^3. \tag{13.2}$$

13.5.1 Inverse Darkness $\frac{\sigma}{M}$

We think that the less the cross section is compared to the mass the less is the interaction - with whatever we may consider - and thus the less the "visibility". It is the lack of visibility which we call darkness just as we call dark matter dark matter because we do not "see" it. So a smaller cross section means darker and thus the ratio with the cross section in the numerator could be called the inverse darkness.

Using the atomic radii we can calculate the cross sections for the following atoms:

$$\text{Hydrogen H: } r_H = 25\text{pm} \Rightarrow \sigma_H = \pi r_H^2 = 1963\text{pm}^2 \tag{13.3}$$

$$\text{Helium He: } r_{He} = 30\text{pm} \Rightarrow \sigma_{He} = \pi * r_{He}^2 = 2827\text{pm}^2 \tag{13.4}$$

$$\text{Carbon C: } r_C = 70\text{pm} \Rightarrow \sigma_C = \pi * r_C^2 = 15394\text{pm}^2 \tag{13.5}$$

$$\text{Silicium Si: } r_{Si} = 110\text{pm} \Rightarrow \sigma_{Si} = \pi * r_{Si}^2 = 38013\text{pm}^2 \tag{13.6}$$

Using that one atomic unit $1u = 1.66 * 10^{-27}$kg we get for the inverse darkness ratios for the atoms mentioned:

$$\text{Hydrogen H: } \frac{\sigma_H}{1u * 1.66 * 10^{-27}\text{kg/u}} = 1.183 * 10^6 \text{m}^2/\text{kg} \tag{13.7}$$

$$\text{Helium He: } \frac{\sigma_{He}}{4u * 1.66 * 10^{-27}\text{kg/u}} = 4.26 * 10^5 \text{m}^2/\text{kg} \tag{13.8}$$

$$\text{Carbon C: } \frac{\sigma_C}{12u * 1.66 * 10^{-27}\text{kg/u}} = 7.73 * 10^5 \text{m}^2/\text{kg} \tag{13.9}$$

$$\text{Silicium Si: } \frac{\sigma_{Si}}{28u * 1.66 * 10^{-27}\text{kg/u}} = 8.18 * 10^5 \text{m}^2/\text{kg} \tag{13.10}$$

In a dust grain say the atoms will typically shadow each other and thus this ratio "the inverse darkness" will be smaller than if the atoms were all exposed to the collision considered. If we denote the average number of atoms lying in the shadow of one atom by "numberthickness" we will have for the ratio for the full grain say

$$\frac{\sigma}{M}\Big|_{grain} = \frac{\frac{\sigma}{M}\big|_{atom}}{\text{"numberthickness"}}. \tag{13.11}$$

If we insert in the grain a mass-wise dominating bubble, the whole object will of course get a small ratio due to the higher mass,

$$\frac{\sigma}{M}\Big|_{composed} = \frac{\sigma}{M}\Big|_{grain} * \frac{M_{grain}}{M}, \tag{13.12}$$

where M is the mass of the bubble or if it dominates the whole composed object, the dark matter particle.

On the average of course the ratio $\frac{M_{grain}}{M}$ of the dust around the bubble and the bubble itself can never be bigger than the ratio of the amount of dust-suitable mass to dark matter in the universe. So noting that the grain should largely be made by the elements heavier than helium, the so called "metals", and that these make up only of the order of 1 % of the ordinary matter which again is only about 1/6 of the mass of the dark matter, we must have

$$\frac{M_{grain}}{M} \leq 1\%/6 = 1/600. \tag{13.13}$$

But really of course not all the "metal" has even reached out to the intergalactic medium, let alone been caught up by the dark matter. So we expect an appreciably

smaller value for this ratio of dust caught by dark matter relative to the dark matter itself.

In earlier papers we have already used the dark matter self-interaction in the low velocity limit extracted from Correa's fit to the dwarf galaxy data shown in Figure 13.4 to give:

$$\frac{\sigma}{M}\Big|_{v-->0} = 15 m^2/kg. \tag{13.14}$$

We now wish to crudely estimate the amount of dust that might pile up around a dark matter bubble with a given velocity during the evolution of the Universe. There are two important effects to be taken into account. First of all the metal density was higher in the past due to the reduction in the "radius" of the Universe by a factor $(1+z)^{-1}$ where z is the red shift. Secondly the metallicity was lower in the past and we use the linear fits of De Cia et al. [22] to its z dependence in our estimate of the rate of collection of metals by our pearls. We found that the most important time for the rate of collection of metals corresponds to $z = 3.3$, when the age of the Universe was 1.52 milliard years. At this time the rate of collecting metals for a given velocity was about 8.4 times bigger than if using the present metallicity and density.

So we might crudely estimate the amount of dust being collected by an 8.4 times bigger density of metals than today in the 8.9 times younger Universe, giving *effective numbers* for the dust settling:

$$\text{"metal density"}_{eff} = 3.71 * 10^{-31} kg/m^3 * 8.4 \tag{13.15}$$
$$= 3.1 * 10^{-30} kg/m^3 \tag{13.16}$$
$$= 1.7 * 10^{-3} GeV/c^2/m^3. \tag{13.17}$$

For orientation we could first ask how much metal-matter at all could be collected by a dust grain while already of the order of 10^{-7} m in size, meaning a cross section of $10^{-14} m^2$ and with a velocity of say 300 km/s = $3 * 10^5$ m/s during an effective age of the Universe of 1.52 milliard years = $4.8 * 10^{16}$ s. We obtain

$$\text{"available metals"} = 3 * 10^5 m/s * 4.8 * 10^{16} s * 10^{-14} m^2 * 3.1 * 10^{-30} kg/m^3$$
$$= 4.4 * 10^{-22} kg \tag{13.18}$$
$$= 2.4 * 10^5 GeV, \tag{13.19}$$

which is to be compared to what the mass of a $(10^{-7} m)^3$ large dust particle with say specific weight 1000 kg/m^3 would be, namely 10^{-18} kg.

So such a "normal" size dust grain could not collect itself in the average conditions in the Universe.

However if the grain to be constructed had lower dimension than 3, then the cross section could be larger for the same hoped for volume and thus mass. Decreasing say the thickness in one of the dimensions from the 10^{-7} m to atomic size 10^{-10} m would for the same collection of matter give a 1000 times smaller mass. This would bring such a "normal size" grain close to being just collectable in the average conditions in the Universe.

Our speculated stronger forces than usual due to the big homolumo gap would not help much, because the grain cannot catch the atoms in intergalactic space which it does not come near enough to touch.

We shall now estimate the inverse darkness for such a dust grain of dimension 2 or less attached to a dark matter bubble. In this case there is no shadowing of the dust atoms and the parameter "numberthickness" in equation (13.11) becomes unity. Also we estimated that in the main period when the dust attached itself to the dark matter bubbles, we had $z = 3.3$ and the age of the Universe was 1.52 milliard years. The density of "metals" at that time was a factor 10^{-1} times the one today. So the factor $1/600$ in equation (13.13) for the "metals" accessible to be caught by the dark matter composite particle becomes

$$\frac{M_{grain}}{M} = 1\%/6/10 = \frac{1}{6000}. \tag{13.20}$$

So taking $\frac{\sigma}{M}|_{atom} = 7 * 10^5 \, m^2/kg$ for the atoms of dust, we obtain our estimate for the inverse darkness of the dark matter particle composed with a dust grain of dimension 2 or less

$$\frac{\sigma}{M}|_{composed} = \frac{\sigma}{M}|_{grain} * \frac{M_{grain}}{M} \tag{13.21}$$

$$= 7 * 10^5 \, m^2/kg/6000 \tag{13.22}$$

$$= 1.2 * 10^2 \, m^2/kg. \tag{13.23}$$

Our expected ratio

$$\frac{\sigma}{M}|_{composed} = 120 \, m^2/kg \tag{13.24}$$

should be compared with the value extracted from the dwarf galaxy data

$$\frac{\sigma}{M}|_{Correa, v \to 0} = 15 \, m^2/kg. \tag{13.25}$$

13.5.2   Size of Individual Dark Matter Particles

In the approximation of only gravitational interaction of dark matter it is well-known that only the *mass density* matters, whereas the number density or the *mass per particle is not observable.*

With other than gravitational interactions one could hope that it would be possible to extract from the fits in say our model, what the particle size should be. But the possibility for that in our model is remarkably bad! The Correa measurement yields just the "inverse darkness" ratio

$$\frac{\sigma}{M} = \frac{\text{"cross section"}}{\text{mass}} \tag{13.26}$$

Our estimate for the rate of 3.5 keV radiation from dark matter seen by DAMA - very crudely - was based on:

- The total kinetic energy of the dark matter hitting the Earth per m^2 per s (but not on how many particles).

- The main part of that energy goes into 3.5 keV radiation of electrons.
- Estimate of a "suppression" factor for how small a part of this electron radiation comes from sufficiently long living excitations to survive down to 1400 m into the Earth.

None of this depends in our estimate on the size of the dark matter particles (provided it lies inside a very broad range)!

If the dark matter particles were so heavy that the number density is so low that the observation over an area of about $1m^2$ would not get an event through every year, then it would contradict the DAMA data.

The rate of dark matter mass hitting a square meter of the Earth is

$$\text{Rate} = 300\text{km/s} * 0.3\text{GeV/cm}^3 \tag{13.27}$$

$$= 3 * 10^5\text{m/s} * 5.34 * 10^{-22}\text{kg/m}^3 \tag{13.28}$$

$$= 1.6 * 10^{-16}\text{kg/m}^2\text{/s} \tag{13.29}$$

$$= 5 * 10^{-9}\text{kg/m}^2\text{/y} \tag{13.30}$$

Taking the DAMA area of observation $\sim 1m^2$ we need to get more than one passage per year and thus

$$M \leq 5 * 10^{-9}\text{kg} \tag{13.31}$$

$$= 3 * 10^{18}\text{GeV.} \tag{13.32}$$

Using the bubble internal mass density as estimated from the 3.5 keV homolumo gap, this upper bound implies that the bubble radius $R \leq 10^{-7}$m.
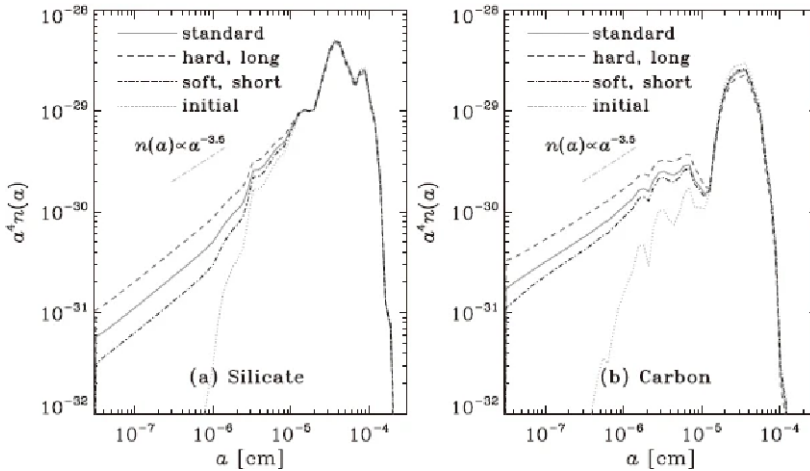
Fig. 13.6: Simulated size distribution for dust grains.

We can assume a typical grain size (see Figure 13.6) of 10^{-7}m, say. Then using the low velocity limit $\frac{\sigma}{M} = 15\text{m}^2\text{/kg}$ gives

$$M = (10^{-7}\text{m})^2/(15\text{m}^2\text{/kg}) \tag{13.33}$$

$$= 7 * 10^{-16}\text{kg.} \tag{13.34}$$

But if now the dust grain is less than 2 dimensional, the area for a grain with the same weight as a massive 3 dimensional one would be more than $\frac{10^{-7}\text{m}}{10^{-10}\text{m}} = 1000$ times bigger, i.e an area bigger than 10^{-11}m^2. Correcting for this would give a bigger mass $M \geq 7 * 10^{-13}\text{kg}$.

13.6 Conclusion

We have reviewed and updated our dark matter model in which the dark matter consists of bubbles of a speculated new phase of the vacuum, in which there has collected so much "ordinary" matter that the surface tension of the separation surface between the two types of vacuum can be spanned out. These pearls are here assumed to be surrounded by a lower than three dimensional grain of dust mainly made from atoms of higher atomic weight than hydrogen and helium.

We suppose that the Hausdorff dimension of the grain of dust is so low that the interaction between the pearls with their dust corresponds to effectively having no shadowing of the grain atoms by each other (with added up dimensionality less than 2). We used the general chemical abundances and estimated a low velocity inverse darkness of $120\text{m}^2/\text{kg}$ for our pearls. This is only one order of magnitude larger - thus it essentially agrees with - the value $15\text{m}^2/\text{kg}$ found by Correa [38]. This is summarized in Table 13.1 as point 1.

In item 2 in the table we see that the estimate for the value v_0 of the velocity at which the inverse darkness falls significantly down as a function of the velocity is 0.7cm/s if we do not take the hardening of the dust grain seriously, while it is 77km/s if we do take this hardening seriously. From the Correa estimate using the dwarf galaxy data one finds $v_0 = 220\text{km/s}$, so only the estimate taking the hardening seriously agrees with experiment.

The rest of the items in Table 13.1 are other order of magnitude estimates checking the viability of our model. Thus item 3 estimates the rate of events in the DAMA-LIBRA experiment formulated in terms of the quantity suppression, which denotes the fraction of the excitations made in the dark matter pearls on entering the Earth, which survive down until the pearl reaches the detector.

The similar item 4 for the XENON1T experiment is now obsolete in as far as the effect found in this experiment was not reproduced after the radon gas was better cleaned away in XENONnT, so it was probably β decay of ^{214}Pb that was responsible for the previous effect.

Item 5 called "Jeltema" represents the very strange observation of the 3.5keV-line from the Tycho Brahe supernova remnant, which should not have enough dark matter to produce the 3.5keV-line so as to be observed at all. But due to our dark matter particles being excitable by the large amount of cosmic rays in the supernova remnant, we indeed could get agreement with the observed rate of $2.2 * 10^{-5}\text{photons/cm}^2$ coming from the supernova remnant.

As item 6 we list the fit of the overall factor in the fit by Cline and Frey to the 3.5keV-line sources together with the very energy 3.5keV by one combination of our parameters for the model $\frac{\xi_{fs}^{1/4}}{\Delta V}$. Actually this combination is essentially the Fermi momentum of the electrons in the highly compressed matter in the

interior of our our bubbles. This fitting is only sensitive to the density of the matter inside the pearls and does not depend on the size of the pearls at the end. So this successful fit actually originates from earlier articles on our model, when we considered the pearls to be cm-sized and so heavy that an impact in Tunguska could have caused a major catastrophe [3].

The last item, item 7, just reviews the fact that we found approximately the same 3.5keV at first in three different places. However now after the sad development for our model in the recent XENONnT experiment [34] only in two places, namely in the satellite etc. observations of the 3.5 keV X-ray line and in the average energy of the modulating part of the DAMA-LIBRA observed events.

In Table 13.2 we present some information on the mass of the single dark matter particle mass M (supposedly dominating the mass of the dust grain).

Table 13.1: Successes

# & exp/th	Quantity	value	related Q.	value
1.	Dwarf Galaxies			
exp	inv. darkness =	$15 m^2/kg$	$\frac{M_{grain}}{M}$	$2 * 10^{-5}$
th	$= \frac{\sigma}{M}\|_{v \to 0}$	$120 m^2/kg$		$1.6 * 10^{-4}$
2.	Dwarf Galaxies			
exp	Velocity par. v_0	$220 km/s$	$4 r_{dust} E$	$8.1 * 10^{13} kg/s^2$
th.	with hardening	$77 km/s$	$4 r_{dust} E$	$1 * 10^{13} kg/s^2$
th.	without hard.	$0.7 cm/s$	$4 r_{dust} E$	$400 kg/s^2$
3.	DAMA-LIBRA			
exp		$0.041 cpd/kg$	suppression	$1.6 * 10^{-10}$
th	air	$0.16 cpd/kg$		$6 * 10^{-10}$
th	stone	$1.6 * 10^{-5} cpd/kg$		$6 * 10^{-14}$
4.	Xenon1T			
exp		$2 * 10^{-4} cpd/kg$	suppression	$6 * 10^{-13}$
th	air	$0.16 cpd/kg$		$6 * 10^{-10}$
th	stone	$1.6 * 10^{-5} cpd/kg$		$6 * 10^{-14}$
5.	Jeltema & P.			
exp	counting rate	$2.2 * 10^{-5} phs/cm^2/s$	$\frac{\sigma}{M}\|_{Tycho}$	$5.6 * 10^{-3} cm^2/kg$
th		$3 * 10^{-6} phs/s/cm^2$	$1\% * \alpha * \frac{\sigma}{M}\|_{nuclear}$	$8 * 10^{-4} cm^2/kg$
6.	Intensity 3.5 kev			
exp	$\frac{N\sigma}{M^2}$	$10^{23} cm^2/kg^2$	$\frac{\xi_{fs}^{1/4}}{\Delta V}$	$0.6 MeV^{-1}$
th		$3.6 * 10^{22} cm^2/kg^2$		$0.5 MeV^{-1}$
7.	Three Energies			
ast	line	3.5 keV		
DAMA	av. en.	3.4 keV		
Xen.	av. en.	3.7 keV		

Table 13.2: Mass M bounds and estimates

Description	R	ΔR	M	ΔM
Faster than year	$\geq 1.0 * 10^{-9}$m		$\geq 2.1 * 10^{-15}$kg	
Corrected	$\geq 3.1 * 10^{-9}$m		$\geq 6.5 * 10^{-14}$kg	
Dust enough	$\geq 1.0 * 10^{-9}$m		$\geq 2 * 10^{-15}$kg	
Velocity dep.	$\approx 10^{-8}$m	big	$\approx 10^{-13}$kg	big
w. E= 400^4	10^{-10}m		$\approx 2 * 10^{-18}$kg	
DAMA stream	$\leq 10^{-7}$m		$\leq 5 * 10^{-9}$kg	
Grain size 10^{-7}m	$7 * 10^{-10}$m		$7 * 10^{-16}$kg	

Acknowledgements

References

1. C. D. Froggatt and H. B. Nielsen, Phys. Rev. Lett. **95** 231301 (2005) [arXiv:astro-ph/0508513].
2. C.D. Froggatt and H.B. Nielsen, Proceedings of Conference: C05-07-19.3 (Bled 2005); arXiv:astro-ph/0512454.
3. C. D. Froggatt and H. B. Nielsen, Int. J. Mod. Phys. A **30** no.13, 1550066 (2015) [arXiv:1403.7177].
4. C. D. Froggatt and H. B. Nielsen, Mod. Phys. Lett. **A30** no.36, 1550195 (2015) [arXiv:1503.01089].
5. H.B. Nielsen, C.D. Froggatt and D. Jurman, PoS(CORFU2017)075.
6. H.B. Nielsen and C.D. Froggatt, PoS(CORFU2019)049.
7. C. D. Froggatt, H. B. Nielsen, "The 3.5 keV line from non-perturbative Standard Model dark matter balls", arXiv:2003.05018.
8. H. B. Nielsen (speaker) and C.D. Froggatt, "Dark Matter Macroscopic Pearls, 3.5 keV -ray Line, How Big?", 23rd Bled Workshop on What comes beyond the Standard Models (2020), arXiv:2012.00445.
9. C. D. Froggatt and H.B.Nielsen, "Atomic Size Dark Matter Pearls, Electron Signal", 24th Bled Workshop on What comes beyond the Standard Models (2021), arXiv:2111.10879.
10. C. D. Froggatt and H.B. Nielsen, "Atomic Size Pearls being Dark Matter giving Electron Signal", arXiv:2203.02779.
11. H. B. Nielsen and C. D. Froggatt, Corfu Summer Institute 2021, "21st Hellenic School and Workshops on Elementary Particle Physics and Gravity", arXiv:2205.08871.
12. D. L. Bennett, C. D. Froggatt and H. B. Nielsen, NBI-HE-94-44, GUTPA-94-09-3, Presented at Conference: C94-07-20 (ICHEP 1994), p.0557-560.
13. D. L. Bennett, C. D. Froggatt and H. B. Nielsen, NBI-95-15, GUTPA-95-04-1, Presented at Conference: C94-09-13 (Adriatic Meeting 1994), p.0255-279 [arXiv:hep-ph/9504294].
14. D. L. Bennett and H. B. Nielsen, Int. J. Mod. Phys. **A9** 5155 (1994).

15. D. L. Bennett, C. D. Froggatt and H. B. Nielsen, NBI-HE-95-07, Presented at Conference: C94-08-30 (Wendisch-Rietz) p.394-412.
16. C. D. Froggatt and H. B. Nielsen, Phys. Lett. **B368** 96 (1996) [arXiv:hep-ph/9511371].
17. H.B. Nielsen (Speaker) and C.D. Froggatt, Presented at Conference: C95-09-03.1 (Corfu 1995); arXiv:hep-ph/9607375.
18. D. S. Akerib et al, Pkys. Rev. Lett. **118**, 2, 021303 (2017) [arXiv:1608.07648].
19. X. Cui et al, Phys. Rev. Lett. **119**, 18, 181302 (2017) [arXiv:1708.06917].
20. E. Aprile et al, Phys. Rev. Lett. **121**, 11, 111302 (2018) [arXiv:1805.12562].
21. F. Calura and F. Matteucci, Mon. Not. R. Astron. Soc. **350**, 351 (2004), [arXiv: astro-ph/0401462].
22. A. De Cia et al., Astron. Astrophys **611**, A76 (2018).
23. D. N. Spergel, and P. J. Steinhardt, Phys. Rev. Lett. **84**, 3760 (2000) [arXiv:astro-ph/9909386].
24. E. Bulbul, M. Markevitch, A. Foster et al., ApJ. **789**, 13 (2014) [arXiv:1402.2301].
25. A. Boyarskiy, O. Ruchayskiy, D. Iakubovskyi and J. Franse, Phys. Rev. Lett. **113**, 251301 (2014) [arXiv:1402.4119].
26. A. Boyarsky, J. Franse, D. Iakubovskyi and O. Ruchayskiy, Phys. Rev. Lett. **115**, 161301 (2015) [arXiv:1408.2503].
27. S. Bhargava et al, MNRAS **497** 656 (2020) [arXiv:2006.13955].
28. D. Sicilian et al, ApJ. **905** 146 (2020) [arXiv:2008.02283].
29. J. W. Foster et al, Phys. Rev. Lett. **127** 051101 (2021) [2102.02207].
30. T. Jeltema and S. Profumo, MNRAS **450**, 2143 (2015) [arXiv:1408.1699].
31. R. Bernabei et al., Eur. Phys. J. **C73**, 2648 (2013). [arXiv:1308.5109].
32. R. Bernabei et al, Prog. Part. Nucl. Phys. **114**, 103810 (2020).
33. E. Aprile et al, Phys. Rev. **D102**, 072004 (2020) [arXiv:2006.09721].
34. E. Aprile et al., Phys. Rev. Lett. **129**, 161805 (2022) [arXiv:2207.11330].
35. R. Hayes and M. Freed, Journal of Young Investigators, March 2007, "The Fractal Dimension and Charging of Preplanetary Dust Aggregates", https://www.jyi.org/2007-march/2017/11/11/the-fractal-dimension-and-charging-of-preplanetary-dust-aggregates.
36. E. L. Wright, ApJ, 320, 818 (1987), htpps://astro.ucla.edu/ wright/dust/
37. J. M. Cline and A. R. Frey, Phys. Rev. D90 123537 (2014) [arXiv:1410.7766]
38. C. A. Correa, MNRAS **503** 920 (2021) [arXiv:2007.02958].

14 What gives a "theory of Initial Conditions" ?

H.B. Nielsen, K. Nagao

Niels Bohr Institute, Copenhagen

Abstract. The present work contains a review of some of the work we have done on complex action or non-Hermitian Hamiltonian theory, especially the result that the anti-Hermitian part of the Hamiltonian functions by determining the actual solution to the equations of motion, that should be realized; this means it predicts the initial conditions. It should be stressed that a major result of ours is that the effective equations of motion will in practice - after long time - be so accurately as if we had indeed a Hermitian Hamiltonian, and so there is at first nothing wrong in assuming a non-Hermitian one. In fact it would practically seem Hermitian anyway. A major new point is that we seek by a bit intuitively arguing to suggest some cosmologically predictions from the mentioned initial conditions predicted: We seek even by assuming essentially nothing but very general properties of the non-Hermitian Hamiltonian that we in practice should find a bottom in the (effective Hermitian) Hamiltonian and that the Universe at some moment should pass through a (multiple) saddle point very closely, so that the time spent at it would be very long.

14.1 Introduction

It would be very nice to unify our knowledge of the equations of motion, or we could say the time-development, with our knowledge about the initial conditions, or as we shall look upon it here, which solutions to the equations of motion is by the initial-condition-physics selected as the one to be realized, the true development. We [9, 11–17, 20, 21, 27, 28, 30–34] and also Masao Ninomiya [1–8, 10] have long worked on the idea that the action should not be real, but rather complex. It has turned out that such theories of complex action or essentially similarly of non-Hermitian [1] in fact lead to a theory in which

- The effect of the non-hermiticity is not seen after appreciable time in the equations of motion, so that effective hermiticity basically came out automatically; and thus this kind of theory is indeed viable!
- But the initial conditions is predicted from such theories.

---

[1] The Hamiltonian is not restricted to the class of PT-symmetric non-Hermitian Hamiltonians that were studied in Refs. [22–26].

But it is then of course very important for whether such a hypothesis of of a complex action or equivalently non-Hermitian Hamiltonian can be upheld, whether the action or the Hamiltonian can be arranged in a reasonable way so as to give some initial condition informations matching with what we know about the initial conditions having governed the world, the universe.

It is the purpose of the present article in addition to reviewing our works on this complex action type of theory to argue even without making any true fitting of the Hamiltonian, except assuming it to have a classical analogue - using in fact a phase space consideration - but rather looking only at an essentially random form of the Hamiltonians, especially the anti-Hermitian part, a not so bad crude picture of the initial condition pops out. In fact what we call this crude success is that the favored or likely initial arrangement becomes that the system - the world - shall pass through and stay *very long* in saddle points. We namely interpret this prediction as being optimistically the prediction of the world going through an in some sense long stage of the inflation situation. An inflaton field having the value equal to the maximum of the (effective) potential for the inflaton field represents namely for each Fourier component of this inflaton field a system sitting at one of its saddle points. So indeed in the phenomenological development of the universe it goes through a state, which is precisely a saddle point, with respect to an infinity of degrees of freedom, namely the various Fourier components. The fact that we predict a very slow going through might be taken as an encouragement by comparison with, that it is a well-known problem, "the slow roll problem", that the inflation for phenomenological reasons should be kept going longer than expected unless the inflaton effective potential is especially (and somewhat in the models constructed) flat. Flatness should help to make the inflation period longer than it would be " naturally". Our long staying prediction might be taken as one of benefits of our model with the complex action seeking to get a long inflation, even with a less flat effective potential.

In the following section 14.2 we shall talk about initial conditions and give very crude arguments for a long staying saddle point being favored. In section 14.3 we draw some crude phase space configurations from which we seek to get an idea about which behavior of the development of the mechanical system with the complex action would be to expect. We end with favoring the long stay at the saddle point and going also to a region near a (local) minimum in the effective Hamiltonian, thereby explaining an effective finding of a bottom of the Hamiltonian. Then, in section 14.4, we allude to our for the belief in our complex action having a chance to be really true most important derivation: that you would not observe any effect (except from the initial conditions) in practice after sufficient time. In section 14.5 we introduce the idea that when one includes the future as one should in our model one may write an expression for the expectation value of a dynamical variable as the by Aharonov et.al. introduced weak value [18,19]. This is a possible scheme for extracting the to be expected average for experiment. A priori this kind of weak values are complex, but we have made theorems which prove reality under some assumptions.

14.2   Hope of Making Theory of Initial Conditions

The laws of physics falls basically in the two classes:

- The equations of motions including the possible states of the universe and thus the types of particles existing. (it is here we find the Standard Model).
- Laws about the initial conditions. Here we may think of the second law of thermodynamics, and perhaps some cosmological laws as the Hubble expansion. Or may be inflation.

We have long worked on the hypothesis that the Hamiltonian were not Hermitian. At first one thinks that this would have been seen immediately, but a major result of ours were:
For the equations of motion there would be no clean signature of the Hamiltonian not being Hermitian left. The only significant revelation of the imaginary part of the Hamiltonian would be **via the initial conditions**.

This then means that by such a non-Hermitian Hamiltonian theory we potentially has found a theory, that could function as a theory behind the initial state laws, we have at present.

14.3   Intuitive Understanding

Let us give the reader an idea about what we have in mind by thinking of a skier with frictionless skies, so that he can only stop when he has run up the hill and lost the kinetic energy. Then there is some given distribution of the quality of the outlook he can enjoy in different places or of some other sort of attraction which the skier would like to enjoy as long as possible.

It is not a good idea to just start at a random attractive outlook point with splendid outlook, because the skier will most likely find that on the hill side and he will rush down and thus away from the attractive outlook point quickly. Even arranging to slide first up with speed as to just stop by loosing the kinetic energy at an attractive point, might not compete with finding an even a bit less attractive outlook but still very attractive outlook point at the "middle" of a pass, in which one can stand seemingly forever.Just a little accidental slide to one side or the other of course in the pass leads to that he slides down and the attractive outlook place soon gets lost. With quantum mechanics such a slight leaving the very metastable saddle point in the pass is unavoidable. So with quantum mechanics the skier has to plan that he cannot be in the saddle point forever, but will slide out some day. Then he has to plan for the next step what is most profitable. Presumably it is best to arrange to find a reasonable attractive outlook place in a little whole in the landscape of only very little less potential energy than the starting situation chosen. Then namely it could be arranged that the skier would only ski little and slowly around when first arriving there. Presumably it would be best to then if possible have arranged to get back again to the first saddle point in the pass and perhaps cyclically repeat again and again a good trip.

Fig. 14.1: This just a skiing terrain, that should really symbolize in our work any state of the whole Universe. We imagine a little skier with frictionless skies, which can ski around but his tour is fixed from where and with what velocity he starts. He cannot stop except if he just runs up the hill and runs out of kinetic energy.
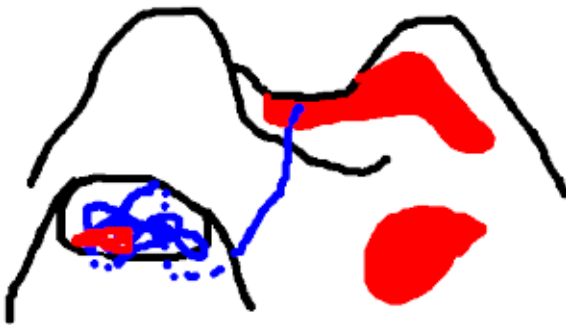

Fig. 14.2: Now we have put on some red spots which are the regions with the best outlooks or for other reasons the best ones to stay in. Now the skier gets the problem of starting in such a clever way that he manages to stay the longest time in these the best regions (marked by red). Going just to a good region at random would probably mean that he very fast would rush out of it and it would only be a short enjoy of the good region. What to do?

14.3.1   Phase space drawings

We now present a few figures supposed to be drawn in phase space, rather than in a geometrical space with mountains, to illustrate again the considerations which the little skier has to do to get the most glorious outlook for so long as possible. One must think of an integral over time of a quantity measuring the beauty of the outlook now in different "places" in phase space because the outlook beauty degree can of course also depend on the momentum, or say the velocity. In our theory with non-Hermitian or in classical thinking complex Hamiltonian the quantity to be identified with the beauty degree for the skier is of course

the imaginary part ImH of the Hamiltonian. This imaginary part ImH namely enhances the normalization of the wave function describing the the skier or in our model say the universe as it moves along classically in the phase space.

Thus the route through phase space which maximizes the time integral over the imaginary part ∫ ImHdt is the one that makes the wave function grow the most. This means that the chance for surviving the tour by the skier or rather the universe the development of which is described by the tour has the largest amplitude for existing at all at the end of the tour, when the integral over time ∫ ImHdt is the largest. It is therefore our theory predicts that what really shall happen most likely is the route through phase space giving this integral the maximal value. So we see that a problem like the one for the little skier is set up.
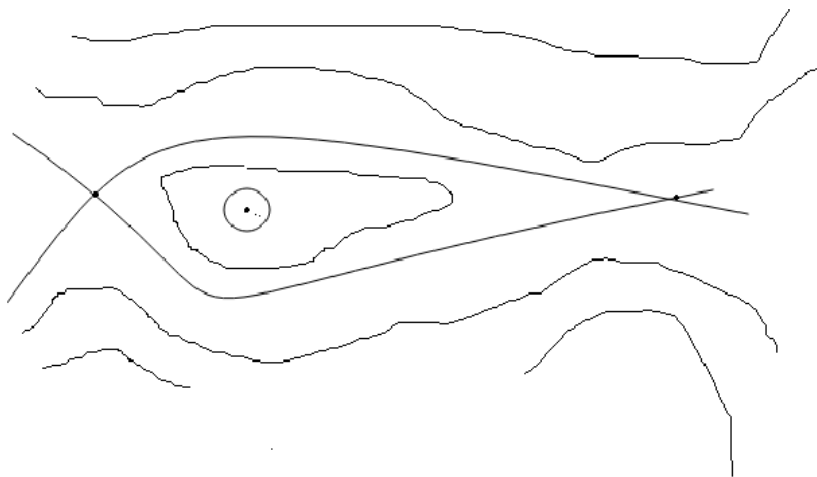
Fig. 14.3: **Symbolic Phase Space for Universe, Level curves for ReH**

Now some are figures formulated in phase space illustrating these consideration: see figures 14.3,...,14.6. How should the system choose to move? To keep red, or yellow, and avoid turquoise ?

- It could start in the red to ensure a favorable Im H in the start, but alas, it comes out in the turquoise and spend a lot of time with very unfavorable Im H.
- It could choose a not too bad, i.e. e.g yellow, place with high stability so that it can stay there forever and enjoy at least the yellow!

What we would like to learn from path favorable for high Im H integrated over time? What we want to learn from this consideration: It will usually be favorable with regard to Im H to choose a very stable place to avoid running around and loosing enormously (the turquoise) with regard to Im H. So this kind of theory predicts:

- Preferably Universe should be just around a very stable, locally ground state, it is the vacuum, with the bottom in the Hamiltonian.
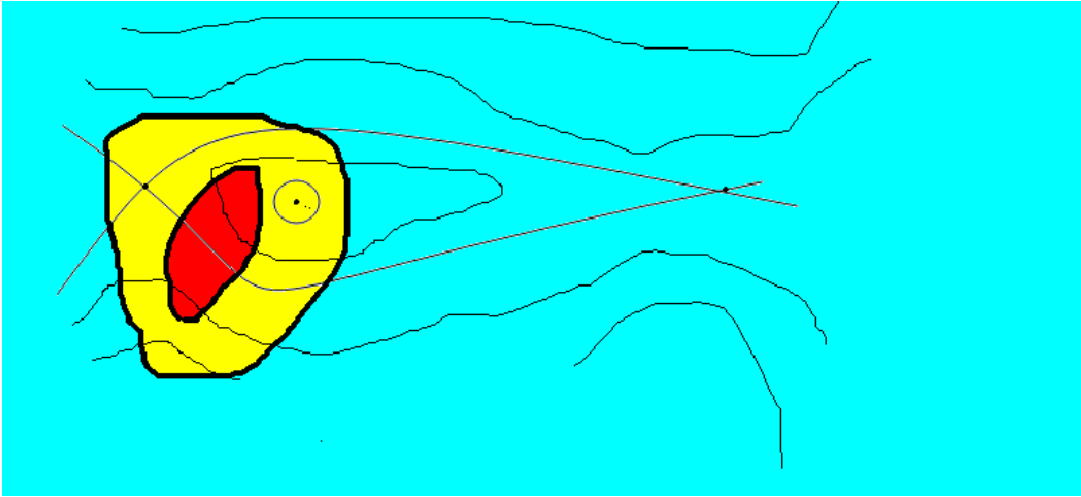
Fig. 14.4: **Symbolic Phase Space for Universe, Level curves for ReH and Color for Im H** Imaginary part Im H symbolized by colors: Red very strongly wished; Yellow also very good, but not the perfect; turquoise strongly to be avoided, bad!
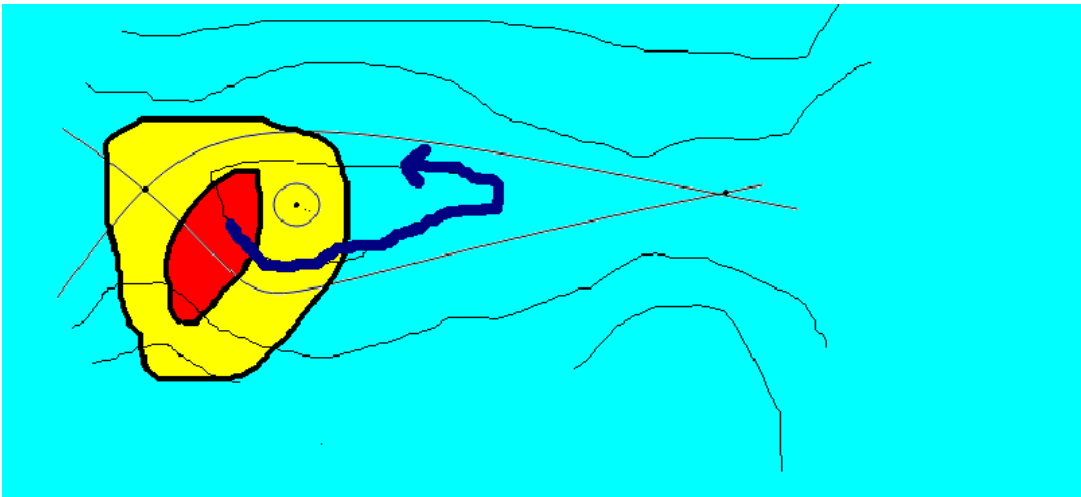
Fig. 14.5: **Symbolic Phase Space for Universe, Level curves for ReH and Color for Im H** Imaginary part Im H symbolized by colors: Red very strongly wished; Yellow also very good, but not the perfect; turquoise strongly to be avoided, bad!

- Even better might be using a saddle point (there are also more of them and so it more likely to be best) and then choose it so that there is a stable local ground state not so far to spend eternity. Such a saddle is the tip of the inflaton effective potential. By choosing just that tip in principle it can stand as long as to be disturbed by quantum mechanics.
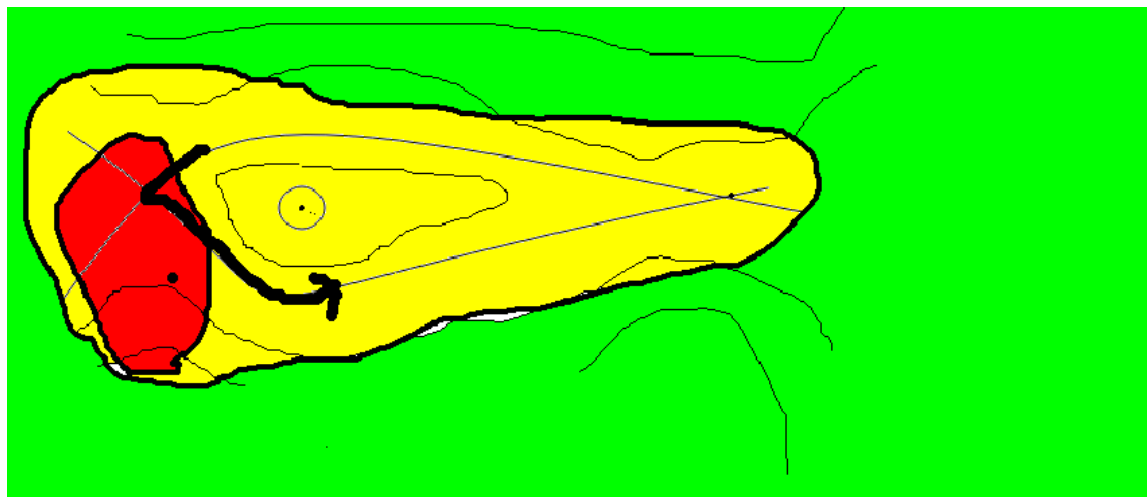
Fig. 14.6: **Symbolic Phase Space for Universe, Level curves for Re H and Color for Im H** Red very strongly wished, the saddle point very good; Yellow also very good, but not the perfect, but on this figure it can circle around more stably in the yellow; turquoise strongly to be avoided, bad, can be avoided by keeping around the fix points!

Results of the intuitive treatment of the non-Hermitian Hamiltonian are as follows:

- The world-system should run around so little as possible to avoid the low Im H places (= the unfavorable ones): It should have small entropy (contrary to the intuitive cosmology of Paul Framptons in the other talk). Rather close to stable point (= ground state). So the model predicts there being a bottom in the effective Hamiltonian locally in phase space.
- The world-system should stay as long as possible at a saddle almost exactly - to keep staying surprisingly long (like a pen standing vertically on its tip in years); but this is in the many degrees of freedom translation a **surprisingly long inflation** era. That is the problem of the too many e-foldings, which we thus at least claimed to have a feature of the initial condition model helping in the right direction (making inflation longer than the potential that should preferably not be flat indicates).

14.4   Main Result

Our main result is that you would not discover from equations of motion that the Hamiltonian had an anti-Hermitian part. The system (the world) would only have significant Hilbert vector components in the states with the very highest imaginary part of the eigenvalues of the non-Hermitian Hamiltonian, since the rest would die out with time. Remember

$$|A(t) >> = \exp(-iHt)|A(0) >> . \tag{14.1}$$

So at least the anti-Hermitian part is near to its (supposed) maximum, and thus at least less significant. We introduce a new inner product making the Hamiltonian H normal, i.e. making the Hermitian and the anti-Hermitian parts commute. So it is unnecessary to assume that the Hamiltonian is Hermitian! It will show up so in practice anyway!

14.5   Weak Value

As a result of our thinking of how to interpret the complex action theory we came to the concept already studied by Aharonov et.al. [18, 19], the weak value:

$$O_{wv}(t) = \frac{< B(t)|O|A(t) >}{< B(t)|A(t) >} \tag{14.2}$$

or better with time development included:

$$O_{wv}(t) = \frac{< B(T_B)|\exp(-i(T_B - t)H)O\exp(-i(t - T_A)H)|A(T_A) >}{< B(T_b)|\exp(-i(T_B - T_A)H)|A(T_A) >}, \tag{14.3}$$

where we have assumed that the states $|B(t) >$ and $|A(t) >$ time-develop according to the following Schrödinger equations:

$$\frac{d}{dt}|B(t) >> = -iH^\dagger|B(t) >>, \tag{14.4}$$

$$\frac{d}{dt}|A(t) >> = -iH|A(t) >> . \tag{14.5}$$

Our idea is to use the weak value instead of the usual operator average:

$$O_{av}(t) = \frac{< A(t)|O|A(t) >}{< A(t)|A(t) >}. \tag{14.6}$$

One motivation is that it may give more natural interpretation of functional integrals. Usually the answer to how to use functional integrals is: "You can use it to calculate a time development operator - e.g an S-matrix - and then use that to propagate the quantum system in the usual Hilbert space formalism." The weak value has a more beautiful functional integral expression:

$$O_{wv}(t) = \frac{\int O\psi_B^*\psi_A \exp(\frac{i}{\hbar}S[path])\mathcal{D}path}{\int \psi_B^*\psi_A \exp((\frac{i}{\hbar}S[path])\mathcal{D}path}, \tag{14.7}$$

where in the numerator the operator O was inserted at the appropriate time, than the usual operator average.

The usual average and the weak value look a priori quite different, but with what we call the maximization principle, that the absolute value of the denominator of Eq.(14.2):

$$| < B(t)|A(t) > | = | < B(T_B)| \exp(-i(T_B - T_A)H)|A(T_A) > | \qquad (14.8)$$

be maximal for fixed normalization of the two states, you may see that (at least for Hermitian Hamiltonian) one gets

$$|B(t) > \propto |A(t) > . \qquad (14.9)$$

In Ref. [13] we have found that one can construct such an inner product $|_Q$ that, even if at first the Hamiltonian H is not normal, i.e. if

$$[H, H^\dagger] \neq 0, \qquad (14.10)$$

then, with regard to this new inner product, it is

$$[H, H^{\dagger Q}] = 0. \qquad (14.11)$$

The new inner product[2] can arrange a normal Hamiltonian.

The inner product can be described as composed from the usual one $|$ and a Hermitian operator Q constructed from H. I.e. $|_Q = |Q$ means

$$< ...|_Q ... > = < ...|Q|... > . \qquad (14.12)$$

One can thus talk about a Q-Hermitian operator O when it obeys

$$O^{\dagger Q} = O \qquad (14.13)$$

where

$$O^{\dagger Q} = Q^{-1}O^\dagger Q. \qquad (14.14)$$

Remember the point of our new inner product was to make the at first not even normal Hamiltonian at least normal, i.e. the Q-Hermitian and the anti-Q-Hermitian parts commute. It is the idea that the physical observables one should use in a world with a non-Hermitian Hamiltonian are Q-Hermitian.

In Ref. [27] we proposed the following theorem "maximization principle in the future-included complex action theory":

As a prerequisite, assume that a given Hamiltonian H is non-normal but diagonalizable and that the imaginary parts of the eigenvalues of H are bounded from above, and define a modified inner product $|_Q$ by means of a Hermitian operator Q arranged so that H becomes

---

[2] Similar inner products are also studied in Refs. [24, 25, 29].

normal with respect to $|_Q$. *Let the two states* $|A(t) >$ *and* $|B(t) >$ *time-develop according to the Schrödinger equations with* H *and* $H^{\dagger_Q}$ *respectively:*

$$|A(t) > = \exp(-iH(t - T_A))|A(T_A) >, \qquad (14.15)$$

$$|B(t) > = \exp(-iH^{\dagger_Q}(t - T_B))|B(T_B) >, \qquad (14.16)$$

and be normalized with $|_Q$ *at the initial time* T_A *and the final time* T_B *respectively:*

$$< A(T_A)|_Q A(T_A) > = 1, \qquad (14.17)$$

$$< B(T_B)|_Q B(T_B) > = 1. \qquad (14.18)$$

Next determine $|A(T_A) >$ *and* $|B(T_B) >$ *so as to maximize the absolute value of the transition amplitude* $| < B(t)|_Q A(t) > | = | < B(T_B)|_Q \exp(-iH(T_B - T_A))|A(T_A) > |$. *Then, provided that an operator* O *is Q-Hermitian, i.e., Hermitian with respect to the inner product* $|_Q$, *i.e.* $O^{\dagger_Q} = O$, *the normalized matrix element of the operator* O *defined by*

$$< O >_Q^{BA} = \frac{< B(t)|_Q O|A(t) >}{< B(t)|_Q A(t) >} \qquad (14.19)$$

becomes real and time-develops under a Q-Hermitian Hamiltonian.

We note that this theorem shows that the complex action theory could make predictions about initial conditions.

14.6   Conclusion

We have put forward our works of looking at a complex action or better a non-Hermitian Hamiltonian. Since it would not be easily seen that the Hamiltonian were indeed non-Hermitian after sufficiently long time and only showing itself up as it were the initial conditions that were influenced by the anti-Hermitian part, and even this influence looks promising, we believe that a complex action of non-Hermitian Hamiltonian model like the one described has indeed a good chance to be the truth. Our complex action theory would make predictions about initial conditions. An intuitive use of non-Hermitian H suggested explanation for: Effective bottom in the Hamiltonian; Long Inflation; Low Entropy.

One should stress that one should consider it a weaker assumption to assume a non-Hermitian Hamiltonian than a Hermitian one, in as far as it is an assumption that the anti-Hermitian part is zero, while assuming the non-Hermitian Hamiltonian is just *allowing the Hamiltonian to be whatever.* It is only because we are taught about the Hermitian Hamiltonian from the tradition that we tend to consider it a new and strange assumption to take the Hamiltonian to be non-Hermitian.

Acknowledgments

References

1. H. B. Nielsen and M. Ninomiya, Proc. Bled 2006: What Comes Beyond the Standard Models, pp.87-124 (2006) [arXiv:hep-ph/0612250].
2. H. B. Nielsen and M. Ninomiya, Int. J. Mod. Phys. A 23, 919 (2008).
3. H. B. Nielsen and M. Ninomiya, Int. J. Mod. Phys. A 24, 3945 (2009).
4. H. B. Nielsen and M. Ninomiya, Prog. Theor. Phys. 116, 851 (2007).
5. H. B. Nielsen and M. Ninomiya, Proc. Bled 2007: What Comes Beyond the Standard Models, pp.144-185 (2007) [arXiv:0711.3080 [hep-ph]].
6. H. B. Nielsen and M. Ninomiya, arXiv:0910.0359 [hep-ph].
7. H. B. Nielsen, Found. Phys. 41, 608 (2011) [arXiv:0911.4005[quant-ph]].
8. H. B. Nielsen and M. Ninomiya, Proc. Bled 2010: What Comes Beyond the Standard Models, pp.138-157 (2010) [arXiv:1008.0464 [physics.gen-ph]].
9. H. B. Nielsen, arXiv:1006.2455 [physic.gen-ph].
10. H. B. Nielsen and M. Ninomiya, arXiv:hep-th/0701018.
11. H. B. Nielsen, arXiv:0911.3859 [gr-qc].
12. H. B. Nielsen, M. S. Mankoc Borstnik, K. Nagao, and G. Moultaka, Proc. Bled 2010: What Comes Beyond the Standard Models, pp.211-216 (2010) [arXiv:1012.0224 [hep-ph]].
13. K. Nagao and H. B. Nielsen, Prog. Theor. Phys. 125, 633 (2011).
14. K. Nagao and H. B. Nielsen, Prog. Theor. Phys. 126, 1021 (2011); 127, 1131 (2012) [erratum].
15. K. Nagao and H. B. Nielsen, Int. J. Mod. Phys. A27, 1250076 (2012); 32, 1792003 (2017)[erratum].
16. K. Nagao and H. B. Nielsen, Prog. Theor. Exp. Phys. 2013, 073A03 (2013); 2018, 029201 (2018)[erratum].
17. K. Nagao and H. B. Nielsen, Prog. Theor. Exp. Phys. 2017, 111B01 (2017).
18. Y. Aharonov, D. Z. Albert, and L. Vaidman, Phys. Rev. Lett. 60, 1351 (1988).
19. Y. Aharonov, S. Popescu, and J. Tollaksen, Phys. Today 63, 27 (2010).
20. K. Nagao and H. B. Nielsen, Prog. Theor. Exp. Phys. 2013, 023B04 (2013); 2018, 039201 (2018)[erratum].
21. K. Nagao and H. B. Nielsen, Proc. Bled 2012: What Comes Beyond the Standard Models, pp.86-93 (2012) [arXiv:1211.7269 [quant-ph]].
22. C. M. Bender and S. Boettcher, Phys. Rev. Lett. 80, 5243 (1998).
23. C. M. Bender, S. Boettcher, and P. Meisinger, J. Math. Phys. 40, 2201 (1999).
24. A. Mostafazadeh, J. Math. Phys. 43, 3944 (2002).
25. A. Mostafazadeh, J. Math. Phys. 44, 974 (2003).
26. C. M. Bender and P. D. Mannheim, Phys. Rev. D 84, 105038 (2011).
27. K. Nagao and H. B. Nielsen, Prog. Theor. Exp. Phys. 2015, 051B01 (2015).
28. K. Nagao and H. B. Nielsen, Prog. Theor. Exp. Phys. 2017, 081B01 (2017).
29. F. G. Scholtz, H. B. Geyer, and F. J. W. Hahne, Ann. Phys. 213, 74 (1992).
30. K. Nagao and H. B. Nielsen, Fundamentals of Quantum Complex Action Theory, (Lambert Academic Publishing, Saarbrucken, Germany, 2017).

31. K. Nagao and H. B. Nielsen, Proc. Bled 2017: What Comes Beyond the Standard Models, pp.121-132 (2017) [arXiv:1710.02071 [quant-ph]].
32. K. Nagao and H. B. Nielsen, Prog. Theor. Exp. Phys. 2019, 073B01 (2019).
33. K. Nagao and H. B. Nielsen, Prog. Theor. Exp. Phys. 2022, 091B01 (2022).
34. K. Nagao and H. B. Nielsen, arXiv:2209.11619 [hep-th].

15   Emergent phenomena in QCD:
The holographic perspective

Guy F. de Téramond

Laboratorio de Física Teórica y Computacional, Universidad de Costa Rica,
11501 San José, Costa Rica
email:gdt@asterix.crnet.cr

Abstract. A basic understanding of the relevant features of hadron physics from first princi-
ples QCD has remained elusive and should be understood as emergent phenomena, which
depend critically on the number of dimensions of Minkowski spacetime. These properties
include the mechanism of color confinement, the origin of the hadron mass scale, chiral
symmetry breaking and the pattern of hadronic bound states. Some of these complex issues
have been recently addressed in an effective computational framework of hadron structure
based on a semiclassical approximation to light-front QCD and its holographic embedding
in AdS space. The framework embodies an underlying superconformal algebraic structure
which leads to the introduction of a mass scale within the superconformal group, and
determines the effective confinement potential of mesons, baryons and tetraquarks, while
keeping the pion massless. This new approach to hadron physics leads to relativistic wave
equations similar in their simplicity to the Schrödinger equation in atomic physics.

15.1   Introduction

The interactions between the fundamental constituents of hadrons, quark and gluons, observed in high energy scattering experiments is described to high precision by Quantum Chromodynamics (QCD), thus establishing QCD as the standard theory of the strong interactions. At large distances, however, the nonperturbative nature of the strong interactions becomes dominant and a basic understanding of the essential features of hadron physics from first principles QCD has remained an important unsolved problem in the standard model of particle physics. Basic hadronic properties are not explicit properties of the QCD Lagrangian but emergent phenomena, among them: The mechanism of color confinement, the origin of the hadron mass scale, the relation between chiral symmetry breaking and confinement, the massless pion *vs.* the massive proton in the chiral limit, bound states and the pattern of hadron excitations. Other important aspects of the strong interaction, such as the emergence of Regge theory, Pomeron physics and the Veneziano amplitude, were introduced in dual models before the advent of QCD, and should also be considered large distance QCD emergent phenomena. Our present goal is trying to understand how emerging QCD properties would appear in an effective computational framework of hadron structure and its dependence on the dimensionality of physical spacetime.

QCD admits an Euclidean lattice formulation [1] which has been established as a rigorous framework to study hadron structure and spectroscopy nonperturbatively. However, dynamical observables in Minkowski spacetime cannot be obtained directly from the Euclidean lattice. Quantum computation of relativistic field theories using the Hamiltonian formalism in light-front quantization [2] represents a promising venue, but its development is still at the exploratory phase [3]. Other nonperturbative methods based on the Schwinger-Dyson and the Bethe-Salpeter equations, and other approximations and models of the strong interactions are described in Ref. [4].

Recent theoretical developments based on AdS/CFT – the correspondence between classical gravity in a higher-dimensional anti-de Sitter (AdS) space and conformal field theories (CFT) in physical space-time [5], have provided a semiclassical approximation for strongly-coupled quantum field theories, giving new insights into nonperturbative dynamics [6]. This approach provides useful tools for constructing dual gravity models in higher dimensions which incorporates confinement and basic QCD properties in physical spacetime. The resulting gauge/gravity duality is broadly known as the AdS/QCD correspondence, or holographic QCD. Or approach to holographic QCD is based on the holographic embedding of Dirac's relativistic *front form* of dynamics [2] into AdS space, thus its name Holographic Light-Front QCD (HLFQCD). This framework leads to relativistic wave equations in physical space-time, similar to the Schrödinger or Dirac wave equations in atomic physics [7–9]. This approach has its origins in the precise mapping between the hadron form factors in AdS space [10] and physical spacetime, which can be carried out for an arbitrary number of quark constituents [11]: It leads to the identification of the invariant transverse impact variable ζ for the n-parton

bound state in physical 3+1 spacetime with the holographic variable z, the fifth dimension of AdS.

A remarkable property of HLFQCD is the embodiment of a superconformal algebraic structure which is responsible for the introduction of a mass scale within the algebra. This symmetry also fixes the confinement interaction leading to a massless pion in the chiral limit (the limit of zero quark masses) and to striking connections between the spectrum of mesons, baryons and tetraquarks [12–17]. Further extensions of HLFQCD provide nontrivial relations between the dynamics of form factors and quark and gluon distributions [18–20] with pre-QCD nonperturbative approaches such as Regge theory and the Veneziano model.

In this introductory presentation I will give an overview of relevant aspects of the semiclassical approximation to QCD quantized in the light front (LF) in 1 + 1 and 3 + 1 spacetime dimensions, followed by the holographic embedding in AdS$_5$ space of the (3 + 1) semiclassical QCD wave equations with an emphasis on the underlying superconformal structure for hadron spectroscopy. Other relevant aspects and applications of the light-front holographic approach have been described in the recent review [21].

15.2 Critical role of the dimensionality of spacetime and QCD emergent phenomena

The number of dimensions of physical spacetime is critical in determining whether hadronic properties are complex emergent phenomena which arise out of the QCD Lagrangian, or can (at least in principle) be computed and expressed in terms of the basic parameters of the QCD Lagrangian [22].

Our starting point is the QCD action in d dimensions with an $SU(N)$ Lagrangian written in terms of the fundamental quark and gluon gauge fields, ψ and A,

$$LS = \int d^d x \left(\bar{\psi} \left(i\gamma^\mu D_\mu - m \right) \psi - \tfrac{1}{4} G^a_{\mu\nu} G^{a\,\mu\nu} \right),$$

where $D_\mu = \partial_\mu - igT^a A^a_\mu$ and $G^a_{\mu\nu} = \partial_\mu A^a_\nu - \partial_\nu A^a_\mu + f^{abc} A^b_\mu A^c_\nu$, with $[T^a, T^b] = if^{abc}$ and a, b, c are $SU(N)$ color indices. A simple dimensional analysis of the QCD action gives

$$[\psi] \sim M^{(d-1)/2}, \tag{15.1}$$
$$[A] \sim M^{(d-2)/2}, \tag{15.2}$$
$$[g] \sim M^{(4-d)/2}.g \tag{15.3}$$

It follows from g that in 1 + 1dimensions, for example, the QCD coupling g has dimensions of mass, $[g] \sim M$. In this case, the theory can be solved for any number of constituents and colors using discrete light-cone quantization (DLCQ) methods [23, 24]. All physical quantities can be computed in terms of the basic 1 + 1 Lagrangian parameters, the coupling and the quark masses, but no emergent phenomena appear.

In contrast, in 3+1 dimensions the coupling g is dimensionless and, in the limit of massless quarks, the QCD Lagrangian is conformally invariant[1]. The need for the renormalization of the theory introduces a scale Λ_{QCD}, which breaks the conformal invariance and leads to the "running coupling" $\alpha_s\left(\mu^2\right) = g^2(\mu)/4\pi$ and asymptotic freedom [25, 26] for large values of μ^2. The scale Λ_{QCD} is determined in high energy experiments: Its origin and the emergence of hadron degrees of freedom out of the constituent quark and gluon degrees of freedom of the QCD Lagrangian in the nonperturbative domain remains a deep unsolved problem.

15.3   Semiclassical approximation to light-front QCD

LF quantization uses the null plane $x^+ = x^0 + x^3 = 0$ tangent to the light cone as the initial surface, thus without reference to a specific Lorentz frame [2]. Evolution in LF time x^+ is given by the Hamiltonian equation

$$\text{LFHE} i\frac{\partial}{\partial x^+}|\psi\rangle = P^-|\psi\rangle, \qquad P^-|\psi\rangle = \frac{P_\perp^2 + M^2}{P^+}|\psi\rangle, \tag{15.4}$$

for a hadron with 4-momentum $P = (P^+, P^-, P_\perp)$, $P^\pm = P^0 \pm P^3$, where the LF Hamiltonian P^- is a dynamical generator and P^+ and $P_\perp$ are kinematical. Hadron mass spectra can be computed from the LF invariant Hamiltonian $P^2 = P_\mu P^\mu = P^+P^- - P_\perp^2$ [9]

$$\text{P2M2} P^2|\psi(P)\rangle = M^2|\psi(P)\rangle. \tag{15.5}$$

The simple structure of the LF vacuum allows for a quantum-mechanical probabilistic interpretation of hadron states in terms of the eigenfunctions of the LF Hamiltonian equation P2M2 in a constituent particle basis, $|\psi\rangle = \sum_n \psi_n|n\rangle$, written in terms of the quark and gluon degrees of freedom in the Fock expansion.
In practice, solving the actual eigenvalue problem P2M2 is a formidable computational task for a non-abelian quantum field theory beyond $1 + 1$ dimensions, and particularly in three and four-dimensional space-time with an unbound particle number with arbitrary momenta and helicities. Consequently, alternative methods and approximations are necessary to tackle the relativistic bound-states in the strong-coupling regime of QCD.

15.3.1   QCD(1 + 1)

The 't Hooft model [27] in one-space and one-time dimensions, constitutes the first example of a semiclassical Hamiltonian wave equation derived from first principles QCD in light-front quantization [2]. This equation is exact in the large-N limit and leads to the computation of a meson spectrum and light front wave functions in terms of the constituent quark and antiquark, while incorporating chiral symmetry breaking (CSB) and confinement.

---

[1] The QED abelian coupling $\alpha = e^2/4\pi$ is also dimensionless, but the physical observables in atomic physics can be computed and, in contrast with the proton, depend critically on the constituent masses in the QED Lagrangian.

In QCD (1 + 1) gluons are not dynamical, there are no gluon self-couplings, and quarks have chirality but no spin. The coupling g has dimension of mass and it is a confining gauge theory for any value of the coupling. We can express the QCD Lagrangian L in 1 + 1 dimensions, with LF coordinates $x^+ = x^0 + x^3$ and $x^- = x^0 - x^3$, in the $A^+ = 0$ gauge in terms of the fields $\psi_\pm \equiv \psi_{R,L}$ and A^-. The LF constraint equations imply that there is only one independent degree of freedom, ψ_+. The hadron 2-momentum generator $P = (P^+, P^-)$, $P^\pm = P^0 \pm P^3$, is then expressed in terms of the field ψ_+ [24,28,29] with

$$\text{Pm11}P^- = \int dx^- \left(\psi_+^\dagger \frac{m^2}{i\partial^+} \psi_+ + g^2 j^{+a} \frac{1}{(i\partial^+)^2} j^{+a} \right), \tag{15.6}$$

for the LF Hamiltonian where $j^{+a} = \psi_+^\dagger T^a \psi_+$. From the inverse derivative in the interaction term in Pm11 (the term with the coupling) there follows the potential V

$$V = -g^2 \int dx^- dy^- j^{+a}(x^-) |x^- - y^-| j^{+a}(y^-). \tag{15.7}$$

The pion mass spectrum can be computed from the LF eigenvalue equation P2M2 for QCD(1+1), namely $P^+ P^- |\chi(P^+)\rangle = M_\pi^2 |\chi(P^+)\rangle$. For the $q\bar{q}$ valence state it leads to [24,29]

$$\text{tHE} \left(\frac{m_q^2}{x} + \frac{m_{\bar{q}}^2}{1-x} \right) \chi(x) + \frac{\lambda_N}{\pi} P \int_0^1 dx' \frac{\chi(x) - \chi(x')}{(x-x')^2} = M_\pi^2 \chi(x), \tag{15.8}$$

the 't Hooft equation [27] with effective coupling $\lambda_N = g^2 (N^2 - 1)/2N$, where x is the longitudinal momentum fraction of the $q\bar{q}$ state. Cancellation of singularities at $x = \epsilon$ and $x = 1 - \epsilon$ for the approximate solution $\chi(x) \sim x^{\beta_q}(1-x)^{\beta_q}$ tHE leads for $m_q^2/\pi\lambda_N \ll 1$ to $\beta_q = \left(3m_q^2/\pi\lambda_N \right)^{1/2}$ and

$$M_\pi^2 = \sqrt{\frac{\pi\lambda_N}{3}} (m_q + m_{\bar{q}}) + \mathcal{O}\left((m_q + m_{\bar{q}})^2 \right). \tag{15.9}$$

In QCD(1+1) both, the value of the CSB "condensate" $\langle \psi\psi \rangle = f_\pi^2 \sqrt{\pi\lambda_N/3}$ and the strength of linear confinement depend on the value of the coupling g in the QCD Lagrangian, and are not emerging properties[2].

15.3.2   3p1QCD(3 + 1)

In 3 + 1 dimensions we also start with the QCD Lagrangian in L and assume that, to a first semiclassical approximation, gluons with small virtualities are non-dynamical and incorporated in the confinement potential [7]. This approximation entails an important simplification of the full LF Hamiltonian P^-, which we express in terms of the dynamical quark field ψ_+, $\psi_\pm = \Lambda_\pm \psi$, $\Lambda_\pm = \gamma^0 \gamma^\pm$ in the $A^+ = 0$ gauge [9]

$$\text{Pm31}P^- = \int dx^- d^2x_\perp \bar{\psi}_+ \frac{(i\nabla_\perp)^2 + m^2}{i\partial^+} \psi_+ + \text{ interactions}, \tag{15.10}$$

---

[2] The glueball spectrum has been computed in a large-N model of QCD in 1 + 1 dimensions [30].

to compute the mass spectrum from the LF eigenvalue Eq. P2M2.

For a $q\bar{q}$ bound state we factor out the longitudinal $X(x)$ and orbital $e^{iL\theta}$ dependence from the LF wave function ψ, $\psi(x, \zeta, \theta) = e^{iL\theta}X(x)\phi(\zeta)/\sqrt{2\pi\zeta}$, where $\zeta^2 = x(1-x)b_{\perp}^2$ is the invariant transverse separation between two quarks, with $b_{\perp}$, the relative impact variable, conjugate to the relative transverse momentum $k_{\perp}$ with longitudinal momentum fraction x. In the ultra-relativistic zero-quark mass limit the invariant LF Hamiltonian Eq. P2M2, with P^- given by Pm31, can be systematically reduced to the wave equation [7]

$$\mathrm{LFWE} \left(-\frac{d^2}{d\zeta^2} - \frac{1 - 4L^2}{4\zeta^2} + U(\zeta) \right) \phi(\zeta) = M^2\phi(\zeta), \qquad (15.11)$$

where the effective potential U comprises all interactions, including those from higher Fock states. The critical value of the LF orbital angular momentum $L = 0$ corresponds to the lowest possible stable solution. The LF equation LFWE is relativistic and frame-independent; It has a similar structure to wave equations in AdS provided that one identifies $\zeta = z$, the holographic variable [7].

15.4   Higher spin wave equations in AdS

The semiclassical LF bound-state wave equation LFWE can be mapped to the equations of motion which describe the propagation of spin-J modes in AdS space [7,8]. To examine this equivalence, we start with the AdS action for a tensor-J field $\Phi_J = \Phi_{N_1...N_J}$ in the presence of a dilaton profile $\varphi(z)$ responsible for the confinement dynamics

$$\mathrm{SAdSS} = \int d^dx\, dz \sqrt{g}\, e^{\varphi(z)} \left(D_M\Phi_J D^M\Phi_J - \mu^2\Phi_J^2 \right), \qquad (15.12)$$

where g is the determinant of the metric tensor g_{MN}, d is the number of transverse coordinates, and D_M is the covariant derivative which includes the affine connection. The variation of the AdS action leads to the wave equation

$$\mathrm{AdSWEJ} \left[-\frac{z^{d-1-2J}}{e^{\varphi(z)}}\partial_z \left(\frac{e^{\varphi(z)}}{z^{d-1-2J}}\partial_z \right) + \frac{(\mu R)^2}{z^2} \right] \Phi_J(z) = M^2\Phi_J(z), \qquad (15.13)$$

after a redefinition of the AdS mass μ, plus kinematical constraints to eliminate lower spin from the symmetric tensor $\Phi_{N_1...N_J}$ [8]. By substituting $\Phi_J(z) = z^{(d-1)/2-J}e^{-\varphi(z)/2}\phi_J(z)$ in AdSWEJ, we find the semiclassical light-front wave equation LFWE with

$$\mathrm{UvarphiU}_J(\zeta) = \frac{1}{2}\varphi''(\zeta) + \frac{1}{4}\varphi'(\zeta)^2 + \frac{2J-3}{2\zeta}\varphi'(\zeta), \qquad (15.14)$$

for $d = 4$ as long as $\zeta = z$. The precise mapping allows us to write the LF confinement potential U in terms of the dilaton profile which modifies the IR region of AdS space to incorporate confinement [9], while keeping the theory conformal invariant in the ultraviolet boundary of AdS for $z \rightarrow 0$, which corresponds to the

4-dimensional physical boundary of AdS space [21]. The separation of kinematic and dynamic components, allows us to determine the mass function in the AdS action in terms of physical kinematic quantities with the AdS mass-radius $(\mu R)^2 = L^2 - (2 - J)^2$ [7,8].

A similar derivation follows from the Rarita-Schwinger action for a spinor field $\Psi_J \equiv \Psi_{N_1 \ldots N_{J-1/2}}$ in AdS with the result [8]

$$\left(-\frac{d^2}{d\zeta^2} - \frac{1 - 4L^2}{4\zeta^2} + U^+(\zeta) \right) \psi_+ = M^2 \psi_+ \text{psi1}, \qquad (15.15)$$

$$\left(-\frac{d^2}{d\zeta^2} - \frac{1 - 4(L+1)^2}{4\zeta^2} + U^-(\zeta) \right) \psi_- = M^2 \psi_- \text{psi2}, \qquad (15.16)$$

with $\zeta = z$, and equal probability $\int d\zeta \, \psi_+^2(\zeta)^2 = \int d\zeta \, \psi_-^2(\zeta)$. The semiclassical LF wave equations for ψ_+ and ψ_- correspond to LF orbital angular momentum L and $L + 1$ with

$$UVU^\pm(\zeta) = V^2(\zeta) \pm V'(\zeta) + \frac{1 + 2L}{\zeta} V(\zeta), \qquad (15.17)$$

a J-independent potential, in agreement with the observed degeneracy in the baryon spectrum.

15.5 Superconformal algebraic structure and emergence of a mass scale

The precise mapping of the semiclassical light-front Hamiltonian equations to the wave equations in AdS space gives important insights into the nonperturbative structure of bound state equations in QCD for arbitrary spin, but it does not answer the question of how the effective confinement dynamics is actually determined, and how it can be related to the symmetries of QCD itself. An important clue, however, comes from the realization that the potential $V(\zeta)$ in Eq. UV plays the role of the superpotential in supersymmetric (SUSY) quantum mechanics (QM) [31]. In fact, the idea to apply an effective supersymmetry to hadron physics is certainly not new [32–34], but failed to account for the special role of the pion. In contrast, as we shall discuss below, in the HLFQCD approach, the zero-energy eigenmode of the superconformal quantum mechanical equations is identified with the pion which has no baryonic supersymmetric partner, a pattern which is observed across the particle families.

Supersymmetric QM is based on a graded Lie algebra consisting of two anticommuting supercharges Q and $Q^\dagger$, $\{Q, Q\} = \{Q^\dagger, Q^\dagger\} = 0$, which commute with the Hamiltonian $H = \frac{1}{2}\{Q, Q^\dagger\}$, $[Q, H] = [Q^\dagger, H] = 0$. If the state $|E\rangle$ is an eigenstate with energy E, $H|E\rangle = E|E\rangle$, then, it follows from the commutation relations that the state $Q^\dagger|E\rangle$ is degenerate with the state $|E\rangle$ for $E \neq 0$, but for $E = 0$ we have $Q^\dagger|E = 0\rangle = 0$, namely the zero mode has no supersymmetric partner [31]; a key result for deriving the supermultiplet structure and the pattern of the hadron spectrum which is observed across the particle families.

Following Ref. [13] we consider the scale-deformed supercharge operator $R_\lambda = Q + \lambda S$, with $K = \frac{1}{2}\{S, S^\dagger\}$ the generator of special conformal transformations. The generator R_λ is also nilpotent, $\{R_\lambda, R_\lambda\} = \{R_\lambda^\dagger, R_\lambda^\dagger\} = 0$, and gives rise to a new scale-dependent Hamiltonian G, $G = \frac{1}{2}\{R_\lambda, R_\lambda^\dagger\}$, which also closes under the graded algebra, $[R_\lambda, G] = [R_\lambda^\dagger, G] = 0$. The new supercharge R_λ has the matrix representation

$$RexR_\lambda = \begin{pmatrix} 0 & r_\lambda \\ 0 & 0 \end{pmatrix}, \quad R_\lambda^\dagger = \begin{pmatrix} 0 & 0 \\ r_\lambda^\dagger & 0 \end{pmatrix}, \tag{15.18}$$

with $r_\lambda = -\partial_x + \frac{f}{x} + \lambda x$, $r_\lambda^\dagger = \partial_x + \frac{f}{x} + \lambda x$. The parameter f is dimensionless and λ has the dimension of $[M^2]$, and thus, a mass scale is introduced in the Hamiltonian without leaving the conformal group. The Hamiltonian equation $G|E\rangle = E|E\rangle$ leads to the wave equations

$$\left(-\frac{d^2}{dx^2} - \frac{1 - 4(f+)^2}{4x^2} + \lambda^2 x^2 + 2\lambda(f-)\right)\phi_+ = E\phi_+, phi1 \tag{15.19}$$

$$\left(-\frac{d^2}{dx^2} - \frac{1 - 4(f-)^2}{4x^2} + \lambda^2 x^2 + 2\lambda(f+)\right)\phi_- = E\phi_-, phi2 \tag{15.20}$$

which have the same structure as the Euler-Lagrange equations obtained from the holographic embedding of the LF Hamiltonian equations, but here, the form of the LF confinement potential, $\lambda^2 x^2$, as well as the constant terms in the potential are completely fixed by the superconformal symmetry [16, 17].

15.5.1 Light-front mapping and baryons

Upon mapping phi1 and phi2 to the semiclassical LF wave equations psi1 and psi2 using the substitutions $x \mapsto \zeta$, $E \mapsto M^2$, $f \mapsto L+$, $\phi_+ \mapsto \psi_-$ and $\phi_- \mapsto \psi_+$, we find the result $U^+ = \lambda^2 \zeta^2 + 2\lambda(L + 1)$ and $U^- = \lambda^2 \zeta^2 + 2\lambda L$ for the confinement potential of baryons [16]. The solution of the LF wave equations for this potential gives the eigenfunctions

$$\psi_+(\zeta) \sim \zeta^{\frac{1}{2}+L} e^{-\lambda\zeta^2/2} L_n^L(\lambda\zeta^2) \tag{15.21}$$

$$\psi_-(\zeta) \sim \zeta^{\frac{3}{2}+L} e^{-\lambda\zeta^2/2} L_n^{L+1}(\lambda\zeta^2) \tag{15.22}$$

with eigenvalues $M^2 = 4\lambda(n + L + 1)$. The polynomials $L_n^L(x)$ are associated Laguerre polynomials, where the radial quantum number n counts the number of nodes in the wave function. We compare in Fig. **??** the model predictions with the measured values for the positive parity nucleons [35] for $\sqrt{\lambda} = 0.485$ GeV.

15.5.2 scMBSuperconformal meson-baryon symmetry

Superconformal quantum mechanics also leads to a connection between mesons and baryons [17] underlying the $SU(3)_C$ representation properties, since a diquark cluster can be in the same color representation as an antiquark, namely $\bar{3} \in 3 \times 3$.
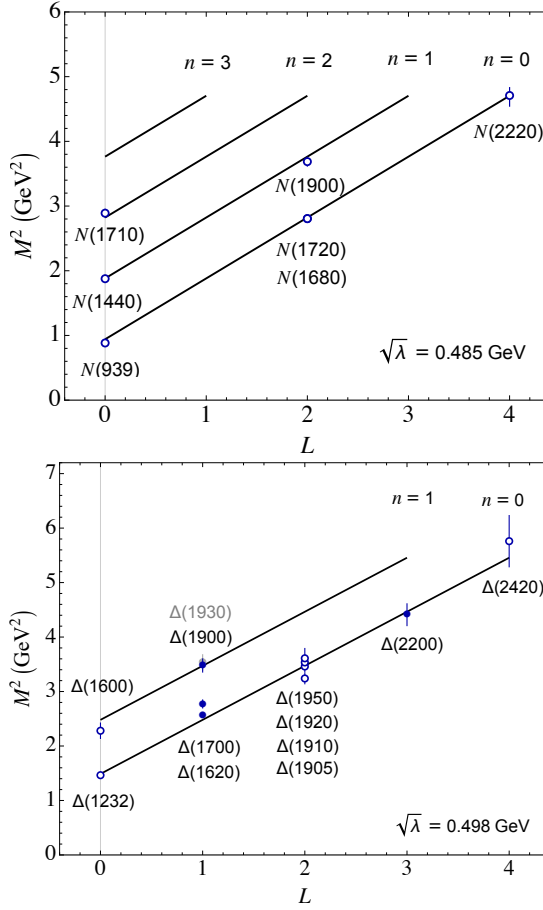
Fig. 15.1: fig:nucleon-delta Model predictions for the orbital and radial positive-parity nucleons (left) and positive and negative parity Δ families (right) compared with the data from Ref. [35]. The values of $\sqrt{\lambda}$ are $\sqrt{\lambda} = 0.485$ GeV for nucleons and $\sqrt{\lambda} = 0.498$ GeV for the deltas.

The specific connection follows from the substitution $x \mapsto \zeta$, $E \mapsto M^2$, $\lambda \mapsto \lambda_B = \lambda_M$, $f \mapsto L_M - = L_B +$, $\phi_+ \mapsto \phi_M$ and $\phi_2 \mapsto \phi_B$ in the superconformal equations phi1 and phi2. We find the LF meson (M) – baryon (B) bound-state equations

$$M\left(-\frac{d^2}{d\zeta^2} - \frac{1 - 4L_M^2}{4\zeta^2} + U_M\right)\phi_M = M^2\,\phi_M, \tag{15.23}$$

$$B\left(-\frac{d^2}{d\zeta^2} - \frac{1 - 4L_B^2}{4\zeta^2} + U_B\right)\phi_B = M^2\,\phi_B, \tag{15.24}$$

with the confinement potentials $U_M = \lambda_M^2\,\zeta^2 + 2\lambda_M(L_M - 1)$ and $U_B = \lambda_B^2\,\zeta^2 + 2\lambda_B(L_B + 1)$.

The superconformal structure imposes the condition $\lambda = \lambda_M = \lambda_B$ and the remarkable relation $L_M = L_B + 1$, where L_M is the LF angular momentum between the

quark and antiquark in the meson, and L_B between the active quark and spectator cluster in the baryon. Likewise, the equality of the Regge slopes embodies the equivalence of the $3_C - \bar{3}_C$ color interaction in the $q\bar{q}$ meson with the $3_C - \bar{3}_C$ interaction between the quark and diquark cluster in the baryon. The mass spectrum from M and B is

$$\text{MNspec} M_M^2 = 4\lambda(n + L_M) \quad \text{and} \quad M_B^2 = 4\lambda(n + L_B + 1). \tag{15.25}$$

The pion has a special role as the unique state of zero mass and, since $L_M = 0$, it has not a baryon partner.
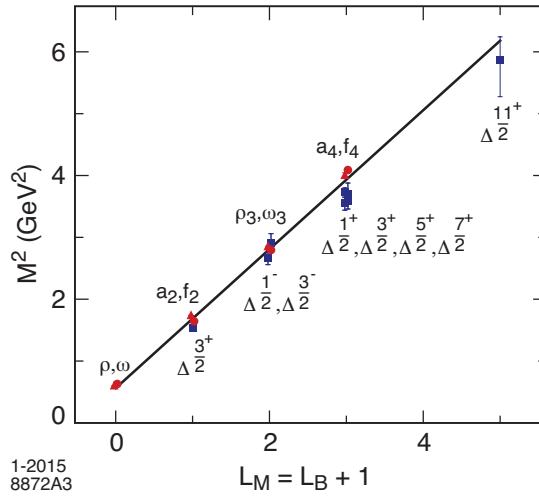
Fig. 15.2: fig:rho-delta Supersymmetric vector meson and Δ partners from Ref. [17]. The experimental values of M^2 from Ref. [35] are plotted vs $L_M = L_B + 1$ for $\sqrt{\lambda} \simeq 0.5$ GeV. The ρ and ω mesons have no baryonic partner, since it would imply a negative value of L_B.

15.5.3 Spin interaction and diquark clusters

Embedding the LF equations in AdS space allows us to extend the superconformal Hamiltonian to include the spin-spin interaction, a problem not defined in the chiral limit by standard procedures. The dilaton profile $\varphi(z)$ in the AdS action SAdS can be determined from the superconformal algebra by integrating Eq. Uvarphi for the effective potential U. One obtains the result $\varphi(z) = \lambda z^2$, which is uniquely determined, provided that it depends only on the modification of AdS space. Since the dilaton profile $\varphi(z) = \lambda z^2$ is valid for arbitrary J, it leads to the additional term 2λ in the LF Hamiltonian for mesons and baryons, which maintains the meson-baryon supersymmetry [36]. The spin $= 0, 1$, is the total internal spin of the meson, or the spin of the diquark cluster of the baryon partner. The effect of the spin term is an overall shift of the quadratic mass as depicted in

Fig. **??** for the spectra of the ρ mesons and Δ baryons [17]. For the Δ baryons the total internal spin S is related to the diquark cluster spin by $S = +\frac{1}{2}(-1)^L$, and therefore, positive and negative Δ baryons have the same diquark spin, $= 1$. As a result, all the Δ baryons lie, for a given n, on the same Regge trajectory, as shown in Fig. **??**.

15.5.4 Inclusion of quark masses

In the usual formulation of bottom-up holographic models one identifies quark mass and chiral condensates as coefficients of a scalar background field $X_0(z)$ in AdS space [37,38]. A heuristic way to take into account the occurrence of quark mass terms in the HLFQCD approach is to include the quark mass dependence in the invariant mass which controls the off-shell dependence of the LF wave function [9]. This substitution leads, upon exponentiation, to a natural factorization of the transverse and the longitudinal wave functions, but it is not a unique prescription [21]. This approach has been consistently applied to the radial and orbital excitation spectra of the light π, ρ, K, K^* and ϕ meson families, as well as to the $N, \Delta, \Lambda, \Sigma, \Sigma^*, \Xi$ and Ξ^* in the baryon sector, giving the value $\sqrt{\lambda} = 0.523 \pm 0.024$ GeV [36].

For heavy quarks the mass breaking effects are large. The underlying hadronic supersymmetry, however, is still compatible with the holographic approach and gives remarkable connections across the entire spectrum of light and heavy-light hadrons [39]. In particular, the lowest mass meson defining the $K, K^*, \eta', \phi, D, D^*, D_s, B, B^*, B_s$ and B_s^* families has no baryon partner, conforming to the SUSY mechanism found for the light hadrons, and depicted in Fig. **??**.

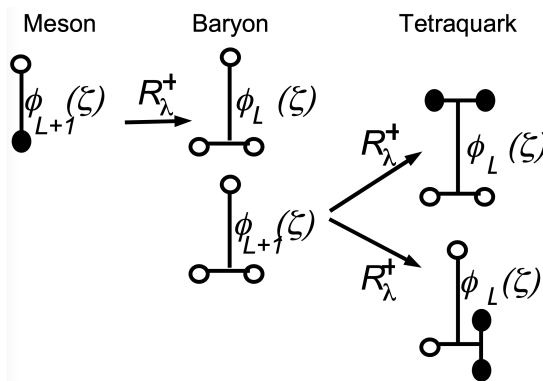### 15.5.5 Completing the supersymmetric hadron multiplet

Fig. 15.3: fig:MBTplet The meson-baryon-tetraquark supersymmetric 4-plet $\{\phi_M, \phi_B^+, \phi_B^-, \phi_T\}$ follows from the two step action of the supercharge operator $R_\lambda^\dagger$: $\bar{3} \to 3 \times 3$ on the pion, followed by $3 \to \bar{3} \times \bar{3}$ on the negative chirality component of the nucleon.

Besides the mesons and the baryons, the supersymmetric multiplet $\Phi = \{\phi_M, \phi_B^+, \phi_B^-, \phi_T\}$ contains a further bosonic partner, a tetraquark, which, as illustrated in Fig. **??**, follows from the action of the supercharge operator $R_\lambda^\dagger$ on the negative-chirality component of a baryon [36]. A clear example is the SUSY positive parity J^P-multiplet $2^+, \frac{3}{2}^+, 1^+$ of states $f_2(1270)$, $\Delta(1232)$, $a_1(1260)$ where the a_1 is interpreted as a tetraquark.

Table 15.1: pred Predicted masses for double heavy bosons from Ref. [43]. Exotics which are predicted to be stable under strong interactions are marked by $^{(!)}$.

quark content	J^P	predicted Mass [MeV]	strong decay	threshold [MeV]
$cq\overline{c}\overline{q}$	0^+	3660	$\eta_c\pi\pi$	3270
$cc\overline{q}\overline{q}^{(!)}$	1^+	3870	D^*D	3880
$bq\overline{b}\overline{q}$	0^+	10020	$\eta_b\pi\pi$	9680
$bb\overline{q}\overline{q}^{(!)}$	1^+	10230	B^*B	10800
$bc\overline{q}\overline{q}^{(!)}$	0^+	6810	BD	7150

Unfortunately, it is difficult to disentangle conventional hadronic quark states from exotic ones and, therefore, no clear-cut identification of tetraquarks for light hadrons, or hadrons with hidden charm or beauty, has been found [36,40,41]. The situation is, however, more favorable for tetraquarks with open charm and beauty which may be stable under strong interactions and therefore easily identified [42]. In Table **??**, the computed masses from Ref. [43] are presented. Our prediction [43] for a doubly charmed stable boson T_{cc} with a mass of 3870 MeV (second row) has been observed at LHCb a year later at 3875 MeV [44], and it is a member of the positive parity J^P-multiplet $2^+, \frac{3}{2}^+, 1^+$ of states $\chi_{c2}(3565)$, $\Xi_{cc}(3770)$, $T_{cc}(3875)$. The possible occurrence of stable doubly beautiful tetraquarks and those with charm and beauty is well founded [42].

15.6   Summary and outlook

Holographic light front QCD is a nonperturbative analytic approach to hadron physics with many applications to spectroscopy and dynamics. In the present overview we have mainly focused on the emerging properties of the holographic QCD approach to describe the hadron spectrum. It originates on a semiclassical approximation to the Hamiltonian equations in light front quantization which leads to relativistic wave equations, similar to the Schrödinger equation in atomic physics. Remarkably, the LF wave equations can be embedded in AdS space, giving a simple procedure to incorporate arbitrary integer or half-integer spin in the bound state equations. The model embodies an underlying superconformal algebraic structure responsible for the introduction of a mass scale within the superconformal group, and determines the effective confinement potential for mesons, nucleons and tetraquarks. It is an effective supersymmetry, not SUSY

QCD. There is a zero eigenmode in the spectrum which is identified with the pion: It is massless in the chiral limit.

There are other aspects and applications of HLFQCD which are not described here but are reviewed in [21]. For example, LF holographic QCD also incorporates important elements for the study of hadron form factors, such as the connection between the twist of the hadron to the fall-off of its current matrix elements for large Q^2, and important aspects of vector meson dominance which are relevant at lower energies. It also incorporates features of pre QCD, such as Veneziano model and Regge theory. Further extensions incorporate the exclusive-inclusive connection in QCD and provide nontrivial relations between hadron form factors and quark distributions. Holographic QCD has also been applied successfully to the description of the gravitational form factors, the hadronic matrix elements of the energy momentum tensor, which provide key information on the dynamics of quarks and gluons within hadrons. Holographic QCD also given new insights on the infrared behavior of the strong coupling in holographic QCD, which is described in [45].

References

1. K. G. Wilson, Confinement of quarks, https://doi.org/10.1103/PhysRevD.10.2445Phys. Rev. D **10**, 2445 (1974).
2. P. A. M. Dirac, Forms of relativistic dynamics, https://doi.org/10.1103/RevModPhys.21.392Rev. Mod. Phys. **21**, 392 (1949).
3. M. Kreshchuk, W. M. Kirby, G. Goldstein, H. Beauchemin and P. J. Love, Quantum simulation of quantum field theory in the light-front formulation, https://doi.org/10.1103/PhysRevA.105.032418Phys. Rev. A **105**, 032418 (2022) [https://arxiv.org/abs/2002.04016arXiv:2002.04016 [quant-ph]].
4. F. Gross and P. Maris, 50 Years of Quantum Chromodynamics, F. Gross and E. Klempt (editors), Sec. 5.3, Eur. Phys. J. C, to be published.
5. J. M. Maldacena, The large-N limit of superconformal field theories and supergravity, https://doi.org/10.1023/A:1026654312961 Adv. Theor. Math. Phys. **2**, 231 (1998) [https://arxiv.org/abs/hep-th/9711200 arXiv:hep-th/9711200].
6. O. Aharony, S. S. Gubser, J. M. Maldacena, H. Ooguri, and Y. Oz, Large N field theories, string theory and gravity, https://doi.org/10.1016/S0370-1573(99)00083-6Phys. Rept. **323**, 183 (2000) [https://arxiv.org/abs/hep-th/9905111 arXiv:hep-th/9905111].
7. G. F. de Téramond and S. J. Brodsky, Light-front holography: A first approximation to QCD, https://doi.org/10.1103/PhysRevLett.102.081601Phys. Rev. Lett. **102**, 081601 (2009) [https://arxiv.org/abs/0809.4899arXiv:0809.4899 [hep-ph]].
8. G. F. de Téramond, H. G. Dosch, and S. J. Brodsky, Kinematical and dynamical aspects of higher-spin bound-state equations in holographic QCD, https://doi.org/10.1103/PhysRevD.87.075005Phys. Rev. D **87**, 075005 (2013) [https://arxiv.org/abs/1301.1651 arXiv:1301.1651 [hep-ph]].

9. S. J. Brodsky, G. F. de Téramond, H. G. Dosch, and J. Erlich, Light-front holographic QCD and emerging confinement, https://doi.org/10.1016/j.physrep.2015.05.001Phys. Rept. **584**, 1 (2015) [https://arxiv.org/abs/1407.8131arXiv:1407.8131 [hep-ph]].

10. J. Polchinski and M. J. Strassler, Deep inelastic scattering and gauge/string duality, https://doi.org/10.1088/1126-6708/2003/05/012JHEP **05**, 012 (2003) [https://arxiv.org/abs/hep-th/0209211arXiv:hep-th/0209211].

11. S. J. Brodsky and G. F. de Téramond, Hadronic spectra and light-front wave functions in holographic QCD, https://doi.org/10.1103/PhysRevLett.96.201601Phys. Rev. Lett. **96**, 201601 (2006) [https://arxiv.org/abs/hep-ph/0602252 arXiv:hep-ph/0602252].

12. V. de Alfaro, S. Fubini, and G. Furlan, Conformal invariance in quantum mechanics, https://doi.org/10.1007/BF02785666Nuovo Cim. A **34**, 569 (1976).

13. S. Fubini and E. Rabinovici, Super conformal quantum mechanics, https://doi.org/10.1016/0550-3213(84)90422-XNucl. Phys. B **245**, 17 (1984).

14. V. P. Akulov and A. I. Pashnev, Quantum superconformal model in $(1, 2)$ space, https://doi.org/10.1007/BF01086252Theor. Math. Phys. **56**, 862 (1983).

15. S. J. Brodsky, G. F. de Téramond, and H. G. Dosch, Threefold complementary approach to holographic QCD, https://doi.org/10.1016/j.physletb.2013.12.044Phys. Lett. B **729**, 3 (2014) [https://arxiv.org/abs/1302.4105 arXiv:1302.4105 [hep-th]].

16. G. F. de Téramond, H. G. Dosch, and S. J. Brodsky, Baryon spectrum from superconformal quantum mechanics and its light-front holographic embedding, https://doi.org/10.1103/PhysRevD.91.045040 Phys. Rev. D **91**, 045040 (2015) [https://arxiv.org/abs/1411.5243 arXiv:1411.5243 [hep-ph]].

17. H. G. Dosch, G. F. de Téramond, and S. J. Brodsky, Superconformal baryon-meson symmetry and light-front holographic QCD, https://doi.org/10.1103/PhysRevD.91.085016Phys. Rev. D **91**, 085016 (2015) [https://arxiv.org/abs/1501.00959arXiv:1501.00959 [hep-th]].

18. G. F. de Téramond, T. Liu, R. S. Sufian, H. G. Dosch, S. J. Brodsky and A. Deur, Universality of generalized parton distributions in light-front holographic QCD, https://journals.aps.org/prl/abstract/10.1103/PhysRevLett.120.182001Phys. Rev. Lett. **120**, 182001 (2018) [https://arxiv.org/abs/1801.09154arXiv:1801.09154 [hep-ph]].

19. T. Liu, R. S. Sufian, G. F. de Téramond, H. G. Dosch, S. J. Brodsky and A. Deur, Unified description of polarized and unpolarized quark distributions in the proton, https://journals.aps.org/prl/abstract/10.1103/PhysRevLett.124.082003Phys. Rev. Lett. **124**, 082003 (2020) [https://arxiv.org/abs/1909.13818arXiv:1909.13818 [hep-ph]].

20. G. F. de Téramond *et al.* [HLFHS], Gluon matter distribution in the proton and pion from extended holographic light-front QCD, https://journals.aps.org/prd/abstract/10.1103/PhysRevD.104.114005Phys. Rev. D **104**, 114005 (2021) [https://arxiv.org/abs/2107.01231arXiv:2107.01231 [hep-ph]].

21. S. J. Brodsky, G. F. de Téramond, and H. G. Dosch, 50 Years of Quantum Chromodynamics, F. Gross and E. Klempt (editors), Sec. 5.5, Eur. Phys. J. C, to be published.

22. G. F. de Téramond, Emergent phenomena in nonperturbative QCD: The holographic light-front perspective, https://www.int.washington.edu/sites/default/files/schedule$_s$ession$_f$iles/deTeramond.pdf, $Origin of the Visible Universe: Unraveling the Proton Mass$, INT Seattle, 13−17 June 2022.

23. H. C. Pauli and S. J. Brodsky, Solving field theory in one space and one time dimension, https://journals.aps.org/prd/abstract/10.1103/PhysRevD.32.1993, Phys. Rev. D **32**, 1993 (1985);

24. K. Hornbostel, The application of light cone quantization to quantum chromodynamics in (1 + 1)-dimensions, Ph. D. thesis Stanford University, https://inspirehep.net/files/5382bfadf6016c08e11430938dd83262SLAC-PUB-0333 (1988).

25. D. J. Gross and F. Wilczek, Ultraviolet behavior of nonabelian gauge theories, http://prl.aps.org/abstract/PRL/v30/i26/p1343₁Phys. Rev. Lett. 30, 1343(1973).

26. H. D. Politzer, Reliable perturbative results for strong interactions?, http://prl.aps.org/abstract/PRL/v30/i26/p1346₁Phys. Rev. Lett. 30, 1346(1973).

27. G. 't Hooft, A two-dimensional model for mesons, https://www.sciencedirect.com/science/article/abs/pii/0550321374900881?via

28. K. Hornbostel, S. J. Brodsky and H. C. Pauli, Light cone quantized QCD in (1+1)-Dimensions, https://journals.aps.org/prd/abstract/10.1103/PhysRevD.41.3814Phys. Rev. D **41**, 3814 (1990).

29. T. Eller, Ph. D. thesis Heidelberg University, unpublished; T. Eller, H. C. Pauli and S. J. Brodsky, Discretized light cone quantization: The massless and the massive Schwinger model, https://journals.aps.org/prd/abstract/10.1103/PhysRevD.35.1493Phys. Rev. D **35**, 1493 (1987).

30. K. Demeterfi, I. R. Klebanov and G. Bhanot, Glueball spectrum in a (1+1)-dimensional model for QCD, https://www.sciencedirect.com/science/article/abs/pii/0550321394902364?via[https://arxiv.org/abs/hep-th/9311015arXiv:hep-th/9311015 [hep-th]].

31. E. Witten, Dynamical breaking of supersymmetry, https://doi.org/10.1016/0550-3213(81)90006-7Nucl. Phys. B **188**, 513 (1981).

32. H. Miyazawa, Baryon number changing currents, https://doi.org/10.1143/PTP.36.1266Prog. Theor. Phys. **36**, 1266 (1966).

33. S. Catto and F. Gursey, Algebraic Treatment of Effective Supersymmetry, https://doi.org/10.1007/BF02902548Nuovo Cim. A **86**, 201 (1985).

34. D. B. Lichtenberg, Whither hadron supersymmetry?, in *International Conference on Orbis Scientiae 1999: Quantum Gravity, Generalized Theory of Gravitation and Superstring Theory Based Unification*, 28th Conference on High-Energy Physics and Cosmology (1999) pp. 203–208, https://arxiv.org/abs/hep-ph/9912280arXiv:hep-ph/9912280.

35. R. L. Workman *et al.* [Particle Data Group], Review of particle physics, https://doi.org/10.1093/ptep/ptac097PTEP **2022**, 083C01 (2022).

36. S. J. Brodsky, G. F. de Téramond, H. G. Dosch, and C. Lorcé, Universal effective hadron dynamics from superconformal algebra, https://doi.org/10.1016/j.physletb.2016.05.068Phys. Lett. B **759** 171 (2016) [https://arxiv.org/abs/1604.06746arXiv:1604.06746 [hep-ph]].

37. J. Erlich, E. Katz, D. T. Son, and M. A. Stephanov, QCD and a holographic model of hadrons, https://doi.org/10.1103/PhysRevLett.95.261602Phys. Rev. Lett. **95**, 261602 (2005) [https://arxiv.org/abs/hep-ph/0501128arXiv:hep-ph/0501128].

38. L. Da Rold and A. Pomarol, Chiral symmetry breaking from five-dimensional spaces, https://doi.org/10.1016/j.nuclphysb.2005.05.009Nucl. Phys. B **72**, 79 (2005) [https://arxiv.org/abs/hep-ph/0501218arXiv:hep-ph/0501218].

39. H. G. Dosch, G. F. de Téramond, and S. J. Brodsky, Supersymmetry across the light and heavy-light hadronic spectrum, https://doi.org/10.1103/PhysRevD.92.074010Phys. Rev. D **92**, 074010 (2015) [https://arxiv.org/abs/1504.05112arXiv:1504.05112 [hep-ph]]; Supersymmetry across the light and heavy-light hadronic spectrum II, https://doi.org/10.1103/PhysRevD.95.034016Phys. Rev. D **95**, 034016 (2017) [https://arxiv.org/abs/1612.02370 arXiv:1612.02370 [hep-ph]].

40. M. Nielsen and S. J. Brodsky, Hadronic superpartners from a superconformal and supersymmetric algebra, https://doi.org/10.1103/PhysRevD.97.114001Phys. Rev. D **97**, 114001 (2018) [https://arxiv.org/abs/1802.09652arXiv:1802.09652 [hep-ph]].

41. M. Nielsen, S. J. Brodsky, G. F. de Téramond, H. G. Dosch, F. S. Navarra, and L. Zou, Supersymmetry in the double-heavy hadronic spectrum, https://doi.org/10.1103/PhysRevD.98.034002Phys. Rev. D **98**, 034002 (2018) [https://arxiv.org/abs/1805.11567arXiv:1805.11567 [hep-ph]].

42. M. Karliner and J. L. Rosner, Discovery of doubly-charmed Ξ_{cc} baryon implies a stable $bb\bar{u}\bar{d}$ tetraquark, https://doi.org/10.1103/PhysRevLett.119.202001Phys. Rev. Lett **119**, 202001 (2017) [https://arxiv.org/abs/1707.07666 arXiv:1707.07666 [hep-ph]].

43. H. G. Dosch, S. J. Brodsky, G. F. de Téramond, M. Nielsen, and L. Zou, Exotic states in a holographic theory, https://doi.org/10.1016/j.nuclphysbps.2021.05.035Nucl. Part. Phys. Proc. **312-317**, 135 (2021) [https://arxiv.org/abs/2012.02496arXiv:2012.02496 [hep-ph]].

44. R. Aaij *et al.* [LHCb], Observation of an exotic narrow doubly charmed tetraquark, https://doi.org/10.1038/s41567-022-01614-yNature Phys. **18**, 751-754 (2022) [https://arxiv.org/abs/2109.01038arXiv:2109.01038 [hep-ex]].

45. A. Deur 50 Years of Quantum Chromodynamics, F. Gross and E. Klempt (editors), Sec. 5.6, Eur. Phys. J. C, to be published.

16   Planetary relationship as the new signature from the dark Universe

Zioutas, K.[1]; Anastassopoulos, V.[1]; Argiriou, A.[1]; Cantatore, G.[2]; Cetin, S.[3]; Gardikiotis, A.[1,4]; Karuza, M.[5]; Kryemadhi, A.[6]; Maroudas, M.[1,4]; Mastronikolis, A.[7]; Ozbozduman, K.[8]; Semertzidis, Y.K.[9]; Tsagris, M.[1,10]; Tsagris, I.[1,10]

[1]University of Patras, physics department, PATRAS, Greece, [2]University and INFN Trieste, Trieste, Italy, [3]Istinye University, Istanbul, Turkiye, [4]University of Hamburg, Hamburg, Germany, [5]University of Rijeka, Rijeka, Croatia, [6]Messiah U., Mechanicsburg, PA, USA, [7]Department of Physics and Astronomy, University of Manchester, Manchester, UK, [8]Bogazici University Physics Department, Istanbul, Turkey, [9]IBS / KAIST, Daejeon, Korea, [10]Present address: Geneva / Switzerland

Abstract. Abstract. Dark Matter (DM) came from unexpected long-range gravitational observations. Even within the solar system, several unexpected phenomena have not conventional explanation. Streaming DM offers a viable common scenario. Gravitational focusing and self-focusing effects, by the Sun or its planets, of DM streams fits as being the underlying process behind otherwise puzzling observations like the 11-year solar cycle, the mysterious heating of the solar corona with its fast

temperature inversion, etc. However, unexpected solar activity or the dynamic Earth's atmosphere and other observations might arise from DM streams. This work is suggestive for an external impact by yet overlooked "streaming invisible matter", which reconciles investigated mysterious observations. Unexpected planetary relationships exist for the dynamic Sun and Earth's upper atmosphere; they are considered as multiple signatures for streaming DM. Then, focusing of DM streams could also occur in exoplanetary systems, suggesting for the first-time investigations by searching for the associated stellar activity as a function of the exoplanetary orbital phases. The entire observationally driven reasoning is suggestive for highly cross-disciplinary approaches including also (puzzling) biomedical phenomena like cancer. Favorite candidates from the dark sector are anti-quark nuggets, magnetic monopoles, but also particles like dark photons or the composite pearls. Thus, insisting anomalies /mysteries within the solar system are the as yet unnoticed manifestation of the dark Universe we are living in.

Povzetek: Na obstoj temne snovi (DM) so že pred skoraj stoletjem opozorila merjenja hitrosti kroženja zvezd okoli centra galaksije. Vendar je tudi v sončnem sistemu več pojavov, ki nimajo razlage in bi jih utegnila povzročiti temna snov.
Avtor predstavi svojo razlago za nekatere pojave, ki so morda povezane z močnim strujanjem temne snovi.

16.1   Introduction

The discovery of dunkle Materie (DM) by ZWICKY came from unexpected cosmological observations. Today we know that our Universe is dominated by a mysterious DM. Its name comes from the widely used definition, namely: DM does not emit or absorb or reflect electromagnetic radiation, making it difficult to detect. Following the observations behind this work, this definition of DM is eventually misleading, because, as we argue in this work, several counter examples might be caused by DM, while, at first sight, contradicting the widely used definition for DM. Our working hypotheses are: Planetary (and solar) gravitational effects on non-relativistic "invisible massive particles" are focused on solar and planetary atmospheres; they also might interact "strongly", while the screening at those places is negligible compared to deep underground locations. With "strongly" is meant that they have large cross section with normal matter and radiation.

With time, during planetary alignment with an invisible stream, that cannot be predicted as long as the streams and their velocity remain unknown, activity enhancement should repeat and might be the novel signature for the dark sector. Fortunately for this approach, the gravitational deflection depends on $1/speed^2$. This favours enormously non-relativistic speeds like the ones widely assumed for the constituents of the dark Universe. This makes any exo-solar planetary systems of potential interest. Because they also consist of a relatively large number of orbiting gravitational lenses for DM constituents (whatever they are made of). After all, what counts in gravitational lensing is mainly the velocity of DM partic. In fact, even the Moon can focus DM particles on Earth with velocities up to about 400 km/s covering thus a large fraction of DM phase space [1,2]. The aforementioned planetary gravitational lensing effects within the solar system becomes enormous if DM consists of streams, at least partly. Recent cosmology publications [3] consider fine grained streams of cosmological origin. Thus, to explain unusual or anomalous observations in our vicinity, we early concluded on the existence of streaming DM following the reasoning of this kind of work (see e.g. [4,5]). Interestingly, the suggested streaming DM scenario is supported also by cosmological considerations following a completely different reasoning [3,4], which was founded on another unbiased approach. A posteriori we find that both findings based on different input converge towards streaming DM.

Figure 1.

Schematic view of planetary gravitational focusing of streaming invisible massive particles (IMM) by the Sun. Free fall can be also strong for low-speed particles toward the Sun [6]. The flux can also be gravitationally modulated by an intervening planet, resulting in a

specific planetary dependence for a putative signature. The size of the planetary orbits is not to scale.

16.2   Signatures

The idea followed in this work goes similarly to the aforementioned reasoning by Zwicky that has led to the discovery of DM on cosmological scales. Namely, the last ˜160 years several unexpected energetic observations have been discovered within the solar system defying explanation (see e.g. [5] and references therein). This could be due to the dark Universe, whose manifestation was overlooked

for long time. Driven by observation, we converge on a class of "invisible" particle candidates from the dark sector, which exclude the parameter phase space of axions and WIMPs following failed direct DM searches since decades. In this work we pinpoint at a simple feature as the common signature from such observations within the solar system. For example, the widely discussed dark sector constituents have a velocity of about 0.001 c (c=velocity of light). As it has been pointed out [4,7,8], streams of "dark" constituents with such velocities can be efficiently gravitationally focused or deflected within a planetary system like ours, including the Sun and the Moon. The aforementioned energetic observations include the unpredictable flaring Sun, its irradiance and more generally its dynamical behaviour [5] as it is manifested by the widely accepted proxy of the solar radio line (F10.7) at 10.7 cm wavelength. The most energetic planetary relationship is Sun's slow size variation during one solar cycle [6]. Because, to lift an 1 km thick layer of the photosphere ($\rho \approx 0.1/cm^3$) by 1 km, the required energy of about 10^{30} ergs is enormous.

In addition, it is also remarkable the planetary dependence of Sun's elemental composition, which makes a widely discussed issue more of a riddle within known physics. Similarly, also the planetary relationship of the many elemental magnetic bright points on the solar surface show planetary relationships [5].

In addition to the unexpected solar observables add up a number of nearby terrestrial anomalous phenomena occurring in the atmosphere while being known since the 1930s. For example, what is beyond ionosphere's dynamical behaviour showing also planetary relationship [8], i.e., why is there annually about 25% more ionosphere around December than six months apart around June? This anomaly is known since 1937 [9]. Two extraordinary facts about the ionosphere are worth mentioning here:

A) the ionosphere is the most outer terrestrial region that is directly exposed to outer space. Then, any so far "invisible" constituents from the dark Universe may appear up there, provided they interact "strongly" (= large cross section) with normal matter. Interestingly, this is possible for DM following recent publications. Then, this requirement has not to be invented for the underlying scenario of this work (see e.g., ref. [10]). By contrast, the deep underground direct DM searches address extremely feebly interacting DM constituents due to the screening of "strongly" interacting dark constituents by the overhead Earth's layers.

B) We also point out here some cross-disciplinary observations of high societal relevance:

1) The not randomly appearing Earthquakes [11]. Probably this happens by some kind of accumulating energy deposition inside the Earth *triggering* finally an Earthquake. Apparently, it is not necessary for the invisible stream(s) or cluster to provide spatiotemporally the entire energy liberated during an Earthquake. It can be final the external trigger for an Earthquake to occur. Remarkably, during the largest Earthquakes, the ionosphere's plasma state changes over long distances as it has been observed by the orbiting GPS system that continuously registers the ionospheric plasma for self-calibration purposes.

2) The observed planetary relationships of melanoma appearance [12-14] following the orbital period of planet Mercury. It has also been observed a periodic modulation of the

daily rate of diagnosed melanoma cases, coinciding with the lunar sidereal periodicity of 27.32 days [14]; this, on its own, points at exo-solar origin, which fits-in the suggested streaming DM scenario.

The observations given above have one common feature. Namely, they all show an otherwise unexpected planetary relationship. Most probably more and more results will emerge following this kind of out-of-the-box thinking, and this might allow to corner the microscopic nature of the suspected streams, being not as "invisible" as widely thought to be.

We also wish to stress here that following the reasoning underlying this work, it is interesting to find out as to whether similar behaviour is encountered in exo-solar planetary systems [15]. With near Earth galactic exo-planetary systems one might be able to establish similar correlations for an exo-planetary system but also a cross-correlation with our solar system. Such observations have the potential to expand our DM horizon within our Galaxy as well as into the dark Universe, establishing the working hypotheses behind such scenarios.

16.3   Summary - conclusion

Observationally driven, we conclude in this work that *a planetary relationship is a key signature pointing on its own at exo-solar origin*. So far, the only viable explanation we can imagine for a plethora of diverse observations showing planetary dependency, is due to gravitational focusing of streaming "invisible" matter. We tentatively identify it with constituents from the dark Universe, interacting eventually also with a large cross section with ordinary matter or radiation. At the moment, we only can speculate about the possible particle candidates (see below), which are suggestive for new searches.

Implications in ongoing or future DM experiments are obvious. Therefore, we urge all experiments and in particular those searching for direct DM signatures, to perform a statistical re-analysis following the reasoning underlying this work (see ref. [5]]). If a planetary dependency is found also in direct DM searches, this will strengthen the concept of "invisible streams" in our vicinity, which can appear either due to tidal forces in our galaxy or others nearby, or, more probably they can be cosmological in origin [2].

We are aiming to widen the appearance of this type of new signatures being probably still hidden also in other observations. One day we might decipher the properties of the invisible stream(s). Along this line of reasoning emerged the medical observations made with long series data of melanoma diagnoses [12-14]. Surprisingly, the main two planetary signatures appeared so far in medicine are:

1) The 88 days orbital periodicity of Mercury using monthly data from the northern hemisphere (USA) [12], which have been independently confirmed [13]. Inconceivably, the author has overlooked his positive result with most cancer types, and

2) The sidereal geocentric lunar periodicity (=27.32 days) using daily melanoma diagnoses data from the southern hemisphere (Australia) [15]. Interestingly, following the planetary scenario and the possible signatures observed [4,5,8,16] the underlying stream(s) can only be exo-solar in origin. Notice by definition, a sidereal periodicity refers to a reference frame fixed to remote stars. Of course, a DM stream is of cosmic origin, even if it happens to be trapped by the solar system during its birth. Also this last scenario is of not minor importance for direct DM searches, or for indirect ones in astrophysical / cosmic observations.

In short, a wide diversity of signatures implying planetary relationships may allow to spot the "invisible" components from the dark Universe we are living in.

Finally, the question arises what can be the first "invisible candidates" favoured by such investigations. The possible candidates are;

a) Anti Quark Nuggets (AQNs) as they have been invented by Ariel ZHITNITSKY (2003) [17-19]. These objects are inspiring many investigations from the origin of the solar corona heating mystery to the direct detection of axions [16].
b) Magnetic monopoles as their interaction with the ubiquitous magnetic fields makes different energy deposition scenarios of potential interest.
c) Dark photons, which can even resonantly convert to real photons if the local plasma density fits-in the rest mass of the hidden photon. Contrary to axions or axion-like particles, the kinetic mixing between real photons with hidden sector photons does not require a magnetic field as catalyst, and this makes them attractive.
d) PEARLs [see Holger Nielsen, this conference]. We suggest that a quantitative investigation as to whether these composite particles fit-in at least some of the observations made so far, as it has been undertaken already with the AQNs, starting for example with the mysterious solar corona heating and the unpredictable solar Flares, seems as an appropriate first step.
e) Some other constituents to be invented yet, remains always an option.

Thus, the mostly inspiring particle constituents fitting-in several observations are *Anti-QuarkNuggets, magnetic monopoles* and *dark photons*. Though, more emerging candidates like the *pearls* (see talk in this conference by Holger Nielsen) are encouraged to investigate whether they fit-in, and, how to identify their possible involvement.

Thus, insisting anomalies / mysteries within the solar system are the unnoticed manifestation of the dark Universe we are living in.

16.4 References:

[1] Sofue, Y. Gravitational Focusing of Low-Velocity Dark Matter on the Earth's Surface. Galaxies, **2020**, 8, 42; https://doi.org/10.3390/galaxies8020042 .
[2] Kryemadhi, A.; Maroudas, M.; Mastronikolis, A.; Zioutas, K. Gravitational focusing effects on streaming dark matter as a new detection concept. Preprint https://doi.org/10.48550/arXiv.2210.07367 (**2022**).
[3] Vogelsberger, M.; White, S.D.M. Streams and caustics: The fine-grained structure of Λ cold dark matter haloes. Mon. Not. R. Astron. Soc. **2011**, 413, 1419. https://academic.oup.com/mnras/article/413/2/1419/1070092 .
[4]   Zioutas, K.; Tsagri, M.; Semertzidis, Y.K.; Papaevangelou,T.; Hoffmann, D.H.H.; Anastassopoulos, V. The 11 years solar cycle as the manifestation of the dark Universe. Mod. Phys. Lett. A **2014**, 29, 1440008; https://doi.org/10.1142/s0217732314400082.
[5] Zioutas, K.; Anastassopoulos, V.; Argiriou, A.; Cantatore, G.; Cetin, S.A.; Gardikiotis, A.; Hoffmann, D.H.H.; Hofmann, S.; Karuza, M.; Kryemadhi, A.; et al. The Dark Universe Is Not Invisible. Phys. Sci. Forum **2021**, 2, 10. https://doi.org/10.3390/ECU2021-09313 .

[6] Zioutas, K.; Maroudas, M.; Kosovichev, A. On the origin of the rhythmic Sun's radius variation. Symmetry **2022**, 14, 325; https://doi.org/10.3390/sym14020325 .

[7] Hoffmann, D.H.H.; Jacoby, J.; Zioutas, K. Gravitational lensing by the Sun of non-relativistic penetrating particles. Astropart. Phys. **2003**, 20, 73. https://doi.org/10.1016/S0927-6505(03)00138-5 .

[8] Bertolucci, S.; Zioutas, K.; Hofmann, S.; Maroudas, M. The sun and its planets as detectors for invisible matter. Phys. Dark Univ. **2017**, 17, 13; https://doi.org/10.1016/j.dark.2017.06.001 .

[9] E.V. Appleton, Regularities and irregularities in the ionosphere, Proc. Roy. Soc. London A162 (1937) 451; http://rspa.royalsocietypublishing.org/content/162/911/451

[10] Emken, T.; Essig, R.; Kouvaris, C.; Sholapurkar, M. Direct Detection of Strongly Interacting SubGeV Dark Matter via Electron Recoils. J. Cosmol. Astropart. Phys. **2019**, 9, 70; https://doi.org/10.1088/1475-7516/2019/09/070 .

[11] Maroudas, M. PhD thesis, University of Patras **2022**.

[12] Zioutas, K.; Valachovic, E. Planetary dependence of melanoma. Biophys. Rev. Lett. **2020**, 13, 75; https://doi.org/10.1142/S179304801850008X .

[13] Zioutas, K.; Valachovic, E.; Maroudas, M. Response to Comment on "Planetary Dependence of Melanoma". Biophys. Rev. Lett. **2019**, 14, 11; https://doi.org/10.1142/S1793048019200029 .

[14] Zioutas, K.; Maroudas, M.; Hofmann, S.; Kryemadhi, A.; Matteson, E.L. Observation of a 27 Days Periodicity in Melanoma Diagnosis. Biophys. Rev. Lett. **2020**, 15, 275; https://doi.org/10.1142/S1793048020500083 .

[15] Perryman, M.; Zioutas, K. Gaia, Fundamental Physics, and Dark Matter,https://arxiv.org/abs/2106.15408 . (**2021**).

[16] Zioutas, K.; Argiriou, A.; Fischer, H.; Hofmann, S.; Maroudas, M.; Pappa, A.; Semertzidis, Y.K. Stratospheric temperature anomalies as imprints from the dark universe. Phys. Dark Univ. 2020, 28, 100497; https://doi.org/10.1016/j.dark.2020.100497 .

[17] Zhitnitsky, A. "Nonbaryonic" Dark Matter as Baryonic Color Superconductor. JCAP **2003**, 310, 10; https://iopscience.iop.org/article/10.1088/1475-7516/2003/10/010 .

[18] Zhitnitsky, A. Solar Flares and the Axion Quark Nugget Dark Matter Model. Phys. Dark Univ. **2018**, 22, 1; https://doi.org/10.1016/j.dark.2018.08.001 .

[19] N. Raza, L. van Waerbeke, A. Zhitnitsky, Solar Corona Heating by the AQN dark matter, Phys. Rev. D, **2018**, 98, 103527; arXiv:1805.01897 .

17 Abstracts of talks presented at the Workshop and in the Cosmovia forum

http://bsm.fmf.uni-lj.si/bled2022bsm/presentations.html
https://bit.ly/bled2022bsm

Not all the talks come as articles in this year's Proceedings, but all the talks can be found on the official website of the Workshop and on the Cosmovia forum:
https://bit.ly/bled2022bsm.
Here are the abstracts of the contributors who did not submit an article.

17.1 T.E. Bikbaev, M.Yu. Khlopov, A.G.Mayorov

National research Nuclear University MEPHI, Moscow, and
Research Institute of Physics, Southern Federal University, Rostov on Don, Russia

Modelling of dark atom interaction with nuclei.

Dark atom interaction with nuclei is the crucial long-standing problem of the composite dark matter solution for the puzzles of direct dark matter searches. This solution assumes existence of stable -2n charged particles bound by Coulomb interaction with n nuclei of primordial helium forming nuclear interacting Bohr-like OHe (n=1) or Thomson-like XHe (n¿1) dark atoms. The puzzles of direct DM searches are then explained by the annual modulation of low-energy binding of dark atom with nuclei in the DAMA/NaI and DAMA/LIBRA detectors, which cannot be detected in direct WIMP searches for recoil nuclei or electrons from WIMP interaction with the matter in other detectors. The continuous approach to the realistic description dark atom interaction with nuclei by the quantum mechanical accomplishment of the numercial study of classical three body problem both for OHe and XHe is now accompanied by the development of methods to solve the Schroedinger equation for the considered problem. The progress in our studies is reported.

Povzetek Avtor predpostavi, da je temna snov iz stabilnih negativno nabitih (-2n) delcev, ki jih poveže elektromagnetna sila sila z n jedri "OHe" ali "XHe" v atome temne snovi. S tem modelom za temno snov išče pojasnilo, zakaj direktnih meritev temne snovi z detektorjem DAMA/NaI in DAMA/LIBRA niso ponovili drugi detektorji, ki tudi merijo sipanje temne snovi na merilnih aparaturah kot funkcijo gibanja Zemlje okoli Sonca. Avtor poroča o napredku pri iskanju stabilnih rešitev njihovega modela temne snovi.

17.2   A. Chaudhuri[1] and J. Das[2]

[1]Discipline of Physics, Indian Institute of Technology, Gandhinagar, Gandhinagar, India.
[2]Department of Physics, University of Delhi, New Delhi, India.

Electroweak phase transition and entropy release in Z2 symmetric extension of the Standard Model

In this work we consider the simple Z2 symmetric extension to the Standard Model (SM) and proceed to study the nature of electroweak phase transition (EWPT) in the early universe. We show that the nature of the phase transition changes from a smooth crossover in the SM to a strong first order with this addition of the real scalar. Furthermore, we show the entropy release in this scenario is higher than that of the SM. This can lead to a strong dilution of frozen out dark matter particles and baryon asymmetry, if something existed before the onset of the phase transition.

Povzetek Avtor razširi standarni model tako, da predpostavi simetrijo Z2 ter uporabi ta model za študij elektrošibkega faznega prehoda v zgodjem vesolju. Pokaže, da se narava faznega prehoda razlikuje od elektrošibkega faznega prehoda v standardnem modelu. Sprosti se več entropije, kar lahko pripelje do manjše gostote nastale temne snovi in do zmanjšane barionske asimetrije, če je ta bila že pred faznim prehodom.

17.3   S. R. Chowdhury, M.Yu. Khlopov

Research Institute of Physics, Southern Federal University, Rostov on Don, Russia

The impact of mass transfer in the formation of compact binary merging.

The binary black hole coalescences GW150914 and GW151226 observed by the LIGO started the gravitational wave (GW) astronomy era. It enabled us to investigate gravity in the strong-
eld regime. In order to resemble the observations, accurate theoretical models are required to compare the results. There are still signi
cant uncertainties about the stability of mass transfer and common envelope evolution in formation models involving isolated binary stars. Large binary population simulations have been used to anticipate the sources for GW. Populations can be produced on timescales of days using a binary population synthesis tool that balances physical modelling and

264

simulation speed. With the help of COSMIC, we simulate the galactic population of compact binaries and their GW signals. Based on the metallicity, the
nal fate of the population has been estimated.

17.4 A. Ghoshal

Sky Meets Laboratory via RGE: Axions, Peccei-Quinn Phase Transitions and Gravitational Waves

As a solution to the SM hierarchy problem, we will discuss model-building with classical scale invariance in 4-dimensional QFT satisfying Total Asymptotic Freedom (TAF): the theory holds up to infifinite energy, where all coupling constants go to zero and is devoid of any Landau poles. Such principles if beyond the reach of LHC (TeV scale) can be tested via Gravitational Waves (GW) in LIGO, etc. As an example, we will discuss a QCD axion in the TAF scenario, with strong fifirst order Peccei-Quinn phase transitions and produces GW. Thus we will conclude by promoting RGE as a novel connection to complement laboratory searches of BSM with cosmological observables as probes of BSM models.

Povzetek Avtor predlaga za rešitev problema hierarhije standardnega modela model z invariantno skalo v štiri-razsežni kvantni teoriji polja s popolno asimptotsko svobodo (TAF), ko so pri neskoncni energiji vse sklopitvene konstante enake nič in ni Landavove singularnosti. Takšni privzetki niso merljivi na LHC (z dosegom TeV), so pa opazljivi pri gravitacijskih valovih v experimentih LIGO in drugih. V tem modelu obravnava avtor axione v kvantni kromodinamiki, ko pride do močnih faznih prehodov prvega reda Peccei-Quinnove vrste, ki povzročijo gravitacijske valove.

17.5 M. Ildes

I Analytic Solutions of Scalar Field Cosmology, Mathematical Structures for Early Inflation and Late Time Accelerated Expansion

We study the most general cosmological model with real scalar field which is minimally coupled to gravity. Our calculations are based on Friedmann-Lemaitre-Robertson-Walker (FLRW) background metric. Field equations consist of three differential equations.

17.6   M. Ildes

II Analytic Solutions of Brans-Dicke Cosmology: Early In ation and Late Time Accelerated Expansion

We investigate the most general exact solutions of Brans- Dicke cosmology by choosing the scale factor "a" as the new independent variable. It is shown that a set of three eld equations can be reduce
d to a constraint equation and a rst order linear dierential equation. Comparison of our results with recent observations of type Ia supernovae indicates that eighty-nine percent of present universe may consist of domain walls while rest is matter.

17.7   S. Kabana

Thermal production of Sexaquarks in Heavy Ion Collisions

Sexaquarks are a hypothetical low mass, small radius uuddss dibaryon which has been proposed recently and especially as a candidate for Dark Matter. The low mass region below 2 GeV escapes upper limits set from experiments which have searched for the unstable, higher mass H-dibaryon and did not fifind it. Depending on its mass, such state may be absolutely stable or almost stable with decay rate of the order of the lifetime of the Universe therefore making it a possible Dark Matter candidate . Even though not everyone agrees its possible cosmological implications as DM candidate cannot be excluded and it has been recently searched in the BaBar experiment. The assumption of a light Sexaquark has been shown to be consistent with observations of neutron stars and the Bose Einstein Condensate of light Sexaquarks has been discussed as a mechanism that could induce quark deconfifinement in the core of neutron stars. S production in heavy ion collisions is expected to be much more favorable than in the only experimental search to date, $Y \rightarrow S\Lambda \rightarrow \lambda$, which is severely suppressed by requiring a low multiplicity exclusive fifinal state. By contrast, parton coalescence and/or thermal production give much larger rates in heavy ion collisions. We use a model which has very successfully described hadron and nuclei production in nucleus-nucleus collisions at the LHC, in order to estimate the thermal production rate of Sexaquarks with characteristics such as discussed previously rendering them DM candidates.
We show new results on the variation of the Sexaquark production rates with mass, radius and temperature and chemical potentials assumed and their ratio to hadrons and nuclei and discuss the consequences.

Povzetek Sexaquarki so hipotetičnini dibarioni uuddss z majhno maso in majhnim radijem. Bili naj bi stabilni ali skoraj stabilni, z življenjsko dobo vesolja in zato kandidati za temno snov. Predpostavka o Sexaquarku z majhno maso se je izkazala za skladno z opazovanji nevtronskih zvezd, kjer naj bi Sexaquarki prožili razgradnjo kvarkov v jedru nevtronskih zvezd. Verjetnost za nastanek Sexaquarkov pri trkih težkih ionov naj bi bila veliko večja kot pri poskusu $Y \rightarrow S\Lambda \rightarrow \lambda$, kjer so ga iskali doslej. Avtorji predlaganega poskusa uporabijo za študij poteka poskusa model, ki je zelo uspešno opisal nastajanje hadronov in jeder v trkih jedro-jedro na pospeševalniku LHC. Z njim ocenjujejo ali imajo Sexaquarki, ki nastajajo pri toplotni produkciji, značilnosti, ki jih morajo imeti kandidati za temno snov.

Predstavljajo nove rezultate o odvisnosti hitrosti nastajanja Sexaquarkov od njihove mase, radija in privzetega kemijskega potenciala v razmerju do hitrosti nastajanja hadronov in jeder.

17.8   A.O.Kirichenko, M.Yu. Khlopov, A.G.Mayorov

National research Nuclear University MEPHI, Moscow, and
Research Institute of Physics, Southern Federal University, Rostov on Don, Russia

Propagation of antinuclei in galactic magnetic field

We model the propagation of antihelium particles in the magnetic fields of the Galaxy from a supposed source of antimatter in the Galactic halo in the form of a globular antistellar cluster. The well-known JF12 model (R. Jansson, G. R. Farrar, 2012) with the addition of an irregular component (A. Beck, A. Strong, 2016) was taken as a magnetic field model. The cutoff energy for the penetration of particles into the disk in the total magnetic field of the Galaxy (of the order of 1000 GeV) is estimated. Particles of low energies (less than 100 GeV) are largely suppressed when they try to penetrate the disk region. The observed suppression is similar to the effect of solar modulation, which occurs when cosmic rays penetrate into the heliosphere. Taking into account expected decreasing power law suppression at the high energies in the source convergence of this cut off with the power law energy dependence favors the energy range which is optimal for search for antihelium component of cosmic rays at the AMS02 experiment

17.9   M. Khlopov

National research Nuclear University MEPHI, Moscow, Russia
Research Institute of Physics, Southern Federal University, Rostov on Don, Russia
Virtual Institute of Astroparticle physics, Paris, France

Cosmological reflection of the BSM physics

The modern cosmology is based on the BSM physics, involved in the mechanisms of inflation, baryosynthesis and the physical nature of dark matter. To specify the parameters of BSM models methods of multimessenger cosmology are developed with special emphasis on the important role of exotic deviations from the now Standard cosmological paradigm, like macroscopic antimatter in baryon asymmetrical Universe, primordial black holes, structures and inhomegeneities in the dark matter distribution as well as Warmer than Cold dark atom scenario of composite dark matter. Positive evidence for such deviations would strongly restrict possible classes of BSM models and provide determination of BSM parameters with "astronomical accuracy".

Povzetek Sodobna kozmologija temelji na fiziki, ki presega oba standardna modela. Zahteva razumevanje pojava eksponentnega širjenja vesolja (inflacije), bariosinteze in razumevanja,

iz česa je temna snov. Da bi lahko določili parametre za za novo teorijo, ki bi presegla oba standardna modela, predlaga avtor modele s posebnim poudarkom na eksotičnih odstopanjih od standardnega kozmološkega modela, kot so makroskopska antimaterija v barionskem asimetričnem vesolju, nastanek črnih lukenj v zgodnjem vesolju, strukture in nehomogenosti v porazdelitvi temne snovi, topli temni atomi, ki da sestavljajo temno snov. Meritve, ki bi potrdile te modele, bi močno omejila izbiro predlogov, ki bi pomenili razširitev obeh standardnih modelov.

17.10   M. Y. Khlopov, O.M. Lecian

Primordial Antimatter and Dark Matter celestial objects

The structure and evolution of Primordial Antimatter domains and Dark matter objects are analysed. Relativistic low- density antimatter domains are described. The Relativistic FRW perfect-fluid solution is found for the characterization of i) ultra- high density antimatter domains, ii) high-density antimatter domains, and iii) dense anti- matter domains. The possible sub-domains structures is analyzed. The structures evolved to the time of galaxy formation are outlined. Comparison is given with other primordial celestial objects. The features of antistars are outlined. In the case of WIMP dark matter clumps, the mechanisms of their survival to the present time are discussed. The cosmological features of neutrino clumping due to fifth force are examined.

Povzetek Članek obravnava strukturo in dinamiko domen anti-snovi majhne gostote in temne snovi v zgodnjem vesolju. Avtorja opišeta domene antisnovi z relativistično idealno tekočino in poiščeta rešitve za majhne, srednje velike in velike gostote tekočine. Dinamiko domen antisnovi spremljata do nastanka galaksij in obravnavata njihovopreživetje do danes. Študirata tudi kozmološke posledice združevanja nevtrinov zaradi pete sile.

17.11   A. Kleppe

Mass matrices in a scenario with only one R-handed state

According to the Standard Model, before the spontaneous symmetry breaking of the electroweak interactions, the fermions were massless Weyl particles, such that states with R-handed helicity were completely separated from particles with L-handed helicity.
After the symmetry breaking, fermions appear as $\psi = \psi_L + \psi_R$, where the L-handed sector is singled out: only L-handed particles appear in the weak interactions.

In our scenario, we take $\psi = \psi_L + \psi_R$ very seriously, perceiving ψ as the sum of two different states ψ_L and ψ_R, which remain just as separate as they were before the SSB. In addition, the singlet state ψ_R is perceived as being the same for all quarks, which means that while the left-handed states take part in charge changing processes, the right-handed states just "stay put".

This assumption has many consequences, and gives rise to mass matrices of a certain, very specific texture.

17.12   A.V. Kravtsova[1], M.Yu. Khlopov[1,2], A.G. Mayorov[1,2]

[1] National research Nuclear University MEPHI, Moscow
[2] Research Institute of Physics, Southern Federal University, Rostov on Don, Russia

Interaction of antinuclei with galactic interstellar gas

Models of strongly inhomogeneous baryosynthesis in the baryon-asymmetric Universe admit the existence of macroscopic domains of antimatter, which could evolve as a globular cluster of antistars in the halo of our Galaxy. Assuming the symmetry of evolution of the globular cluster of stars and antistars on the basis of symmetry of matter and antimatter properties, such an object could be the source of anthelium nuclei in galactic cosmic rays. This allows us to the prediction of the expected fraction from the luxes of cosmic antinuclei propagation in the magnetic field of the Galaxy, taking into account the inelastic interaction with interstellar matter, in which destruction of antiHe-4 can result in creation of anti-He3. Assuming that interstellar gas predominantly contains different components of hydrogen we formulate the problem of cosmic ray enrichment by anti-He3, which will be important for interpretation of the coming AMS02 data.

Discussion section

The discussion contributions are not arranged alphabetically

18   Discussion of cosmological acceleration and dark energy

Felix M Lev

Artwork Conversion Software Inc.
509 N. Sepulveda Blvd Manhattan Beach CA 90266 USA
Email: felixlev314@gmail.com

Abstract. The title of this workshop is: "What comes beyond standard models?". Standard models are based on Poincare invariant quantum theory. However, as shown in the famous Dyson's paper "Missed Opportunities" and in my publications, such a theory is a special degenerate case of de Sitter invariant quantum theory. I argue that the phenomenon of cosmological acceleration has a natural explanation as a consequence of quantum de Sitter symmetry in semiclassical approximation. The explanation is based only on universally recognized results of physics and does not involve models and/or assumptions the validity of which has not been unambiguously proved yet (e.g., dark energy and quintessence). I also explain that the cosmological constant problem and the problem why the cosmological constant is as is do not arise.

Povzetek: Avtor razloži kozmolški pospešek s pomočjo kvantne de Sitterjeve simetrije v polklasičnem približku. Temne energije in drugih eksotičnih konceptov njegova razlaga ne vključuje.

Keywords: quantum de Sitter symmetry; cosmological acceleration; irreducible representations; dark energy

18.1   Introduction

The title of this workshop is: "What comes beyond standard models?". Standard models are based on Poincare invariant quantum theory. However, as shown in the famous Dyson's paper "Missed Opportunities" and in my publications, such a theory is a special degenerate case of de Sitter invariant quantum theory.
The problem of cosmological acceleration is an example where the approach based on de Sitter symmetry solves the problem proceeding only from universally recognized results of physics without involving models and/or assumptions the validity of which has not been unambiguously proved yet (e.g., dark energy and quintessence). This problem was

considered in my papers published in known journals, and in the book recently published by Springer.

My publications are based on large calculations. To understand them, the readers must be experts not only in quantum theory, but also in the theory of representations of Lie algebras in Hilbert spaces. Therefore, understanding my results can be a challenge for many physicists. Since the problem of cosmological acceleration is very important and my approach considerably differs from approaches of other authors, in this presentation to the 25th Bled workshop I outline only the ideas of my approach without calculations.

18.2   History of dark energy

This history is well-known. First Einstein introduced the cosmological constant Λ because he believed that the universe was stationary and his equations can ensure this only if $\Lambda \neq 0$. But when Friedman found his solutions of equations of General Relativity (GR) with $\Lambda = 0$, and Hubble found that the universe was expanding, Einstein said (according to Gamow's memories) that introducing $\Lambda \neq 0$ was the biggest blunder of his life. After that, the statement that Λ must be zero was advocated even in textbooks.

The explanation was that, according to the philosophy of GR, matter creates a curvature of space-time, so when matter is absent, there should be no curvature, i.e., space-time should be the flat Minkowski space. That is why when in 1998 it was realized that the data on supernovae could be described only with $\Lambda \neq 0$, the impression was that it was a shock of something fundamental. However, the term with Λ in the Einstein equations has been moved from the left hand side to the right hand one, it was declared that in fact $\Lambda = 0$, but the impression that $\Lambda \neq 0$ was the manifestation of a hypothetical field which, depending on the model, was called dark energy or quintessence. In spite of the fact that, as noted in wide publications (see e.g., [1] and references therein), their physical nature remains a mystery, the most publications on the problem of cosmological acceleration involve those concepts.

Several authors criticized this approach from the following considerations. GR without the contribution of Λ has been confirmed with a good accuracy in experiments in the Solar System. If Λ is as small as it has been observed, then it can have a significant effect only at cosmological distances while for experiments in the Solar System the role of such a small value is negligible. The authors of [2] titled "Why All These Prejudices Against a Constant?" note that it is not clear why we should think that only a special case $\Lambda = 0$ is allowed. If we accept the theory containing the gravitational constant G, which cannot be calculated and is taken from outside, then why can't we accept a theory containing two independent constants?

Let us note that currently there is no physical theory which works under all conditions. For example, it is not correct to extrapolate nonrelativistic theory to the cases when speeds are comparable to c, and it is not correct to extrapolate classical physics for describing energy levels of the hydrogen atom. GR is a successful classical (i.e., non-quantum) theory for describing macroscopic phenomena where large masses are present, but extrapolation of GR to the case when matter disappears is not physical. One of the principles of physics is that a definition of a physical quantity is a description how this quantity should be measured. The concepts of space and its curvature are pure mathematical. Their aim is to describe the motion of real bodies. But the concepts of empty space and its curvature should not be used in physics because nothing can be measured in a space which exists only in our imagination. Indeed, in the limit of GR when matter disappears, space remains and has a curvature (zero curvature when $\Lambda = 0$, positive curvature when $\Lambda > 0$ and negative

curvature when $\Lambda < 0$) while, since space is only a mathematical concept for describing matter, a reasonable approach should be such that in this limit space should disappear too. A common principle of physics is that when a new phenomenon is discovered, physicists should try to first explain it proceeding from the existing science. Only if all such efforts fail, something exotic can be involved. But in the case of cosmological acceleration, an opposite approach was adopted: exotic explanations with dark energy or quintessence were accepted without serious efforts to explain the data in the framework of existing science.

18.3   Elementary particles in relativistic and de Sitter-invariant theories

In the problem of cosmological acceleration, only large macroscopic bodies are involved and that is why one might think that for considering this problem, there is no need to involve quantum theory. Most works on this problem proceed from GR with additional assumptions the validity of which has not been unambiguously proved yet (see e.g. [1] and references therein).

However, ideally, the results for every classical (i.e., non-quantum) problem should be obtained from quantum theory in semiclassical approximation. We will see that considering the problem of cosmological acceleration from the point of view of quantum theory, sheds a new light on understanding this problem.

Standard particle theory and standard models are based on Poincare symmetry where elementary particles are described by irreducible representations (IRs) of the Poincare group or its Lie algebra. The representation generators of the Poincare algebra commute according to the commutation relations

$$[P^\mu, P^\nu] = 0, \quad [P^\mu, M^{\nu\rho}] = -i(\eta^{\mu\rho}P^\nu - \eta^{\mu\nu}P^\rho),$$
$$[M^{\mu\nu}, M^{\rho\sigma}] = -i(\eta^{\mu\rho}M^{\nu\sigma} + \eta^{\nu\sigma}M^{\mu\rho} - \eta^{\mu\sigma}M^{\nu\rho} - \eta^{\nu\rho}M^{\mu\sigma}) \tag{18.1}$$

where $\mu, \nu = 0, 1, 2, 3$, P^μ are the operators of the four-momentum, $M^{\mu\nu}$ are the operators of Lorentz angular momenta and $\eta^{\mu\nu}$ is such that $\eta^{00} = -\eta^{11} = -\eta^{22} = -\eta^{33} = 1$ and $\eta^{\mu\nu} = 0$ if $\mu \neq \nu$.

Although the Poincare group is the group of motions of Minkowski space, the description in terms of relations (18.1) does not involve Minkowski space at all. It involves only representation operators of the Poincare algebra, and *those relations can be treated as a definition of relativistic invariance on quantum level* (see the discussion in [3, 3]). In particular, the fact that $\eta^{\mu\nu}$ formally coincides with the metric tensor in Minkowski space does not imply that this space is involved.

In classical field theories, the background space (e.g., Minkowski space) is an auxiliary mathematical concept for describing real fields and bodies. In quantum theory, any physical quantity should be described by an operator, but there is no operator corresponding to the coordinate x of the background space. In quantum field theory, Minkowski space is an auxiliary mathematical concept for describing interacting fields. Here a local Lagrangian L(x) is used, and x is only an integration parameter. The goal of the theory is to construct the S-matrix in momentum space, and, when this construction has been accomplished, one can forget about space-time background. This is in the spirit of the Heisenberg S-matrix program according to which in quantum theory one can describe only transitions of states from the infinite past when $t \to -\infty$ to the distant future when $t \to +\infty$.

The fact that the S-matrix is the operator in momentum space does not exclude a possibility that, in semiclassical approximation, it is possible to have a space-time description with some accuracy but not with absolute accuracy (see e.g., [3] for a detailed discussion).

For example, if p is the momentum operator of a particle then, in the nonrelativistic approximation, the position operator of this particle in momentum representation *can be defined* as $r = i\hbar\partial/\partial p$. In this case, r is a physical quantity characterizing a given particle and is different for different particles.

In relativistic quantum mechanics, for considering a system of noninteracting particles, there is no need to involve Minkowski space. A description of a single particle is fully defined by its IR by the operators commuting according to Eq. (18.1) while the representation describing several particles is the tensor product of the corresponding single-particle IRs. This implies that the four-momentum and Lorenz angular momenta operators for a system are sums of the corresponding single-particle operators. In the general case, representations describing systems with interaction are not tensor products of single-particle IRs, but there is no law that the construction of such representations should necessarily involve a background space-time.

In his famous paper "Missed Opportunities" [5] Dyson notes that de Sitter (dS) and anti-de Sitter (AdS) theories are more general (fundamental) than Poincare one even from pure mathematical considerations because dS and AdS groups are more symmetric than Poincare one. The transition from the former to the latter is described by a procedure called contraction when a parameter R (see below) goes to infinity. At the same time, since dS and AdS groups are semisimple, they have a maximum possible symmetry and cannot be obtained from more symmetric groups by contraction.

The paper [5] appeared in 1972 (i.e., more than 50 years ago) and, in view of Dyson's results, a question arises why general theories of elementary particles (QED, electroweak theory and QCD) are still based on Poincare symmetry and not dS or AdS ones. Probably, physicists believe that, since the parameter R is much greater than even sizes of stars, dS and AdS symmetries can play an important role only in cosmology and there is no need to use them for describing elementary particles. We believe that this argument is not consistent because usually more general theories shed a new light on standard concepts. The discussion in our publications and, in particular, in this paper is a good illustration of this point.

By analogy with relativistic quantum theory, the definition of quantum dS symmetry should not involve dS space. If M^{ab} ($a, b = 0, 1, 2, 3, 4$, $M^{ab} = -M^{ba}$) are the operators describing the system under consideration, then, *by definition of dS symmetry on quantum level*, they should satisfy the commutation relations *of the dS Lie algebra* so(1,4), *i.e.*,

$$[M^{ab}, M^{cd}] = -i(\eta^{ac}M^{bd} + \eta^{bd}M^{ac} - \eta^{ad}M^{bc} - \eta^{bc}M^{ad}) \tag{18.2}$$

where η^{ab} is such that $\eta^{00} = -\eta^{11} = -\eta^{22} = -\eta^{33} = -\eta^{44} = 1$ and $\eta^{ab} = 0$ if $a \neq b$. The *definition* of AdS symmetry on quantum level is given by the same equations but $\eta^{44} = 1$. The procedure of contraction from dS and AdS symmetries to Poincare one is defined as follows. If we *define* the operators P^{μ} as $P^{\mu} = M^{4\mu}/R$ where R is a parameter with the dimension length then in the formal limit when $R \to \infty$, $M^{4\mu} \to \infty$ but the quantities P^{μ} are finite, Eqs. (18.2) become Eqs. (18.1). This procedure is the same for the dS and AdS symmetries and *it has nothing to do with the relation between the Minkowski and dS/AdS spaces*. In [3, 6] it has been proposed the following

Definition: *Let theory A contain a finite nonzero parameter and theory B be obtained from theory A in the formal limit when the parameter goes to zero or infinity. Suppose that, with any desired accuracy, theory A can reproduce any result of theory B by choosing a value of the parameter. On the contrary, when the limit is already taken, one cannot return to theory A, and theory B cannot reproduce all results of theory A. Then theory A is more general than theory B and theory B is a special degenerate case of theory A.*

As argued in [3,6], in contrast to Dyson's approach based on Lie groups, the approach to symmetry on quantum level should be based on Lie algebras. Then it has been proved

that, on quantum level, dS and AdS symmetries are more general (fundamental) than Poincare symmetry, *and this fact has nothing to do with the comparison of dS and AdS spaces with Minkowski space*. It has been also proved that classical theory is a special degenerate case of quantum one in the formal limit $\hbar \to 0$, and nonrelativistic theory is a special degenerate case of relativistic one in the formal limit $c \to \infty$. In the literature the above facts are explained from physical considerations but, as shown in [3, 6], they can be proved mathematically by using properties of Lie algebras.

Physicists usually understand that physics cannot (and should not) derive that $c \approx 3 \cdot 10^8$m/s and $\hbar \approx 1.054 \cdot 10^{-34}$kg·m^2/s. At the same time, they usually believe that physics should derive the value of Λ, and that the solution of the dark energy problem depends on this value. However, background space in GR is only a classical concept, while on quantum level symmetry is defined by a Lie algebra of basic operators.

The parameters $(c, \hbar, R)$ are on equal footing because each of them is the parameter of contraction from a more general Lie algebra to a less general one, and therefore those parameters must be finite. In particular, the formal case $c = \infty$ corresponds to the situation when the Poincare algebra does not exist because it becomes the Galilei algebra, and the formal case $R = \infty$ corresponds to the situation when the de Sitter algebras do not exist because they become the Poincare algebra.

Quantum de Sitter theories do not need the dimensionful parameters $(c, \hbar, R)$ at all. They arise in less general theories, and the question why they are as are does not arise because the answer is: $\hbar$ is as is because people want to measure angular momenta in kg·m^2/s, c is as is because people want to measure velocities in m/s, and R is as is because people want to measure distances in meters. The values of the parameters $(c, \hbar, R)$ in (kg, m, s) have arisen from people's macroscopic experience, and there is no guaranty that those values will be the same during the whole history of the universe (see e.g., [3] for a more detailed discussion). The fact that particle theories do not need the quantities $(c, \hbar)$ is often explained such that the system of units $c = \hbar = 1$ is used. However, the concept of systems of units is purely classical and is not needed in quantum theory.

It is difficult to imagine standard particle theories without IRs of the Poincare algebra. Therefore, when Poincare symmetry is replaced by a more general dS one, dS particle theories should be based on IRs of the dS algebra. However, as a rule, physicists are not familiar with such IRs. The mathematical literature on such IRs is wide but there are only a few papers where such IRs are described for physicists. For example, an excellent Mensky's book [7] exists only in Russian.

18.4   Explanation of cosmological acceleration

In this section we explain that, *as follows from quantum theory, the value of Λ in classical theory must be non-zero and the question why Λ is as is does not arise*.

Consider a system of free macroscopic bodies, i.e., we do not consider gravitational, electromagnetic and other interactions between the bodies. Suppose that distances between the bodies are much greater than their sizes. Then the motion of each body as a whole can be formally described in the same way as the motion of an elementary particle with the same mass. In semiclassical approximation, the spin effects can be neglected, and we can consider our system in the framework of dS quantum mechanics of free particles.

The explicit expressions for the operators M^{ab} in IRs of the dS Lie algebra have been derived in [8] (see also [3, 6, 9]). In contrast to standard quantum theory where the mass m of a particle is dimensionful, in dS quantum theory, the mass m_{dS} of a particle is dimensionless. In the approximation when Poincare symmetry works with a high accuracy, these masses in units $c = \hbar = 1$ are related as $m_{dS} = Rm$. Also, in dS quantum theory, the Hilbert space of

functions in IRs is the space of functions depending not on momenta but on four-velocities $v = (v_0, v)$ where $v_0 = (1 + v^2)^{1/2}$. Then in the spinless case, the explicit expressions for the operators M^{ab} are (see e.g., Eq. (3.16) in [3]):

$$J = l(v), \quad N = -iv_0 \frac{\partial}{\partial v}, \quad \mathcal{E} = m_{ds} v_0 + iv_0 (v \frac{\partial}{\partial v} + \frac{3}{2})$$
$$B = m_{ds} v + i[\frac{\partial}{\partial v} + v(v \frac{\partial}{\partial v}) + \frac{3}{2} v] \tag{18.3}$$

where $J = \{M^{23}, M^{31}, M^{12}\}$, $N = \{M^{01}, M^{02}, M^{03}\}$, $B = \{M^{41}, M^{42}, M^{43}\}$, $l(v) = -iv \times \partial/\partial v$ and $\mathcal{E} = M^{40}$. *The important observation is that, at this stage, we have no coordinates yet.* For describing the motion of the particle in terms of coordinates, we must define the position operator. If Poincare symmetry works with a high accuracy, the momentum of the particle can be defined as $p = mv$ and, as noted above, the position operator can be defined as $r = i\hbar \partial/\partial p$.

In semiclassical approximation, we can treat p and r as usual vectors. Then, if $E = \mathcal{E}/R$, $P = B/R$ and the classical nonrelativistic Hamiltonian is defined as $H = E - mc^2$, it follows from Eq. (18.3) that

$$H(P, r) = \frac{P^2}{2m} - \frac{mc^2 r^2}{2R^2} \tag{18.4}$$

Here the last term is the dS correction to the non-relativistic Hamiltonian.

The representation describing a free N-body system is a tensor product of the corresponding single-particle IRs. This means that every N-body operator M^{ab} is a sum of the corresponding single-particle operators.

Consider a system of two free particles described by the quantities P_j and r_j ($j = 1, 2$). Define standard nonrelativistic variables

$$P = P_1 + P_2, \quad q = (m_2 P_1 - m_1 P_2)/(m_1 + m_2)$$
$$R = (m_1 r_1 + m_2 r_2)/(m_1 + m_2), \quad r = r_1 - r_2 \tag{18.5}$$

Here P and R are the momentum and position of the system as a whole, and q and r are the relative momentum and relative radius-vector, respectively. Then as follows from Eqs. (18.4) and (18.5), the internal two-body Hamiltonian is

$$H_{nr}(r, q) = \frac{q^2}{2m_{12}} - \frac{m_{12} c^2 r^2}{2R^2} \tag{18.6}$$

where m_{12} is the reduced two-particle mass. Then, as follows from the Hamilton equations, in semiclassical approximation the relative acceleration is given by

$$a = rc^2/R^2 \tag{18.7}$$

where a and r are the relative acceleration and relative radius vector of the bodies, respectively.

The fact that the relative acceleration of noninteracting bodies is not zero does not contradict the law of inertia, because this law is valid only in the case of Galilei and Poincare symmetries. At the same time, in the case of dS symmetry, noninteracting bodies necessarily repulse each other. In the formal limit $R \to \infty$, the acceleration becomes zero as it should be.

Equations of relative motion derived from Eq. (18.6) are the same as those derived from GR if $\Lambda \neq 0$. In particular, the result (18.7) coincides with that in GR if the curvature of dS space equals $\Lambda = 3/R^2$, where R is the radius of this space. *Therefore the cosmological constant has a physical meaning only on classical level, the parameter of contraction from dS symmetry to Poincare one coincides with R and, as noted above, a question why R is as is does not arise.*

In GR, the result (18.7) does not depend on how Λ is interpreted, as the curvature of empty space or as the manifestation of dark energy or quintessence. However, in quantum theory, there is no freedom of interpretation. Here R is the parameter of contraction from the dS Lie algebra to the Poincare one, it has nothing to do with dark energy or quintessence and it must be finite because dS symmetry is more general than Poincare one.

Every dimensionful parameter cannot have the same numerical values during the whole history of the universe. For example, at early stages of the universe such parameters do not have a physical meaning because semiclassical approximation does not work at those stages. In particular, the terms "cosmological constant" and "gravitational constant" can be misleading. General Relativity successfully describes many data in the approximation when Λ and G are constants but this does not mean that those quantities have the same numerical values during the whole history of the universe.

18.5   Discussion and conclusion

In view of the problem of cosmological acceleration, the cosmological constant problem is widely discussed in the literature. This problem arises as follows.

One starts from Poincare invariant quantum field theory (QFT) of gravity defined on Minkowski space. This theory contains only one phenomenological parameter — the gravitational constant G, and the cosmological constant Λ is defined by the vacuum expectation value of the energy-momentum tensor. The theory contains strong divergencies which cannot be eliminated because the theory is not renormalizable. Therefore, the results for divergent integrals can be made finite only with a choice of the cutoff parameter. Since G is the only parameter in the theory, a reasonable choice of the cutoff parameter in momentum space is the Planck momentum $\hbar/l_P$ where l_P is the Plank length. In units $\hbar = c = 1$, G has the dimension $1/\mathrm{length}^2$ and Λ has the dimension length^2. Therefore, the value of Λ obtained in this approach is of the order of $1/G$. However, this value is more than 120 orders of magnitude greater than the experimental one.

In view of this situation, the following remarks can be made. As explained in Sec. 18.3, Poincare symmetry is a special degenerate case of dS symmetry in the formal limit $R \to \infty$. Here R is a parameter of contraction from dS algebra to Poincare one. This parameter has nothing to do with the relation between Poincare and dS spaces. The problem why R is as is does not arise by analogy with the problem why c and $\hbar$ are as are. As explained in Sec. 18.4, the cosmological constant Λ has a physical meaning only in semiclassical approximation and here it equals $3/R^2$. Therefore the cosmological constant problem and the problem why the cosmological constant is as is do not arise.

As noted in Sec. 18.3, the background space-time is only a mathematical concept which has a physical meaning only in classical theory. This concept turned out to be successful in QED. In particular, the results for the electron and muon magnetic moments agree with experiments with the accuracy of eight decimal digits. However, QED works only in perturbation theory because the fine structure constant is small. There is no law that the ultimate quantum theory will necessarily involve the concept of background space-time. QFTs of gravity (for example, Loop Quantum Gravity) usually assume that in semiclassical approximation, the background space in those theories should become the background space in GR. However, in Sec. 18.4, the result for the cosmological acceleration in semiclassical approximation has been obtained without space-time background and this result is the same as that obtained in GR.

Although the physical nature of dark energy remains a mystery, there exists a wide literature where the authors propose QFT models of dark energy. These models are based on Poincare symmetry with the background Minkowski space. So, the authors do not take into account

the fact that de Sitter symmetry is more general (fundamental) than Poincare symmetry and that the background space is only a classical concept. While in most publications, only proposals about future discovery of dark energy are considered, the authors of [1] argue that dark energy has been already discovered by the XENON1T collaboration. In June 2020, this collaboration reported an excess of electron recoils: 285 events, 53 more than the expected 232 with a statistical significance of 3.5σ. However, in July 2022, a new analysis by the XENONnT collaboration discarded the excess [10].

As shown in Sec. 18.4, the result (18.7) has been derived without using dS space and its geometry (metric and connection). It is simply a consequence of dS quantum mechanics in semiclassical approximation. We believe that this result is more important than the result of GR because any classical result should be a consequence of quantum theory in semiclassical approximation.

Therefore, the phenomenon of cosmological acceleration has nothing to do with dark energy or other artificial reasons. This phenomenon is purely a kinematical consequence of dS quantum mechanics in semiclassical approximation.

References

1. S. Vagnozzi, L. Visinelli, P. Brax, A-Ch. Davis and J. Sakstein: Direct detection of dark energy: the XENON1T excess and future prospects, Phys. Rev. **D104**, 063023 (2021).
2. E. Bianchi and C. Rovelli: Why All These Prejudices Against a Constant, arXiv:1002.3966v3 (2010).
3. F.M. Lev: de Sitter Symmetry and Quantum Theory, Phys. Rev. **D85**, 065003 (2012).
4. F.M. Lev: Finite Mathematics as the Foundation of Classical Mathematics and Quantum Theory. With Application to Gravity and Particle theory. ISBN 978-3-030-61101-9. Springer, Cham, 2020.
5. F. G. Dyson: Missed Opportunities, Bull. Amer. Math. Soc. **78**, 635-652 (1972).
6. F.M. Lev: Cosmological Acceleration as a Consequence of Quantum de Sitter Symmetry, Physics of Particles and Nuclei Letters **17**, 126-135 (2020).
7. M.B. Mensky: Method of Induced Representations. Space-time and Concept of Particles. Nauka, Moscow (1976).
8. F.M. Lev: Finiteness of Physics and its Possible Consequences, J. Math. Phys. **34**, 490-527 (1993).
9. F.M. Lev: Could Only Fermions Be Elementary? J. Phys. **A37**, 3287-3304 (2004).
10. E. Aprile, K. Abe, F. Agostini *et. al.*: Search for New Physics in Electronic Recoil Data from XENONnT, arXiv:2207.11330 (2022).

19 Clifford odd and even objects in even and odd dimensional spaces

N. S. Mankoč Borštnik

Department of Physics, University of Ljubljana
SI-1000 Ljubljana, Slovenia
norma.mankoc@fmf.uni-lj.si

Abstract. In a long series of works I demonstrated, together with collaborators, that the model named the *spin-charge-family* theory offers the explanation for all in the *standard model* assumed properties of the second quantized fermion and boson fields, offering several predictions as well as explanations for several of the observed phenomena. The theory assumes a simple starting action in even dimensional spaces with $d \geq (13+1)$ with massless fermions interacting with gravity only. The internal spaces of fermion and boson fields are described by the Clifford odd and even objects, respectively. This note discusses properties of the internal spaces in odd dimensional spaces, d, $d = (2n + 1)$, which differ essentially from the properties in even dimensional spaces.

Povzetek:
V dolgem nizu člankov sem skupaj s sodelavci pokazala, da ponuja teorija , imenovana *spin-charge-family*, razlago za vse v *standardnem modelu* privzete lastnosti fermionskih in bozonskih polj (v drugi kvantizaciji), ponuja pa poleg napovedi tudi razlago za marsikatero od opaženih kozmoloških pojavov. Teorija predlaga preprosto akcijo v sodo-razsežnih prostorih, $d \geq (13 + 1)$, za brezmasne fermione v interakciji samo z gravitacijskim poljem. Notranje prostore fermionskih in bozonskih polj opišejo Cliffordovi lihi oziroma sodi objekti. Ta prispevek obravnava lastnosti notranjega prostora fermionov in bozonov v prostorih z lihimi razsežnostimi d, $d = (2n + 1)$.

19.1 introduction

My working hypothesis is that "Nature knows all the mathematics", which we have and possibly will ever invent, and "she uses it where needed". Recognizing that there are two kinds of the Clifford algebra objects, γ^a's and $\tilde{\gamma}^a$'s [2], each of them of odd and even

character, I use them to describe the internal spaces of fermion and boson fields [5–9] in even dimensional spaces.

The Clifford odd objects, if they are superposition of odd products of γ^a's, explain in even $d = 2n$ properties of fermion fields. The second kind of the Clifford odd objects, $\tilde{\gamma}^a$'s, can be used, after defining their application on the polynomials of γ^a's (Eq. (7) of my talk in this Proceedings [4]), to equip the irreducible representations of odd polynomials of γ^a's with the family quantum numbers.

The Clifford even objects, if they are superposition of even products of γ^a's, explain in even d properties of boson fields, the gauge fields of the corresponding fermion fields. They do not appear in families [4–9].

In $d = (13 + 1)$ the Clifford odd objects manifest all the properties of the internal space of fermions — of the observed quarks and leptons and antiquarks and antileptons with their families included — and the Clifford even objects explain the gauge fields of the corresponding fermion fields, as well as the Higgs' scalars and Yukawa couplings. The internal space of fermion and boson fields, described by "basis vectors" (they are chosen to be eigenvectors of all the members of the Cartan subalgebra members of the Lorentz group in the internal space of fields), demonstrate properties of the postulates of the second quantization of fermion and boson fields, explaining these postulates [4,6].

I demonstrate in this note that also in odd dimensional spaces the Clifford odd and the Clifford even objects exist. However, the eigenstates of the operator of handedness are in odd dimensional spaces the superposition of the Clifford odd and the Clifford even objects. This seems to explain the ghost fields appearing in several theories for taking care of the singular contributions in evaluating Feynman graphs.

Next section presents the internal spaces, described by the Clifford odd and the Clifford even "basis vectors" for fermion and boson fields in even dimensional spaces, for $d = (1+1)$ and $d = (3 + 1)$, as well as in odd dimensional spaces, for $d = (0 + 1)$ and $d = (2 + 1)$. This simple cases are chosen to easier demonstrate the difference in properties in even and odd dimensional spaces.

In Refs. [10–12] from 20years ago the authors discuss the question of q time and $d − q$ dimensions in odd and even dimensional spaces, for any q. Using the requirements that the inner product of two fermions is unitary and invariant under Lorentz transformations the authors conclude that odd dimensional spaces are not appropriate due to the existence of fermions of both handedness and correspondingly not mass protected.

In this note the comparison of properties of fermion and boson fields in odd and in even dimensional spaces are made, using the Clifford algebra objects to describe the internal spaces of fermion and boson fields. The recognition of this note might further clarify the "effective" choice of Nature for one time and three space dimensions.

The reader can find more explanation about the properties of internal spaces of fermion and boson fields in even dimensional spaces in my contribution in this proceedings [4].

19.2   "Basis vectors" in $d = 2n$ and $d = 2n + 1$ for $n = 0, 1, 2$

In Ref. [4–9] the reader can find the definition of the "basis vectors" as the eigenstates of the Cartan subalgebra of the Lorentz algebra in internal spaces of fermion and boson fields. "Basis vectors" are written as superposition of the Clifford odd (for fermions) and the Clifford even (for bosons) products of γ^a's. "Basis vectors" for fermions have either left or right handedness, $\Gamma^{(}d)$ (the handedness is defined in Eq. (19.2)), and appear in families (the family quantum numbers are determined by $\tilde{\gamma}^a$'s, with $\tilde{S}^{ab} = \frac{i}{4}\{\tilde{\gamma}^a, \tilde{\gamma}^b\}_-$). The Clifford odd "basis vectors" have their Hermitian conjugated partners in a separate group. "Basis

vectors" for bosons have no families and have their Hermitian conjugated partners within the same group.

Properties of the "basis vectors" in odd dimensional spaces have completely different properties: Only the superposition of the Clifford odd and the Clifford even"basis vectors" have a definite handedness. Correspondingly the eigenvectors of the Cartan subalgebra members have both handedness, $\Gamma^{(2n+1)} = \pm 1$.

19.2.1   Even dimensional spaces $d = (1+1), (3+1)$

To simplify the comparison between even and odd dimensional spaces, simple cases for either even or odd dimensional spaces are discussed. The definition of nilpotents and projectors and the relations among them can be found in App. 19.4.

$d = (1+1)$

There are $4\,(2^{d=2})$ "eigenvectors" of the Cartan subalgebra members, Eq. (19.4), S^{01} and $\mathcal{S}^{01}$ of the Lorentz algebra S^{ab} and $\mathcal{S}^{ab} = S^{01} + \tilde{S}^{01}$ ($S^{ab} = \frac{i}{4}\{\gamma^a, \gamma^b\}_-$ $\tilde{S}^{ab} = \frac{i}{4}\{\tilde{\gamma}^a, \tilde{\gamma}^b\}_-$) representing one Clifford odd "basis vector" $\hat{b}_1^{1\dagger} = \overset{01}{(+i)}$ (m=1), appearing in one family (f=1) and correspondingly one Hermitian conjugated partner $\hat{b}_1^1 = \overset{01}{(-i)}$ [1] and two Clifford even "basis vector" $^{I}\mathcal{A}_1^{1\dagger} = \overset{01}{[+i]}$ and $^{II}\mathcal{A}_1^{1\dagger} = \overset{01}{[-i]}$, each of them is self adjoint.

Correspondingly we have two Clifford odd, Eqs. (19.3, 19.7)

$$\hat{b}_1^{1\dagger} = \overset{01}{(+i)}, \quad \hat{b}_1^1 = \overset{01}{(-i)}$$

and two Clifford even

$$^{I}\mathcal{A}_1^{1\dagger} = \overset{01}{[+i]}, \quad ^{II}\mathcal{A}_1^{1\dagger} = \overset{01}{[-i]}$$

"basis vectors".

The two Clifford odd "basis vectors" are Hermitian conjugated to each other. I make a choice that $\hat{b}_1^{1\dagger}$ is the "basis vector", the second Clifford odd object is its Hermitian conjugated partner. Defining the handedness as $\Gamma^{(1+1)} = \gamma^0\gamma^1$, Eq. (19.2), it follows, using Eq. (19.5), that $\Gamma^{(1+1)}\,\hat{b}_1^{1\dagger} = \hat{b}_1^{1\dagger}$, which means that $\hat{b}_1^{1\dagger}$ is the right handed "basis vector".

We could make a choice of left handed "basis vector" if choosing $\hat{b}_1^{1\dagger} = \overset{01}{(-i)}$, but the choice of handedness would remain only one.

Each of the two Clifford even "basis vectors" is self adjoint $((^{I,II}\mathcal{A}_1^{1\dagger})^\dagger = {}^{I,II}\mathcal{A}_1^{1\dagger})$.

Let us notice, taking into account Eqs. (19.5, 19.9), that

$$\{\hat{b}_1^1(\equiv \overset{01}{(-i)}) *_A \hat{b}_1^{1\dagger}(\equiv \overset{01}{(+i)})\}|\psi_{oc}> = {}^{II}\mathcal{A}_1^{1\dagger}(\equiv \overset{01}{[-i]})|\psi_{oc}> = |\psi_{oc}>,$$

$$\{\hat{b}_1^{1\dagger}(\equiv \overset{01}{(+i)}) *_A \hat{b}_1^1(\equiv \overset{01}{(-i)})\}|\psi_{oc}> = 0,$$

---

[1] It is our choice which one, $\overset{01}{(+i)}$ or $\overset{01}{(-i)}$, we chose as the "basis vector" $\hat{b}_1^{1\dagger}$ and which one is its Hermitian conjugated partner. The choice of the "basis vector" determines the vacuum state $|\psi_{oc}>$. For $\hat{b}_1^{1\dagger} = \overset{01}{(+i)}$, the vacuum state is $|\psi_{oc}> = \overset{01}{[-i]}$ (due to the requirement that $\hat{b}_1^{1\dagger}|\psi_{oc}>$ is nonzero), which is the Clifford even object.

$$^I\mathcal{A}_1^{1\dagger}(\equiv[\overset{01}{+i}]) *_A \hat{b}_1^1(\equiv(\overset{01}{+i}))|\psi_{oc}> = \hat{b}_1^1(\equiv(\overset{01}{+i}))|\psi_{oc}>,$$

$$^I\mathcal{A}_1^{1\dagger}(\equiv[\overset{01}{+i}]) \hat{b}_1^1(\equiv(\overset{01}{-i}))|\psi_{oc}> = 0.$$

We find that

$$^I\mathcal{A}_1^{1\dagger} *_A {}^{II}\mathcal{A}_1^{1\dagger} = 0 = {}^{II}\mathcal{A}_1^{1\dagger} *_A {}^I\mathcal{A}_1^{1\dagger}.$$

From the case $d = (3 + 1)$ we can learn a little more:

$d = (3 + 1)$

There are 16 ($2^{d=4}$) "eigenvectors" of the Cartan subalgebra members (S^{03}, S^{12}) and ($\mathcal{S}^{03}, \mathcal{S}^{12}$) of the Lorentz algebras S^{ab} and $\mathcal{S}^{ab}$, Eq. (19.4), in $d = (3 + 1)$.

There are two families ($2^{\frac{4}{2}-1}$, f=(1,2)) with two ($2^{\frac{4}{2}-1}$, m=(1,2)) members each of the Clifford odd "basis vectors" $\hat{b}_f^{m\dagger}$, with $2^{\frac{4}{2}-1} \times 2^{\frac{4}{2}-1}$ Hermitian conjugated partners $\hat{b}_f^m$ in a separate group (not reachable by S^{ab}).

There are $2^{\frac{4}{2}-1} \times 2^{\frac{4}{2}-1}$ members of the group of $^I\mathcal{A}_f^{m\dagger}$, which are Hermitian conjugated to each other or are self adjoint, all reachable by $\mathcal{S}^{ab}$ from any starting "basis vector $^I\mathcal{A}_1^{1\dagger}$.

And there is another group of $2^{\frac{4}{2}-1} \times 2^{\frac{4}{2}-1}$ members of $^{II}\mathcal{A}_f^{m\dagger}$, again either Hermitian conjugated to each other or are self adjoint. All are reachable from the starting vector $^{II}\mathcal{A}_1^{1\dagger}$ by the application of $\mathcal{S}^{ab}$.

Again we can make a choice of either right or left handed Clifford odd "basis vectors", but not of both handedness. Making a choice of the right handed "basis vectors"

$$
\begin{array}{ccc}
f = 1 & f = 2 & \\
\tilde{S}^{03} = \frac{i}{2}, \tilde{S}^{12} = -\frac{1}{2}, & \tilde{S}^{03} = -\frac{i}{2}, \tilde{S}^{12} = \frac{1}{2}, & S^{03}, \quad S^{12} \\
\hat{b}_1^{1\dagger} = \overset{03}{(+i)}\overset{12}{[+]} & \hat{b}_2^{1\dagger} = \overset{03}{[+i]}\overset{12}{(+)} & \frac{i}{2} \quad \frac{1}{2} \\
\hat{b}_1^{2\dagger} = \overset{03}{[-i]}\overset{12}{(-)} & \hat{b}_2^{2\dagger} = \overset{03}{(-i)}\overset{12}{[-]} & -\frac{i}{2} \quad -\frac{1}{2},
\end{array}
$$

we find for the Hermitian conjugated partners of the above "basis vectors"

$$
\begin{array}{ccc}
S^{03} = -\frac{i}{2}, S^{12} = \frac{1}{2}, & S^{03} = \frac{i}{2}, S^{12} = -\frac{1}{2}, & \tilde{S}^{03}, \tilde{S}^{12} \\
\hat{b}_1^1 = \overset{03}{(-i)}\overset{12}{[+]} & \hat{b}_2^1 = \overset{03}{[+i]}\overset{12}{(-)} & -\frac{i}{2} \quad -\frac{1}{2} \\
\hat{b}_1^2 = \overset{03}{[-i]}\overset{12}{(+)} & \hat{b}_2^2 = \overset{03}{(+i)}\overset{12}{[-]} & \frac{i}{2} \quad \frac{1}{2}.
\end{array}
$$

Let us notice that if we look at the subspace $SO(1, 1)$, with the Clifford odd "basis vector" with the Cartan subalgebra member S^{03} of the space $SO(3, 1)$, and neglect the values of S^{12}, we do have $\hat{b}_1^{1\dagger} = \overset{03}{(+i)}$ and $\hat{b}_2^{2\dagger} = \overset{03}{(-i)}$, which have opposite handedness $\Gamma^{(1,1)}$ in $d = (1+1)$, but they have different "charges" S^{12} in $d = (3 + 1)$. In the whole internal space all the Clifford odd "basis vectors" have only one handedness.

We further find that $|\psi_{oc}> = \frac{1}{\sqrt{2}}(\overset{03}{[-i]}\overset{12}{[+]} + \overset{03}{[+i]}\overset{12}{[+]})$. All the Clifford odd "basis vectors" are orthogonal: $\hat{b}_f^{m\dagger} *_A \hat{b}_{f'}^{m'\dagger} = 0$.

For the Clifford even "basis vectors" we find two groups of either self adjoint members or with the Hermitian conjugated partners within the same group. The members of one group are not reachable by the application of $\mathcal{S}^{03}$ on members of another group. We have for $^I\mathcal{A}_f^{m\dagger}$, $m = (1, 2), f = (1, 2)$

$$
\begin{array}{lcccccc}
 & & \mathcal{S}^{03} & \mathcal{S}^{12} & & & \mathcal{S}^{03}\ \ \mathcal{S}^{12} \\
^{I}\mathcal{A}_1^{1\dagger} = \overset{03}{[+i]}\overset{12}{[+]} & & 0 & 0 & , & ^{I}\mathcal{A}_2^{1\dagger} = \overset{03}{(+i)}\overset{12}{(+)} & i \quad 1 \\
^{I}\mathcal{A}_1^{2\dagger} = \overset{03}{(-i)}\overset{12}{(-)} & & -i & -1 & , & ^{I}\mathcal{A}_2^{2\dagger} = \overset{03}{[-i]}\overset{12}{[-]} & 0 \quad 0,
\end{array}
$$

and for $^{II}\mathcal{A}_f^{m\dagger}$, $\mathfrak{m} = (1,2)$, $\mathfrak{f} = (1,2)$

$$
\begin{array}{lcccccc}
 & & \mathcal{S}^{03} & \mathcal{S}^{12} & & & \mathcal{S}^{03}\ \ \mathcal{S}^{12} \\
^{II}\mathcal{A}_1^{1\dagger} = \overset{03}{[+i]}\overset{12}{[-]} & & 0 & 0 & , & ^{II}\mathcal{A}_2^{1\dagger} = \overset{03}{(+i)}\overset{12}{(-)} & i \quad 1 \\
^{II}\mathcal{A}_1^{2\dagger} = \overset{03}{(-i)}\overset{12}{(+)} & & -i & 1 & , & ^{II}\mathcal{A}_2^{2\dagger} = \overset{03}{[-i]}\overset{12}{[+]} & 0 \quad 0.
\end{array}
$$

The Clifford even "basis vectors" have no families.

$$^{I}\mathcal{A}_f^{m\dagger} *_A {}^{I}\mathcal{A}_{f'}^{m'\dagger} = 0, \text{ for any } (m, m', f, f').$$

Even dimensional spaces have the properties of the fermion and boson second quantized fields, as explained in Ref. [4].

19.2.2   Odd dimensional spaces $d = (0+1), (2+1)$

In odd dimensional spaces fermions have handedness defined with the odd products of γ^a's, Eq. (19.2). Correspondingly the operator of handedness transforms the Clifford odd "basis vectors" into Clifford even "basis vectors" and the description of either fermions or bosons with the Clifford even and odd "basis vectors" have in odd dimensional spaces different meaning than in even dimensional spaces:

i. While in even dimensional spaces the Clifford odd "basis vectors", $\hat{b}_f^{m\dagger}$, have $2^{\frac{d}{2}-1}$ members, $\mathfrak{m}$, in $2^{\frac{d}{2}-1}$ families, $\mathfrak{f}$, and their Hermitian conjugated partners appear in a separate group of $2^{\frac{d}{2}-1}$ members in $2^{\frac{d}{2}-1}$ families, there are in odd dimensional spaces some of the $2^{\frac{d}{2}-1} \times 2^{\frac{d}{2}-1} = 2^{d-2}$ Clifford odd "basis vectors" self adjoint and yet they have some of the Hermitian conjugated partners in another group with 2^{d-2} members.

ii. In even dimensional spaces the Clifford even "basis vectors" $^{i}\hat{\mathcal{A}}_f^{m\dagger}$, $i = (I, II)$, appear in two mutually orthogonal groups, each with $2^{\frac{d}{2}-1} \times 2^{\frac{d}{2}-1}$ members and each with the Hermitian conjugated partners within the same group, $2^{\frac{d}{2}-1}$ of them are self adjoint.

In odd dimensional spaces the Clifford even "basis vectors" appear in two groups, each with $2^{\frac{d}{2}-1} \times 2^{\frac{d}{2}-1} = 2^{d-2}$ members, which are either self adjoint or have their Hermitian conjugated partners in another group. Not all the members of one group are orthogonal to the members of another group, only the self adjoint ones are.

iii. While $\hat{b}_f^{m\dagger}$ have in even dimensional spaces one handedness only (either right or left, depending on the definition of handedness), in odd dimensional spaces the operator of handedness is a Clifford odd object — the product of an odd number of γ^a's, Eq. (19.2), (still commuting with S^{ab}) — transforming the Clifford odd "basis vectors" into Clifford even "basis vectors" and opposite. Correspondingly are the eigenvectors of the operator of handedness the superposition of the Clifford odd and the Clifford even "basis vectors", offering in odd dimensional spaces the right and left handed eigenvectors of the operator of handedness.

Let us illustrate the above mentioned properties of the "basis vectors" in odd dimensional spaces, starting with the simplest case:

d=(0+1)

There is one Clifford odd "basis vector", which is self adjoint

$$\hat{b}_1^{1\dagger} = \gamma^0 = (\hat{b}_1^{1\dagger})^\dagger = \hat{b}_1^1$$

and one Clifford even "basis vectors"

$$^i\hat{\mathcal{A}}_1^{1\dagger} = 1 \,.$$

The operator of handedness $\Gamma^{(0+1)} = \gamma^0$ transforms $\hat{b}_1^{1\dagger}$ into identity $^i\hat{\mathcal{A}}_1^{1\dagger}$ and $^i\hat{\mathcal{A}}_1^{1\dagger}$ into $\hat{b}_1^{1\dagger}$.

The two eigenvectors of the operator of handedness are

$$\frac{1}{\sqrt{2}}(\gamma^0 + 1) \,, \quad \frac{1}{\sqrt{2}}(\gamma^0 - 1) \,,$$

with the handedness $(+1, -1)$, that is of right and left handedness. respectively.

d=(2+1)

There are twice $2^{d=(3-2)} = 2$ Clifford odd "basis vectors". We chose as the Cartan subalgebra member S^{01} of S^{ab}, Eq (19.4): $\hat{b}_1^{1\dagger} = [\overset{01}{-i}]\gamma^2$, $\hat{b}_1^{2\dagger} = (\overset{01}{+i})$, $\hat{b}_2^{1\dagger} = (\overset{01}{-i})$, $\hat{b}_2^{2\dagger} = [\overset{01}{+i}]\gamma^2$, with the properties

$$
\begin{array}{ccc}
f = 1 & f = 2 & \\
\tilde{S}^{01} = \frac{i}{2} & \tilde{S}^{01} = -\frac{i}{2}, & S^{01} \\
\hat{b}_1^{1\dagger} = [\overset{01}{-i}]\gamma^2 & \hat{b}_2^{1\dagger} = (\overset{01}{-i}) & -\frac{i}{2} \\
\hat{b}_1^{2\dagger} = (\overset{01}{+i}) & \hat{b}_2^{2\dagger} = [\overset{03}{+i}]\gamma^2 & \frac{i}{2},
\end{array}
$$

$\hat{b}_1^{1\dagger}$ and $\hat{b}_2^{2\dagger}$ are self adjoint (up to a sign), $\hat{b}_1^{2\dagger} = (\overset{01}{+i})$ and $\hat{b}_2^{1\dagger} = (\overset{01}{-i})$ are Hermitian conjugated to each other.

In odd dimensional spaces the Clifford odd "basis vectors" describing fermions are not separated from their Hermitian conjugated partners, as it is the case in even dimensional spaces, and do not appear in families. $\hat{b}_1^{1\dagger}$ are either self adjoint or have their Hermitian conjugated partners in another family.

The operator of handedness is (chosen up to a sign to be) $\Gamma^{(2+1)} = i\gamma^1\gamma^2\gamma^2$, Eq. (19.2).

There are twice $2^{(d=3)-2} = 2$ Clifford even "basis vectors". We choose as the Cartan subalgebra member $\mathcal{S}^{01}$: $^I\hat{\mathcal{A}}_1^{1\dagger} = [\overset{01}{+i}]$, $^I\hat{\mathcal{A}}_1^{2\dagger} = (\overset{01}{-i})\gamma^2$, $^{II}\hat{\mathcal{A}}_2^{1\dagger} = [\overset{01}{-i}]$, $^{II}\hat{\mathcal{A}}_2^{2\dagger} = (\overset{01}{+i})\gamma^2$, with the properties

$$
\begin{array}{cccc}
& \mathcal{S}^{01} & & \mathcal{S}^{01} \\
^I\hat{\mathcal{A}}_1^{1\dagger} = [\overset{01}{+i}] & 0 & ^{II}\hat{\mathcal{A}}_2^{1\dagger} = [\overset{01}{-i}] & 0 \\
^I\hat{\mathcal{A}}_1^{2\dagger} = (\overset{01}{-i})\gamma^2 & -i & ^{II}\hat{\mathcal{A}}_2^{2\dagger} = (\overset{03}{+i})\gamma^2 & i,
\end{array}
$$

$^I\hat{\mathcal{A}}_1^{1\dagger} = [\overset{01}{+i}]$ and $^{II}\hat{\mathcal{A}}_2^{1\dagger} = [\overset{01}{-i}]$ are self adjoint, $^I\hat{\mathcal{A}}_1^{2\dagger} = (\overset{01}{-i})\gamma^2$ and $^{II}\hat{\mathcal{A}}_2^{2\dagger} = (\overset{03}{+i})\gamma^2$ are Hermitian conjugated to each other.

In odd dimensional spaces the two groups of the Clifford even "basis vectors" are not orthogonal.

Let us find the eigenvectors of the operator of handedness $\Gamma^{(2+1)} = i\gamma^0\gamma^1\gamma^2$. Since it is the Clifford odd object its eigenvectors are superposition of Clifford odd and Clifford even "basis vectors".

It follows

$$\Gamma^{(2+1)}\{\overset{01}{[-i]} \pm i \overset{01}{[-i]} \gamma^2\} = \mp\{\overset{01}{[-i]} \pm i \overset{01}{[-i]} \gamma^2\},$$

$$\Gamma^{(2+1)}\{\overset{01}{(+i)} \pm i \overset{01}{(+i)} \gamma^2\} = \mp\{\overset{01}{(+i)} \pm i \overset{01}{(+i)} \gamma^2\},$$

$$\Gamma^{(2+1)}\{\overset{01}{[+i]} \pm i \overset{01}{[+i]} \gamma^2\} = \pm\{\overset{01}{[+i]} \pm i \overset{01}{[+i]} \gamma^2\},$$

$$\Gamma^{(2+1)}\{\overset{01}{(-i)} \gamma^2 \pm i \overset{01}{(-i)}\} = \pm\{\overset{01}{(-i)} \gamma^2 \pm i \overset{01}{(-i)}\},$$

We can conclude that neither Clifford odd nor Clifford even "basis vectors" have in odd dimensional spaces the properties which they do demonstrate in even dimensional spaces, the properties which empower the Clifford odd "basis vectors" to represent fermions and the Clifford even "basis vectors" to represent the corresponding gauge fields.

i. In odd dimensional spaces the Clifford odd "basis vectors" are not separated from their Hermitian conjugated partners, they instead are either self adjoint or have their Hermitian conjugated in another family. We can not define creation and annihilation operators as a tensor products of "basis vectors" and basis in momentum space so that they would manifest the creation and annihilation operators fulfilling the postulates of the second quantized fermions.

In odd dimensional spaces the two groups of the Clifford even "basis vectors" are not orthogonal, only the self adjoint "basis vectors" are orthogonal, the rest of "basis vectors" have their Hermitian conjugated partners in another group.

ii. The Clifford odd operator of handedness allows left and right handed superposition of Clifford odd and Clifford even "basis vectors".

19.3   Discussion

This note discusses the properties of the internal spaces of fermion and boson fields in even and odd dimensional spaces, if the internal spaces are described by the Clifford odd and even "basis vectors", which are the superposition of odd or even products of operators γ^a's. "Basis vectors" are arranged into algebraic products of nilpotents and projectors, which are eigenvectors of the Cartan subalgebra of the Lorentz algebra S^{ab} in the internal space of fermions and bosons.

The Clifford odd "basis vectors", which are products of an odd number of nilpotents and the rest of projectors, offer in even dimensional spaces the description of the internal space of fermion fields.

Each irreducible representation of the Lorentz algebra is equipped with the family quantum number determined by the second kind of the Clifford operators $\tilde\gamma^a$'s. The Clifford odd "basis vectors" anticommute. Their Hermitian conjugated partners appear in a different group. In a tensor product with the basis in ordinary space the "basis vectors" and their Hermitian conjugated partners form the creation and annihilation operators which fulfil the anticommutation relations postulated for second quantized fermion fields.

In $d = 2(2n+1), n \geq 7$, these creation and annihilation operators, applying on the vacuum state, or on the Hilbert space, offer the description of all the properties of the observed

quarks and leptons and antiquarks and antileptons. The massless fermion fields are of one handedness only.

The Clifford even "basis vectors", which are products of an even number of nilpotents and the rest of projectors, offer in even dimensional spaces the description of the internal space of boson fields, the gauge fields of the corresponding fermion fields. The Clifford even "basis vectors" commute. They do not appear in families and have their Hermitian conjugated partners in the same group. In a tensor product with the basis in ordinary space the "basis vectors" form the creation and annihilation operators which fulfil the commutation relations postulated for second quantized boson fields fields. In $d = 2(2n + 1), n \geq 7$, these creation and annihilation operators offer the description of all the properties of the observed gauge fields as well as of the scalar Higgs's field, explaining also the Yukawa couplings.

This way of describing internal space of boson fields with the Clifford even "basis vectors", although very promising, needs further studies to understand what new it can bring into second quantization of fermion and boson fields. In particular, it must be understood what does it bring if we replace in a simple starting action in $d = 2(2n + 1), n \geq 7$

$$\mathcal{A} = \int d^d x \, E \, \frac{1}{2} \, (\bar{\psi} \, \gamma^a p_{0a} \psi) + h.c. +$$
$$\int d^d x \, E \, (\alpha \, R + \tilde{\alpha} \, \tilde{R}) \, ,$$
$$p_{0a} = f^\alpha{}_a p_{0\alpha} + \frac{1}{2E} \{p_\alpha, E f^\alpha{}_a\}_- \, ,$$
$$p_{0\alpha} = p_\alpha - \frac{1}{2} S^{ab} \omega_{ab\alpha} - \frac{1}{2} \tilde{S}^{ab} \tilde{\omega}_{ab\alpha} \, ,$$
$$R = \frac{1}{2} \{f^{\alpha[a} f^{\beta b]} \, (\omega_{ab\alpha,\beta} - \omega_{ca\alpha} \omega^c{}_{b\beta})\} + h.c. \, ,$$
$$\tilde{R} = \frac{1}{2} \{f^{\alpha[a} f^{\beta b]} \, (\tilde{\omega}_{ab\alpha,\beta} - \tilde{\omega}_{ca\alpha} \tilde{\omega}^c{}_{b\beta})\} + h.c. \, . \qquad (19.1)$$

Here [2] $f^{\alpha[a} f^{\beta b]} = f^{\alpha a} f^{\beta b} - f^{\alpha b} f^{\beta a}$. $f^a{}_\alpha$, and the two kinds of the spin connection fields, $\omega_{ab\alpha}$ (the gauge fields of S^{ab}) and $\tilde{\omega}_{ab\alpha}$ (the gauge fields of $\tilde{S}^{ab}$), manifest in $d = (3 + 1)$ as the known vector gauge fields and the scalar gauge fields taking care of masses of quarks and leptons and antiquarks and antileptons and the weak boson fields [3], if we replace the covariant derivative $p_{0\alpha}$

$$p_{0\alpha} = p_\alpha - \frac{1}{2} S^{ab} \omega_{ab\alpha} - \frac{1}{2} \tilde{S}^{ab} \tilde{\omega}_{ab\alpha}$$

in Eq. (19.1) with

---

[2] $f^\alpha{}_a$ are inverted vielbeins to $e^a{}_\alpha$ with the properties $e^a{}_\alpha f^\alpha{}_b = \delta^a{}_b$, $e^a{}_\alpha f^\beta{}_a = \delta^\beta_\alpha$, $E = \det(e^a{}_\alpha)$. Latin indices $a, b, .., m, n, .., s, t, ..$ denote a tangent space (a flat index), while Greek indices $\alpha, \beta, .., \mu, \nu, ..\sigma, \tau, ..$ denote an Einstein index (a curved index). Letters from the beginning of both the alphabets indicate a general index ($a, b, c, ..$ and $\alpha, \beta, \gamma, ..$), from the middle of both the alphabets the observed dimensions $0, 1, 2, 3$ ($m, n, ..$ and $\mu, \nu, ..$), indexes from the bottom of the alphabets indicate the compactified dimensions ($s, t, ..$ and $\sigma, \tau, ..$). We assume the signature $\eta^{ab} = diag\{1, -1, -1, \cdots, -1\}$.

[3] Since the multiplication with either γ^a's or $\tilde{\gamma}^a$'s changes the Clifford odd "basis vectors" into the Clifford even objects, and even "basis vectors" commute, the action for fermions can not include an odd numbers of γ^a's or $\tilde{\gamma}^a$'s, what the simple starting action of Eq. (19.1) does not. In the starting action γ^a's and $\tilde{\gamma}^a$'s appear as $\gamma^0 \gamma^a \hat{p}_a$ or as $\gamma^0 \gamma^c \, S^{ab} \omega_{abc}$ and as $\gamma^0 \gamma^c \, \tilde{S}^{ab} \tilde{\omega}_{abc}$.

$$p_{0\alpha} = p_\alpha - \sum_{mf} {}^{I}\hat{\mathcal{A}}_f^{m\dagger} {}^{I}\mathcal{C}_{f\alpha}^m - \sum_{mf} {}^{I}\widehat{\widetilde{\mathcal{A}}}_f^{m\dagger} {}^{I}\widetilde{\mathcal{C}}_{f\alpha}^m ,$$

where the relation among ${}^{I}\widehat{\widetilde{\mathcal{A}}}_f^{m\dagger} {}^{I}\widetilde{\mathcal{C}}_{f\alpha}^m$ and ${}^{II}\widehat{\widetilde{\mathcal{A}}}_f^{m\dagger} {}^{II}\widetilde{\mathcal{C}}_{f\alpha}^m$ with respect to $\omega_{ab\alpha}$ and $\tilde{\omega}_{ab\alpha}$, not discussed directly in this article, needs additional study and explanation.

While in any even dimensional space the superposition of odd products of γ^a's, forming the Clifford odd "basis vectors", offer the description of the internal space of fermions with the half integer spins (manifesting in $d = (3 + 1)$ properties of quarks and leptons and antiquarks and antileptons, with the families included if $d = (13 + 1)$), the superposition of even products of γ^a's, forming the Clifford even "basis vectors", offer the description of the internal space of boson fields with integer spins, manifesting as gauge fields of the corresponding Clifford odd "basis vectors".

The Clifford odd and even "basis vectors" exist also in odd dimensional spaces. In this case their properties differ a lot from the "basis vectors" in even dimensional spaces. The eigenvectors of the operator of handedness are the superposition of the odd and even "basis vectors", offering both handedness, left and right. These basis vectors resembles the ghosts, needed in Feynman diagrams to get read of singularities. This study just starts and needs further comments and understanding.

19.4   Some useful formulas

This appendix contains some equations, needed in this note. More detailed explanations can be found in this proceedings in my talk [4].

The operator of handedness Γ^d is for fermions determined as follows

$$\Gamma = \prod_a (\sqrt{\eta^{aa}}\gamma^a) \cdot \begin{cases} (i)^{\frac{d}{2}}, & \text{for } d \text{ even}, \\ (i)^{\frac{d-1}{2}}, & \text{for } d \text{ odd}, \end{cases} \tag{19.2}$$

The Clifford objects γ^a's and $\tilde{\gamma}^a$'s fulfil the relations

$$\{\gamma^a, \gamma^b\}_+ = 2\eta^{ab} = \{\tilde{\gamma}^a, \tilde{\gamma}^b\}_+ ,$$
$$\{\gamma^a, \tilde{\gamma}^b\}_+ = 0 , \quad (a, b) = (0, 1, 2, 3, 5, \cdots, d) ,$$
$$(\gamma^a)^\dagger = \eta^{aa} \gamma^a , \quad (\tilde{\gamma}^a)^\dagger = \eta^{aa} \tilde{\gamma}^a . \tag{19.3}$$

The choice of the Cartan subalgebra members is made

$$\mathcal{S}^{03}, \mathcal{S}^{12}, \mathcal{S}^{56}, \cdots, \mathcal{S}^{d-1\,d} ,$$
$$S^{03}, S^{12}, S^{56}, \cdots, S^{d-1\,d} ,$$
$$\tilde{S}^{03}, \tilde{S}^{12}, \tilde{S}^{56}, \cdots, \tilde{S}^{d-1\,d} ,$$
$$\mathcal{S}^{ab} = S^{ab} + \tilde{S}^{ab} = i(\theta^a \frac{\partial}{\partial\theta_b} - \theta^b \frac{\partial}{\partial\theta_a}) . \tag{19.4}$$

Nilpotents and projectors are defined as follows [2, 13, 14]

$$\overset{ab}{(k)} := \frac{1}{2}(\gamma^a + \frac{\eta^{aa}}{ik}\gamma^b) , \quad \overset{ab}{[k]} := \frac{1}{2}(1 + \frac{i}{k}\gamma^a\gamma^b) , \tag{19.5}$$

with $k^2 = \eta^{aa}\eta^{bb}$.

One finds, taking Eq. (19.3) into account and the assumption

$$\{\tilde{\gamma}^a B = (-)^B i B\gamma^a\}|\psi_{oc} >,\tag{19.6}$$

with $(-)^B = -1$, if B is (a function of) an odd products of γ^a's, otherwise $(-)^B = 1$ [14], $|\psi_{oc} >$ is defined in Eq. (19.8), the eigenvalues of the Cartan subalgebra operators

$$S^{ab}\overset{ab}{(k)}= \frac{k}{2}\overset{ab}{(k)}, \qquad \tilde{S}^{ab}\overset{ab}{(k)}= \frac{k}{2}\overset{ab}{(k)},$$

$$S^{ab}\overset{ab}{[k]}= \frac{k}{2}\overset{ab}{[k]}, \qquad \tilde{S}^{ab}\overset{ab}{[k]}= -\frac{k}{2}\overset{ab}{[k]}.\tag{19.7}$$

The vacuum state for the Clifford odd "basis vectors", $|\psi_{oc} >$, is defined as

$$|\psi_{oc} >= \sum_{f=1}^{2^{\frac{d}{2}-1}} \hat{b}_f^m{}_{*_A} \hat{b}_f^{m\dagger} |1 > .\tag{19.8}$$

Taking into account Eq. (19.3) it follows

$$\gamma^a\overset{ab}{(k)} = \eta^{aa}\overset{ab}{[-k]}, \quad \gamma^b\overset{ab}{(k)}= -ik\overset{ab}{[-k]}, \quad \gamma^a\overset{ab}{[k]}=\overset{ab}{(-k)}, \quad \gamma^b\overset{ab}{[k]}= -ik\eta^{aa}\overset{ab}{(-k)},$$

$$\tilde{\gamma}^a\overset{ab}{(k)} = -i\eta^{aa}\overset{ab}{[k]}, \quad \tilde{\gamma}^b\overset{ab}{(k)}= -k\overset{ab}{[k]}, \quad \tilde{\gamma}^a\overset{ab}{[k]}= i\overset{ab}{(k)}, \quad \tilde{\gamma}^b\overset{ab}{[k]}= -k\eta^{aa}\overset{ab}{(k)},$$

$$\overset{ab}{(k)}^{\dagger} = \eta^{aa}\overset{ab}{(-k)}, \quad (\overset{ab}{(k)})^2 = 0, \quad \overset{ab}{(k)}\overset{ab}{(-k)}= \eta^{aa}\overset{ab}{[k]},$$

$$\overset{ab}{[k]}^{\dagger} = \overset{ab}{[k]}, \quad (\overset{ab}{[k]})^2 =\overset{ab}{[k]}, \quad \overset{ab}{[k]}\overset{ab}{[-k]}= 0,$$

$$\overset{ab}{(k)}\overset{ab}{[k]} = 0, \quad \overset{ab}{[k]}\overset{ab}{(k)}=\overset{ab}{(k)}, \quad \overset{ab}{(k)}\overset{ab}{[-k]}=\overset{ab}{(k)}, \quad \overset{ab}{[k]}\overset{ab}{(-k)}= 0,$$

$$\overset{ab}{(\tilde{k})}^{\dagger} = \eta^{aa}\overset{ab}{(-\tilde{k})}, \quad (\overset{ab}{(\tilde{k})})^2 = 0, \quad \overset{ab}{(\tilde{k})}\overset{ab}{(-\tilde{k})}= \eta^{aa}\overset{ab}{[\tilde{k}]},$$

$$\overset{ab}{[\tilde{k}]}^{\dagger} = \overset{ab}{[\tilde{k}]}, \quad (\overset{ab}{[\tilde{k}]})^2 =\overset{ab}{[\tilde{k}]}, \quad \overset{ab}{[\tilde{k}]}\overset{ab}{[-\tilde{k}]}= 0,$$

$$\overset{ab}{(\tilde{k})}\overset{ab}{[\tilde{k}]} = 0, \quad \overset{ab}{[\tilde{k}]}\overset{ab}{(\tilde{k})}=\overset{ab}{(\tilde{k})}, \quad \overset{ab}{(\tilde{k})}\overset{ab}{[-\tilde{k}]}=\overset{ab}{(\tilde{k})}, \quad \overset{ab}{[\tilde{k}]}\overset{ab}{(-\tilde{k})}= 0.\tag{19.9}$$

19.5   Acknowledgment

References

1. N. Mankoč Borštnik, "Spin connection as a superpartner of a vielbein", *Phys. Lett.* **B 292** (1992) 25-29.

2. N. Mankoč Borštnik, "Spinor and vector representations in four dimensional Grassmann space", *J. of Math. Phys.* **34** (1993) 3731-3745.
3. N. Mankoč Borštnik, "Unification of spin and charges in Grassmann space?", hep-th 9408002, IJS.TP.94/22, Mod. Phys. Lett.**A (10)** No.7 (1995) 587-595.
4. N. Mankoč Borštnik, "Clifford odd and even objects, offering description of internal space of fermion and boson fields, respectively, open new insight into next step beyond standard model", contribution in this proceedings .
5. N. S. Mankoč Borštnik, H. B. Nielsen, "How does Clifford algebra show the way to the second quantized fermions with unified spins, charges and families, and with vector and scalar gauge fields beyond the *standard model*", Progress in Particle and Nuclear Physics, http://doi.org/10.1016.j.ppnp.2021.103890 .
6. N. S. Mankoč Borštnik, "How Clifford algebra can help understand second quantization of fermion and boson fields", [arXiv: 2210.06256. physics.gen-ph].
7. N. S. Mankoč Borštnik, "Clifford odd and even objects offer description of internal space of fermions and bosons, respectively, opening new insight into the second quantization of fields", The 13th Bienal Conference on Classical and Quantum Relativistic Dynamics of Particles and Fields IARD 2022, Prague, $6 - 9$ June [http://arxiv.org/abs/2210.07004].

8. N.S. Mankoč Borštnik, H.B.F. Nielsen, "Understanding the second quantization of fermions in Clifford and in Grassmann space", *New way of second quantization of fermions — Part I and Part II*, in this proceedings [arXiv:2007.03517, arXiv:2007.03516].
9. N. S. Mankoč Borštnik, "How do Clifford algebras show the way to the second quantized fermions with unified spins, charges and families, and to the corresponding second quantized vector and scalar gauge field ", Proceedings to the 24rd Workshop "What comes beyond the standard models", 5 - 11 of July, 2021, Ed. N.S. Mankoč Borštnik, H.B. Nielsen, D. Lukman, A. Kleppe, DMFA Založništvo, Ljubljana, December 2021, [arXiv:2112.04378] .
10. N.S. Mankoč Borštnik, H.B. Nielsen, "Why odd space and odd time dimensions in even dimensional spaces?" Phys. Lett. B 486 (2000)314-321.
11. N.S.Mankoč Borštnik, H.B.Nielsen, "Why Nature has made a choice of one time and three space coordinates?", [hep-ph/0108269], *J. Phys. A:Math. Gen.* **35** (2002) 10563-10571.
12. N.S. Mankoč Borštnik, H.B. Nielsen, D. Lukman, "Unitary representations, noncompact groups SO(q, d-q) and more than one time", Proceedings to the 5th International Workshop "What Comes Beyond the Standard Model", 13 -23 of July, 2002, VolumeII, Ed. Norma Mankoč Borštnik, Holger Bech Nielsen, Colin Froggatt, Dragan Lukman, DMFA Založništvo, Ljubljana December 2002, hep-ph/0301029.
13. N.S. Mankoč Borštnik, H.B.F. Nielsen, *J. of Math. Phys.* **43**, 5782 (2002) [arXiv:hep-th/0111257].
14. N.S. Mankoč Borštnik, H.B.F. Nielsen, "How to generate families of spinors", *J. of Math. Phys.* **44** 4817 (2003) [arXiv:hep-th/0303224].

20 Modules over Clifford algebras as a basis for the theory of second quantization of spinors

V. V. Monakhov

Ulyanovskaya 1, Saint Petersburg, 198504, Russia
Saint Petersburg State University, v.v.monahov@spbu.ru

Abstract. We have studied the properties of the fundamental constructions of QFT - algebraic spinors, Clifford vacua generated by primitive idempotents of the Clifford algebra of arbitrary even dimension, and the large Clifford algebra in the momentum phase space generated by the creation and annihilation operators of spinors.
We have proved that a connected Lie group of Lorentz transformations that preserves relations of the CAR algebra of spinor operators of creation and annihilation leads to the appearance of a small Clifford algebra. In it, basis Clifford vectors are gamma operators, whose matrix representation are Dirac gamma matrices, as well as two additional gamma operators corresponding to the internal degrees of freedom of spinors.
We have constructed a Lorentz-invariant spinor vacuum operator of the small Clifford algebra from the product of the Clifford vacua operators of the large Clifford algebra.

20.1 Introduction

In 1913 Eli Cartan discovered spinors as two-valued irreducible complex representations of simple Lie groups [1]. The importance of spinors in physics was realized after the appearance in 1927 of Pauli's work on the spin of the electron [2] and in 1928 of the Dirac equation explaining the relativistic properties of the electron [3]. Brauer and Weil in 1935 laid down an approach to the theory of spinors based on Clifford algebras [4].
Pauli in 1940 proved an unambiguous connection between spin and statistics of particles in the presence of Lorentz covariance [5]. He proved that if the vacuum energy is assumed to be zero, then under the requirement that the energy be positive, particles with half-integer spins must satisfy the Fermi-Dirac statistics. And that from the requirement of relativistic causality (commutation of operators of observables at points separated by spacelike intervals) follows the Bose-Einstein statistics for particles with an arbitrary integer spin. Since then, the concepts of "spinor" and "fermion" have been considered identical.

Nevertheless, the term "fermion" is usually used for physical particles with a half-integer spin, and "spinor" for mathematical objects that are two-valued representations of groups of pseudo-orthogonal rotations (we will call them rotations below without indicating pseudo-orthogonality). Since, mathematically, states with half-integer spin greater than ½ can be expressed in terms of the product of an odd number of states with spin ½, it suffices to consider only spinors with spin ½. Therefore, below the word "spinor" will mean a spinor with spin ½.

A mathematically rigorous theory of spinors as representations of Clifford algebras was formulated by Chevalley [6]. Lounesto and a number of other authors developed the theory of spinors as elements of left ideals of Clifford algebras ([7–10] and so on). Such spinors are called algebraic [8–10]. The theory of algebraic spinors in the modern formulation is the theory of spinor modules. In this article, we will show that the solution of a number of problems, both in the theory of spinors as elements of ideals of Clifford algebras, and in the theory of second quantization based on CAR algebras, lies in considering spinors as elements of a module over Clifford algebra.

20.2   Spinor modules

A spinor module (a spinor space) is a module over the Clifford algebra. The theory of such modules as the most general mathematical theory of spinors was developed relatively recently [11, 12] and therefore is usually not familiar to physicists using Clifford algebras. Let M be an Abelian group, K a ring, $m, m_1, m_2 \in M$, $k, k_1, k_2 \in K$. A left module M over K is an Abelian group with the operation of left multiplication of elements of M by elements of the ring K, satisfying the relations

$$
\begin{aligned}
(k_1 k_2)m &= k_1(k_2 m), \\
1m &= m, \\
k(m_1 + m_2) &= km_1 + km_2, \\
(k_1 + k_2)m &= k_1 m + k_2 m.
\end{aligned}
\tag{20.1}
$$

For the right module, the relations are similar, but the multiplication by the elements of the ring is carried out on the right. For a two-sided module, multiplication by ring elements can be done both on the left and on the right.

If the ring K is an algebra, then the module is a module over this algebra. In this case, relations (20.1) define a homomorphism of the algebra K into the module M. An algebra homomorphism is a mapping that preserves the basic operations and basic relations of the given algebra. In particular, the Clifford algebra is a two-sided module over itself.

An important consequence of the theory of modules is that there is a one-to-one correspondence (up to isomorphism) between linear representations of any associative algebra and modules over this algebra. This means that the results obtained for matrix representations of algebras are of much greater significance than one might expect – they are applicable to any linear representations of these algebras. The question of the equivalence or non-equivalence of certain algebraic constructions for the representation of spinors is also removed – they are equivalent if their matrix representations coincide (up to isomorphism).

Thus, the matrix algebra generated by the Dirac gamma matrices is equivalent to the corresponding Clifford algebra, and the spinor space in the form of a matrix column is equivalent to the minimal ideal of the Clifford algebra generated using a primitive idempotent. In addition, when trying to create algebraic constructions describing spinors (for example, in [13]), in order to verify the correctness of the algebraic constructions and

the physical interpretation of the results, one should either explicitly check the presence of an algebra homomorphism (20.1) or check the corresponding matrix representations [14]. Consider now the application of modules over algebra in physics. Physicists began to actively use the work with modules over algebras after the creation of quantum mechanics. Paul Dirac called the left modules of the algebra of operators of quantum mechanics ket-vectors $\mid \xi >$, while the right modules are bra-vectors $< \xi \mid$. A feature of a one-sided (left or right) module is that the elements of the module can only be added, but not multiplied. Although elements of the left module can be multiplied by elements of the algebra on the left, and elements of the right module can be multiplied on the right. The principle of superposition in quantum mechanics is a manifestation of the fact that state vectors are elements of a module.

Working with modules over matrix algebra is used in the theory of Dirac spinors. In matrix representation, the Dirac spinor is a column with four components

$$\Psi_D = \begin{pmatrix} \psi^1 \\ \psi^2 \\ \psi^3 \\ \psi^4 \end{pmatrix}. \tag{20.2}$$

It is a left module over the algebra of 4×4 matrices.

20.3   Algebraic spinors

An algebraic spinor Ψ in the matrix representation can be given by a 4×4 matrix. It has four columns

$$\Psi = \begin{pmatrix} \psi_1^1 & \psi_2^1 & \psi_3^1 & \psi_4^1 \\ \psi_1^2 & \psi_2^2 & \psi_3^2 & \psi_4^2 \\ \psi_1^3 & \psi_2^3 & \psi_3^3 & \psi_4^3 \\ \psi_1^4 & \psi_2^4 & \psi_3^4 & \psi_4^4 \end{pmatrix}. \tag{20.3}$$

corresponding to the four Dirac spinors

$$\Psi_1 = \begin{pmatrix} \psi_1^1 \\ \psi_1^2 \\ \psi_1^3 \\ \psi_1^4 \end{pmatrix}, \ \Psi_2 = \begin{pmatrix} \psi_2^1 \\ \psi_2^2 \\ \psi_2^3 \\ \psi_2^4 \end{pmatrix}, \ \Psi_3 = \begin{pmatrix} \psi_3^1 \\ \psi_3^2 \\ \psi_3^3 \\ \psi_3^4 \end{pmatrix}, \ \Psi_4 = \begin{pmatrix} \psi_4^1 \\ \psi_4^2 \\ \psi_4^3 \\ \psi_4^4 \end{pmatrix}. \tag{20.4}$$

A left ideal of an algebra A is a subalgebra that is closed under multiplication by elements of the algebra A. An ideal is called minimal if it does not contain subideals. That is, if it cannot be decomposed into the sum of two or more ideals. The minimal ideal is generated by the product of all elements of the algebra by a primitive idempotent. An idempotent is said to be primitive if it cannot be decomposed into two (or more) orthogonal idempotents. In the Clifford algebra, the spaces of spinors (minimal left ideals) corresponding to Dirac spinors are generated by four primitive idempotents I_j, $j = 1, 2, 3, 4$, having the idempotent property

$$(I_j)^2 = I_j, \tag{20.5}$$

and the orthogonality property

$$I_j I_k = 0, \ j \neq k. \tag{20.6}$$

In the matrix representation, matrices with one unit element on the diagonal can be chosen as such idempotents [10]:

$$I_1 = \begin{pmatrix} 1 & 0 & 0 & 0 \\ 0 & 0 & 0 & 0 \\ 0 & 0 & 0 & 0 \\ 0 & 0 & 0 & 0 \end{pmatrix}, I_2 = \begin{pmatrix} 0 & 0 & 0 & 0 \\ 0 & 1 & 0 & 0 \\ 0 & 0 & 0 & 0 \\ 0 & 0 & 0 & 0 \end{pmatrix}, I_3 = \begin{pmatrix} 0 & 0 & 0 & 0 \\ 0 & 0 & 0 & 0 \\ 0 & 0 & 1 & 0 \\ 0 & 0 & 0 & 0 \end{pmatrix}, I_4 = \begin{pmatrix} 0 & 0 & 0 & 0 \\ 0 & 0 & 0 & 0 \\ 0 & 0 & 0 & 0 \\ 0 & 0 & 0 & 1 \end{pmatrix}. \tag{20.7}$$

Left multiplication of any general matrix (20.3) by idempotents (20.7) leaves nonzero only the columns corresponding to the Dirac spinors (20.4):

$$\Psi I_1 = \begin{pmatrix} \psi_1^1 & 0 & 0 & 0 \\ \psi_1^2 & 0 & 0 & 0 \\ \psi_1^3 & 0 & 0 & 0 \\ \psi_1^4 & 0 & 0 & 0 \end{pmatrix}, \Psi I_2 = \begin{pmatrix} 0 & \psi_2^1 & 0 & 0 \\ 0 & \psi_2^2 & 0 & 0 \\ 0 & \psi_2^3 & 0 & 0 \\ 0 & \psi_2^4 & 0 & 0 \end{pmatrix},$$

$$\Psi I_3 = \begin{pmatrix} 0 & 0 & \psi_3^1 & 0 \\ 0 & 0 & \psi_3^2 & 0 \\ 0 & 0 & \psi_3^3 & 0 \\ 0 & 0 & \psi_3^4 & 0 \end{pmatrix}, \Psi I_4 = \begin{pmatrix} 0 & 0 & 0 & \psi_4^1 \\ 0 & 0 & 0 & \psi_4^2 \\ 0 & 0 & 0 & \psi_4^3 \\ 0 & 0 & 0 & \psi_4^4 \end{pmatrix}. \tag{20.8}$$

It is easy to see that further multiplication ΨI_j on the left by an arbitrary number of 4×4 matrices keeps only column number j nonzero. These columns are left ideals of the algebra, the spinor spaces.

In the case of d-dimensional spinors, for even $d = 2n$, there are 2^n columns in a column of 2^n components (that is, 2^n independent spinors), and the matrix corresponding to the algebraic spinor has size $2^n \times 2^n$. In what follows, we will consider only the case of even d, since in the odd-dimensional case the center of Clifford algebra is nontrivial, and the similarity transformation is not an inner automorphism of the algebra. Therefore, in this case, a number of properties of the spaces of vectors and spinors differ from those observed physically.

For even d, it is possible to pass to the equivalent matrix representation of the idempotents of the Clifford algebra using the similarity transformation

$$I_j' = BI_j B^{-1}, \tag{20.9}$$

along with all other elements A of the given matrix representation

$$A' = BAB^{-1}, \tag{20.10}$$

for an arbitrary invertible matrix B. Without loss of generality, we can assume that its determinant is equal to 1. Moreover, it is obvious that, as a result of transformation (20.9), the idempotents retain properties (20.5) and (20.6).

It was shown in [10] that by a similarity transformation of the form (20.10), a set of primitive idempotents of the matrix representation of any complex Clifford algebra for even dimension d can be reduced to the form (20.7). Therefore, for spinor modules, it is sufficient to consider only idempotents of the form (20.7) and spaces of spinors of the form (20.8).

Basis orthonormal vectors e_i of the d-dimensional Clifford algebra in the matrix representation are usually called d-dimensional Dirac gamma matrices γ_i. The group of Clifford rotations and reflections in the case of the signature of the Clifford algebra $(p, q) = (1, d-1)$

or $(p, q) = (d − 1, 1)$ is usually called Lorentz d-dimensional group. Here p is the number of basis vectors with a positive signature, and q with a negative one. Due to the fact that rotations groups are isomorphic for $(p, q) = (1, d−1)$ and $(p, q) = (d−1, 1)$, and reflections from the full Lorentz group are not included in the transformations of the Poincaré group, we will consider only the signature $(p, q) = (1, d − 1)$. The results obtained can be easily generalized to spaces of even dimension of arbitrary signature.

The Cartan subgroup of a connected Lie group is the maximal connected Abelian subgroup of this group. Its Lie algebra is called the Cartan subalgebra of the Lie algebra of the given group. The Cartan subgroup of the Lie algebra of the Lorentz group is the Lie group generated by the maximum possible number of linearly independent commuting elements of the corresponding Clifford algebra. In this case, the Clifford algebra acts as a universal enveloping algebra for the Lie algebra of the Lorentz group.

Each Lie algebra can be uniquely associated with a universal enveloping algebra (up to isomorphism), a Cartan subalgebra can be uniquely associated in the Clifford algebra with a subalgebra of the Clifford algebra generated by the maximum possible number of linearly independent commuting elements of the Clifford algebra. It is universal enveloping algebra of the Cartan subalgebra. In the matrix representation, the basis of this algebra can be transformed by a similarity transformation to a diagonal form. We choose the generators of the Lorentz group $\gamma^0\gamma^3, \gamma^1\gamma^2, \cdots, \gamma^{d−1}\gamma^d$ as the basis of this algebra. They commute, and in the chiral representation of the gamma matrices are diagonal. Using them, we construct 2^n idempotents

$$I_{\pm 03, \pm 12, \cdots, \pm(d−1)d} = \frac{1 \pm \gamma^0\gamma^3}{2} \frac{1 \pm \gamma^1\gamma^2}{2} \cdots \frac{1 \pm \gamma^{d−1}\gamma^d}{2}. \tag{20.11}$$

It is easy to see that idempotents (20.11) will have a form similar to (20.7), but for $2^n \times 2^n$ matrices, with one unit element on the diagonal and with zero other elements of the matrix. It is also easy to check that if we denote the idempotents (20.11) as I_j, then

$$1 = \sum_{j=1}^{2^n} I_j. \tag{20.12}$$

Idempotents (20.11) were constructed in [16, 17], and decomposition (20.12) for Clifford algebras was obtained in [12]. It was used implicitly in [17] and explicitly by us in [15] to decompose algebraic spinors into spinor modules in RQFT.

Note that due to the presence of an imaginary unit in idempotents (20.11), they are admissible only in the complex Clifford algebra $Cl^{1,d−1}(\mathbb{C})$ and are inadmissible in the real algebra $Cl^{1,d−1}(\mathbb{R})$. However, the multiplication of elements $Cl^{1,d−1}(\mathbb{R})$ by any of the idempotents (20.11) is a homomorphism of the algebra $Cl^{1,d−1}(\mathbb{R})$. Therefore, the construction of spinor modules over this algebra using them is correct. Similarly, it is not a problem that Dirac gamma matrices are complex, although the corresponding Clifford algebra is real. Corresponding mapping from the Clifford algebra to the algebra generated by Dirac gamma matrices is a homomorphism. This matrix algebra is a two-sided module over the Clifford algebra. But at the same time, it is impossible to multiply the elements of this matrix algebra by an imaginary unit, since this violates the homomorphism.

20.4   Problems of the theory of algebraic spinors

Despite being more general than previous theories of spinors, there are a number of problems in the theory of algebraic spinors.

The first of them is the presence of 2^n independent spinors. They have been interpreted in a variety of ways, from completely ignoring "extra" spinors [9, 18] to considering them as independent spinor fields [17] and even interpreting them as states of fermions and bosons of the Standard Model [13]. In [21] and our work [15], an approach was found to solve this problem, which consists in the fact that these spinors belong to states with different vacua. In [21], the author proposed various expressions for Clifford vacua and indicated the fact that swapping the creation and annihilation operators changes one Clifford vacuum for another. In [15] we made a correct construction of the Clifford vacua and showed that they have the properties of spinors. However, as will be shown below, the spinor vacuum has a more complex structure than the Clifford vacuum. The correct construction of spinor vacua will be given below when considering the properties of the CAR algebra.

The second problem in the theory of algebraic spinors is related to conjugate spinors. Each fermion, described by the matrix column Ψ, has an antiparticle, which in Dirac's theory is described by the Dirac conjugate quantity – the matrix row $\bar{\Psi} = (\gamma^0 \Psi)^+$. The matrix column and the matrix row exist in different spaces, and the corresponding states cannot be added. However, algebraic spinors belong to the same Clifford algebra, and their matrix representations belong to the same matrix algebra. So the question arises why they can not mix. Moreover, the Dirac conjugation of a matrix of the form (20.3) gives a matrix of a similar form. That is, the antispinor state is a superposition of spinor states. The solution of this problem, as we show below, follows from the construction of spinors and spinor vacua in the framework of the CAR algebra.

The third problem is related to the impossibility of constructing the spinor vacuum as a scalar. The Clifford vacuum cannot be a scalar. Under Lorentz transformations, it transforms as a spinor. Due to the presence of decomposition (20.12), the unit 1 in the one-sided spinor module is decomposed into 2^n spinors and has the property of a spinor. Therefore, it also cannot be a scalar. We will consider this problem below.

The fourth problem is related to the physics of actually observed fermions. Fermions, as you know, can be created and annihilated. To describe these processes, the so-called theory of second quantization was developed, the mathematical basis of which is the theory of CAR algebras. The study of the CAR algebra together with the Clifford algebra corresponding to the Lorentz group will be done next.

20.5   Clifford vacuum

In accordance with [19–21], the Clifford vacuum Ψ_V is built using the creation a_k^+ and annihilation a_k operators built from the basic Clifford vectors, in this case, from the gamma matrices

$$a_1 = \frac{\gamma^0 + \gamma^3}{2}, a_1^+ = \frac{\gamma^0 - \gamma^3}{2}, a_2 = \frac{\gamma^1 - i\gamma^2}{2}, a_2^+ = \frac{-\gamma^1 - i\gamma^2}{2}, \ldots,$$

$$a_n = \frac{\gamma^{d-1} - i\gamma^d}{2}, a_n^+ = \frac{-\gamma^{d-1} - \gamma^d}{2}. \tag{20.13}$$

as a state for which

$$a_k \Psi_V = 0 \tag{20.14}$$

for every k.

Note that for $d > 2$, such an operation is possible only in the complex Clifford algebra $Cl^{1,d-1}(\mathbb{C})$, or in the complex module over the real algebra $Cl^{1,d-1}(\mathbb{R})$, or in the real Clifford algebra $Cl^{d/2,d/2}(\mathbb{R})$.

It is obvious that

$$\Psi_V = a_1 a_2 \cdots a_n A \tag{20.15}$$

where A is an arbitrary nonzero element of the algebra that does not annihilate $a_1 a_2 \cdots a_n$. Operators (20.13) satisfy the anticommutation relations

$$\{a_j^+, a_k\} = \delta_j^k,$$
$$\{a_j, a_k\} = \{a_j^+, a_k^+\} = 0. \tag{20.16}$$

There are various options for specifying the factor A in (20.15) [21]. It was noted in [21] that the action $a_j^+ \Psi_V$ of the spinor creation operator a_j^+ on the vacuum Ψ_V for any j should create a state with one spinor. This spinor must belong to the spinor space, that is, the minimal left ideal. Therefore, AV in (20.15) should be represented as a product of some element A_1 of the algebra and a primitive idempotent I. That is why

$$\Psi_V = a_1 a_2 \cdots a_n A_1 I. \tag{20.17}$$

Any primitive idempotent can be chosen as I [21]. However, it is natural to require that the action of the vacuum operator on itself leaves the vacuum invariant

$$\Psi_V \Psi_V = (\Psi_V)^2 = \Psi_V. \tag{20.18}$$

Requirement (20.18) means that Ψ_V must be an idempotent.

Let us show the uniqueness of the Clifford vacuum for operators (20.13) under conditions (20.15) and (20.18). We decompose A into a sum of monoms in terms of the basis of the Clifford algebra, for which we use sums and products of operators (20.13). In this case, in the monoms, all operators a_k can be placed to the left of a_k^+ using relations (20.16). Since

$$\Psi_V \Psi_V = (\Psi_V)^2 = \Psi_V = a_1 a_2 \cdots a_n A a_1 a_2 \cdots a_n A, \tag{20.19}$$

all monoms, at least one element of which commutes or anticommutes with any of the operators a_k, will give a zero contribution on the right side of (20.19). Only a_k^+ does not commute and does not anticommute with a_k. Therefore, a nonzero contribution to Ψ_V gives only $\pm a_1^+ a_2^+ \cdots a_n^+$, and we can assume up to a sign that

$$\Psi_V = a_1 a_1^+ a_2 a_2^+ \cdots a_n a_n^+. \tag{20.20}$$

From (20.13) it follows that

$$a_1 a_1^+ = \frac{1 - \gamma^0 \gamma^3}{2}, \, a_2 a_2^+ = \frac{1 - i\gamma^1 \gamma^2}{2}, \ldots, a_n a_n^+ = \frac{1 - i\gamma^{d-1} \gamma^d}{2}. \tag{20.21}$$

Wherein

$$(a_j a_j^+)^2 = a_j a_j^+,$$
$$(a_j^+ a_j)^2 = a_j^+ a_j \tag{20.22}$$

for each j. Here and below there is no summation over repeated indices.

From (20.20), (20.21) and (20.11) we obtain

$$\Psi_V = I_{-03,-12,\cdots,-(d-1)d} = \frac{1 - \gamma^0 \gamma^3}{2} \frac{1 - \gamma^1 \gamma^2}{2} \cdots \frac{1 - \gamma^{d-1} \gamma^d}{2}. \tag{20.23}$$

Such a definition is ambiguous due to the arbitrariness in (20.11), (20.13) and (20.23) the signs in front of the gamma matrices. That is, in the choice of which operator to consider as the operator of creation, and which one as the operator of annihilation. In accordance with [15], each of the primitive idempotents (20.11) is a Clifford vacuum, but in different idempotents the role of some of the creation and annihilation operators has changed. Therefore, in d-dimensional space, where $d = 2n$, there are 2^n independent Clifford vacua.

The idempotents (20.11) are Hermitian. Therefore, when choosing any of them as the Clifford vacuum, we automatically obtain that all Clifford vacua operators are Hermitian

$$\Psi_V = \Psi_V^+. \tag{20.24}$$

Conditions (20.24) and (20.15) imply

$$\Psi_V^+ = A^+ a_n^+ \cdots a_2^+ a_1^+ = a_1 a_2 \cdots a_n A. \tag{20.25}$$

That is why

$$A = A_2 a_n^+ \cdots a_2^+ a_1^+, \tag{20.26}$$

where A_2 is some element of the algebra.

From (20.24)-(20.26) we obtain

$$\Psi_V = a_1 a_2 \cdots a_n A_2 a_n^+ \cdots a_2^+ a_1^+, \tag{20.27}$$

As before, we expand A2 in terms of monoms with operators a_j to the left of a_j^+. The contribution on the right side of (20.27) of all monoms other than 1 with some numerical factor, is equal to zero. Therefore

$$\Psi_V = \pm a_1 a_2 \cdots a_n a_n^+ \cdots a_2^+ a_1^+, \tag{20.28}$$

Taking into account (20.16), we have obtained formula (20.20) up to sign. Based on this, at first glance, conditions (22.11) and (20.24) rather than (22.11) and (20.18) can be used to choose the Clifford vacuum formula. However, when transforming elements of the algebra according to formulas (20.9)-(20.10), conditions (22.11) and (20.18) will be preserved, but condition (20.24) will be violated in the case of non-unitary matrices B. Therefore, to specify the Clifford vacuum operator, one should choose conditions (22.11) and (20.18).

Consider a left ideal (that is, the spinor space) formed by left multiplying the elements of the Clifford algebra by the primitive idempotent (20.23). Such a mapping is a homomorphism and defines a Clifford module. In it, the unit 1 of the Clifford algebra goes into the idempotent (20.23), that is, this idempotent is the unit 1_m of this module. That is why

$$1_m = \Psi_V,$$
$$a_j 1_m = 0, \ \forall j. \tag{20.29}$$

Therefore, we can designate the creation operators as Grassmann variables, and the annihilation operators as derivatives with respect to them

$$a_j^+ = \theta^j,$$
$$a_j = \frac{\partial}{\partial \theta^j}. \tag{20.30}$$

In this case, conditions

$$a_j^+ 1_m = \theta^j 1_m = \theta^j \neq 0,$$
$$a_j 1_m = \frac{\partial}{\partial \theta^j} 1_m = 0 \tag{20.31}$$

are satisfied.

The anti-Hermitian operator $S_{03} = \frac{i\gamma^0 \gamma^3}{2}$ is a d-dimensional boost operator in the plane γ^0, γ^3, and the Hermitian operators

$$S_{12} = \frac{i\gamma^1 \gamma^2}{2}, \ldots, S_{d-1,d} = \frac{i\gamma^{d-1} \gamma^d}{2} \tag{20.32}$$

are d-dimensional spin operators and correspond to rotations in the planes $\gamma^1, \gamma^2, .., \gamma^d$. These operators have eigenvalues $-i/2, -1/2, \ldots, -1/2$ on the eigenvector (20.15) for any A. That is, Clifford vacuum corresponds to the state with the lowest (lowest sign) half-integer spin. That is, it is a spinor.

Obviously, the Clifford vacuum Ψ_V cannot be a scalar, since the requirement $\Psi_V = 1$ is incompatible with conditions (20.13)-(22.11). Therefore, it is not invariant under Lorentz transformations and cannot be considered as a spinor vacuum (or, what is the same one, fermionic vacuum), corresponding to actually observed spinors. We have constructed such a vacuum in the framework of the theory of CAR-algebraic spinors (previously we called them superalgebraic) [22–24]. In this paper, we have studied the properties of spinors based on the theory of CAR algebras.

20.6   Second quantization and CAR algebra

The development of the mathematical theory of second quantization followed a parallel branch with the theory of algebraic spinors and practically did not intersect with it. Fermion field quantization based on canonical anticommutation relations (CAR) was introduced by Jordan and Wigner in 1928 [25]. In modern quantum field theory, the algebra of canonical anticommutation relations (CAR algebra) is considered as fundamental in describing the properties of spinors. Relativistic quantum field theory (RQFT) uses the second quantization method to describe systems with the creation and annihilation of field quanta. Its foundations for spinors were formulated by Schwinger in 1951-1953 [26, 27]. Mathematical substantiation of the theory of second quantization was developed on the basis of the theory of CAR algebras in the works of Gårding and Wightman [28], Araki and Wyss [29], Berezin [30] and so on. RQFT is based on the theory of second quantization and canonical anticommutation relations, as well as on infinitesimal transformations of fields and operators. In the modern mathematical interpretation, these are transformations of the Poincaré group and the Lie algebra corresponding to it.

Anticommutation relations for the fermion creation operator $a_j(p)^+$ (with number j and spatial momentum p) and the fermion annihilation operator $a_k(p')$ (with number k and spatial momentum p') acting on the Hilbert space can be written as [31]

$$\{a_k(p)^+, a_l(p')\} = \delta_l^k \delta(p - p'), \tag{20.33}$$

$$\{a_k(p), a_l(p')\} = \{a_k(p)^+, a_l(p')^+\} = 0. \tag{20.34}$$

In fact, the momentum spectrum of fermions in the free state is not continuous, but quasi-continuous discrete, with very small distances between discrete levels. The size L of the flat space (the Universe) is very large, and we can assume that it tends to infinity $L \to \infty$. In this case, cyclic Born-von Karman boundary conditions can be set, and a discrete spectrum of momenta pi is obtained with an infinitely small momentum step $\Delta p = 2\pi\hbar/L \to 0$.

Let us replace equations (20.33)–(20.34) for the continuous spectrum with equations for the discrete quasi-continuous spectrum [22]. In this case, the Dirac delta function in (20.33) must be replaced by its discrete analog, and we obtain discrete relations [22]

$$\{a_k(p_i)^+, a_l(p_j)\} = \frac{1}{\Delta^3 p} \delta_l^k \delta_j^i, \tag{20.35}$$

$$\{a_k(p_i), a_l(p_j)\} = \{a_k(p_i)^+, a_l(p_j)^+\} = 0. \tag{20.36}$$

For operators related to the same value of the spatial momentum $p_i = p_j$, they coincide, up to normalization, with conditions (20.16), where the discrete value of the momentum is one of the parts of the particle-type multi-index.

Let us introduce the normalization of the creation and annihilation operators so

$$A_k(p_i) = \sqrt{\Delta^3 p} \; a_k(p_i), \tag{20.37}$$

that their anticommutation relations

$$\{A_k(p_i)^+, A_l(p_j)\} = \delta_l^k \delta_j^i, \tag{20.38}$$

$$\{A_k(p_i), A_l(p_j)\} = \{A_k(p_i)^+, A_l(p_j)^+\} = 0. \tag{20.39}$$

completely coincide in form with (20.16).
Infinite-dimensional algebra of operators (20.37) is called the CAR algebra [28, 29].
Let us introduce operators

$$\begin{aligned} \Gamma_{+ki} &= A_k(p_i)^+ + A_l(p_i), \\ \Gamma_{-ki} &= A_k(p_i)^+ - A_l(p_i). \end{aligned} \tag{20.40}$$

From (20.40) it follows that

$$\begin{aligned} (\Gamma_\alpha)^2 &= 1, \quad \alpha = +ki, \\ (\Gamma_\alpha)^2 &= -1, \quad \alpha = -ki, \\ \{\Gamma_\alpha, \Gamma_\beta\} &= 0, \; \alpha \neq \beta. \end{aligned} \tag{20.41}$$

Formulas (20.41) can be generalized as

$$\{\Gamma_\alpha, \Gamma_\beta\} = 2\eta_{\alpha\beta}, \; \eta_{\alpha\beta} = \mathrm{diag}(+1, -1, +1, -1, \ldots). \tag{20.42}$$

Formula (20.42) shows that CAR algebra is an infinite-dimensional countable Clifford algebra whose operators are defined on a Hilbert space. This fact is well known [32] and is even used as one of the ways to define CAR algebras instead of specifying canonical anticommutation relations [33]. We called this algebra large Clifford algebra [24].
Let us find out the transformation laws for operators $a_k(p_i)$ and $a_k(p_i)^+$ under Lorentz transformations by analogy with [31], pp.192-193. But, in contrast to [31], we take into account that during boosts, the positive-frequency and negative-frequency components of the spinor must mix. Therefore, relations (20.35)–(20.36) are true only for $p_i \to 0$. Let us denote for this case

$$\begin{aligned} a_k(p_i)^+ &= \theta^k(p_i), \\ a_k(p_i) &= \frac{\partial}{\partial\theta^k(p_i)}, \\ \Gamma_{+ki} &= \sqrt{\Delta^3 p} \; (\theta^k(p_i) + \frac{\partial}{\partial\theta^k(p_i)}), \\ \Gamma_{-ki} &= \sqrt{\Delta^3 p} \; (\theta^k(p_i) - \frac{\partial}{\partial\theta^k(p_i)}). \end{aligned} \tag{20.43}$$

Then

$$\begin{aligned} \{\frac{\partial}{\partial\theta^k(p_i)}, \theta^l(p_j)\} &= \frac{1}{\Delta^3 p} \delta_l^k \delta_j^i, \\ \{\frac{\partial}{\partial\theta^k(p_i)}, \frac{\partial}{\partial\theta^l(p_j)} &= \{\theta^k(p_i), \theta^l(p_j)\} = 0. \end{aligned} \tag{20.44}$$

Relations (20.44) are just another form of relations (20.42) of the CAR algebra as a Clifford algebra. We require that Lorentz boosts transform the creation and annihilation operators for momentum p_i into the creation and annihilation operators for another momentum. That

is, we require that Lorentz boosts transform the relations (20.44) for momentum pi into relations (20.44) for another momentum. Hence, relations (20.42) of the Clifford algebra transform to

$$\{\Gamma'_\alpha, \Gamma'_\beta\} = 2\eta_{\alpha\beta}, \tag{20.45}$$

where Γ'_α and Γ'_β are transformed Dirac matrices.

It follows from the generalized Pauli theorem [34] that matrices Γ'_λ and Γ_λ are related by the formula

$$\Gamma'_\alpha = B\Gamma_\alpha B^{-1}, \tag{20.46}$$

where B is some invertible element of the Clifford algebra.

Consider infinitesimal transformations when

$$B = 1 + dG = e^{dG}, \tag{20.47}$$

where dG is some infinitesimal element of the large Clifford algebra.

Denote a commutator of dG with following elements as $d\hat{G} = [dG, \cdot]$, the operator $\frac{\partial}{\partial\theta^k(0)}$ after the boost to the finite momentum p_i as $b_k(p_i)$, and the operator $\theta^k(0)$ after the boost as $\bar{b}_k(p_i)$.

Then

$$\Gamma'_\lambda = (1 + dG)\Gamma_\lambda(1 - dG) = (1 + d\hat{G})\Gamma_\lambda = e^{d\hat{G}}\Gamma_\lambda. \tag{20.48}$$

We have obtained infinitesimal transformations of the Lie group. By integrating these transformations, we obtain similar formulas for the finite values of the rotation angles. In this case, the formulas for the operators after the Lorentz transformation will look like

$$b_k(p_i) = e^{\hat{G}}\frac{\partial}{\partial\theta^k(0)},$$
$$\bar{b}_k(p_i) = e^{\hat{G}}\theta^k(0). \tag{20.49}$$

and relations (20.44) will look

$$\{b_k(p_i), \bar{b}_l(p_j)\} = \frac{1}{\Delta^3 p}\delta_l^k\delta_j^i,$$
$$\{b_k(p_i), b_l(p_j)\} = \{\bar{b}_k(p_i), \bar{b}_l(p_j)\} = 0. \tag{20.50}$$

In [23], we proved that the rotations $e^{\hat{G}}$ are generated by the operators $\hat{\gamma}^{\mu\nu} = \frac{1}{2}(\hat{\gamma}^\mu\hat{\gamma}^\nu - \hat{\gamma}^\nu\hat{\gamma}^\mu)$, $\mu, \nu = 0, 1, 2, 3$, where gamma operators $\hat{\gamma}^\mu$ are the operator analogs of the corresponding Dirac matrices γ_D^μ. Therefore, (20.49) can be rewritten as

$$b_k(p_i) = e^{\frac{1}{2}\hat{\gamma}^{0r}\omega_{0r}}\frac{\partial}{\partial\theta^k(0)},$$
$$\bar{b}_k(p_i) = e^{\frac{1}{2}\hat{\gamma}^{0r}\omega_{0r}}\theta^k(0). \tag{20.51}$$

where ω_{0r} are parameters of the boost to the momentum p_i.

Also, there are two additional gamma operators $\hat{\gamma}^6$ and $\hat{\gamma}^7$ compared to the Dirac's theory, which correspond to the internal degrees of freedom of spinors [23, 24, 35–38], and the Clifford pseudovector $\hat{\gamma}^5$, corresponding to the Dirac matrix γ_D^5. The algebra generated by the gamma operators $\hat{\gamma}^\mu$, $\hat{\gamma}^6$ and $\hat{\gamma}^7$, we called the small Clifford algebra [24].

The operator $\bar{b}_k(p_i)$ in (20.51), as it is easy to check, is obtained using the generalized Dirac conjugation of the field operator $b_k(p_i)$

$$\bar{b}_k(p_i) = (\hat{\gamma}^0 b_k(p_i))^+. \tag{20.52}$$

Thus, we have substantiated the formulas for superalgebraic spinors that we obtained earlier [22–24, 35–38]. As is clear from the above, it is more correct to call them CAR algebraic spinors.

20.7   Spinor vacuum

In the theory of second quantization, an important role is played by the spinor (fermionic) vacuum as a state in which there are no spinors. In most studies it is assumed that it is unique. However, such an assumption contradicts the theory of CAR algebras. It has been proven that there are an infinite number of physically equivalent vacua, only one of which is the Fock vacuum (in which the particle number operator is meaningful) [28]. However, an explicit algebraic formula for the spinor vacuum has not been obtained in the framework of the theory of CAR algebras. At the same time, in a few attempts [13,17,21], including our own [15], to explicitly construct an algebraic expression for the spinor vacuum, the authors tried to identify the physical vacuum of spinors with the Clifford one. This, as shown above, is wrong.

In [22], we obtained an explicit expression for the spinor vacuum in terms of the field operators (20.49). For a state with momentum p_i, we introduce the operator

$$\Psi_{V_i} = (\Delta^3 p)^4 b_1(p_i)\bar{b}_1(p_i)b_2(p_i)\bar{b}_2(p_i)b_3(p_i)\bar{b}_3(p_i)b_4(p_i)\bar{b}_4(p_i). \tag{20.53}$$

Since, according to (20.50), $(\bar{b}_k(p_i))^2 = 0$, then

$$(\Delta^3 p \, b_k(p_i)\bar{b}_k(p_i))^2 = (\Delta^3 p)^2 b_k(p_i)\bar{b}_k(p_i)(\frac{1}{\Delta^3 p} - \bar{b}_k(p_i)b_k(p_i)) =$$
$$= \Delta^3 p \, b_k(p_i)\bar{b}_k(p_i). \tag{20.54}$$

From (20.53) and (20.54) it follows that $\Psi_{V_i}^2 = \Psi_{V_i}$, that is, Ψ_{V_i} is an idempotent. It is easy to verify that this is the Clifford vacuum (20.23) for the Clifford algebra corresponding to a given value of p_i. All Ψ_{V_i} for different i commute with each other. Therefore, the operator

$$\Psi_V = \prod_i \Psi_{V_i} \tag{20.55}$$

is an idempotent. It is invariant with respect to Lorentz rotations, since Clifford vacua Ψ_{V_i} simply change the place as a factor in (20.55) under such rotations.
Since

$$b_k(p_i)\bar{b}_k(p_i)\bar{b}_k(p_i) = 0$$
$$\bar{b}_k(p_i)b_k(p_i)\bar{b}_k(p_i) = \bar{b}_k(p_i)(\frac{1}{\Delta^3 p} - \bar{b}_k(p_i)b_k(p_i)) = \frac{1}{\Delta^3 p}\bar{b}_k(p_i), \tag{20.56}$$

operators $b_k(p_i)$ play the role of annihilation operators, operators $\bar{b}_k(p_i)$ play the role of creation operators

$$b_k(p_i)\Psi_V = b_k(p_i)\prod_j \Psi_{V_j} = \prod_{j<i}\Psi_{V_j} \, b_k(p_i)\Psi_{V_i} \prod_{j>i}\Psi_{V_j} = 0,$$
$$\bar{b}_k(p_i)\Psi_V = \bar{b}_k(p_i)\prod_j \Psi_{V_j} = \prod_{j<i}\Psi_{V_j} \, \bar{b}_k(p_i)\Psi_{V_i} \prod_{j>i}\Psi_{V_j} \neq 0, \tag{20.57}$$

and

$$N(p_i) = \Delta^3 p \, \bar{b}_k(p_i)b_k(p_i) \tag{20.58}$$

the role of operator of the number of particles with momentum p_i

$$N(p_i)\Psi_V = 0$$
$$N(p_i)\bar{b}_k(p_j)\Psi_V = 0, \; i \neq j,$$
$$N(p_i)\bar{b}_k(p_i)\Psi_V = \bar{b}_k(p_i)\Psi_V. \tag{20.59}$$

20.8   Conclusions

We have proved that modules over Clifford algebras are a basis for the theory of second quantization of spinors. We developed the theory of algebraic spinors as left modules over d-dimensional Clifford algebra and showed the presence in it of $2^{d/2}$ equivalent Clifford vacua, which differ in the role of $2^{d/2}$ creation operators and 2d/2 annihilation operators. We have proved that transformations of the connected Lie group of Lorentz transformations that preserve relations of the CAR algebra lead to the appearance of a small Clifford algebra. In it, the basis Clifford vectors are four gamma operators $\hat{\gamma}^{\mu}$, $\mu = 0, 1, 2, 3$, whose matrix representation are Dirac gamma matrices γ_D^{μ}, as well as two additional gamma operators $\hat{\gamma}^6$ and $\hat{\gamma}^7$, corresponding to the internal degrees of freedom of the spinors. For CAR algebraic spinors, a spinor (fermionic) vacuum is constructed in explicit form. It is a 4-scalar and is invariant under the Lorentz transformations and gauge transformations corresponding to the internal degrees of freedom of these spinors.

References

1. E. Cartan: Les groupes projectifs qui ne laissent invariante aucune multiplicité plane, Bull. Soc. Math. France **41**, 53-96 (1913).
2. W. Pauli: Zur Quantenmechanik des magnetischen Elektrons, Zeitschrift für Physik **43**, 601–632 (1927).
3. P. Dirac: The quantum theory of the electron, Proc. of the Royal Society of London. Series A **117**, 610–624 (1928).
4. R. Brauer, H. Weyl: Spinors in n dimensions, American J. of Mathematics **57**, 425–449 (1935).
5. W. Pauli: The Connection Between Spin and Statistics, Phys. Rev. **58**, 716–722 (1940).
6. C. Chevalley: *The Algebraic Theory of Spinors and Clifford Algebras*, Columbia University Press, 1954.
7. P. Lounesto, G. P. Wene: Idempotent structure of Clifford algebras, Acta Applicandae Mathematica **9**, 165–173 (1987).
8. P. Lounesto: *Clifford Algebras and Spinors*, Cambridge University Press, 2001.
9. V. L. Figueiredo, C. E. de Oliveira, W. A. Rodrigues, Covariant, algebraic, and operator spinors. Int. J. of Theor. Phys. **29**, 371–395 (1990).
10. Jr. J. Vaz, Jr. R. da Rocha: *An introduction to Clifford algebras and spinors*, Oxford University Press, 2016.
11. M. F. Atiyah, R. Bott, A. Shapiro: Clifford modules, Topology **3**, 3–38 (1964).
12. H. B. Lawson, M.-L.Michelsohn: *Spin Geometry*, Princeton University Press, 1989.
13. N. M. Borštnik, H. B. Nielsen: How does Clifford algebra show the way to the second quantized fermions with unified spins, charges and families, and with vector and scalar gauge fields beyond the standard model, Progress in Particle and Nuclear Physics **121**, 103890 (2021).
14. V. V. Monakhov: Remarks to the published review article of Susana Norma Mankoc Borstnik and Holger Nielsen in PPNP 121 103890 (2021), Progress in Particle and Nuclear Physics **125**, 103961 (2022).
15. V. V. Monakhov: Construction of a fermionic vacuum and the fermionic operators of creation and annihilation in the theory of algebraic spinors, Physics of Particles and Nuclei **48**, 836–838 (2017).
16. P. Lounesto: On primitive idempotents of Clifford algebras, Report-HTKK-Mat , Helsinki University of Technology **A-113** (1977).
17. K. Bugajska: Internal structure of fermions, J. of Math. Phys. **26**, 1111–1117 (1985).

18. P. Lounesto: Clifford algebras and Hestenes spinors, Foundations of physics **23**, 1203–1237 (1993).
19. A. Salam, J. Strathdee: Unitary representations of super-gauge symmetries, Nuclear Physics B **80**, 499–505 (1974).
20. S. Weinberg: *The Quantum Theory of Fields: Supersymmetry (Volume III)*, Cambridge University Press, 2000.
21. M. Pavšič: A theory of quantized fields based on orthogonal and symplectic Clifford algebras, Advances in Applied Clifford Algebras **22**, 449–481 (2012).
22. V. Monakhov: Superalgebraic structure of Lorentz transformations, J. of Physics: Conf. Series **1051**, 012023 (2018).
23. V. Monakhov: Generalization of Dirac conjugation in the superalgebraic theory of spinors, Theor. and Math. Phys. **200**, 1026–1042 (2019).
24. V. Monakhov: Vacuum and spacetime signature in the theory of superalgebraic spinors, Universe **5**, 162 (2019).
25. P. Jordan, E. P. Wigner: Uber das Paulische Aquivalenzverbot, Z. Phys. **47**, 631–651 (1928).
26. J. Schwinger: The Theory of Quantized Fields. I, Phys. Rev. **82**, 914–927 (1951).
27. J. Schwinger: The Theory of Quantized Fields. II, Phys. Rev. **91**, 713–728 (1953).
28. L. Gårding, A. Wightman: Representations of the anticommutation relations, Proc. Nat. Acad. Sci. USA **40**, 617–621 (1954).
29. H. Araki, W. Wyss: Representations of canonical anticommutation relations, Helvetica Physica Acta **37**, 136–159 (1964).
30. F. A. Berezin: *The method of second quantization*, Academic Press, New York, 1966.
31. S. Weinberg: *The Quantum Theory of Fields:Foundations (Volume I)*, Cambridge University Press, 1995.
32. V. Ya. Golodets: Classification of representations of the anticommutation relations, Russian Math. Surveys **24**, 1–63 (1969).
33. C. Binnenhei: Charged quantum fields associated with endomorphisms of CAR and CCR algebras, PhD dissertation, arXiv preprint math/9809035 (1998). https://arxiv.org/pdf/math/9809035
34. D. S. Shirokov: Pauli theorem in the description of n-dimensional spinors in the Clifford algebra formalism, Theor. and Math. Phys. **175**, 454–474 (2013).
35. V. Monakhov, A.Kozhedub: Algebra of Superalgebraic Spinors as Algebra of Second Quantization of Fermions, Geom. Integrability & Quantization **22**, 165–187 (2021).
36. V. Monakhov: Spacetime and inner space of spinors in the theory of superalgebraic spinors, J. of Physics: Conf. Series **1557**, 12031 (2020).
37. V. Monakhov: Generation of Electroweak Interaction by Analogs of Dirac Gamma Matrices Constructed from Operators of the Creation and Annihilation of Spinors, Bull. of Russian Acad. of Sciences: Physics **84**, 1216–1220 (2020).
38. V. Monakhov: The Dirac Sea, T and C Symmetry Breaking, and the Spinor Vacuum of the Universe, Universe **7**, 124 (2021).

BLED WORKSHOPS
IN PHYSICS
VOL. 23, NO. 1

Proceedings to the 25*th [Virtual]*
Workshop
What Comes Beyond . . . *(p. 304)*
Bled, Slovenia, July 4–10, 2022

21 A new view on cosmology, with non-translational invariant Hamiltonian

H. B. Nielsen[1], M. Ninomiya[2]

[1]Bohr Institute, Copenhagen
[2]Yuji Sugawara Lab., Science and Engineering, Department of Physics Sciences, Ritumeikan university, Japan

Abstract. The idea of this contribution is to suggest a way to get rid of gravity as a dynamical space time approximately in cosmology and thus be able to use Hamiltonian formulation ignoring the gravitational degrees of freedom, treating them just as background. Concretely we suggest to use a back groud De Sitter space time and then instead of the usual choice of coordinates leading to a picture in which the Universe Hubble expands, we propose to identify the time translation in the new coordinate system with a Killing form transformation for the De Sitter space time. This then leads to unwanted features like the descripton being formally not translational invariant, but we have in mind just to get in a simple way time translation and its associated Hamiltonian, and shall then in word give some ideas of the from this point of view way of looking at the usual cosmology.

21.1 Introduction

In quantum mechanics and in analytical mechanics one works with very general mechanical systems using a Hamiltonian formalism, in which the time t is taken as a parameter as a function of which then the state $|\psi(t)>$ is considered. In relativity theory and especially in general relativity the time concept is complicated by being at the end a general coordinate, which one has to **choose**, and it cannot be treated correctly unless one includes the gravitational field degrees of freedom.
But if we have some ideas developed in analytical mechanics or quantum regi with a simple Hamiltonian not including gravitational degrees of freedom and would like at a first crude stage to apply it to cosmology, then we would like to be allowed to have at least a crude cosmology, in which the gravitational field is considered a static background, so that most importantly an expansion of space can be ignored. Of course one could alternatively introduce as a dynamical variable the size of the Universe, a say, but that is really beginning to approximate a *dynamical* gravity, which it is the purpose of the present idea to avoid.

Let us at least state, that we want in the "central region" in 3-space to have a flat space approximation like one really in a short distance perspective usually work with in the neighborhood of our Milky Way. Then other usual requirements which may not be so important for making a Hamiltonian description o.k., such as the translational invariance or the associated asssumption, that crudely there is the same density of galaxies etc. all over on a very large scale, we do not need, if it is troublesome to obtain.

Let us take as a first approximation cosmological model the De Sitter space time model. (You may actually choose between taking the cosmological constant either the effective one in the inflation era or the present effective value.)

Let us resume and concretize our "model":

- We take a De Sitter space time.
- We take the time development to be identified with a Killing transformation of the space time approximating the cosmology (i.e. a Killing transformation for the De Sitter space time.
- We arrange the Milky Way to be, where the "new" time translation operation deviates the least from the "usual" FLRW (Friedmann–Lemaître–Robertson–Walker metric) parametrization "time".

21.1.1   Why we Like Hamiltonian formalism, but Trouble with Gravity

- From quantum mechanics we get (historically ?) accustomed to work with theories described by a Hamiltonian.
- In general relativity the for the Hamiltonian so basic concept, the energy E becomes strongly gauge dependent in the for cosmology interesting situations.
- So it looks at first, that one needs a quantum gravity; but that is awfull, because many colleagues work on that without being even themselves convinced so much. May be string theory is good but not immediately usefull for cosmology?

21.1.2   Our Suggestion: Use a Killing Symmetry for "Time Translation" in Approximate Cosmology

The main suggestion of the present work/talk is:

- Get rid of gravity by taking the gravitational field - the geometry - as only a background field. I.e. do not include gravity in the dynamical degrees of freedom being treated by the Hamiltonian.
- But then we need the time translation symmetry to be at least an approximate symmetry of the gravitational degrees of freedom.
- So choose an approximately cosmologically correct geometry and identify the "time translation symmetry" with a Killing transformation symmetry of the approximate geometry.

21.2   DeSitter space time

To obtain a pictorial image of de Sitter space time we want to present a perspective picture in 3 dimensions to illustrate the imbedding of the 3+1 dimensional De Sitter space into a 4+1 dimensional space-time, just for giving the illustration. But to do that we then need to simply remove 2 of the spatial dimentions so as to reduce 4+1 to 2+1 (correponding to what humans can conceive of as perpective drawing): See fig **??**.

.
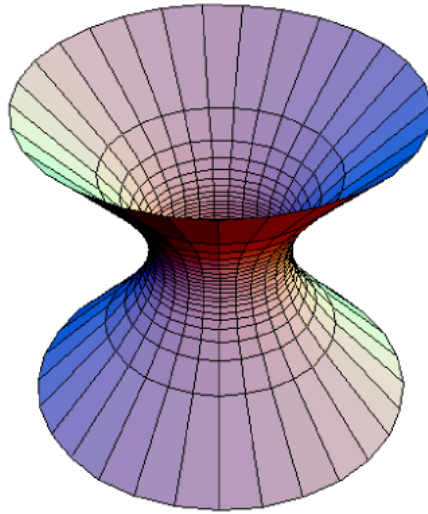
Fig. 21.1: The imbedded 1+1 DeSitter space time made to really represent the physically relevant 4+1 imbedding of the 3+1 dimensional De Sitter space time, which may be a crudely good cosmology. Here the coordinates drawn on the figure are the usual FLRW coordinates, in which the universe in the upper (= late time part) is expanding. The lower part will in most sensible models be considered so wrong that we should ignore it.

21.3   Coordinates

In the De Sitter model the space had at a certain time in the usual FLRW (fig.**??**) coodinates a most narrow i.e. least spatial size (radius R) moment of time. This is of course not true if one believes in a genuine Big Bang model, so it is only the time somewhat after that moment of the narrow space that should be taken approximately seriously. Also in the Killing form suggested coordinates as on the figure **??** the region below the narrow neck is of course presumably not to be taken seriosly.

Denoting the radius of the universe at the most narrow moment by R we can write in the imbedding coordinates the equation for the De Sitter space time surface as imbedded in the 4+1 dimensional space time, with the time -like coordinate X^0 going upwards on the shown figures. Introducing of course an extra coordinate compared to usual 3+1 space time, say X^4 we have the following equation for the imbedded surface to be identified with the universe space time:

$$(X^1)^2 + (X^2)^2 + (X^3)^2 + (X^4)^2 - (X^0)^2 = R^2. \tag{21.1}$$

We put the Milky Way at the maximal value of X^4 for a given value of X^0, i.e. indeed, for Milky Way:

$$X^4 = \sqrt{R^2 + (X^0)^2} \text{ for Milky Way} . \tag{21.2}$$

If we now want to keep to our wish to let the time at the Milky Way be the eigentime there, then we are forced to both in usual coordinates and in the "new "ones to have

$$\sqrt{\frac{(dX^0)^2 - (dX^4)^2}{dt^2}} = 1 \text{ along the track of Milky Way} \tag{21.3}$$

dS and AdS QFT: What Are the Problems?
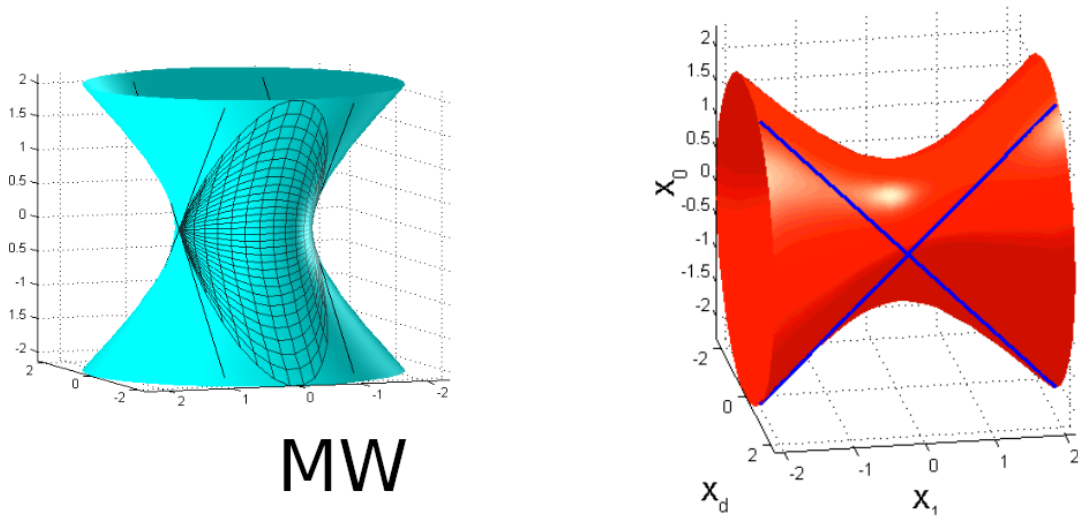
Fig. 21.2: In this figure we see both a de Sitter space time imbedding and an anti-Desitter space time imbedding. In both figures the time in the front region goes upwards on the figures. But we are in the present article really only interested in the De Sitter space-time in green to the left - and also do not care for the problem of what is wrong with quantum field theories -, and this figure illustrates **De Sitter space with 1+1 dimension (instead of 3+1)**. On the one side of it is drawn a lap with coordinates, illustrating those coordinates we propose here: the coordinate curves going upward are the time coordinates and as such in the 1+1 dimension each represent a point in space. The more horizontal coordinate lines are "parallel" to the space coordinate and each of the lines represent a moment of time in the " our " coordinate system. The region below/earlier than the narrow neck is not to be taken seriously in usual cosmology, since it would be before the **smoothed out big bang**.

This in fact leads to

$$X^4(t)_{MW} = R * \cosh \frac{t}{R} \qquad (21.4)$$

$$X^0(t)_{MW} = R * \sinh \frac{t}{R}. \qquad (21.5)$$

where t stands for the time coordinate t_u of the usual FLRW coordinates or in the "new" proposal t_n. In the "usual" FLRW model we keep the equation (21.5) to be valid not only for the Milky way, but all over. Usually one then defines the radius of the Universe at the time $t_n = t$ by the equation for a S^3-sphere representing the space at that time:

$$(X^1)^2 + (X^2) + (X^3)^2 + (X^4)^2 = a^2 \qquad (21.6)$$

$$\text{so that } a = R * \cosh \frac{t_u}{R}. \qquad (21.7)$$

In the "new", here suggested coordinates, we rather let the "momement of time" cut straight back in "usual" time to the S^2-sphere given by

$$\text{"Axis sphere" } X^0 = X^4 = 0 \qquad (21.8)$$

$$\text{or } (X^1)^2 + (X^2)^2 + (X^3)^2 = R^2. \qquad (21.9)$$

That is to say, that

$$\frac{X^0(t_n)}{X^4(t_n)} = \tanh \frac{t_n}{R} \text{ for "new" system.} \qquad (21.10)$$

$$\text{so that for } t_n \text{ fixed } \frac{dX^0}{dX^4} = \frac{t_n}{R}. \qquad (21.11)$$

Let us also define a distance $DisttoMW_n$ from the Milky Way along the equal time t_n in the "new" coordinate system out to a running point counted spacelike by

$$d\text{Dist to } MW_n^2 = da^2 + (dX^4)^2 - (dX^0)^2 \qquad (21.12)$$

$$\text{as function of the angle } \theta_n = \arccos \frac{X^4}{X^4_{MW}} = \arccos \frac{X^4}{R * \cosh \frac{t_n}{R}} \qquad (21.13)$$

$$\text{giving Dist to } MW_n = R\theta_n. \qquad (21.14)$$

$$\text{In fact using for fixed } t_n \text{ that } (dX^4)^2 - (dX^0)^2 = \frac{1}{\cosh^2 \frac{t}{R}} * (dX^4)^2 \qquad (21.15)$$

$$\text{and } a^2 + (X^4)^2 = (X^4_{MW})^2 = R^2 (\cosh \frac{t_n}{R})^2 \qquad (21.16)$$

$$\text{one gets } X^4 = \cos(\theta_n) * R * \cosh \frac{t_n}{R} \qquad (21.17)$$

$$\text{and } a = \sin(\theta_n) * R \cosh \frac{t_n}{R} \qquad (21.18)$$

$$(21.19)$$

21.3.1   How to consider the Killing transformation in the Imbedding

If we consider how a fixed point in the "space" in the 'new' coordinates move as function of the time t_n we can use that it is rotated in the imbedding space time with its indefinite metric - the X^0 being a time coordinate - around the three-space given as $X^4 = X^0 = 0$. That is to say that the distance to this three-space is constant as long as an event is moved just by progressing the "new" time t_t. The rate of running of the local eigentime relative to the coordinate time in our "new" system is thus proportional to the (Lorentz) invariant distance from the three-space to the point.

21.3.2 Developping coordinate transformation

In the "new" coordinates the Milky Way coordinates in the imbedding system are given as

$$(X_{MW}^4, X_{MW}^0) = (R * \cosh \frac{t_n}{T_H}, R \sinh \frac{t_n}{T_H}) \tag{21.20}$$

and thus for running point

$$(X^4, X^0) = ((\cos(\theta_n) * R * \cosh \frac{t_n}{T_H}, \cos(\theta_n) * R \sinh \frac{t_n}{T_H}) \tag{21.21}$$

Since in the usual FLRW we have $X^0 = R \sinh \frac{t_u}{T_H}$ we can put up the equation

$$\sinh \frac{t_u}{T_H} = \cos(\theta_n) \sinh \frac{t_n}{T_H}. \tag{21.22}$$

(Here we have written T_H for Hubble time, a constant parameter of dimension time. The simplest is to take $T_H = R$.)

Except at the Milky Way where $t_u = t_n$ we have in the whole (half) space $t_u < t_n$ meaning that the events with which we today see as simultaneous with our time in the "new" coordinates belong to the past in the usual FLRW scheme.

In the usual scheme

$$X^4 = R * \cos(\theta_u) * \cosh \frac{t_u}{T_H} \tag{21.23}$$

and so $R * \cos(\theta_u) * \cosh \frac{t_u}{T_H} = \cos(\theta_n) * R * \cosh \frac{t_n}{T_H}. \tag{21.24}$

Since we already saw that $t_u < t_n$ almost anywhere in the positive X^0 and thus relevant region, we have also here

$$\cos(\theta_u) > \cos(\theta_n) \tag{21.25}$$

$$\text{and thus } \theta_u < \theta_n, \tag{21.26}$$

where the difference between the two angles though gets smaller in absolute value (but we shall see below not relatively) the smaller the θ angles, and goes to equality at the Milky Way at the θs being zero.

Because the time development in the "new" scheme is given as a Killing transformation the spatial geometric structure in this "new" coordinate system is constant as a function of the time t_n, so that say the radius $\frac{\pi}{2} * R$ of the "half"-space remains of this value at all times t_n, while the corresponding radius of the "half"-space in the "usual" FLRW coordinates grows with the time t_u as

$$\text{"half"-space radius}_u = \frac{\pi}{2} * R * \cosh \frac{t_u}{T_H}$$

so that the logarithmic derivative $\dfrac{d\text{"half"-space radius}_u}{\text{"half"-space radius}_u \, dt_u} = \dfrac{1}{T_H} * \tanh \dfrac{t_u}{T_H}$

so T_H is Hubble time for $\tanh \dfrac{t_u}{T_H} \approx 1.$

21.3.3 Only a lap is in both coordinates

As one may see from the figure ?? also it is not the whole usual De Sitter space which is described in the "new" coordinates, but rather only a lap, because late in the "new" system one looks the simultaneity surface in the "new" coordinates must still be a space-like

surface, and thus seen from the usual system the point motion represented by the t_n fixed to a value, must run with bigger than light speed. For late t_n times however it goes very close to the speed of light, except near the Milky Way, where t_n and t_u are approximately equal. But this means that there is no way to get an event so close to $(\theta_u = 0, t_u = 0)$ that it could be reached by a signal from $(\theta_u = 0, t_u = 0)$ represented in the "new" system. This limit means that in order, that an event can be represented in the "new" coordinateswe must have

$$t_u \leq R * (\frac{\pi}{2} - \theta_u) \text{ approximately for small } t_u \quad (21.27)$$

$$\text{or more exactly: } \cos(\theta_u) * \cosh \frac{t_u}{T_H} \geq \sinh \frac{t_u}{T_H} \quad (21.28)$$

$$\text{or } 1 \geq \cos \theta_u > \tanh \frac{t_u}{T_H} \quad (21.29)$$

$$1 \geq \cos \frac{\text{Dist to } MW_u}{R \cosh \frac{t_u}{T_H}} > \tanh \frac{t_u}{T_H} \approx 1 \text{ for large } t_u$$

$$(21.30)$$

For very late times, i.e. $t_u \to \infty$ we have

$$\tanh \frac{t_u}{T_H} \approx 1 - 2 \exp(-2\frac{t_u}{T_H}) \quad (21.31)$$

$$\cos \frac{\text{Dist to } MW_u}{R \cosh \frac{t_u}{T_H}} \approx 1 - 2 * \left(\frac{\text{Dist to } MW_u^2}{R^2 \exp(-2\frac{t_u}{T_H})} \right) \quad (21.32)$$

$$(21.33)$$

Inserting these approximations of late time into the inequlity yields

$$\text{Dist to } MW_u < R \text{ for large } t_u. \quad (21.34)$$

That is to say that for late times there is still a constant - of magnitude R the most narrow size of the De Sitter Universe - radius region around the Milky Way in which transition to the "new" coordinates is possible. Regions in the usual coordinates further away than that cannot be transformed into the "new" coordinates. The angle θ_u describing this transformable region of course falls exponentially with time t_u, which is natural since the size of the unviverse grow exponentially.

21.3.4   Develloping formulae

By division of our coordinate relations (21.22) and (21.24) we obtain

$$\cos \theta_u = \frac{\tanh \frac{t_u}{T_H}}{\tanh \frac{t_n}{T_H}} \quad (21.35)$$

We can also just write (21.22) and (21.24) as respectively

$$(21.22) \text{ as } \cos \theta_n = \frac{\sinh \frac{t_u}{T_H}}{\sinh \frac{t_n}{T_H}} \quad (21.36)$$

$$\text{and } (21.24): \frac{\cos \theta_u}{\cos \theta_n} = \frac{\cosh \frac{t_n}{T_H}}{\cosh \frac{t_u}{T_H}} \quad (21.37)$$

21.3.5 Near Milky way

For small θ_u and θ_n, i.e. near the Milky way we can of course approximate

$$\cos\theta \approx 1 - \frac{1}{2}\theta^2 \tag{21.38}$$

and if we are mainly interested in late times we may also use approximations like

$$\cosh\frac{t}{T_H} \approx \sinh\frac{t}{T_H} \approx \frac{1}{2} * \exp(\frac{t}{T_H}) \tag{21.39}$$

$$\tanh\frac{t}{T_H} \approx 1 - 2\exp(-2\frac{t}{T_H}). \tag{21.40}$$

Note that in the same approximation as the sinh and cosh ones given here the tanh would be exactly 1.

In these approximations of late time and small angles we get

$$\frac{1}{2}\theta_u^2 \approx 2\exp(-2\frac{t_u}{T_H}) - 2\exp(-2\frac{t_n}{T_H}) \tag{21.41}$$

$$\text{or } \theta_u \approx 2\sqrt{\exp(-2\frac{t_u}{T_H}) - \exp(-2\frac{t_n}{T_H})} \tag{21.42}$$

$$1 - \frac{1}{2}\theta_n^2 = \exp(\frac{t_u - t_n}{T_H}) \tag{21.43}$$

$$\text{Taking } \ln: \ -\frac{1}{2}\theta_n^2 = \frac{t_u - t_n}{T_H} \tag{21.44}$$

$$\frac{\cos\theta_u}{\cos\theta_n} \approx 1 - \frac{1}{2}(\theta_u^2 - \theta_n^2) = \frac{\cosh\frac{t_n}{T_H}}{\cosh\frac{t_u}{T_H}} \approx \exp(\frac{t_n - t_u}{T_H}) \tag{21.45}$$

$$\text{taking } \ln: \ -\frac{1}{2}(\theta_u^2 - \theta_n^2) = \frac{t_n - t_u}{T_H}. \tag{21.46}$$

We see that here

$$\theta_u << \theta_n \tag{21.47}$$

Indeed :

$$\theta_u \ \sim \ \sqrt{\exp(-2t/T_H)} \sim \exp(-t) \tag{21.48}$$

$$\text{while } \theta_n \ \sim \ \frac{t_n - t_u}{T_H} \text{ (much bigger)} \tag{21.49}$$

Really in the region near the Milky Way the two times t_u and t_n only deviate little compared to their approximately common zize the age of the universe at the time considered, which here was taken to be large. We should have in mind that distance between galaxies or galaxy clusters are roughly constant in the angular coordinate θ_u in the usual coordinates, so that the diminishing exponentially as $\propto \exp(-t/T_H)$ of θ_u relative to the "new" θ_n in the region around the Milky Way means that the galaxies - to keep their fixed coordinates in θ_u - seen in θ_n moves away as with a Hubble expansion as if the "new" angular coordinate meant a genuine distance. Actually θ_n means a genuine distnace since we already noted that

$$\text{Dist to MW}_n = \theta_n * R. \tag{21.50}$$

It is namely so in the beginning at $t_n = 0$, but since the development in the "new" coordinates is of Killing form transformation type, the spatial structure and metric does not change under the t_n time development. So not surprisingly we see the Hubble expansion

in the distance as seen in the "new" coordinates. Of course *this* Hubble epansion can*not* continue at longer distances from the Milky Way, since the whole spatial universe in the "new" coordinate system is bounded of the size R. So the galaxies must seen in the "new" system somehow collect up in the large θ_n region. We can consider this large θ_n region as a kind of garbage place where galaxies expelled from the neighborhood of the Milky Way are thrown in, and get concentrated there. These regions also contribute relatively less to the Hamiltonian, so it is natural to consider them not so important and a kind of garbage place.

21.4 Hubble Expansion

Having in mind that in the "new" coordinates radius of the treated part of the universe remains R = the narrowest size in the "usual" coordinates, there is no possibility for a true expanding universe as a whole.

But of course translated back to the "usual" LFRW coordinates we assume that there is the usual type of Hubble expansion. So what happens in our "new" coordinate system?

To orient ourselves let us start by estimating the rather easy to calculate relative velocity of the galaxies or pregalactic material in the region near the $\theta = \frac{\pi}{2}$ boundary. Here the usual time t_u never gets very big even for huge times t_n in our new coordinate system. The "new" system locally in this boundary region moves with velocity corresponding to a "hyperbolic angle" $\frac{t}{R}$, meaning that the relative velocity is

$$v = \tanh \frac{t}{R} \tag{21.51}$$

so that "Lorentz contraction factor" $= \gamma^{-1} = \sqrt{1 - v^2} = \dfrac{1}{\cosh \frac{t}{R}} \tag{21.52}$

$$\text{To compare to } \frac{a}{R} = \cosh \frac{t}{R}. \tag{21.53}$$

That is to say: The Lorentz contraction - for the moment in the region where it is most easy to calculate it - is just of the size needed to Lorentz contract the Hubble expansion away and to put the universe as conceived in the "usual" LFRW coordinates of radius a into the universe as seen at all times in our "new" scheme as having the radius only R (remember $R < a$ all the time except in the first moment).

Very close to the Milky Way the velocity of the "new" versus the "usual" local frames goes through zero and thus here the relative frame velocity is small. Thus very close to the Milky Way the Lorentz contraction is also small.

Rather the Hubble expansion means that the galaxies move away from the Milky Way more and more into the boundary region close to $\theta_n \approx \frac{\pi}{2}$. So the major part as seen in the "new" coordinates gets more and more empty/vacuum, only the Milky Way because of our choice stands back in the midle.

Here a shorter attempt on Hubble Expansion in our system:

In the usual coordinates of course the galaxies are static in the sense of having e.g. staionary θ_u values ideally. The distance along space in the usual coordinates are:

$$\text{Dist to MW}_u = \theta_u * R * \cosh \frac{t_u}{T_H} \tag{21.54}$$

$$\text{Dist to MW}_n = \theta_n * R. \tag{21.55}$$

Thus in the usual frame the expansion of the distance from the Milky Way to a galaxy at θ_u goes as

$$\text{Dist to MW}_u = \theta_u * R * \cosh \frac{t_u}{T_H} \tag{21.56}$$

$$\text{and log-derivative } \frac{\text{dDist to MW}_u}{\text{Dist to MW}_u\, dt} = \frac{1}{T_H} \tanh \frac{t_u}{T_H} \tag{21.57}$$

$$\approx \frac{1}{T_H} \text{ for late times.} \tag{21.58}$$

21.5 Time

It should be pointed out that the simulatneity in our "new" coordinates is closer to the way astronomers have to think about the happenings in practice: Because of the time it takes the light or also gravitational waves say to run we would be tempted to think of what in usual coordinates happened as long a go as the happening is light years away,as if it happened now. In our "new" coordinates the simultaneity sufaces are much closer to this tempting point of view. In our scheme there is a part of the big bang creation still present very far out near the bourder of $\theta_n = \frac{\pi}{2}$.

21.6 The Non-translatioanl invariant Hamiltonian

It was the major disadvantage of our proposal that we should give up translational invariance along space. In fact the point is that the time progress in the "new" coordinate system to be conceived of as the development due to the Hamiltonian should represent a Killing form development corresponding in the imbedding we have used so much to a space time rotation (so it is really boosting). The crux of the matter now is the genuine time progress is thus much smaller in the region around which the rotation goes. Thus not unexpected the original Hamiltonian which would crudely to be used in the FLRW system should be deminished in this region where the timeprogressing is slow. In fact this diminishing goes proportional $\cos \theta_n$ or equivalently $\cos \frac{\text{Dist to MW}_n}{R}$. Thus the Hamiltonian to be used would rather be:

To be Used Hamiltonian

$$H = \int \cos\left(\frac{\text{"Dist to MW}_n''}{R}\right)\mathcal{H}(x)\,d^3\Omega \tag{21.59}$$

where "Dist to MW$_n''$is the distance to the Milky Way, R the radius parameter in the De Sitter space used, $\mathcal{H}(x)$ the Hamiltonian density in a usual sense. Note that only half the De Sitter space is in the proposed region, or rather in the other half the usual energy is counted with a **negative** weight factor!

21.7 Conclusion

We have proposed to use a De Sitter approximation as a back ground ansatz for the gravitational fields metric tensor so that back reaction can, although rather approximately only be ignored, and thus gravity can be kept out of the study provided one can get rid of such to non-gravitational theory not usual effects as the Hubble expansion as a room expansion. The proposal is to get rid of the Hubble expansion as an effect from space

expansion by choosing a coordinate system corresponding to the Killing transformation of one of the symmetries of the De Sitter space-time to be identified with the time progress transformation. The price of this choice is, that we loose translational invariance in space, although gaining it in time to make up for it (time translation symmetry is of course violated if the varying size of the universe is considered a back ground effect.) But for using the usual quantum mechanics formalism with a conserved Hamiltonian a scheme as the one here with broken translational invariance in space but unbroken in time is preferable. Around the Milky Way we could arrange to have approximately the special relativity in the coordinates of the "new" system. The region most far away from this Milky Way has very strongly suppressed Hamiltonian and thereby time development and remain at the satge of the ealy universe almost forever. We suggested treating these far away from Milky way places as kind of garbage place in which more and more of Hubble expanded material will end up, and since it contributes suppressed to the energy it is not so bad to suggest to ignore these far away regions nearer $\theta_n = \frac{\pi}{2}$.

Acknowledgements

References

1. de Sitter, W. (1917), "On the relativity of inertia: Remarks concerning Einstein's latest hypothesis" (PDF), Proc. Kon. Ned. Acad. Wet., 19: 1217–1225, Bibcode:1917KNAB...19.1217D de Sitter, W. (1917), "On the curvature of space" (PDF), Proc. Kon. Ned. Acad. Wet., 20: 229–243 Levi-Civita, Tullio (1917), "Realtà fisica di alcuni spazî normali del Bianchi", Rendiconti, Reale Accademia dei Lincei, 26: 519–31
   See e.g. also: Yoonbai Kima, Chae Young Oha, and Namil Parka, hep-th/0212326, "Classical Geometry of De Sitter Spacetime : An Introductory Review"
2. L. Susskind, "De Sitter Holography: Fluctuations, Anomalous Symmetry, and Wormholes," Universe **7**, no.12, 464 (2021), [arXiv:2106.03964 [hep-th]]

22   A new Paradigm for the Dark Matter Phenomenon

P. Salucci

SISSA,Via Bonomea 265, Trieste, Italy
salucci@sissa.it

Abstract. The phenomenon of the Dark matter baffles the researchers: the underlying dark particle has escaped so far the detection and its astrophysical role appears complex and entangled with that of the standard luminous particles. We propose that, in order to act efficiently, alongside with abandoning the current ΛCDM scenario, we need also to shift the Paradigm from which it emerges.

22.1   The Phenomenon of Dark Matter

The phenomenon of the Dark Matter is one of the most intriguing mysteries in the Universe. In fact, not only it implies the existence of unknown Physics, but it concerns the fabrics itself of the Universe. A new Law of Nature, yet to be discovered, seems to be at work. As Zwicky found back in the 30's and Vera Rubin in the late 70's [1], the law of Gravity seems to fail in Clusters of Galaxies and in (Disk) Galaxies. One detects large anomalous motions: the stars in a galaxy do not move as they should do under their own gravity, but as they were attracted by something of invisible.

Disk systems can be divided in normal spirals, dwarf irregulars and Low Surface Brightness galaxies. Here, the equilibrium between the gravity force and the motions that oppose to it has a simple realization: the stars (and the HI gaseus disk) rotate around the galaxy center. However, we realize that such rotation is very much unrelated with the spatial distribution of the stars and gas, contrary to what should be according to Newton Law. The objects of this most populated type of galaxies are relatively simple to investigate in that we have:

$$R\frac{d\Phi(R)}{dR} = V^2(R) \tag{22.1}$$

where the (measured) circular velocity and the galaxy total gravitational potential are indicated by: $V(R)$ and $\Phi(R)$. A disk of stars is their main luminous component whose surface mass density $\Sigma_D(R)$, proportional to the surface luminosity measured by the photometry, takes the form ([2]):

$$\Sigma_\star(r) = \frac{M_D}{2\pi R_D^2} \, e^{-R/R_D} , \tag{22.2}$$

where M_D is the mass of the stellar disk to be determined and R_D is its scale length measured from the photometry. At $R \geq 3 R_D$ this component rapidly disappears, so that R_D plays as the characteristic radius of the stellar disk. Eq(1) with the Poisson equation for this component (in cylindrical coordinates, δ is the Kronedeker function):

$$\nabla^2 \Phi(R) = 4\pi G \, \Sigma_\star(R)\delta(z)$$

yields $V_\star(y)$ the luminous matter contribution to the circular velocity ($y \equiv R/R_D$). $v_\star^2(y) \equiv \frac{G^{-1}V_\star^2(y)R_D}{M_D}$ takes the form (I, K are the Bessel functions):

$$v_\star(y)^2 = \frac{1}{2} \, y^2 (I_0 \, K_0 - I_1 \, K_1)_{y/2} \tag{22.3}$$

Defining $\nabla \equiv d\log V/d\log R$, from Eq.(3) we have: $\nabla_\star(y) \simeq 0.87 - 0.5 \, y + 0.043 \, y^2$. According to Newtonian gravity one expects: $\nabla(y) = \nabla_\star(y)$, instead, almost always we have: $\nabla(y) > \nabla_\star(y)$ see Fig.(1). In order to restore the law of Gravity one adds a "dark halo" component with:

$$\nabla_h(y) = \frac{\nabla(y) \, V^2(y) - \nabla_\star(y) \, V_\star^2(y)}{V^2(y) - V_\star^2(y)} \tag{22.4}$$

and:

$$V^2(R) = V_\star^2(R) + V_h^2(R) \tag{22.5}$$

in Eq (5), for simplicity, we have neglected the small contribution of the HI gaseous disk and we have: $V_h^2(R) = G \frac{\int 4\pi \rho_h(R)R^2 \, dR}{R}$ where $\rho_h(R)$ is the DM halo density. From the above equations the DM halo density reads:

$$\rho_h(y) = \left(G^{-1}V^2(y) - \frac{M_D}{R_D}v_\star^2(y) \right) \left(\frac{1 + 2\,\nabla_h(y)}{4\pi R_D^2 \, y^2} \right) \tag{22.6}$$

and can be determined, once we measure R_D and $V(R)$ and we estimate M_D sufficiently well.
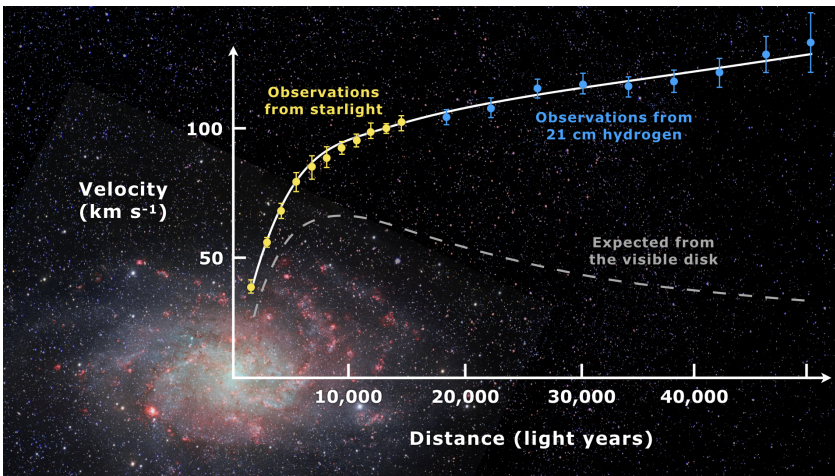
Fig. 22.1: M33: the profile of the stellar disk contribution to the circular velocity does not coincide with that of the latter ($\nabla > \nabla_\star$). [3].

It is well known that the dark matter reveals itself also in the other types of galaxies (see, e.g. [4]) and that the presence of this non- interacting massive particle is necessary to explain a number of cosmological observations such as the rate of the expansion of the universe, the anisotropies in the Cosmic Background Radiation, the evolution of the large scale structures and the existence itself of galaxies (e.g. see [6]). The starting point to account for all this has been to postulate the ubiquitous presence in the Universe of massive particles that emit radiation at a level totally negligible with respect to that emitted by the Standard Model (SM) particles. Then, this particle, necessarily outside the SM, unlike its particles, is hidden to us also when it aggregates in vast amounts. We take this dark particle option as a foundation of Physics and Cosmology. However, it is important to stress that this does not automatically determine the mass or the nature of such a particle. Furthermore, the present status of "darkness" means that the particle has a very small, but not necessarily zero, self- interactions or interactions with the SM particles and this can have various cosmological, physical and astrophysical consequences.

22.2   The Standard Paradigm

The next step has been to provide the particle with a theoretical scenario. Let us introduce the concept of the Paradigm for the Dark Matter Phenomenon. Here, for Paradigm we intend a set of properties that the actual DM scenario must possess and that, in turn, reveals the nature of the particle. After the first "detections" of DM in the Universe, a Paradigm has, indeed, emerged lasting until today. According to this, the *scenario* behind the DM Phenomenon must have the following properties:

1) it connects the (new) Dark Matter physics with the (known) physics of the Early Universe; it introduces in a natural way the required massive dark particle and relates it with the value of the cosmological mass density of the expanding Universe.

2) it is mathematically described by a very small number of parameters and by a very well known and specific initial conditions, while having, at the same time, a strong predictive power on the evolution of the structures of the Universe. Furthermore, these latter can be thoroughly followed by proper numerical simulations.

3) its (unique) dark particle can be detected by experiments and observations with present technology.

4) it sheds light on issues of the Standard Model particle physics.

5) it provides us with hints for solving long standing big issues of Physics.

In other words, the ruling paradigm heads us towards scenarios for the dark matter phenomenon that are very beautiful, and hopefully towards the most beautiful one, where beauty is in the sense of simplicity, naturalness, usefulness, achieving expectations and harmonically extending our knowledge. For definiteness and clarity of the discussion, we name it as: "The Apollonian paradigm". Let us point out that here we just *name* concepts emerged and solidified in the mid 80' and that since then have served as lighthouses in the investigation of the DM mystery. This Paradigm has straightforwardly led the Cosmologists to one particular scenario: the well known ΛCDM scenario (e.g. [6]). Not only the Apollonian paradigm has identified the possible scenario for the dark particle, but it is directly responsible for large part of its claimed successes, so that, to adopt the above scenario or to adhere to the originating paradigm is the same thing. Finally, the ΛCDM scenario is rather unique: in the past 30 years no other scenario has emerged with such complete Apollonian status.

Λ stays for the Dark Energy having 70% of the total energy of the Universe and CDM for Cold Dark Matter. Cold refers to the fact that the dark matter particles move very slow compared to the speed of light. Dark means that these particles, in normal circumstances,

do not interact with the ordinary matter via electromagnetic force but very feebly with a cross section of the order of $3 \times 10^{-26} \text{cm}^2$ characteristic of the Weak Force. This specific value of the cross section inserted in the Physics of the early Universe, makes the predicted WIMP (Weak Interacting Massive Particles) relic density compatible with the observed value of about $3 \times 10^{-30} \text{g/cm}^3$ (e.g. [6]). It is well known that in this scenario the density perturbations evolve through a series of halos mergings from the smallest to the biggest in mass and the final state is a matrioska of halos with smaller halos inside bigger ones. Very distinctively, these dark halos show an universal spherical spatial density [7]:

$$\rho_{\text{NFW}}(r) = \frac{\rho_s}{(r/r_s)(1 + r/r_s)^2}, \tag{22.7}$$

where r_s is a characteristic inner radius, and ρ_s the related density. Notably, this scenario confirms its beauty resulting extremely falsifiable since in all the Universe and throughout its history, the related dark component creates structures with the same one configuration. The well known evidence is that no such dark particle has been detected in the past 30 years. This has occurred in experiments at underground laboratories, searching for the soft scatter of these particles with particular nucleus, in particle collisions at LHC collider with a general search for Super-Symmetric partners or more exotic invisible particles to be seen as missing momentum of unbalanced events; in measurements at space observatories as gamma rays coming from dense regions of the Universe where the dark particle annihilates with its antiparticle (see e.g. [?, 8]). Furthermore, the current upper limits for the energy scale of SuSy, as indicated by LHC experiments, rules out the Neutralino as the DM particle. It is, however, important to notice that, in the attempts made so far, only WIMP particles have been thoroughly searched. The search for particles related to other DM scenarios has been very limited and almost no blind searches have been performed. Thus, the lack of detection of the dark particle so far, in no way indicates that this does not exist, but only the failure of certain detection strategies related to particular scenarios.

In recent years, at different cosmological scales, observational evidence in strong tension with the above scenario has emerged (e.g. [5]). Here, we focus on the distribution of dark matter in galaxies, a topic for which the failure of the ΛCDM scenario is the most eventful ([9]). Dark Matter is, in fact, located mostly in galaxies that come with very large ranges of total masses, luminosities, sizes, dynamical state and morphologies. This diversity of the properties of their luminous components is an asset for the investigation of their dark components.
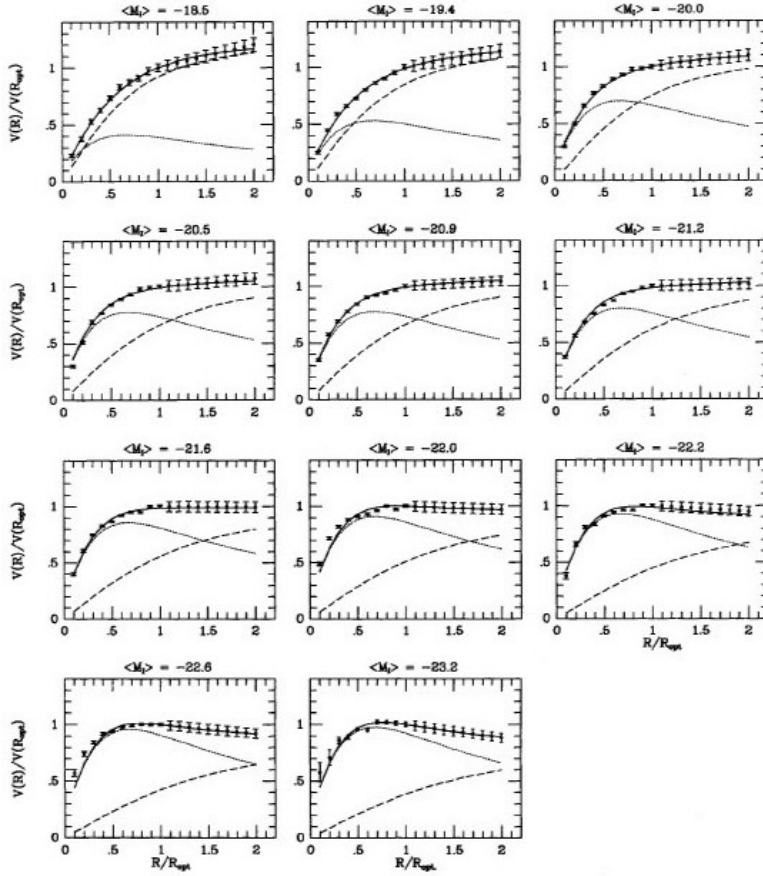
Fig. 22.2: Stacking of 1000 individual RCs in 11 luminosity bins. The coadded curves $V(R/R_{opt})/V(R_{opt})$ *(points with errorbars)* are fitted with the URC model *(solid line)*: a cored DM halo *(dashed line)* + a Freeman Disk *(dotted line)* ([13, 16])

22.3   The cored DM halos

The rotation curves of disk systems are well measured from the Doppler measurements of the H_α and the 21cm galaxy emission lines. They extend in many cases well beyond the stellar disk edge and in some case out to 20% of the halo size. By investigating several thousands RCs covering: a) all the morphologies of the disk systems: normal spirals, dwarf Irregulars and low surface brightness galaxies and b) all the magnitudes from the faintest to the most luminous objects, one finds that the RCs, from the center of the galaxies out to the edge of the dark matter halo, combine in an Universal Rotation Curve (see [4]). That is, in order of retrieving the galaxy dark and luminous mass distributions from their circular velocity $V(R)$, the latter can be represented by an unique function $V_{URC}(R/R_D, Mag, c, T)$, where R_D is the disk length scale of Eq. (2), Mag is the magnitude, c indicates how compact is of the distribution of light and T the galaxy morphology [10, 11, 13–15]).
$V_{coadd}(R/R_D, P_i)$ the coadded velocity data (and the related r.m.s.) (see Fig. 2) are obtained by stacking with a proper procedure a large number of individual RCs in bins of the

observed quantity(ies) P_i, (e.g. Mag and T) . $V_{URC}(R/R_D, P_i)$ (The ensemble of solid lines in Fig. 2) is an analytical function found to fit the above V_{coadd} data (see [13]). V_{coadd} is a crucial kinematical quantity, any values and their r.m.s. would take, moreover, since the latter are found very small, they are good templates of the large majority of individual RCs. On the other hand, the function V_{URC} allows one to interpret the V_{coadd} data in terms of a universal mass model.

Remarkably, all the RCs identifier quantities belong to the *stellar* component of the galaxies despite that the *dark* component dominates the mass distribution. This is a first indication of a *direct coupling* between the dark and luminous components. The proposed mass model features the following two components: the above stellar disk of mass M_D as a free parameter and a dark halo with the Burkert density distribution [16]:

$$\rho_B(r) = \frac{\rho_0}{(1 + r/r_0)(1 + (r/r_0)^2)} \tag{22.8}$$

The latter has 2 free parameters: the central density ρ_0 and the core radius r_0 that marks the edge of the region in which the DM density is roughly constant. This model well reproduces the coadded RCs [13–16], so as the individual RCs of disk galaxies (see also [4]) and it is dubbed as the URC model. Notably, its success faces the failure of the NFW halo + stellar disk mass model in the *coadded* RCs [17].
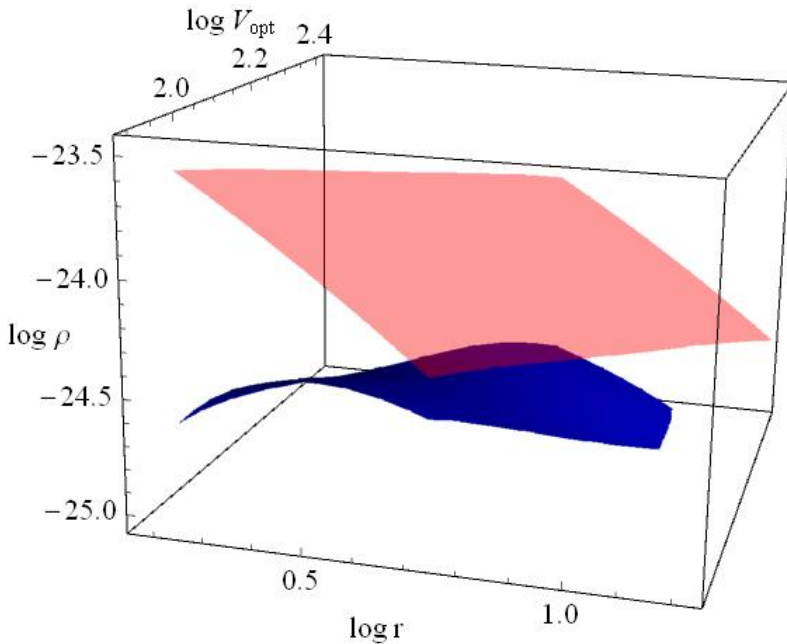
Fig. 22.3: The halo density from Eq. (6) *blue* as function radius R for galaxies with different values of $\log V_{opt}$. The disagreement with the predicted NFW one *red* is evident

Importantly, the same outcome occurs also for the control sample of high quality *individual* RCs (e.g. [19–22,26]). This disagreement is serious, model independent and emerges directly

from Eq(6) in combination with: $M_D \simeq (0.72-0.95\nabla)G^{-1}V_{opt}^2 R_{opt}$ [18] with $R_{opt} \equiv 3.2\ R_D$ (see Fig. 5).

Furthermore, in the framework of ΛCDM cuspy halos model, we also find implausible best-fitting values for the masses of the stellar disk and dark halo and for the two structural parameters of the NFW halo (e.g. [17]).

This raises strong doubts about the collisionless status of the DM particles in galaxies, a fundamental aspect of the ΛCDM scenario. Moreover, at radii $r >> r_0$, the density profile of the dark matter in disk galaxies returns to be that of the collisionless particles [11](see Fig. 4).

This fits well with the above observational scenario: in the external regions of halos, the luminous and dark matter are so rarefied that, in the past 10 Gyrs, had no time to interact among themselves, also if this was physically allowed. Thus, on the scale of the halo's virial radius, the standard physics of galaxy formation is not in tension with the observed distribution of dark matter. Differently, on the scale of the distribution of the luminous component, the observations imply that the DM halo density have undergone to a significant and not yet well understood evolution over the Hubble time (see also [27])
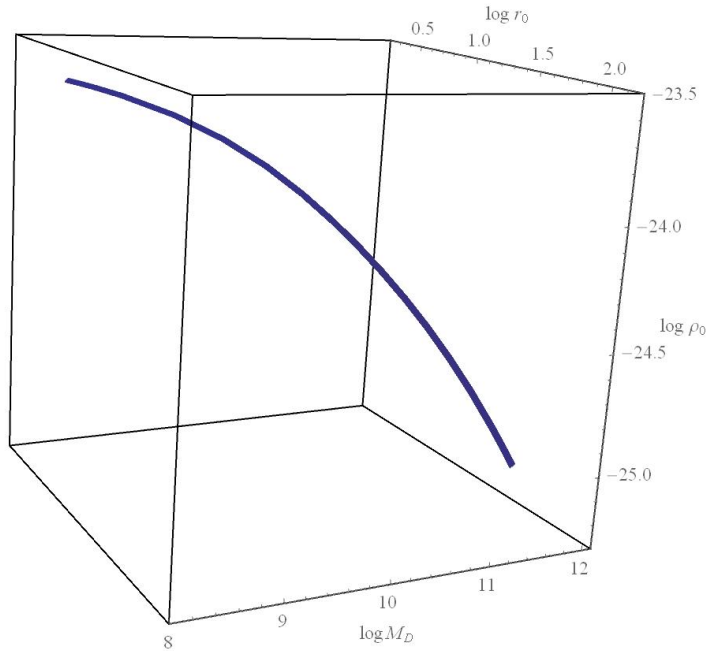
Fig. 22.4: The relationship among the DM and LM structural parameters ρ_0, r_0, M_D (see [11]). Log-units: $M_\odot$, kpc, g/cm^3.

Therefore, the mass distribution of a disk galaxy is described, in principle, by one parameter belonging to the luminous world and two to the dark world which represent structural quantities (not defined in the standard ΛCDM scenario). In disk galaxies and extraordinary observational evidence adds up: the three parameters r_0, ρ_0 and M_D result well correlated among themselves (see Fig. 5, [11] and Fig. 11 in [4]). This, obviously, cannot occur in the

standard ΛCDM scenario; then, we focus on this evidence ad we directly investigate the structural physical properties of disk galaxies.
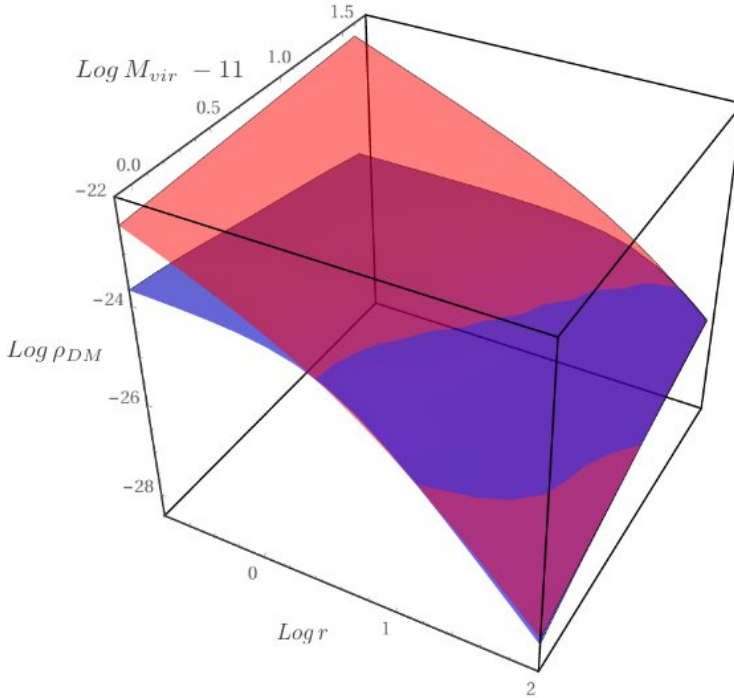
Fig. 22.5: The density of the DM halos today *(blue)* and the primordial one *(red)* as function of radius and mass. The agreement of the two profiles at outer radii reveals a time evolution of the DM in the central regions of the halos. Log-units: kpc g/cm^3 10^{11}M$_\odot$

22.4 Unexpected relationships

We remark that the properties of the internal structure of the disk galaxies, at the basis of this work, have been previously discovered and independently confirmed (references in this work and the review [4]). Here we *use* them as motivation for proposing a paradigm shift in the way we investigate the dark matter mystery.

22.4.1 Central halo surface density

The quantity $\mu_0 \equiv \rho_0 r_0$, i.e. the central surface density of the DM halo, is found constant in objects of any magnitude and disk morphology (see Fig. 6) [16, 28–30] (see also [4]):

$$\log \frac{\mu_0}{M_\odot pc^{-2}} = 2.2 \pm 0.25 \tag{22.9}$$

this means that ρ_0, the value of the DM halo density at the center of galaxy, is inversely proportional to the size r_0 of the region in which the density is about constant. This seems to imply that the dark particle possesses some form of self-interaction of unspecified nature.
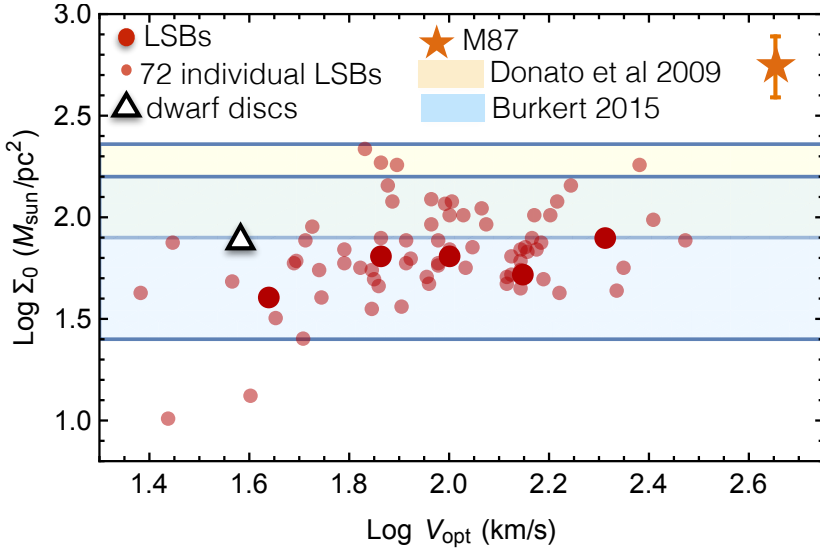
Fig. 22.6: The dark halo central surface density μ_0 as a function of the reference velocity V_{opt} in disk systems and in the giant elliptical M87

22.4.2   DM core radii vs. disk length scales

Amazingly, r_0 tightly correlates with the stellar disc scale length R_D [13–15, 24, 25] :

$$\log r_0 = (1.38 \pm 0.15) \log R_D + 0.47 \pm 0.03 \qquad (22.10)$$

see Fig. (7).

This relationship, found for the first time in a large sample of Spirals by [13], is present also in LSBs and Dwarf Irregulars and in the giant elliptical M 87 (see Fig. 7). Overall, it extends in objects whose luminosities span over five orders of magnitudes. Then, the size of the region in which the DM density does not (much) change with radius results related with the size of the stellar disk R_D. It is very difficult to understand such tight correlation between very different quantities without postulating that dark and luminous matter are able to interact more directly than via the gravitational force.
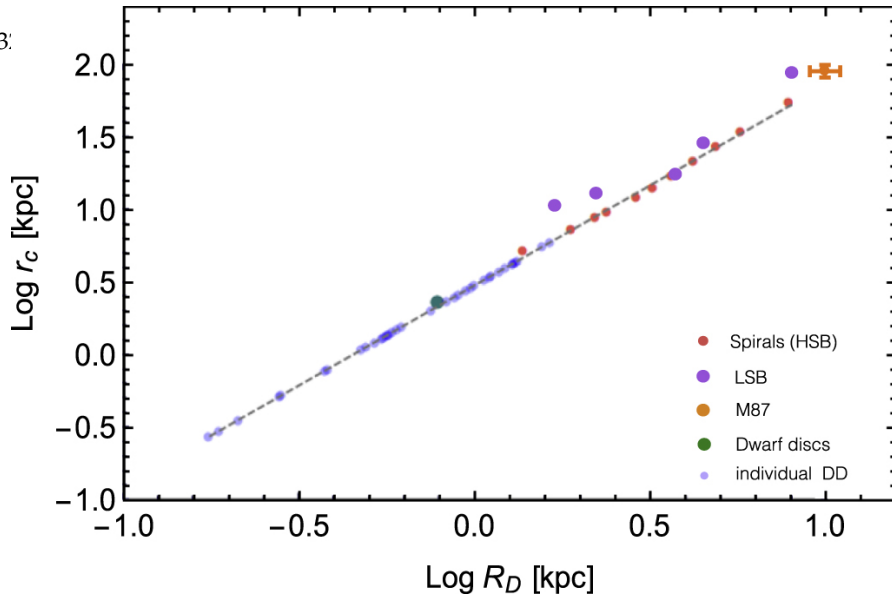
Fig. 22.7: DM halo core radius r_c (= r_0 for Burkert profile) vs. the stellar disk length scale R_D (from Eq. (2)) in galaxies of different morphology

.

22.4.3 Stellar disks vs. DM halos compactness

Similar mysterious entanglement emerges also from the evidence that, in galaxies with the same stellar disk mass, the more compact is the stellar disk, i.e. the larger is the value of M_D/R_D^2, the more compact is the 2-D projected DM core region, i.e. the larger is the value of M_h/r_0^2 (see Fig. 8) ([14], Fig. (15) in [15],. Moreover the stellar and the DM surface brightness, once averaged inside r_0, are found to be proportional [23]). Dark and luminous world seem to have communicated in an unknown language.

22.4.4 Total vs. baryonic radial accelerations

Also without assuming a-priori the presence of a dark halo in galaxies, this emerges and results mysteriously entangled with the baryonic component. $V^2(y)/y \equiv g$ is the radial acceleration of a point mass in rotational equilibrium at a distance y from the center of a disk galaxy and $V_b^2(y)/y \equiv g_b$ is its baryonic (stellar) component. In spiral galaxies we find: $g(y) > g_b(y)$, that calls for a dark component, but also: $g = g(g_b)$: the two accelerations are related by a tight relationship [31].
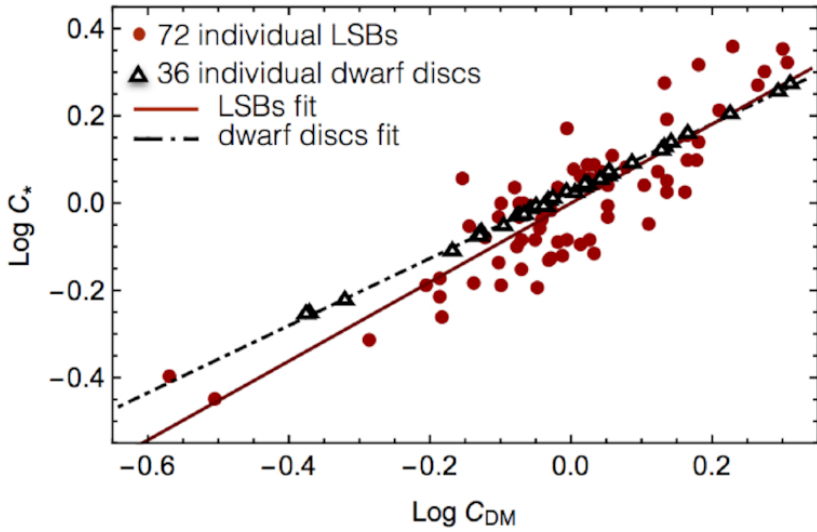
Fig. 22.8: Compactness of the stellar disk vs that of the cored DM region

Including in the game also dwarf Irregulars and Low Surface Brightness galaxies, the above relation gains an other parameter, the radius $y \equiv R/R_D$ and form a surface $\log g = g(\log g_b, y)$ around which, within a very small r.m.s. distance of 0.04 dex, the accelerations at all radii and in all galaxies lay [32] (see Fig. (9)). The origin of this surface of hybrid dark-luminous quantities is difficult even to frame in a pure collisionless scenario.

22.4.5 The crucial role of r_0

The relationships above indicate the quantity r_0 as the radius of the region inside which the DM–LM interaction has taken place so far. Here, we show a direct support for such identification. In the case of self-annihilating DM the number of interactions per unit of time has a dependence on the DM halo density given by: $K_{SA}(R) = \rho_{DM}^2(R)$, here we take $K_C(R) \equiv \rho_{DM}(R)\rho_\star(R)$ as the analogue quantity in a scenario with DM-baryons interactions. K_C has no physical meaning in a collisionless DM particle scenario. From the above URC mass model we get:

$$K_C(r_0) \simeq \text{const} = 10^{-47.5\pm0.3} g^2 cm^{-6} \quad . \tag{22.11}$$
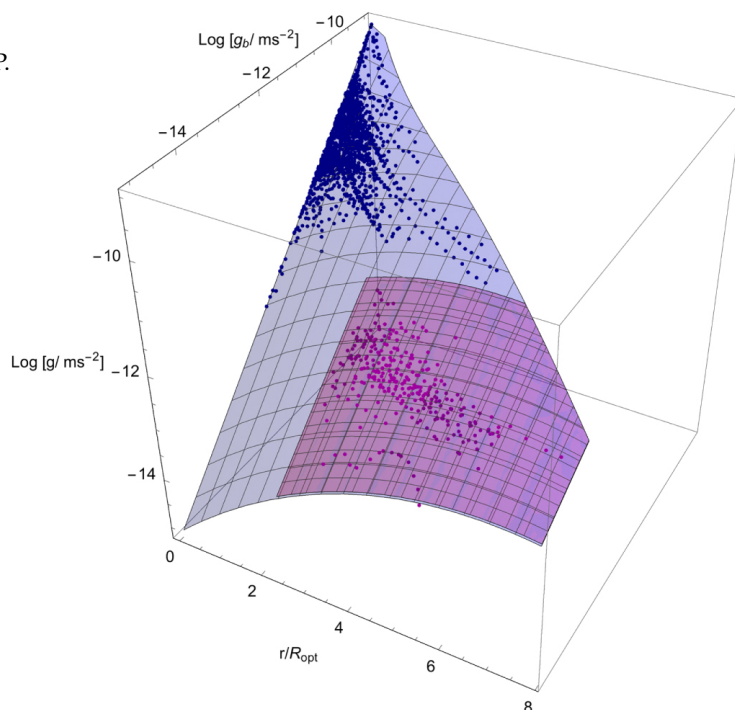
Fig. 22.9: The relationship in dwarf and LSB galaxies among the total and the baryonic accelerations at y and y.

We see in Fig.(10) that the kernel $K_C(R)$, at a same physical radius R, varies largely among galaxies of different mass, and, in each galaxy, varies largely at different radii. But, at $R \simeq r_0$ and only there, this quantity takes the same value in all galaxies. In the scenario of interacting dark matter, this clearly suggests the radius r_0 as the edge of the region inside which interactions between dark matter particles and a Standard Model particles have taken place so far, flattening the original halo cusp.

22.5   A new Paradigm

Dark Matter particles have been thought, as their main characteristic, to interact with the rest of the Universe essentially only by Gravity. However, in such a framework, the properties of the mass distribution in galaxies do not make much sense. Observations, therefore, appear to strongly call for a new interaction, negligible on time scales of the order of the galaxy free fall time, like the WIMP one, but, unlike the latter, able to modify the dark halo density distribution within a timescale as long as the age of the Universe.
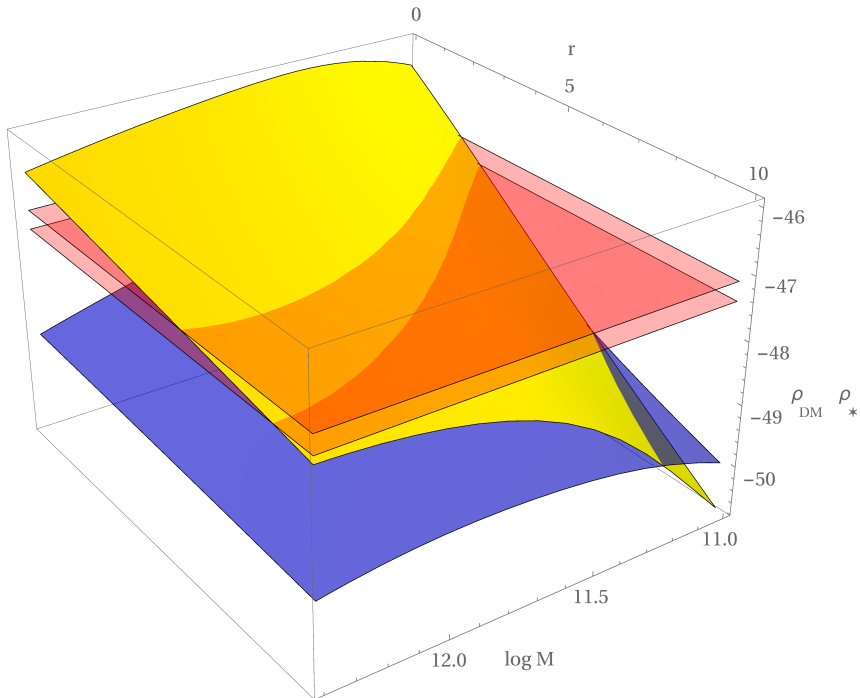
Fig. 22.10: $\rho_{DM}(r)\rho_{LM}(r)$ as function of radius and halo mass (*yellow*). $\rho_{DM}(r_0)\rho_{LM}(r_0)$ resides, for all the objects, inside the two red planes. Shown (*blue*) also the analogue of the the dark particle annihilation, $\rho_{DM}(r)^2$. Log Units: $M_\odot$, kpc, $g^2\ cm^{-6}$.

It is certain that the impact of these observational evidences goes beyond the falsification of the ΛCDM WIMP scenario and proceeds till to rule out the entire Apollonian paradigm from which such scenario has emerged. The defining criteria of the paradigm, in fact, appear unaccountable by the above evidences. Thus, the spectacular DM–LM entanglement found in galaxies, allied with the fact that the WIMP particle has escaped detection, become a strong motivation for a change of the Paradigm with which to approach the dark matter Phenomenon and determine the nature of the dark particle and its Cosmological History. Reflecting upon the failure of the current paradigm we realize that it stems from the adopted correlation between truth and beauty in solving the DM mystery. Instead, the observational properties of the dark and luminous matter in galaxies tell another story that bends towards the triumph of ugliness. Observational relationships and galaxy properties seem to indicate scenarios with a large number of free unexplained parameters, with no much predictive power, no obvious connection with known Physics, let alone with the theoretically expected new physics and no help in resolving well known big problems of Physics, but actually an addition of new ones. Then, we need a new Paradigm that opens the road to "ugliness" and prefers scenarios with properties unacceptable by the Apollonian Paradigm. Many philosophers have expressed their opinion for this situation, but it is fair to acknowledge that F. Nietzsche has been obsessed by the concepts of beauty and ugliness in relation to those of truth and falsity, so we name after him the proposed new Paradigm, that allows

the building of scenarios that seriously follow the observational evidences how ugly the former and the latter can appear.

Let us to remind that to work in the ΛCDM scenario yields to clear advantages : - The underlying Physics is solid, undisputed and rather simple but also capable to lead one to new results in the fields of Cosmology and Physics of the Elementary particles. -In this scenario the initial conditions and the general knowledge at the basis of any new investigation is well-known and generally agreed upon. -The scenario has inbuilt a clear agenda for the investigation of dark matter mystery which is already in use in the scientific community and that fosters a global spirit of research.-The scenario has a fundamental and straightforward connection with "state of the art" computer simulations, observations and experiments and requires always better performances. Therefore, to abandon such scenario has important consequences in the investigation of the DM phenomenon. In the complexity that the new scenario may have. In understanding and in generally agreeing on its basic physics, in the contribution that computer simulations, observations and experiments may provide in the investigation of the DM Mystery. Given this, it is simply not possible to sneak away from the ΛCDM to some other scenario without performing a deep reflection on what we are leaving, why and what we are looking for. Then, in order to value and protect by biases the seemingly exotic, mysteriously entangled and ad hoc scenarios that the observations seem to indicate, we claim that an explicit switch to the Nietzschean paradigm is necessary.

Within this new Paradigm the exploration of DM mystery proceeds according to the following loop: available observations suggest us a scenario which, once verified by other purposely planned observations, is thought to provide us with the nature of the dark particle and the theoretical background of the DM Phenomenon that, once we arrive at this point, certainly will appear very beautiful.

22.6   Conclusions

Here, we have motivated and proposed that, in the investigation of the complex and entangled world of the phenomenon of the Dark matter in galaxies we take a new and tailored approach. In detail, while abandoning the failing ΛCDM scenario, we must be poised to search for scenarios without requiring that: a) they naturally come from (known) "first principles" b) they obey to the Occam razor idea c) they have the bonus to lead us towards the solution of presently open issues of the SM of the Elementary particles. On the other side, such search must: i) follow the observations and the experiments wherever they may lead ii) consider the possibility that the Physics behind the Dark Matter phenomenon be disconnected from the Physics we know and iii) does not comply with the usual canons of beauty. Finally, for the goal of this work with respect to the scientific community, it is irrelevant whether such a search is undertaken after an individual convincement or to follow a generally agreed new paradigm.

References

1. Rubin, V. C., Ford Jr, W. K. and Thonnard, N., Rotational properties of 21 SC galaxies *ApJ* ,**1980**, *238*, 471–487
2. Freeman, K.C, . On the Disks of Spiral and S0 Galaxies *ApJ*, **1970**, *160*,811
3. Corbelli, E. and Salucci, P. The extended rotation curve and the dark matter halo of M33 *MNRAS*, **2000**, *311*, 441-447

4. Salucci, P. The distribution of dark matter in galaxies *AARv*, **2019**, *27*, 2
5. Abdalla, E. etal Cosmology intertwined: A review of the particle physics, astrophysics, and cosmology associated with the cosmological tensions and anomalies *JHEAp* ,**2022**, *34*, 49A2022/06
6. Kolb, E. and Turner, M. The Early Universe, Addison Wesley, **1990**
7. Navarro J. F. Frenk, C. S. and White, S. D. M., The Structure of Cold Dark Matter Halos *ApJ*, **1996**, *462*, 563
8. Arcadi, G. etal The waning of the WIMP? A review of models, searches, and constraints *European Phys. J. C*, **2018**, *78*, 203
9. Salucci, P., Turini,N., Di Paolo C. Paradigms and scenarios for the dark matter phenomenon *Universe*, **2020**, *6*, 118
10. Persic, M, Salucci,P. The universal galaxy rotation curve *ApJ*, **1991**, *368*, 60-65
11. Salucci, P. etal The universal rotation curve of spiral galaxies–II. The dark matter distribution out to the virial radius *MNRAS*, **2007**, *378*, 41–47
12. Yegorova IA, Salucci P (2007) The radial Tully–Fisher relation for spiral galaxies— *MNRAS* ,**2007**, *377*, 507
13. Persic, M., Salucci, P. and Stel, F., The universal rotation curve of spiral galaxies—I. The dark matter connection *MNRAS*, **1966**, *281*, 27–47
14. Di Paolo, C, Salucci, P and Erkurt, A., The universal rotation curve of low surface brightness galaxies - IV. The interrelation between dark and luminous matter *MNRAS*, **2019**, *490*, 5451-5477
15. Karukes, E. V., Salucci P. The universal rotation curve of dwarf disc galaxies *MNRAS* ,**2017**, *465*, 4703–4722
16. Salucci, P. and Burkert, A., Dark matter scaling relations *ApJ* ,**2000**, *537*, 9
17. Dehghani, R., Salucci, P., Ghaffarnejad, H., Navarro-Frenk-White dark matter profile and the dark halos around disk systems *AA* ,**2020**, *643*, 161
18. Persic, M. Salucci, P. Mass decomposition of spiral galaxies from disc kinematics *MN* ,**1990**, *245*, 577
19. Gentile, G. et al The cored distribution of dark matter in spiral galaxies *MNRAS* ,**2004**, *351*, 903-922
20. Oh, S. etal Dark and Luminous Matter in THINGS Dwarf Galaxies *AJ* ,**2011**, *193*, 45
21. Karukes,E. V. , Salucci, P. , Gentile P. The dark matter distribution in the spiral NGC 3198 out to 0.22 Rvir *AA*, **2015**, *578*, 13
22. Lelli F, McGaugh SS, Schombert JM SPARC: mass models for 175 disk galaxies with Spitzer photometry and accurate rotation curves. *AJ* ,**2016**, *152*, 157
23. Gentile G. et al Universality of galactic surface densities within one dark halo scale-length *Nature* ,**2009**, *461*, 627
24. De Laurentis, MF, Salucci.P The accurate mass distribution of M87, the Giant Galaxy with imaged shadow of its supermassive black hole, as a portal to new Physics *ApJ* ,**2022**, *l 929*, 17
25. Donato, F, Gentile, G., Salucci P Cores of dark matter haloes correlate with stellar scalelengths *MNRAS* ,**2004**, *353*, 17-22
26. Salucci P The constant-density region of the dark halos of spiral galaxies. *MNRAS*, **2001**, *320*, 1
27. Sharma, G Salucci, P. van de Ven G. Observational evidence of evolving dark matter profiles at z= 1 *AA* ,**2022**, *659*, 40
28. Burkert, A. The Structure and Dark Halo Core Properties of Dwarf Spheroidal Galaxies *ApJ* ,**2015**, *808*, 158
29. Kormendy J, Freeman KC Scaling laws for dark matter halos in late-type and dwarf spheroidal galaxies.. *IAU 220S*, **2004**, *377*

30. Donato, F et al A constant dark matter halo surface density in galaxies *MNRAS* ,**2009**, *397*, 1169-1176
31. McGaugh S., Lelli F. and Schombert J. Radial Acceleration Relation in Rotationally Supported Galaxies *PhRvL*, **2016**, *117* ,201101
32. Di Paolo, C. , Salucci,P. , Fontaine JP The radial acceleration relation (RAR): crucial cases of dwarf disks and low-surface-brightness galaxies *ApJ*, **2019**, *873*, 106

23   On the construction of artificial empty space

Elia Dmitrieff

elia@quantumgravityresearch.org

Abstract. We consider principles of four-dimensional tessellation model of physical vacuum, and suggest a concept of experimental hardware equipment intended to reproduce some of its properties.

Povzetek Avtor uporabi princip štiri-razsežnega teselacijskega modela fizičnega vakuuma, da predlaga model osnovih fermionov in ustreznih umeritvenih polj standarnega modela.

- The basic structure for our model is the 4D space-filling by *26-cell 'satori' polytopes*. It is the Voronoi diagram of tesseract grid $\mathbb{Z}^4$ having all its nodes shifted in four orthogonal directions on length of $\frac{1}{2}$ along the crystallographic axes. Each node is considered having a *parity*, either *even* or *odd*, according to product of its coordinates in the original tesseract lattice.
- We postulate the changeable and discrete electrical *charge* of node, and its initial equality to the *parity* bit. Doing so, we can consider the grid as a kind of memory, storing the data locally in nodes, one bit per node.
- While the *parity* of nodes is fixed by their position in the lattice, their *charge* can be exchanged between immediate neighbors. This exchange produces a pair of anti-structural defects. Being separated, these opposite-charged defects, having also opposite parity, are recognized as a particle and anti-particle. It reflects the known natural charge-parity (CP) symmetry. To be exact, this symmetry needs also a Translation operation, since opposite defects exist in different (even or odd) sub-lattices.
- The electrical *charge* associated with node is $\pm\frac{1}{6}e$. Consequential inverses of several node's *charge* changes the total charge with steps of $\frac{1}{3}e$, which is in accordance with known particle charges. The single defect carries $\pm\frac{1}{3}e$, corresponding to down quarks/anti-quarks. The double defect is an up quark with $\pm\frac{2}{3}3e$, and the triple defect is a charged lepton with $\pm e$. The estimated physical scale (cell radius), based on Higgs expectation value, is about 10^{-21} m.
- The data in grid is stored both in nodes and edges. The edges are more conservative than nodes in sense that modifications (rewritings) of edges are associated with more energetic processes, like Universe formation, Big Bang, inflation, bariogenesis, vacuum phase transitions. In the modern Universe (maybe excepting black holes) the geometrical structure of edges is fixed. It determines the emergent space dimension count, its

symmetry, and the rules of node data exchanges. However, the orientation of edge is not so conservative because it is determined by the data in nodes thaw it connects

- The node data is represented by *charge* bits. It is more volatile than edges. It describes individual particles and defines their behavior. The node data is assumed to be 1 bit per node. Or, one may say that the node is one bit and the whole tessellation is a form of a binary memory.

- The *compactification* of grid together with *charge-parity* concept can explain why the observable space is isotropic while grids, that are supposed to be the background structure of space, are not. For 4D space curled with the minimal radius into 5D cylinder, one of 4 dimensions effectively vanishes and the space looks like it is flat 3D. However, the space is *doubled* in the following sense: every 3D point corresponds to two points on different surfaces of the cylinder. They are seen from different sides, so the *parity* difference is compensated, and opposite *charges* cancel each other. As the result, the electrical charge (in absence of defects) is exactly 0 everywhere, so nodes are not observable, and the projected space appears isotropic and empty.

- However, all nodes still exist in the 4D space and they can participate in time clock movement and cellular-automaton-like evolution. Defects cause the de-compensations of charges. They are observable as particles (charged or not charged) on the 'empty' background.

- The 4D tesseract grid translation unit, as well as the unit of 'satori' structure, has the equal lengths of its main diagonal and of the edge. Also, the both ends of the main diagonal have the same parity. So, this grid can be compactified in two ways using the same radius. It is possible that there are other ways of compactification.

- The cellular automaton's cell may be equipped with a *simple hardware circuit* to apply the evaluating rule locally. Running the evaluation asynchronously is supposed to have some competitive effects that cannot be achieved when using dedicated CPU that runs simple program rule for all the cells in turn. The simple circuit approach allows to get rid of computational resources limitations and of lowering performance on big arrays.

- In the 26-cell 'satori' filling, there are no straight (geodesic) paths, but there are *forks* with equal angles. They need a choice to be made. In backward direction, they are *junctions*. So, each path is a combination of *junctions* and *forks* with some rate, that is always non-negative. The *proper time* for the propagating defect may be effectively defined on the basis of this forks count. Zero proper time, corresponding to the light-speed movement, is presumably caused by *no forks* on 5D helical paths having the maximal possible pitch. With this definition of the proper time, there cannot be any tachyons.

- There is another geometrical *time* that is the compactified dimension. It is of very short length that is one translation unit. The T symmetry is connected to reflection in this direction. not with the proper time (that is a positive count). The movement along it in both directions is as free as in other three dimensions. But since it is compactified, both results have just minor differences that are observable as rare cases of CP symmetry violations.

- The compactification of the 4th dimension down to 3D makes the modeling much easier. It allows using existing 3D hardware technology. Exploiting the edge conservatism, a fixed 3D circuit of PLA chips can be built. This hardware model would not be able to reproduce gravity, black holes and other special cases without additional tricks, but it might be useful in demonstration of propagation, scattering and decay of macroscopic artificial particles.

24   Virtual Institute of Astroparticle physics as the online platform for studies of BSM physics and cosmology

Maxim Yu. Khlopov[1,2,3]

[1] *Centre for Cosmoparticle Physics "Cosmion"*
National Research Nuclear University MEPHI", 115409 Moscow, Russia
[2] *Virtual Institute of Astroparticle physics, 75018, Paris, France*
[3] *Institute of Physics, Southern Federal University*
Stachki 194, Rostov on Don 344090, Russia

Abstract. The relaxation of pandemia conditions is not complete and the meetings in person are to be still accompanied by online sessions, leading to their hybrid forms. The unique multi-functional complex of Virtual Institute of Astroparticle Physics (VIA) operating on website **http://viavca.in2p3.fr/site.html**, provides the platform for online virtual meetings. We review VIA experience in presentation online for the most interesting theoretical and experimental results, participation online in conferences and meetings, various forms of collaborative scientific work as well as programs of education at distance, combining online videoconferences with extensive library of records of previous meetings and Discussions on Forum. Since 2014 VIA online lectures combined with individual work on Forum acquired the form of Open Online Courses. Aimed to individual work with students the Course is not Massive, but the account for the number of visits to VIA site converts VIA in a specific tool for MOOC activity. VIA sessions, being a traditional part of Bled Workshops' program, have converted at XXV Bled Workshop "What comes beyond the Standard models?" into the hybrid format, combining streaming of the presentations in the Plemelj House (Bled, Slovenia) with distant talks, preserving the traditional creative nonformal atmosphere of Bled Workshop meetings. We openly discuss the state of art of VIA platform.

Keywords: astroparticle physics, physics beyond the Standard model, e-learning, e-science, MOOC

24.1   Introduction

Studies in astroparticle physics link astrophysics, cosmology, particle and nuclear physics and involve hundreds of scientific groups linked by regional networks (like ASPERA / ApPEC [1,2]) and national centers. The exciting progress in these studies will have impact on the knowledge on the structure of microworld and Universe in their fundamental relationship and on the basic, still unknown, physical laws of Nature (see e.g. [3,4] for review). The

progress of precision cosmology and experimental probes of the new physics at the LHC and in nonaccelerator experiments, as well as the extension of various indirect studies of physics beyond the Standard model involve with necessity their nontrivial links. Virtual Institute of Astroparticle Physics (VIA) [5] was organized with the aim to play the role of an unifying and coordinating platform for such studies.

Starting from the January of 2008 the activity of the Institute took place on its website [6] in a form of regular weekly videoconferences with VIA lectures, covering all the theoretical and experimental activities in astroparticle physics and related topics. The library of records of these lectures, talks and their presentations was accomplished by multi-lingual Forum. Since 2008 there were **220 VIA online lectures**, VIA has supported distant presentations of **192 speakers at 32 Conferences** and provided transmission of talks at **78 APC Colloquiums**. In 2008 VIA complex was effectively used for the first time for participation at distance in XI Bled Workshop [7]. Since then VIA videoconferences became a natural part of Bled Workshops' programs, opening the virtual room of discussions to the world-wide audience. Its progress was presented in [8–20].

Here the current state-of-art of VIA complex, integrated in 2009 - 2022 in the structure of APC Laboratory, is presented in order to clarify the way in which discussion of open questions beyond the standard models of both particle physics and cosmology were supported by the platform of VIA facility at the hybrid Memorial XXV Bled Workshop. The relaxation of the conditions of pandemia, making possible offline meetings, is still not complete, preventing many participants to attend these meetings. In this situation VIA videoconferencing became the only possibility to continue in 2022 traditions of open discussions at Bled meetings combining streams of the offline presentations and support of distant talks and involving distant participants in these discussions.

24.2   VIA structure and activity

24.2.1   The problem of VIA site

The structure of the VIA site was based on Flash and is virtually ruined now in the lack of Flash support. This original structure is illustrated by the Fig. 24.1. The home page, presented on this figure, contained the information on the coming and records of the latest VIA events. The upper line of menu included links to directories (from left to right): with general information on VIA (About VIA); entrance to VIA virtual rooms (Rooms); the library of records and presentations (Previous), which contained records of VIA Lectures (Previous → Lectures), records of online transmissions of Conferences (Previous → Conferences), APC Colloquiums (Previous → APC Colloquiums), APC Seminars (Previous → APC Seminars) and Events (Previous → Events); Calendar of the past and future VIA events (All events) and VIA Forum (Forum). In the upper right angle there were links to Google search engine (Search in site) and to contact information (Contacts). The announcement of the next VIA lecture and VIA online transmission of APC Colloquium occupied the main part of the homepage with the record of the most recent VIA events below. In the announced time of the event (VIA lecture or transmitted APC Colloquium) it was sufficient to click on "to participate" on the announcement and to Enter as Guest (printing your name) in the corresponding Virtual room. The Calendar showed the program of future VIA lectures and events. The right column on the VIA homepage listed the announcements of the regularly up-dated hot news of Astroparticle physics and related areas.

In the lack of Flash support this system of links is ruined, but fortunately, they continue to operate separately and it makes possible to use VIA Forum, by direct link to it, as well as direct inks to virtual room of adobeConnect used for regular Laboratory meetings and
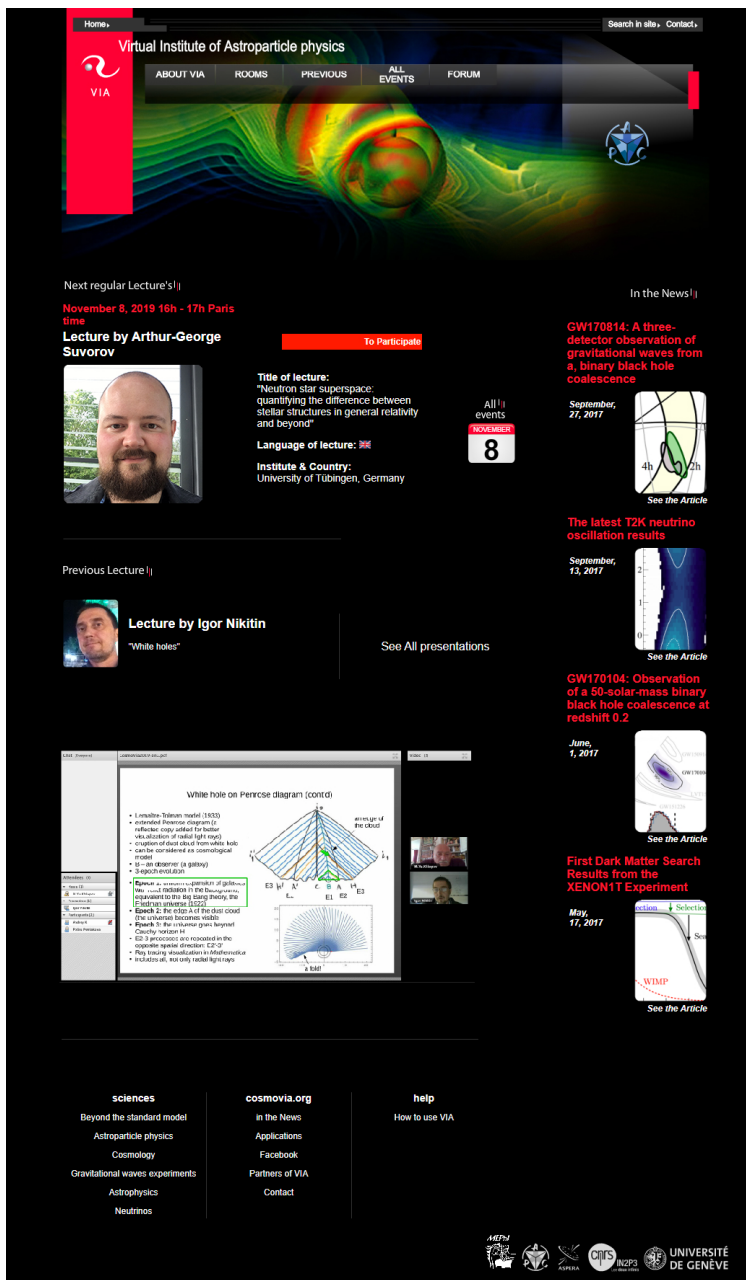
Fig. 24.1: The original home page of VIA site

Seminar and to Zoom (see Fig 24.2). The necessity to restore all the links within VIA complex is a very important task to revive the full scale of VIA activity. Another problem is the necessity to convert .flv files of records in mp4 format.

24.2.2   VIA activity

In 2010 special COSMOVIA tours were undertaken in Switzerland (Geneva), Belgium (Brussels, Liege) and Italy (Turin, Pisa, Bari, Lecce) in order to test stability of VIA online transmissions from different parts of Europe. Positive results of these tests have proved the stability of VIA system and stimulated this practice at XIII Bled Workshop. The records of the videoconferences at the XIII Bled Workshop were put on VIA site [21].

Since 2011 VIA facility was used for the tasks of the Paris Center of Cosmological Physics (PCCP), chaired by G. Smoot, for the public program "The two infinities" conveyed by J.L.Robert and for effective support a participation at distance at meetings of the Double Chooz collaboration. In the latter case, the experimentalists, being at shift, took part in the collaboration meeting in such a virtual way.

The simplicity of VIA facility for ordinary users was demonstrated at XIV Bled Workshop in 2011. Videoconferences at this Workshop had no special technical support except for WiFi Internet connection and ordinary laptops with their internal webcams and microphones. This test has proved the ability to use VIA facility at any place with at least decent Internet connection. Of course the quality of records is not as good in this case as with the use of special equipment, but still it is sufficient to support fruitful scientific discussion as can be illustrated by the record of VIA presentation "New physics and its experimental probes" given by John Ellis from his office in CERN (see the records in [22]).

In 2012 VIA facility, regularly used for programs of VIA lectures and transmission of APC Colloquiums, has extended its applications to support M.Khlopov's talk at distance at Astrophysics seminar in Moscow, videoconference in PCCP, participation at distance in APC-Hamburg-Oxford network meeting as well as to provide online transmissions from the lectures at Science Festival 2012 in University Paris7. VIA communication has effectively resolved the problem of referee's attendance at the defence of PhD thesis by Mariana Vargas in APC. The referees made their reports and participated in discussion in the regime of VIA videoconference. In 2012 VIA facility was first used for online transmissions from the Science Festival in the University Paris 7. This tradition was continued in 2013, when the transmissions of meetings at Journées nationales du Développement Logiciel (JDEV2013) at Ecole Politechnique (Paris) were organized [24].

In 2013 VIA lecture by Prof. Martin Pohl was one of the first places at which the first hand information on the first results of AMS02 experiment was presented [23].

In 2014 the 100th anniversary of one of the foundators of Cosmoparticle physics, Ya. B. Zel-dovich, was celebrated. With the use of VIA M.Khlopov could contribute the programme of the "Subatomic particles, Nucleons, Atoms, Universe: Processes and Structure International conference in honor of Ya. B. Zeldovich 100th Anniversary" (Minsk, Belarus) by his talk "Cosmoparticle physics: the Universe as a laboratory of elementary particles" [25] and the programme of "Conference YaB-100, dedicated to 100 Anniversary of Yakov Borisovich Zeldovich" (Moscow, Russia) by his talk "Cosmology and particle physics".

In 2015 VIA facility supported the talk at distance at All Moscow Astrophysical seminar "Cosmoparticle physics of dark matter and structures in the Universe" by Maxim Yu. Khlopov and the work of the Section "Dark matter" of the International Conference on Particle Physics and Astrophysics (Moscow, 5-10 October 2015). Though the conference room was situated in Milan Hotel in Moscow all the presentations at this Section were given at distance (by Rita Bernabei from Rome, Italy; by Juan Jose Gomez-Cadenas, Paterna,
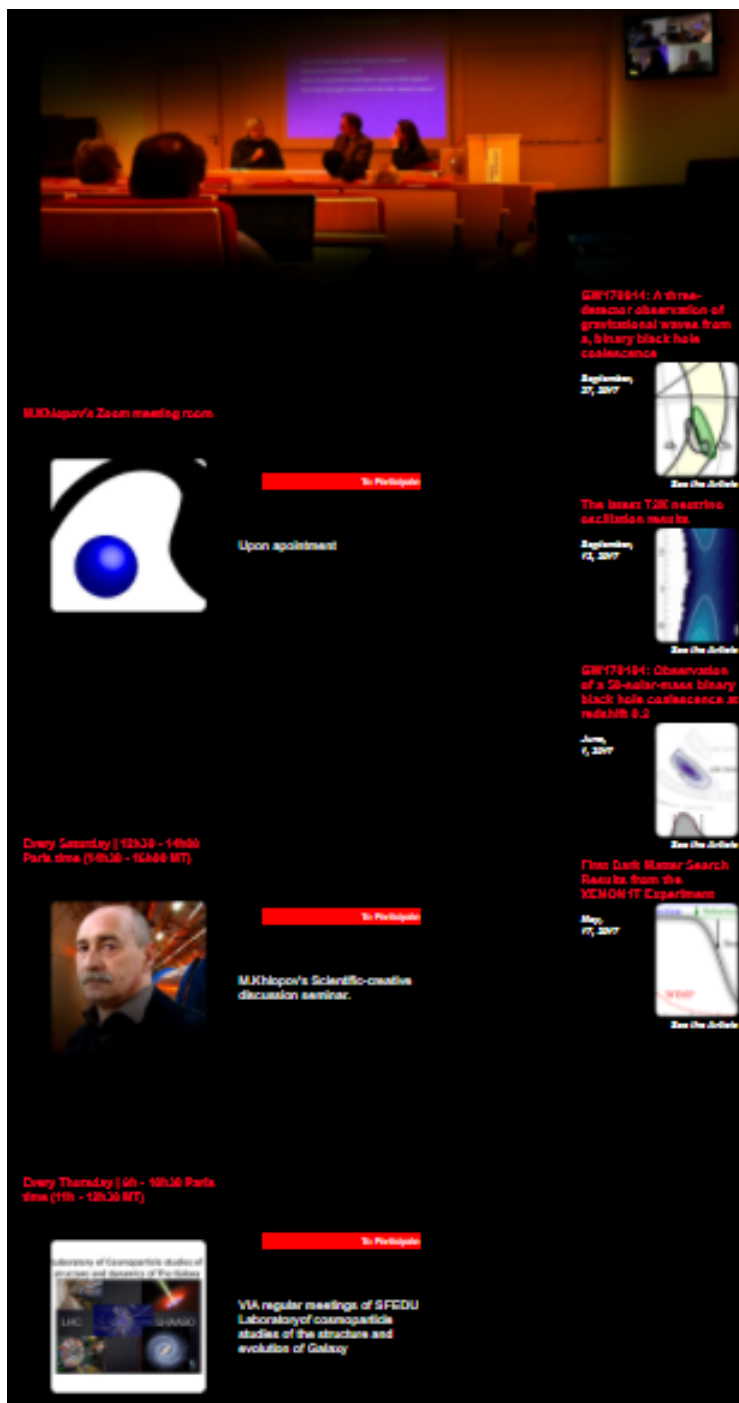
Fig. 24.2: The current home page of VIA site

University of Valencia, Spain and by Dmitri Semikoz, Martin Bucher and Maxim Khlopov from Paris) and its proceeding was chaired by M.Khlopov from Paris. In the end of 2015 M. Khlopov gave his distant talk "Dark atoms of dark matter" at the Conference "Progress of Russian Astronomy in 2015", held in Sternberg Astronomical Institute of Moscow State University.

In 2016 distant online talks at St. Petersburg Workshop "Dark Ages and White Nights (Spectroscopy of the CMB)" by Khatri Rishi (TIFR, India) "The information hidden in the CMB spectral distortions in Planck data and beyond", E. Kholupenko (Ioffe Institute, Russia) "On recombination dynamics of hydrogen and helium", Jens Chluba (Jodrell Bank Centre for Astrophysics, UK) "Primordial recombination lines of hydrogen and helium", M. Yu. Khlopov (APC and MEPHI, France and Russia)"Nonstandard cosmological scenarios" and P. de Bernardis (La Sapiensa University, Italy) "Balloon techniques for CMB spectrum research" were given with the use of VIA system. At the defense of PhD thesis by F. Gregis VIA facility made possible for his referee in California not only to attend at distance at the presentation of the thesis but also to take part in its successive jury evaluation.

Since 2018 VIA facility is used for collaborative work on studies of various forms of dark matter in the framework of the project of Russian Science Foundation based on Southern Federal University (Rostov on Don). In September 2018 VIA supported online transmission of **17 presentations** at the Commemoration day for Patrick Fleury, held in APC.

The discussion of questions that were put forward in the interactive VIA events is continued and extended on VIA Forum. Presently activated in English,French and Russian with trivial extension to other languages, the Forum represents a first step on the way to multi-lingual character of VIA complex and its activity. Discussions in English on Forum are arranged along the following directions: beyond the standard model, astroparticle physics, cosmology, gravitational wave experiments, astrophysics, neutrinos. After each VIA lecture its pdf presentation together with link to its record and information on the discussion during it are put in the corresponding post, which offers a platform to continue discussion in replies to this post.

24.2.3   VIA e-learning, OOC and MOOC

One of the interesting forms of VIA activity is the educational work at distance. For the last eleven years M.Khlopov's course "Introduction to cosmoparticle physics" is given in the form of VIA videoconferences and the records of these lectures and their ppt presentations are put in the corresponding directory of the Forum [26]. Having attended the VIA course of lectures in order to be admitted to exam students should put on Forum a post with their small thesis. In this thesis students are proposed to chose some BSM model and to study the cosmological scenario based on this chosen model. The list of possible topics for such thesis is proposed to students, but they are also invited to chose themselves any topic of their own on possible links between cosmology and particle physics. Professor's comments and proposed corrections are put in a Post reply so that students should continuously present on Forum improved versions of work until it is accepted as admission for student to pass exam. The record of videoconference with the oral exam is also put in the corresponding directory of Forum. Such procedure provides completely transparent way of evaluation of students' knowledge at distance.

In 2018 the test has started for possible application of VIA facility to remote supervision of student's scientific practice. The formulation of task and discussion of progress on work are recorded and put in the corresponding directory on Forum together with the versions of student's report on the work progress.

Since 2014 the second semester of the course on Cosmoparticle physics is given in English and converted in an Open Online Course. It was aimed to develop VIA system as a possible accomplishment for Massive Online Open Courses (MOOC) activity [27]. In 2016 not only students from Moscow, but also from France and Sri Lanka attended this course. In 2017 students from Moscow were accompanied by participants from France, Italy, Sri Lanka and India [28]. The students pretending to evaluation of their knowledge must write their small thesis, present it and, being admitted to exam, pass it in English. The restricted number of online connections to videoconferences with VIA lectures is compensated by the wide-world access to their records on VIA Forum and in the context of MOOC VIA Forum and videoconferencing system can be used for individual online work with advanced participants. Indeed Google Analytics shows that since 2008 VIA site was visited by more than **250 thousand** visitors from **155** countries, covering all the continents by its geography (Fig. 24.3). According to this statistics more than half of these visitors continued to enter VIA site after the first visit. Still the form of individual educational work makes VIA facility most

Fig. 24.3: Geography of VIA site visits according to Google Analytics

appropriate for PhD courses and it could be involved in the International PhD program on Fundamental Physics, which was planned to be started on the basis of Russian-French collaborative agreement. In 2017 the test for the ability of VIA to support fully distant education and evaluation of students (as well as for work on PhD thesis and its distant defense) was undertaken. Steve Branchu from France, who attended the Open Online Course and presented on Forum his small thesis has passed exam at distance. The whole procedure, starting from a stochastic choice of number of examination ticket, answers to ticket questions, discussion by professors in the absence of student and announcement of result of exam to him was recorded and put on VIA Forum [29].

In 2019 in addition to individual supervisory work with students the regular scientific and creative VIA seminar is in operation aimed to discuss the progress and strategy of students scientific work in the field of cosmoparticle physics.

In 2020 the regular course now for M2 students continued, but the problems of adobe Connect, related with the lack of its support for Flash in 2021 made necessary to use the platform of Zoom, This platform is rather easy to use and provides records, as well as whiteboard tools for discussions online can be solved by accomplishments of laptops by

graphic tabloids. In 2022 the Open Online Course for M2 students was accompanied by special course "Cosmoparticle physics", given in English for English speaking M1 students.

24.2.4   Organisation of VIA events and meetings

First tests of VIA system, described in [5,7–9], involved various systems of videoconferencing. They included skype, VRVS, EVO, WEBEX, marratech and adobe Connect. In the result of these tests the adobe Connect system was chosen and properly acquired. Its advantages were: relatively easy use for participants, a possibility to make presentation in a video contact between presenter and audience, a possibility to make high quality records, to use a whiteboard tools for discussions, the option to open desktop and to work online with texts in any format. The lack of support for Flash, on which VIA site was originally based, made necessary to use Zoom, which shares all the above mentioned advantages.

Regular activity of VIA as a part of APC included online transmissions of all the APC Colloquiums and of some topical APC Seminars, which may be of interest for a wide audience. Online transmissions were arranged in the manner, most convenient for presenters, prepared to give their talk in the conference room in a normal way, projecting slides from their laptop on the screen. Having uploaded in advance these slides in the VIA system, VIA operator, sitting in the conference room, changed them following presenter, directing simultaneously webcam on the presenter and the audience. If the advanced uploading was not possible, VIA streaming was used - external webcam and microphone are directed to presenter and screen and support online streaming. This experience has found proper place in the current weakening of the pandemic conditions and regular meetings in real can be streamed. Moreover, such streaming can be made without involvement of VIA operator, by direction of webcam towards the conference screen and speaker.

24.2.5   VIA activity in the conditions of pandemia

The lack of usual offline connections and meetings in the conditions of pandemia made the use of VIA facility especially timely and important. This facility supports regular weekly meetings of the Laboratory of cosmoparticle studies of the structure and dynamics of Galaxy in Institute of Physics of Southern Federal University (Rostov on Don, Russia) and M.Khlopov's scientific - creative seminar and their announcements occupied their permanent position on VIA homepage (Fig. 24.2), while their records were put in respective place of VIA forum, like [31] for Laboratory meetings.

The platform of VIA facility was used for regular Khlopov's course "Introduction to Cosmoparticle physics" for M2 students of MEPHI (in Russian) and in 2020 supported regular seminars of Theory group of APC.

The programme of VIA lectures continued to present hot news of astroparticle physics and cosmology, like talk by Zhen Cao from China on the progress of LHAASO experiment or lecture by Sunny Vagnozzi from UK on the problem of consistency of different measurements of the Hubble constant.

The results of this activity inspired the decision to hold in 2020 XXIII Bled Workshop online on the platform of VIA [19].

The conditions of pandemia continued in 2021 and VIA facility was successfully used to provide the platform for various online meetings. 2021 was announced by UNESCO as A.D.Sakharov year in the occasion of his 100th anniversary VIA offered its platform for various events commemorating A.D.Sakharov's legacy in cosmoparticle physics. In the framework of 1 Electronic Conference on Universe ECU2021), organized by the MDPI journal "Universe" VIA provided the platform for online satellite Workshop "Developing A.D.Sakharov legacy in cosmoparticle physics" [32].
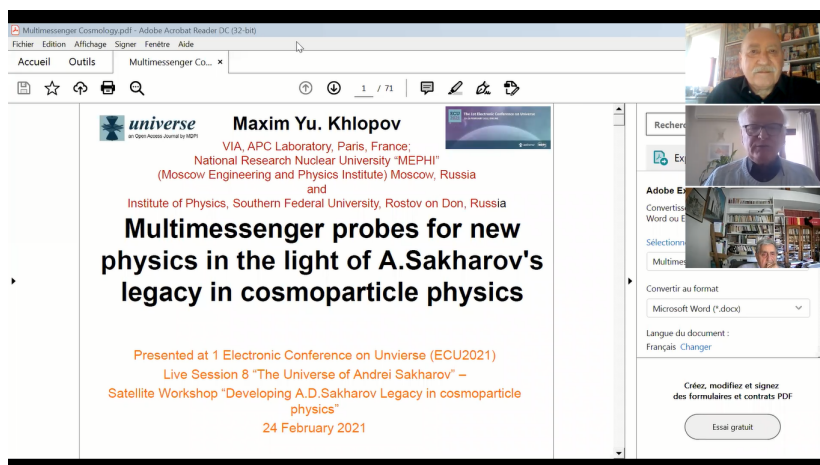
Fig. 24.4: M.Khlopov's talk "Multimessenger probes for new physics in the light of A.D.Sakharov legacy in cosmoparticle physics" at the satellite Workshop "Developing A.D.Sakharov legacy in cosmoparticle physics" of ECU2021.

24.3   VIA platform at Hybrid Memorial XXV Bled Workshop

VIA sessions at Bled Workshops continued the tradition coming back to the first experience at XI Bled Workshop [7] and developed at XII, XIII, XIV, XV, XVI, XVII, XVIII, XIX, XX, XXI and XXII Bled Workshops [8–18]. They became a regular but supplementary part of the Bled Workshop's program. In the conditions of pandemia it became the only form of Workshop activity in 2020 [19] and in 2021 [20].

During the XXV Bled Workshop the announcement of VIA sessions was put on VIA home page, giving an open access to the videoconferences at the Workshop sessions. The preliminary program as well as the corrected program for each day were continuously put on Forum with the slides and records of all the talks and discussions [33].

VIA facility tried to preserve the creative atmosphere of Bled discussions. The program of XXV Bled Workshop combined talks presented in Plemelj House in Bled, which were streamed by VIA facility, as the talk "Understanding nature with the spin-charge- family theory, New way of second quantization of fermions and bosons" by Norma Mankoc-Borstnik (Fig. 24.5) with talks given in the format videoconferences "Recent results and empowered perspectives of DAMA/LIBRA-phase2" by R.Bernabei, (Fig. 24.6), from Rome University, Italy (see records in [33]).

During the Workshop the VIA virtual room was open, inviting distant participants to join the discussion and extending the creative atmosphere of these discussions to the world-wide audience. The participants joined these discussions from different parts of world. The talk "A Nietzschean paradigm for the dark matter phenomenon" was given by Paolo Salucci from Italy (Fig. 24.7). R.Mohapatra and S. Brodsky gave their talks from US and E.Kiritsis from from Paris. The online talks were combined with presentations in Bled such as "Dusty dark matter pearls developed" by H.B. Nielsen (Fig. 24.8) or "Cosmological reflection of the BSM physics" by M.Y. Khlopov (Fig. 24.9).
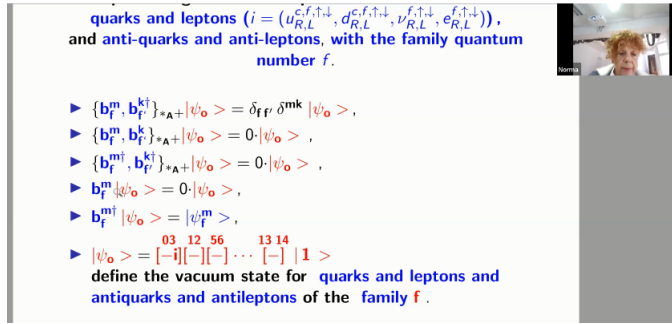
Fig. 24.5: VIA stream of the talk "Understanding nature with the spin-charge-family theory, New way of second quantization of fermions and bosons" by Norma Mankoc-Borstnik at XXV Bled Workshop

Fig. 24.6: VIA talk "Recent results and empowered perspectives of DAMA/LIBRA-phase2" by R.Bernabei from Rome at XXV Bled Workshop

The distant VIA talks highly enriched the Workshop program and streaming of talks from Bled involved distant participants in fruitful discussions. The use of VIA facility has provided remote presentation of students' scientific debuts in BSM physics and cosmology. The records of all the talks and discussions can be found on VIA Forum [33].

VIA facility has managed to join scientists from Mexico, USA, France, Italy, Russia, Slovenia, India and many other countries in discussion of open problems of physics and cosmology beyond the Standard models.

24.4   Conclusions

The Scientific-Educational complex of Virtual Institute of Astroparticle physics provides regular communication between different groups and scientists, working in different sci-

13:30 - 15:00 P. Salucci: A Nietzschean paradigm for the dark matter phenomenon, I, ZOOM

Fig. 24.7: VIA talk "A Nietzschean paradigm for the dark matter phenomenon" by Paolo Salucci at XXV Bled Workshop

Fig. 24.8: VIA stream of talk "Dusty dark matter pearls developed" by Holger Bech Nielsen at XXV Bled Workshop

entific fields and parts of the world, the first-hand information on the newest scientific results, as well as support for various educational programs at distance. This activity would easily allow finding mutual interest and organizing task forces for different scientific topics of cosmology, particle physics, astroparticle physics and related topics. It can help in the elaboration of strategy of experimental particle, nuclear, astrophysical and cosmological studies as well as in proper analysis of experimental data. It can provide young talented people from all over the world to get the highest level education, come in direct interactive contact with the world known scientists and to find their place in the fundamental research. These educational aspects of VIA activity can evolve in a specific tool for International PhD program for Fundamental physics. Involvement of young scientists in creative discussions was an important aspect of VIA activity at XXV Bled Workshop. VIA applications can go far

12.00 - 13.30 M.Y. Khlopov: Cosmological reflection of the BSM physics, I
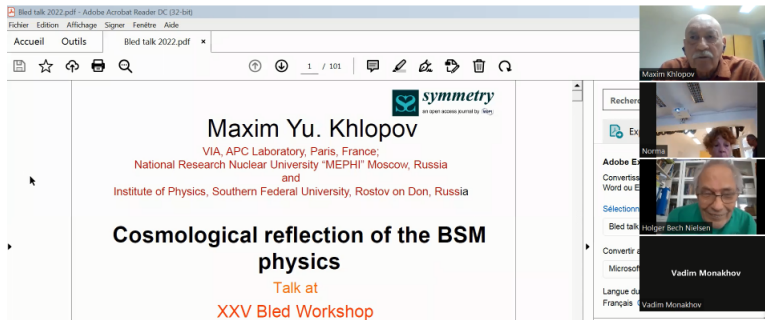
Fig. 24.9: VIA stream of talk "Cosmological reflection of the BSM physics" by Maxim Yu. Khlopov at XXV Bled Workshop

beyond the particular tasks of astroparticle physics and give rise to an interactive system of mass media communications.

VIA sessions, which became a natural part of a program of Bled Workshops, maintained in 2022 the platform for online discussions of physics beyond the Standard Model involving distant participants from all the world in the fruitful atmosphere of Bled offline meeting. This discussion can continue in posts and post replies on VIA Forum. The experience of VIA applications at Bled Workshops plays important role in the development of VIA facility as an effective tool of e-science and e-learning.

One can summarize the advantages and flaws of online format of Bled Workshop. It makes possible to involve in the discussions scientists from all the world (young scientists, especially) free of the expenses related with meetings in real (voyage, accommodation, ...), but loses the advantage of nonformal discussions at walks along the beautiful surrounding of the Bled lake and other places of interest. The improvement of VIA technical support by involvement of Zoom provided better platform for nonformal online discussions, but in no case can be the substitute for offline Bled meetings and its creative atmosphere in real, which has revived at the offline XXV Bled Workshop. One can summarize that VIA facility provides important tool of the offline Bled Workshop, involving world-wide participants in its creative and open discussions.

Acknowledgements

complex. The work was financially supported by Southern Federal University, 2020 Project VnGr/2020-03-IF. I express my gratitude to the Organizers of Bled Workshop N.S. Mankoč Borštnik, A.Kleppe and H.Nielsen or cooperation in the organization of VIA online Sessions at XXV Bled Workshop. I am grateful to T.E.Bikbaev for technical assistance and help. I am grateful to Sandi Ogrizek for creation of compact links to VIA Forum.

References

1. http://www.aspera-eu.org/
2. http://www.appec.org/
3. M.Yu. Khlopov: *Cosmoparticle physics*, World Scientific, New York -London-Hong Kong - Singapore, 1999.
4. M.Yu. Khlopov: *Fundamentals of Cosmic Particle Physics*, CISP-Springer, Cambridge, 2012.
5. M. Y. Khlopov, Project of Virtual Institute of Astroparticle Physics, arXiv:0801.0376 [astro-ph].
6. http://viavca.in2p3.fr/site.html
7. M. Y. Khlopov, Scientific-educational complex - virtual institute of astroparticle physics, 981–862008.
8. M. Y. Khlopov, Virtual Institute of Astroparticle Physics at Bled Workshop, 10177–1812009.
9. M. Y. Khlopov, VIA Presentation, 11225–2322010.
10. M. Y. Khlopov, VIA Discussions at XIV Bled Workshop, 12233–2392011.
11. M. Y. .Khlopov, Virtual Institute of astroparticle physics: Science and education online, 13183–1892012.
12. M. Y. .Khlopov, Virtual Institute of Astroparticle physics in online discussion of physics beyond the Standard model, 14223–2312013.
13. M. Y. .Khlopov, Virtual Institute of Astroparticle physics and "What comes beyond the Standard model?" in Bled, 15285-2932014.
14. M. Y. .Khlopov, Virtual Institute of Astroparticle physics and discussions at XVIII Bled Workshop, 16177-1882015.
15. M. Y. .Khlopov, Virtual Institute of Astroparticle Physics — Scientific-Educational Platform for Physics Beyond the Standard Model, 17221-2312016.
16. M. Y. .Khlopov: Scientific-Educational Platform of Virtual Institute of Astroparticle Physics and Studies of Physics Beyond the Standard Model, 18273-2832017.
17. M. Y. .Khlopov: The platform of Virtual Institute of Astroparticle physics in studies of physics beyond the Standard model, 19383-3942018.
18. M. Y. .Khlopov: The Platform of Virtual Institute of Astroparticle Physics for Studies of BSM Physics and Cosmology, Journal20249-2612019.
19. M. Y. .Khlopov: Virtual Institute of Astroparticle Physics as the Online Platform for Studies of BSM Physics and Cosmology, Journal21249-2632020.
20. M. Y. .Khlopov: Challenging BSM physics and cosmology on the online platform of Virtual Institute of Astroparticle physics, Journal22160-1752021.
21. $http://viavca.in2p3.fr/what_comes_beyond_the_standard_models_xiii.html$
22. $http://viavca.in2p3.fr/what_comes_beyond_the_standard_models_xiv.html$
23. $http://viavca.in2p3.fr/pohl_martin.html$
24. In http://viavca.in2p3.fr/ Previous - Events - JDEV 2013
25. $http://viavca.in2p3.fr/zeldovich_100_meeting.html$
26. In https://bit.ly/bled2022bsm Forum- Discussion in Russian - Courses on Cosmoparticle physics

27. In https://bit.ly/bled2022bsm Forum - Education - From VIA to MOOC
28. In https://bit.ly/bled2022bsm Forum - Education - Lectures of Open Online VIA Course 2017
29. In https://bit.ly/bled2022bsm Forum - Education - Small thesis and exam of Steve Branchu
30. $http://viavca.in2p3.fr/john_ellis.html$
31. In https://bit.ly/bled2022bsm Forum - LABORATORY OF COSMOPARTICLE STUDIES OF STRUCTURE AND EVOLUTION OF GALAXY
32. In https://bit.ly/bled2022bsm Forum - CONFERENCES - CONFERENCES ASTROPARTICLE PHYSICS - The Universe of A.D. Sakharov at ECU2021
33. In https://bit.ly/bled2022bsm Forum - CONFERENCES BEYOND THE STANDARD MODEL - XXV Bled Workshop "What comes beyond the Standard model?"

25   A poem

When I met Elia Dmitrieff in Bled, he told me that he has a datcha by the Lake Baikal.
"Really?" I said, "o, I would love to visit you and see the Baikal!"
He smiled and nodded, and I thought of the Trans-Siberian railway, and made a vague plan
to one day visit him.
Some years later, when the war in Ukraine started, I was in total shock, and soon thereafter,
I went into a depression. I thought of the Ukrainians, and I thought of Elia, and I thought
of all my Russians friends. And then I wrote this poem.

Voyage to Irkutsk

I thought I one day
would pay you a visit, take the train
many days
through the large waste land woods

We would go to your datcha
chop some wood, make a fire,
drink our tea
and discuss the meaning of charge!

By the hearth you would tell me
your binary codes
of the innermost parts, of your
Glasperlenspiel,

while over the house the moon
would sail,
and mirror its light
in the Lake Baikal,
And you'd say: If you pray, pray
for healing and reason, and if
you believe,
believe
in the good!

I will, I would say, but I want you to tell me
a story where all goes well!
I want it to be in a grandiose land
where oceans are pure, since pollution is banned.

And there must be a house with a garden and trees
with apples and plums, and flowers and bees
And children shall play in the neighbouring wood
and nobody barks, and people are good!

Do you hear, I will come
and visit you soon! Then we'll talk
about binary codes.
When the devils
are gone and the light is restored,
and the roads are repaired
and the flowers all bloom,
I will visit you soon, very soon!

Astri Kleppe